
Anionic Polymerization of Terpenes and Bio-Based Thermoplastic Elastomers

Dissertation zur Erlangung des Grades
„Doktor der Naturwissenschaften“
im Promotionsfach Chemie

am Fachbereich Chemie, Pharmazie und Geowissenschaften der
Johannes Gutenberg-Universität Mainz

vorgelegt von

Christian Wahlen
geboren in Mainz

Mainz, Oktober 2020

JOHANNES GUTENBERG
UNIVERSITÄT MAINZ



Die als Dissertation vorgelegte Arbeit wurde in der Zeit von April 2017 bis Oktober 2020 am Department Chemie der Johannes Gutenberg-Universität Mainz im Arbeitskreis von [REDACTED] angefertigt.

1. Berichterstatter: [REDACTED]

2. Berichterstatter: [REDACTED]

Tag der mündlichen Prüfung: 16.11.2020

Hiermit versichere ich gemäß § 10 Abs. 3d der Promotionsordnung vom 24.07.2007:

Ich habe die jetzt als Dissertation vorgelegte Arbeit selbst angefertigt und alle benutzten Hilfsmittel (Literatur, Apparaturen, Material) in der Arbeit angegeben.

Ich habe oder hatte die jetzt als Dissertation vorgelegte Arbeit nicht als Prüfungsarbeit für eine andere staatliche oder andere wissenschaftliche Prüfung eingereicht.

Ich hatte weder die jetzt als Dissertation vorgelegte Arbeit noch Teile davon bei einer anderen Fakultät bzw. einem anderen Fachbereich als Dissertation eingereicht.

Christian Wahlen

Für



Danksagung

Zum Gelingen dieser Dissertation haben in den letzten Jahren zahlreiche Menschen beigetragen, bei denen ich mich hiermit herzlich bedanken möchte.

An erster Stelle möchte ich besonders meinem Doktorvater [REDACTED] für die Möglichkeit danken, meine Doktorarbeit in seinem Arbeitskreis anfertigen zu dürfen. Vielen Dank für die Freiheiten, welche Sie mir bei der Entwicklung und Umsetzung meiner Forschungsprojekte gegeben haben. Dieses entgegengebrachte Vertrauen ist nicht selbstverständlich. Ohne Ihre uneingeschränkte Unterstützung während meiner Promotion, wäre die Umsetzung meiner Projektideen nicht möglich gewesen.

In der heutigen Forschung ist die interdisziplinäre Zusammenarbeit mit Kooperationspartnern unerlässlich. Ich hatte das Glück, während meiner Promotion mit zahlreichen hoch renommierten Wissenschaftlern zusammenarbeiten zu dürfen, denen ich an dieser Stelle danken möchte.

Besonderer Dank gilt dabei [REDACTED], ohne dessen Einsatz und Expertise im Bereich der Rheologie und des Phasenseparationsverhalten von Copolymeren zahlreiche meiner Projekte nicht in diesem Umfang möglich gewesen wären.

Bei [REDACTED] möchte ich mich für die erfolgreiche Zusammenarbeit und die sehr konstruktiven Diskussionen bezüglich der Copolymerisations-Kinetik bedanken, welche meine Dissertation sehr bereichert haben.

[REDACTED], [REDACTED] und [REDACTED] danke ich für die erfolgreiche Zusammenarbeit hinsichtlich Electrospinning, Phasenseparationsverhalten und Materialeigenschaften von Multiblock-Copolymeren. In diesem Zusammenhang möchte ich auch [REDACTED] für die Unterstützung bei den Zug-Dehnungs-Versuchen danken.

Ganz besonders danke ich [REDACTED], für die herausragende freundschaftliche und kollegiale Zusammenarbeit im Bereich der Copolymerisations-Kinetik. Diese hat mir sehr viel Freude beim Erstellen dieser Arbeit bereitet.

Bei [REDACTED] möchte ich mich herzlich für die Einführung in die Thematik der carbanionischen Polymerisation und Multiblockstrukturen während meiner Masterarbeit und zu Beginn meiner Promotion, sowie für die erfolgreiche Zusammenarbeit bedanken.

Des Weiteren danke ich [REDACTED] für die Unterstützung bei der Durchführung und Auswertung der Copolymerisations-Kinetik-Messungen, [REDACTED] für die Durchführung der Electrospinning-Experimente, sowie [REDACTED] und [REDACTED] für das Korrekturlesen von Teilen dieser Arbeit.

Vielen lieben Dank an [REDACTED] und [REDACTED], dass ihr den Laden zusammenhaltet und für die lustigen gemeinsamen Momente. Eure Leistung und Unterstützung im Laboralltag kann man gar nicht genug würdigen. Ebenso möchte ich [REDACTED] für die Hilfe bei scheinbar unlösbaren organisatorischen Aufgaben bedanken. Bei [REDACTED] möchte ich mich für die Koordination der Laborbestellungen und die angenehme Arbeitsatmosphäre bedanken.

Ich danke [REDACTED] und [REDACTED] für die gute Zusammenarbeit im Rahmen ihrer Bachelorarbeit, sowie [REDACTED] für die erfolgreiche Zusammenarbeit im Rahmen seines Forschungsmoduls. In diesem Zusammenhang danke ich auch [REDACTED] für die unkomplizierte und erfolgreiche gemeinsame Betreuung von Milena Hesse.

Nach der Arbeit kommt das Vergnügen. Dementsprechend möchte ich mich bei allen bedanken, die mir den Arbeitsalltag erleichtert, und meine Freizeit bereichert haben:

Ich möchte mich bei [REDACTED]
[REDACTED]
[REDACTED]
[REDACTED] und [REDACTED] für die lustige Zeit im Arbeitskreis und das freundschaftliche Verhältnis bedanken. Allein wegen euch haben sich die 3,5 Jahre Promotion bereits gelohnt!

Die unzähligen AK-Aktivitäten wie das Hüttenseminar im Kleinwalsertal, Konferenzbesuche in Freiburg und Durham, die AK-Fassenacht, die Seewochenenden, die Betriebsausflüge, die gemeinsamen Teilnahmen am Mainzer Firmenlauf und die anderen Feierlichkeiten werden für immer unvergesslich bleiben. Ich danke allen Beteiligten!

Ein sportlicher Dank geht an die **AK-Kicker** (vor allem an das Stammpersonal: [REDACTED] [REDACTED]) und [REDACTED]. Fußball und Entertainment auf allerhöchstem Niveau, mehr gibt es dazu nicht zu sagen. Ich hoffe dieses hohe Gut wird weiterhin gewahrt. Es gibt genug neue junge Talente im Arbeitskreis. Die Kapitänsbinde gebe ich hiermit an [REDACTED] weiter. Es war mir eine Freude!

Die Corona-Krise hat die letzten Monate meiner Promotion etwas anders gestaltet als ursprünglich geplant. Dank Freunden, wie meinem „Corona-Buddy“ [REDACTED], konnte ich jedoch das Beste aus dieser schwierigen Zeit machen.

Mit meinem Abschied aus dem Arbeitskreis verabschiede ich mich auch von meinem guten Freund [REDACTED]. Du bist der Beste!

[REDACTED] möchte ich für die Unterstützung und den Rückhalt während einem Großteil meiner Promotion danken.

Ein ganz besonderer Dank geht an meine langjährigen Freunde [REDACTED] [REDACTED]. Danke für die gelegentliche Ablenkung vom Arbeitsalltag und entschuldigt, dass die Arbeit manchmal wichtiger schien als das Vergnügen.

Ein herzlicher Dank geht an dieser Stelle an [REDACTED] und [REDACTED]. Vielen Dank für das Vertrauen und die Freude, welche ihr mir mit meinem Patenkind [REDACTED] geschenkt habt.

Zu guter Letzt danke ich [REDACTED], insbesondere [REDACTED], für die bedingungslose Unterstützung während meines gesamten Studiums. Danke!

Ich wünsche allen genannten Personen alles Gute und freue mich auf zukünftige Begegnungen und gemeinsame Erlebnisse!

Table of Contents

Motivation and Objectives	2
Abstract	6
Zusammenfassung	9
Graphical Abstract	13
Chapter 1 Introduction to the Living Anionic Polymerization of Terpenes.....	17
Chapter 2 β -Myrcenol-Based Monomer for Living Anionic Polymerization	49
Chapter 3 Influence of Silyl Protective Groups on Polymyrcenol Microstructure	101
Chapter 4 Terpene-Based Thermoplastic Elastomers	143
Chapter 5 Tapered Multiblock Copolymers of Isoprene and 4-Methylstyrene.....	211
Appendix	
Chapter A1 Tapered Diblock Copolymers of Isoprene and 4-Methylstyrene	251
Curriculum Vitae	286
List of Publications	288

Motivation and Objectives

The success story of rubbery materials started with the vulcanization of natural rubber in 1839 by Charles Goodyear, resulting in the first tires for automobile industry.¹ Nowadays, elastomers enrich our everyday life in manyfold ways. The biomass-derived polyterpene *cis*-1,4-polyisoprene, commonly referred to as natural rubber, still presents the most consumed rubber worldwide.² The increased demand on natural rubber caused a growing industrial production volume of alternative petrochemical-based elastomers. However, today's society desires a reduction on its fossil resource dependence, drawing attention to current research for the use of biomass-derived chemicals and materials.³ Terpenes represent a large-scale available and structural versatile class of bio-based compounds, which covers a wide range of applications from fragrances to rubber.⁴ Due to their large variety of polymerizable moieties, terpenes offer a versatile library of renewable monomers for polymerization.⁵

The living anionic polymerization of isoprene in apolar solvents results in polyisoprene with high content of 1,4-regioisomers, showing highly similar elasticity to natural rubber. In recent years, the vast potential of the biomass-derived 1,3-diene monomers β -myrcene and β -farnesene as alternatives for fossil-based isoprene has been explored. Today, β -myrcene as well as β -farnesene are produced in large scale from biomass.^{6,7} Consequently, the polymerization of those renewable monomers is attracting increased interest.

Nevertheless, there is a lack of functional groups in the polydiene backbone with exception of their double bonds. Functionalized polydienes are of industrial relevance because of their improved interaction with functional fillers, resulting in a reinforcement in mechanical, electrical and thermal properties at low costs.^{8,9} Additional to the polymerizable 1,3-diene moiety, β -myrcene offers an additional double bond in the isopropylidene pendant group. Those addressable double bonds allow functionalization of polymyrcene by postpolymerization modification reactions. Nevertheless, postmodification reactions exhibit a lack of regioselectivity of the functionalization, which is key for the synthesis of well-defined polymer architectures. A potential alternative for the regioselective introduction of functional groups is the utilization of functional monomers. Due to the high susceptibility of the 1,3-diene moiety to side reactions in the living anionic polymerization, the diversity of suitable functional

1,3-diene monomers, is strongly limited.¹⁰ In publications to date, hydroxyl groups were attached to polymyrcene via post-polymerization modification reactions, leading imprecise defined polymer structures. This lack of tools for the adjustment of well-defined hydroxyl-functionalized polymer architectures, results in the following question:

“Is it possible to introduce hydroxyl functionalities to the polydiene backbone in a regiospecific fashion, by using a biomass-derived functional diene-monomer for the living anionic polymerization?”

Besides their application as elastomers, polydienes represent suitable rubbery building blocks for so-called thermoplastic elastomers (TPEs). Cross-linking in elastomers is obtained by irreversible chemical cross-linking of flexible polymer chains, exhibiting low glass transition temperatures (T_g). However, the cross-linking in TPEs is achieved by reversible physical crosslinking. Thereby the linkage of glassy end blocks (A) and a flexible rubbery midblock (B) in a single polymer chain in form of ABA triblock copolymers combines the advantages of commonly incompatible materials.¹¹ Bridge formation and entangled loops of the flexible rubbery midblock enhances the mechanical properties of the materials in comparison to AB diblock copolymers.¹² The thermodynamic immiscibility of the polymer blocks induces the formation of rubbery and glassy domains. The phase separation behavior dictates the outstanding mechanical properties of the ABA triblock copolymers.¹³ Living anionic polymerization is the method of choice for the synthesis of well-defined and complex block copolymer architectures with high molecular weights, due to its unique sequence control by sequential monomer addition, in both the polymer industry and academia.^{14,15} The living anionic polymerization of 1,3-dienes and styrene is commonly used for the synthesis of highly industrial relevant block copolymer architectures. Their application varies from daily life articles like footwear, toothbrushes, food packaging, automotive products to advanced technologies like polymeric actuators and separation membranes.^{16,17} The mechanical properties of TPEs are improved by the synthesis of multiblock copolymers, due to multiple bridging polydiene segments in a single polymer chain.¹²

In general, the replacement of the fossil sourced TPEs by renewable alternatives is a current objective in academic and industrial research. The previously discussed terpene-based 1,3-diene monomers β -myrcene and β -farnesene are ideal candidates for low T_g rubbery building blocks of thermoplastic elastomers.¹⁸ In contrast to the linear polyisoprene chains, polyfarnesene exhibits a bottlebrush-like structure, which

influences the molecular dynamics of the polymer chains and induces an increase in the entanglement molecular weight. Thus, the terpene-based polydiene blocks are expected to influence the thermal, morphological and mechanical properties of TPEs when compared to conventional isoprene-based analogs. The investigation of the influence of the polydiene architecture on the properties of TPEs is a neglected topic in academic research and literature, which raises the question:

“How does the replacement of fossil feedstock-based 1,3-diene monomers by biomass-derived terpene-based monomers influence the thermal, morphological and mechanical properties of thermoplastic elastomers?”

References

- (1) Calzonetti, J. A.; Laursen, C. J. Patents of Charles Goodyear: His International Contributions to the Rubber Industry. *Rubber Chem. Technol.* **2010**, *83*, 303–321.
- (2) Sarkar, P.; Bhowmick, A. K. Sustainable rubbers and rubber additives. *J Appl Polym Sci* **2018**, *135*, 45701.
- (3) Corma, A.; Iborra, S.; Velty, A. Chemical routes for the transformation of biomass into chemicals. *Chem. Rev.* **2007**, *107*, 2411–2502.
- (4) Breitmaier, E. *Terpenes: Flavors, fragrances, pharmaca, pheromones*; Wiley-VCH: Weinheim, 2006.
- (5) Zhao, J.; Schlaad, H. Synthesis of Terpene-Based Polymers; *Adv. Polym. Sci.* **2013**, *253*, 151-190.
- (6) Behr, A.; Johnen, L. Myrcene as a natural base chemical in sustainable chemistry: a critical review. *ChemSusChem* **2009**, *2*, 1072–1095.
- (7) Benjamin, K. R.; Silva, I. R.; Cherubim, J. P.; McPhee, D.; Paddon, C. J. Developing Commercial Production of Semi-Synthetic Artemisinin, and of β -Farnesene, an Isoprenoid Produced by Fermentation of Brazilian Sugar. *J. Braz. Chem. Soc.* **2016**, *27*, 1339–1345.
- (8) Bokobza, L. Mechanical and Electrical Properties of Elastomer Nanocomposites Based on Different Carbon Nanomaterials. *C—J. Carbon Res.* **2017**, *3*, 10.
- (9) Najam, M.; Hussain, M.; Ali, Z.; Maafa, I. M.; Akhter, P.; Majeed, K.; Ahmed, A.; Shehzad, N. Influence of silica materials on synthesis of elastomer nanocomposites: A review. *J. Elastomers Plast.* **2020**, *52* (8), 1-25.
- (10) Hadjichristidis, N.; Hirao, A., Eds. *Anionic Polymerization: Principles, Practice, Strength, Consequences and Applications*, 1st ed.; Springer: Tokyo, 2015.
- (11) Knoll, K.; Nießner, N. Styrolux and styroflex - from transparent high impact polystyrene to new thermoplastic elastomers: Syntheses, applications and blends with other styrene based polymers. *Macromol. Symp.* **1998**, *132*, 231–243.

- (12) Smith, S. D.; Spontak, R. J.; Satkowski, M. M.; Ashraf, A.; Heape, A. K.; Lin, J. S. Microphase-separated poly(styrene-*b*-isoprene)_n multiblock copolymers with constant block lengths. *Polymer* **1994**, *35*, 4527–4536.
- (13) Adhikari, R.; Godehardt, R.; Lebek, W.; Weidisch, R.; Michler, G. H.; Knoll, K. Correlation Between Morphology and Mechanical Properties of Different Styrene/Butadiene Triblock Copolymers: A Scanning Force Microscopy Study. *J. Macromol. Sci., Part B* **2001**, *40*, 833–847.
- (14) Hirao, A.; Goseki, R.; Ishizone, T. Advances in Living Anionic Polymerization: From Functional Monomers, Polymerization Systems, to Macromolecular Architectures. *Macromolecules* **2014**, *47*, 1883–1905.
- (15) Hadjichristidis, N.; Iatrou, H.; Pitsikalis, M.; Mays, J. Macromolecular architectures by living and controlled/living polymerizations. *Prog. Polym. Sci.* **2006**, *31* (12), 1068–1132.
- (16) Shankar, R.; Ghosh, T. K.; Spontak, R. J. Dielectric elastomers as next-generation polymeric actuators. *Soft matter* **2007**, *3*, 1116–1129.
- (17) Wang, W.; Lu, W.; Goodwin, A.; Wang, H.; Yin, P.; Kang, N.-G.; Hong, K.; Mays, J. W. Recent advances in thermoplastic elastomers from living polymerizations: Macromolecular architectures and supramolecular chemistry. *Progr. Polym. Sci.* **2019**, *95*, 1–31.
- (18) Bolton, J. M.; Hillmyer, M. A.; Hoye, T. R. Sustainable Thermoplastic Elastomers from Terpene-Derived Monomers. *ACS Macro Lett.* **2014**, *3*, 717–720.

Abstract

This thesis describes the introduction of a novel bio-based hydroxyl-functionalized 1,3-diene monomer to the field of the living anionic polymerization, which enables the functionalization of polymyrcene. Furthermore, the thesis investigates the influence of the replacement of fossil feedstock-based 1,3-diene monomers by terpene-based alternatives in regards to the thermal, morphological and mechanical properties of tapered multiblock copolymers.

Chapter 1 gives an introduction to the living anionic polymerization of terpene-based 1,3-diene monomers. In general, biomass-derived monomers have been attracting attention in recent years due to dwindling fossil resources as well as a growing environmental awareness in society. The structural similarity of terpenes to isoprene opens a versatile library of various 1,3-diene monomers. Nevertheless, to date the carbanionic polymerization of terpenes is limited to the two 1,3-diene monomers β -myrcene and β -farnesene. In this chapter, an overview over the industrial large-scale production of both biomass-derived monomers is presented. The structural differences of polyterpenes compared to commercial fossil-based (thermoplastic) elastomers are key to tailor future materials for specialized applications. Furthermore, the huge structural variety of terpenes provides potential cyclic 1,3-diene monomers, which may enable the synthesis of bio-based rigid polymers with high glass transition temperatures. Those glassy polymer structures may represent bio-based alternatives to commercial fossil-based polystyrene. Additionally, the functionalization of the bio-based polydiene backbone by postpolymerization modification reactions is reviewed. In this context, the vast potential of the functionalized polydienes as macro-precursors for the synthesis of bio-based TPEs with complex polymer architectures is highlighted.

Chapter 2 presents a novel silyl-protected hydroxyl functionalized monomer (MyrOSi), derived from the terpenoid β -myrcenol, and its anionic polymerization to polymyrcenol (MyrOH). The removal of the *tert*-butyldimethyl silyl (TBDMS) protective group after polymerization results in well-defined polymyrcenol homopolymers. Additionally, the copolymerization kinetics with β -myrcene (Myr) were investigated by ^1H NMR spectroscopy, resulting in a random copolymer composition. Due to its polar silyl ether moiety, MyrOSi exhibits a “self-modifier” ability, which influences the polydiene microstructure during the copolymerization as typically known for polar additives

(modifier) like THF. The influence of the “self-modifier” effect on the polydiene microstructure as well as the thermal properties were investigated by a series of P(Myrc-co-MyrOH) copolymers, varying the monomer ratios. The introduction of hydroxyl functionalities by the (co)polymerization of a functionalized monomer (MyrOSi) enables unique control of the regiospecificity of the functionalization, which is not attainable by a postmodification functionalization of polymyrcene. Graft copolymer architectures are presented after using a P(Myrc-co-MyrOH) copolymer as macro-precursor in the “grafting from” approach for the polymerization of L-lactide. The adjustable random distribution of the hydroxyl groups in the polydiene backbone leads to a well-controlled poly(L-lactide) graft density. Those graft copolymers are promising candidates for fully bio-based thermoplastic elastomers.

In **Chapter 3**, the influence of silyl protective groups on the polymyrcenol microstructure is investigated. Surprisingly, only a few investigations on the protective group-controlled regio- and stereochemistry of polymers have been reported in literature. Therefore, the library of β -myrcenol-based monomers for the living anionic polymerization is expanded by using different silyl protective groups with varying steric bulk. An increasing steric bulk of the protective groups leads to a higher content of 1,4-units in the polymyrcenol backbone, resulting in a lower glass transition temperature. Consequently, the selectivity of the “self-modifier” effect of MyrOSi is strongly influenced by the steric volume of the protective group. The decreasing glass transition temperature, with increasing content of 1,4-units, is desirable for potential application as soft compounds of thermoplastic elastomers or low-temperature flexible rubbers.

In **Chapter 4**, the influence of the replacement of fossil feedstock-based 1,3-diene monomers by biomass-derived terpene-based monomers on the material properties of thermoplastic elastomers is investigated. In this context, the fundamental copolymerization kinetics of the bio-based monomer β -farnesene and styrene were investigated by *in-situ* ^1H NMR spectroscopy. The copolymerization results in a tapered copolymer composition with highly diverging reactivity ratios of the monomers, similar to other 1,3-diene/styrene copolymerizations. Additionally, an in-depth understanding of the applicability of copolymerization models is obtained. The one-pot tapered copolymer approach was used for the synthesis of tapered tri- (ABA) and pentablock (ABABA) copolymers of β -farnesene (B) and styrene (A). Furthermore, analog isoprene and β -myrcene series of styrenic tri- and -pentablock copolymers were synthesized, keeping

the total polydiene volume fraction constant. The equal polydiene volume fractions resulted in identical morphologies of the phase separated multiblock copolymers. The morphology unity enables a valid comparison of thermal and mechanical properties of the multiblock copolymers, while they are based on different polydiene architectures. The bottlebrush-like structure of the polyfarnesene blocks exhibit a higher entanglement molecular weight in comparison to the linear polyisoprene analogs and therefore influences the mechanical properties of the multiblock copolymers. In addition, the processing behavior of the unique polyfarnesene-based block copolymers was investigated by electrospinning.

In order to gain a deeper understanding of the influence of block number and molecular weight of tapered multiblock copolymers on their phase separation behavior and their thermomechanical properties, a series of tapered multiblock copolymers is discussed in detail in **Chapter 5**. For this purpose, three tapered multiblock copolymer series with constant molecular weights of 80, 120 and 240 kg mol⁻¹ and block numbers of 2, 4, 6, 8 and 10 were synthesized, using the monomers isoprene (I) and 4-methylstyrene (4MS). In contrast to the well investigated copolymerization of isoprene and styrene, the I/4-MS copolymerization results in a tapered copolymer with shorter tapered interface. Regarding the phase separation behavior, the shorter taper is counterbalanced by the lower effective interaction parameter, resulting in similar domain spacing. The mechanical properties of the multiblock copolymers can be fine-tuned by the judicious selection of molecular weight and number of blocks.

A detailed comparison of the living anionic copolymerization of isoprene (I)/styrene (S) and isoprene (I)/4-methylstyrene (4MS) is given in **Chapter A1**. The statistical copolymerization of the monomer pairs is investigated by real-time ¹H NMR spectroscopy. The extremely slow crossover from isoprene to the styrenic monomer results in a tapered copolymer composition. The effect of the methyl group in *para*-position of 4-methylstyrene is observable in form of a shorter taper in comparison to I/S. Additionally, Kinetic Monte Carlo simulations were used to confirm the tapered copolymer structures. The presented unique combination of experimental methods and simulation enables in-depth understanding of the copolymerization kinetics and the copolymer composition

Zusammenfassung

Die vorliegende Arbeit beschreibt die Entwicklung eines neuartigen biobasierten hydroxyl-funktionalisierten 1,3-Dien-Monomers für die lebende anionische Polymerisation, welches die Funktionalisierung von Polymyrcen ermöglicht. Darüber hinaus wird in dieser Arbeit der Einfluss von Terpen-basierten Monomeren auf die thermischen, morphologischen und mechanischen Eigenschaften von verjüngten Multiblock Copolymeren im Vergleich zu bisherigen, auf fossilen Rohstoffen basierten, thermoplastischen Elastomeren untersucht.

Kapitel 1 gibt eine Einführung in die lebende anionische Polymerisation von 1,3-Dien-Monomeren auf Terpenbasis. Im Allgemeinen haben aus Biomasse gewonnene Monomere in den letzten Jahren aufgrund schwindender fossiler Ressourcen sowie eines wachsenden Umweltbewusstseins in der Gesellschaft verstärkt Aufmerksamkeit erhalten. Die strukturelle Ähnlichkeit von Terpenen mit Isopren eröffnet eine große Bandbreite an verschiedenen 1,3-Dienmonomeren. Bisher ist die carbanionische Polymerisation von Terpenen jedoch auf die beiden 1,3-Dien-Monomere β -Myrcen und β -Farnesen beschränkt. In diesem Kapitel wird ein Überblick über die industrielle Produktion beider aus Biomasse gewonnener Monomere gegeben. Die strukturellen Unterschiede von Polyterpenen im Vergleich zu kommerziellen fossilen (thermoplastischen) Elastomeren bieten neuartige Struktur-Eigenschafts-Beziehungen für zukünftiges Materialdesign. Die große strukturelle Vielfalt der Terpene bietet u.a. potentielle cyclische 1,3-Dien-Monomere, welche die Synthese von starren biobasierten Polymeren mit hohen Glasübergangstemperaturen ermöglichen. Diese glasartigen Polymerstrukturen könnten zukünftig biobasierte Alternativen zu kommerziellem fossil-basiertem Polystyrol darstellen. Des Weiteren wird ein Überblick über die Funktionalisierung des biobasierten Polydien-Rückgrats mittels Postpolymerisations-Modifikation gegeben. In diesem Zusammenhang wird das enorme Potenzial der funktionalisierten Polydiene als Makro-Präkursor für die Synthese biobasierter TPEs mit komplexen Polymerarchitekturen hervorgehoben.

In **Kapitel 2** wird ein neues silyl-geschütztes hydroxyl-funktionalisiertes Monomer (MyrOSi), welches auf dem Terpenoid β -Myrcenol basiert, für die anionische Polymerisation vorgestellt. Die Entfernung der *tert*-Buthyldimethylsilyl-Schutzgruppe (TBDMS) nach der Polymerisation resultiert in wohldefinierten Polymyrcenol-

Homopolymeren. Zusätzlich wurde die Copolymerisations-Kinetik mit β -Myrcen (Myr) mittels $^1\text{H-NMR}$ Spektroskopie untersucht, wodurch eine statische Verteilung der Copolymerzusammensetzung ermittelt wurde. Aufgrund der polaren Silylethereinheiten weist MyrOSi eine „Selbst-Modifikator“-Fähigkeit auf, welche die Polydien-Mikrostruktur während der Polymerisation beeinflusst, wie es typischerweise für polare Additive (Modifikatoren) wie THF bekannt ist. Der Einfluss des „Selbst-Modifikator“-Effekts auf die Polydiene-Mikrostruktur, sowie auf die thermischen Eigenschaften der Polymere wurde anhand einer Reihe von P(Myrcen-co-MyrOH)-Copolymeren untersucht, wobei die Monomerverhältnisse variiert wurden. Die Einführung von Hydroxylfunktionalitäten mittels Copolymerisation eines funktionalisierten Monomers (MyrOSi) ermöglicht eine einzigartige Kontrolle der Regiospezifität der Funktionalisierung von Polymyrcen, die durch Postmodifikations-Funktionalisierung nicht erreichbar ist. Zudem werden Pfropfcopolymerstrukturen auf Basis der P(Myrcen-co-MyrOH)-Copolymere vorgestellt, wobei die Copolymere als Makro-Präkursoren für die Polymerisation von L-lactide mittels „grafting from“ Methode eingesetzt wurden. Die über das Monomerverhältnis justierbare Verteilung der Hydroxylgruppen der Copolymere ermöglicht eine gezielte Einstellung der Pfropfdichte der Pfropfcopolymere. Derartige Pfropfcopolymere sind vielversprechende Kandidaten hinsichtlich vollständig biobasierter thermoplastischer Elastomere.

In **Kapitel 3** wird der Einfluss von Silyl-Schutzgruppen auf die Polymyrcenol-Mikrostruktur untersucht. Erstaunlicherweise wurden in der Literatur bisher nur wenige Untersuchungen zur schutzgruppen-gesteuerten Regio- und Stereochemie von Polymeren veröffentlicht. Daher wird in diesem Kapitel der Baukasten von Monomeren auf β -Myrcenol-Basis für die lebende anionische Polymerisation unter Verwendung verschiedener Silyl-Schutzgruppen mit unterschiedlichem sterischem Anspruch erweitert. Ein zunehmendes sterisches Volumen der Schutzgruppen führt zu einem höheren Gehalt an 1,4-Einheiten im Polymyrcenol-Rückgrat, was wiederum zu einer niedrigeren Glasübergangstemperatur führt. Folglich wird die Selektivität des „Selbst-Modifikator“-Effekts von MyrOSi stark vom sterischen Volumen der Schutzgruppe beeinflusst. Die abnehmende Glasübergangstemperatur mit zunehmendem Gehalt von 1,4-Einheiten ist für mögliche Anwendungen als elastische Komponente in thermoplastischen Elastomeren oder in flexiblen Niedertemperaturkautschuken wünschenswert.

In **Kapitel 4** wird der Einfluss von Terpen-basierten Monomeren auf Materialeigenschaften von thermoplastischen Elastomeren im Vergleich zu bisherigen, auf fossilen Rohstoffen basierten, Materialien untersucht. In diesem Zusammenhang wird zunächst grundlegend die Copolymerisations-Kinetik der Copolymerisation von β -Farnesen und Styrol mittels *in-situ* $^1\text{H-NMR}$ -Spektroskopie untersucht. Die Copolymerisation führt zu einer verjüngten Copolymerzusammensetzung mit stark divergierenden Reaktivitätsparametern der Monomere, ähnlich wie bei anderen 1,3-Dien/Styrol-Copolymerisationen. Zusätzlich wird ein tiefgreifendes Verständnis der Anwendbarkeit von Copolymerisations-Modellen erhalten. Die Ein-Topf-Methode zur Synthese verjüngter Diblockcopolymer wurde zur Synthese von verjüngten Tri- (ABA) und Pentablockcopolymeren (ABABA) von β -Farnesen (B) und Styrol (A) verwendet. Darüber hinaus wurden analoge Isopren- und β -Myrcen-Reihen von Styrol-basierten verjüngten Tri- und Pentablock-Copolymeren synthetisiert, wobei der gesamte Polydienvolumenanteil konstant gehalten wurde. Die gleichen Polydienvolumenfraktionen führen zu identischen morphologischen Strukturen der phasenseparierten Multiblockcopolymeren. Die Einheitlichkeit in der Morphologie ermöglicht einen validen Vergleich der thermischen und mechanischen Eigenschaften der Multiblockcopolymeren, die auf verschiedenen Polydienbausteinen basieren. Die flaschenbürstenartige Struktur der Polyfarnesenblöcke weist im Vergleich zum linearen Polyisopren ein höheres Verschlaufungsmolekulargewicht auf und beeinflusst daher die mechanischen Eigenschaften der Multiblockcopolymeren. Zusätzlich wurde das Verarbeitungsverhalten der Blockcopolymeren auf Polyfarnesen-Basis mittels Elektrosponnen untersucht.

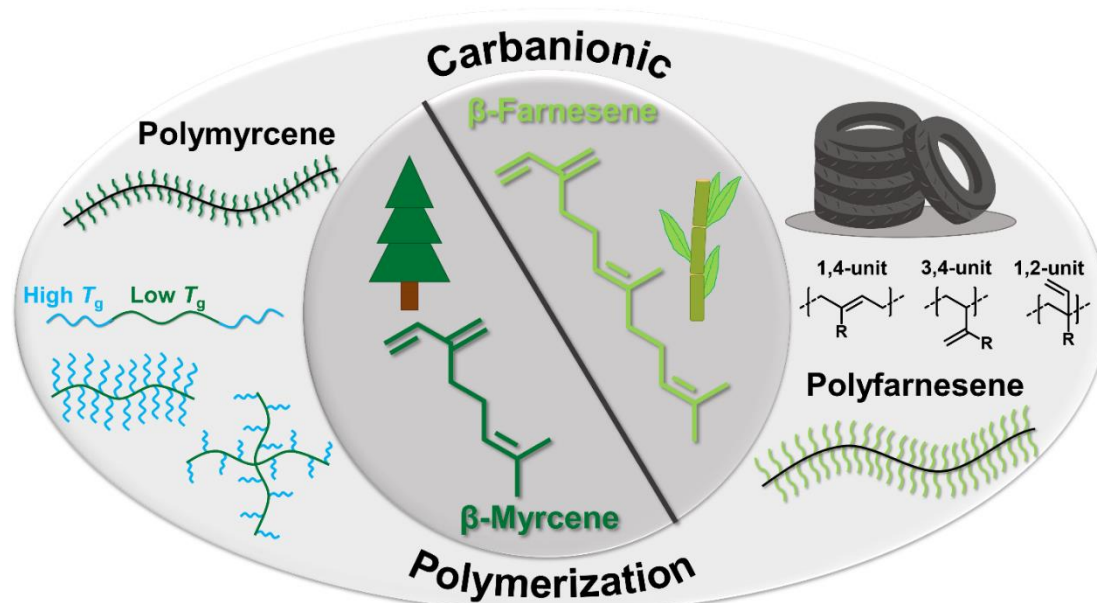
Um den Einfluss der Blockanzahl und des Molekulargewichts von verjüngten Multiblockcopolymeren auf ihr Phasenseparationsverhalten und ihre thermomechanischen Eigenschaften besser zu verstehen, wird in **Kapitel 5** eine Reihe von verjüngten Multiblockcopolymeren diesbezüglich detailliert untersucht. Zu diesem Zweck wurden drei verjüngte Multiblockcopolymer-Reihen mit konstanten Molekulargewichten von 80, 120 und 240 kg mol⁻¹ und Blockanzahlen von 2, 4, 6, 8 und 10 unter Verwendung der Monomere Isopren (I) und 4-Methylstyrol (4MS) synthetisiert. Im Gegensatz zur gut untersuchten Copolymerisation von Isopren und Styrol führt die I/4-MS-Copolymerisation zu verjüngten Diblockcopolymeren mit kürzerer verjüngender Copolymersequenz. In Bezug auf das Phasenseparationsverhalten wird die kürzere

Grenzfläche durch den niedrigeren effektiven Wechselwirkungsparameter ausgeglichen, was zu einem ähnlichen Domänenabstand führt. Die mechanischen Eigenschaften der Multiblockcopolymeren können durch die Auswahl des Molekulargewichts und der Anzahl der Blöcke feinjustiert werden.

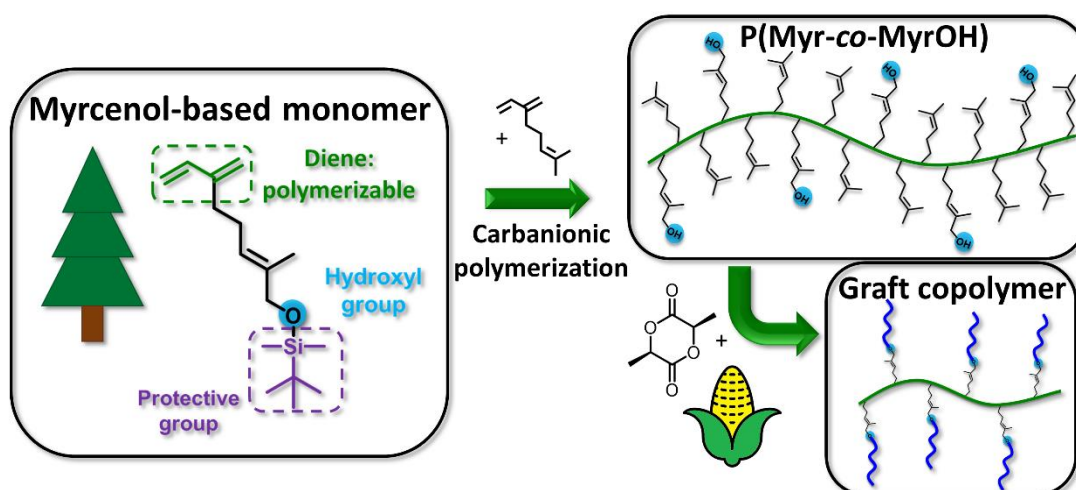
Ein detaillierter Vergleich der lebenden anionischen Copolymerisation von Isopren (I)/Styrol (S) und Isopren (I)/4-Methylstyrol (4MS) ist in **Kapitel A1** aufgeführt. Die anionische Copolymerisation der Monomerpaaire wird durch Echtzeit-¹H-NMR-Spektroskopie untersucht. Der langsame Übergang von Isopren zum Styrol-Monomer führt zu einer verjüngten Copolymerzusammensetzung. Der Effekt der Methylgruppe in *para*-Position von 4-Methylstyrol ist in Form einer kürzeren verjüngenden Copolymersequenz im Vergleich zu I/S zu beobachten. Zusätzlich wurden kinetische Monte-Carlo-Simulationen verwendet, um die verjüngten Diblockcopolymerstrukturen zu bestätigen. Die vorgestellte einzigartige Kombination von experimenteller Methode und Simulation ermöglicht ein detailliertes Verständnis der Copolymerisationskinetik und der Copolymerzusammensetzung.

Graphical Abstract

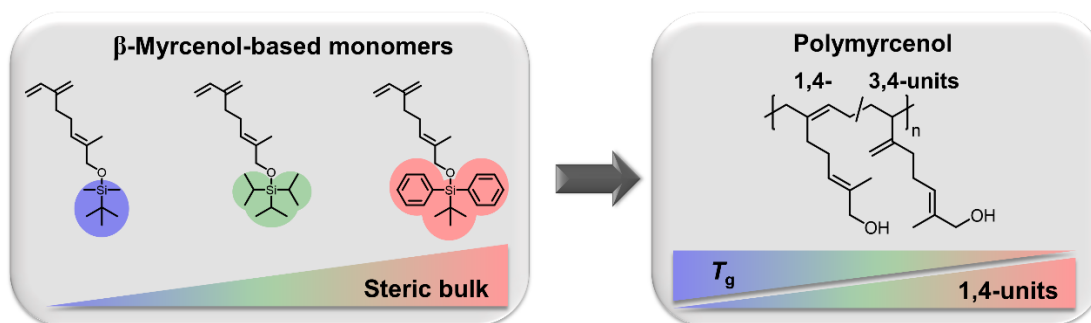
CHAPTER 1: Introduction to the Living Anionic Polymerization of Terpenes



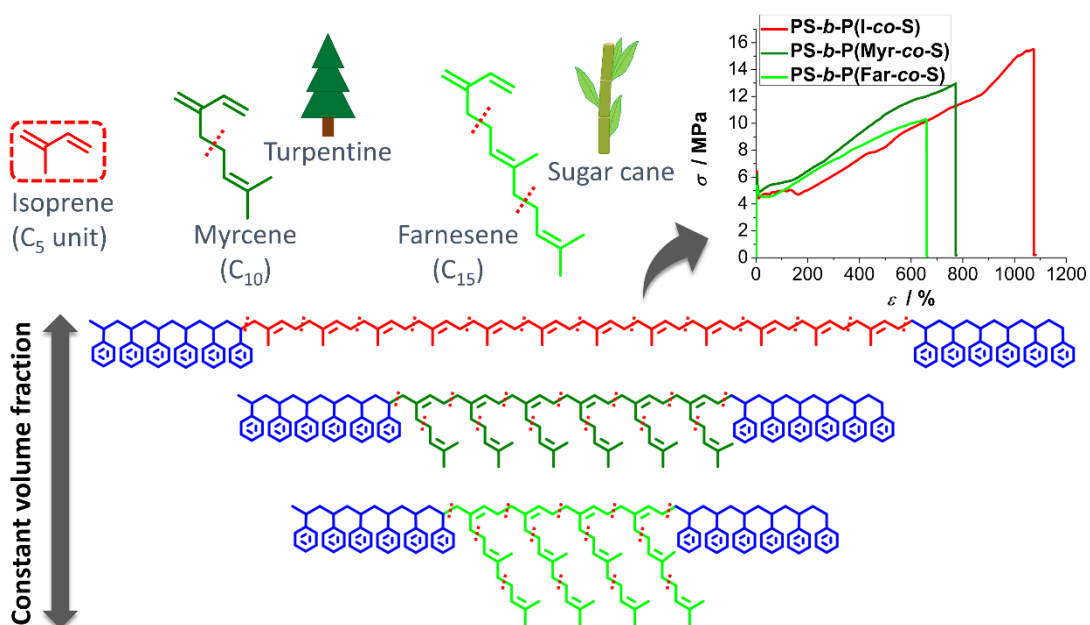
CHAPTER 2: β -Myrcenol-Based Monomer for Living Anionic Polymerization



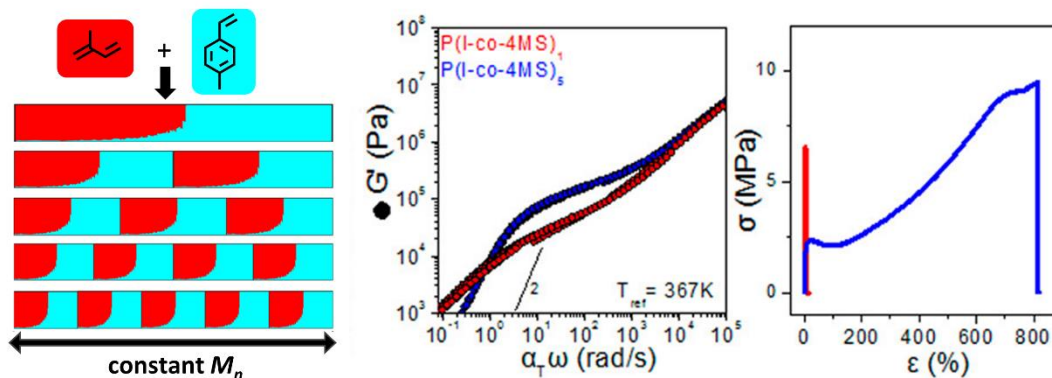
CHAPTER 3: Influence of Silyl Protective Groups on Polymyrcenol Microstructure



CHAPTER 4: Terpene-Based Thermoplastic Elastomers

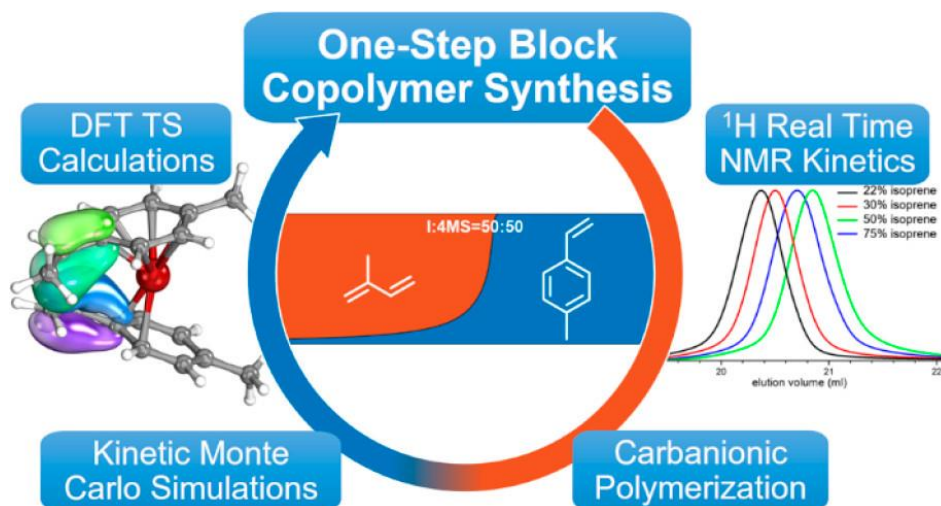


CHAPTER 5: Tapered Multiblock Copolymers of Isoprene and 4-Methylstyrene



Appendix

CHAPTER A1: Tapered Diblock Copolymers of Isoprene and 4-Methylstyrene



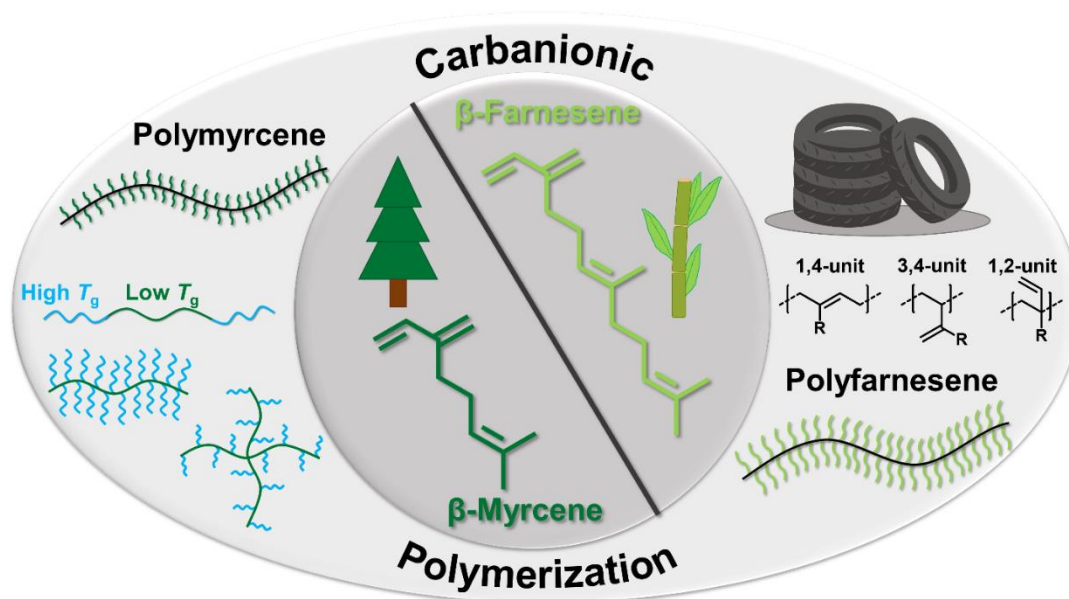
CHAPTER 1

Introduction to the Living Anionic Polymerization of Terpenes

CHAPTER 1

Anionic Polymerization of Terpenes –
Perspectives for Bio-Based ElastomersChristian Wahlen^a and Holger Frey^{*,a}^a Department of Chemistry, Johannes Gutenberg University, Duesbergweg 10-14, 55128 Mainz, Germany

To be submitted.



Abstract

Biomass-derived materials possess vast potential for material science and industry for the next decades. Dwindling fossil resources and an increasing environmental awareness increase the demand for sustainable feedstock-based alternatives. In addition to natural rubber (*cis*-polyisoprene), the class of terpenes offers a large variety of renewable monomers, like the 1,3-diene monomers β -myrcene and β -farnesene. Living anionic polymerization of the bio-based 1,3-diene monomers enables the synthesis of well-defined, high molecular weight block- and copolymers with unique control over polymer architecture and polydiene microstructure. The resulting materials can be used for a variety of technical products. For instance, polyfarnesene has been introduced as an additive in tire mixtures and replaces fossil resource-based rubbery building blocks in styrenic thermoplastic materials that enrich our everyday life. Furthermore, the unsaturated nature of polymyrcene and polyfarnesene renders them accessible for functionalization by postmodification reactions, which results e.g. in improved interaction with functional fillers. (End-)functionalized polyterpenes are promising candidates as macro-precursors for the synthesis of fully bio-based thermoplastic elastomeric materials. In this review we give an overview of the recent developments regarding the anionic polymerization of terpenes and the considerable potential the resulting polymer architectures offer for material science and a more sustainable future.

Introduction

Polymer-based materials possess key relevance in a vast range of applications and enable our high economic status in many ways. Nevertheless, plastics disposal poses one of the significant global challenges for the next decades.¹ The accumulation of plastic waste in the environment is visibly evident in the great pacific garbage patch.^{2,3} On the other hand, decreasing fossil resources, which are required for the production of plastics such as styrene-butadiene-based rubbers (SBR), presents additional challenges for the plastics industry. For this reason, improved recycling of plastics, as well as the substitution of fossil resources by renewable resources are receiving increased attention, and there is a quest for a “circular economy”.⁴⁻⁶ Accordingly, there is an increase of the production volume of chemicals from biomass during the last years, highlighted by the comprehensive review of Bhowmick and Sarkar.^{7,8} An important class of biomass-based chemicals are terpenes, which offer an extensive variety of chemical structures. Terpenes are naturally abundant compounds originating from plants, which are employed as fragrances, spices, pharmaceutical products and pheromones in everyday life.⁹ The cyclic and linear terpene monomers differ in the size of the carbon framework, which fulfills the “isoprene rule” of Ruzicka, consisting of C₅ units (isoprene units).⁹⁻¹² Additionally, a wide range of functionalized terpene-based structures, so-called terpenoids (or isoprenoids) are also obtainable from biomass. Monoterpenes (C₁₀) and sesquiterpenes (C₁₅) exhibit special significance as monomers in polymer and material science.¹³⁻¹⁵ A growing library of monoterpene-based monomers already exists in literature.¹⁶ The most prominent C₁₀ monomers are β -myrcene,^{17,18} β -pinene,¹⁹ limonene^{20,21} and limonene oxide.^{22,23} Furthermore, terpenes can be utilized to design novel renewable monomers by chemical transformation, e.g. thiol-ene modification of limonene results in a suitable monomer for polycondensation.²⁴ In contrast, the vast potential of sesquiterpenes as monomers has been hardly exploited to date. There are few publications that deal with the polymerization of β -farnesene^{17,25} as well as the ring opening metathesis polymerization of humulene and caryophyllene.²⁶

Cis-polyisoprene (natural rubber) is the most important polyterpene, obtained from *hevea brasiliensis*. It accounts for around 46 % of the total worldwide rubber consumption. The similarity of synthetically produced polydienes to natural rubber illustrates the relevance of alternative bio-based 1,3-diene synthons for rubber materials.⁷ In particular, the 1,3-diene-based terpenes β -myrcene and β -farnesene are promising bio-based

alternatives for the large scale industrial used 1,3-diene monomers butadiene and isoprene. Due to the structural similarity, polyfarnesene has already partially replaced synthetic and natural rubber in commercial products like chewing gum and tires (up to around 6 % of polyfarnesene content).^{27,28} The monoterpene β -myrcene naturally occurs in wild thyme, ylang-ylang fruits, bay leaves, hop and other plant materials.²⁹ Due to the uneconomical direct extraction of β -myrcene from plant materials, β -myrcene is industrial basically produced in large scales from turpentine oil, which has an annually worldwide production scale of 330 000 t. The pyrolysis of β -pinene, which can be easily obtained from turpentine oil by fractional distillation, at temperatures of 450 – 600 °C results in β -myrcene with yields up to 85 % (as shown in Figure 1), described in detail in the comprehensive review of Behr and Johnen.²⁹ The commercial production of β -farnesene by Amyris Inc., is described in the review of Paddon et al., as schematically shown in Figure 1.³⁰ The fermentation of sugar, obtained from Brazilian sugar cane with engineered yeast enables the large scale production of β -farnesene. For this process, the yeast is engineered by the introduction of the enzyme β -farnesene synthase. The enzyme generates β -farnesene from farnesyl diphosphate, which occurs in the biosynthesis of isoprenoids by the mevalonate pathway (MVA).³⁰ Alternatively, β -farnesene can be synthesized on small scale by dehydration of farnesol, which is obtainable from rose oil.^{9,31,32}

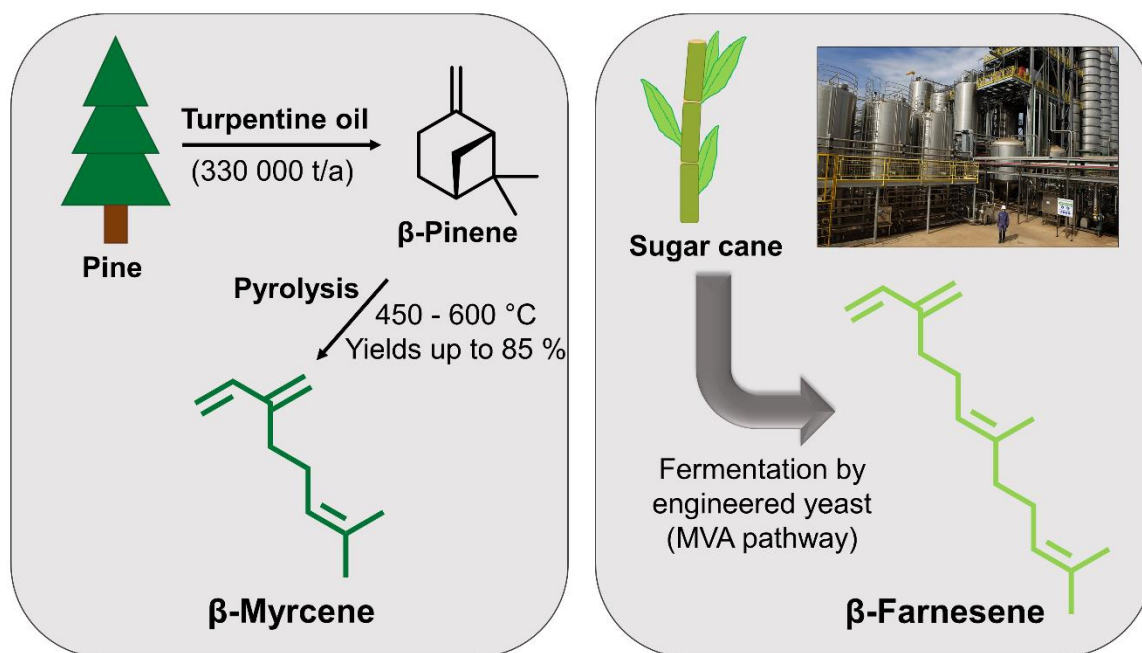


Figure 1. Industrial large-scale production pathways of β -myrcene, based on turpentine oil (left) and β -farnesene based on fermentation technology of sugar cane (right) by Amyris Inc. The fermentation tanks of Amyris in Brotas, SP, Brazil, are shown at the picture on the right side (Photo by Paddon et al. / CC BY 4.0).³⁰

Anionic polymerization of terpenes. The key requirement for an aliphatic monomer to be suitable for living anionic polymerization is the existence of a 1,3-diene (butadiene) moiety in the monomer structure. Various alkyl-substituted 1,3-diene monomers have been polymerized by carbanionic polymerization so far. Isoprene represents the simplest alkyl-substituted 1,3-diene monomer. Terpenes, which are formed accordingly via the isoprenoid biosynthesis, formally consist of isoprene units, represent a promising monomer toolbox for the anionic polymerization. Nevertheless, to date merely β -myrcene and β -farnesene that show a high structural similarity to isoprene but differ in the length of the alkenyl side chains, have been reported as monomers for carbanionic polymerization. However, there are other promising terpene-based monomers, which are potentially suitable for the living anionic polymerization, as outlined in Figure 2. Acyclic terpenes with a different alkyl substituent pattern of the 1,3-diene moiety are also promising candidates for living anionic polymerization, but to date have been polymerized by other polymerization methods. β -Ocimene has been reported to be polymerizable by catalytic polymerization methods.^{17,33} Furthermore, alloocimene is polymerizable by the utilization of a catalyst system of sodium and aliphatic ether.³⁴ An additional potential monomer class for carbanionic polymerization are cyclic terpenes

that contain a 1,3-diene moiety inside the cyclic structure. For instance, the cyclic terpene (*R*)-(-)- α -phellandrene offers promising structural similarities to cyclohexadiene, which is polymerizable by living anionic polymerization, using alkyllithium initiators.^{35,36} In contrast to acyclic flexible polydienes (low T_g), cyclic polydienes exhibit a rigid structure resulting in high glass transition temperatures (T_g) above 100 °C.³⁷ Consequently, these rigid polymers offer potential regarding their application as glassy building blocks in thermoplastic elastomers. In addition to the naturally available 1,3-diene terpenes, there are several possibilities to transform terpenes by simple chemical modification reactions into 1,3-diene compounds.³⁸ α,β -Unsaturated carbonyl compounds like carvone can be transformed into the corresponding cyclic 1,3-diene structure by the Wittig reaction, as shown in Figure 2.³⁹ Hydroxyl functional terpenes (so-called terpenoids) also offer promise regarding the application as renewable functional 1,3-diene monomers for living anionic polymerization. They offer a possibility to overcome the lack of functional 1,3-diene monomers for the living anionic polymerization, caused by synthetic difficulties due to the high reactivity of the 1,3-diene entity. By protecting the hydroxyl groups of terpenoids like β -myrcenol with appropriate protective groups for the living anionic polymerization (e.g. silyl groups), a novel type of monomers is obtained.^{40,41} In recent works myrcenol was copolymerized with β -myrcene or isoprene, using neodymium or cobalt catalyzed polymerization.^{42,43}

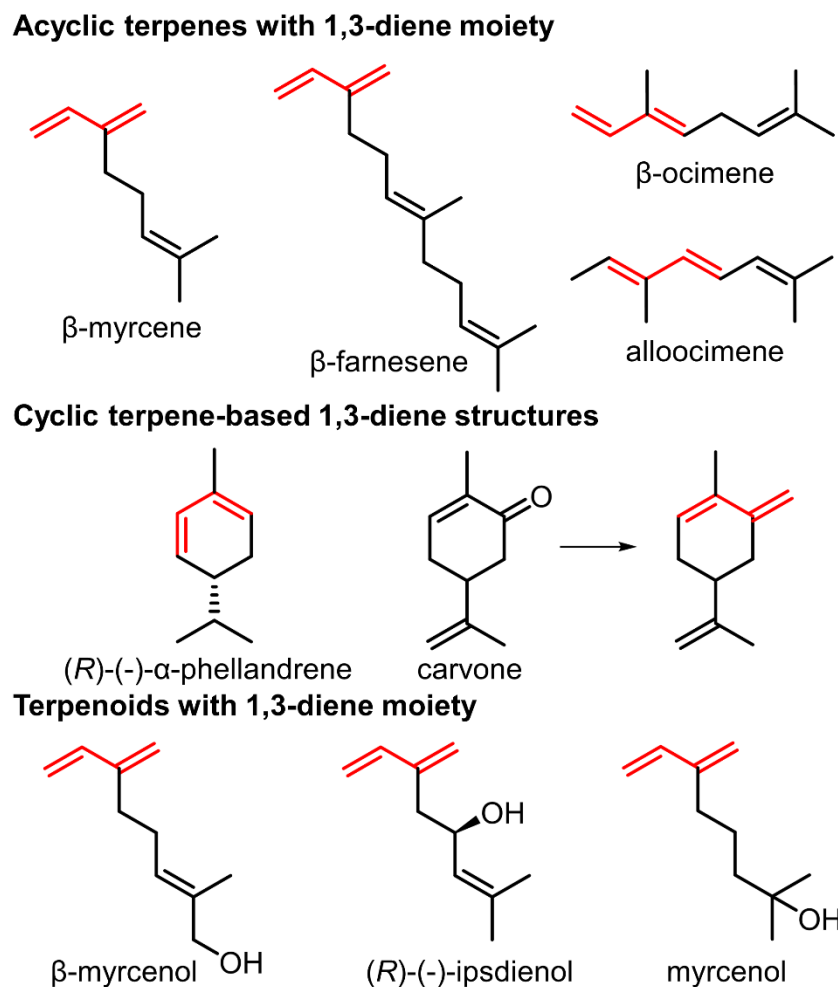


Figure 2. Overview of terpenes containing (perspectively) polymerizable 1,3-diene moieties (red).

The bio-based 1,3-diene monomers β -myrcene and β -farnesene are known to be polymerizable by free radical,^{25,44,45} controlled radical,^{25,46,47} cationic,^{48,49} coordination^{17,42,50} and living anionic polymerization.^{51,52} The living anionic polymerization exhibits key benefits over most other polymerization methods. It enables the synthesis of high molecular weight homo- and (block) copolymers with well-defined complex polymer architectures and complete monomer conversion, adjustable polymer microstructure and introduction of functional (end-)groups (all discussed in detail below).^{53,54} In comparison, the free and controlled radical polymerization of β -myrcene and β -farnesene results in incomplete conversion, the reported results ranging from 65 % to 80 %, respectively. Furthermore, cross-linking occurs, due to the double bond of the alkenyl side chain of the β -myrcene and β -farnesene units in the polymer backbone.^{25,47,55} The coordination polymerization, using rare-earth catalysts, results in polyterpenes with

complete monomer conversion and high molecular weights, but the synthesized polyterpenes exhibit high dispersities ($D > 1.3$).^{17,56} Furthermore the coordination polymerization cannot offer control of polymer microstructure, as is possible with the living anionic polymerization.^{17,42,50,56} In general, the polymerization of 1,3-diene monomers results in an heterogenous polydiene microstructure in form of *cis*- and *trans*-1,4-, 3,4- and 1,2-units, as it is shown as an example for polymyrcene in Figure 3.⁵⁷ The polydiene microstructure plays a key role for the adjustment of the glass transition temperature and the elastic properties of materials, as discussed in detail below.

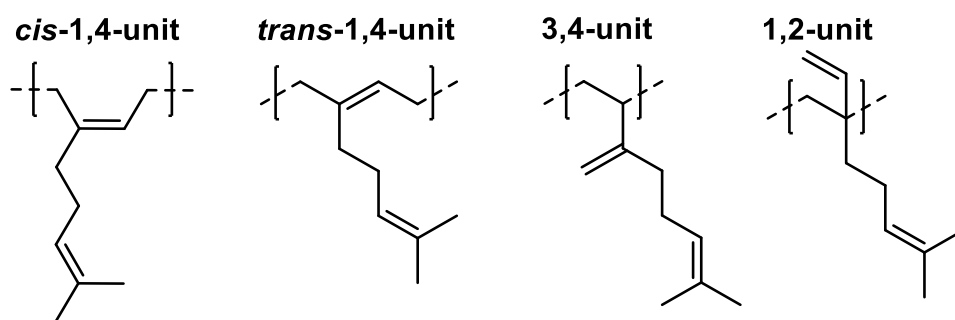


Figure 3. Possible polydiene microstructures of polymyrcene, resulting from anionic polymerization. The incorporation mode is controlled by solvent, temperature and added modifiers.

NMR analysis enables the determination of the polydiene microstructure, i.e. the mode of monomer incorporation, as first published by Newmark and Majumdas for polymyrcene and polyfarnesene.^{52,58} In material science (*cis*-)1,4-polydienes are preferred for most elastomer applications, due to their low glass transition temperatures and their similarity to natural rubber in their elastic behavior.^{59,60} The similarity of synthetically produced polydienes to the naturally occurring polyterpene *cis*-polyisoprene (natural rubber, obtained from the rubber tree *Hevea brasiliensis*), points at the relevance of alternative bio-based synthons for elastomers.⁷ Recently, polyfarnesene has been established on a technical scale and is used on small scale to replace natural rubber in commercial products as diverse as chewing gum and tires.^{27,28} In the field of carbanionic polymerization, the polydiene microstructure is mainly influenced by the solvent, polar additives, the counter ion, as well as chain end concentration and the temperature.^{61,62} The carbanionic *sec*-BuLi-initiated polymerization of β -myrcene in cyclohexane results in polymyrcene with 94 % of the preferred 1,4- and 6 % 3,4 units,⁴¹ while the polymerization in the more polar solvent THF results in 30 % 1,4-, 57 % 3,4-, and 13 % 1,2 units.⁶³ A high content of 1,4-units of polydienes results in a low glass transition temperature and improved

elasticity when compared to polydienes with increased 3,4-content.^{60,64} The glass transition temperature of polydienes generally increases in a linear fashion with increasing vinyl content (1,2 and 3,4 units).^{64,65} As demonstrated by Henning et al.,⁶⁶ the slope of the linear correlation strongly correlates with the polydiene architecture, as shown in Figure 4.

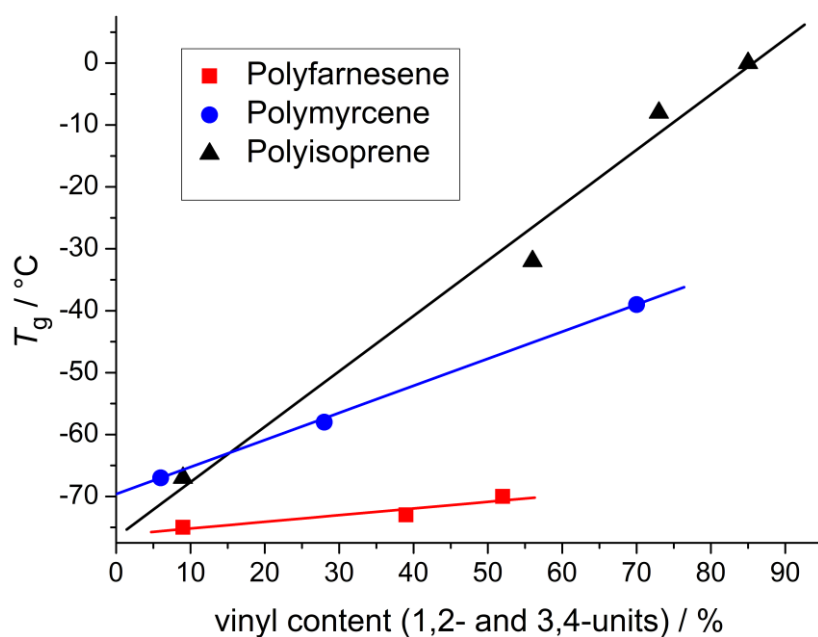


Figure 4. Glass transition temperature as a function of vinyl content for polyisoprene, polymyrcene and polyfarnesene reproduced from Henning et al. and expanded by data available for polymyrcene from literature.^{41,63,66,67}

While the slope of the linear dependency increases strongly for linear polyisoprene, a significant decrease of the gradient from polyisoprene > polymyrcene > polyfarnesene is observable, i.e. related to the terpene chain length. This translates to a nearly constant glass transition temperature of polyfarnesene, even for increasing vinyl content (Figure 4). The gradient change can be contributed to the different polydiene structures. While polyisoprene can be considered as a linear polymer with methyl side groups, the length of the side chain increases from polymyrcene (C_6/C_8 , depending on the polydiene microstructure (1,4- or 3,4-units)) to polyfarnesene (C_{11}/C_{13}), which exhibits an almost bottlebrush-like structure, as illustrated in Figure 5. The additional vinyl groups in the side chain of the 3,4- and 1,2-units limit molecular motion and decrease the free volume of polyisoprene. In comparison, the low T_g values of polyfarnesene, showing a weak vinyl unit dependency, can be attributed to the bottlebrush-like

structure results in a hindered tight packing of the polymer chains, resulting in a higher free volume and consequently in a lower T_g . The influence of the 3,4- and 1,2-units in the side chain is increasingly overcompensated with longer side chain, corresponding to a more bottlebrush-like structure.⁶⁶ In addition the bottlebrush-like structure of polyfarnesene causes a significantly higher entanglement molecular weight ($M_e(\text{PFar}) = 50 \text{ kg}\cdot\text{mol}^{-1}$)⁶⁸ in comparison to polymyrcene ($M_e(\text{PMyr}) = 18 \text{ kg}\cdot\text{mol}^{-1}$) and polyisoprene ($M_e(\text{PI}) = 5.4 \text{ kg}\cdot\text{mol}^{-1}$), which is attributed to the increased persistence length of polyfarnesene.⁶⁹ The decrease in entanglement molecular weight follows the trend of decreasing side chain length, in the order $\text{PFar} > \text{PMyr} > \text{PI}$. Runt et al. studied in detail the influence of the bottlebrush-like structure of polyfarnesene on its molecular dynamics.⁶⁸ Below the critical molecular weight ($M_c(\text{PFar}) = 100 \text{ kg}\cdot\text{mol}^{-1}$) polyfarnesene behaves like a bottlebrush-like polymer and exhibits Rouse-like melt dynamics. However, above the high critical molecular weight, polyfarnesene behaves like an entangled polymer melt.⁶⁸ In general, bottlebrush-like or branched structures show reduced melt and solution viscosity in comparison to linear analogues, which renders polyfarnesene a useful alternative for linear polyisoprene to improve the processing of styrenic thermoplastic elastomers.⁷⁰⁻⁷²

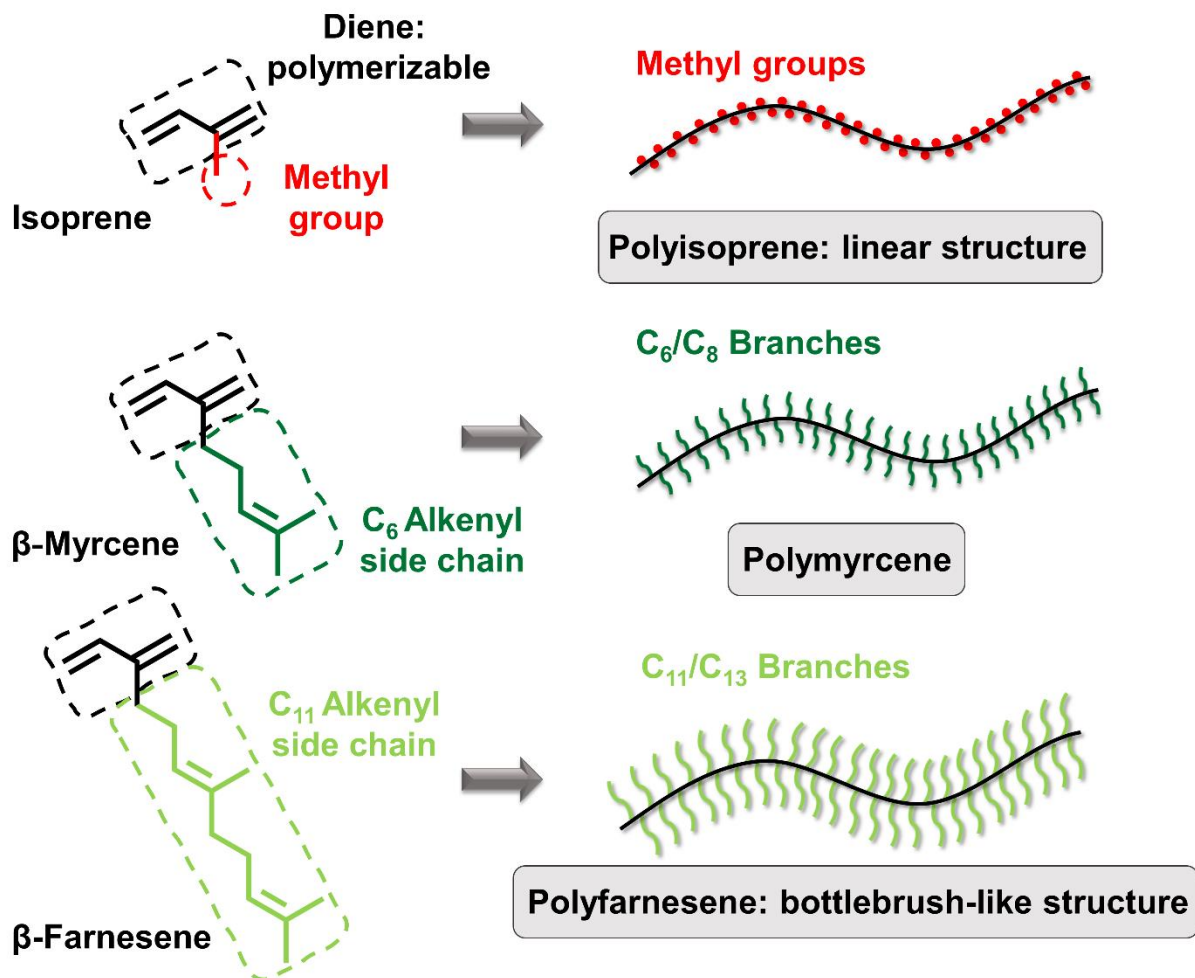


Figure 5. Schematic illustration of the polydiene architectures of polyisoprene (linear), polymyrcene and polyfarnesene (bottlebrush-like).

Copolymerization with styrene derivatives. The statistical anionic polymerization of 1,3 diene and styrene derivatives in cyclohexane is commonly used for the synthesis of tapered copolymers and multiblock copolymers.^{73–75} Tapered multiblock copolymers present a unique alternative for well-established isoprene/styrene-based thermoplastic elastomers consisting of ABA triblock copolymers with flexible midblock structure.^{76–78} β -Myrcene and β -farnesene are promising bio-based candidates for the replacement of the fossil-sourced 1,3-diene monomers butadiene or isoprene in styrene-based thermoplastic materials.^{63,70} Even if there are several alternative routes to produce the fossil source-based monomers isoprene and styrene from biomass, these approaches are currently not scalable to an industrially relevant production volume.^{79–82} In several recent, fundamental works the copolymerization of β -myrcene and styrene was studied.^{67,83–85} The copolymerization of β -myrcene and styrene in cyclohexane results in

tapered copolymers (as shown in Figure 6 (top)), with an even steeper gradient than observed for isoprene and styrene, expressed by the more disparate reactivity ratios ($r_{\text{Myrcene}} = 36$, $r_{\text{Styrene}} = 0.028$ and $r_{\text{Isoprene}} = 12.8$, $r_{\text{Styrene}} = 0.051$).^{83,86} Whilst the copolymerization with styrene results in tapered copolymers, the statistical copolymerization of β -myrcene with 4-methylstyrene results in block-like copolymers, due to the extremely steep gradient formed.⁸³ The copolymer microstructure can be controlled both by the polarity of the solvent and by adding polar or complexing additives. In several works the dependency on the polarity of the solvent was used to adjust the copolymer microstructure.⁶² Polar modifiers like ethyl tetrahydrofurfuryl ether (ETE) or tetramethylethylenediamine (TMEDA) have been added to the anionic copolymerization of β -myrcene and styrene in cyclohexane, resulting in random copolymers (as shown in Figure 6 (middle)), albeit the corresponding works lack in-depth investigation of the copolymerization kinetics.^{67,84} In a completely different approach, Gallei et al. capitalized on the unreactive nature of β -myrcene in polar solvents (THF) at $-78\text{ }^{\circ}\text{C}$ for the formation of well-defined block copolymers with styrene directly from a monomer mixture.⁸⁵ They initiated the comonomer mixture in THF at $-78\text{ }^{\circ}\text{C}$, resulting in the formation of a pure polystyrene block. The cross-over from the living polystyrene chains to β -myrcene was induced by a temperature increase up to $10\text{ }^{\circ}\text{C}$, resulting in a polystyrene-*block*-polymyrcene block copolymers (as shown in Figure 6 (bottom)). The sec-butyllithium-initiated copolymerization of β -farnesene and styrene in cyclohexane results in in a tapered copolymer as well, with strongly disparate reactivity ratios of $r_{\text{Far}} = 27$ and $r_{\text{S}} = 0.037$.⁷⁰

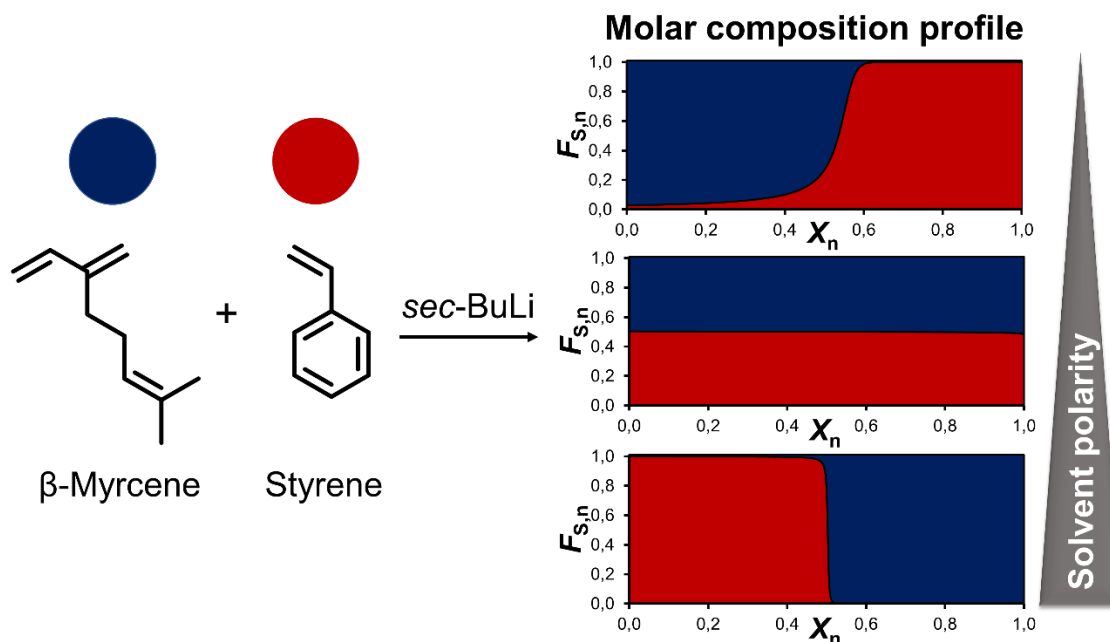


Figure 6. Molar composition profiles⁷⁰ of copolymers of β -myrcene and styrene ($F_{S,n}$: instantaneous styrene incorporation; X_n : molar-based chain position), synthesized by anionic polymerization. The anionic copolymerization results in dependency of the polarity of the solvent in tapered copolymers (top, solvent: cyclohexane),⁸³ random copolymers (middle, solvent: cyclohexane and polar additives)^{67,84} and inverse block-like copolymers (bottom, solvent: THF, temperature induced).⁸⁵

In addition, the terpolymerization of β -myrcene, isoprene and 4-methylstyrene was investigated, resulting in a tapered copolymer with mixed polydiene block, exhibiting a gradient composition of β -myrcene and isoprene ($r_{\text{Myrcene}} = 4.4$, $r_{\text{isoprene}} = 0.23$), followed by a taper and a pure polystyrene block. Han and coworkers investigated the influence of the alkenyl side chains of the myrcene units of poly(myrcene-*co*-butadiene-*co*-styrene) terpolymers in comparison to commercial used styrene-butadiene rubbers (SBR).⁶⁷ The pendant alkenyl side chain of the myrcene units improved the carbon black dispersibility in rubber, commonly used in tire mixtures, as well as the wet grip resistance without affecting the low rolling resistance. Accordingly, the replacement of butadiene by bio-based β -myrcene in styrenic rubbers is a promising approach for the development of more sustainable tires.^{67,87} Similar effects are observable for polyfarnesene, so consequently Kuraray Co, Ltd. and Amyris, Inc. have commercialized rubber compositions for tires containing polyfarnesene compounds.²⁸

Functionalization of polyterpenes. The potential for functionalization, provided by unsaturated polyterpenes like polymyrcene and polyfarnesene vastly expands their range

of applications. There are basically three approaches to introduce functionality to a polymer backbone: i) introduction of a functional end-group by using functional end-capping agents and/or initiators; ii) postmodification reactions; iii) utilization of functional monomers.⁶⁰ The living character of the anionic polymerization enables the introduction of functional end-groups by termination of the living polymer chains using a suitable end-capping agent. Commonly applied end-capping agents for the quantitative implementation of terminal hydroxyl groups are epoxides, such as ethylene oxide (EO) and propylene oxide, resulting in primary (EO) or secondary (PO) hydroxyl end-groups.^{88,89} Li and coworkers synthesized α,ω -hydroxyl functionalized polymyrcene by the use of a silyl-protected alkyllithium initiator for the hydroxyl group in α -position, while the primary hydroxyl group in ω -position was implemented by end-capping with EO (Figure 7a).⁹⁰ In a different approach by Henning et al., the heterobifunctional α,ω -functionalization was introduced by end-capping of the bifunctional initiated polymerization of β -farnesene with PO, using a proprietary dilithio initiator (Figure 7b).⁶⁶ Those α,ω -functionalized polydienes are promising building blocks (macro-precursors) for the synthesis of triblock copolymers, which are discussed below in the section “Thermoplastic elastomers”. Furthermore, amine ω -terminated polymyrcene was synthesized by the usage of *N*-benzylidenetriethylsilylamine as end-capping agent with a degree of functionalization up to 87 %, as shown in Figure 7c.⁹¹

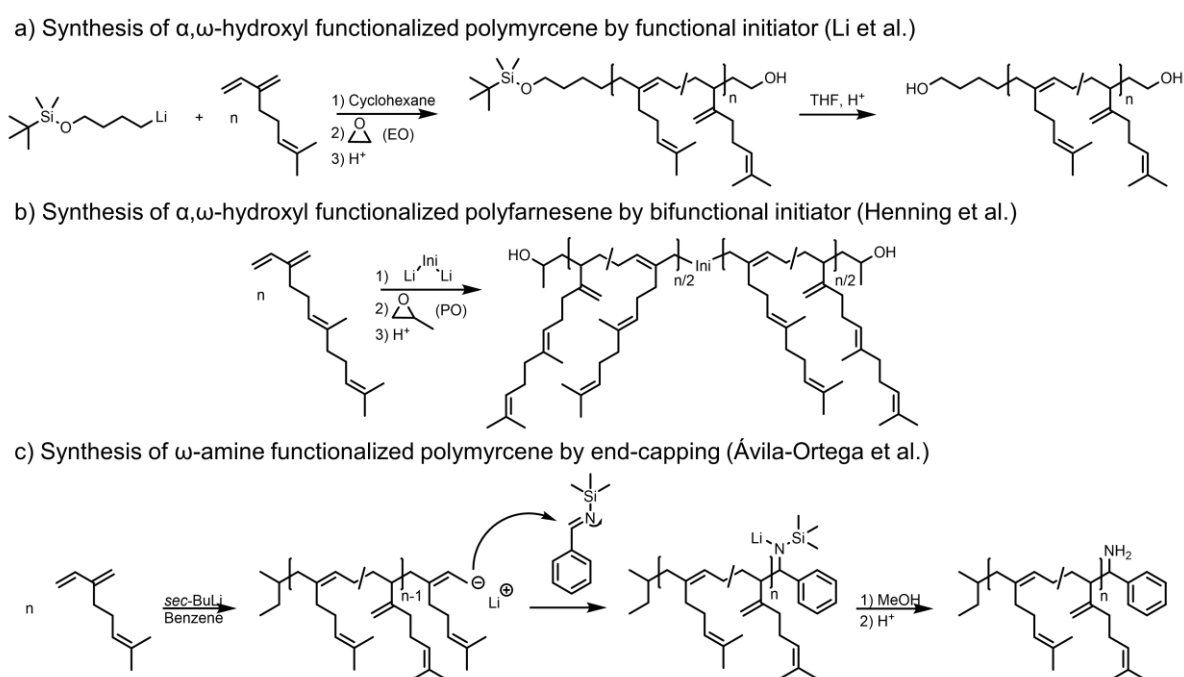


Figure 7. End-functionalization strategies for polymyrcene and polyfarnesene.^{66,90,91}

The double bonds of the polymyrcene and polyfarnesene backbone as well as in the alkenyl side chains offer promising potential regarding postpolymerization reactions. There are several approaches for the postmodification of double bonds, which have already been applied for polymyrcene. Schlaad et al. investigated the regiospecificity of the thiol-ene reaction and epoxidation of polymyrcene.^{92,93} Close to quantitative degrees of postmodification by thiol-ene click (side chain double bonds up to 24 times faster), allows a regiospecific functionalization, controlled by the degree of conversion/functionalization. In addition, the regioselectivity was found to increase from secondary (2) to primary thiols (1), while tertiary thiols (3) resulted in low conversion (exemplary thiol structures are shown in Figure 8, assigned by numbers 1-3). This effect is attributed both to their chemical structure and steric hindrance, which results in a different accessibility of the double bonds.⁹² In a further postmodification reaction, saponification of thiol functionalized polymyrcene resulted in amphiphilic polyelectrolytes.⁹² Furthermore, thiol-ene modification of polymyrcene enables its application as a 3D printing material (printable photopolymer resin component) by photo-cross-linking, using the tetrafunctional thiol-compound pentaerythritol tetrakis(3-mercaptopropionate) (PETMP) (thiol (5) in Figure 8).⁹⁴ The surface hydrophobicity of 3D printed materials is adjustable by using different thiols, from superhydrophobic when using a long alkyl chain thiol (thiol (4) in Figure 8) to more hydrophilic in case of a more polar thiol (e.g. thiol (1) in Figure 8).⁹⁴

Complete epoxidation of the unsaturated polymyrcene was achieved by Schlaad and coworkers.⁹³ The degree of epoxidation was adjustable in the range from 0 to 100 %. Additionally, a stereoselectivity of the epoxidation at the side chain was observed, although less pronounced than in comparison to the thiol-ene modification. Complete epoxidation of polymyrcene leads to an increase of the glass transition temperature from -64 °C up to 14 °C. Hydrolysis of the epoxidized polymyrcene results in a diol-moiety (polyol) as shown in Figure 8. However, the ring opening reaction is generally incomplete (conversion only around 72%).⁹³ The introduction of epoxide or hydroxyl groups at the polymyrcene backbone improves the interaction with functional fillers, which is highly relevant for silica reinforced tires.^{43,95} Furthermore, epoxidized myrcene cross-links under acidic conditions or by annealing at 260 °C, resembling an epoxy resin.⁹³ The epoxidation of polyfarnesene was also performed by Chao et al..⁹⁶

Leaving aside the advantages the double bonds of polymyrcene and polyfarnesene offer for postmodification, it is obvious that the unsaturated nature of polydienes makes them vulnerable to oxidation and cross-linking processes. To overcome the limited stability of polydienes, hydrogenation of the polymer backbone is often utilized for industrial applications, as shown exemplary for polymyrcene in Figure 8. The hydrogenation is performed with palladium carbon catalysts under high pressure, which is highly relevant for industrial application.⁹⁷ On a lab scale, the hydrogenation can be performed by the diimide method, using *p*-toluenesulfonyl hydrazide.^{62,92} In comparison to 1,4-polymyrcene ($T_g = -68\text{ }^\circ\text{C}$), the hydrogenation results in an increase of the glass transition temperature up to $-54\text{ }^\circ\text{C}$.⁵¹

Triazolinedione (TAD) click chemistry represents a further powerful tool for the postpolymerization modification reaction of unsaturated polymers. The terpene-based polymer poly(citronellyl glycidyl ether) (CitroGE) was quantitatively modified within short reaction times (< 1 hour). The similarity of the functionalized isopropylidene side chains of (PCitroGE) to polymyrcene promises a vast potential for the postmodification of polymyrcene by TAD click chemistry. The large library of triazolinediones enables a versatile functionalization as well as crosslinking by using a bisfunctional TAD, resulting in bio-based elastomers.⁹⁸

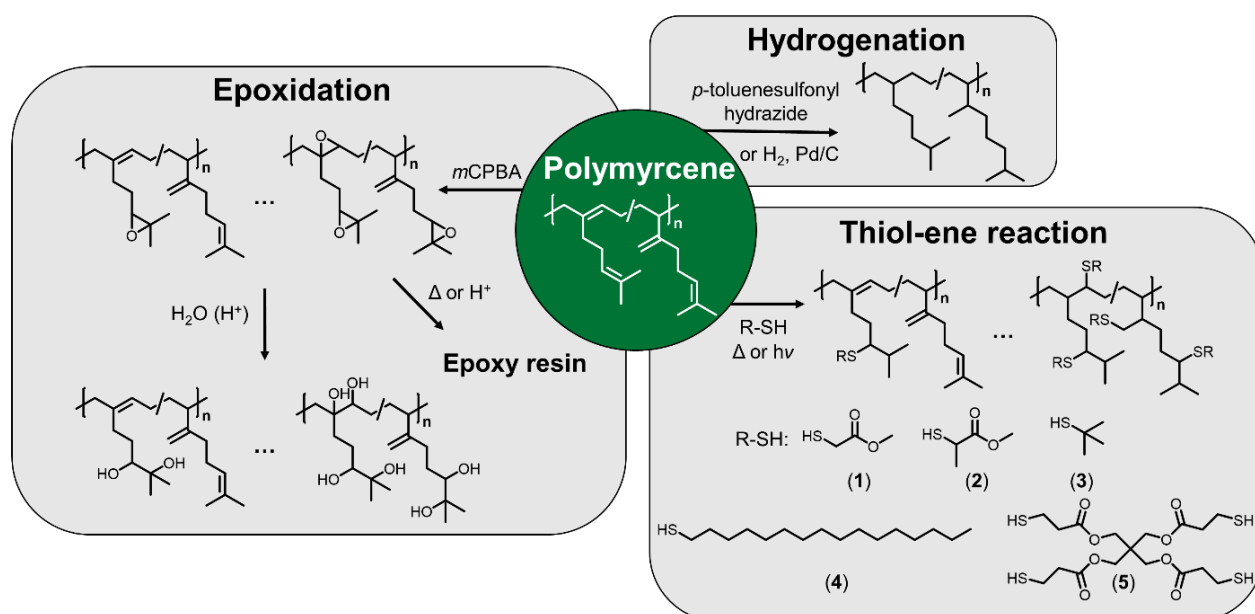


Figure 8. Postmodification reactions established for polymyrcene.

The functionalization of polymyrcene using a functional monomer in the living anionic polymerization is strongly limited, due to the high susceptibility of functionalized dienes to the Diels-Alder reaction. Furthermore, protecting functional groups is mandatory to prevent proton abstraction by the living carbanionic chain end, which results in the termination of the polymerization.⁶⁰ In the field of coordination polymerization there are several recent works by Gong et al., in which a hydroxyl myrcene derivative (2-methyl-6-methyleneoct-7-en-2-ol) was copolymerized with β -myrcene or isoprene, applying neodymium or cobalt catalyzed polymerization.^{42,43} In recent work, we were able to introduce the first reported hydroxyl group containing 1,3-diene monomer for the living anionic polymerization, based on β -myrcenol (2-methyl-6-methylideneocta-2,7-dienol), which was obtained by allylic oxidation of β -myrcene.⁴¹ The protection of the hydroxyl unit with a silyl protective group (TBDMS-, *tert*-butyldimethylsilyl-group) enables the carbanionic polymerization of silyl protected β -myrcenol (MyrOSi). The protective group was quantitatively removed after polymerization by treatment with tetra-*n*-butylammonium fluoride (TBAF). In comparison to the epoxidation which results in a regioselective functionalization, the introduction of hydroxyl groups to the polymyrcene backbone is regiospecific at the alkenyl side chains of the myrcene units. Additionally, the random anionic copolymerization of MyrOSi with β -myrcene enables precise adjustment of the degree of functionalization by changing the comonomer ratio. Furthermore, functional monomers enable the selective functionalization of single polymer segments when employing sequential monomer addition.⁴¹

Thermoplastic elastomers. Thermoplastic elastomers (TPEs) combine the typical properties of rubbers, behaving as viscoelastic liquids (low T_g) and stiff thermoplasts (high T_g). Block copolymers of at least three blocks, with the sequence hard-soft-hard (ABA), enable physical crosslinking of the hard domains, resulting in dimensional stability of the elastic material without additional vulcanization. Currently, commercial thermoplastic elastomers are based on monomers derived from fossil resources like isoprene, butadiene and styrene.⁹⁹ Due to dwindling fossil feedstocks, academic and industrial research is increasingly focused on potentially sustainable alternatives. The first step towards the development of fully sustainable thermoplastic elastomers, synthesized by carbanionic polymerization, from terpene-derived monomers was undertaken by Bolton et al..⁶³ In addition to β -myrcene, α -methyl-*p*-methylstyrene (AMMS) was used as bio-based styrene derivative. α -Methyl-*p*-methylstyrene is obtained from the pyrolysis of β -pinene and can

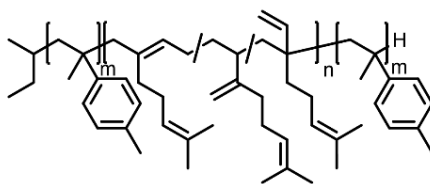
be alternatively derived from limonene by dehydrogenation.⁷⁸ Triblock copolymers were synthesized by the sequential anionic polymerization in THF at low temperatures, followed by dichlorodimethylsilane coupling (Figure 9a).⁶³ The triblock copolymers show phase separation (hexagonally packed cylinders) with a rubbery low T_g polymyrcene phase ($T_{g,PMYR} = -39\text{ }^\circ\text{C}$), and hard, high T_g poly(α -methyl-*p*-methylstyrene) cylinders ($T_{g,PAMMS} = 160 - 182\text{ }^\circ\text{C}$), which cause physical cross-linking. However, the exceptionally high glass transition temperature of PAMMS is unfavorable for processing of the material. The sustainable thermoplastic elastomers are competitive to fossil resource-based styrenic TPEs, as highlighted by a tensile strength of up to 10 MPa and ultimate elongations of up to 1300 %. However, due to the polymerization in THF, an increased vinyl content (1,2- and 3,4-units) is of the polymyrcene block cannot be avoided, resulting in an increased glass transition temperature of $-39\text{ }^\circ\text{C}$.⁶³ The glass transition temperature of the bio-based polydiene block can be decreased by performing the anionic polymerization in apolar solvents (e.g. cyclohexane). Kuraray Co, Ltd. and Amyris, Inc. developed the first ABA triblock copolymers based on styrene (A) and the bio-based monomer β -farnesene (B) synthesized by sequential anionic polymerization in cyclohexane, followed by hydrogenation of the polyfarnesene midblock (Figure 9b).^{97,100} In a recent study by our group, the influence of the bio-based monomers β -myrcene and β -farnesene in styrenic tapered tri- and pentablock copolymers on the mechanical properties was investigated. Processing via electrospinning was also investigated (tapered triblock structure is shown in Figure 9c).⁷⁰ The bio-based tri- and pentablock copolymers were compared to the isoprene-based analogues. As a function of the entanglement molecular weight of the polydiene blocks, decreasing in the row polyfarnesene > polymyrcene > polyisoprene, the ultimate toughness of the styrenic multiblock copolymers decreased with increasing side chain length at the polydiene backbone.⁷⁰

Another approach for the synthesis of fully bio-based thermoplastic elastomers is the utilization of hydroxyl functionalized polymyrcene as a macro-precursor for the synthesis of L-lactide-based block or graft copolymers, reported in several works by Li and coworkers.^{90,101,102} On the one hand, linear poly(L-lactide)-*block*-polymyrcene-*block*-poly(L-lactide) triblock copolymers were synthesized, starting from a hydroxyl α,ω -functionalized polymyrcene precursor (as shown in Figure 7a). The poly(L-lactide) end blocks were synthesized by TBD (1,5,7-Triazabicyclo-[4.4.0]dec-5-ene) catalyzed polymerization of L-lactide. The polymyrcene middle block of the L-lactide-based triblock

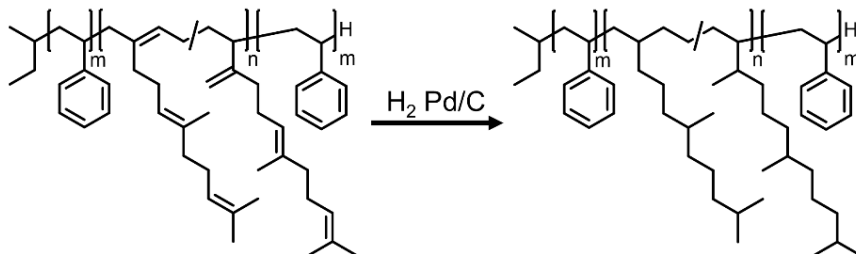
copolymers results in a toughening in comparison to pure poly(L-lactide), due to the flexible, low T_g polymyrcene backbone. The coexistence of a glass transition of the polymyrcene backbone ($T_g \approx -60$) and the semicrystalline thermal behavior of the poly(L-lactide) (PLLA) domains with glass transition temperatures in the range of 49 °C to 53 °C and melting temperatures between 152 °C and 160 °C, indicates phase separation of the triblock copolymers.⁹⁰ On the other hand, the epoxidation approach (Figure 8) was used for the synthesis of linear and star-shaped polymyrcene-*graft*-poly(L-lactide) graft copolymers (an overview of the L-lactide-based polymer architecture is given in Figure 9d).^{101,102} In dependence of the graft length and graft density, the crystallization of the poly(L-lactide) grafts was suppressed by the flexible polymyrcene backbone for several samples, resulting in completely amorphous materials with two glass transition temperatures due to the polymyrcene backbone ($T_{g,PMYR} = -45 - -52$ °C) and the PLLA grafts ($T_{g,PLLA} = 39 - 54$ °C). However, due to the variation of both composition and molecular weights of the different polymyrcene/poly(L-lactide) block copolymer structures, a correlation of the polymer architecture with material properties is not possible.^{101,102}

In recent works, the potential of hydroxyl α,ω -functionalized polyfarnesene building blocks (polydiol, shown in Figure 7b) for hydrolysis-resistant polyurethane elastomers (shown in Figure 9e) was pointed out.¹⁰³ The hydrophobic polyfarnesene diol soft segment reduces the amount of adsorbed water of the polyurethane elastomers (water contact angle of 100°), increasing the hydrolytic resistance. The bottlebrush-like structure of the polyfarnesene diol shields the hydrolytically cleavable carbamate bond of the polyurethane elastomers, resulting in improved hydrolysis-resistance in comparison with linear polyolefine-based diol soft segments (e.g. hydroxyl-telechelic polyisobutylene or polybutadiene). Consequently, the physical properties of the polyurethane elastomers remained constant after prolonged storage in water. Additionally, the bottlebrush-like structure of the polyfarnesene diol soft segment results in lower glass transition temperatures ($T_{g,PFar} = -66$ °C) in contrast to linear polyolefine-based diols, leading to low temperature flexible polyurethane elastomers.¹⁰³

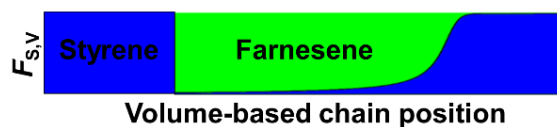
a) Sustainable β -myrcene-based thermoplastic elastomers (Bolton et al.)



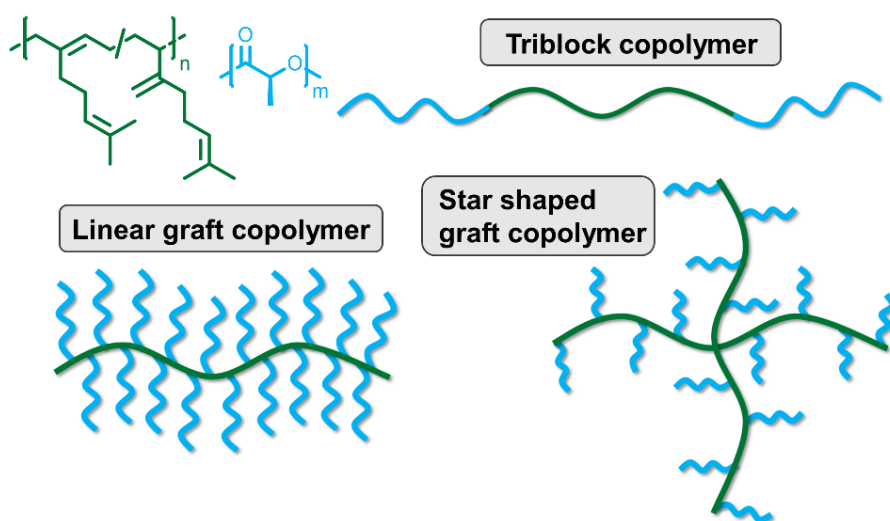
b) Hydrogenated farnesene-based triblock copolymers (Kuraray Co; Ltd.)



c) β -Farnesene-based tapered triblock copolymer (Frey et al.)



d) L-Lactide-based triblock and graft copolymers (Li et al.)



e) β -Farnesene-based polyurethane elastomers (Ma et al.)

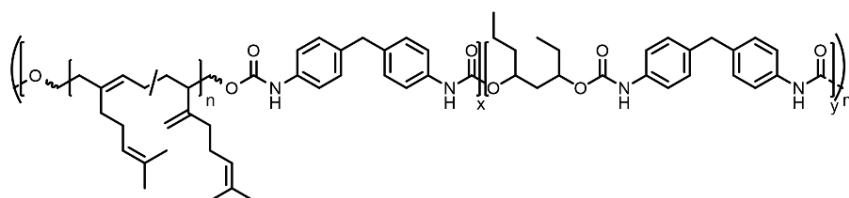


Figure 9. Examples of polymyrcene- and polyfarnesene based thermoplastic elastomers (TPEs).^{63,70,90,97,101–103}

Conclusion and Perspective

The versatile bio-based class of terpenes offers a variety of hidden treasures for various polymerization methods, which are currently revealed and exploited to an increasing extent. Their structural similarity to isoprene opens a toolbox of various 1,3-diene monomers. The immense structural variety of terpenes, ranging from acyclic to cyclic structures, as well as functional derivatives (terpenoids) is crucial to produce tailor-made, bio-based materials.⁹ To date, the living anionic polymerization of terpenes is limited to the 1,3-diene monomers β -myrcene- and β -farnesene, which are widely present in bio-based feedstocks and are already produced on industrial scale from biomass.³⁰ The similarity of the chemical structure of polymyrcene and polyfarnesene to natural rubber (*cis*-polyisoprene) renders them a promising bio-based alternative for other fossil resource-based rubber materials. However, there are also promising cyclic 1,3-diene structures among terpenes that are yet unexplored. These structures may enable the synthesis of bio-based rigid polymers with high glass transition temperature, for instance as a bio-based alternative for polystyrene. In addition, several functional terpenes are suitable candidates for living anionic polymerization, like β -myrcenol.⁴¹ In contrast to established postpolymerization modification reactions, the introduction of functionality by a monomer enables unique regiospecificity as well as a selective functionalization of single polymer blocks by sequential monomer addition. Furthermore, there are several yet unexplored postmodification approaches, which enable fast and efficient modification or cross-linking of double bonds, like the triazolinedione (TAD) click chemistry.⁹⁸ The structural peculiarity of terpenes is also reflected in the polymer properties. In case of polyfarnesene, the bottlebrush-like structure results in a reduced entanglement molecular weight in comparison to its linear fossil-based analog polyisoprene, affecting physical properties like viscosity and glass transition temperature.⁶⁸ Remarkably, in contrast to polyisoprene, the glass transition temperature is nearly unaffected by the polydiene microstructure, which establishes new opportunities regarding structure-property relationship in materials.⁶⁶ The structural differences of polyterpenes compared to commercial fossil-based (thermoplastic) elastomers are key to tailor future elastomers for specialized high-performance applications.

Acknowledgments

The authors thank Sandra Schüttner and Christoph Hahn for the critical reading of the manuscript.

References

- (1) Mühlaupt, R. Green Polymer Chemistry and Bio-based Plastics: Dreams and Reality. *Macromolecular Chemistry and Physics*, 214(2), 159-174. *Macromol. Chem. Phys.* **2013**, 214, 159–174.
- (2) Suaria, G; Avio, C. G.; Mineo, A.; Lattin, G. L.; Magaldi, M. G.; Belmonte, G.; Moore, C. J.; Regoli, F.; Aliani, S. The Mediterranean Plastic Soup: synthetic polymers in Mediterranean surface waters. *Sci. Rep.*, 6, 1–10.
- (3) Lebreton, L.; Slat, B.; Ferrari, F.; Sainte-Rose, B.; Aitken, J; Marthouse, R.; Hajbane, S.; Cunsolo, S.; Schwarz, A.; Levivier, A. Evidence that the Great Pacific Garbage Patch is rapidly accumulating plastic. *Sci. Rep.*, 8, 1–15.
- (4) Gandini, A. Polymers from Renewable Resources: A Challenge for the Future of Macromolecular Materials. *Macromolecules* **2008**, 41, 9491–9504.
- (5) Keijer, T.; Bakker, V.; Slootweg, J. C. Circular chemistry to enable a circular economy. *Nature Chem* **2019**, 11, 190–195.
- (6) Sheldon, R. A. Metrics of Green Chemistry and Sustainability: Past, Present, and Future. *ACS Sustain. Chem. Eng.* **2018**, 6(1), 32-48.
- (7) Sarkar, P.; Bhowmick, A. K. Sustainable rubbers and rubber additives. *J Appl Polym Sci* **2018**, 135, 45701.
- (8) Corma, A.; Iborra, S.; Velty, A. Chemical routes for the transformation of biomass into chemicals. *Chem. Rev.* **2007**, 107, 2411–2502.
- (9) Breitmaier, E. *Flavors, fragrances, pharmaca, pheromones*; Wiley-VCH: Weinheim, 2006.
- (10) Winnacker, M.; Rieger, B. Recent progress in sustainable polymers obtained from cyclic terpenes: synthesis, properties, and application potential. *ChemSusChem* **2015**, 8, 2455–2471.
- (11) Della Monica, F.; Kleij, A. W. From terpenes to sustainable and functional polymers. *Polymer Chemistry. Polym. Chem.*, **2020**, 11, 5109-5127.
- (12) L. Ruzicka. The isoprene rule and the biogenesis of terpenic compounds. *Experientia* **1953**, 9, 357–367.
- (13) Zhu, Y.; Romain, C.; Williams, C. Sustainable polymers from renewable resources. *Nature* **2016**, 354–362.
- (14) Sahu, P.; Bhowmick, A. K.; Kali, G. Terpene Based Elastomers: Synthesis, Properties, and Applications. *Processes* **2020**, 8, 553.

- (15) Wilbon, P. A.; Chu, F.; Tang, C. Progress in renewable polymers from natural terpenes, terpenoids, and rosin. *Macromol. Rapid Commun.* **2013**, *34*, 8–37.
- (16) Tang, C.; Ryu, C. Y. *Sustainable Polymers from Biomass*, 1. Aufl.; Wiley-VCH: Weinheim, 2017.
- (17) Lamparelli, D. H.; Paradiso, V.; Della Monica, F.; Proto, A.; Guerra, S.; Giannini, L.; Capacchione, C. Toward More Sustainable Elastomers: Stereoselective Copolymerization of Linear Terpenes with Butadiene. *Macromolecules* **2020**, *53*, 1665–1673.
- (18) Marvel, C. S.; Hwa, C. C. L. Polymyrcene. *J. Polym. Sci.* **1960**, *45*, 25–34.
- (19) Winnacker, M. Pinenes: Abundant and Renewable Building Blocks for a Variety of Sustainable Polymers. *Angew. Chem. Int. Ed.* **2018**, *57*, 14362–14371.
- (20) Ojika, M.; Satoh, K.; Kamigaito, M. BAB-random-C Monomer Sequence via Radical Terpolymerization of Limonene (A), Maleimide (B), and Methacrylate (C): Terpene Polymers with Randomly Distributed Periodic Sequences. *Angew. Chem. Int. Ed.* **2017**, *56*.
- (21) Sibaja, B.; Sargent, J.; Auad, M. L. Renewable thermoset copolymers from tung oil and natural terpenes. *J. Appl. Polym. Sci.* **2014**, *131*.
- (22) Parrino, F.; Fidalgo, A.; Palmisano, L.; Ilharco, L. M.; Pagliaro, M.; Ciriminna, R. Polymers of Limonene Oxide and Carbon Dioxide: Polycarbonates of the Solar Economy. *ACS Omega* **2018**, *3*, 4884–4890.
- (23) Neumann, S.; Leitner, L.-C.; Schmalz, H.; Agarwal, S.; Greiner, A. Unlocking the Processability and Recyclability of Biobased Poly(limonene carbonate). *ACS Sustain. Chem. Eng.* **2020**, *8*, 6442–6448.
- (24) Firdaus, M.; Montero de Espinosa, L.; Meier, M. A. R. Terpene-Based Renewable Monomers and Polymers via Thiol–Ene Additions. *Macromolecules*, **2011**, *44*(18), 7253–7262.
- (25) Sahu, P.; Bhowmick, A. K. Redox Emulsion Polymerization of Terpenes: Mapping the Effect of the System, Structure, and Reactivity. *Ind. Eng. Chem. Res.* **2019**, *58*, 20946–20960.
- (26) Grau, E.; Mecking, S. Polyterpenes by ring opening metathesis polymerization of caryophyllene and humulene. *Green Chemistry*, **2013**, *15*, 1112–1115.
- (27) Mo, X; Greenberg, M. J. Chewing Gum base Containing Polyfarnesene and Chewing Gum Products Made therefrom. U.S. Patent 2013/0251846A1, Sep 26, 2013.
- (28) Kuwahara, S.; Hirata, K.; Koda D. Rubber Composition and Tire. U.S. Patent 8785542B2, Jul 22, 2014.
- (29) Behr, A.; Johnen, L. Myrcene as a natural base chemical in sustainable chemistry: a critical review. *ChemSusChem* **2009**, *2*, 1072–1095.
- (30) Benjamin, K. R.; Silva, I. R.; Cherubim, J. P.; McPhee, D.; Paddon, C. J. Developing Commercial Production of Semi-Synthetic Artemisinin, and of β -Farnesene, an

Isoprenoid Produced by Fermentation of Brazilian Sugar. *J. Braz. Chem. Soc.* **2016**, *27*, 1339–1345.

(31) Brieger, G.; Nestruck, T. J.; McKenna, C. Synthesis of trans, trans- α -farnesene. *J. Org. Chem.* **1969**, *34*, 3789–3791.

(32) Arkoudis, E.; Stratakis, M. Synthesis of cordiaquinones B, C, J, and K on the basis of a bioinspired approach and the revision of the relative stereochemistry of cordiaquinone C. *J. Org. Chem.* **2008**, *73*, 4484–4490.

(33) Naddeo, M.; Buonerba, A.; Luciano, E.; Grassi, A.; Proto, A.; Capacchione, C. Stereoselective polymerization of biosourced terpenes β -myrcene and β -ocimene and their copolymerization with styrene promoted by titanium catalysts. *Polymer* **2017**, *131*, 151–159.

(34) Veazey, R. L. Polyalloocimene and Method for the Preparation thereof. U.S. Patent 4694059, Sept 15, 1987.

(35) Hong, K.; Mays, J. W. 1,3-Cyclohexadiene Polymers. 1. Anionic Polymerization. *Macromolecules* **2001**, *34*, 782–786.

(36) Inoue, N. Anionic Polymerization of 1,3-Cyclohexadiene with Alkylolithium/Amine Systems. Characteristics of n-Butyllithium/N,N,N',N'-Tetramethylethylenediamine System for Living Anionic Polymerization. *Macromolecules* **1998**, *31*, 4687–4694.

(37) Williamson, D. T.; Elman, J. F.; Madison, P. H.; Pasquale, A. J.; Long, T. E. Synthesis and Characterization of Poly(1,3-cyclohexadiene) Homopolymers and Star-Shaped Polymers. *Macromolecules* **2001**, *34*, 2108–2114.

(38) Lajunen, M. Synthesis of some conjugated caradienes from 3-carene by the Wittig reaction and their reactivity in the diels-alder reaction. *Tetrahedron* **1994**, *50*, 13181–13198.

(39) Büchi, G.; Hofheinz, W.; Paukstelis, J. V. The total synthesis of (-)-aromadendrene. *J. Am. Chem. Soc.* **1966**, *88*, 4113–4114.

(40) Hirao, A.; Loykulnant, S.; Ishizone, T. Recent advance in living anionic polymerization of functionalized styrene derivatives. *Progr. Polym. Sci.* **2002**, *27*, 1399–1471.

(41) Wahlen, C.; Rauschenbach, M.; Blankenburg, J.; Kersten, E.; Ender, C. P.; Frey, H. Myrcenol-based Monomer for Carbanionic Polymerization: Funtional Copolymers with Myrcene and Bio-based Graft Copolymers. *Macromolecules*, **2020** DOI: 10.1021/acs.macromol.0c01734.

(42) Gan, Q.; Xu, Y.; Huang, W.; Luo, W.; Hu, Z.; Tang, F.; Jia, X.; Gong, D. Utilization of bio-sourced myrcene for efficient preparation of highly cis-1,4 regular elastomer via a neodymium catalyzed copolymerization strategy. *Polym. Int* **2020**, *69*, 763–770.

(43) Xu, Y.; Zhao, J.; Gan, Q.; Ying, W.; Hu, Z.; Tang, F.; Luo, W.; Luo, Y.; Jian, Z.; Gong, D. Synthesis and properties investigation of hydroxyl functionalized polyisoprene prepared by cobalt catalyzed co-polymerization of isoprene and hydroxylmyrcene. *Polym. Chem.* **2020**, *11*, 2034–2043.

- (44) J. L. Cawse; J. L. Stanford; R. H. Still. Polymers from renewable sources. III. Hydroxy-terminated myrcene polymers. *J. Appl. Polym. Sci.* **1986**, *31*, 1963–1975.
- (45) Johanson, A. J.; McKennon, F. L.; Goldblatt, L. A. Emulsion Polymerization of Myrcene. *Ind. Eng. Chem.* **1948**, *40*, 500–502.
- (46) Luk, S. B.; Marić, M. Nitroxide-Mediated Polymerization of Bio-Based Farnesene with a Functionalized Methacrylate. *Macromol. React. Eng.* **2019**, *13*, 1800080.
- (47) Bauer, N.; Brunke, J.; Kali, G. Controlled Radical Polymerization of Myrcene in Bulk: Mapping the Effect of Conditions on the System. *ACS Sustain. Chem. Eng.* **2017**, *5*, 10084–10092.
- (48) Hulnik, M. I.; Vasilenko, I. V.; Radchenko, A. V.; Peruch, F.; Ganachaud, F.; Kostjuk, S. V. Aqueous cationic homo- and co-polymerizations of β -myrcene and styrene: a green route toward terpene-based rubbery polymers. *Polym. Chem.* **2018**, *9*, 5690–5700.
- (49) Nishida, T.; Satoh, K.; Nagano, S.; Seki, T.; Tamura, M.; Li, Y.; Tomishige, K.; Kamigaito, M. Biobased Cycloolefin Polymers: Carvone-Derived Cyclic Conjugated Diene with Reactive exo -Methylene Group for Regioselective and Stereospecific Living Cationic Polymerization. *ACS Macro Lett.* **2020**, *9*, 1178–1183.
- (50) Laur, E.; Welle, A.; Vantomme, A.; Brusson, J.-M.; Carpentier, J.-F.; Kirillov, E. Stereoselective Copolymerization of Styrene with Terpenes Catalyzed by an Ansa-Lanthanidocene Catalyst: Access to New Syndiotactic Polystyrene-Based Materials. *Catalysts* **2017**, *7*, 361.
- (51) Hattam, P.; Gauntlett, S.; Mays, J. W.; Hadjichristidis, N.; Young, R. N.; Fetters, L. J. Conformational characteristics of some model polydienes and polyolefins. *Macromolecules* **1991**, *24*, 6199–6209.
- (52) Newmark, R. A.; Majumdar, R. N. ¹³C-NMR spectra of cis-polymyrcene and cis-polyfarnesene. *J. Polym. Sci. A Polym. Chem.* **1988**, *26*, 71–77.
- (53) Leibig, D.; Morsbach, J.; Grune, E.; Herzberger, J.; Müller, A. H.E.; Frey, H. Die lebende anionische Polymerisation. *ChiuZ* **2017**, *51*, 254–263.
- (54) Baskaran, D.; Müller, A. H. E. Anionic vinyl polymerization—50 years after Michael Szwarc. *Progr. Polym. Sci.* **2007**, *32*, 173–219.
- (55) Métafiot, A.; Kanawati, Y.; Gérard, J.-F.; Defoort, B.; Marić, M. Synthesis of β -Myrcene-Based Polymers and Styrene Block and Statistical Copolymers by SG1 Nitroxide-Mediated Controlled Radical Polymerization. *Macromolecules* **2017**, *50*, 3101–3120.
- (56) Liu, B.; Li, L.; Sun, G.; Liu, D.; Li, S.; Cui, D. Ioselective 3,4-(co)polymerization of bio-renewable myrcene using NSN-ligated rare-earth metal precursor: an approach to a new elastomer. *Chem. Comm.* **2015**, *51*, 1039–1041.
- (57) Zhao, J.; Schlaad, H. Synthesis of Terpene-Based Polymers; *Adv. Polym. Sci.* **2013**, *253*, 151–190.

(58) Georges, S.; Bria, M.; Zinck, P.; Visseaux, M. Polymyrcene microstructure revisited from precise high-field nuclear magnetic resonance analysis. *Polymer* **2014**, *55*, 3869–3878.

(59) Schoenberg, E.; Marsh, H. A.; Walters, S. J.; Saltman, W. M. Polyisoprene. *Rubber Chem. Technol.* **1979**, *52*, 526–604.

(60) Hadjichristidis, N.; Hirao, A., Eds. *Anionic Polymerization: Principles, Practice, Strength, Consequences and Applications*, 1st ed. 2015; Springer: Tokyo, 2015.

(61) Hsieh, H. L.; Quirk, R. P. *Anionic Polymerization: Principles and Practical Applications*; *Plastics Engineering* 34; Dekker: New York, 1996.

(62) Steube, M.; Johann, T.; Hübner, H.; Koch, M.; Dinh, T.; Gallei, M.; Floudas, G.; Frey, H.; Müller, A. H. E. Tetrahydrofuran: More than a “Randomizer” in the Living Anionic Copolymerization of Styrene and Isoprene: Kinetics, Microstructures, Morphologies, and Mechanical Properties. *Macromolecules* **2020**, *53*, 5512–5527.

(63) Bolton, J. M.; Hillmyer, M. A.; Hoye, T. R. Sustainable Thermoplastic Elastomers from Terpene-Derived Monomers. *ACS Macro Lett.* **2014**, *3*, 717–720.

(64) Widmaier, J. M.; Meyer, G. C. Glass transition temperature of anionic polyisoprene. *Macromolecules* **1981**, *14*, 450–452.

(65) Lal, J.; Mark, J. E., Eds. *Advances in Elastomers and Rubber Elasticity*; Springer US: Boston, 1986.

(66) Yoo, T.; Henning, S. K. Synthesis and Characterization of Farnesene-based Polymers. *Rubber Chem. Technol.* **2017**, *90*, 308–324.

(67) Zhang, J.; Lu, J.; Su, K.; Wang, D.; Han, B. Bio-based β -myrcene-modified solution-polymerized styrene–butadiene rubber for improving carbon black dispersion and wet skid resistance. *J Appl Polym Sci* **2019**, *136*, 48159.

(68) Iacob, C.; Yoo, T.; Runt, J. Molecular Dynamics of Polyfarnesene. *Macromolecules* **2018**, *51*, 4917–4922.

(69) Fetters, L. J.; Lohse, D. J.; Richter, D.; Witten, T. A.; Zirkel, A. Connection between Polymer Molecular Weight, Density, Chain Dimensions, and Melt Viscoelastic Properties. *Macromolecules* **1994**, *27*, 4639–4647.

(70) Wahlen, C.; Blankenburg, J.; von Tiedemann, P.; Ewald, J.; Sajkiewicz, P.; Müller, A. H. E.; Floudas, G.; Frey, H. Tapered Multiblock Copolymers based on Farnesene and Styrene: Impact of Bio-based Polydiene Architectures on Material Properties. *submitted to Macromolecules*.

(71) Zhang, J.; Li, T.; Mannion, A. M.; Schneiderman, D. K.; Hillmyer, M. A.; Bates, F. S. Tough and Sustainable Graft Block Copolymer Thermoplastics. *ACS Macro Lett.* **2016**, *5*, 407–412.

(72) Jakobi, B.; Bichler, K. J.; Sokolova, A.; Schneider, G. J. Dynamics of PDMS-g-PDMS Bottlebrush Polymers by Broadband Dielectric Spectroscopy. *Macromolecules* **2020**, DOI: 10.1021/acs.macromol.0c01277.

- (73) Grune, E.; Johann, T.; Appold, M.; Wahlen, C.; Blankenburg, J.; Leibig, D.; Müller, A. H. E.; Gallei, M.; Frey, H. One-Step Block Copolymer Synthesis versus Sequential Monomer Addition: A Fundamental Study Reveals That One Methyl Group Makes a Difference. *Macromolecules* **2018**, *51*, 3527–3537.
- (74) Steube, M.; Johann, T.; Plank, M.; Tjaberings, S.; Gröschel, A. H.; Gallei, M.; Frey, H.; Müller, A. H. E. Kinetics of Anionic Living Copolymerization of Isoprene and Styrene Using in Situ NIR Spectroscopy: Temperature Effects on Monomer Sequence and Morphology. *Macromolecules* **2019**, *52*, 9299–9310.
- (75) Grune, E.; Appold, M.; Müller, A. H. E.; Gallei, M.; Frey, H. Anionic Copolymerization Enables the Scalable Synthesis of Alternating (AB)_n Multiblock Copolymers with High Molecular Weight in $n/2$ Steps. *ACS Macro Lett.* **2018**, *7*, 807–810.
- (76) Galanos, E.; Grune, E.; Wahlen, C.; Müller, A. H. E.; Appold, M.; Gallei, M.; Frey, H.; Floudas, G. Tapered Multiblock Copolymers Based on Isoprene and 4-Methylstyrene: Influence of the Tapered Interface on the Self-Assembly and Thermomechanical Properties. *Macromolecules* **2019**, *52*, 1577–1588.
- (77) Steube, M.; Johann, T.; Galanos, E.; Appold, M.; Rüttiger, C.; Mezger, M.; Gallei, M.; Müller, A. H. E.; Floudas, G.; Frey, H. Isoprene/Styrene Tapered Multiblock Copolymers with up to Ten Blocks: Synthesis, Phase Behavior, Order, and Mechanical Properties. *Macromolecules* **2018**, *51*, 10246–10258.
- (78) Tiedemann, P. von; Yan, J.; Barent, R. D.; Spontak, R. J.; Floudas, G.; Frey, H.; Register, R. A. Tapered Multiblock Star Copolymers: Synthesis, Selective Hydrogenation, and Properties. *Macromolecules* **2020**, *53*, 4422–4434.
- (79) Abdelrahman, O. A.; Park, D. S.; Vinter, K. P.; Spanjers, C. S.; Ren, L.; Cho, H. J.; Zhang, K.; Fan, W.; Tsapatsis, M.; Dauenhauer, P. J. Renewable Isoprene by Sequential Hydrogenation of Itaconic Acid and Dehydro-Decyclization of 3-Methyl-Tetrahydrofuran. *ACS Catal.* **2017**, *7*, 1428–1431.
- (80) Yang, J.; Zhao, G.; Sun, Y.; Zheng, Y.; Jiang, X.; Liu, W.; Xian, M. Bio-isoprene production using exogenous MVA pathway and isoprene synthase in *Escherichia coli*. *Bioresour. Technol.* **2012**, *104*, 642–647.
- (81) Azeem, M.; Borg-Karlson, A. K.; Rajarao, G. K. Sustainable bio-production of styrene from forest waste. *Bioresour. Technol.* **2013**, *144*, 684–688.
- (82) McKenna, R.; Nielsen, D. R. Styrene biosynthesis from glucose by engineered *E. coli*. *Metab. Eng.* **2011**, *13*, 544–554.
- (83) Grune, E.; Bareuther, J.; Blankenburg, J.; Appold, M.; Shaw, L.; Müller, A. H. E.; Floudas, G.; Hutchings, L. R.; Gallei, M.; Frey, H. Towards bio-based tapered block copolymers: the behaviour of myrcene in the statistical anionic copolymerisation. *Polym. Chem.* **2019**, *10*, 1213–1220.
- (84) Zhang, S.; Han, L.; Ma, H.; Liu, P.; Shen, H.; Lei, L.; Li, C.; Yang, L.; Li, Y. Investigation on Synthesis and Application Performance of Elastomers with Biogenic Myrcene. *Ind. Eng. Chem. Res.* **2019**, *58*, 12845–12853.

- (85) Bareuther, J.; Plank, M.; Kuttich, B.; Kraus, T.; Frey, H.; Gallei, M. Temperature Variation Enables the Design of Bio-Based Block Copolymers via One-Step Anionic Copolymerization. *Macromol. Rapid Commun.*, **2020**, DOI: 10.1002/marc.202000513
- (86) Quinebèche, S.; Navarro, C.; Gnanou, Y.; Fontanille, M. In situ mid-IR and UV-visible spectroscopies applied to the determination of kinetic parameters in the anionic copolymerization of styrene and isoprene. *Polymer* **2009**, *50*, 1351–1357.
- (87) Zhang, J.; Lu, J.; Wang, D.; Han, B. Preparation, carbon black dispersibility and performances of novel biobased integral solution-polymerized styrene–butadiene rubber with β -myrcene bottlebrush segments. *J. Mater. Sci.* **2020**, *55*, 16544–16560.
- (88) Quirk, R. P.; Ma, J.-J. Characterization of the functionalization reaction product of poly(styryl)lithium with ethylene oxide. *J. Polym. Sci. A Polym. Chem.* **1988**, *26*, 2031–2037.
- (89) Quirk, R. P.; Lizárraga, G. M. Investigation of the Reaction of Poly(styryl)lithium with Propylene Oxide. *Macromolecules* **1998**, *31*, 3424–3430.
- (90) Zhou, C.; Wei, Z.; Lei, X.; Li, Y. Fully biobased thermoplastic elastomers: synthesis and characterization of poly(l -lactide)-b-polymyrcene-b-poly(l -lactide) triblock copolymers. *RSC Adv.* **2016**, *6*, 63508–63514.
- (91) Ávila-Ortega, A.; Aguilar-Vega, M.; Loría Bastarrachea, M. I.; Carrera-Figueiras, C.; Campos-Covarrubias, M. Anionic synthesis of amine ω -terminated β -myrcene polymers. *J Polym Res* **2015**, *22*.
- (92) Matic, A.; Schlaad, H. Thiol-ene photofunctionalization of 1,4-polymyrcene. *Polym. Int* **2018**, *67*, 500–505.
- (93) Matic, A.; Hess, A.; Schanzenbach, D.; Schlaad, H. Epoxidized 1,4-polymyrcene. *Polym. Chem.* **2020**, *11*, 1364–1368.
- (94) Weems, A. C.; Delle Chiaie, K. R.; Yee, R.; Dove, A. P. Selective Reactivity of Myrcene for Vat Photopolymerization 3D Printing and Postfabrication Surface Modification. *Biomacromolecules* **2020**, *21*, 163–170.
- (95) Sahu, P.; Sarkar, P.; Bhowmick, A. K. Design of a Molecular Architecture via a Green Route for an Improved Silica Reinforced Nanocomposite using Bioresources. *ACS Sustain. Chem. Eng.* **2018**, *6*, 6599–6611.
- (96) Chao, H.; Yoo, T.; Nehache, S. Epoxidized Polyfarnesene and Methods for Producing the same. U.S. Patent 2019/0055336A1, Feb 21, 2019.
- (97) Sasaki, H.; Uehara, Y.; Kato, M; Thermoplastic elastomer composition and molded body. U.S. Patent 9752027B2, Sep 5, 2017.
- (98) Tobias Johann; Hannes A. Houck; Thi Dinh; Ulrike Kemmer-Jonas; Filip E. Du Prez; Holger Frey. Multi-olefin containing polyethers and triazolinediones: a powerful alliance. *Polym. Chem.* **2019**, *10*, 4699–4708.
- (99) Knoll, K.; Nießner, N. Styrolux and styroflex - from transparent high impact polystyrene to new thermoplastic elastomers: Syntheses, applications and blends with other styrene based polymers. *Macromol. Symp.* **1998**, *132*, 231–243.

(100) McPhee, D. J.; Graham, M. J. Adhesive Compositions Comprising a Polyfarnesene. U.S. Patent 7655739B1, Feb 2, 2010.

(101) Zhou, C.; Wei, Z.; Jin, C.; Wang, Y.; Yu, Y.; Leng, X.; Li, Y. Fully biobased thermoplastic elastomers: Synthesis of highly branched linear comb poly(β -myrcene)-graft-poly(l-lactide) copolymers with tunable mechanical properties. *Polymer* **2018**, *138*, 57–64.

(102) Zhou, C.; Wei, Z.; Wang, Y.; Yu, Y.; Leng, X.; Li, Y. Fully biobased thermoplastic elastomers: Synthesis of highly branched star comb poly(β -myrcene)-graft-poly(l-lactide) copolymers with tunable mechanical properties. *Eur. Polym. J.* **2018**, *99*, 477–484.

(103) Zhang, J.; Chen, J.; Yao, M.; Jiang, Z.; Ma, Y. Hydrolysis-resistant polyurethane elastomers synthesized from hydrophobic bio-based polyfarnesene diol. *J. Appl. Polym. Sci.* **2019**, *136*, 47673.

CHAPTER 2

β -Myrcenol-Based Monomer for Living Anionic Polymerization

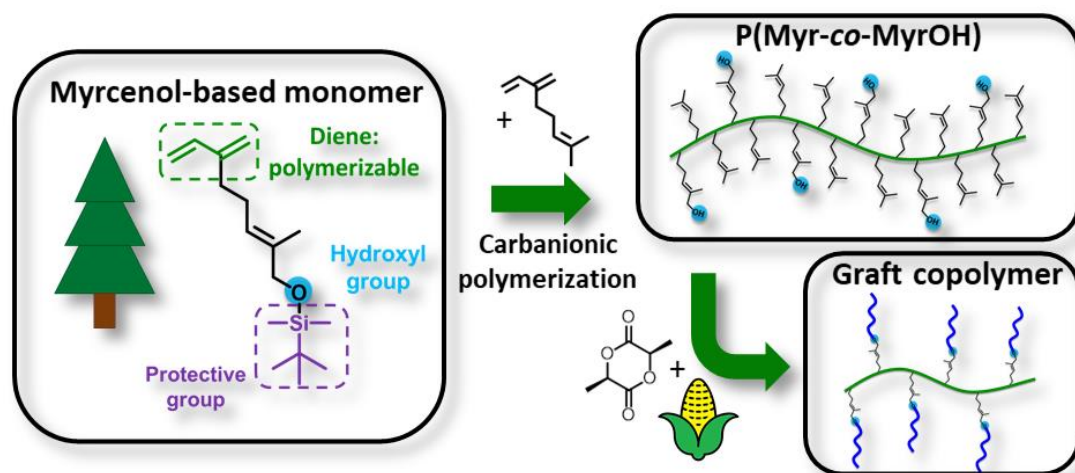
CHAPTER 2

Myrcenol-Based Monomer for Carbanionic Polymerization: Functional Copolymers with Myrcene and Bio-Based Graft Copolymers

Christian Wahlen,^a Moritz Rauschenbach,^a Jan Blankenburg,^a Erik Kersten,^a
Christopher P. Ender^a and Holger Frey^{*,a}

^a Department of Chemistry, Johannes Gutenberg University, Duesbergweg 10-14, 55128 Mainz, Germany

Published in *Macromolecules* 2020. DOI: 10.1021/acs.macromol.0c01734



Abstract

A bio-based hydroxyl group-containing diene monomer, silyl-protected β -myrcenol (MyrOSi), is introduced to the field of carbanionic polymerization. The polymerization of MyrOSi in cyclohexane, using *sec*-butyllithium as an initiator, resulted in homopolymers with well-controlled molecular weights in the range of 7.9 to 31.3 kg mol⁻¹ and dispersities between 1.10 to 1.27. The silyl protective groups can be removed quantitatively under mild conditions, using tetra-*n*-butylammonium fluoride (TBAF), resulting in well-defined polymyrcenol. The statistical copolymerization of MyrOSi with β -myrcene was also investigated. The monomer sequence distribution of the copolymers was evaluated by ¹H NMR kinetic studies. Random copolymerization was observed for the β -myrcene/MyrOSi copolymerization. Copolymers with varying MyrOH content, in the full range between 0 and 100 mol% MyrOH, were synthesized ($D \leq 1.11$) and characterized regarding their glass transition temperatures and polydiene-microstructure. With increasing MyrOH content in the polymer backbone, an increasing number of 3,4-units was observed, resulting in an increasing T_g from -67 to -23 °C. The P(Myrc-*co*-MyrOH) copolymers are valuable building blocks for the synthesis of more complex polymer architectures, such as graft copolymers. The P(Myrc-*co*-MyrOH) copolymers were used for the synthesis of graft copolymers consisting of a flexible polymyrcene backbone and poly(L-lactide) side chains by using the “grafting from” approach. The graft copolymers are promising candidates for bio-based thermoplastic elastomers.

Introduction

Bio-based polymers have been attracting increased attention both in academic and industrial research in recent years.¹⁻³ This trend is caused by an intensified environmental awareness as well as the desire to substitute dwindling fossil resources by sustainable alternatives.⁴⁻⁷ The development of innovative synthetic strategies for bio-based advanced materials, associated with the usage of novel renewable monomers, is considered a key point for a sustainable future.¹ In this context, terpenes are a promising class of renewable monomers due to their large variety of functional and polymerizable groups as well as their bioavailability.^{8,9} There has been rapid progress in manufacturing natural terpenes from biomass on large scales in the last decade.^{10,11} β -Myrcene is currently one of the most popular terpenes in material science. It is technically obtained by pyrolysis of β -pinene, which is a naturally occurring component of turpentine.¹¹⁻¹³ The diene entity of several terpenes, such as β -myrcene, renders them suitable for the living carbanionic polymerization. The polymerization of β -myrcene results in a microstructure consisting of *trans*- and *cis*-1,4, 1,2 and 3,4 units, with the relative amounts depending on the polymerization method, solvent and temperature.^{8,14} In the case of anionic polymerization of β -myrcene in apolar solvents (e.g. benzene), polymyrcene with a high amount (89%) of the preferable 1,4-units is obtained.⁸ In recent fundamental works the copolymerization kinetics of β -myrcene with several comonomers and the synthesis of fully bio-based thermoplastic elastomers were studied.¹⁵⁻¹⁸

The isopropylidene groups of the myrcene units play an important role in the postmodification of polymyrcene, as they offer a side-chain double bond in addition to the polymer backbone. In several works, the immense potential of polymyrcene for postmodification was exploited, e.g. by thiol-ene “click” chemistry, which offers the possibility to introduce a variety of functional groups.¹⁹ Another modification reaction is the epoxidation of polymyrcene, which was already applied in several works.²⁰⁻²³ Epoxidized polymyrcene can be used as precursor to build up more complex architectures, e.g., graft copolymers. In previous works, this approach was used for example to prepare polymyrcene-*graft*-poly(L-lactide) graft copolymers.^{21,22,24} A disadvantage of the postmodification reactions of polymyrcene is the lack of regioselectivity. In addition to the double bonds in the side chain, also modification of the double bonds in the polymer backbone takes place.^{19,21} An alternative approach to introduce functional groups into the polymer backbone is the utilization of suitable functional diene monomers. Compared to

postmodification reactions, functional monomers enable a quantitative and regiospecific functionalization of the polymer as well as sequence control of the functionalized monomer units by copolymerization with other monomers.²⁵ In recent works β -myrcene was copolymerized with functional monomers like dibutyl itaconate and glycidyl methacrylate via radical emulsion polymerization.^{26,27} In other current works by Gong et al., a hydroxyl myrcene derivative (2-methyl-6-methyleneoct-7-en-2-ol) was copolymerized with β -myrcene or isoprene, using neodymium or cobalt catalyzed polymerization.^{28,29} The resulting hydroxyl functionalized elastomers show improved interaction with SiO₂ fillers.

However, the vast potential that terpenes offer for material science, is by no means exhausted. Especially in the field of carbanionic polymerization the utilization of functional terpene-based monomers, the so-called terpenoids, is a rather neglected topic. The accessibility of functional diene monomers for carbanionic polymerization is strongly limited, due to synthetic difficulties and the high susceptibility of the structures to the Diels-Alder reaction.³⁰ Merely a few functional diene monomers have been reported to date, containing silyl or amine groups.³¹⁻³⁴ Furthermore, it was demonstrated that the highly reactive carbanionic chain end induces an elimination reaction of 2-alkoxy-1,3-butadienes, which leads to an unexpected transformation of the monomer structure under the polymerization conditions, the so called “back side collapse”. This can be circumvented by the introduction of an alkyl spacer, that is naturally present in β -myrcene.^{35,36} Terpenoids with a polymerizable diene unit are conveniently accessible compounds, which are prospective candidates for bio-based monomers for carbanionic polymerization. One of the potential candidates is β -myrcenol (2-methyl-6-methylideneocta-2,7-dienol), which is a natural compound that is found in thyme oil, but also synthetically accessible by allylic oxidation of β -myrcene.^{37,38} In this work we present a novel hydroxyl group containing, silyl protected, diene monomer, based on the bio-based compound β -myrcenol, which allows to introduce hydroxyl functionalities to polymyrcene both in a randomly distributed and regiospecific fashion. Furthermore, the hydroxyl groups in the polymer backbone permit a large variety of postmodification reactions, like the synthesis of graft copolymers. In the current work we chose to graft semicrystalline poly(L-lactide) from the P(Myrc-co-MyrOH) copolymers to demonstrate the potential of the novel myrcene building blocks, e.g. for the synthesis of well-defined bio-based thermoplastic elastomeric materials.

Experimental Section

Reagents. β -Myrcene ($\geq 95\%$), selenium dioxide, salicylic acid and tetrabutylammonium fluoride, as a 1 M solution in THF, were purchased from Sigma Aldrich. *Tert*-butyldimethylsilyl chloride (TBDMSCl) was received from Carbolution Chemicals GmbH. *Tert*-butyl hydroperoxide (TBHP, 70% solution in H₂O), *sec*-butyllithium as a 1.3 M solution in cyclohexane/hexane (92/8), imidazole and calcium hydride were purchased from Acros Organics. Dichloromethane and cyclohexane were acquired from Fisher Scientific. Chloroform-*d*₁ and tetrahydrofuran-*d*₈ were received from Deutero GmbH. Cyclohexane was dried using *sec*-butyllithium and 1,1-diphenylethylene (DPE) as an indicator (*sec*-BuLi-DPE-anion shows red color).

Instrumentation. SEC measurements were performed in THF as the mobile phase (flow rate 1 mL min⁻¹) on an SDV column set from PSS (SDV 10³, SDV 10⁵, SDV 10⁶) and a RI detector. Calibration was carried out by using polyisoprene (PI) standards, provided by PSS Polymer Standard Service GmbH. NMR spectra were recorded on a Bruker Avance II 400 spectrometer with 400 MHz (¹H NMR) or 101 MHz (¹³C NMR). All spectra are referenced internally to the residual proton signals of the deuterated solvent. The thermal properties of the polymers were studied with a Q2000 (TA Instruments) differential scanning calorimeter (DSC). Two heating and cooling cycles were performed in a temperature range between -90 °C and 130 °C (-90 °C and 180 °C for graft copolymers). Heating and cooling rates are given under the corresponding DSC curves. The glass transition temperatures (*T*_g) were determined from the second cycle.

Monomer synthesis. *2-Methyl-6-methylideneocta-2,7-dienol* (β -Myrcenol, *MyrOH*). 402 mL of *tert*-butyl hydroperoxide solution (70% in water, 2.9 mol, 4.0 equiv) was added dropwise to a stirred solution of 2.44 g (22.0 mmol, 0.03 equiv) of selenium dioxide and 10.12 g (73.3 mmol, 0.1 equiv) of salicylic acid in 660 mL dichloromethane. After 15 min of vigorous stirring, 99.8 g (732 mmol, 1 equiv) of β -myrcene was added dropwise at 0 °C, and the solution was stirred for 48 h under an argon atmosphere. The solution was diluted with benzene and concentrated under vacuum. The residue was diluted with diethyl ether and washed twice with an aqueous NaOH solution (10%) and subsequently with a Brine solution. The organic layer was dried over MgSO₄ and the solvent was evaporated. After column chromatography (silica, *n*-hexane/ethyl acetate (4/1), *R*_f = 0.25) 22.3 g (147 mmol) of pure β -myrcenol were obtained (yield = 20%). ¹H NMR (400 MHz, CDCl₃): δ (ppm) =

6.38 (dd, 17.6, 10.8 Hz, 1H, CH=CH₂), 5.44 (m, 1H, CH=C), 5.24 (d, 17.6 Hz, 1H, CH₂=CH), 5.06 (d, 1H, CH₂=CH), 5.02 (s, 1H, CH₂=C), 5.00 (s, 1H, CH₂=C), 4.00 (s, 2H, CH₂-OH), 2.31 – 2.15 (m, 4H, CH₂-CH₂), 1.67 (s, 3H, CH₃-C). ¹H and ¹³C NMR spectra are attached to the Supporting Information (Figures S1 and S2).

(*Tert*-butyldimethylsiloxy)-2-methyl-6-methylideneocta-2,7-diene (MyrOSi). 7.6 g (50 mmol) of β-myrcenol and 8.51 g (125 mmol, 2.5 equiv) imidazole were dissolved in 15 mL dichloromethane. A solution of 7.2 g (48 mmol, 0.95 equiv) *tert*-butyldimethylsilyl chloride in 15 mL dichloromethane was added dropwise to the β-myrcenol containing solution, which was cooled to 0 °C. The solution was stirred for 24 h under argon atmosphere. Afterwards the solution was washed with 50 mL of aqueous NaHCO₃ solution (5%). The organic layer was separated, and the aqueous layer was washed several times with *n*-hexane (3 × 20 mL). The combined organic layers were dried with MgSO₄. The solvent was evaporated under vacuum to obtain the crude product. After column chromatography (silica, toluene, R_f = 0.89) 12.8 g (47.9 mmol) of pure MyrOSi were obtained (yield = 96%). ¹H NMR (400 MHz, CDCl₃): δ (ppm) = 6.38 (dd, 17.6, 10.8 Hz, 1H, CH=CH₂), 5.43 (m, 1H, CH=C), 5.24 (d, 17.6 Hz, 1H, CH₂=CH), 5.06 (d, 10.8 Hz, 1H, CH₂=CH), 5.02 (s, 1H, CH₂=C), 5.00 (s, 1H, CH₂=C), 4.02 (s, 2H, CH₂-OSi), 2.29 – 2.23 (m, 4H, CH₂-CH₂), 1.60 (s, 3H, CH₃-C), 0.91 (s, 9H, (CH₃)₃-C-Si), 0.07 (s, 6H, (CH₃)₂-Si). ¹H, ¹³C, COSY, HSQC, HMBC and ²⁹Si NMR spectra are attached to the Supporting Information (Figures S4 – S9).

Homo- and copolymerization. The polymerizations were carried out in a glove box in glass vessels (25 mL) with septum. Dry and degassed cyclohexane was distilled into a Schlenk flask equipped with a Teflon stopper. The monomer(s) (MyrOSi and β-myrcene) were dried 24 h over CaH₂, degassed and finally distilled into another Schlenk flask with Teflon stopper. Inside the glove box the monomer(s) and cyclohexane were added into glass vessel with septum. For the synthesis of a homopolymer (shown as an example for $M_n^{\text{th}} = 17.5 \text{ kg mol}^{-1}$) 1.13 g MyrOSi (4.2 mmol, [MyrOSi]₀ = 0.84 mol L⁻¹) in 5 mL cyclohexane was initiated with 0.05 mL of *sec*-butyllithium (0.065 mmol). In case of a copolymerization (shown as an example for $M_n^{\text{th}} = 14.5 \text{ kg mol}^{-1}$, with 50 mol% MyrOSi) a mixture of 0.61 g MyrOSi (2.27 mmol, [MyrOSi]₀ = 0.45 mol L⁻¹) and 0.37 g of β-myrcene (2.27 mmol, [Myr]₀ = 0.45 mol L⁻¹) in 5 mL cyclohexane was initiated with 0.05 mL *sec*-butyllithium (0.065 mmol). All homo- and copolymers were synthesized on a 1 g scale. After initiation both the homo- and copolymerization solution turned pale yellow. The

solution was stirred for 2 h at RT, and then the polymerization was terminated by adding degassed 2-propanol. Subsequently the polymer was precipitated in 2-propanol and dried under vacuum. The average molecular weights were determined by SEC (polyisoprene standards) and, after removal of the protective group, by ^1H NMR-spectroscopy end group analysis. The product was a colorless, highly viscous material with yields > 90%. NMR spectra are attached to the Supporting Information (Figures 1, S10 – S13 and S20).

Deprotection. Homopolymer. 400 mg of P(MyrOSi) was dissolved in 10 mL THF and afterwards tetra-*n*-butylammonium fluoride (1 M solution in THF, 7.5 equivalents related to MyrOSi units) was added under argon atmosphere. After 0.5 h, 4 mL 2-propanol was added to the cloudy solution. The solution was stirred for 0.5 h at 40 °C and quenched by the addition of 4 mL of a saturated aqueous NH_4Cl solution. The organic layer was washed with brine. The polymer was precipitated from the organic layer in cyclohexane via centrifugation at -10 °C. The polymer was washed with water and precipitated twice from a 2-propanol solution in cyclohexane. The colorless highly viscous product was dried under vacuum, yielding > 85% of the hydroxyl-functional polymer. ^1H and ^{13}C NMR spectra are attached to the Supporting Information (Figures S14 and S15).

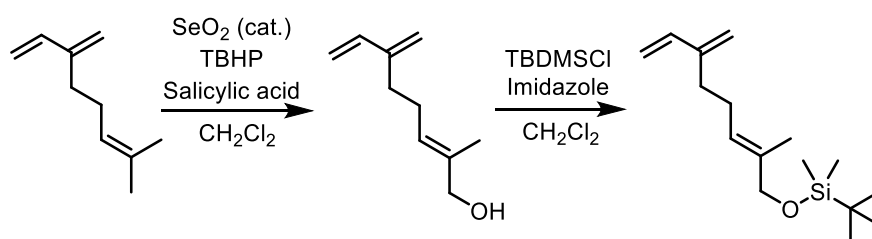
Copolymers. 400 mg of P(Myr-co-MyrOSi) was dissolved in 10 mL THF and afterwards tetra-*n*-butylammonium fluoride (1 M solution in THF, 7.5 equiv with respect to MyrOSi units) was added under argon atmosphere. The solution was stirred for 1 h at RT. The polymer was precipitated from the solution in 2-propanol. The precipitation was repeated twice from a cyclohexane solution in 2-propanol, and the product was dried under vacuum, yielding > 90% of the deprotected copolymer. Copolymers with MyrOH-content exceeding 50 mol% were deprotected according to the procedure for the homopolymer. ^1H NMR spectrum is attached to the Supporting Information (Figures S21).

General procedure for the “grafting from” approach of P(Myr_{0.89}-co-MyrOH_{0.11}) with L-lactide. The polymerization of LLA using 1,8-diazabicyclo[5.4.0]undec-7-ene (DBU) as a catalyst was performed according to the work of Hedrick and Waymouth.³⁹ The hydroxyl functional copolymer P(Myr_{0.89}-co-MyrOH_{0.11}) and LLA were dissolved in dry (molecular sieves 3 Å) benzene and dried *in vacuo* overnight, prior to use. DBU was stirred over CaH_2 and distilled into a Schlenk flask. The polymerization was performed in a glovebox (MBraun UNILAB, < 0.1 ppm of O_2 and < 0.1 ppm of H_2O). LLA (330 mg, 2.3 mmol) and the macroinitiator (96 mg, 0.005 mmol) were added to a screw cap vial and

dissolved in 1 mL of dry chloroform. A stock solution of DBU was prepared by dissolving 0.1 mL of DBU in 4.9 mL of dry chloroform. Subsequently, 0.05 mL (2.2 mg, 0.01 mmol) of the stock solution was added to start the polymerization. After stirring at room temperature for 1 h the polymerization was quenched by adding 5 mg of benzoic acid. The polymer was precipitated in cold methanol, centrifuged and dried *in vacuo*. The polymer was obtained with quantitative yield as a colorless solid.

Results and Discussion

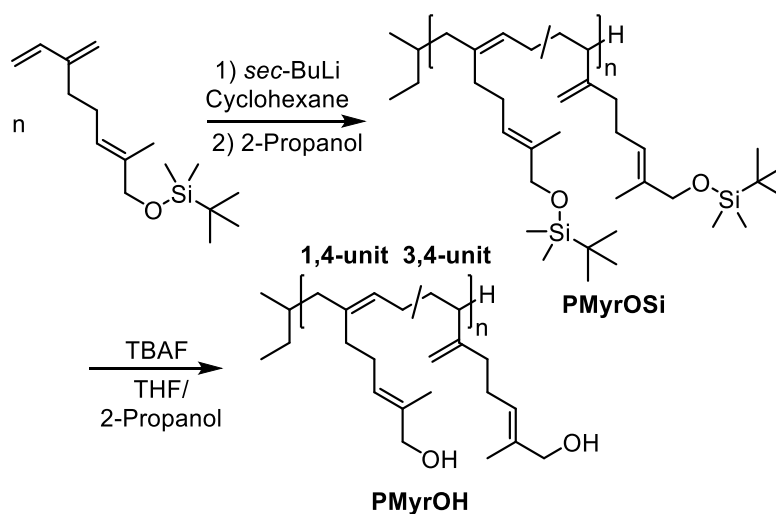
Monomer synthesis. The synthesis of functional diene monomers is a challenging objective, due to the high reactivity of the diene structure, resulting in a high susceptibility to side reactions.³⁰ We have developed a functional diene monomer for carbanionic polymerization, synthesized by a two-step strategy (Scheme 1). The allylic oxidation of the bio-based compound β -myrcene results in β -myrcenol. For the allylic oxidation selenium dioxide was used in catalytic amounts, which reduces toxicity and waste, resulting in a simple work-up.⁴⁰ THBP (*tert*-butyl hydroperoxide) was used as a primary oxidant, which is known as an environmentally friendly reactant, because of the reduction product *tert*-butanol, which is easily removable from the reaction products and can be regenerated to THBP.⁴¹ Low conversion of β -myrcene results in low yields, in agreement with literature.⁴² The conversion was determined from the ¹H NMR spectrum of the crude product (shown in Figure S3), resulting in 70 % of unreacted β -myrcene, albeit this can be recycled for further monomer synthesis. The use of protective group chemistry resulted in a novel monomer, *tert*-butyldimethylsilyl (TBDMS) protected β -myrcenol (MyrOSi), suitable for carbanionic polymerization.



Scheme 1. Synthesis route of TBDMS-protected β -myrcenol based on β -myrcene.

Homopolymerization. The polymerization of MyrOSi was carried out in cyclohexane, using *sec*-butyllithium as an initiator. The synthesis strategy, including subsequent removal of the protective groups, is outlined in Scheme 2. Homopolymers with molecular weights up to 31.3 kg mol^{-1} and dispersities in a range of 1.10 to 1.27 were obtained

(Table 1). Molecular weights and the degree of polymerization were determined by SEC measurements (SEC traces are shown in Figure 2).



Scheme 2. Synthesis strategy for polymyrcenol.

Table 1. Characterization data of the synthesized homopolymers, before (PMyrOSi) and after (PMyrOH) removal of protective groups.

sample	M_n^{th} (kg mol ⁻¹)	M_n^a (kg mol ⁻¹)	M_n^b (kg mol ⁻¹)	\bar{D}^a
PMyrOSi ₂₈	8.75	7.9	7.5	1.10
PMyrOSi ₅₁	17.5	12.8	13.6	1.12
PMyrOSi ₇₈	35.0	21.2	20.8	1.24
PMyrOSi ₁₂₆	52.5	31.3	- ^c	1.27
PMyrOH ₂₈	5	4.5	4.3	1.10
PMyrOH ₅₁	10	8.1	7.8	1.11
PMyrOH ₇₈	20	15.2	11.9	1.20
PMyrOH ₁₂₆	30	19.2	- ^c	1.26

Degrees of polymerization were determined by M_n^a (SEC). ^aDetermined by SEC measurements (eluent: THF, calibration: polyisoprene standards). ^bDetermined by ¹H NMR spectra, by end-group analysis of the corresponding PMyrOH (400 MHz, THF-*d*₈). ^cMolecular weight too high for end-group analysis.

The determination of the molecular weight of the silyl-protected homopolymers by end-group analysis via ¹H NMR spectrum was not directly possible, because of the overlapping proton signals of the methyl groups of the initiator and the *tert*-butyl groups of the protective groups at 0.91 ppm (a ¹H NMR spectrum of PMyrOSi₇₈ is shown in Figure 1). Hence, the molecular weights of the silyl-protected homopolymers (shown in Table 1) were extrapolated from the molecular weights of the corresponding deprotected

homopolymers. The dispersity of the polymers increases with molecular weight, which indicates side reactions during the polymerization. Possible side reactions of the carbanionic chain ends with the TBDMS protective groups were described by Hirao and coworkers for related styrene derivatives (Scheme S1) and include the nucleophilic attack of the living carbanionic species on the silyl-center of the protective group, resulting in the cleavage and a stable oxyanion-lithium-aggregate.⁴³ In addition, the content of the 3,4-units in the polymer backbone was determined from ¹H NMR spectra (according to eq. S1), resulting in 31 % 3,4 units (and 69 % 1,4 units) for all homopolymers. The higher amount of 3,4-units of polymyrceinol in comparison to polymyrce (6 % 3,4-units, Table 3), synthesized under the same conditions, is discussed below with respect to (co)polymer composition and thermal properties.

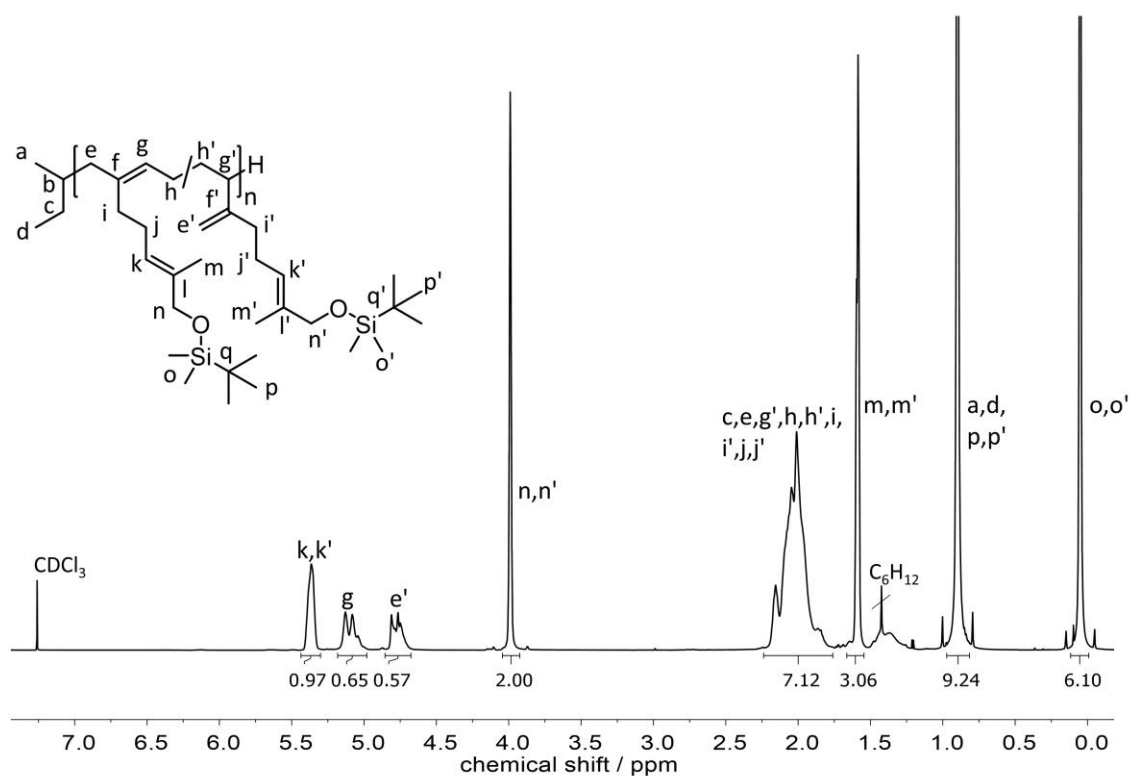


Figure 1. ¹H NMR spectrum (600 MHz) of PMyrOSi₇₈ in CDCl₃.

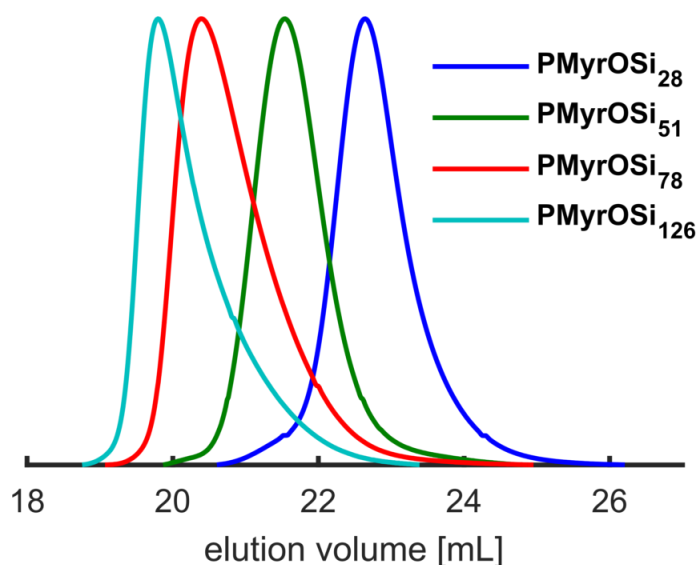


Figure 2. SEC traces (THF, PI standard, RI signal) of PMyrOSi homopolymers.

The protective groups could be removed under mild conditions, using TBAF (tetra-*n*-butylammonium fluoride) in a THF/2-propanol mixture, resulting in quantitative deprotection of the hydroxyl groups. In the SEC traces, a shift of the molecular weight distributions to higher elution volume can be observed, which translates to lower molecular weight (Figure 3). However, the removal of the protective groups involves a low extent of chain coupling reactions that is observable as a small distribution mode with double molecular weight (M_n) in the SEC trace (Figures 3 and S16). Such chain coupling side reactions are a common problem of postmodification reactions of polmyrcene.¹⁹ Several concentration dependent SEC measurements (eluent: THF) of PMyrOH₂₈, as well as SEC-measurements in DMF were performed, permitting to exclude aggregation phenomena as a reason for the bimodal distribution, which are show in Figures S17 and S18.

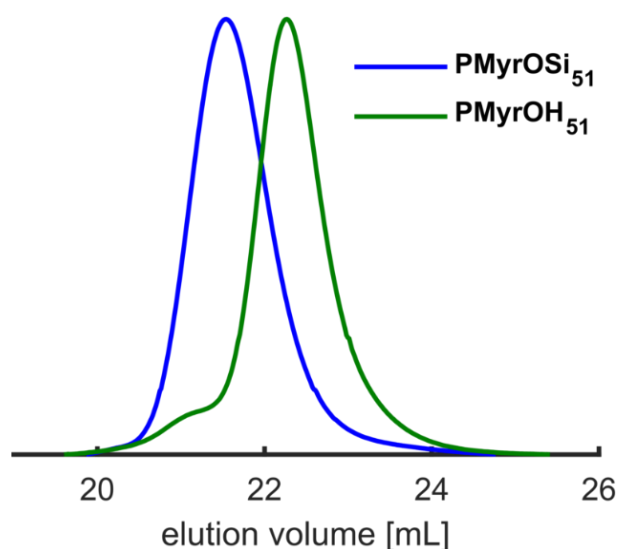


Figure 3. SEC traces (THF, PI standard, RI signal) before (PMyrOSi, blue line) and after (PMyrOH, green line) removal of the protective groups.

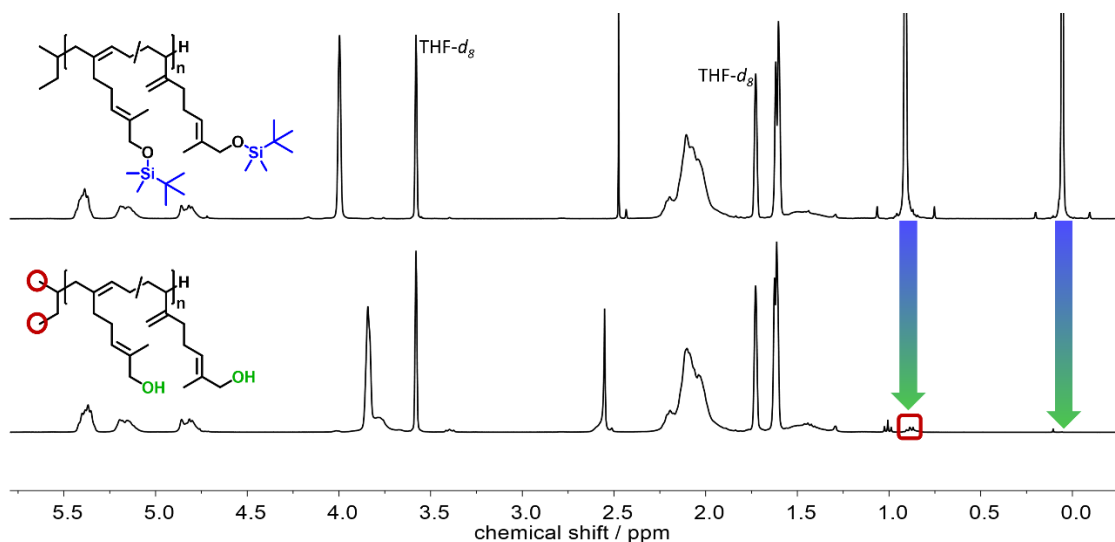


Figure 4. ^1H NMR Spectra (400 MHz, $\text{THF-}d_8$) before (top) and after (bottom) quantitative cleavage of the silyl protective group of the homopolymer.

Quantitative deprotection is proven by ^1H NMR spectroscopy, showing the complete disappearance of the proton signals of the TBDMS protective group at 0.91 and 0.05 ppm, which overlapped with the proton signals of the methyl groups of the initiator, as shown in Figure 4. Due to the disappearance of the proton signals of the silyl protective groups, the molecular weight of deprotected polymyrcenol can be determined by end-group analysis relying on the ^1H NMR spectrum (Figure 4). Nevertheless, even minor residues of the protective group (^1H NMR signals overlap with the initiator signals at 0.91 ppm) result in an apparent decrease of the molecular weight determined from the ^1H NMR spectrum. The molecular weights determined by ^1H NMR spectroscopy are in good agreement with the values obtained from SEC in THF with polyisoprene standards. In all

cases the determined molecular weights are lower than the theoretical values, which can be tentatively ascribed to systematic errors, like a variation of the concentration of *sec*-butyllithium. Furthermore, a polyisoprene standard was applied for the SEC characterization, which could result in an underestimation of the molecular weight due to different solubility behavior of polymyrcenol (potential aggregation effects), resulting in a different hydrodynamic radius in comparison to polyisoprene with the same molecular weight. The removal of the protective group results in an increase of the glass transition temperature from $T_{g,PMyrOSi} = -53\text{ }^{\circ}\text{C}$ to $T_{g,PMyrOH} = -23\text{ }^{\circ}\text{C}$ (DSC results are shown in Figure 5), which is attributed to the increased chain interaction, due to the polar hydroxyl groups, which reduces the polymer chain mobility. Further evidence for the cleavage of the protective group is the appearance of an O-H band in the IR-spectra (Figure S19).

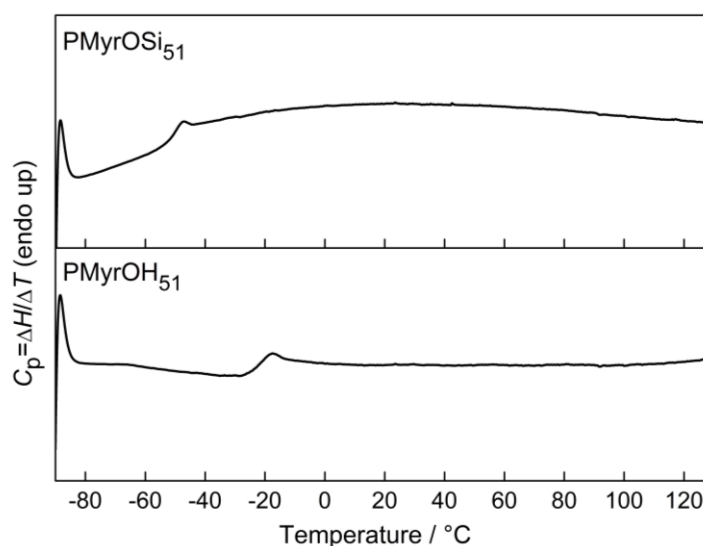


Figure 5. DSC measurements of PMyrOSi₅₁ (top) and of PMyrOH₅₁ (bottom) after removal of the protective groups (second heating curves, heating and cooling rate of 10 °C min⁻¹).

Table 2. Solubility of PMyrOSi and PMyrOH (10 mg in 1 mL solvent at RT).

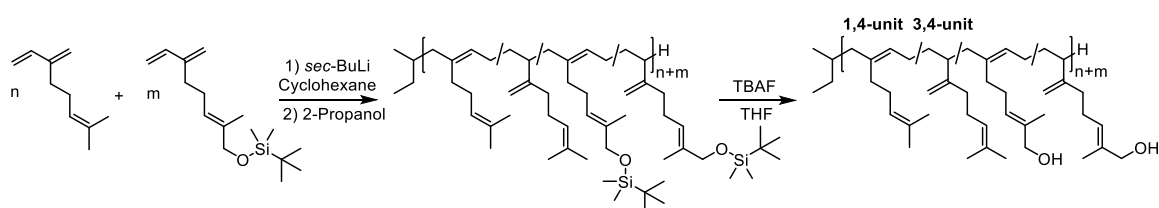
sample	H ₂ O	MeOH	ⁱ PrOH	THF	CHCl ₃	C ₆ H ₁₂
PMyrOSi ₅₁	-	-	-	+	+	+
PMyrOH ₅₁	-	+	+	+	±	-

+: soluble, ±: partial soluble, -: insoluble

The removal of the protective groups results in a change of the solubility behavior of the polymer. While the silyl-protected polymers show similar solubility behavior as

polymyrcene, which is soluble in apolar solvents like cyclohexane or polar aprotic solvents like THF, polymyrcenol is soluble in more polar, protic solvents (e.g. methanol or 2-propanol), but as expected not soluble in water (Table 2). Due to the different solubility behavior of polymyrcene and polymyrcenol, the copolymerization of β -myrcene and MyrOSi, described in the following, enables to adjust the solubility / polarity of the copolymers by varying the monomer ratio. This is attractive for solution applications of rubbery materials or to adjust the interaction of β -myrcene-derived elastomers materials with functional fillers. The altered solubility behavior with increasing β -myrcenol content of the copolymers has to be considered for the choice of solvents for the deprotection procedure, as reported in the Experimental Section.

Statistical copolymerization with β -myrcene. A series of copolymers with constant molecular weight of 10 kg mol^{-1} and monomer ratio varied over the whole range from 0 to 100 mol% of β -myrcenol was synthesized (Scheme 3). An overview of all protected P(Myrc-co-MyrOSi) copolymers is given in Table S1, and the corresponding SEC traces are shown in Figure S22. While the copolymers with M_n up to 10 kg mol^{-1} show monomodal molecular weight distributions, copolymers with M_n exceeding 10 kg mol^{-1} exhibited a low extent of chain coupling, which is a common side reaction of the polymerization of myrcene.^{19,44} In analogy to the homopolymers quantitative removal of the protective groups was achieved, as confirmed in the $^1\text{H NMR}$ spectrum shown in Figure S21. Well-defined P(Myrc-co-MyrOH) copolymers with dispersities between 1.07 and 1.19 were obtained (Table 3). In comparison to the deprotection of the homopolymers, chain coupling induced by the deprotection of the copolymers is less pronounced and decreases with decreasing MyrOSi content (SEC traces in Figure S23). The molecular weights determined by $^1\text{H NMR}$ and SEC are in good agreement, indicating that the polyisoprene calibration can be applied both for homo- and copolymers. Copolymers with molecular weights up to 46 kg mol^{-1} and dispersities lower than 1.19 were successfully synthesized.



Scheme 3. Synthesis strategy for copolymers of β -myrcenol and β -myrcene.

Table 3. Characterization data of (co)polymers of β -myrcene and β -myrcenol with different monomer ratios

Sample	MyrOH content ^b (mol%)	M_n^{th} (kg mol ⁻¹)	M_n^a (kg mol ⁻¹)	M_n^b (kg mol ⁻¹)	\bar{D}^a	T_g^c (°C)	3,4-units ^b (%)
PMyr ₇₀	0	10	9.9	9.5	1.09	-67	6
P(Myr _{0.94-co-MyrOH} _{0.06}) ₆₃	6	10	8.6	8.4	1.08	-65	9
P(Myr _{0.86-co-MyrOH} _{0.14}) ₄₈	14	10	6.6	5.5	1.07	-60	10
P(Myr _{0.73-co-MyrOH} _{0.27}) ₆₃	27	10	8.8	9.3	1.07	-53	14
P(Myr _{0.40-co-MyrOH} _{0.60}) ₄₇	60	10	6.9	6.4	1.07	-40	21
P(Myr _{0.25-co-MyrOH} _{0.75}) ₅₉	75	10	8.7	6.3	1.08	-33	26
PMyrOH ₅₁	100	10	8.1	7.8	1.11	-23	31
P(Myr _{0.89-co-MyrOH} _{0.11}) ₁₅₇	11	20	21.6	- ^d	1.16	-59	8
P(Myr _{0.87-co-MyrOH} _{0.13}) ₃₃₄	13	30	46.2	- ^d	1.19	-60	9

Degrees of polymerization were determined by SEC (M_n^a). ^aDetermined by SEC measurements in THF at 25 °C with PI standard. ^bDetermined from ¹H NMR spectra (400 MHz, CDCl₃). ^cDetermined in DSC measurements. ^dMolecular weight too high for end-group analysis.

Thermal properties and polydiene microstructure. As expected, the thermal properties of the copolymers are strongly dependent on the content of β -myrcenol in the polymer backbone. With increasing β -myrcenol content the glass transition temperature of the (co)polymers increased from -67 °C (0 mol% of MyrOH) to -23 °C (100 mol% of MyrOH). There is a linear dependency of the incorporated monomer ratio on the T_g , as shown in Figure 6 (red). According to the Fox-equation (eq S1, Figure S25),⁴⁵ the linear dependency indicates a random distribution of the monomers along the polymer chains, which is confirmed by ¹H NMR kinetic studies shown below. The increasing T_g is basically caused by two effects: (i) polarity of hydroxyl groups, resulting in increased interaction of the polymer chains and (ii) increased amount of 3,4-units. The apparently linear increase of T_g with increasing content of 3,4-units is in line with literature (Figure S26).⁴⁶ The stereochemistry of carbanionic diene polymerization generally depends on the solvent, the presence of polar additives, the counter ion, the chain end concentration and the temperature.⁴⁷ During the anionic polymerization MyrOSi acts both as a monomer as well as a polar additive (modifier), capable of coordinating the lithium counter ion by the silyl protected hydroxyl group. Polar additives are well known to increase the 3,4-unit content of the anionic polymerization of polydienes like polymyrcene.^{17,48,49}

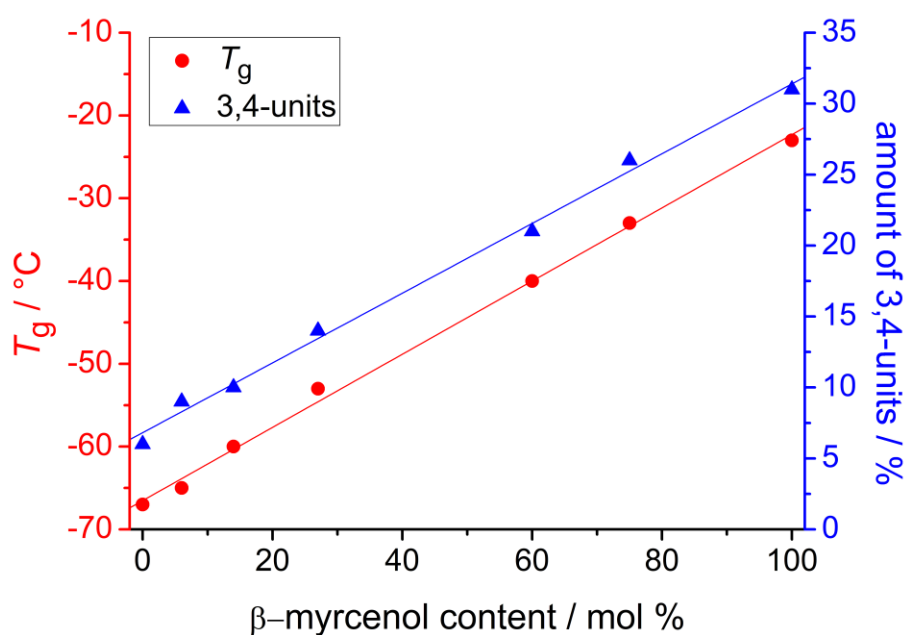


Figure 6. Variation of T_g (red) and polydiene microstructure (3,4-units, blue) of the (co)polymers with MyrOH content (linear fit).

^1H NMR copolymerization kinetic study. ^1H NMR kinetics measurements are known to be a powerful tool for understanding of the polymer microstructure and to determine reactivity ratios.²⁵ Due to a lack of separated signals of β -myrcene and MyrOSi in cyclohexane- d_{12} (Figure S27), their copolymerization cannot be followed by *in situ* ^1H NMR kinetics experiments. Only when CDCl_3 is used as a solvent, the proton signal of the MyrOSi monomer, with a chemical shift of 4.0 ppm, is separated from the corresponding signal of the polymer (as shown in Figure S28). However, since the carbanionic polymerization is not performable in a protic solvent like chloroform, for the considered monomer pair a ^1H NMR kinetic study was performed by taking aliquots. For this purpose, sample were taken every 10 minutes and terminated with degassed methanol. After evaporation of the solvents, ^1H NMR spectra of the samples were measured in CDCl_3 , to follow monomer incorporation during copolymerization (stacked ^1H NMR spectra are shown in Figure S28). In Figure 7a, the observed linear decrease of both monomer concentrations by increasing conversion is shown, which indicates a random copolymerization. Due the very small composition shift, only the Jaacks method (Wall's non-terminal model)⁵⁰ was used, resulting in reactivity ratios of $r_{\text{Myr}} = 1.1$ and $r_{\text{MyrOSi}} = 0.9$ (Figure S29), which correspond to the expected, almost perfectly random copolymerization.^{51,52} The linear trend of the logarithmic monomer conversion versus

time plot (Figure S30) confirms the living character of the copolymerization.⁵³ The corresponding copolymerization diagram shows a random copolymerization (Figure S31). The reactivity ratios were used to simulate the composition profile, as shown in Figure 7b. Note that in the case of a living copolymerization the total conversion translates to the normalized chain position (Supp. Inf., eq S7). The amount of MyrOSi-units is constant along the copolymer chain. In summary, the copolymerization of β -myrcene and MyrOSi allows to design copolymers with a defined and constant density of functional groups along the chain by varying the comonomer ratio. This can be used for instance to adjust the grafting density of brush copolymers.

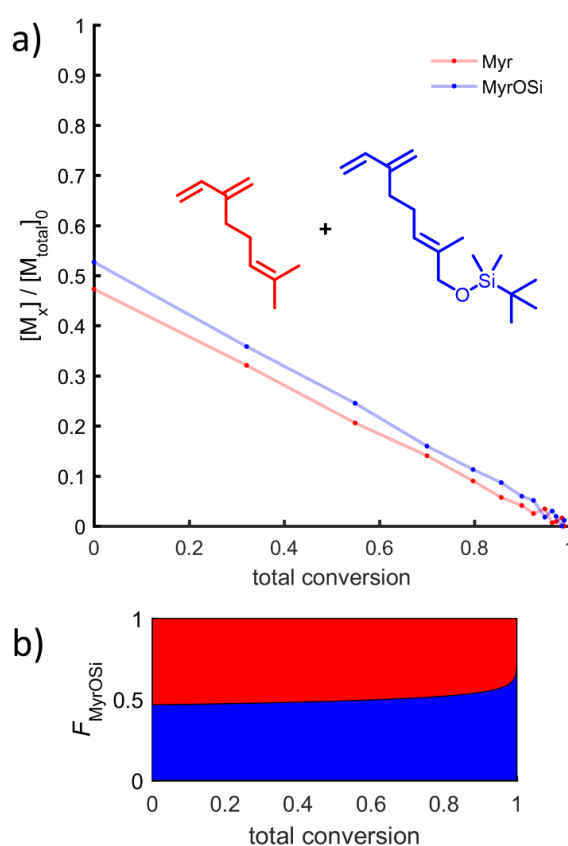


Figure 7. (a) Monomer concentration plotted vs total conversion of the copolymerization of Myr (red) and MyrOSi (blue), determined by ^1H NMR spectroscopy in CDCl_3 . (b) Simulation of the molar composition profile: distribution of β -myrcenol units along the polymer chain, 50:50 copolymer of Myr and MyrOSi.

Graft copolymers. The synthesized copolymers of β -myrcene and β -myrcenol are promising candidates for postmodification reactions. Copolymers with randomly distributed functional groups are ideal building blocks for the synthesis of graft polymers. The low melt viscosity of graft copolymers in comparison to their linear analogs has resulted in an increased popularity of these architectures both in academia and for

commercial utilization.^{54,55} The degree of functionalization of the precursor P(Myrc-co-MyrOH), which is correlated with the degree of branching of the corresponding graft copolymer, is adjustable by varying the monomer ratio of the copolymerization. The rubbery nature of the P(Myrc-co-MyrOH) copolymers renders them suitable building blocks for bio-based thermoplastic elastomers. The “grafting from” approach allows to graft poly(L-lactide) from the hydroxyl groups of the linear copolymer backbone. Poly(L-lactide) is a semicrystalline polymer, known for its bio-renewability, biodegradability and mechanical properties similar to polystyrene.^{56,57} In previous works polymyrcene-*graft*-poly(L-lactide) graft copolymers were synthesized by epoxidation of polymyrcene, followed by acid catalyzed hydrolysis, resulting in two hydroxyl groups per double bond.^{21,22} The epoxidation of polymyrcene is not regiospecific, resulting in transformation of the double bonds of the side chain as well as partial reaction of the double bonds of the polymer backbone.¹⁹ In comparison to these works, the current copolymers, utilizing MyrOSi as a functional comonomer, offer more precise placement of the hydroxyl groups, resulting in well-defined building blocks for the synthesis of graft copolymers. In a proof of concept reaction, the P(Myrc_{0.89}-co-MyrOH_{0.11})₁₅₇ copolymer ($M_n=21.6\text{ kg mol}^{-1}$) was used as a precursor to graft poly(L-lactide) from the hydroxyl groups. Complete conversion of the hydroxyl groups of the macroinitiator is proven by the shift of the proton signal in the ¹H NMR spectrum of the methylene group next to the hydroxyl group from 4.0 ppm to 4.5 ppm (Figure 8). Well-defined graft copolymers with dispersities < 1.1 and molecular weights up to 72.5 kg mol⁻¹ were obtained (characterization data shown in Table 4 and SEC curves in Figure 9). The graft copolymer composition was determined by the ¹H NMR spectrum according to eq. S8 and S9.

Table 4: Characterization data of synthesized PLLA graft copolymers using $P(\text{Myr}_{0.89}\text{-co-MyrOH}_{0.11})_{157}$ ($M_n = 21.6 \text{ kg mol}^{-1}$) as polymer precursor.

Sample	M_n^{th} (kg mol^{-1})	M_n^a (kg mol^{-1})	D^a	$M_{n,branch}^a$ (kg mol^{-1})	yield (%)	T_{g1}^b ($^{\circ}\text{C}$)	T_{g2}^b ($^{\circ}\text{C}$)	T_m^b ($^{\circ}\text{C}$)	ΔH_m^a (J g^{-1})	X_c^c (%)
$\text{PMyr}_{0.35}\text{-graft-PLLA}_{0.65}$	55	51.9	1.09	1.8	95	-	24	-	-	-
$\text{PMyr}_{0.20}\text{-graft-PLLA}_{0.80}$	85	72.5	1.06	3.0	92	-	34	110	9.8	10.5

^aDetermined by SEC measurements in THF at 25 $^{\circ}\text{C}$ with PI standard. ^bDetermined by DSC measurements with a rate of 5 $^{\circ}\text{C min}^{-1}$. ^c Degree of crystallization of copolymers (ΔH_m of 100% crystalline PLLA is 93.7 J g^{-1}).²²

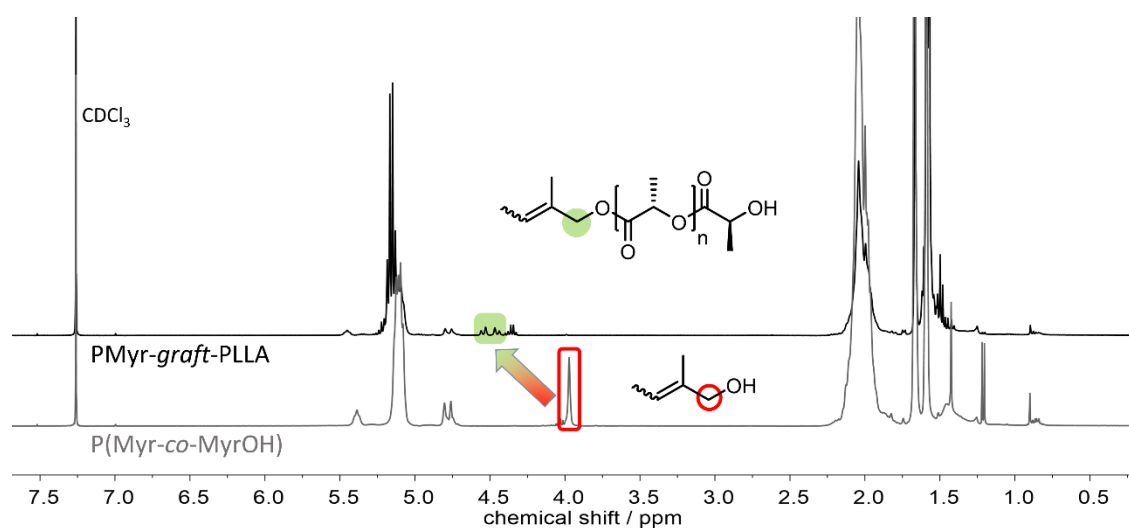


Figure 8. ^1H NMR Spectra (400 MHz, CDCl_3) of the macro-precursor $P(\text{Myr}_{0.89}\text{-co-MyrOH}_{0.11})_{157}$ (grey) and the corresponding graft copolymer $\text{PMyr}_{0.35}\text{-graft-PLLA}_{0.65}$ (black).

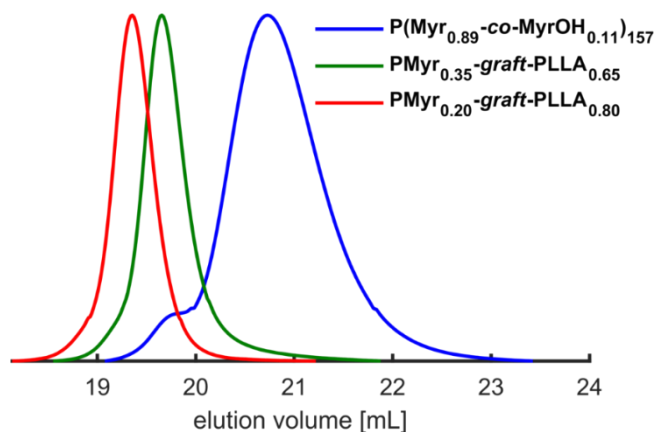


Figure 9. SEC traces (THF, PI standard, RI signal) of the β -myrcene/ β -myrcenol-based macroinitiator (blue) and lactide graft copolymers (red and green).

The thermal properties of the graft copolymers were investigated by DSC measurements. Poly(L-lactide) typically exhibits a glass transition temperature in the range of 50 °C to 65 °C and a melting point at 160°C.⁵⁸ In comparison to the homopolymer of poly(L-lactide), the synthesized graft copolymers show a reduced T_g and reduced degree of crystallization of the poly(L-lactide) branches. While the graft copolymer with 65 mol% of PLLA (with a molecular weight of a single PLLA branch of $M_{n,branch} = 1.8 \text{ kg mol}^{-1}$) shows no crystallization, the graft copolymer with 80 mol% PLLA ($M_{n,branch} = 3 \text{ kg mol}^{-1}$) shows a melting point at 110 °C, which is strongly reduced in comparison to PLLA homopolymer (DSC results shown in Figures S33-S36). The graft copolymer PMyr_{0.20-graft}-PLLA_{0.80} exhibits a low crystallinity ($X_c = 10.5 \%$), which was determined from the melting enthalpy ($\Delta H_m = 9.8 \text{ J g}^{-1}$) obtained from the DSC measurements. The attachment of rather short PLLA chains to the flexible polymyrcene backbone impedes crystallization of PLLA. On the other hand, the polymyrcene backbone reduces the glass transition temperature of polylactide (plasticizer effect). Graft architectures with flexible backbone offer promising potential to increase the toughness of polylactide.^{21,22} The adjustable molecular weight and degree of functionalization of the P(Myrc-co-MyrOH) copolymer precursor offer a unique control over the grafting density and graft length of the graft copolymers.

Conclusion

To the best of our knowledge, this work presents the first example of a hydroxyl group containing diene monomer for carbanionic polymerization, employing the biobased compound β -myrcenol, which is synthesized by the allylic oxidation of β -myrcene. However, the low conversion of β -myrcene (around 30 %), which can be recycled for further monomer synthesis, resulted in low yields of β -myrcenol of 20 % after purification. Silyl-protective group chemistry was used to transform β -myrcenol to the anionic polymerizable monomer MyrOSi. The structure of the terpene structure of β -myrcenol, in which the polymerizable 1,3-diene entity is separated from the functional hydroxyl group by an alkyl spacer, enables controlled anionic polymerization of the monomer with a silyl-protected hydroxyl group. Homo- and copolymers with β -myrcene have been obtained with low to moderate dispersities between 1.08 and 1.27 and molecular weights up to 46.2 kg mol⁻¹. As expected, the solubility behavior of polymyrcenol differs significantly from polymyrcene. The influence of the β -myrcenol content of the copolymers on the thermal properties and on the polydiene microstructure was investigated. An increasing glass transition temperature, due to 3,4-units formed

with increasing amount of β -myrcenol in the copolymer backbone, was observed, demonstrating the effect of the protected MyrOSi monomer as a modifier on the incorporation mode. The random copolymerization with β -myrcene, studied via ^1H NMR measurements on samples taken from the copolymerization, allows to design copolymers with well-defined sequence distributions of the hydroxyl groups along the polymer backbone. This control of the functional group distribution of polymyrcene is not accessible by postmodification of polymyrcene via established methods like epoxidation or thiol-ene click chemistry. The hydroxyl groups as well as the two double bonds per β -myrcene and β -myrcenol unit enable diverse postmodification reactions. To demonstrate the promising potential of P(Myrc-co-MyrOH) copolymers for postmodification reactions, usage of the copolymers as multifunctional macroinitiators for the synthesis of polymyrcene-*graft*-poly(L-lactide) copolymers was demonstrated. Attachment of PLLA to the flexible polymyrcene backbone of the graft copolymers impedes the crystallization of poly(L-lactide) and results in a reduced glass transition temperature (plasticizer effect) in comparison to pure poly(L-lactide). The graft-copolymers offer potential regarding the synthesis of bio-based thermoplastic elastomers, varying both graft density and graft length, which is currently studied.

Acknowledgments

The authors thank Monika Schmelzer for the valuable support with the SEC measurements and Christoph Hahn for critical evaluation of this article.

References

- (1) Winnacker, M.; Rieger, B. Recent progress in sustainable polymers obtained from cyclic terpenes: synthesis, properties, and application potential. *ChemSusChem* **2015**, *8*, 2455–2471.
- (2) Gallezot, P. Conversion of biomass to selected chemical products. *Chem. Soc. Rev.* **2012**, *41*, 1538–1558.
- (3) Babu, R. P.; O'Connor, K.; Seeram, R. Current progress on bio-based polymers and their future trends. *Prog. Biomater.* **2013**, *2*, 8.
- (4) Holmberg, A. L.; Reno, K. H.; Wool, R. P.; Epps, T. H. Biobased building blocks for the rational design of renewable block polymers. *Soft matter* **2014**, *10*, 7405–7424.
- (5) Mühlhaupt, R. Green Polymer Chemistry and Bio-based Plastics: Dreams and Reality. *Macromol. Chem. Phys.* **2013**, *214*, 159–174.

- (6) Gandini, A. Polymers from Renewable Resources: A Challenge for the Future of Macromolecular Materials. *Macromolecules* **2008**, *41*, 9491–9504.
- (7) Yao, K.; Tang, C. Controlled Polymerization of Next-Generation Renewable Monomers and Beyond. *Macromolecules* **2013**, *46*, 1689–1712.
- (8) Zhao, J.; Schlaad, H. Synthesis of Terpene-Based Polymers; *Adv. Polym. Sci.* **2013**, *253*, 151–190.
- (9) Yunqing Zhu, Charles Romain, Charlotte K. Williams. Sustainable polymers from renewable resources. *Nature* **2016**, 354–362.
- (10) Corma, A.; Iborra, S.; Velty, A. Chemical routes for the transformation of biomass into chemicals. *Chem. Rev.* **2007**, *107*, 2411–2502.
- (11) Behr, A.; Johnen, L. Myrcene as a natural base chemical in sustainable chemistry: a critical review. *ChemSusChem* **2009**, *2*, 1072–1095.
- (12) Wilbon, P. A.; Chu, F.; Tang, C. Progress in renewable polymers from natural terpenes, terpenoids, and rosin. *Macromol. Rapid Commun.* **2013**, *34*, 8–37.
- (13) Thomsett, M. R.; Storr, T. E.; Monaghan, O. R.; Stockman, R. A.; Howdle, S. M. Progress in the synthesis of sustainable polymers from terpenes and terpenoids. *Green Mater.* **2016**, *4*, 115–134.
- (14) Sarkar, P.; Bhowmick, A. K. Synthesis, characterization and properties of a bio-based elastomer: polymyrcene. *RSC Adv* **2014**, *4*, 61343–61354.
- (15) Grune, E.; Bareuther, J.; Blankenburg, J.; Appold, M.; Shaw, L.; Müller, A. H. E.; Floudas, G.; Hutchings, L. R.; Gallei, M.; Frey, H. Towards bio-based tapered block copolymers: the behaviour of myrcene in the statistical anionic copolymerisation. *Polym. Chem.* **2019**, *10*, 1213–1220.
- (16) Bolton, J. M.; Hillmyer, M. A.; Hoye, T. R. Sustainable Thermoplastic Elastomers from Terpene-Derived Monomers. *ACS Macro Lett.* **2014**, *3*, 717–720.
- (17) Zhang, J.; Lu, J.; Su, K.; Wang, D.; Han, B. Bio-based β -myrcene-modified solution-polymerized styrene–butadiene rubber for improving carbon black dispersion and wet skid resistance. *J Appl Polym Sci* **2019**, *136*, 48159.
- (18) Zhou, C.; Wei, Z.; Lei, X.; Li, Y. Fully biobased thermoplastic elastomers: synthesis and characterization of poly(l -lactide)-b-polymyrcene-b-poly(l -lactide) triblock copolymers. *RSC Adv.* **2016**, *6*, 63508–63514.
- (19) Matic, A.; Schlaad, H. Thiol-ene photofunctionalization of 1,4-polymyrcene. *Polym. Int* **2018**, *67*, 500–505.
- (20) Ren, X.; Guo, F.; Fu, H.; Song, Y.; Li, Y.; Hou, Z. Scandium-catalyzed copolymerization of myrcene with ethylene and propylene: convenient syntheses of versatile functionalized polyolefins. *Polym. Chem.* **2018**, *9*, 1223–1233.
- (21) Zhou, C.; Wei, Z.; Jin, C.; Wang, Y.; Yu, Y.; Leng, X.; Li, Y. Fully biobased thermoplastic elastomers: Synthesis of highly branched linear comb poly(β -myrcene)-graft-poly(l-lactide) copolymers with tunable mechanical properties. *Polymer* **2018**, *138*, 57–64.

- (22) Cheng Zhou, Zhiyong Wei, Yanshai Wang, Yang Yu, Xuefei Leng, Yang Li. Fully biobased thermoplastic elastomers: Synthesis of highly branched star comb poly(β -myrcene)-graft-poly(l-lactide) copolymers with tunable mechanical properties. *Eur. Polym. J.* **2018**, 477–484.
- (23) Matic, A.; Hess, A.; Schanzenbach, D.; Schlaad, H. Epoxidized 1,4-polymyrcene. *Polym. Chem.* **2020**, 11, 1364–1368.
- (24) Gramlich, W. M.; Theryo, G.; Hillmyer, M. A. Copolymerization of isoprene and hydroxyl containing monomers by controlled radical and emulsion methods. *Polym. Chem.* **2012**, 3, 1510.
- (25) Leibig, D.; Müller, A. H. E.; Frey, H. Anionic Polymerization of Vinylcatechol Derivatives: Reversal of the Monomer Gradient Directed by the Position of the Catechol Moiety in the Copolymerization with Styrene. *Macromolecules* **2016**, 49, 4792–4801.
- (26) Sarkar, P.; Bhowmick, A. K. Green Approach toward Sustainable Polymer: Synthesis and Characterization of Poly(myrcene- co -dibutyl itaconate). *ACS Sustain. Chem. Eng.* **2016**, 4, 2129–2141.
- (27) Sahu, P.; Sarkar, P.; Bhowmick, A. K. Design of a Molecular Architecture via a Green Route for an Improved Silica Reinforced Nanocomposite using Bioresources. *ACS Sustain. Chem. Eng.* **2018**, 6, 6599–6611.
- (28) Gan, Q.; Xu, Y.; Huang, W.; Luo, W.; Hu, Z.; Tang, F.; Jia, X.; Gong, D. Utilization of bio-sourced myrcene for efficient preparation of highly cis -1,4 regular elastomer via a neodymium catalyzed copolymerization strategy. *Polym. Int* **2020**, 69, 763–770.
- (29) Xu, Y.; Zhao, J.; Gan, Q.; Ying, W.; Hu, Z.; Tang, F.; Luo, W.; Luo, Y.; Jian, Z.; Gong, D. Synthesis and properties investigation of hydroxyl functionalized polyisoprene prepared by cobalt catalyzed co-polymerization of isoprene and hydroxylmyrcene. *Polym. Chem.* **2020**, 11, 2034–2043.
- (30) Hadjichristidis, N.; Hirao, A., Eds. *Anionic Polymerization: Principles, Practice, Strength, Consequences and Applications*, 1st ed. 2015; Springer: Tokyo, 2015.
- (31) Petzhold, C.; Morschhaeuser, R.; Kolshorn, H.; Stadler, R. On the Anionic Polymerization of (Dialkylamino)isoprenes. 2. Influence of the Tertiary Amino Group on the Polymer Microstructure. *Macromolecules* **1994**, 27, 3707–3713.
- (32) Hirao, A.; Hiraishi, Y.; Nakahama, S.; Takenaka, K. Polymerization of Monomers Containing Functional Silyl Groups. 13. Anionic Polymerization of 2-[(N, N -Dialkylamino)dimethylsilyl]-1,3-butadiene Derivatives. *Macromolecules* **1998**, 31, 281–287.
- (33) Ding, Y. X.; Weber, W. P. Regio- and stereospecific 1,4-polymerization of 2-(triethylsilyl)-1,3-butadiene. *Macromolecules* **1988**, 21, 530–532.
- (34) Takenaka, K.; Hattori, T.; Hirao, A.; Nakahama, S. Polymerization of monomers containing functional silyl groups. 6. Anionic polymerization of 2-(trialkoxysilyl)-1,3-butadiene. *Macromolecules* **1989**, 22, 1563–1567.

- (35) Takenaka, K.; Nakashima, D.; Miya, M.; Takeshita, H.; Shiomi, T. Anionic polymerization of 2-(N,N-bis(trimethylsilylamino)methyl)-1,3-butadiene and 2-(4-(N,N-bis(trimethylsilylamino)butyl)-1,3-butadiene. *e-J. Soft Mater.* **2013**, *9*, 14–19.
- (36) Takenaka, K.; Akagawa, Y.; Takeshita, H.; Miya, M.; Shiomi, T. Polymerization of 1,3-Dienes Containing Functional Groups 6: Unexpected Collapse of Monomer Structure in the Anionic Polymerization of 2-Ethoxymethyl-1,3-butadiene. *Polym. J.* **2009**, *41*, 106–107.
- (37) Breitmaier, E. *Terpene: Aromen, Düfte, Pharmaka, Pheromone*; Teubner Studienbücher Chemie; Vieweg+Teubner Verlag: Wiesbaden, 1999.
- (38) Kauh, U.; Andernach, L.; Weck, S.; Sandjo, L. P.; Jacob, S.; Thines, E.; Opatz, T. Total Synthesis of (-)-Hymenoseetin. *J. Org. Chem.* **2016**, *81*, 215–228.
- (39) Lohmeijer, B. G. G.; Pratt, R. C.; Leibfarth, F.; Logan, J. W.; Long, D. A.; Dove, A. P.; Nederberg, F.; Choi, J.; Wade, C.; Waymouth, R. M.; *et al.* Guanidine and Amidine Organocatalysts for Ring-Opening Polymerization of Cyclic Esters. *Macromolecules* **2006**, *39*, 8574–8583.
- (40) Nakamura, A.; Nakada, M. Allylic Oxidations in Natural Product Synthesis. *Synthesis* **2013**, *45*, 1421–1451.
- (41) Młochowski, J.; Wójtowicz-Młochowska, H. Developments in Synthetic Application of Selenium(IV) Oxide and Organoselenium Compounds as Oxygen Donors and Oxygen-Transfer Agents. *Molecules* **2015**, *20*, 10205–10243.
- (42) Büchi, G.; Wüest, H. Eine Synthese des β -Sinensals. *Helv. Chim. Acta* **1967**, *50*, 2440–2445.
- (43) Hirao, A.; Kitamura, K.; Takenaka, K.; Nakahama, S. Protection and polymerization of functional monomers. 18. Syntheses of well-defined poly(vinylphenol), poly[(vinylphenyl)methanol], and poly[2-vinylphenylethanol] by means of anionic living polymerization of styrene derivatives containing tert-butyldimethylsilyl ethers. *Macromolecules* **1993**, *26*, 4995–5003.
- (44) Zhang, S.; Han, L.; Ma, H.; Liu, P.; Shen, H.; Lei, L.; Li, C.; Yang, L.; Li, Y. Investigation on Synthesis and Application Performance of Elastomers with Biogenic Myrcene. *Ind. Eng. Chem. Res.* **2019**, *58*, 12845–12853.
- (45) Fox, T. G. Influence of Diluent and of Copolymer Composition on the Glass Temperature of a Polymer System. *Bull. Am. Phys. Soc.*, **1956**, 123.
- (46) Lal, J.; Mark, J. E. *Advances in Elastomers and Rubber Elasticity*; Springer US, 2013.
- (47) Hsieh, H. L.; Quirk, R. P. *Anionic Polymerization: Principles and Practical Applications*; *Plastics Engineering* 34; Dekker: New York, 1996.
- (48) Widmaier, J. M.; Meyer, G. C. Glass transition temperature of anionic polyisoprene. *Macromolecules* **1981**, *14*, 450–452.
- (49) Steube, M.; Johann, T.; Hübner, H.; Koch, M.; Dinh, T.; Gallei, M.; Floudas, G.; Frey, H.; Müller, A. H. E. Tetrahydrofuran: More than a “Randomizer” in the Living Anionic

Copolymerization of Styrene and Isoprene: Kinetics, Microstructures, Morphologies, and Mechanical Properties. *Macromolecules* **2020**, *53*, 5512–5527.

(50) Wall, F. T. The Structure of Vinyl Copolymers. *J. Am. Chem. Soc.* **1941**, *63*, 1862–1866.

(51) Blankenburg, J.; Maciol, K.; Hahn, C.; Frey, H. Poly(ethylene glycol) with Multiple Aldehyde Functionalities Opens up a Rich and Versatile Post-Polymerization Chemistry. *Macromolecules* **2019**, *52*, 1785–1793.

(52) Jaacks, V. A novel method of determination of reactivity ratios in binary and ternary copolymerizations. *Macromol. Chem. Phys.* **1972**, *161*, 161–172.

(53) Blankenburg, J.; Kersten, E.; Maciol, K.; Wagner, M.; Zarbakhsh, S.; Frey, H. The poly(propylene oxide- co -ethylene oxide) gradient is controlled by the polymerization method: determination of reactivity ratios by direct comparison of different copolymerization models. *Polym. Chem.* **2019**, *10*, 2863–2871.

(54) Zhang, J.; Schneiderman, D. K.; Li, T.; Hillmyer, M. A.; Bates, F. S. Design of Graft Block Polymer Thermoplastics. *Macromolecules* **2016**, *49*, 9108–9118.

(55) Zhang, J.; Li, T.; Mannion, A. M.; Schneiderman, D. K.; Hillmyer, M. A.; Bates, F. S. Tough and Sustainable Graft Block Copolymer Thermoplastics. *ACS Macro Lett.* **2016**, *5*, 407–412.

(56) Tschan, M. J.-L.; Brulé, E.; Haquette, P.; Thomas, C. M. Synthesis of biodegradable polymers from renewable resources. *Polym. Chem.* **2012**, *3*, 836–851.

(57) Garlotta, D. A Literature Review of Poly(Lactic Acid). *J. Polym. Environ.* **2001**, *9*, 63–84.

(58) Di Lorenzo, M. L.; Androsch, R., Eds. *Synthesis, structure and properties of poly(lactic acid)*; Advances in Polymer Science 279; Springer: Cham 2018.

Supporting Information

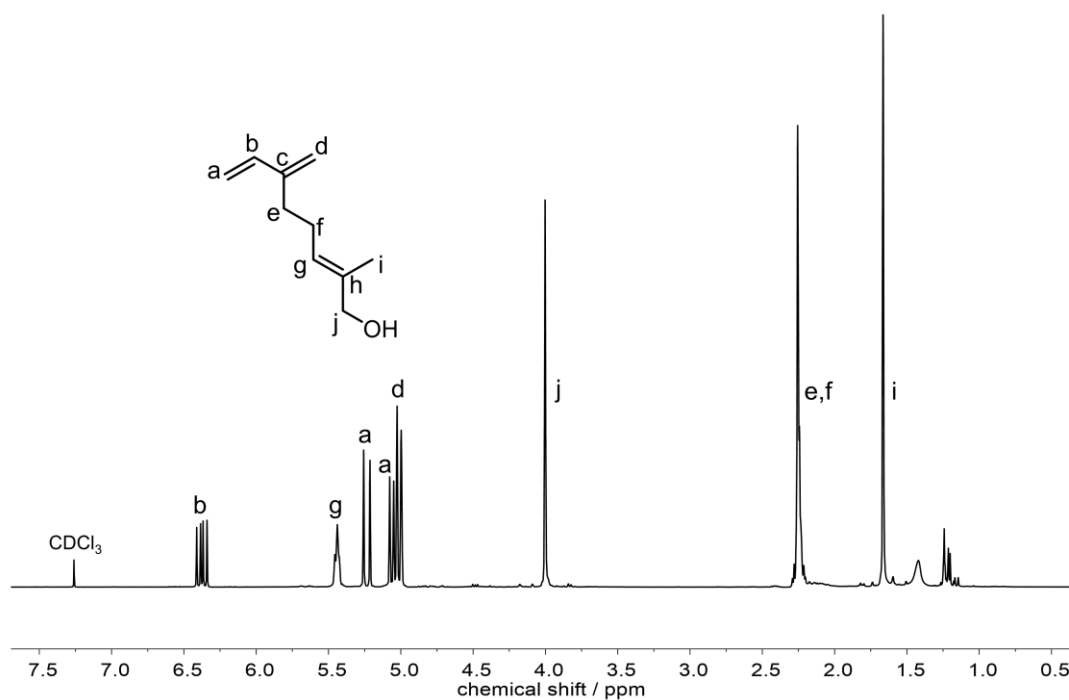
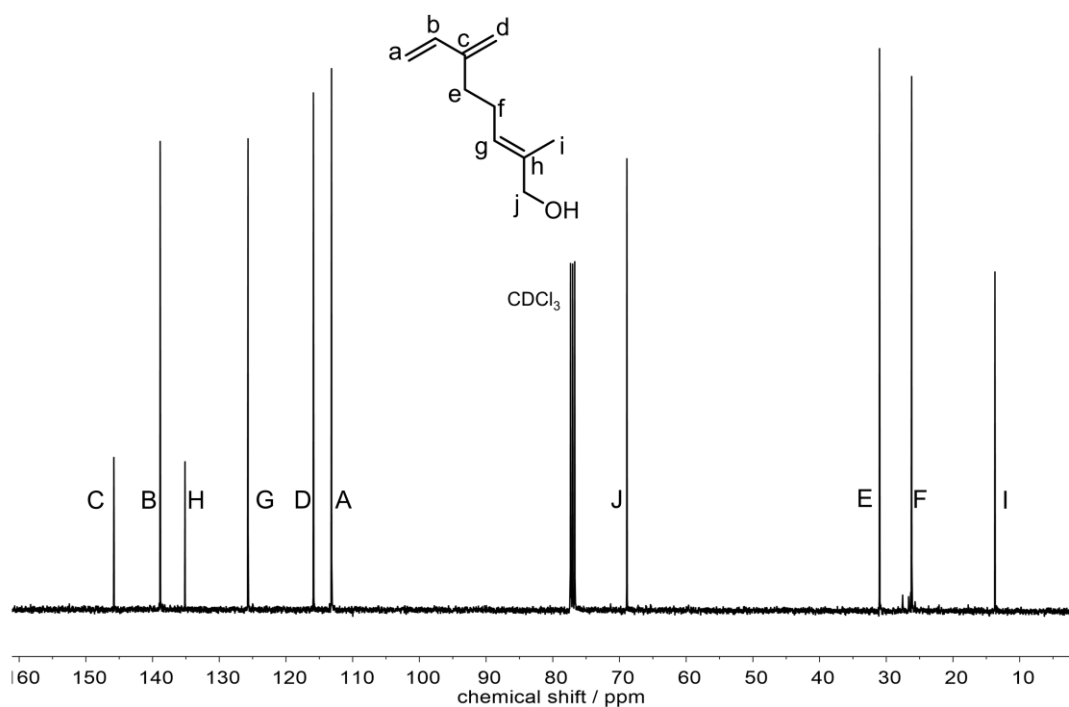
Myrcenol-Based Monomer for Carbanionic Polymerization: Functional Copolymers with Myrcene and Bio-Based Graft Copolymers

Christian Wahlen, Moritz Rauschenbach, Jan Blankenburg, Erik Kersten, Christopher P. Ender and Holger Frey*

Table of Contents

1	Monomer characterization.....	77
2	Homopolymer characterization.....	81
2.1	NMR spectra of PMyrOSi and PMyrOH.....	81
2.2	Determination of polydiene microstructure of homopolymers (content of 3,4-units).....	84
2.3	SEC measurements of PMyrOH.....	85
2.4	IR spectra of PMyrOSi and PMyrOH.....	87
3	Potential side reaction during polymerization.....	87
4	Characterization of copolymers.....	88
4.1	¹ H NMR spectra of copolymers.....	88
4.2	SEC results of copolymers.....	89
4.3	Determination of molecular weight of homo and copolymers by ¹ H NMR spectrum.....	90
4.4	Determination of copolymer composition.....	91
4.5	Determination of polydiene microstructure of copolymers (content of 3,4-units).....	91
4.6	DSC measurements of copolymers.....	92
4.7	Fox equation.....	92
4.8	¹ H NMR copolymerization kinetic experiment.....	94
5	Characterization of PMyr- <i>graft</i> -PLLA graft copolymers.....	97
5.1	¹ H NMR spectrum of PMyr- <i>graft</i> -PLLA.....	97
5.2	Determination of polymer composition of PMyr- <i>graft</i> -PLLA.....	97
5.3	DSC measurements of PMyr- <i>graft</i> -PLLA.....	98
	References.....	101

1 Monomer characterization

**Figure S1.** ^1H NMR spectrum (400 MHz) of β -myrcenol in CDCl_3 .**Figure S2.** ^{13}C NMR spectrum (101 MHz) of β -myrcenol in CDCl_3 .

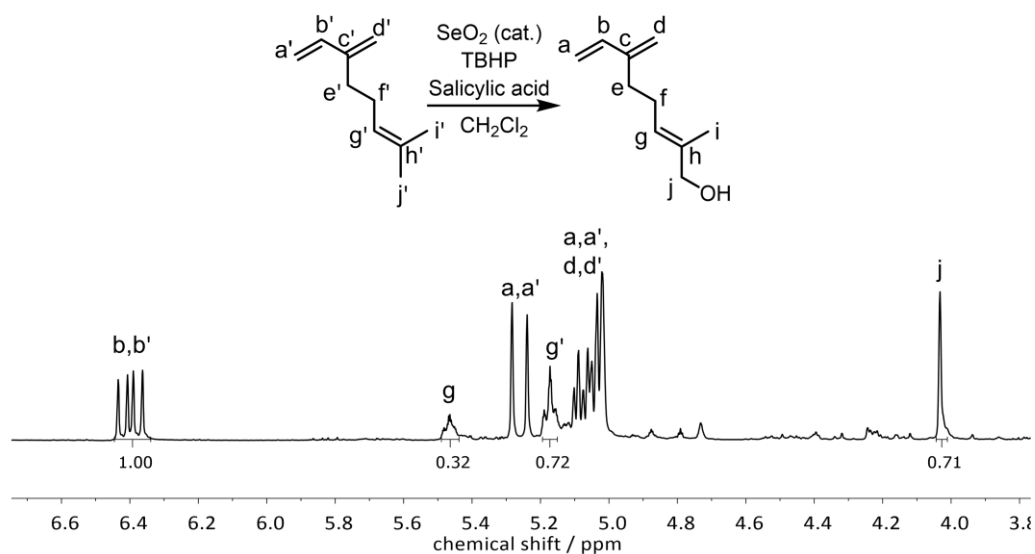


Figure S3. ^1H NMR spectrum (400 MHz) of the crude product of the β -myrcenol synthesis; determination of the conversion of β -myrcene by integration of the signals (b,b') and (g').

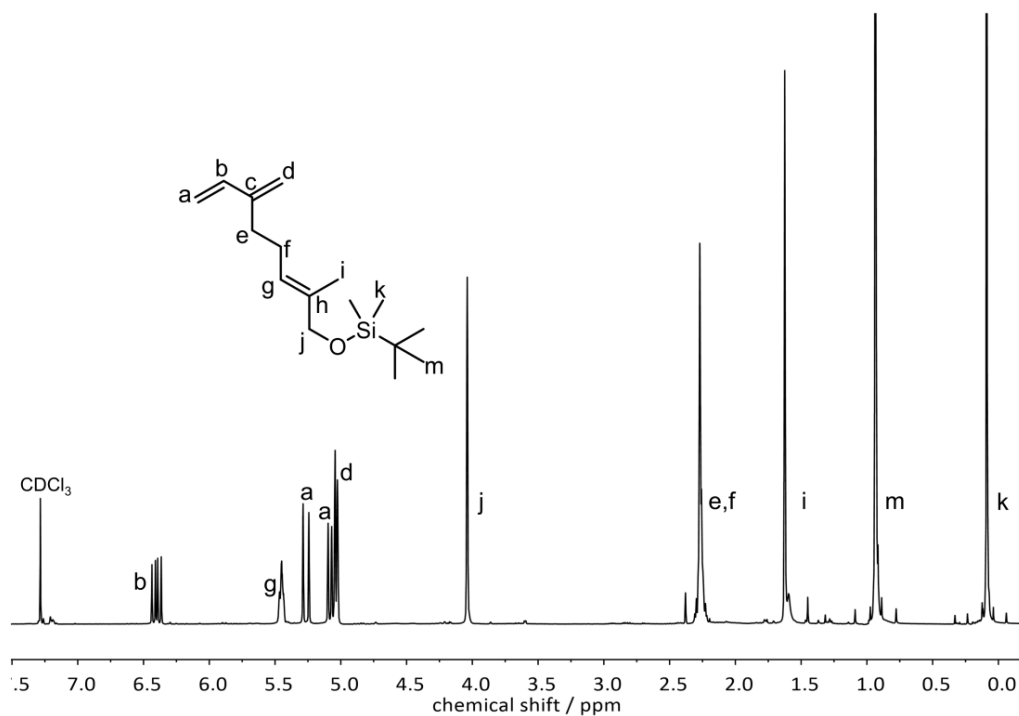


Figure S4. ^1H NMR spectrum (400 MHz) of MyrOSi in CDCl_3 .

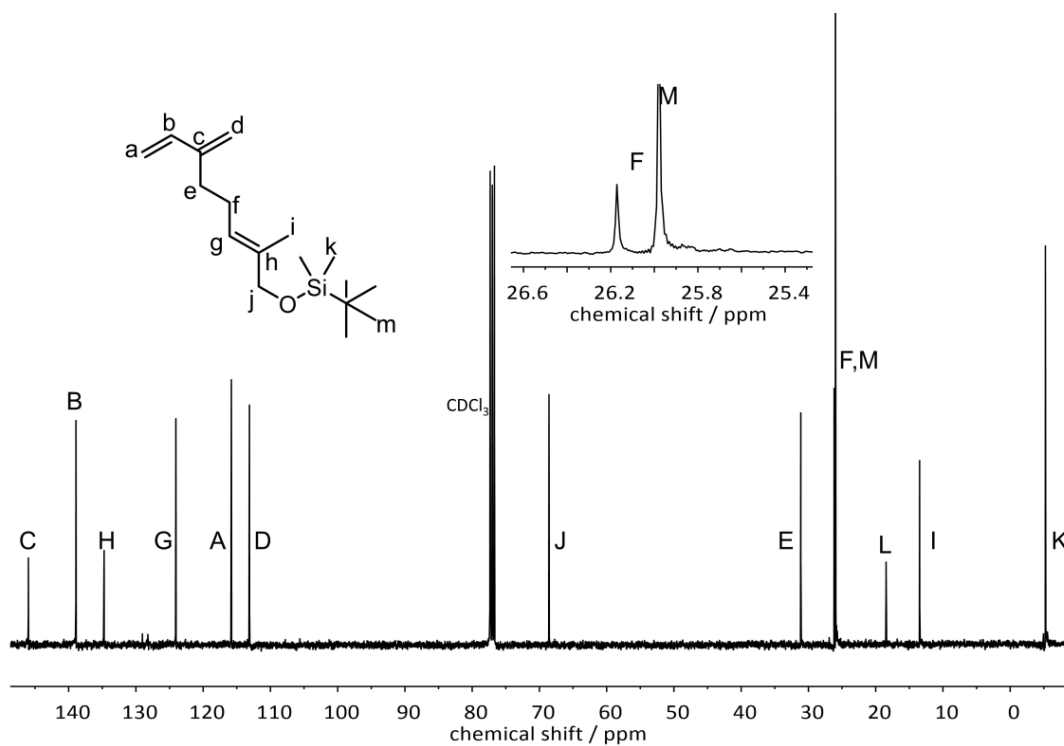


Figure S5. ^{13}C NMR spectrum (101 MHz) of MyrOSi in CDCl_3 .

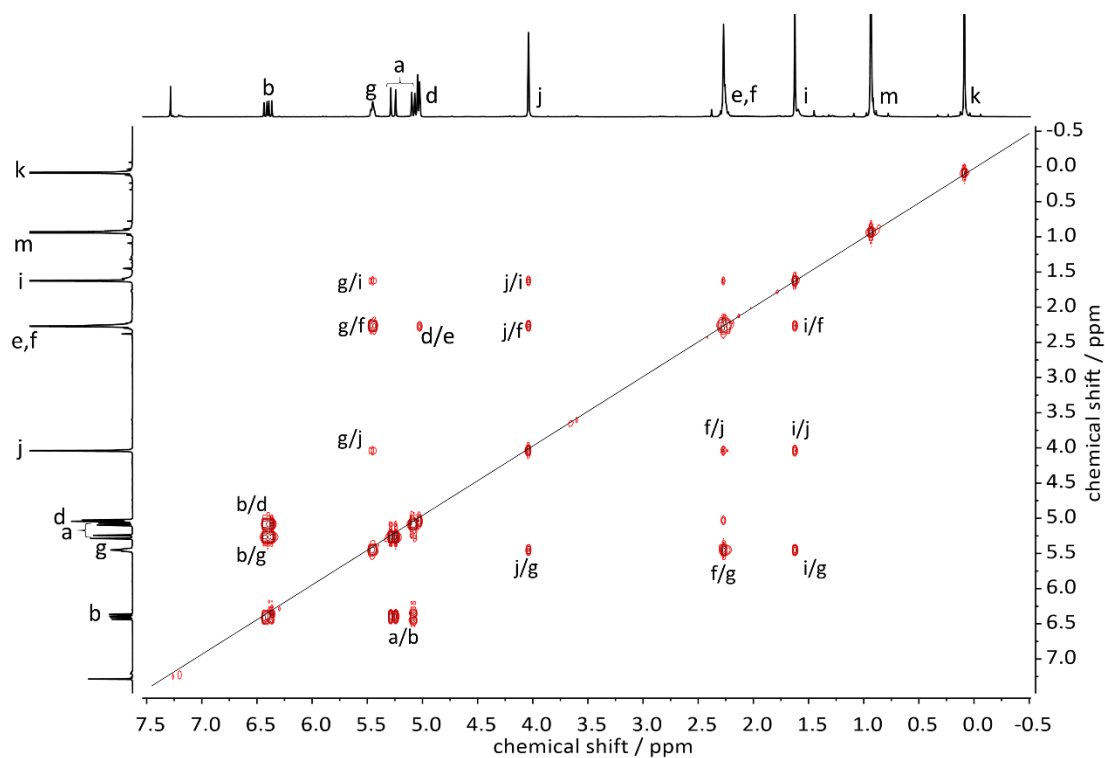


Figure S6. COSY NMR spectrum (400 MHz) of MyrOSi in CDCl_3 .

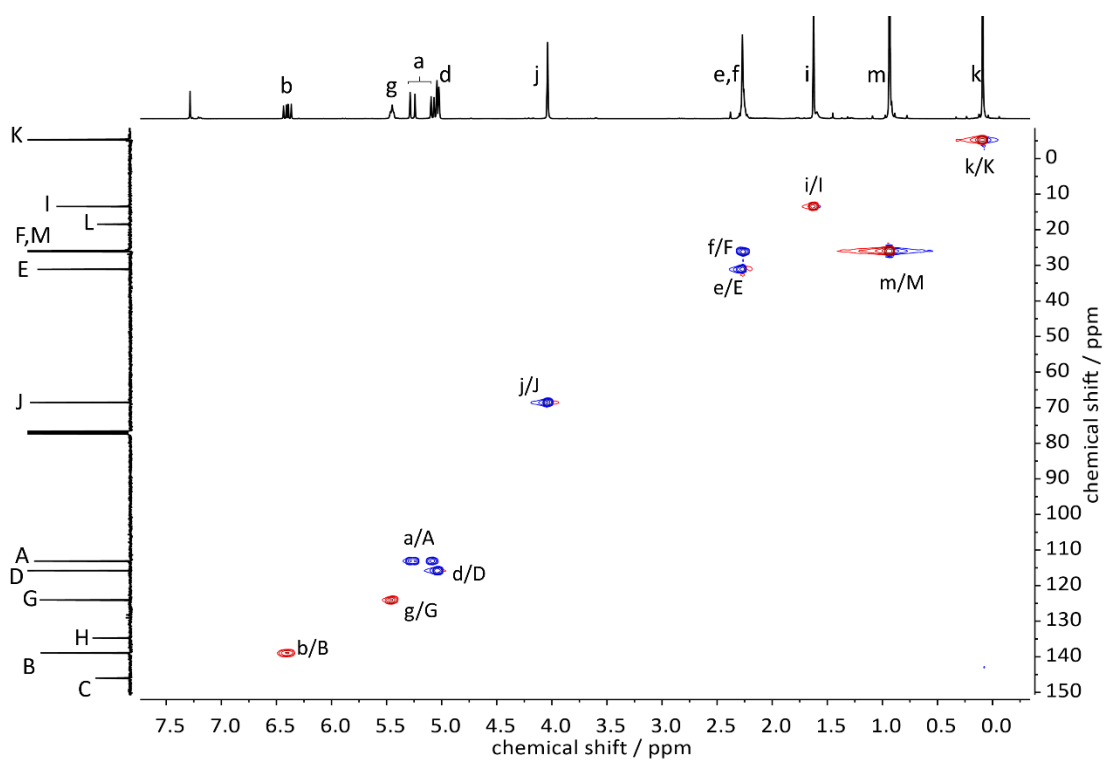


Figure S7. HSQC NMR spectrum (101 MHz / 400 MHz) of MyrOSi in CDCl_3 .

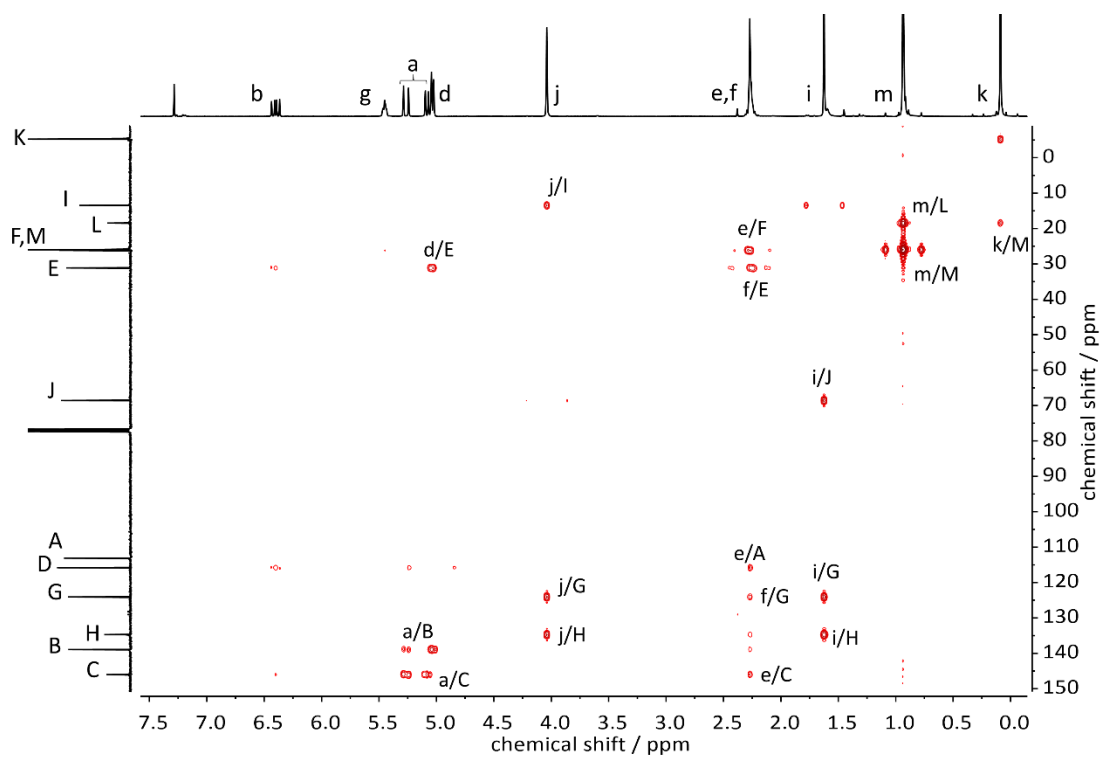


Figure S8. HMBC NMR spectrum (101 MHz / 400 MHz) of MyrOSi in CDCl_3 .

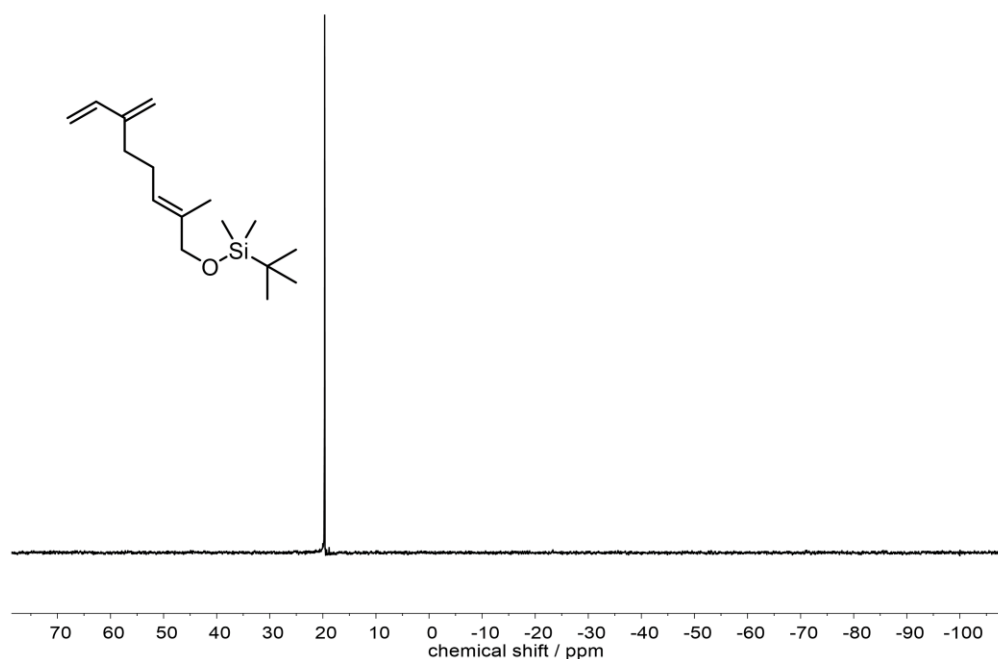


Figure S9. ^{29}Si NMR spectrum (400 MHz) of MyrOSi in CDCl_3 .

2. Homopolymer characterization

2.1 NMR spectra of PMyrOSi and PMyrOH

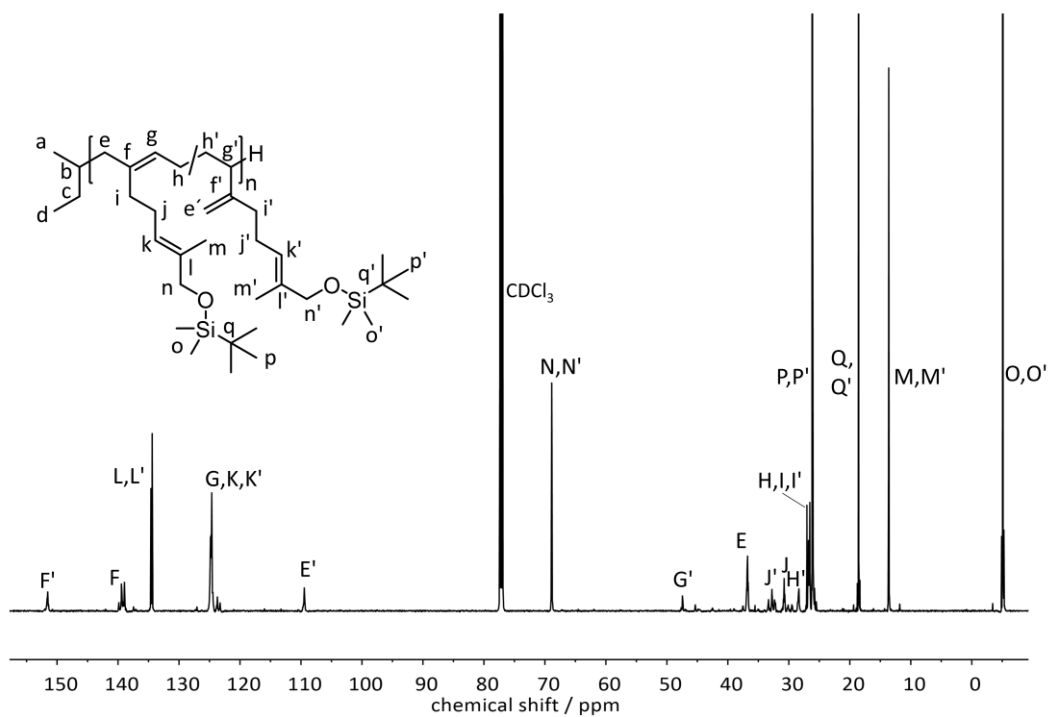


Figure S10. ^{13}C NMR *inverse gated* (IG) spectrum (150 MHz) of PMyrOSi in CDCl_3 .

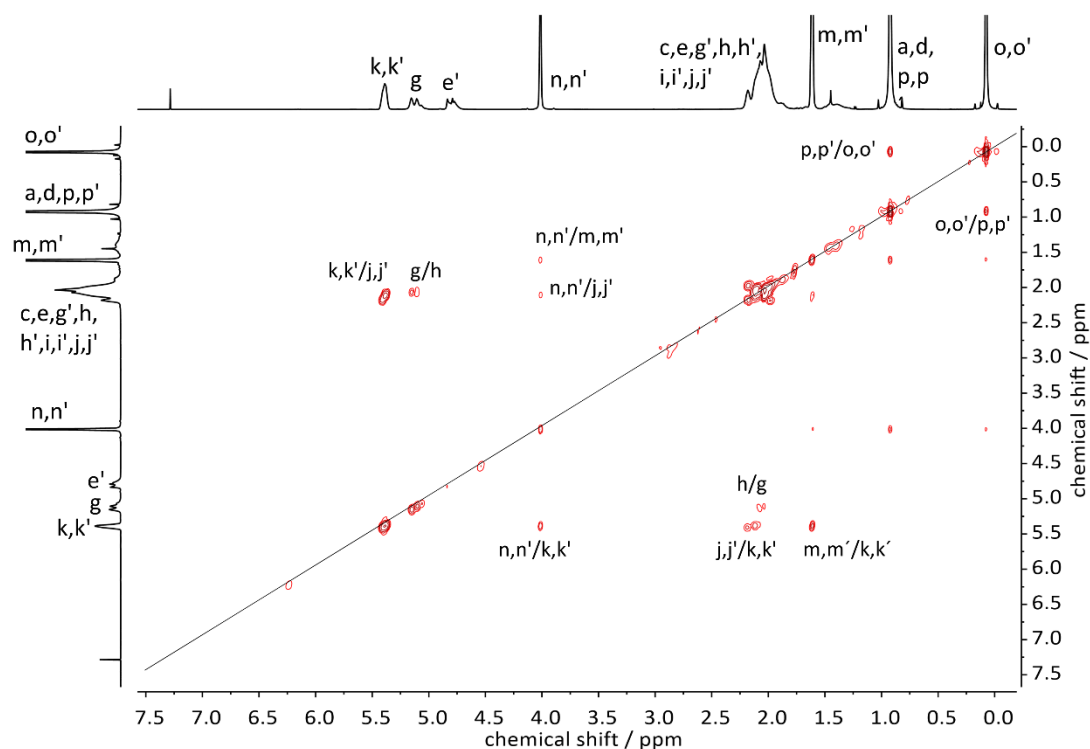


Figure S11. COSY NMR spectrum (600 MHz) of PMyrOSi in CDCl_3 .

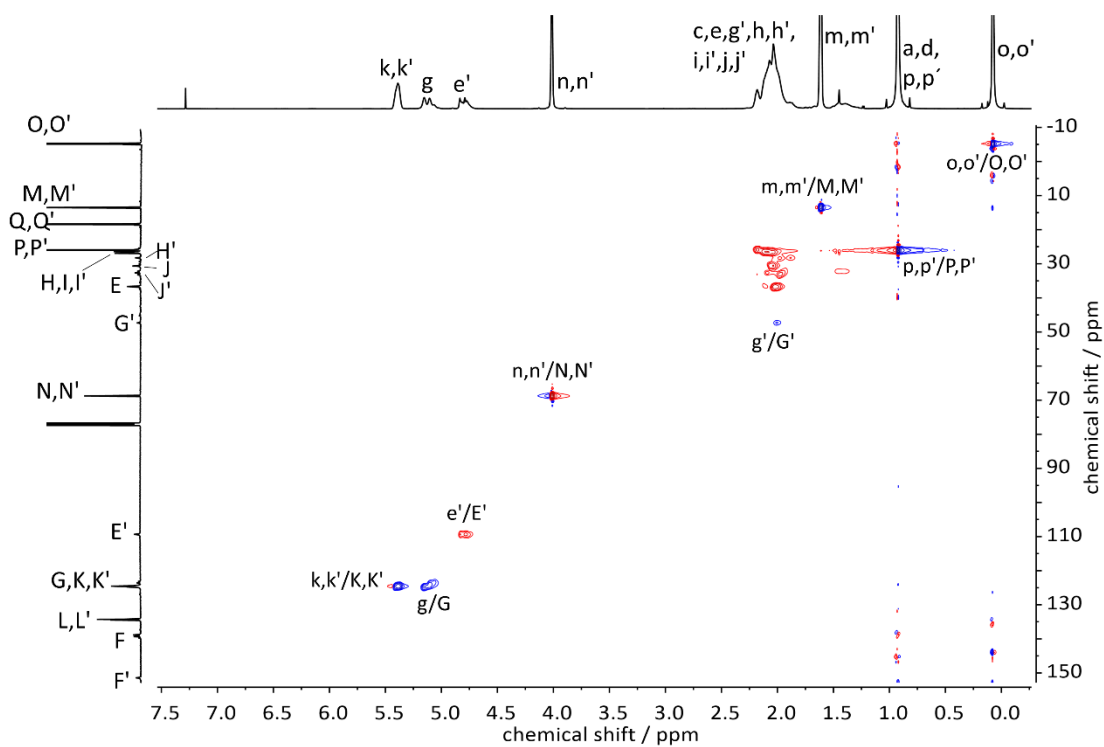


Figure S12. HSQC NMR spectrum (150 MHz / 600 MHz) of PMyrOSi in CDCl_3 .

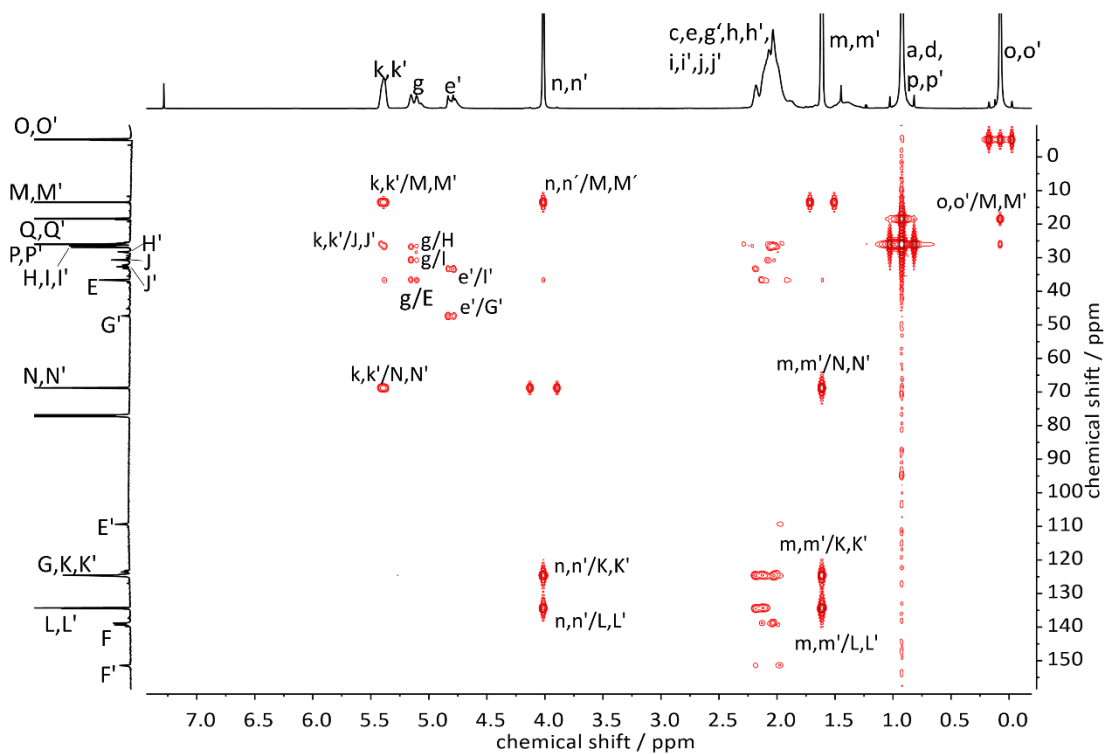


Figure S13. HMBC NMR spectrum (150 MHz / 600 MHz) of PMyOSi in CDCl₃.

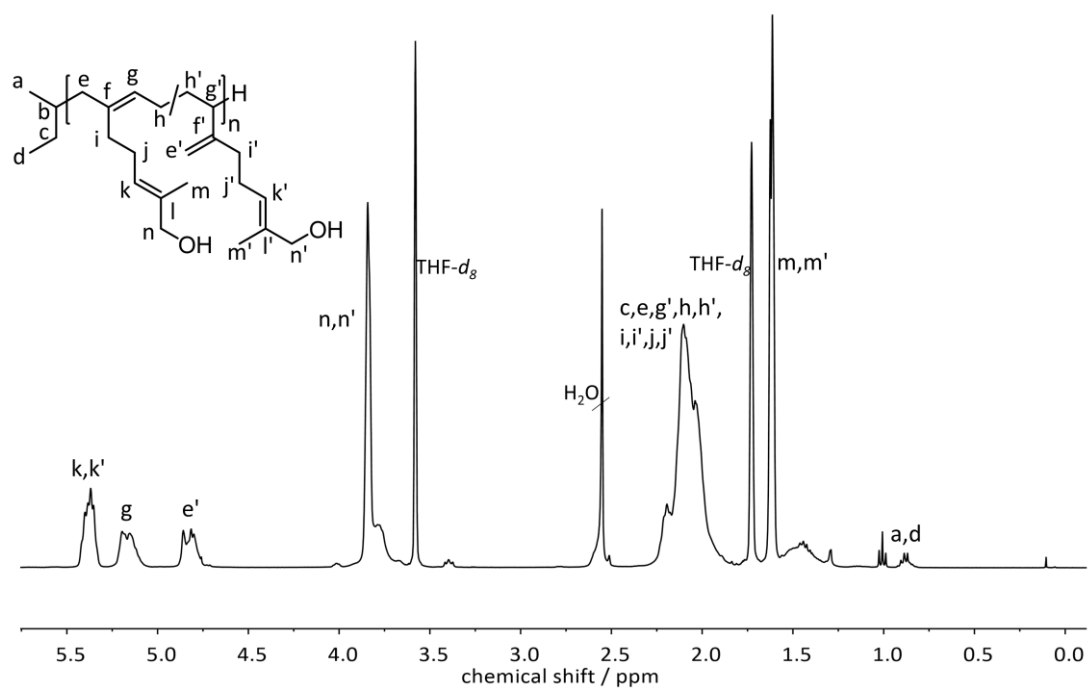


Figure S14. ¹H NMR spectrum (400 MHz) of PMyOH in THF-*d*₈.

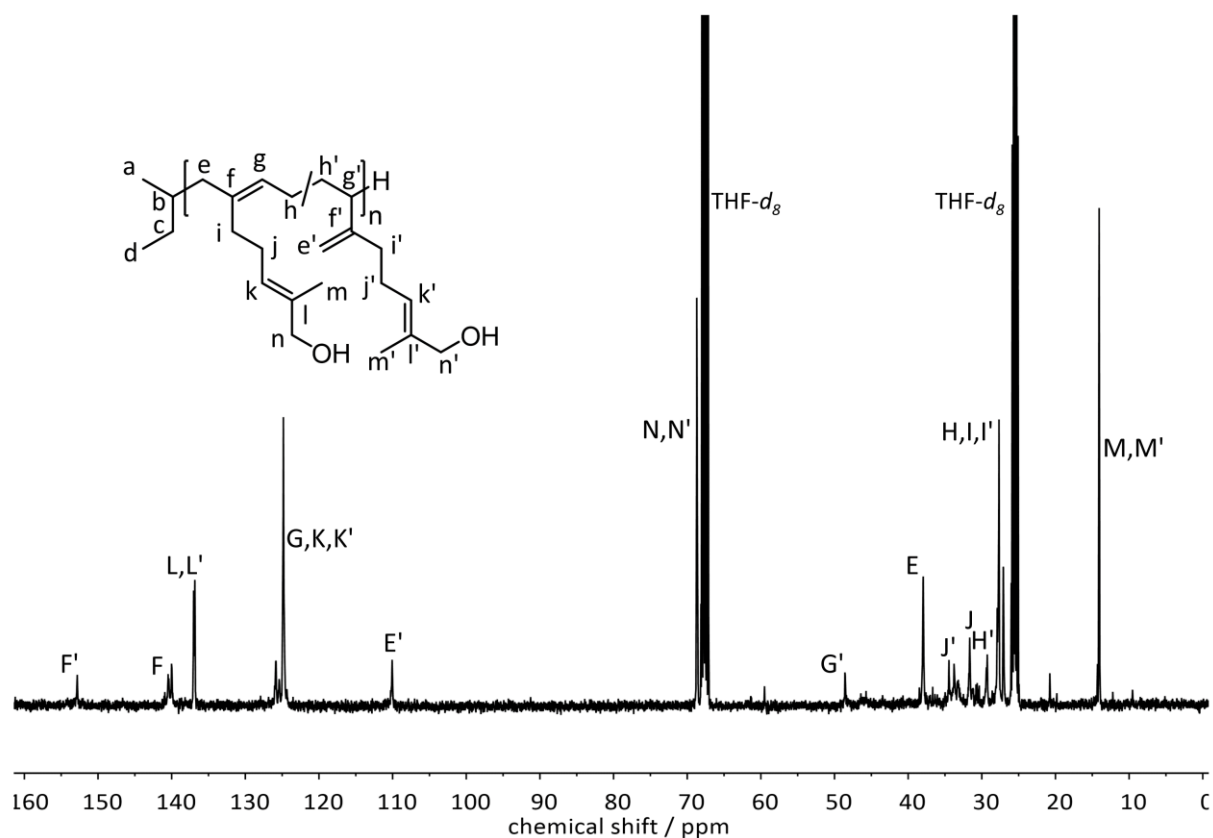


Figure S15. ^{13}C NMR *inverse gated* spectrum (101 MHz) of PMyrOH in $\text{THF-}d_8$.

2.2 Determination of polydiene microstructure of homopolymers (content of 3,4-units)

The content of 3,4-units in the homopolymer backbone was calculated from the integrals (*I*) of the proton signals *e'* and *g* of the ^1H NMR spectrum (Figure S1 or Figure S14) as follows:

$$3,4 \text{ content (\%)} = \frac{\frac{I(e', e''')}{2}}{I(g) + \frac{I(e', e''')}{2}} \quad (\text{S1})$$

2.3 SEC measurements of PMyrOH

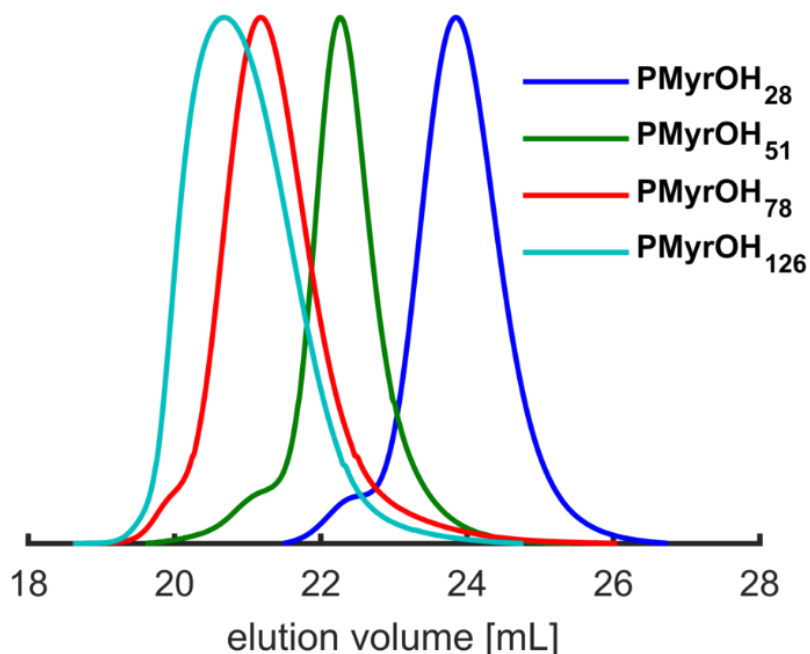


Figure S16. SEC traces (THF, PI standard, RI signal) of PMyrOH homopolymers, after removal of the silyl protective groups.

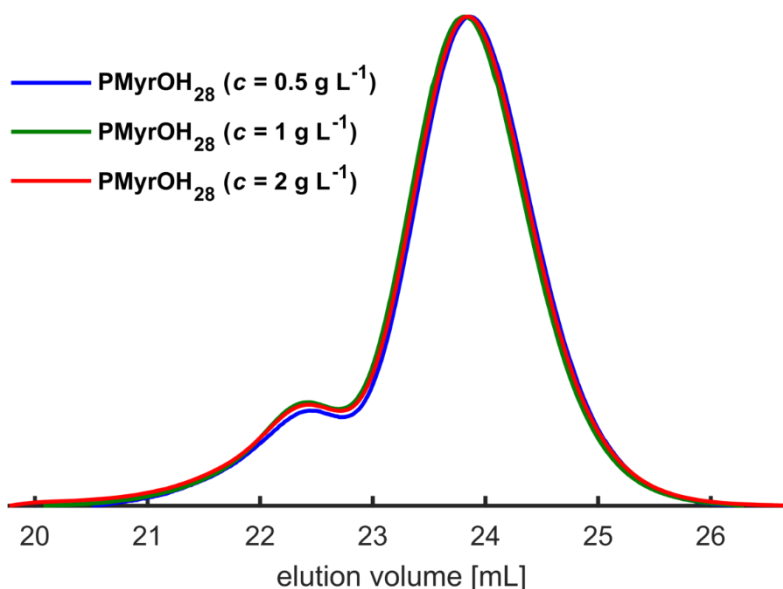


Figure S17. SEC traces (THF, PI standard, RI signal) of PMyrOH₂₈ with different concentrations (normalized to the intensity of the low molecular weight distribution), to investigate the concentration dependency of the high molecular weight distribution. No significant concentration dependency of the SEC diagrams is observable, indicating chain coupling as a cause of the high molecular weight distribution (i.e. aggregation is negligible).

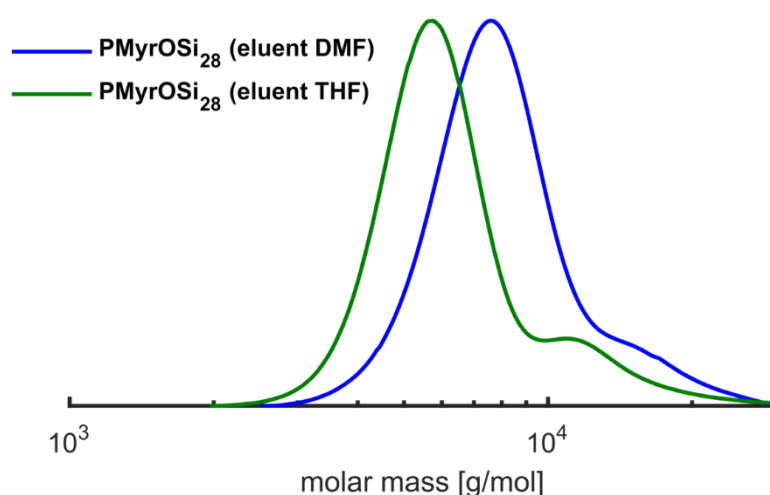


Figure S18. SEC traces in THF (green) and DMF (blue) (PS standards, RI signal) of PMyrOH₂₈ (with equal concentrations of 1 g L⁻¹) to investigate solvent dependency. The high molecular weight distribution appears in THF as well as in DMF, confirming chain coupling as the reason of the high molecular weight distribution (not aggregation). The SEC shift and difference in molecular weight indicates a strong solvent dependency of the hydrodynamic volume.

2.4 IR spectra of PMyrOSi and PMyrOH

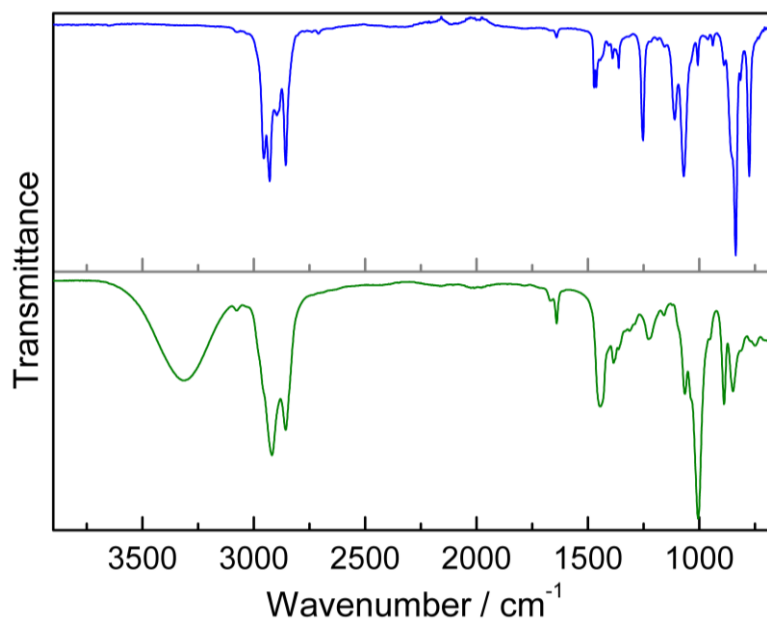
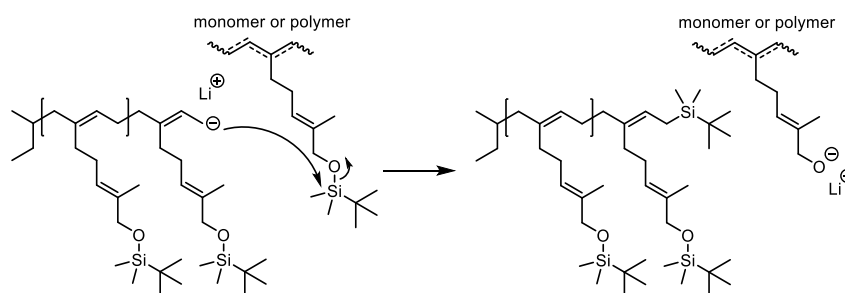


Figure S19. IR spectra of PMyrOSi₅₁ (blue) and the corresponding PMyrOH₅₁ (green), after removal of the protective groups

3 Potential side reaction during polymerization

The increasing dispersity of the homo- and copolymers with increasing molecular weight / degree of polymerization suggests the occurrence of side reactions during the polymerization. Hirao and coworkers reported for TBDMS-protected, hydroxyl group containing styrene derivatives the cleavage of the protective group by a nucleophilic attack of the living carbanionic chain end (as shown in Scheme S1), transferred to the MyrOSi monomer.¹



Scheme S1. Possible Side Reaction During the Anionic Polymerization of MyrOSi.

4 Characterization of copolymers

Table S1. Characterization data of copolymers of β -myrcene and MyrOSi with different monomer ratio and molecular weights.

Sample	MyrOSi content th (mol%)	MyrOSi content ^b (mol%)	[M] ₀ /[I] ₀ th	M_n^{th} (kg mol ⁻¹)	M_n^a (kg mol ⁻¹)	M_n^b (kg mol ⁻¹)	\bar{D}^a
P(Myrc _{0.94} -co-MyrOSi _{0.06}) ₆₃	5	6	73	10.4	8.6	8.4	1.09
P(Myrc _{0.86} -co-MyrOSi _{0.14}) ₄₈	10	14	73	10.8	7.1	5.5	1.07
P(Myrc _{0.73} -co-MyrOSi _{0.27}) ₆₃	25	27	71	12.0	11.8	9.3	1.07
P(Myrc _{0.40} -co-MyrOSi _{0.60}) ₄₇	50	60	69	13.9	8.8	6.4	1.07
P(Myrc _{0.25} -co-MyrOSi _{0.75}) ₅₉	75	75	67	15.8	12.1	6.3	1.09
P(Myrc _{0.89} -co-MyrOSi _{0.11}) ₁₅₇	10	11	145	21.7	22.2	- ^c	1.15
P(Myrc _{0.87} -co-MyrOSi _{0.13}) ₃₃₄	10	13	218	32.5	47.1	- ^c	1.16

^aDetermined by SEC measurements in THF at 25 °C with PI standard. ^bDetermined by ¹H NMR spectra (400 MHz, CDCl₃). ^cMolecular weight too high for end-group analysis.

4.1 ¹H NMR spectra of copolymers

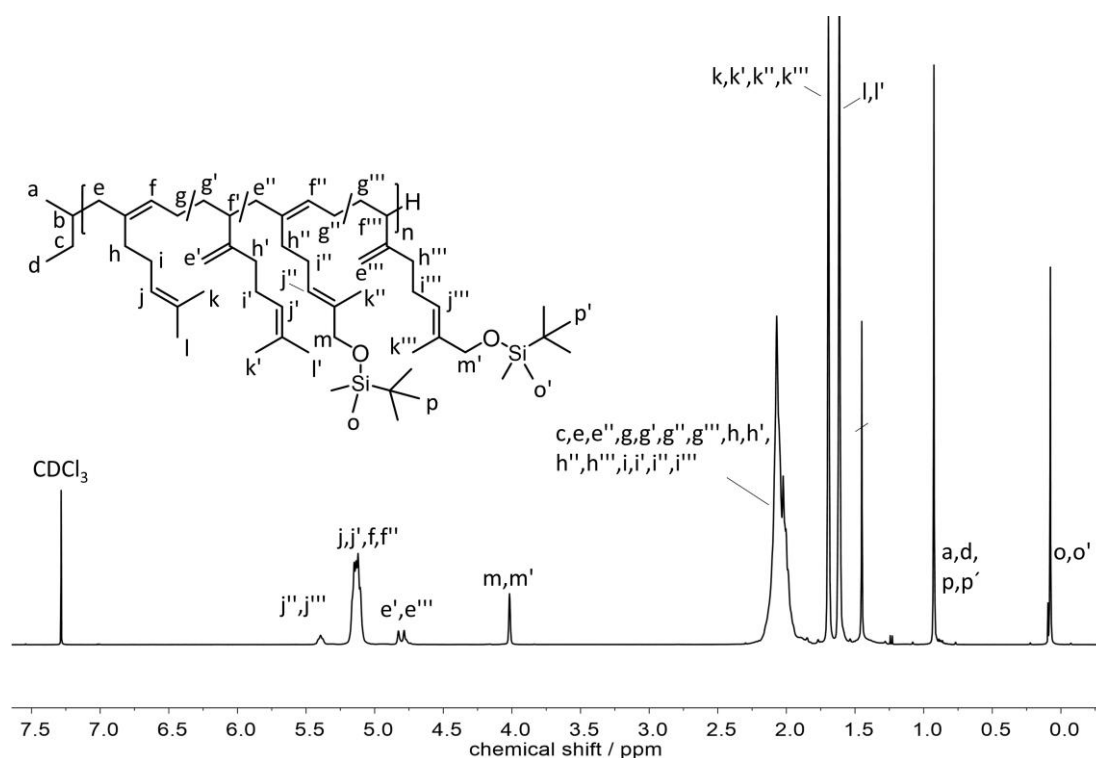


Figure S20. ¹H NMR spectrum (400 MHz) of P(Myrc_{0.89}-co-MyrOSi_{0.11})₁₅₇ in CDCl₃.

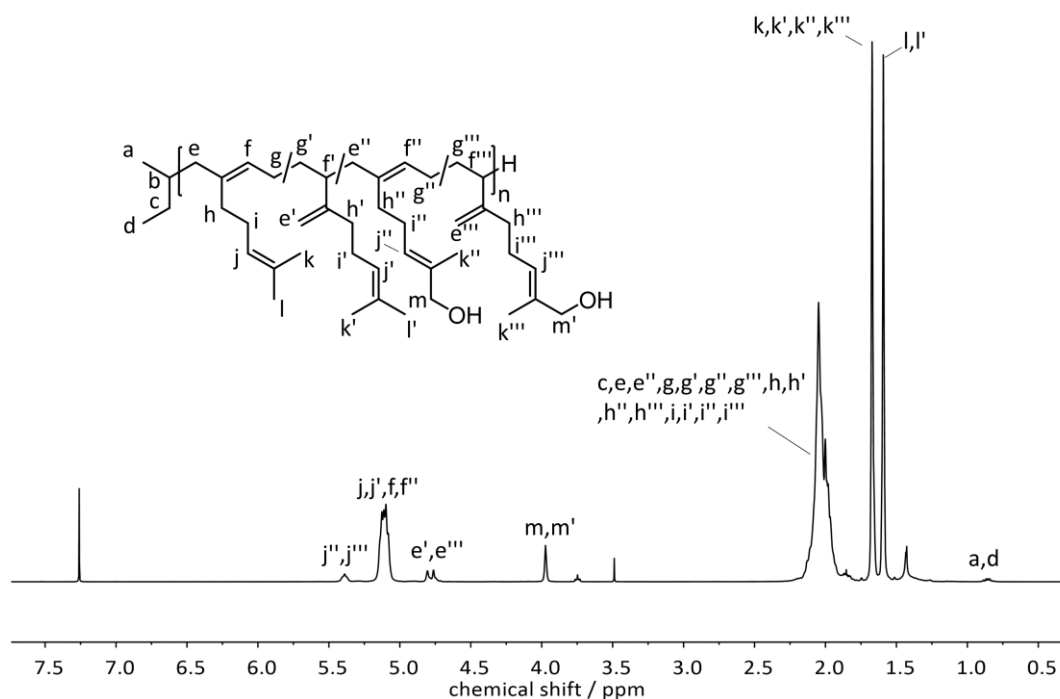


Figure S21. ^1H NMR spectrum (400 MHz) of $\text{P}(\text{Myr}_{0.89}\text{-co-MyrOH}_{0.11})_{157}$ in CDCl_3 .

4.2 SEC results of copolymers

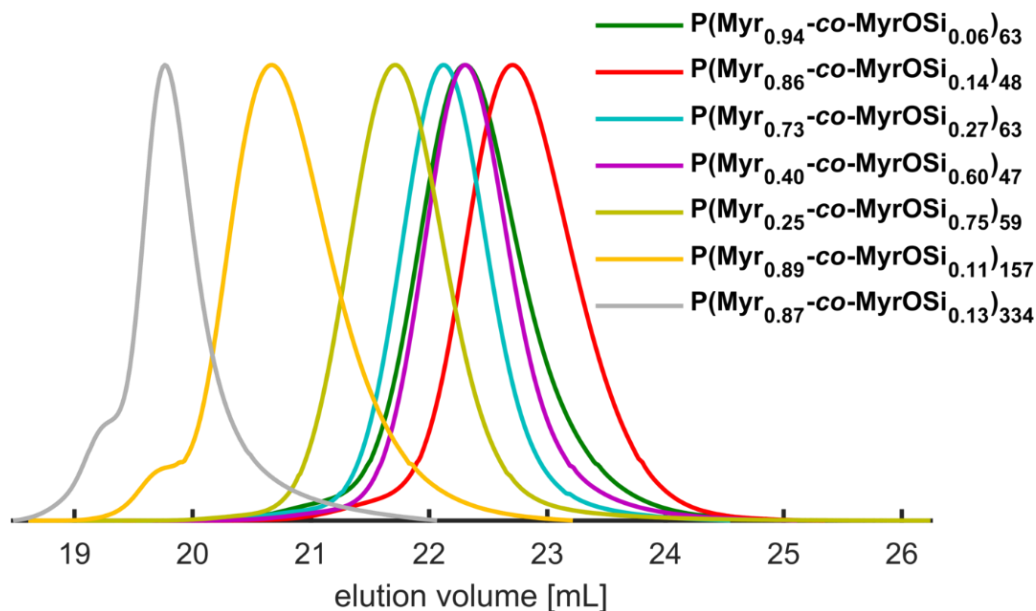


Figure S22. SEC traces (THF, PI standard, RI signal) of statistical copolymers of β -myrcene and MyrOSi with varying monomer composition and molecular weights ($M_n^{\text{th}} = 10, 20$ (orange) and 30 (grey) kg/mol) (color codes corresponding to Figure S22).

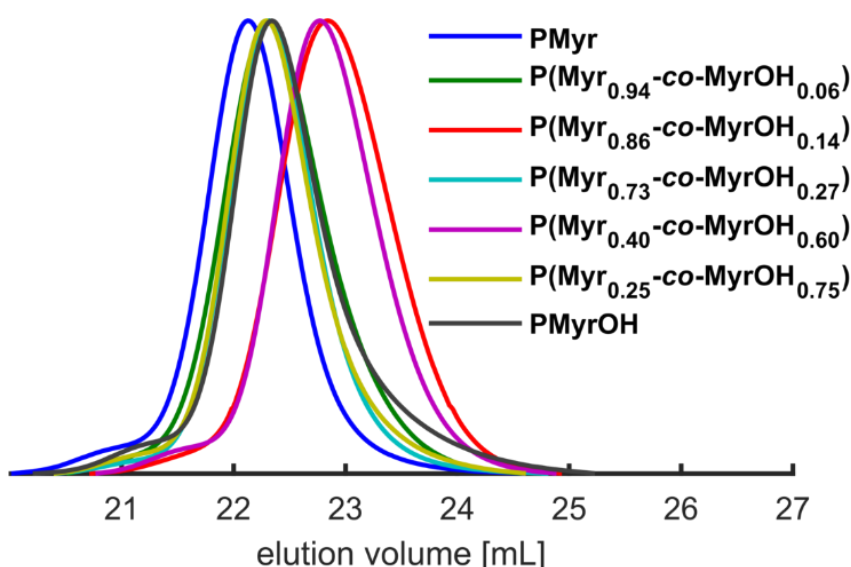


Figure S23. SEC traces (THF, PI standard, RI signal) of statistical (co)polymers of β -myrcene and β -myrcenol after removal of protective group with varied monomer composition ($M_n^{\text{th}} = 10 \text{ kg/mol}$) (color codes corresponding to Figure S21).

4.3 Determination of molecular weight of homo and copolymers by ^1H NMR spectrum

After removal of the protective groups the molecular weights of the homo- and copolymers were calculated by evaluation of the ^1H NMR spectra. Exemplary described for the copolymers, the signal of the six methyl protons of the initiator (signal a,d in Figure S21) was used as a reference, and the molecular weight was determined from the integrals (I) of the protons in the region of the unsaturated double bonds (4.5-5.5 ppm) as follows (Figure S21):

$$M_{n,\text{P(MyrOH)}} = I(k, k') \cdot 152.24 \frac{\text{g}}{\text{mol}} \quad (\text{S2})$$

$$M_{n,\text{Copolymer}} = \frac{I(j'', j''') + I(j, j', f, f') + \frac{I(e', e''')}{2}}{2} \cdot \left(x_{\text{MyrOH}} \cdot 152.24 \frac{\text{g}}{\text{mol}} + (1 - x_{\text{MyrOH}}) \cdot 136.24 \frac{\text{g}}{\text{mol}} \right) \quad (\text{S3})$$

4.4 Determination of copolymer composition

The copolymer composition (molar fraction of myrcenol) was calculated from the integrals (I) of the proton signals e', e''', f, f', j, j', j'', j''' of the ^1H NMR spectrum (Figure S21) as follows:

$$x_{MyrOH} = \frac{I(j'', j''')}{\frac{I(j'', j''') + I(j, j', f, f'') + \frac{I(e', e''')}{2}}{2}} \quad (\text{S4})$$

4.5 Determination of polydiene microstructure of copolymers (content of 3,4-units)

The content of 3,4-units in the copolymer backbone was calculated from the integrals (I) of the proton signals e', e''', f, f', j, j', j'', j''' of the ^1H NMR spectrum (Figure S21) as follows:

$$3,4 \text{ content (\%)} = \frac{\frac{I(e', e''')}{2}}{\frac{I(j'', j''') + I(j, j', f, f'') + \frac{I(e', e''')}{2}}{2}} \cdot 100 \quad (\text{S5})$$

4.6 DSC measurements of copolymers

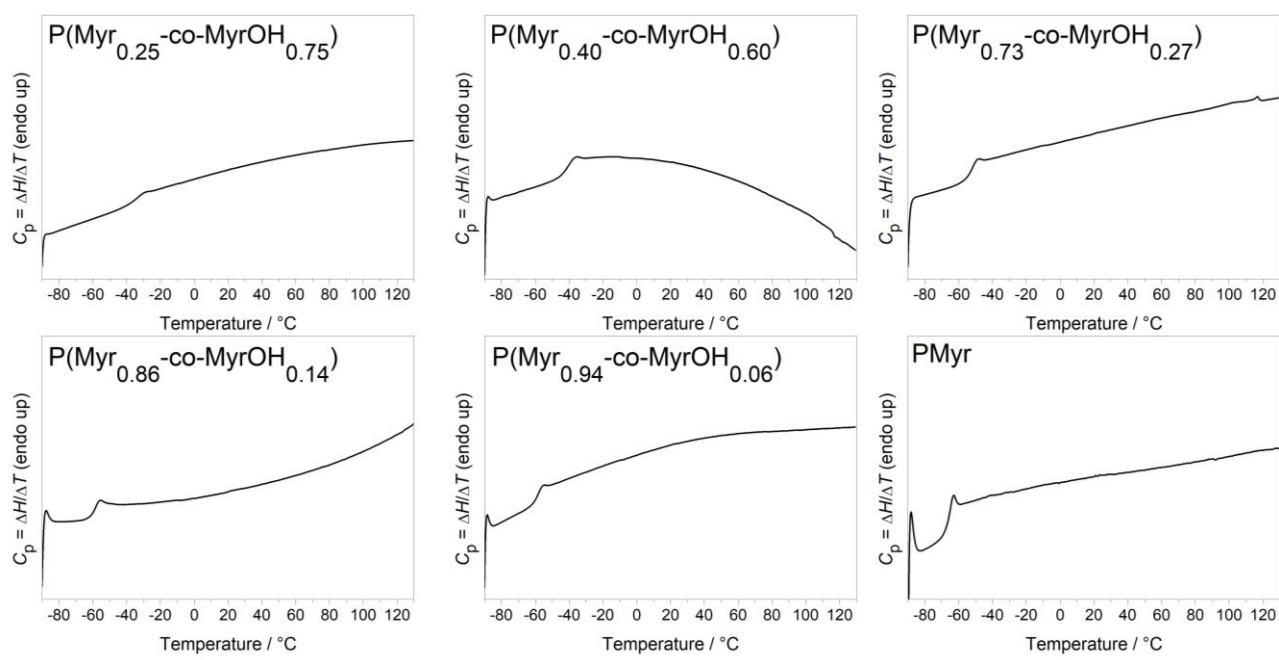


Figure S24. DSC-Curves of statistical (co)polymers of β -myrcene and β -myrcenol (second heating curves, heating and cooling rate of 10 K min^{-1}) with monomer composition varied from 0 to 75 mol% of incorporated MyrcOH (DSC curve of 100 mol% MyrcOH is shown in Figure S19) ($M_n^{\text{th}} = 10 \text{ kg/mol}$).

4.7 Fox equation

The Fox equation (eq 1) was used for evaluation of the plotted glass-transition temperatures vs the incorporated weight fraction of β -myrcene in the polymer backbone, shown in Figure S25.² For copolymers with randomly distributed monomer sequence, the glass-transition temperature depends on the weight fraction of the incorporated monomer in a linear fashion and can be predicted by the T_g s of the homopolymers. The single glass-transition temperature of the copolymer will be consequently between the T_g s of the homopolymers.³

$$\frac{1}{T_g} = \frac{w_1}{T_{g1}} + \frac{w_2}{T_{g2}} \quad (\text{S6})$$

In Figure S26 the literature known linear dependency of the glass-transition temperature with the amount of 3,4 units is shown.⁴

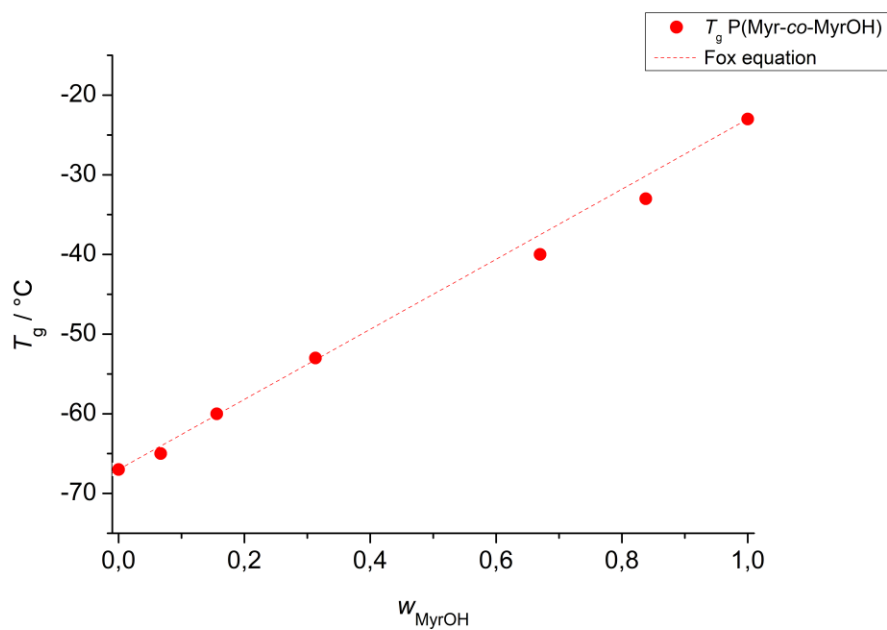


Figure S25. Glass-transition temperature (T_g) plotted vs weight fraction of incorporated MyrOH (w_{MyrOH}) and plotted line of Fox equation (dashed line).

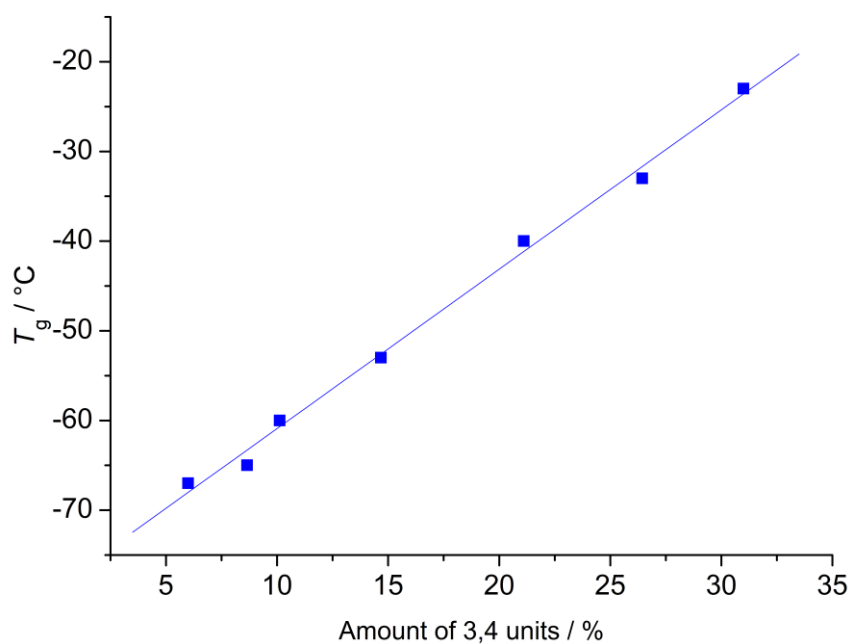


Figure S26. Glass-transition temperature (T_g) plotted vs amount of 3,4 units in the polydiene backbone and linear fit (blue line).

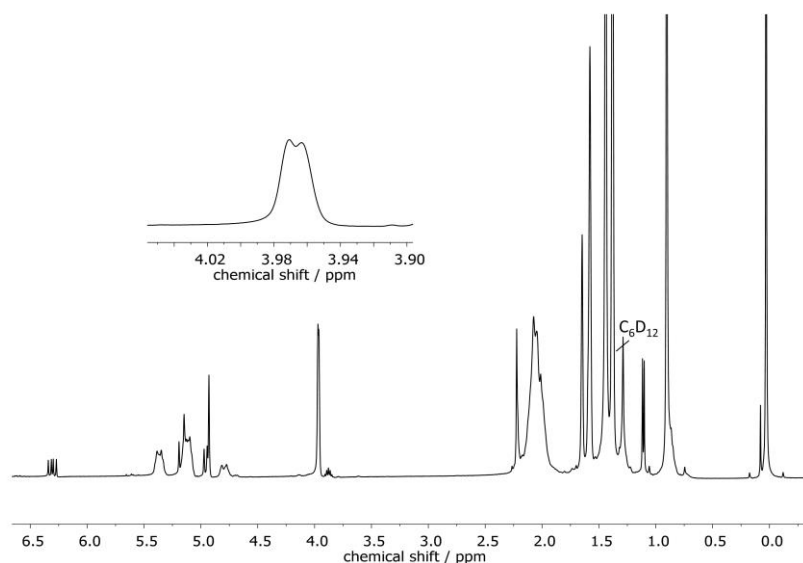
4.8 ^1H NMR copolymerization kinetic experiment

Figure S27. ^1H NMR (400 MHz, C_6D_{12}) spectrum of a mixture of MyrOSi and PMyrOSi, showing an overlap of the signals of the monomer mixture, which prohibits *in situ* ^1H NMR kinetic experiments of the copolymerization.

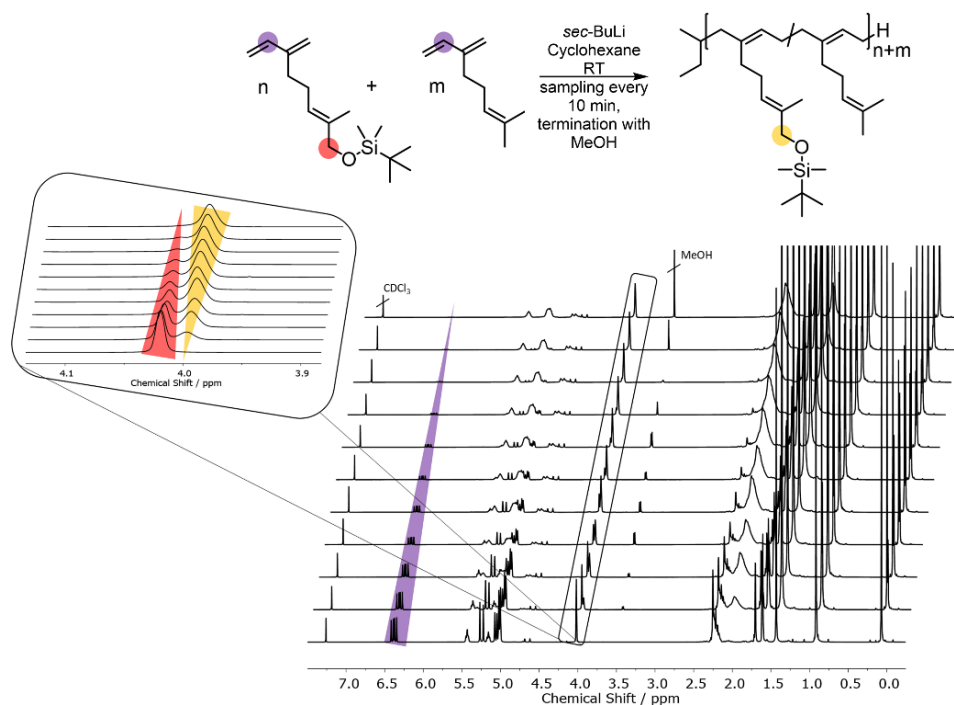


Figure S28. Stacked ^1H NMR spectra (400 MHz, CDCl_3) of the NMR kinetic experiment of the copolymerization of β -myrcene and β -myrcenol at 23 $^\circ\text{C}$, (spectrum every 10 min, conversion of MyrOSi followed by the red colored signal, total monomer conversion followed by decrease of the purple signal)

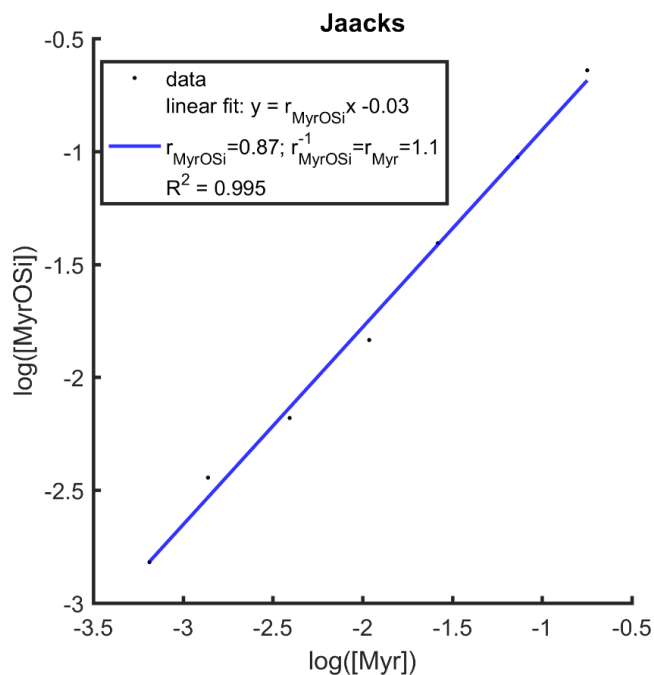


Figure S29. Jaacks fit⁵ of the copolymerization of Myr and MyrOSi.

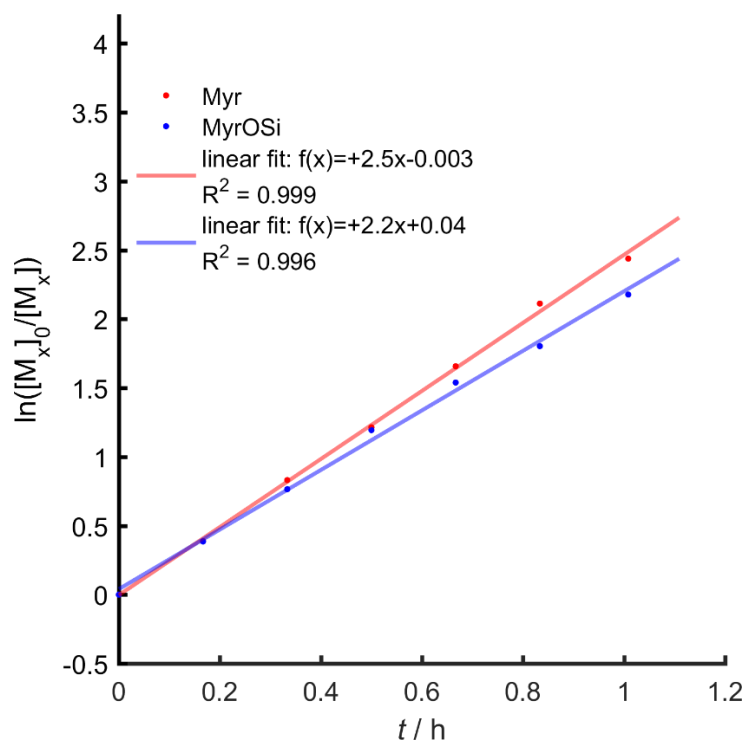


Figure S30. Pseudo first order time-conversion plot of the copolymerization of Myr and MyrOSi.

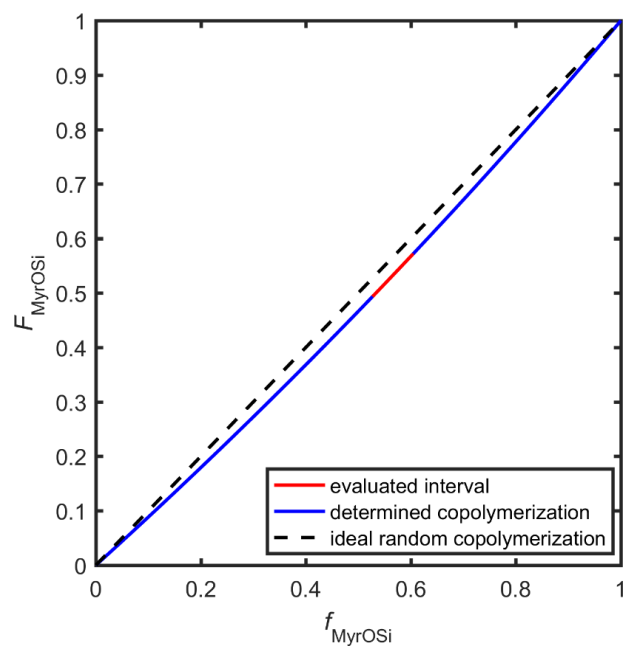


Figure S31. Copolymerization diagram of β -myrcene and MyrOSi obtained from ^1H NMR kinetic studies.

Under the conditions of the living anionic polymerization, the total conversion X is a linear function of the degree of polymerization (P_n), with the constant factor of the initiator concentration $[\text{I}]_0$ and total initial monomer concentration $[\text{M}]_0$.^{6,7} In this case the total conversion X can be interchanged with the normalized chain length, as shown in eq 5.

$$\begin{aligned}
 P_n &= \frac{[\text{M}]_0 - [\text{M}]}{[\text{I}]_0} \\
 X &= \frac{[\text{M}]_0 - [\text{M}]}{[\text{M}]_0} = \frac{[\text{I}]_0}{[\text{M}]_0} P_n
 \end{aligned}
 \tag{S7}$$

5 Characterization of PMyr-graft-PLLA graft copolymers

5.1 ^1H NMR spectrum of PMyr-graft-PLLA

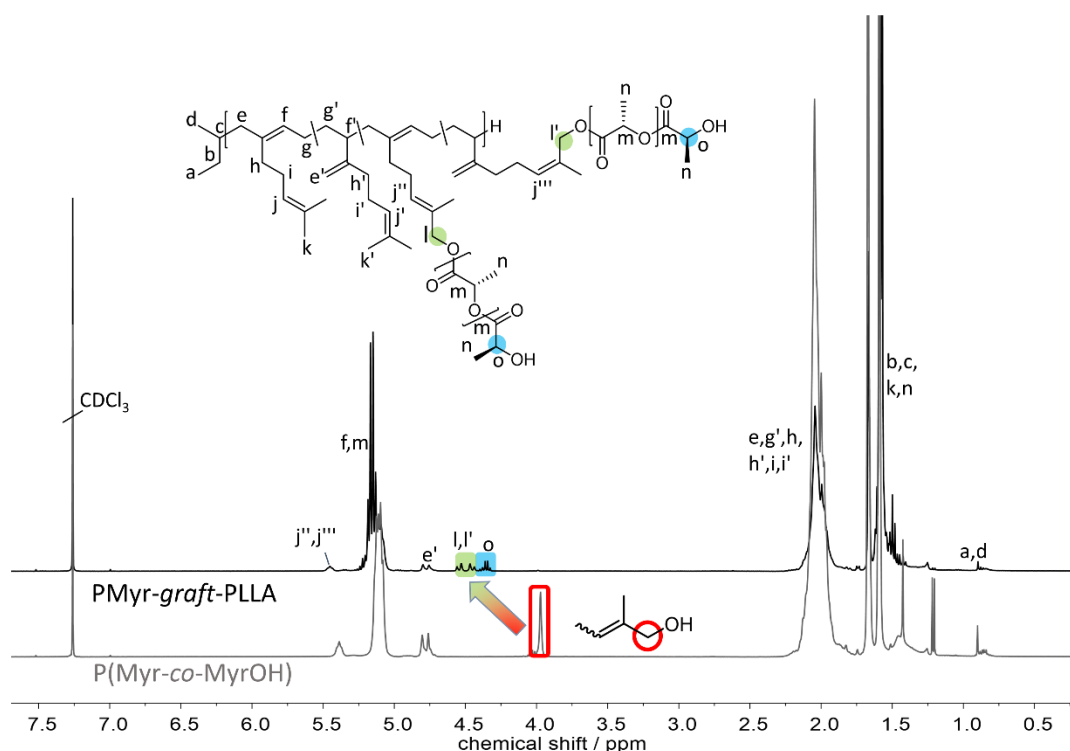


Figure S32: ^1H NMR spectra (400 MHz, CDCl_3) of the copolymer precursor $\text{P}(\text{Myr}_{0.89}\text{-co-MyrOH}_{0.11})$ (grey) and the corresponding graft copolymer $\text{PMyr}_{0.35}\text{-graft-PLLA}_{0.65}$ (black) with signal assignment.

5.2 Determination of polymer composition of PMyr-graft-PLLA

For the determination of the incorporated monomer ratio of the PMyr-graft-PLLA copolymers, the molar fraction of incorporated β -myrcenol (x_{MyrOH}), determined from the corresponding spectrum of $\text{P}(\text{Myr-co-MyrOH})$ (grey spectrum in Figure S32), of the precursor copolymer was used.

$$I(m) = I(f, j, j', m) - \left(2 \frac{I(j'', j''')}{x_{\text{MyrOH}}} - I(j'', j''') - \frac{I(e')}{2} \right) \quad (\text{S8})$$

$$x_{\text{LLA}} = \frac{I(m)}{I(j'', j''') + \left(I(f, j, j', m) - I(m) \right) + \frac{I(e', e)}{2} + I(m)} \quad (\text{S9})$$

5.3 DSC measurements of PMyr-graft-PLLA

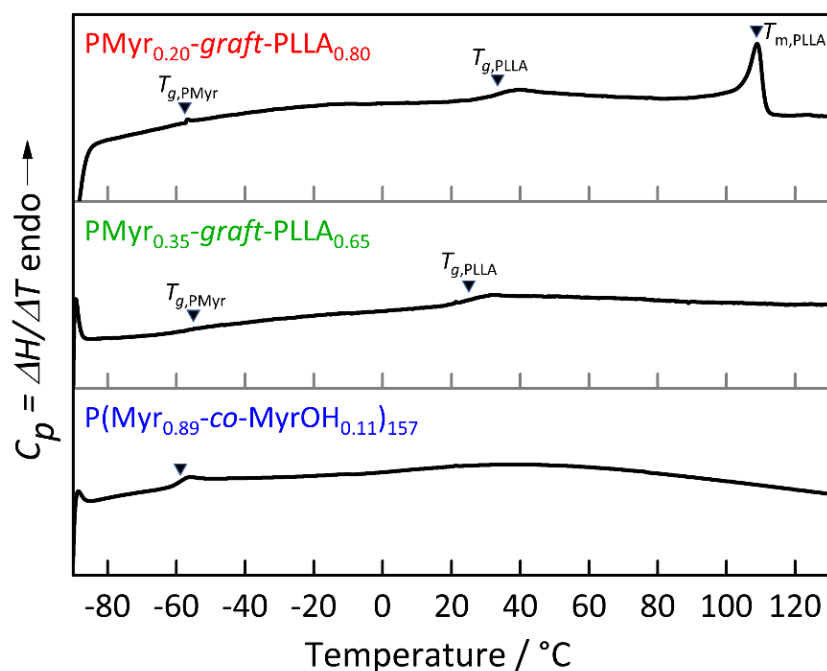


Figure S33. DSC curves (second heating curves, heating and cooling rate of 5 K min^{-1}) of the lactide graft copolymers and the corresponding macroinitiator (color codes corresponding to Figure 9).

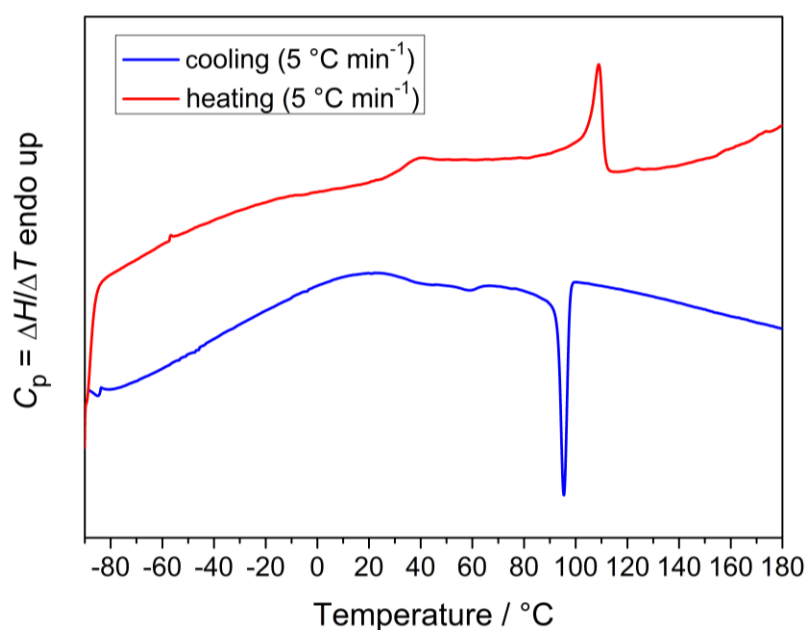


Figure S34. DSC cooling (blue) and heating (red) curves of $\text{PMyr}_{0.20}\text{-graft-PLLA}_{0.80}$ (second cycle with heating and cooling rates of 5 K min^{-1}).

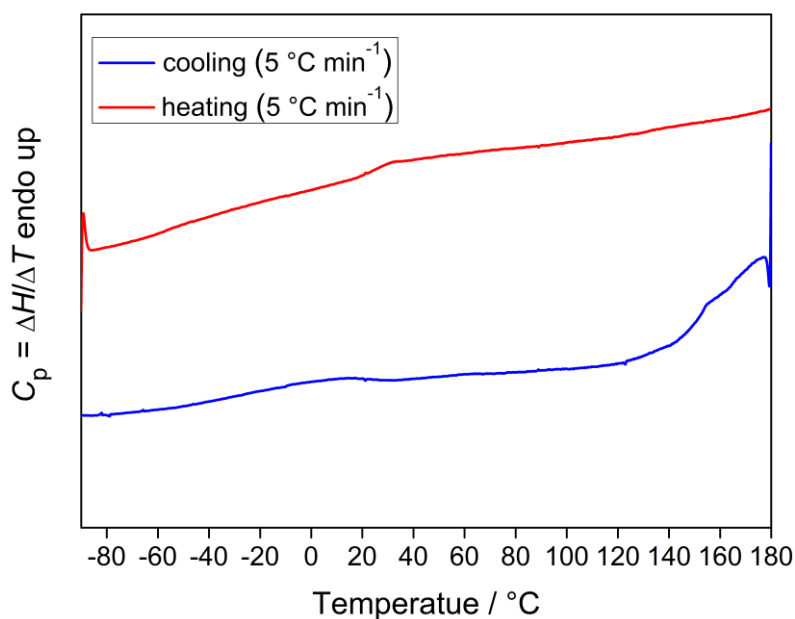


Figure S35. DSC cooling (blue) and heating (red) curves of PMyr_{0.35}-*graft*-PLLA_{0.65} (second cycle with heating and cooling rates of 5 K min⁻¹).

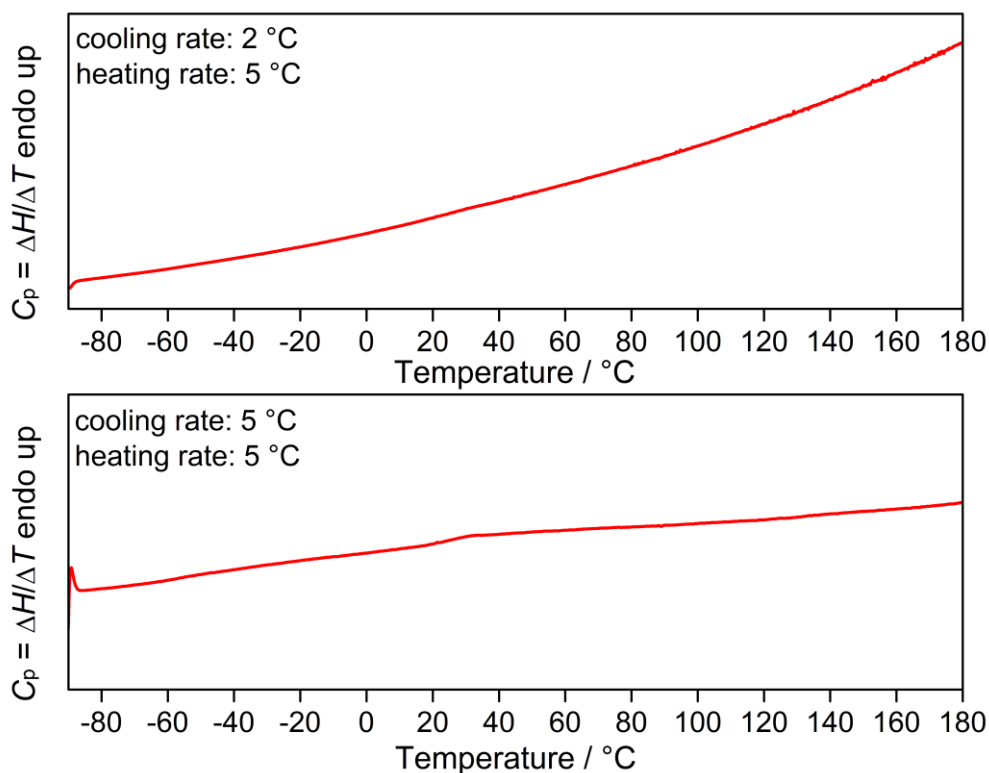


Figure S 36. DSC curves of PMyr_{0.35}-*graft*-PLLA_{0.65} (second heating curves, heating rate 5K/min) with varying cooling rates (2 °C (up) and 5 °C (bottom)).

References

- (1) Hirao, A.; Kitamura, K.; Takenaka, K.; Nakahama, S. Protection and polymerization of functional monomers. 18. Syntheses of well-defined poly(vinylphenol), poly[(vinylphenyl)methanol], and poly[2-vinylphenyl]ethanol] by means of anionic living polymerization of styrene derivatives containing tert-butyldimethylsilyl ethers. *Macromolecules* **1993**, *26*, 4995–5003.
- (2) Fox, T. G. Influence of Diluent and of Copolymer Composition on the Glass Temperature of a Polymer System. *Bull. Am. Phys. Soc.*, **1956**, 123.
- (3) Sarkar, P.; Bhowmick, A. K. Terpene Based Sustainable Elastomer for Low Rolling Resistance and Improved Wet Grip Application: Synthesis, Characterization and Properties of Poly(styrene- co -myrcene). *ACS Sustain. Chem. Eng.* **2016**, *4*, 5462–5474.
- (4) Lal, J.; Mark, J. E. *Advances in Elastomers and Rubber Elasticity*; Springer US, 2013.
- (5) Jaacks, V. A novel method of determination of reactivity ratios in binary and ternary copolymerizations. *Macromol. Chem. Phys.* **1972**, *161*, 161–172.
- (6) Waack, R.; Rembaum, A.; Coombes, J. D.; Szwarc, M. Molecular Weights of “Living” Polymers *J. Am. Chem. Soc.* **1957**, *79*, 2026–2027.
- (7) Webster, O. W. Living polymerization methods. *Science* **1991**, *251*, 887–893.

CHAPTER 3

Influence of Silyl Protective Groups on Polymyrcenol Microstructure

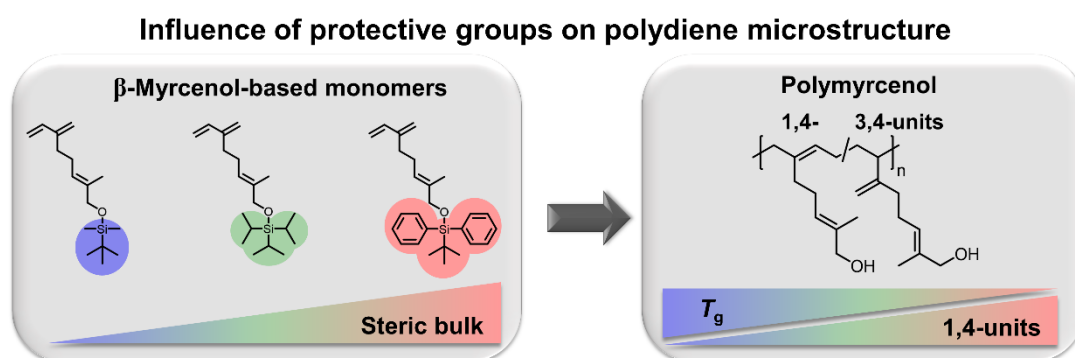
CHAPTER 3

Protective Groups Make the Difference: Influence of Silyl Protective Groups on the Polydiene Microstructure of Polymyrcenol

Christian Wahlen,^a Christopher P. Ender^a and Holger Frey^{*,a}

^aDepartment of Chemistry, Johannes Gutenberg University, Duesbergweg 10-14, 55128 Mainz, Germany

To be submitted.



Abstract

Two novel β -myrcenol-based diene monomers carrying different silyl-protective groups, triisopropylsilyl (TIPS) and *tert*-butyldiphenylsilyl (TBDPh) groups, are introduced for carbanionic polymerization. The *sec*-butyllithium initiated polymerization of the monomers in cyclohexane resulted in homopolymers with molecular weights in the range of 12.8 to 24.0 kg mol⁻¹ and dispersities between 1.12 and 1.41. The removal of the silyl protective groups can be achieved under mild conditions, using tetra-*n*-butylammonium fluoride (TBAF), and results in well-defined polymyrcenol. The polymers were characterized by ¹H NMR spectroscopy, size exclusion chromatography (SEC) and differential scanning calorimetry (DSC). The monomers were found to act as “self-modifier” of the polydiene microstructure. The amount of 3,4-units in the polydiene backbone was found to be dependent on the type of silyl group. The 3,4-unit content decreases in the following order TBDMS < TIPS < TBDPhS, which correlates directly with the increasing steric bulk of the respective protective groups. The T_g of the corresponding polymyrcenol increases expectedly with increasing 3,4-vinyl content. The increased content of 1,4-units, in comparison to the so far published *tert*-butyldimethylsilyl (TBDMS) protected polymyrcenol, renders the polymyrcenol building blocks interesting candidates for bio-based thermoplastic elastomers.

Introduction

The living anionic polymerization of 1,3-diene monomers is highly relevant for the synthesis of elastomers. Unique control over the polydiene microstructure enables the synthesis of polydienes with high 1,4-stereoregularity. Due to their similarity to natural rubber (*cis*-1,4-polyisoprene), which accounts for around 46 % of the total worldwide rubber consumption, there is a large demand for synthetic and bio-based 1,3-diene monomers.¹ Besides the common fossil feedstock-based monomers (butadiene and isoprene), there is an increasing number of biomass-derived alternatives, such as β -myrcene and β -farnesene.^{2,3} These renewable monomers enable the synthesis of bio-based thermoplastic elastomers (TPEs), which potentially substitute fossil source-based TPEs, for instance polystyrene-*block*-polyisoprene-*block*-polystyrene triblock copolymers (SBS).⁴⁻⁶ In general, the polymerization of 1,3-dienes results in an inhomogeneous microstructure, consisting of *cis*-1,4-, *trans*-1,4-, 3,4- and 1,2-units.⁷ Since the glass transition temperature as well as the elastic properties strongly depend on the polydiene microstructure, there are numerous studies focusing on the control of the microstructure.⁸⁻¹⁸ In the living anionic polymerization, the polydiene microstructure is influenced by temperature, polarity of the solvent, polar additives (modifier), concentration and the pendant moiety.^{19,20}

The accessibility of functional 1,3-diene monomers is limited due to synthetic difficulties, caused by the susceptibility of the diene-moiety to side reaction, in particular the Diels-Alder reaction.²⁰ Terpenes like β -myrcene and β -farnesene are potentially convenient synthons for the synthesis of functional 1,3-diene monomers. However, the regiospecific functionalization of the double bond of the isopropylidene side chain is a non-trivial objective, as reported in several works.²¹⁻²⁴ Nevertheless, some silyl- and amine-functionalized diene-monomers, suitable for carbanionic polymerization, have been reported so far. In this context, an effect of the functional groups on the polydiene microstructure was observed, i.e. an increased vinyl-content (1,2- and 3,4-units).²⁵⁻²⁷ Stadler et al. described the effect of the bulkiness of the alkyl moieties of 5-(*N,N*-dialkylamino)isoprenes on the polydiene microstructure.²⁵ The alkyl substituents influence the ratio of *cis*- and *trans*-1,4 units formed during the anionic polymerization in apolar solvents (benzene), while the fraction of 3,4-units is comparatively small (< 12 %). The modifier effect of the amino-based isoprene monomers on the polydiene

microstructure is significantly weaker than of the corresponding common polar modifier tetramethylethylenediamine (TMEDA) or triethylamine (TEA).²⁵

However, the influence of protective groups has rarely been investigated in literature. In general, protective groups are necessary for the carbanionic polymerization of most functional monomers to prevent proton abstraction of the functional group by the living carbanionic chain end.²⁸ Silyl groups are well-established protective groups for hydroxyl moieties in the field of carbanionic polymerization. The stability of the silyl ether bond of the protected monomer is determined by the steric bulk of the silyl group.²⁹ In several approaches the steric bulk of protective groups was exploited to adjust the stereochemistry of the resulting polymers. In free radical and RAFT copolymerization the tacticity of poly(methacrylic acid) (PMMA) was adjusted by the steric bulk of various silyl-protective groups, resulting in syndiotactic, atactic or highly isotactic PMMA.³⁰ Another work by Kamigaito et. al. investigated the influence of silyl groups on the tacticity of bio-based vinyl catechol monomers in living anionic polymerization.³¹

The influence of the protective group structure on the (co)polymerization behavior of functional monomers was also investigated in a previous work of our group.³² The living anionic copolymerization of styrene and protected vinyl catechol monomers results in different gradient copolymer compositions, depending on the length of the pendant alkyl chains of the acetal protective group. Accordingly, the approach of protective group-controlled monomer sequence enables unique control over the copolymer gradient.³²

In recent works, Liu et al. demonstrated the influence of a silyl-protected hydroxyl functionalized alkyllithium initiator on the microstructure of polybutadiene.^{33,34} The authors illustrated the increasing content of 1,4-units with increasing steric bulk of the protective group of the functional initiator. With increasing steric bulk of the protective group (TMS < TBDMS < TIPS) of the hydroxyl propyllithium initiator, the content of 1,4-units increased from 79 to 91 %.³⁴

Recently, we presented the first silyl-protected hydroxyl functionalized 1,3-diene monomer for living carbanionic polymerization, based on the terpenoid β -myrcenol.³⁵ The polymerization and subsequent deprotection results in polymyrcenol with an increased content of 3,4-units (31 %) in contrast to polymyrcene (only 6% of 3,4-units), polymerized under the same conditions in cyclohexane.³⁵ The difference in microstructure is attributed to the “self-modifier” effect, caused by the polar silyl-

protected hydroxyl group in the alkenyl side chain. The protected hydroxyl group enables coordination of the lithium ions at the living chain ends by the monomer. Similar effects occur for polar additives like tetrahydrofuran (THF), TMEDA, TEA and ethyl tetrahydrofurfuryl ether (ETE), which act as a modifier during the (co)polymerization.^{17,18,36–38} In this work we expand the investigation of the effect of the steric bulk of the silyl protective groups on the polydiene microstructure, by varying the silyl protective groups of the β -myrcenol-based monomer.

Experimental Section

Reagents. β -Myrcene ($\geq 95\%$), selenium dioxide, salicylic acid, triisopropylsilyl chloride (TIPSCl), and tetrabutylammonium fluoride, as a 1 M solution in THF, were purchased from Sigma Aldrich. *Tert*-butyldimethylsilyl chloride (TBDMSCl) was received from Carbolution Chemicals GmbH. *Tert*-butyldiphenylsilyl chloride (TBDPhCl) was acquired from Alfa Aesar. *Tert*-butyl hydroperoxide (TBHP, 70% solution in H₂O), *sec*-butyllithium as a 1.3 M solution in cyclohexane/hexane (92/8), imidazole and calcium hydride were purchased from Acros Organics. Dichloromethane and cyclohexane were acquired from Fisher Scientific. Chloroform-*d*₁ and tetrahydrofuran-*d*₈ were received from Deutero GmbH. Cyclohexane was dried using *sec*-butyllithium and 1,1-diphenylethylene (DPE) as an indicator (the *sec*-BuLi-DPE-anion shows red color).

Instrumentation. SEC measurements were performed in THF as the mobile phase (flow rate 1 mL min⁻¹) on an SDV column set from PSS (SDV 10³, SDV 10⁵, SDV 10⁶) and a RI detector. Calibration was carried out by using PI standards, provided by PSS Polymer Standard Service GmbH. NMR spectra were recorded on a Bruker Avance II 400 spectrometer with 400 MHz (¹H NMR) or 101 MHz (¹³C NMR). All spectra are referenced internally to the residual proton signals of the deuterated solvent. The thermal properties of the polymers were studied with a Q2000 (TA Instruments) differential scanning calorimeter (DSC). Two cooling and heating cycles were performed with a rate of 10 K min⁻¹ in a temperature range between -90 °C and 100 °C. The glass transition temperatures (*T*_g) were determined from the second cycle.

Monomer Synthesis. *2-Methyl-6-methylideneocta-2,7-dienol* (β -Myrcenol, *MyrOH*). 402 mL of *tert*-butyl hydroperoxide solution (70% in water, 2.9 mol, 4.0 equiv) was added dropwise to a stirred solution of 2.44 g (22.0 mmol, 0.03 equiv) of selenium dioxide and 10.12 g (73.3 mmol, 0.1 equiv) of salicylic acid in 660 mL dichloromethane. After 15 min

of vigorous stirring, 99.8 g (732 mmol, 1 equiv) of β -myrcene was added dropwise at 0 °C, and the solution was stirred for 48 h under an argon atmosphere. The solution was diluted with benzene and concentrated under vacuum. The residue was diluted with diethyl ether and washed twice with an aqueous NaOH solution (10%) and subsequently with a Brine solution. The organic layer was dried over MgSO₄ and the solvent was evaporated. After column chromatography (silica, *n*-hexane/ethyl acetate (4/1), R_f = 0.25) 22.3 g (147 mmol) of pure β -myrcenol were obtained (yield = 20%). ¹H NMR (400 MHz, CDCl₃): δ (ppm) = 6.38 (dd, 17.6, 10.8 Hz, 1H, CH=CH₂), 5.44 (m, 1H, CH=C), 5.24 (d, 17.6 Hz, 1H, CH₂=CH), 5.06 (d, 1H, CH₂=CH), 5.02 (s, 1H, CH₂=C), 5.00 (s, 1H, CH₂=C), 4.00 (s, 2H, CH₂-OH), 2.31 – 2.15 (m, 4H, CH₂-CH₂), 1.67 (s, 3H, CH₃-C). ¹H and ¹³C NMR spectra are attached to the Supporting Information (Figures S1 and S2).

(*Tert*-butyldimethylsiloxy)-2-methyl-6-methylideneocta-2,7-diene (*MyrOSi^{TBDM}*). 7.6 g (50 mmol) of β -myrcenol and 8.51 g (125 mmol, 2.5 equiv) imidazole were dissolved in 15 mL dichloromethane. A solution of 7.2 g (48 mmol, 0.95 equiv) *tert*-butyldimethylsilyl chloride in 15 mL dichloromethane was added dropwise to the β -myrcenol containing solution, which was cooled to 0 °C. The solution was stirred under argon atmosphere for 24 h. Subsequently, the solution was washed with 50 mL of aqueous NaHCO₃ solution (5%). The organic layer was separated, and the aqueous layer was washed several times with *n*-hexane (3 × 20 mL). The combined organic layers were dried over MgSO₄. The solvent was evaporated under vacuum to obtain the crude product. After column chromatography (silica, toluene, R_f = 0.89) 12.8 g (47.9 mmol) of pure *MyrOSi^{TBDM}* were obtained (yield = 96%). ¹H NMR (400 MHz, CDCl₃): δ (ppm) = 6.38 (dd, 17.6, 10.8 Hz, 1H, CH=CH₂), 5.43 (m, 1H, CH=C), 5.24 (d, 17.6 Hz, 1H, CH₂=CH), 5.06 (d, 10.8 Hz, 1H, CH₂=CH), 5.01 (d, 4.5 Hz, 2H, CH₂=C), 4.02 (s, 2H, CH₂-OSi), 2.29 – 2.23 (m, 4H, CH₂-CH₂), 1.60 (s, 3H, CH₃-C), 0.91 (s, 9H, (CH₃)₃-C-Si), 0.07 (s, 6H, (CH₃)₂-Si). ¹H and ¹³C NMR spectra are attached to the Supporting Information (Figures S3 and S4).

(*Triisopropylsiloxy*)-2-methyl-6-methylideneocta-2,7-diene (*MyrOSi^{TIP}*). The same procedure as for *MyrOSi^{TBDM}* was applied, replacing *tert*-butyldimethylsilyl chloride by triisopropylsilyl chloride (TIPSCl), with a yield of 90% of pure *MyrOSi^{TIP}*. ¹H NMR (400 MHz, CDCl₃): δ (ppm) = 6.38 (dd, 17.6, 10.8 Hz, 1H, CH=CH₂), 5.48 (m, 1H, CH=C), 5.24 (d, 17.6 Hz, 1H, CH₂=CH), 5.06 (d, 10.8 Hz, 1H, CH₂=CH), 5.01 (d, 4.5 Hz, 2H, CH₂=C), 4.09 (s, 2H, CH₂-OSi), 2.25 (s, 4H, CH₂-CH₂), 1.60 (s, 3H, CH₃-C), 1.15 – 0.97 (m, 21H, ((CH₃)₂-CH)₃-

Si). ^1H , ^{13}C , COSY, HSQC, HMBC and ^{29}Si NMR spectra are attached to the Supporting Information (Figures S5 – S10).

(*Tert-butyl*diphenylsiloxy)-2-methyl-6-methylideneocta-2,7-diene ($\text{MyrOSi}^{\text{TBDPh}}$). The same procedure as for $\text{MyrOSi}^{\text{TBDM}}$ was applied, replacing *tert*-butyldimethylsilyl chloride by *tert*-butyldiphenylsilyl chloride (TBDPhCl), with a yield of 96% of pure $\text{MyrOSi}^{\text{TBDPh}}$. ^1H NMR (400 MHz, CDCl_3): δ (ppm) = 7.69 (dd, 4H, 7.9, 1.6 Hz, *m*-Ar-*H*), 7.40 (m, 6H, *o,p*-Ar-*H*), 6.39 (dd, 17.6, 10.8 Hz, 1H, $\text{CH}=\text{CH}_2$), 5.48 (m, 1H, $\text{CH}=\text{C}$), 5.26 (d, 17.6 Hz, 1H, $\text{CH}_2=\text{CH}$), 5.08 (d, 10.8 Hz, 1H, $\text{CH}_2=\text{CH}$), 5.02 (d, 4.5 Hz, 2H, $\text{CH}_2=\text{C}$), 4.06 (s, 2H, $\text{CH}_2\text{-OSi}$), 2.26 (s, 4H, $\text{CH}_2\text{-CH}_2$), 1.61 (s, 3H, $\text{CH}_3\text{-C}$), 1.07 (s, 9H, $(\text{CH}_3)_3\text{-C-Si}$). ^1H , ^{13}C , COSY, HSQC, HMBC and ^{29}Si NMR spectra are attached to the Supporting Information (Figures S11 – S16).

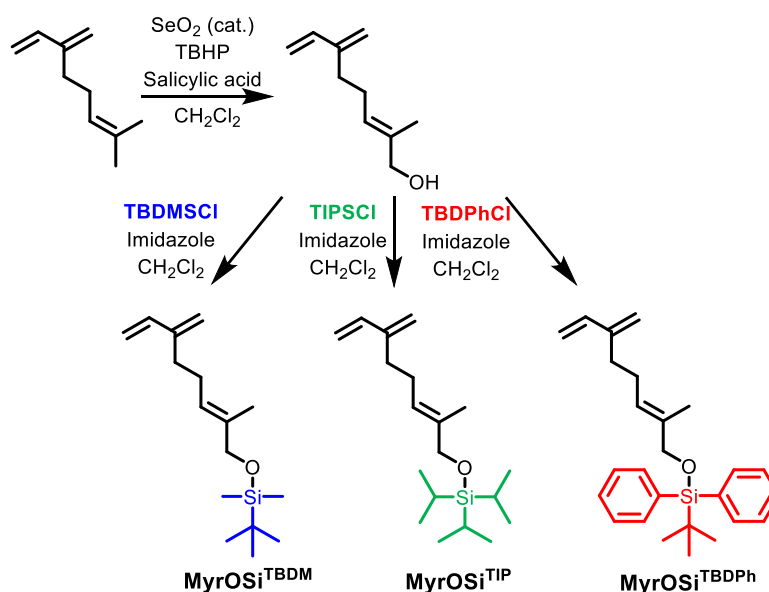
Homopolymerization. The polymerizations were carried out in a glove box in glass vessels (25 mL) with septum. Dry and degassed cyclohexane was distilled into a Schlenk flask equipped with a Teflon stopper. The monomer was dried for 24 h over CaH_2 , degassed and finally distilled into another Schlenk flask with Teflon stopper. The monomer and cyclohexane were added into glass vessel with septum inside the glove box. The polymerization was initiated with *sec*-butyllithium and the solution turned pale yellow shortly after initiation. After stirring the solution for 2 h at RT the polymerization was terminated by adding degassed 2-propanol. Subsequently the polymer was precipitated in 2-propanol and dried under vacuum. The average molecular weights were determined by SEC (polyisoprene standards). The product was a colorless, highly viscous material with yields > 90%. NMR spectra are attached to the Supporting Information (Figures S17 – S29).

Deprotection. 400 mg of PMyrOSi was dissolved in 10 mL THF. Subsequently, tetra-*n*-butylammonium fluoride (1 M solution in THF, 7.5 equiv related to MyrOSi units) was added under argon atmosphere. After 1 h, 4 mL 2-propanol was added to the cloudy solution. The solution was stirred for 0.5 h at RT and quenched by the addition of 4 mL of a saturated aqueous NH_4Cl solution. The organic layer was washed with brine. The polymer was precipitated from the organic layer in cyclohexane via centrifugation at $-10\text{ }^\circ\text{C}$. The polymer was washed with water and precipitated twice from a 2-propanol solution in cyclohexane. The colorless highly viscous product was dried under vacuum,

yielding > 80% of the hydroxyl-functional polymer. ¹H NMR spectra are attached to the Supporting Information (S31 and S32).

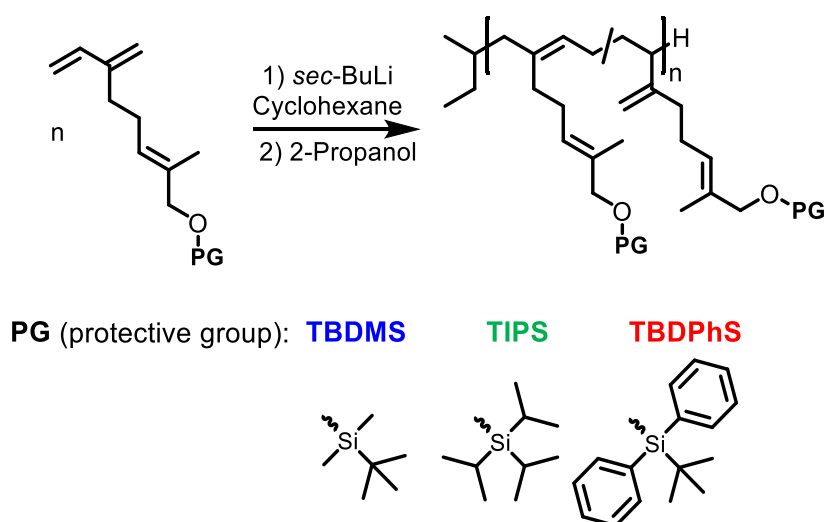
Results and Discussion

Monomer Synthesis. As reported in our recent study, a two-step strategy (outlined in Scheme 1) enables access to the hydroxyl-functionalized myrcene derivative for carbanionic polymerization.³⁵ Via conventional petrochemical synthetic routes, the synthesis of functional 1,3-diene derivatives is limited due to the high susceptibility of the diene moiety to side reactions.²⁰ By using the biomass-derived compound β -myrcene, the challenge of the synthesis of functional 1,3-diene monomers can be overcome. The allylic oxidation of β -myrcene results in β -myrcenol with yields of 20 %. The low yield is caused by incomplete conversion of β -myrcene (conversion of 30 %) and can be recycled for further monomer synthesis.²⁴ In contrast to our previous work, we introduce two different protective groups to the hydroxyl group of β -myrcenol, using the corresponding silyl chlorides. In addition to the *tert*-butyldimethylsilyl (TBDMS) group, the triisopropylsilyl (TBDMS) and *tert*-butyldiphenylsilyl (TBDMS) protective groups were introduced.



Scheme 1. Synthesis route of silyl-protected β -myrcenol (MyrOSi), with different silyl protective groups (TBDMS, TIPS and TBDPhs), based on β -myrcene.

Homopolymerization. The polymerization of MyrOSi with different protective groups (TBDMS, TIPS and TBDPhs) was carried out in cyclohexane, using *sec*-butyllithium as an initiator. The synthesis strategy is outlined in Scheme 2. Homopolymers with molecular weights up to 24 kg mol^{-1} and dispersities in a range of 1.12 to 1.41 were obtained (Table 1). Molecular weights and the degree of polymerization were determined by SEC measurements (SEC traces are shown in Figure 1). The molecular weight determined by SEC differs from the theoretical values. The deviation is attributed to the applied polyisoprene standard, which results in an underestimation of the molecular weight due to a different hydrodynamic radius of PMyrOSi in comparison to polyisoprene with the same molecular weight. Furthermore, systematic errors, e.g. in form of slight variation of the *sec*-butyllithium concentrations, are possible reasons for the deviation in molecular weight.



Scheme 2. Polymerization of silyl-protected β -myrcenol (MyrOSi) with varying silyl protective groups, which differ in steric bulk (TBDMS, TIPS and TBDPhS).

Table 1. Characterization data of the synthesized homopolymers (PMyrOSi) with varying silyl protective groups.

sample	M_n^{th} (kg mol^{-1})	M_n^a (kg mol^{-1})	D^a	T_g^b ($^{\circ}\text{C}$)	3,4-units (%)
PMyrOSi ^{TBDM} ₄₈	17.5	12.8	1.12	-53	31
PMyrOSi ^{TBDM} ₇₉	35	21.2	1.24		31
PMyrOSi ^{TIP} ₄₃	20.3	13.4	1.12	-67	18
PMyrOSi ^{TIP} ₇₈	40.5	24.0	1.41		18
PMyrOSi ^{TBDPh} ₂₇	25.7	10.6	1.41	-14	15

^aDetermined by SEC measurements (eluent: THF, calibration: polyisoprene standards). ^bDetermined by DSC measurements (heating rate of 10 K min⁻¹).

The TIPS-protected polymyrcenol (PMyrOSi^{TIP}) shows similar characteristics as the corresponding TBDMS-protected analogue (PMyrOSi^{TBDM}) (Table 1). While the dispersity is low ($D = 1.12$) for a molecular weight of 13.4 kg mol⁻¹, with increasing molecular weight ($M_n = 24$ kg mol⁻¹) the dispersity of PMyrOSi^{TIP} increases up to 1.41. In accordance with the previously reported TBDMS-protected polymyrcenol (PMyrOSi^{TBDM}), increasing broadening (i.e. tailing to lower molecular weight, observable in the SEC traces in Figure 1) of the molecular weight distribution with increasing molecular weight is assigned to potential side reactions. Hirao et al. reported the nucleophilic attack of the living carbanionic chain end at the silyl protective group for TBDMS-protected hydroxyl functionalized styrene derivatives, resulting in its cleavage.³⁹ Accordingly, the side reaction is not inhibited by the larger steric bulk of the TIPS protective group in

comparison to the TBDMS protective group. In contrast to $\text{MyrOSi}^{\text{TBDM}}$ and $\text{MyrOSi}^{\text{TIP}}$, the anionic polymerization of TBDPhS-protected β -myrcenol ($\text{MyrOSi}^{\text{TBDPh}}$) is hindered by the high boiling point of $\text{MyrOSi}^{\text{TBDPh}}$, which impedes the common monomer purification by drying over CaH_2 and distillation *in vacuo* (thermally induced autopolymerization at around $140\text{ }^\circ\text{C}$ at 10^{-3} mbar occurs before boiling). Instead, $\text{MyrOSi}^{\text{TBDPh}}$ was dried over molecular sieve (3 \AA). Nevertheless, the described purification of $\text{MyrOSi}^{\text{TBDPh}}$ was insufficient for the synthesis of well-defined polymers by living anionic polymerization, resulting in a broad molecular weight distribution ($\mathcal{D} = 1.41$, Figure 1) and incomplete monomer conversion, as shown in the ^1H NMR spectrum of the crude product in Figure S30.

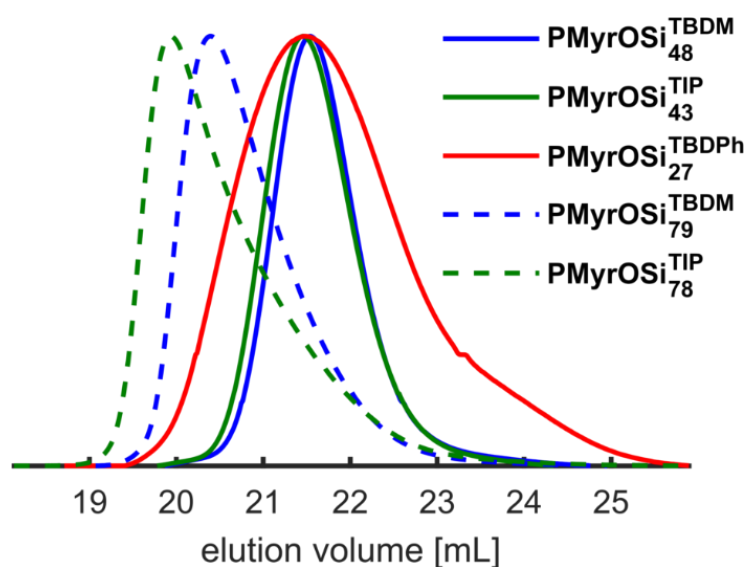


Figure 1. SEC traces (THF, PI standard) of PMyrOSi homopolymers with different protective groups (TBDMS, TIPS and TBDPhS).

Polydiene microstructure. In recent works the influence of the steric bulk of different silyl protective groups of a hydroxyl functionalized alkyllithium initiator on the polydiene microstructure was investigated.^{33,34} In this work, we expand the approach of protective group-control of the polydiene microstructure by investigating the influence of the steric bulk of the silyl protective groups, attached to a functional 1,3 diene monomer (β -myrcenol), to the polydiene microstructure of polymyrcenol. The polydiene microstructure (content of 1,4- and 3,4-units) was determined by ^1H NMR spectra, on the basis of the specific proton signals of the 1,4- and 3,4-units, shown in Figure 2.

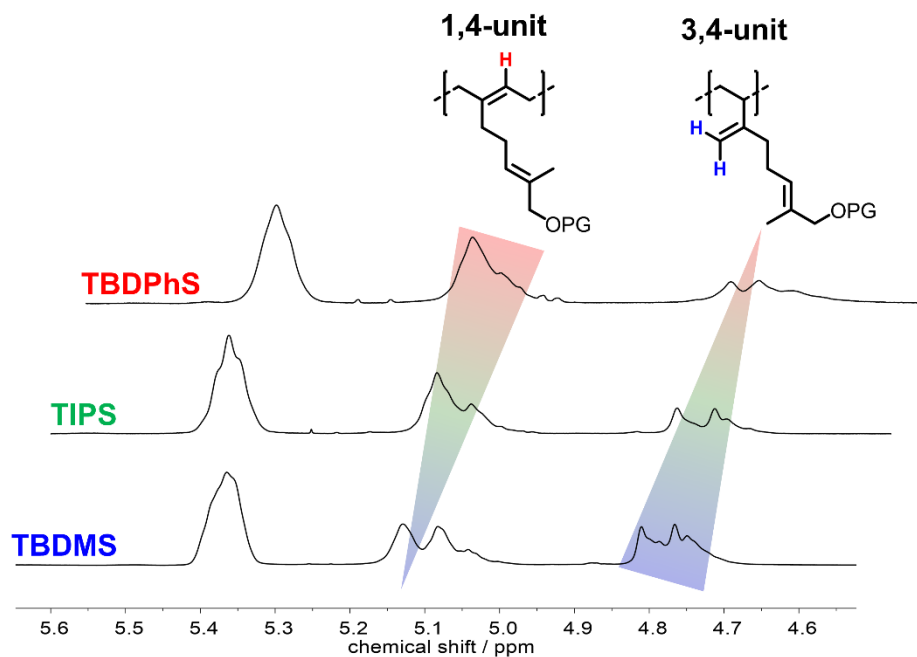


Figure 2. ^1H NMR spectra (zoom in of the region between 4.6 and 5.6 ppm) of silyl-protected polymyracenol (PMrOSi) with different silyl protective groups (TBDMS, TIPS and TBDPhS), showing the different ratios of 1,4- and 3,4-units.

Similar to the works by Li et al., which are based on silyl-protected initiators, a decrease of 3,4-units with increasing steric bulk of the silyl protective group (TBDMS < TIPS < TBDPhS) was observed, as shown in Figure 3. In general, polar additives are well known to increase the 3,4-unit content of the anionic polymerization of polydienes like polymyracene.^{10,17,37} We explain these observations with increasing steric bulk of the silyl protective group, since the oxygen atom is increasingly shielded, resulting in a reduced coordination strength of the lithium counter ions at the living carbanionic polymer chain end. Consequently, the microstructure modifier strength decreases with increasing steric bulk. The observed trend confirms the assumption of the microstructure modifier effect of MyrOSi^{TBDM} during polymerization, which is reported in our previous study.³⁵ In contrast to the silyl-protected hydroxyl propyllithium initiator, the modifier effect by using silyl-protected β -myrcenol monomers is more pronounced (higher amounts of 3,4 units are accessible, up to 31 % vs. 15 % for the corresponding TBDMS-based hydroxyl propyllithium initiator). The stronger modifier effect is basically caused by the higher concentration of a monomer in comparison to an initiator.

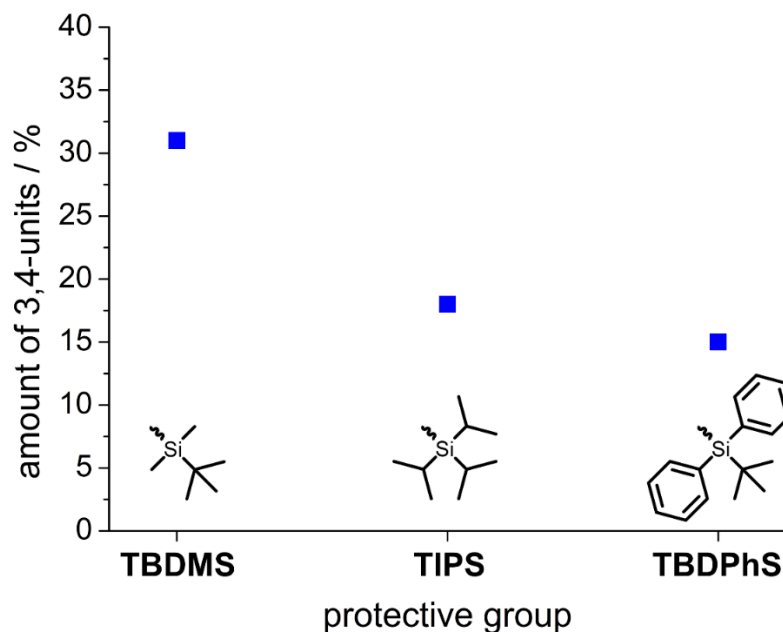
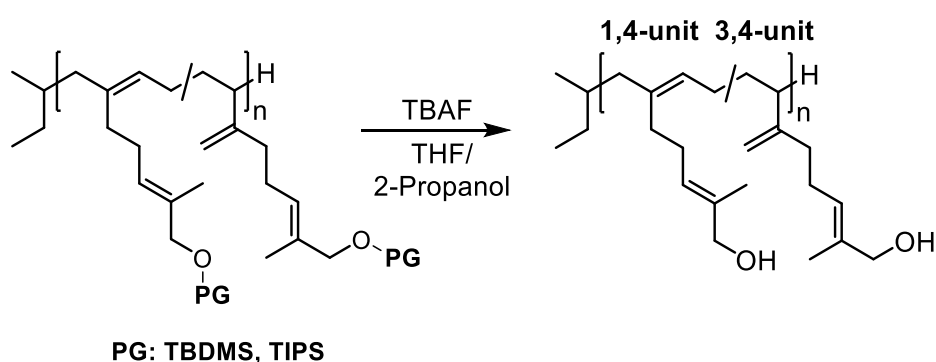


Figure 3. Influence of the silyl protective group on the polydiene microstructure (amount of 3,4-units). Steric bulk of protective groups increases in the order TBDMS < TIPS < TBDPhS.

The influence of the protective groups on the thermal properties of silyl-protected polymyrcenol was investigated by DSC-measurements (DSC-curves are shown in Figures S34-36). The glass transition temperatures (shown in Table 1) are basically influenced by two effects: (i) the content of 3,4-units in the polymer backbone and (ii) the steric bulk of the silyl protective groups. The TIPS protected polymyrcenol exhibits the lowest glass transition temperature observed at $-67\text{ }^{\circ}\text{C}$, which is mainly caused by the low content of 3,4-units (18 %) and the larger steric bulk of the silyl group in comparison to $\text{PMyrOSi}^{\text{TBDMS}}$. The larger steric bulk of the silyl protective group increases the free volume of the polymer chains and consequently reduces the T_g . In addition to the amount of 3,4-units and the steric bulk, the thermal properties of the silyl-protected polymers strongly depend on the chemical nature of the silyl protective group. While $\text{PMyrOSi}^{\text{TBDMS}}$ and $\text{PMyrOSi}^{\text{TIP}}$ show low T_g s below $-53\text{ }^{\circ}\text{C}$, in the typical range of polydienes as polymyrcene ($T_{g,\text{PMyr}} = -67\text{ }^{\circ}\text{C}$, 6% 3,4 units), the glass transition temperature of $\text{PMyrOSi}^{\text{TBDPh}}$ is significantly higher ($T_{g,\text{PMyr}} = -14\text{ }^{\circ}\text{C}$). The higher glass transition temperature is caused by the phenyl moieties of the TBDPhSi protective groups, resulting in a decreased chain mobility.

Polymyrcenol. To demonstrate the influence of the silyl protective group on polymyrcenol, two exemplary samples ($\text{PMyrOSi}^{\text{TBDMS}}_{48}$ and $\text{PMyrOSi}^{\text{TIP}}_{43}$) were

deprotected, as outlined in Scheme 3. The protective groups could be removed under mild conditions, using TBAF (tetra-*n*-butylammonium fluoride) in a THF/2-propanol mixture. Quantitative removal of the protective groups in all cases is proven by the complete disappearance of the proton signals of the protective groups in the corresponding ^1H NMR spectra (Figures S31 and S32). Well-defined polymyracenol homopolymers with low dispersities ($\mathcal{D} = 1.08\text{--}1.11$) were obtained. In contrast to the previously reported deprotection of $\text{PMyrOSi}^{\text{TBDMS}}$,³⁵ the deprotection of $\text{PMyrOSi}^{\text{TIP}}$ results in a monomodal molecular weight distribution, without any evidence for chain coupling side reactions, as shown in the SEC trace in Figure 4.



Scheme 3. Removal of the silyl protective groups (TBDMS and TIPS) of PMyrOSi , resulting in polymyracenol (PMyrOH).

Table 2. Characterization data of polymyracenol (PMyrOH), synthesized with different protective groups (TBDMS and TIPS).

sample	M_n^{th} (kg mol^{-1})	M_n^a (kg mol^{-1})	\mathcal{D}^a	T_g^a ($^{\circ}\text{C}$)	$\Delta T_{g,\text{deprot.}}^a$ ($^{\circ}\text{C}$)	3,4- units (%)
$\text{PMyrOH}^{\text{TBDMS}}_{48}$	10	8.1	1.11	-23	30	31
$\text{PMyrOH}^{\text{TIPS}}_{43}$	10	8.4	1.08	-46	21	18

^aDetermined by SEC measurements (eluent: THF, calibration: polyisoprene standards). ^bDetermined by DSC measurements (heating rate of 10 K min^{-1}).

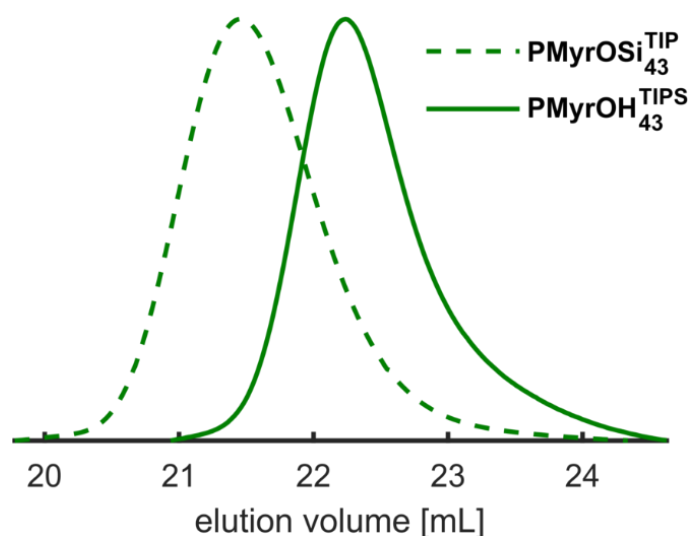


Figure 4. SEC traces (THF, PI standard, RI signal) before (PMyrOSi^{TIP}₄₃, dashed line) and after (PMyrOH^{TIPS}₄₃, green line) removal of the protective groups.

The protective group-controlled polydiene microstructure strongly influences the thermal properties of the resulting deprotected polymyrcenol. The removal of the protective groups results in an increase of the glass transition temperature ($\Delta T_{g,\text{deprot}}$), which is significantly higher for the deprotection of the TIPS-protected polymyrcenol than for the TBDMS-protected polymer, as shown in Table 2. The difference in $\Delta T_{g,\text{deprot}}$ is attributed to the higher steric bulk of the TIPS-group and the corresponding higher content of 1,4-units. The higher glass transition temperature of polymyrcenol with high content of 3,4-units is observable in the DSC-curves shown in Figure 5. Polymyrcenol, synthesized with the TIPS protective group (PMyrOH^{TIPS}₄₃, $T_g = -46$) exhibits a significantly lower glass transition temperature, in comparison to its analog synthesized with the TBDMS protective group (PMyrOH^{TBDMS}₄₈, $T_g = -23$). The reduced content of 3,4-units, yielding a lower glass transition temperature, renders PMyrOH^{TIPS} more interesting as a highly flexible building blocks for thermoplastic elastomers, as well for low temperature applications of rubbers, exhibiting improved interaction with functional fillers in comparison to non-functionalized polydienes.^{40,41}

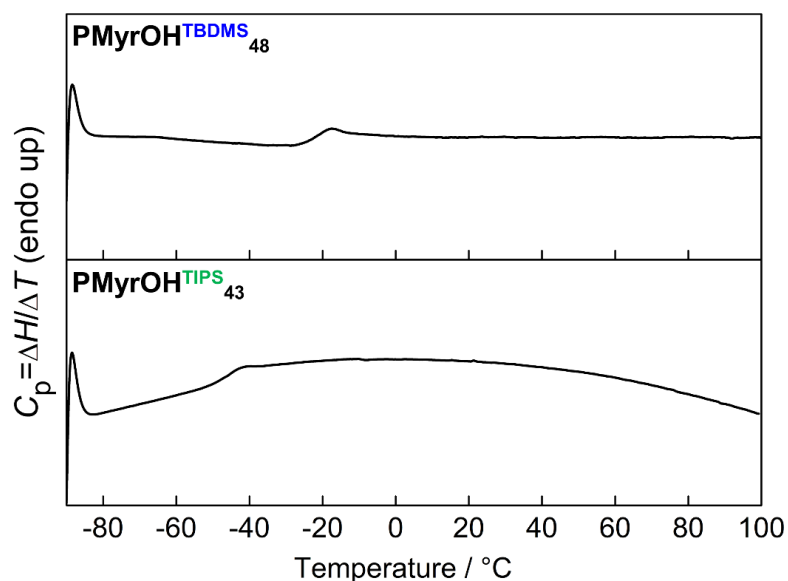


Figure 5. DSC curves of PMyrOH (top) and of PMyrOH (bottom) after removal of the protective groups (second heating curves, heating and cooling rate of 10 K min⁻¹).

Conclusion

In this work we established a protective group-controlled polydiene microstructure of polymyrcenol by the application of different silyl-protective groups, which differ in steric bulk. An increasing steric bulk of the protective group lead to a higher content of 1,4-units. To the best of our knowledge this work shows the first control of the polydiene microstructure by use of different protective groups of a functionalized 1,3-diene monomer. In comparison to a similar approach, using silyl-protected functionalized alkyllithium initiators, the effect of the silyl protected β -myrcenol monomer on the polydiene microstructure is stronger, resulting in an adjustable polydiene microstructure over a wide range (31 to 15 % of 3,4-units). The protective groups can be removed under mild conditions using TBAF. In contrast to the deprotection of TBDMS-protected polymyrcenol, the removal of TIPS protective group results in polymyrcenol with a monomodal molecular weight distribution without any evidence of chain coupling. A key observation is the TIPS group derived polymyrcenol's lower glass transition temperature at -46 °C, in comparison to the TBDMS protective group derived polymyrcenol ($T_g = -23$ °C). The lower glass transition temperature improves the potential of polymyrcenol for prospective applications as low T_g flexible component, both in thermoplastic elastomers and in vulcanized rubbers.

Acknowledgments

The authors thank Monika Schmelzer for the valuable support with the SEC measurements and Christoph Hahn for critical evaluation of this article.

References

- (1) Sarkar, P.; Bhowmick, A. K. Sustainable rubbers and rubber additives. *J Appl Polym Sci* **2018**, *135*, 45701.
- (2) Behr, A.; Johnen, L. Myrcene as a natural base chemical in sustainable chemistry: a critical review. *ChemSusChem* **2009**, *2*, 1072–1095.
- (3) Benjamin, K. R.; Silva, I. R.; Cherubim, J. P.; McPhee, D.; Paddon, C. J. Developing Commercial Production of Semi-Synthetic Artemisinin, and of β -Farnesene, an Isoprenoid Produced by Fermentation of Brazilian Sugar. *J. Braz. Chem. Soc.* **2016**, *27*, 1339–1345.
- (4) Bolton, J. M.; Hillmyer, M. A.; Hoye, T. R. Sustainable Thermoplastic Elastomers from Terpene-Derived Monomers. *ACS Macro Lett.* **2014**, *3*, 717–720.
- (5) Zhou, C.; Wei, Z.; Lei, X.; Li, Y. Fully biobased thermoplastic elastomers: synthesis and characterization of poly(l -lactide)-b-polymyrcene-b-poly(l -lactide) triblock copolymers. *RSC Adv.* **2016**, *6*, 63508–63514.
- (6) Sasaki, H.; Uehara, Y.; Kato, M. Thermoplastic elastomer composition and molded body.
- (7) Zhao, J.; Schlaad, H. Synthesis of Terpene-Based Polymers; *Adv. Polym. Sci.* **2013**, *253*, 151–190.
- (8) Hattam, P.; Gauntlett, S.; Mays, J. W.; Hadjichristidis, N.; Young, R. N.; Fetters, L. J. Conformational characteristics of some model polydienes and polyolefins. *Macromolecules* **1991**, *24*, 6199–6209.
- (9) Bywater, S.; Johnson, A. F.; Worsfold, D. J. The Electronic Spectra of Some Anionic Polymerization Systems. *Can. J. of Chem.* **1964**, *42* (6), 1255–1260.
- (10) Widmaier, J. M.; Meyer, G. C. Glass transition temperature of anionic polyisoprene. *Macromolecules* **1981**, *14*, 450–452.
- (11) Henry Hsieh; Arthur V. Tobolsky. Polymerization of isoprene by n-butyl lithium. *J Polym. Sci.* **1957**, *25*, 245–247.
- (12) Morita, H.; Tobolsky, A. V. Isoprene Polymerization by Organometallic Compounds. I. *J. Am. Chem. Soc.* **1957**, *79*, 5853–5855.
- (13) Jia, X.; Zhang, X.; Gong, D. 1,2 Enriched polymerization of isoprene by cobalt complex carrying aminophosphory fused (PN 3) ligand. *J. Polym. Sci. Part A: Polym. Chem.* **2018**, *56*, 2286–2293.
- (14) Burfield, D. R. Polymer glass transition temperatures. *J. Chem. Educ.* **1987**, *64*, 875.

- (15) Zhang, L.; Luo, Y.; Hou, Z. Unprecedented isospecific 3,4-polymerization of isoprene by cationic rare earth metal alkyl species resulting from a binuclear precursor. *J. Am. Chem. Soc.* **2005**, *127*, 14562–14563.
- (16) Lal, J.; Mark, J. E. *Advances in Elastomers and Rubber Elasticity*; Springer US, 2013.
- (17) Steube, M.; Johann, T.; Hübner, H.; Koch, M.; Dinh, T.; Gallei, M.; Floudas, G.; Frey, H.; Müller, A. H. E. Tetrahydrofuran: More than a “Randomizer” in the Living Anionic Copolymerization of Styrene and Isoprene: Kinetics, Microstructures, Morphologies, and Mechanical Properties. *Macromolecules* **2020**, *53*, 5512–5527.
- (18) Kim, J. M.; Chakrapani, S. B.; Beckingham, B. S. Tuning Compositional Drift in the Anionic Copolymerization of Styrene and Isoprene. *Macromolecules*, *53* (10), 3814–3821.
- (19) Hsieh, H. L.; Quirk, R. P. *Anionic Polymerization: Principles and Practical Applications*; *Plastics Engineering* 34; Dekker: New York, 1996.
- (20) Hadjichristidis, N.; Hirao, A., Eds. *Anionic Polymerization: Principles, Practice, Strength, Consequences and Applications*, 1st ed. 2015; Springer: Tokyo, 2015.
- (21) Nakamura, A.; Nakada, M. Allylic Oxidations in Natural Product Synthesis. *Synthesis* **2013**, *45*, 1421–1451.
- (22) Hioki, H.; Ooi, H.; Hamano, M.; Mimura, Y.; Yoshio, S.; Kodama, M.; Ohta, S.; Yanai, M.; Ikegami, S. Enantioselective total synthesis and absolute stereostructure of hippospongiic acid A. *Tetrahedron* **2001**, *57*, 1235–1246.
- (23) Gautam, V. K.; Singh, J.; Dhillon, R. S. Selective hydroboration studies with acetoxyborohydride. *J. Org. Chem.* **1988**, *53*, 187–189.
- (24) Büchi, G.; Wüest, H. Eine Synthese des β -Sinensals. *HCA* **1967**, *50*, 2440–2445.
- (25) Petzhold, C.; Morschhaeuser, R.; Kolshorn, H.; Stadler, R. On the Anionic Polymerization of (Dialkylamino)isoprenes. 2. Influence of the Tertiary Amino Group on the Polymer Microstructure. *Macromolecules* **1994**, *27*, 3707–3713.
- (26) Hirao, A.; Hiraishi, Y.; Nakahama, S.; Takenaka, K. Polymerization of Monomers Containing Functional Silyl Groups. 13. Anionic Polymerization of 2-[(N, N - Dialkylamino)dimethylsilyl]-1,3-butadiene Derivatives. *Macromolecules* **1998**, *31*, 281–287.
- (27) Ding, Y. X.; Weber, W. P. Regio- and stereospecific 1,4-polymerization of 2-(triethylsilyl)-1,3-butadiene. *Macromolecules* **1988**, *21*, 530–532.
- (28) Hirao, A.; Loykulnant, S.; Ishizone, T. Recent advance in living anionic polymerization of functionalized styrene derivatives. *Prog. Polym. Sci.* **2002**, *27*, 1399–1471.
- (29) Greene, T. W.; Wuts, P. G. M. *Protective Groups In Organic Synthesis*, 3rd ed. John Wiley & Sons: New York, 1991.
- (30) Ishitake, K.; Satoh, K.; Kamigaito, M.; Okamoto, Y. Stereospecific Free Radical and RAFT Polymerization of Bulky Silyl Methacrylates for Tacticity and Molecular Weight Controlled Poly(methacrylic acid). *Macromolecules* **2011**, *44*, 9108–9117.

- (31) Takeshima, H.; Satoh, K.; Kamigaito, M. Scalable Synthesis of Bio-Based Functional Styrene: Protected Vinyl Catechol from Caffeic Acid and Controlled Radical and Anionic Polymerizations Thereof. *ACS Sustainable Chemistry & Engineering*, **6**(11), 13681-13686.
- (32) Leibig, D.; Lange, A.-K.; Birke, A.; Frey, H. Capitalizing on Protecting Groups to Influence Vinyl Catechol Monomer Reactivity and Monomer Gradient in Carbanionic Copolymerization. *Macromol. Chem. Phys.* **2017**, *218*, 1600553.
- (33) Min, X.; Fan, X.; Liu, J. Utilization of steric hindrance of alkyl lithium-based initiator to synthesize high 1,4 unit-containing hydroxyl- terminated polybutadiene. *R. Soc. Open Sci.* **2018**, *5*, 180156.
- (34) Zhu, X.-z.; Fan, X.-d.; Zhao, N.; Min, X.; Liu, J.; Wang, Z.-c. Influence of mono-lithium based initiators with different steric bulks on 1,4 unit content of hydroxyl terminated polybutadiene using anionic polymerization. *RSC Adv.* **2017**, *7*, 52712–52718.
- (35) Wahlen, C.; Rauschenbach, M.; Blankenburg, J.; Kersten, E.; Ender, C. P.; Frey., H. Myrcenol-Based Monomer for Carbanionic Polymerization: Functional Copolymers with Myrcene and Bio-Based Graft Copolymers. *Macromolecules* **2020**, <https://doi.org/10.1021/acs.macromol.0c01734>.
- (36) T. A. Antkowiak; A. E. Oberster; A. F. Halasa; D. P. Tate. Temperature and concentration effects on polar-modified alkyllithium polymerizations and copolymerizations. *J. Polym. Sci. Part A-1: Polym. Chem.* **1972**, *10*, 1319–1334.
- (37) Zhang, J.; Lu, J.; Su, K.; Wang, D.; Han, B. Bio-based β -myrcene-modified solution-polymerized styrene–butadiene rubber for improving carbon black dispersion and wet skid resistance. *J Appl Polym Sci* **2019**, *136*, 48159.
- (38) Zhang, S.; Han, L.; Ma, H.; Liu, P.; Shen, H.; Lei, L.; Li, C.; Yang, L.; Li, Y. Investigation on Synthesis and Application Performance of Elastomers with Biogenic Myrcene. *Ind. Eng. Chem. Res.* **2019**, *58*, 12845–12853.
- (39) Hirao, A.; Kitamura, K.; Takenaka, K.; Nakahama, S. Protection and polymerization of functional monomers. 18. Syntheses of well-defined poly(vinylphenol), poly[(vinylphenyl)methanol], and poly[2-vinylphenyl]ethanol by means of anionic living polymerization of styrene derivatives containing tert-butyldimethylsilyl ethers. *Macromolecules* **1993**, *26*, 4995–5003.
- (40) Xu, Y.; Zhao, J.; Gan, Q.; Ying, W.; Hu, Z.; Tang, F.; Luo, W.; Luo, Y.; Jian, Z.; Gong, D. Synthesis and properties investigation of hydroxyl functionalized polyisoprene prepared by cobalt catalyzed co-polymerization of isoprene and hydroxylmyrcene. *Polym. Chem.* **2020**, *11*, 2034–2043.
- (41) Sahu, P.; Sarkar, P.; Bhowmick, A. K. Design of a Molecular Architecture via a Green Route for an Improved Silica Reinforced Nanocomposite using Bioresources. *ACS Sustain. Chem. Eng.* **2018**, *6*, 6599–6611.

Supporting Information

Protective Groups Make the Difference: Influence of Silyl Protective Groups on the Polydiene Microstructure of Polymyrcenol

Christian Wahlen, Christopher P. Ender and Holger Frey*

Table of Contents

1	Monomer characterization.....	123
2	Homopolymer characterization.....	131
2.1	NMR spectra of PMyrOSi ^{TBDM}	131
2.2	NMR spectra of PMyrOSi ^{TIP}	131
2.3	NMR spectra of PMyrOSi ^{TBDPh}	134
2.4	NMR spectra of PMyrOH.....	138
2.5	Determination of polydiene microstructure of homopolymers (content of 3,4-units).....	139
2.6	DSC measurements.....	140

1 Monomer characterization

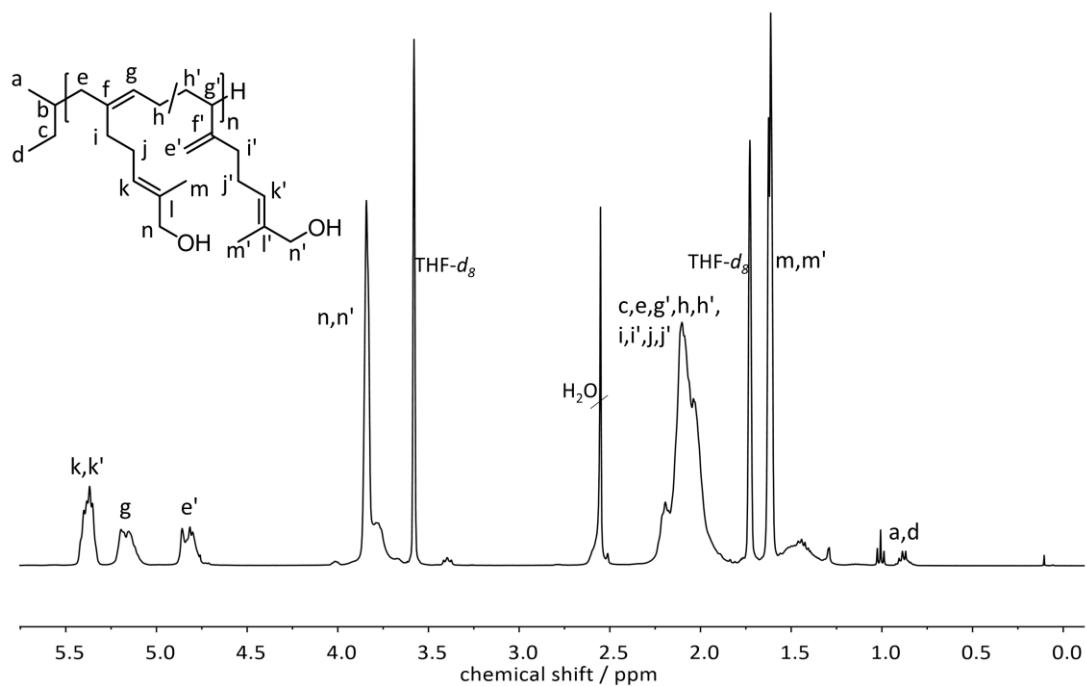


Figure S1. ^1H NMR spectrum (400 MHz) of β -myrcenol in CDCl_3 .

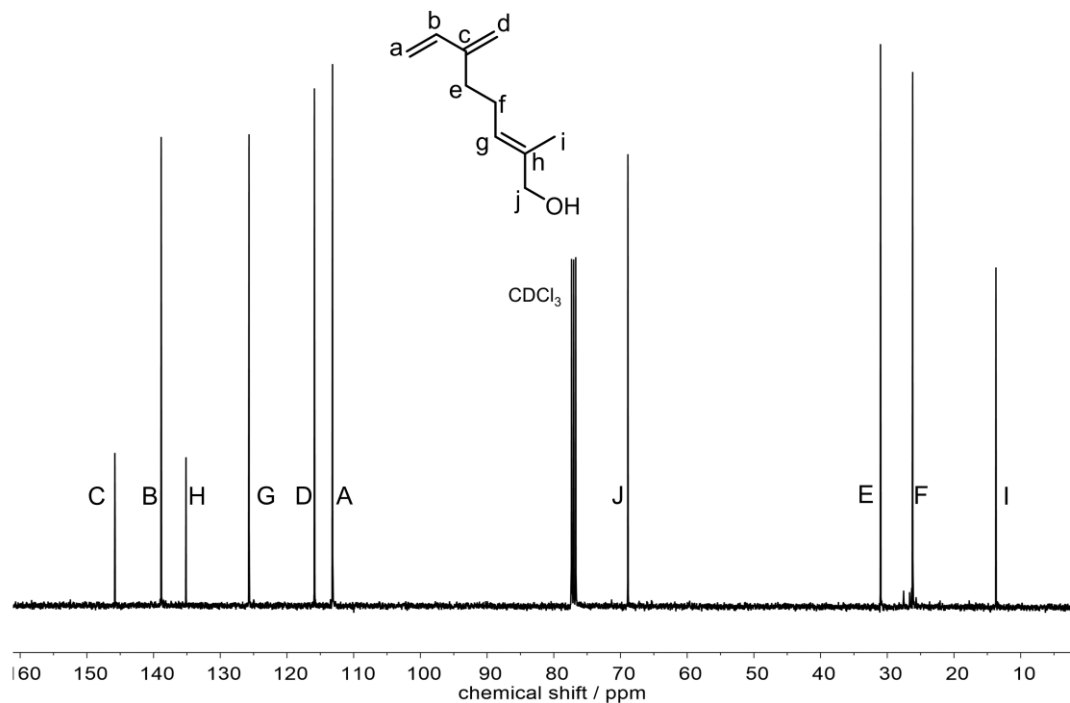


Figure S2. ^{13}C NMR spectrum (101 MHz) of β -myrcenol in CDCl_3 .

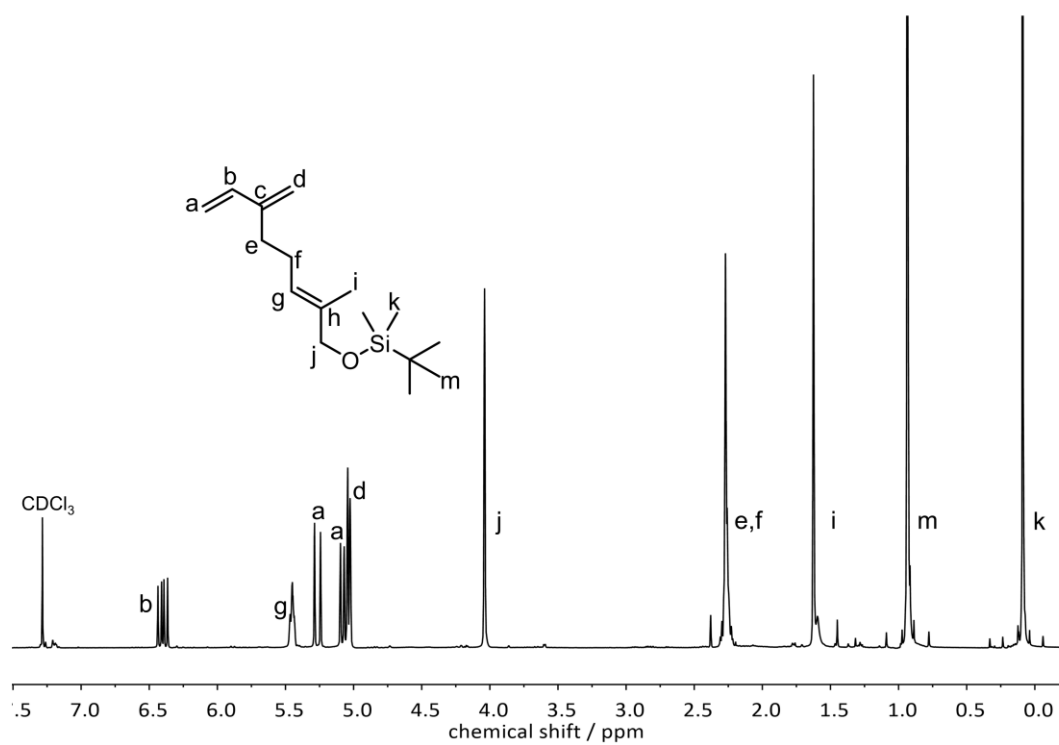


Figure S3. ¹H NMR spectrum (400 MHz) of MyrOSi^{TBDM} in CDCl₃.

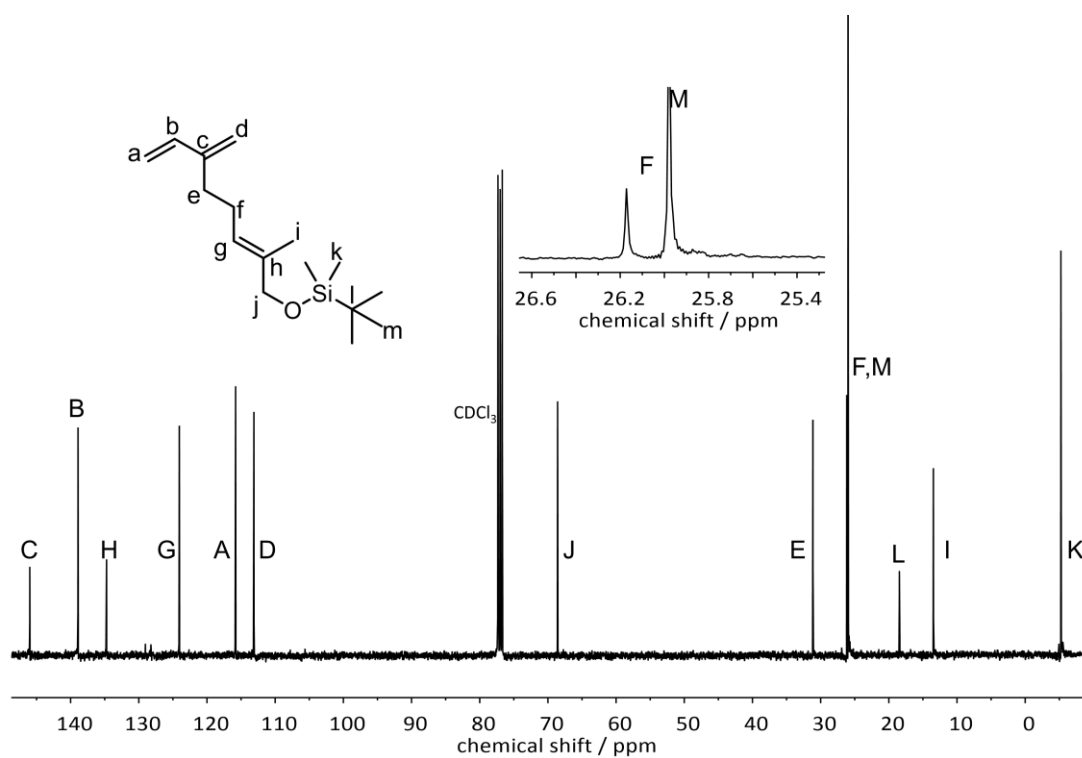


Figure S4. ¹³C NMR spectrum (101 MHz) of MyrOSi^{TBDM} in CDCl₃.

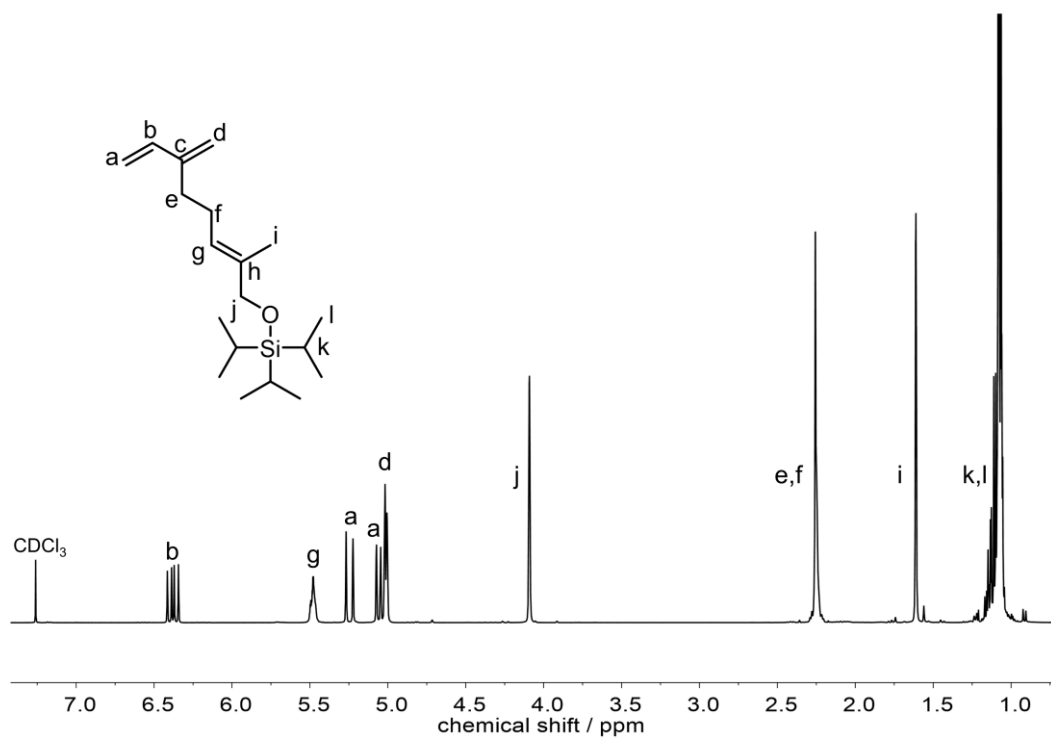


Figure S5. ^1H NMR spectrum (400 MHz) of MyrOSi^{TIP} in CDCl_3 .

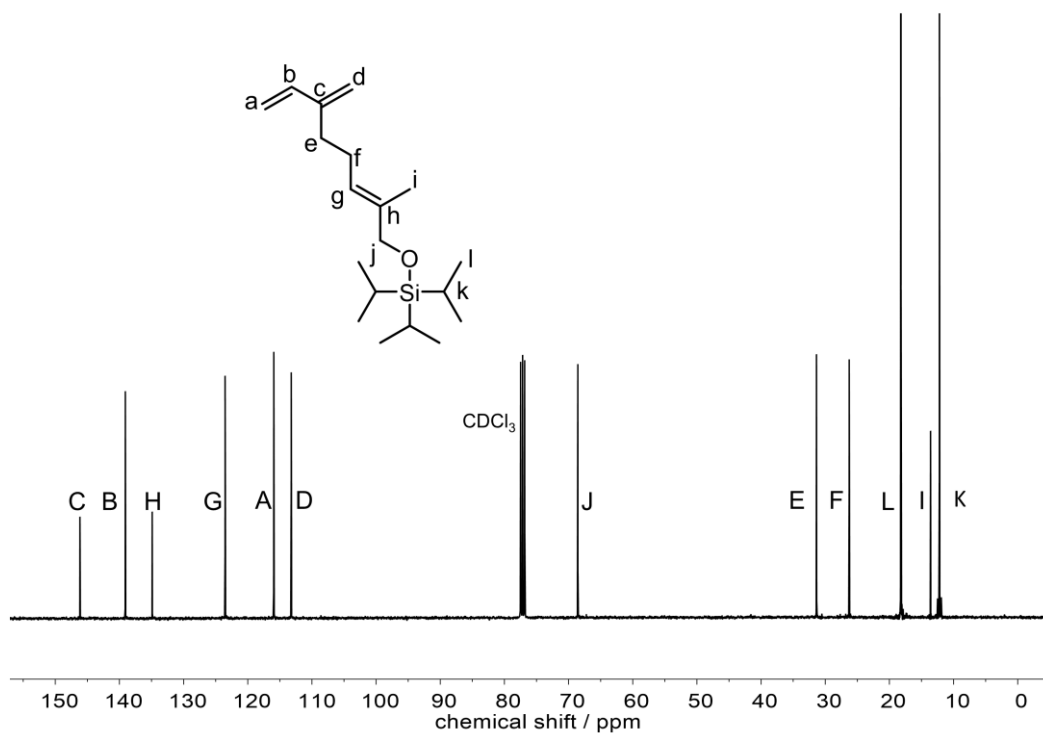


Figure S6. ^{13}C NMR spectrum (101 MHz) of MyrOSi^{TIP} in CDCl_3 .

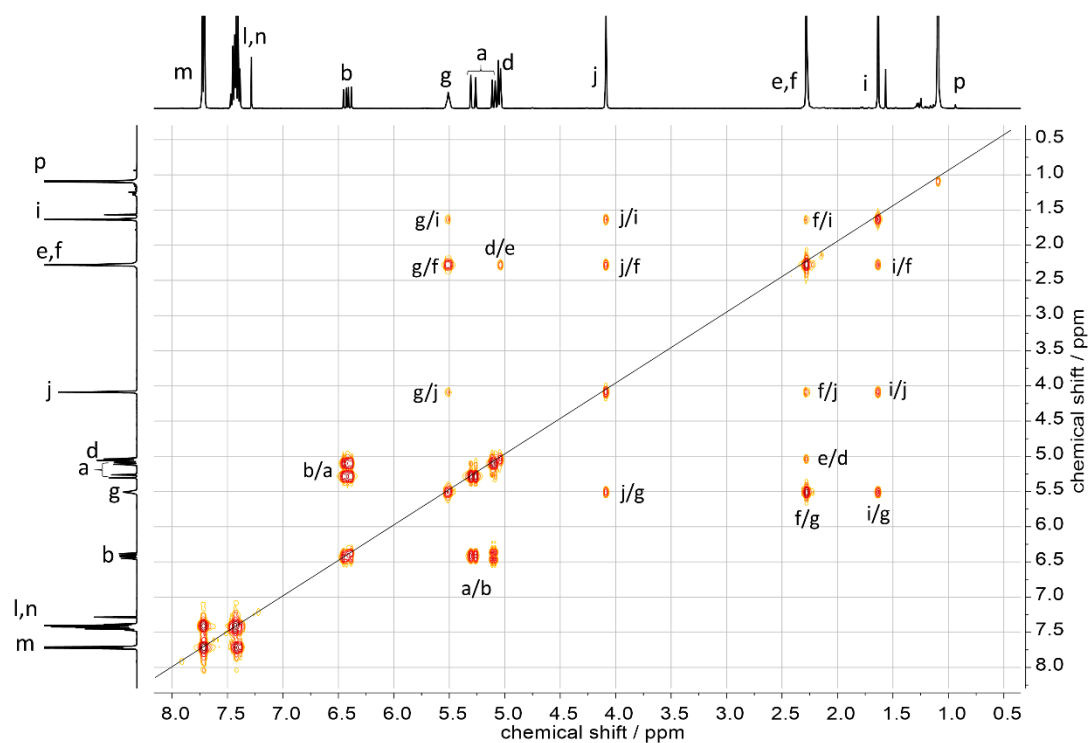


Figure S7. COSY NMR spectrum (400 MHz) of MyrOSi^{TIP} in CDCl₃.

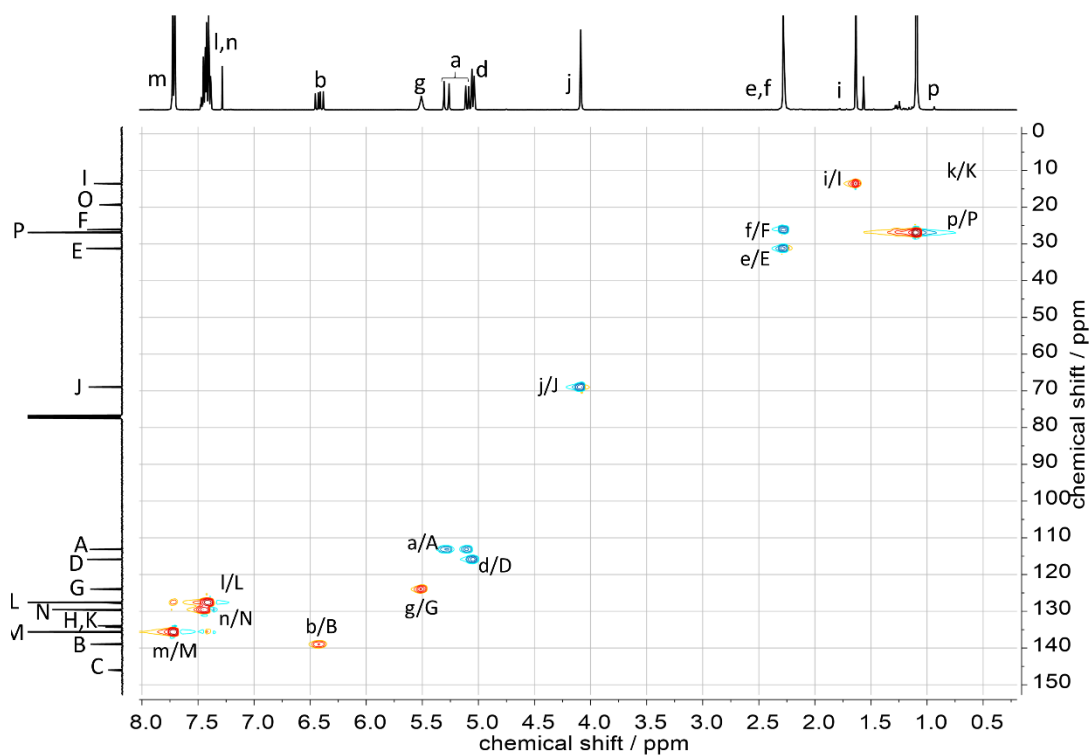


Figure S8. HSQC NMR spectrum (101 MHz / 400 MHz) of MyrOSi^{TIP} in CDCl₃.

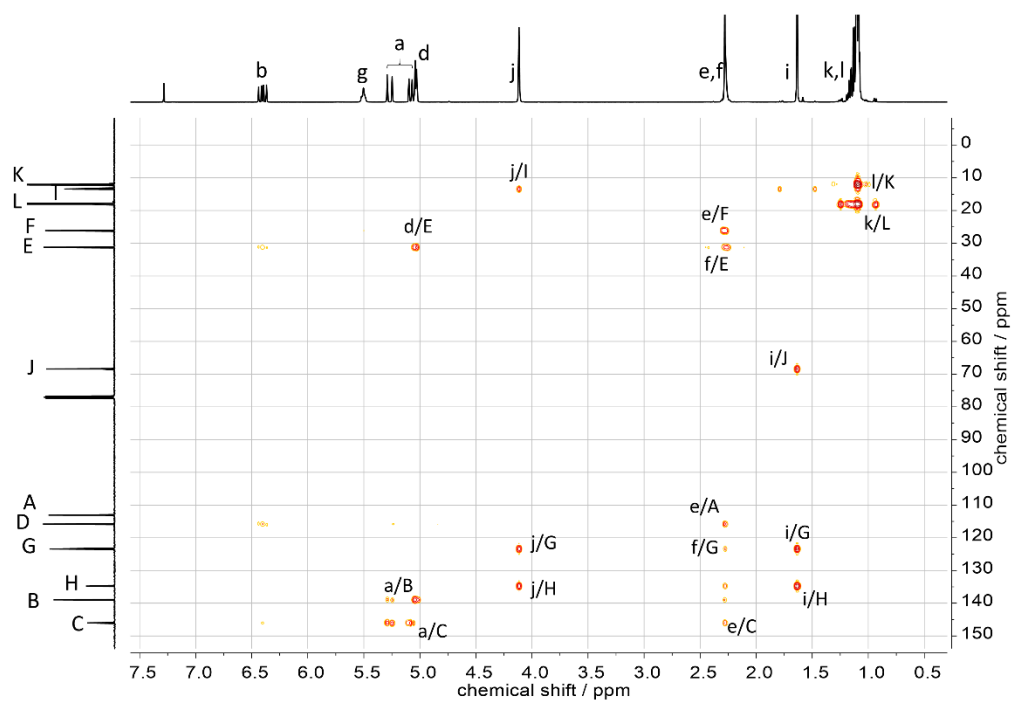


Figure S9. HMBC NMR spectrum (101 MHz / 400 MHz) of MyrOSi^{TIP} in CDCl₃.

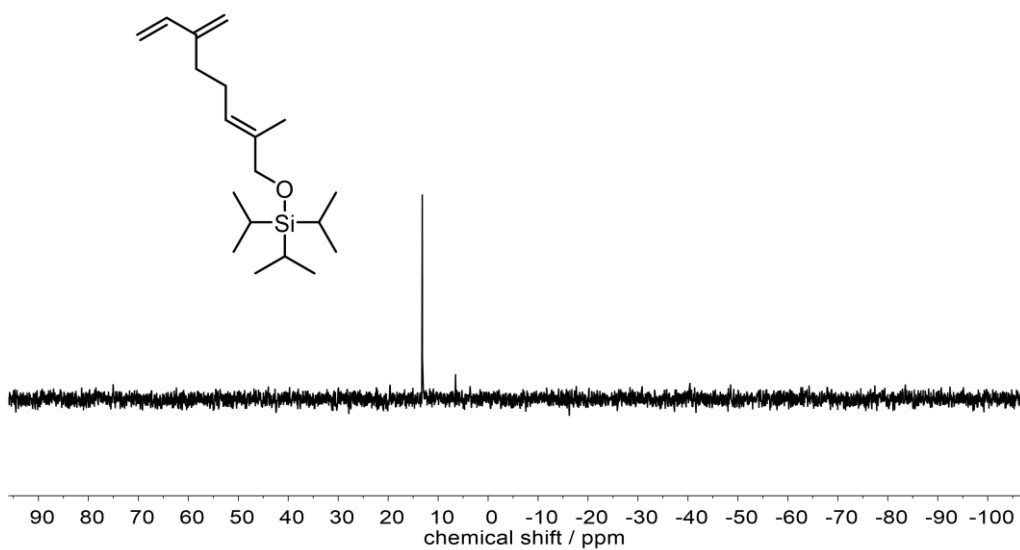


Figure S10. ²⁹Si NMR spectrum (400 MHz) of MyrOSi^{TIP} in CDCl₃.

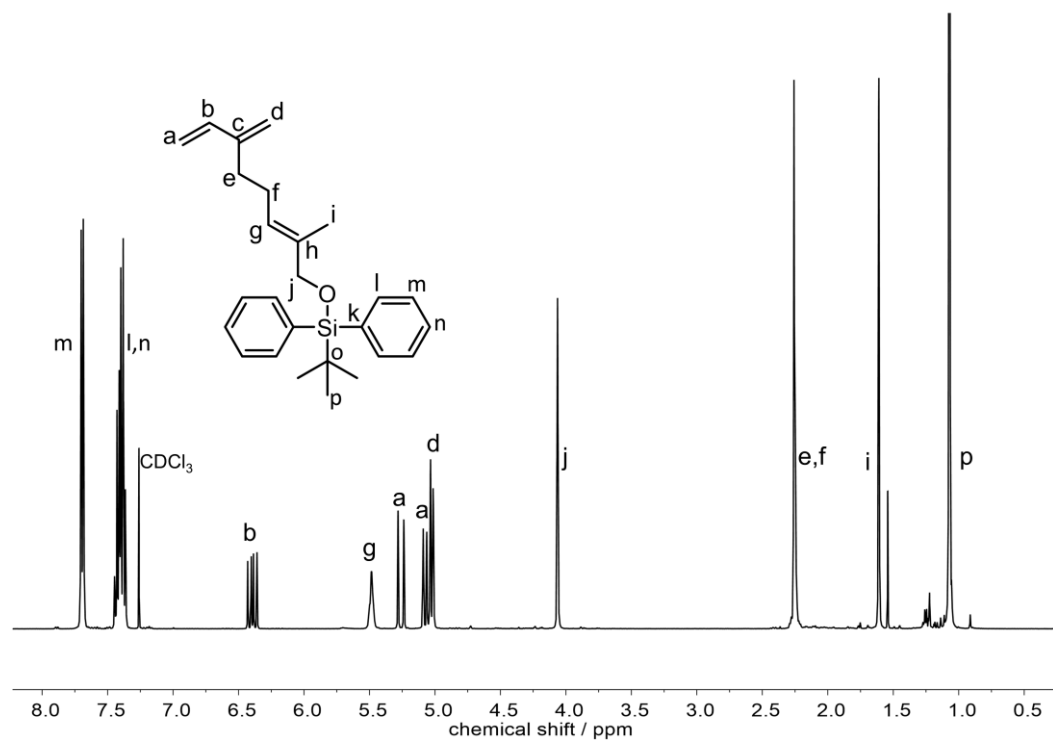


Figure S11. ¹H NMR spectrum (400 MHz) of MyrOSi^{TBDPh} in CDCl₃.

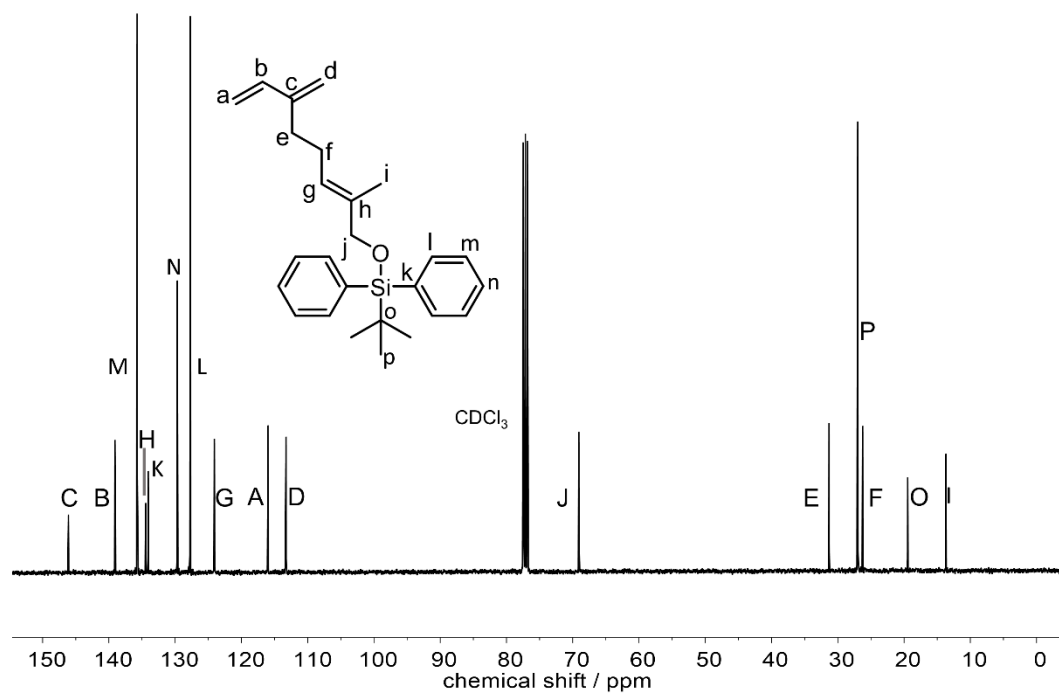


Figure S12. ¹³C NMR spectrum (101 MHz) of MyrOSi^{TBDPh} in CDCl₃.

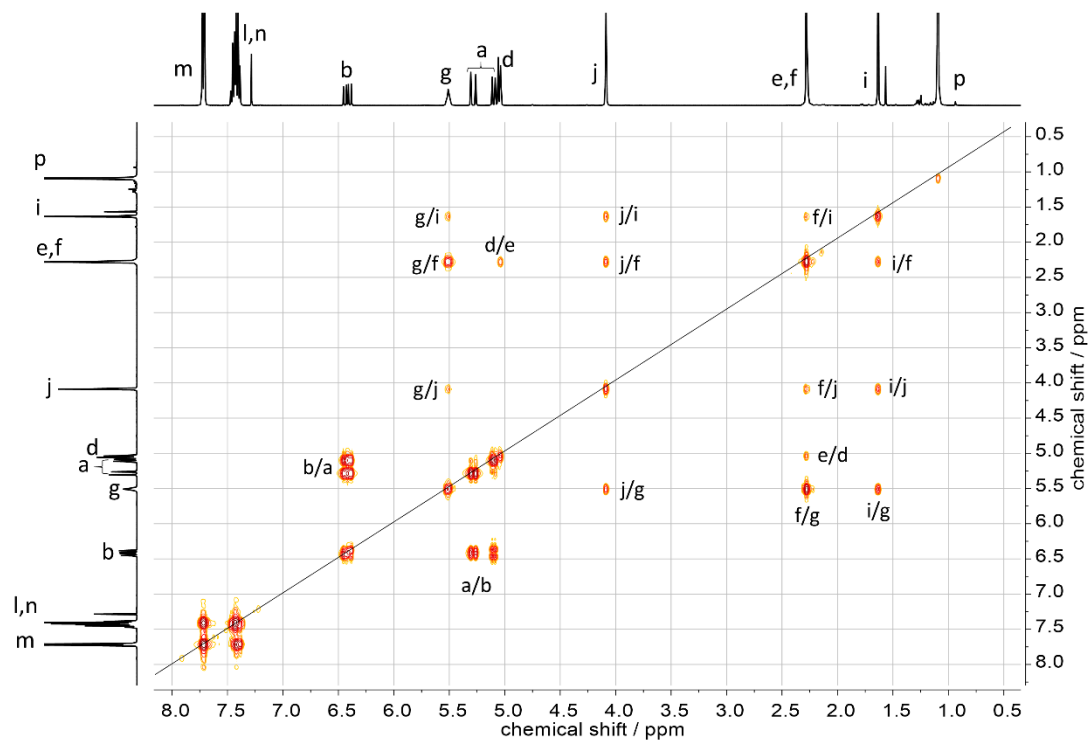


Figure S13. COSY NMR spectrum (400 MHz) of MyrOSi^{TBDPh} in CDCl₃.

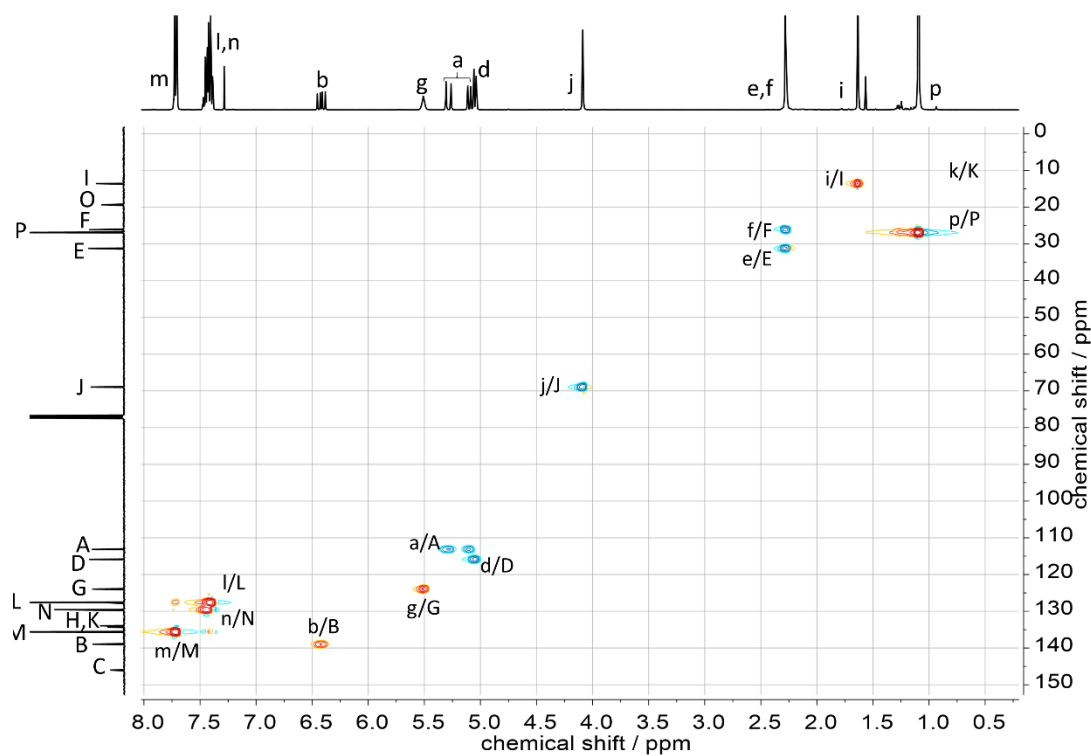


Figure S14. HSQC NMR spectrum (101 MHz / 400 MHz) of MyrOSi^{TBDPh} in CDCl₃.

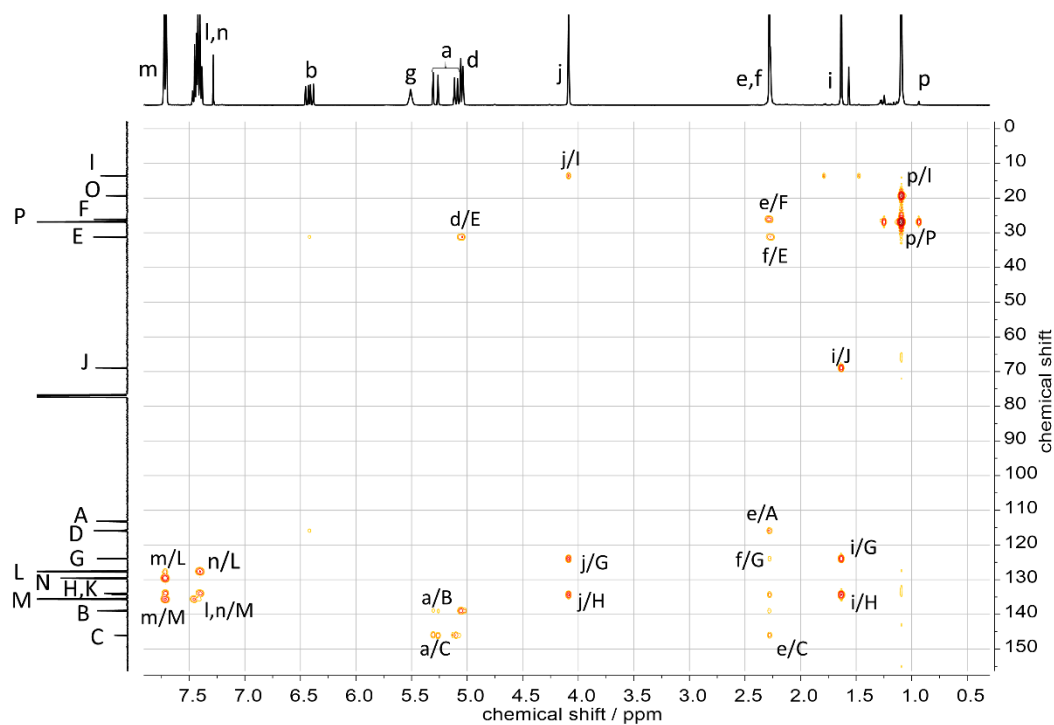


Figure S15. HMBC NMR spectrum (101 MHz / 400 MHz) of MyrOSi^{TBDPh} in CDCl₃.



Figure S16. ²⁹Si NMR spectrum (400 MHz) of MyrOSi^{TBDPh} in CDCl₃.

2 Homopolymer characterization

2.1 NMR spectra of PMyrOSiTBDM

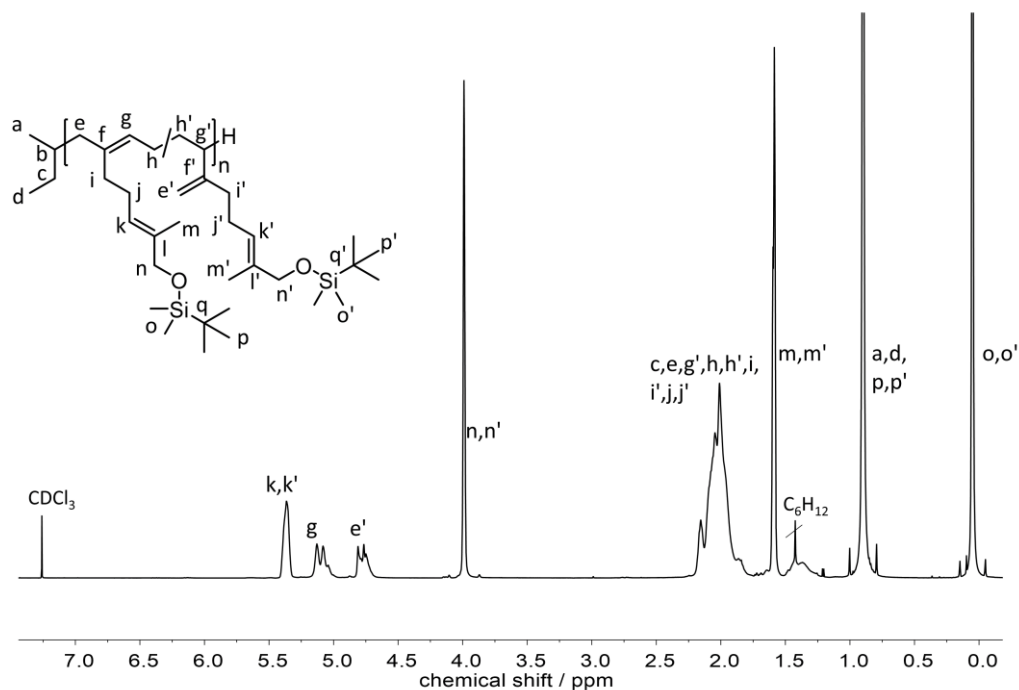


Figure S17. ¹H NMR spectrum (600 MHz) of PMyrOSi^{TBDM} in CDCl₃.

2.2 NMR spectra of PMyrOSiTIP

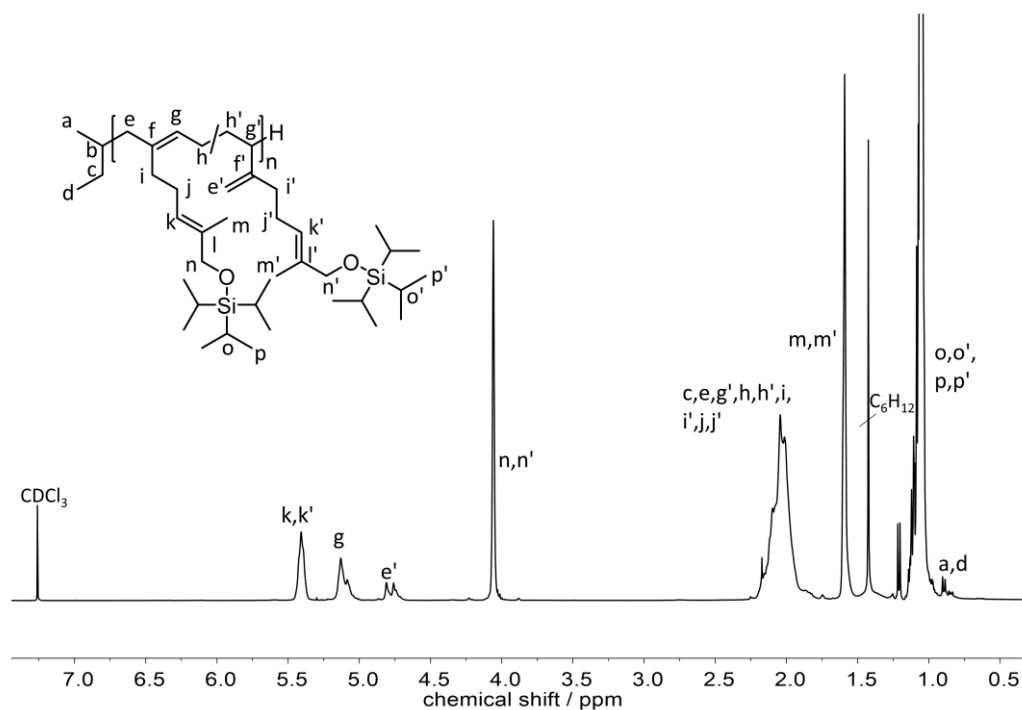


Figure S18. ¹H NMR spectrum (400 MHz) of PMyrOSi^{TIP} in CDCl₃.

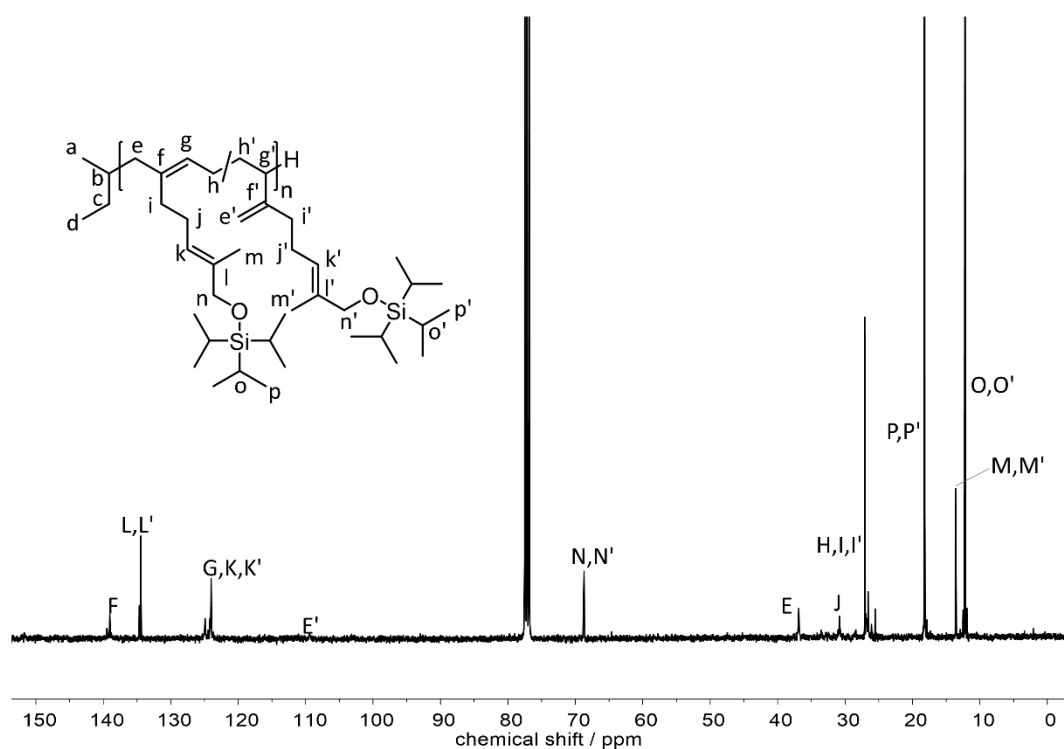


Figure S19. ^{13}C NMR inverse gated (IG) spectrum (101 MHz) of PMyrosi-TIP in CDCl_3 .

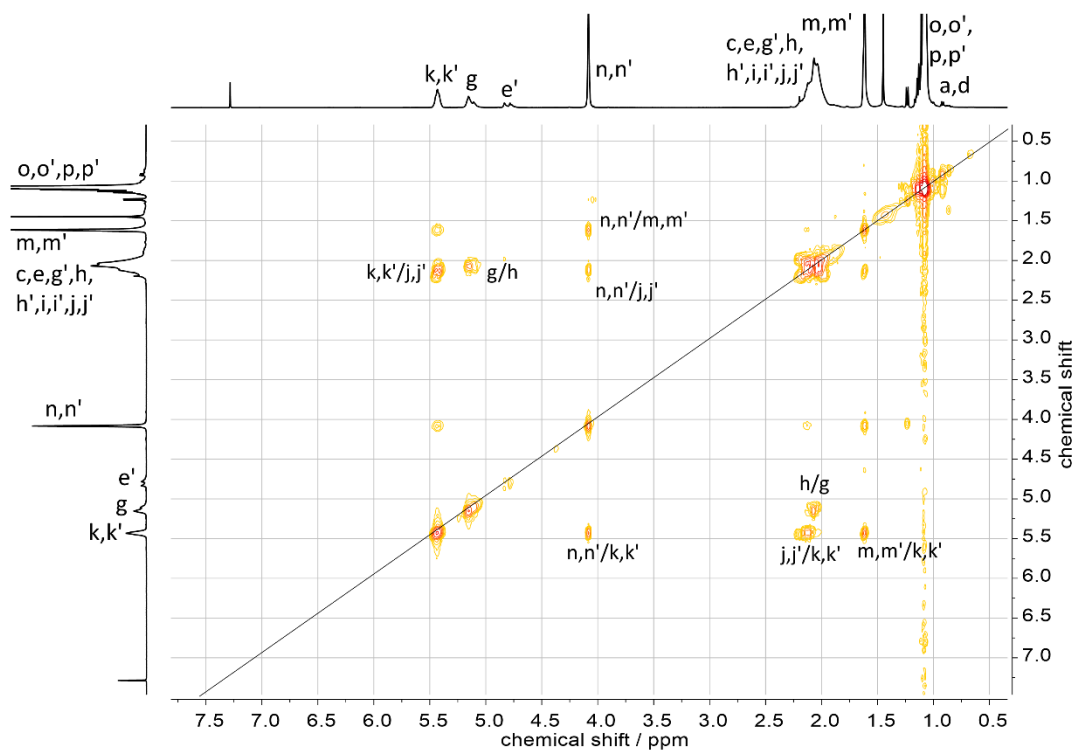


Figure S20. COSY NMR spectrum (400 MHz) of PMyrosi-TIP in CDCl_3 .

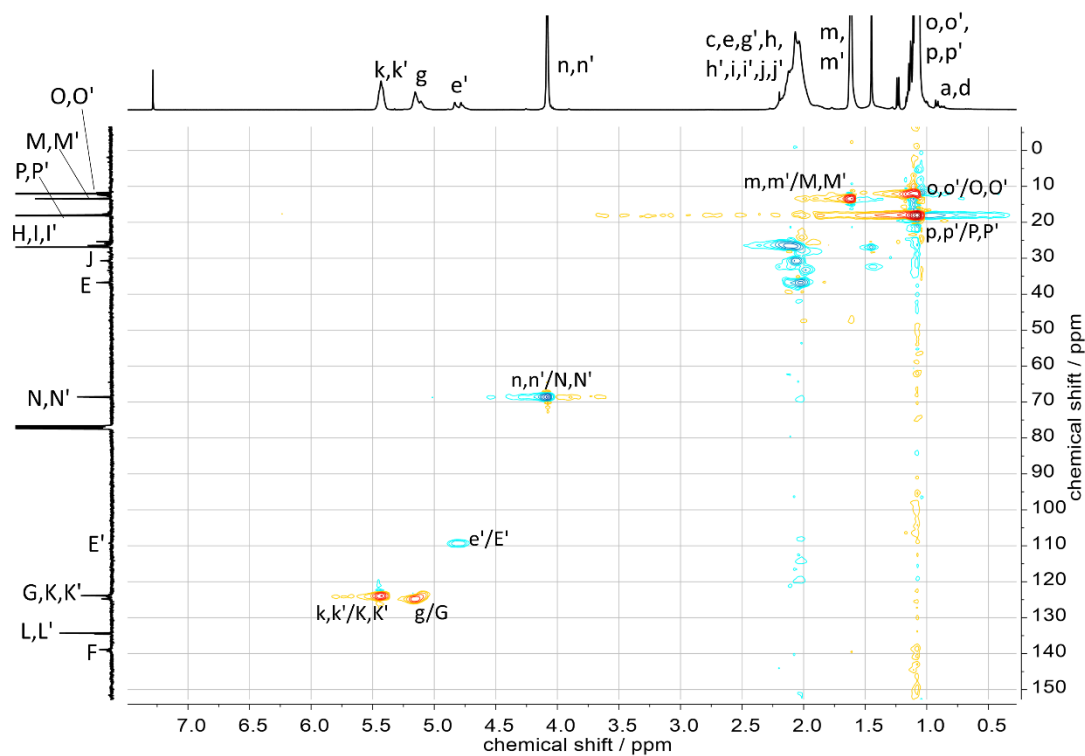


Figure S21. HSQC NMR spectrum (101 MHz / 400 MHz) of PMyrOSi^{TIP} in CDCl₃.

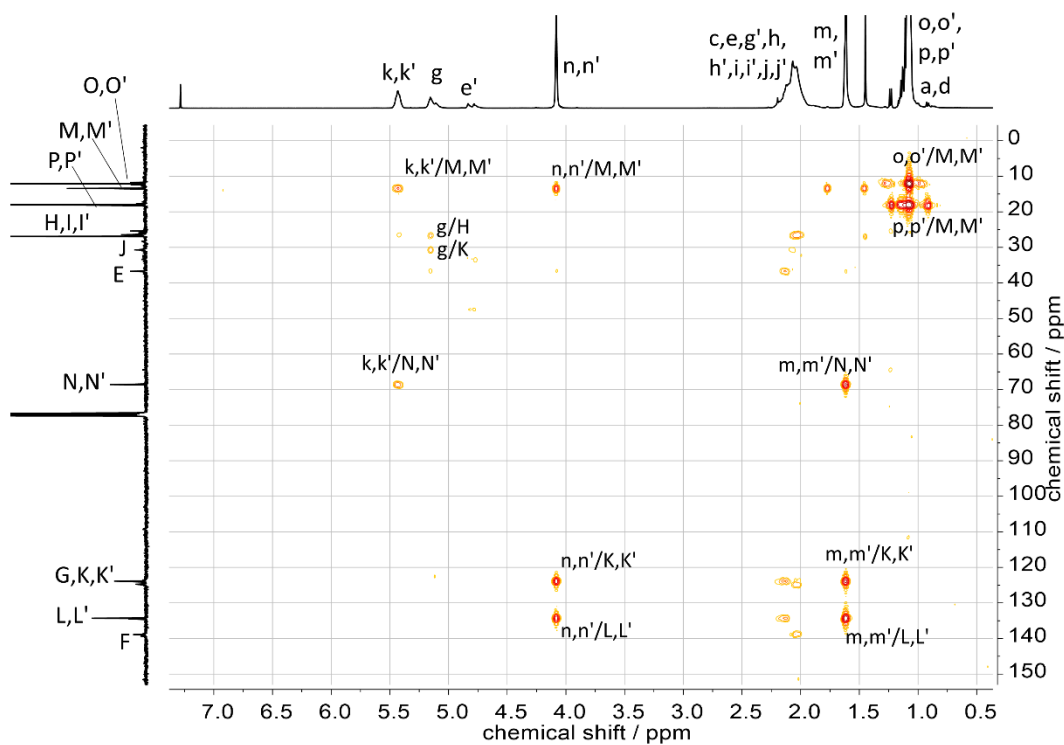


Figure S22. HMBC NMR spectrum (101 MHz / 400 MHz) of PMyrOSi^{TIP} in CDCl₃.

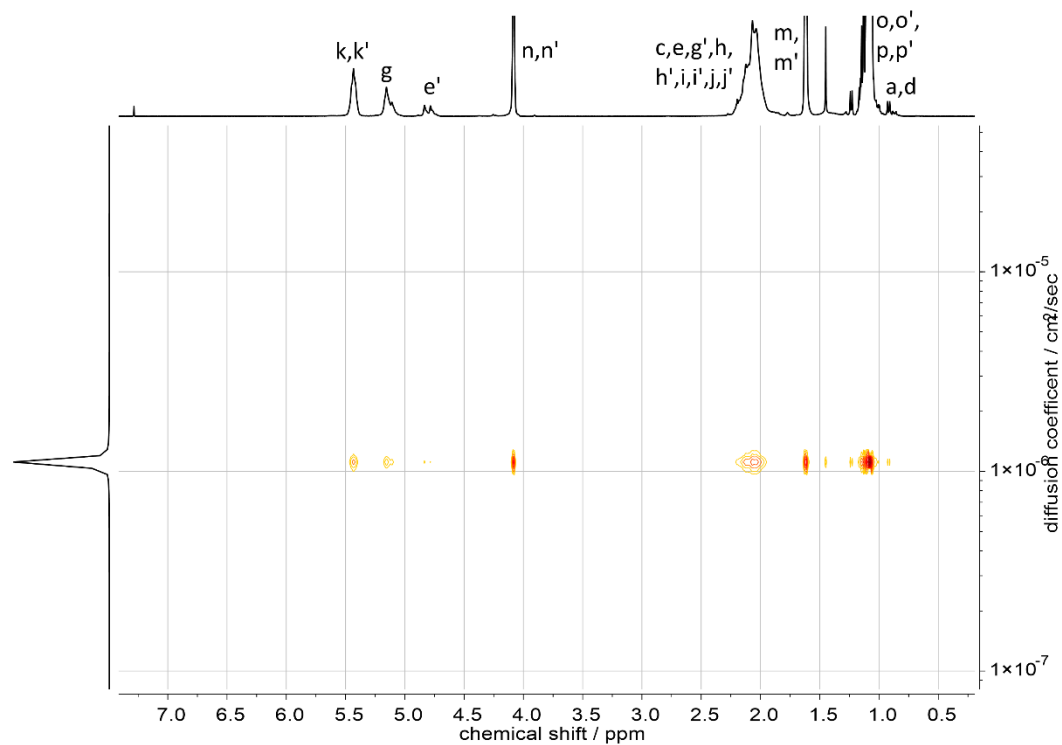


Figure S23. DOSY spectrum (400 MHz) of PMyOSi^{TIP} in CDCl₃.

2.3 NMR spectra of PMyOSiTBDPh

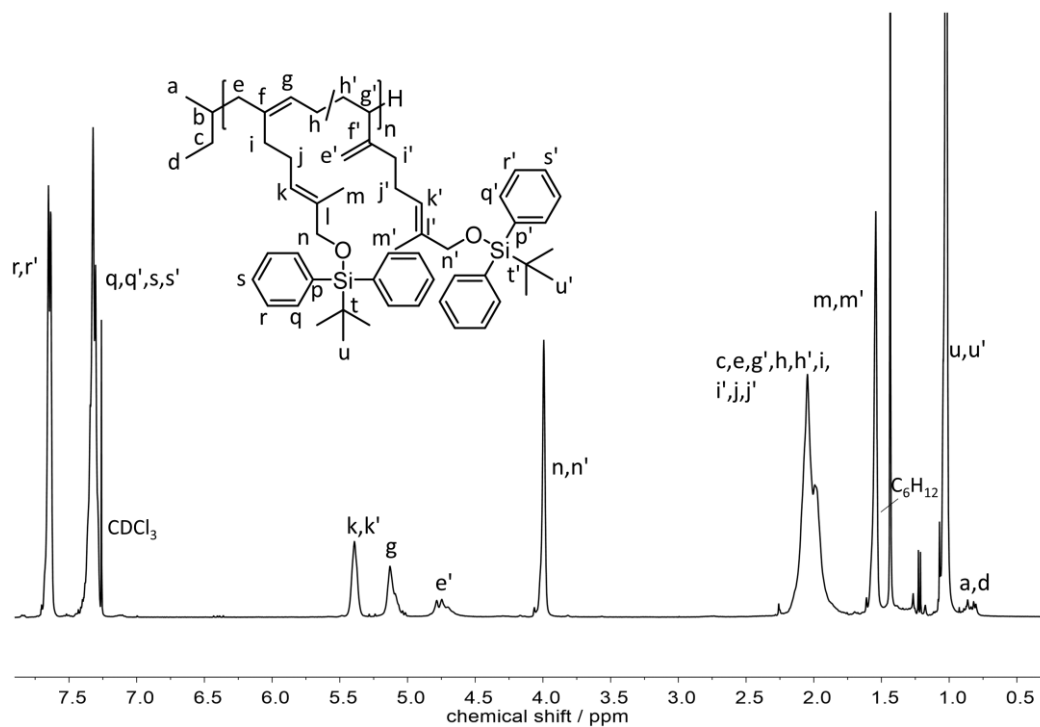


Figure S24. ¹H NMR spectrum (400 MHz) of PMyOSi^{TBDPh} in CDCl₃.

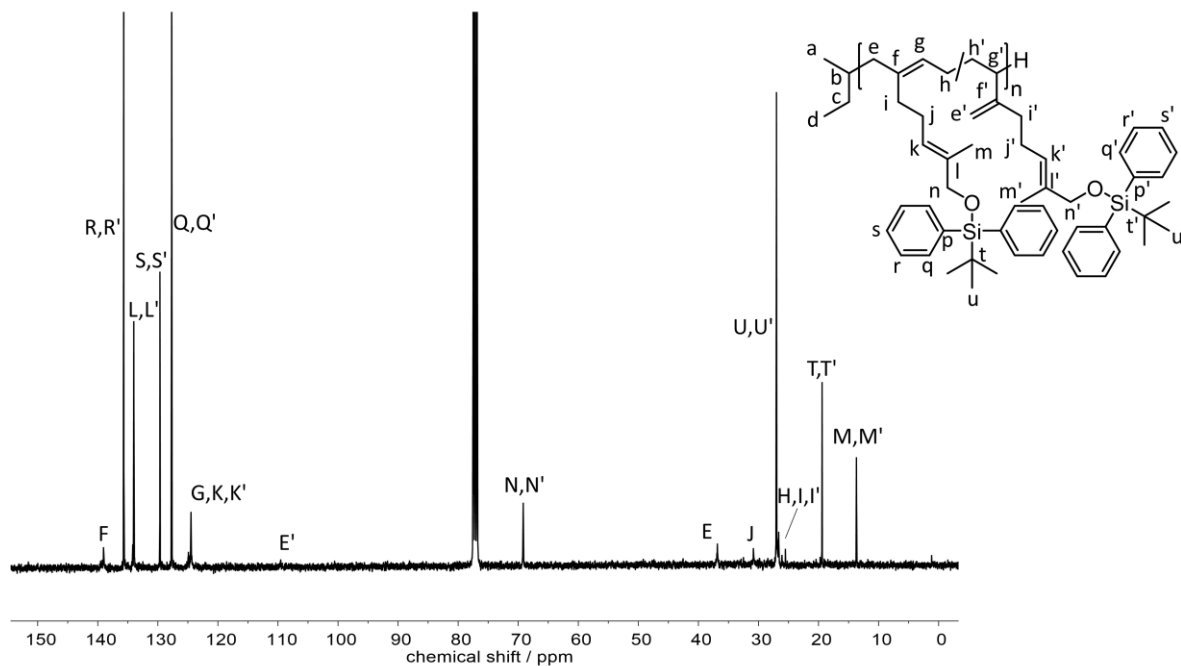


Figure S25. ^{13}C NMR *inverse gated* (IG) spectrum (101 MHz) of $\text{PMyOSi}^{\text{TBDDPh}}$ in CDCl_3 .

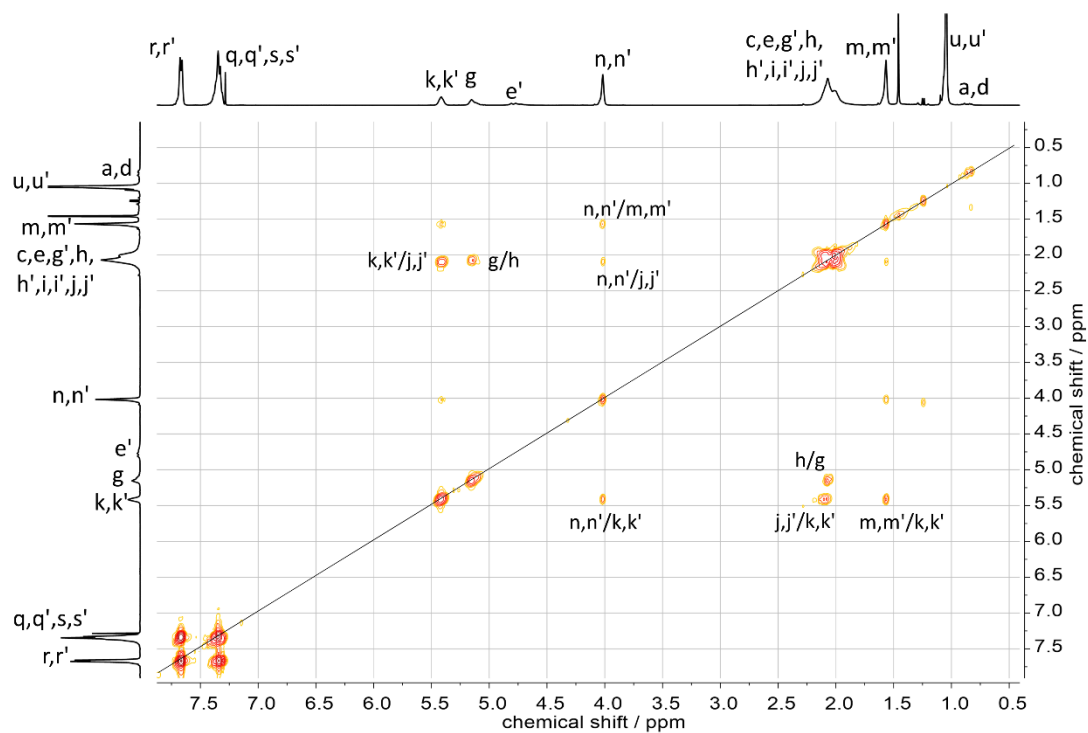


Figure S26. COSY spectrum (400 MHz) of $\text{PMyOSi}^{\text{TBDDPh}}$ in CDCl_3 .

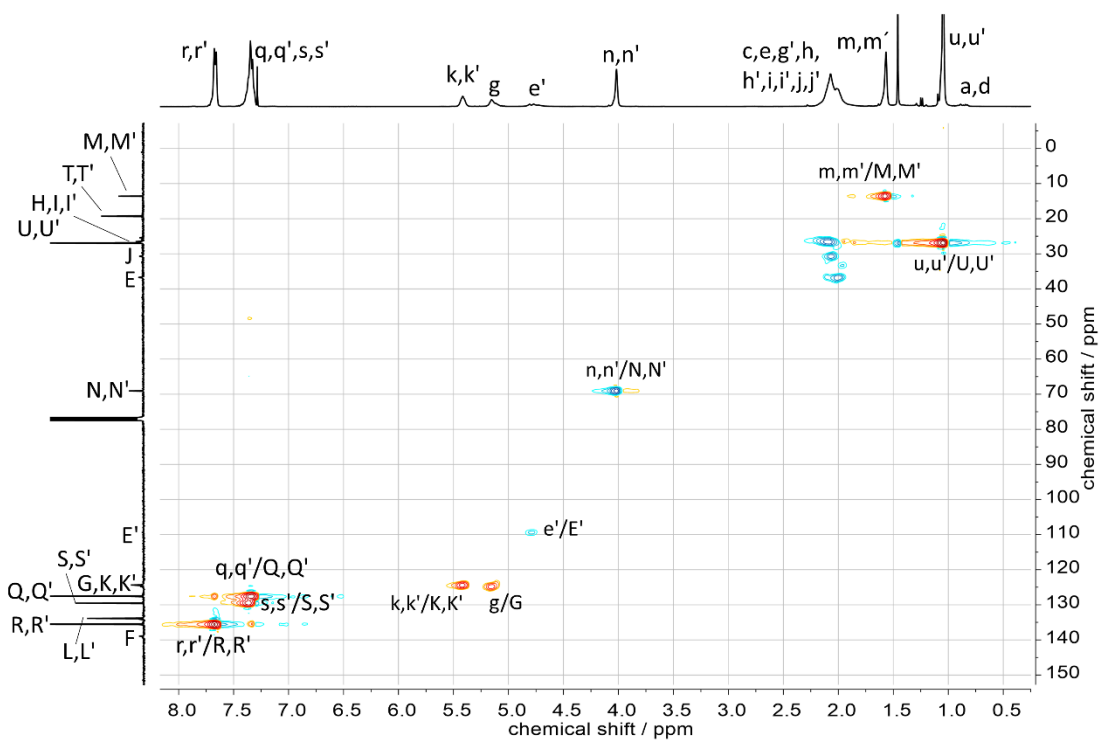


Figure S27. HSQC NMR spectrum (101 MHz / 400 MHz) of PMyrOSi^{TBDPh} in CDCl₃.

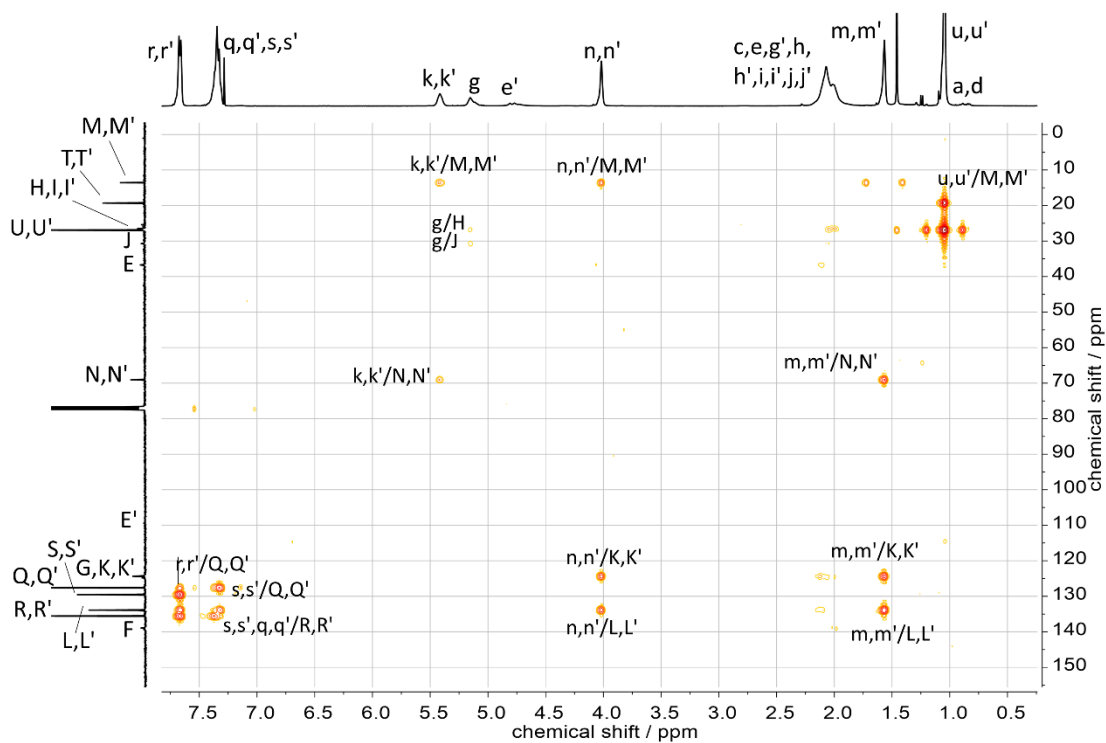


Figure S28. HMBC NMR spectrum (101 MHz / 400 MHz) of PMyrOSi^{TBDPh} in CDCl₃.

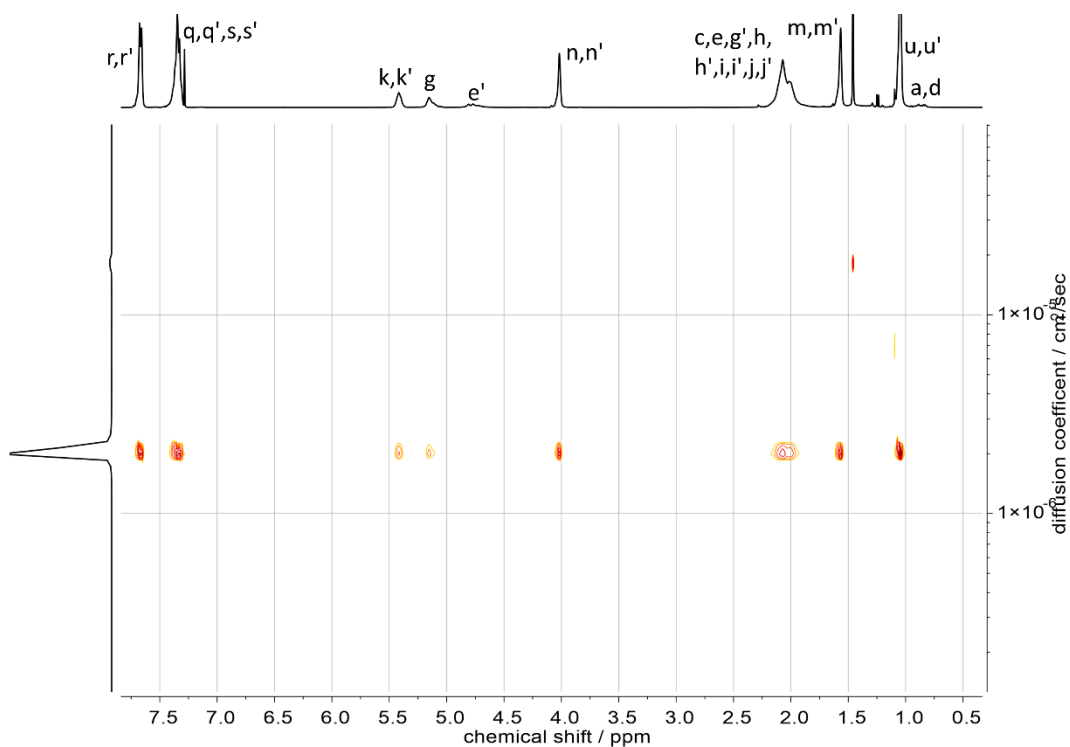


Figure S29. DOSY spectrum (400 MHz) of PMyrOSi^{TBDPh} in CDCl₃.

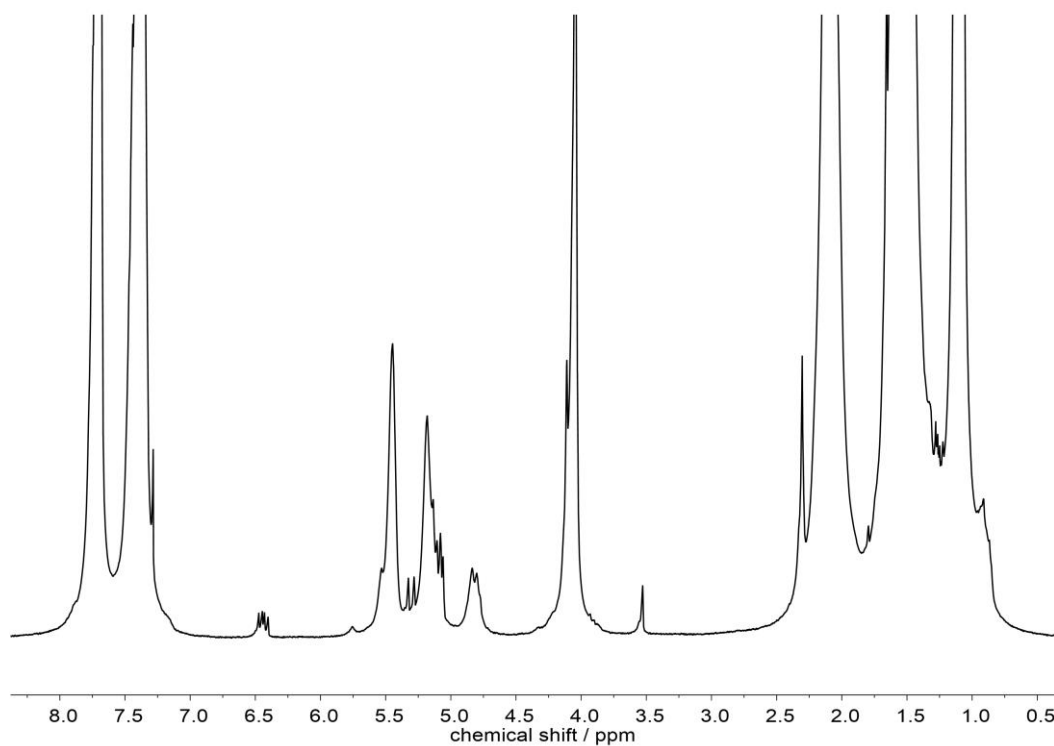


Figure S30. ¹H NMR spectrum (400 MHz) of the crude PMyrOSi^{TBDPh} in CDCl₃, showing an incomplete monomer conversion (e.g. monomer residues in form of proton signal at 6.41 ppm).

2.4 NMR spectra of PMyrOH

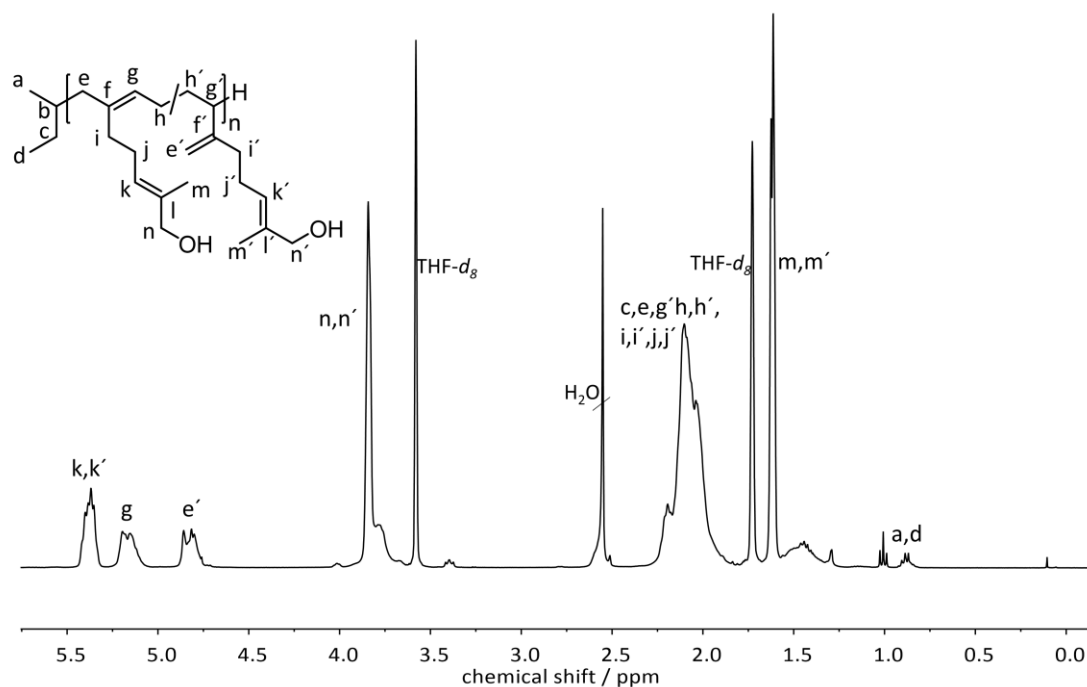


Figure S31. ¹H NMR spectrum (400 MHz) of PMyrOH (synthesized with TBDMS protective group) in THF-*d*₈.

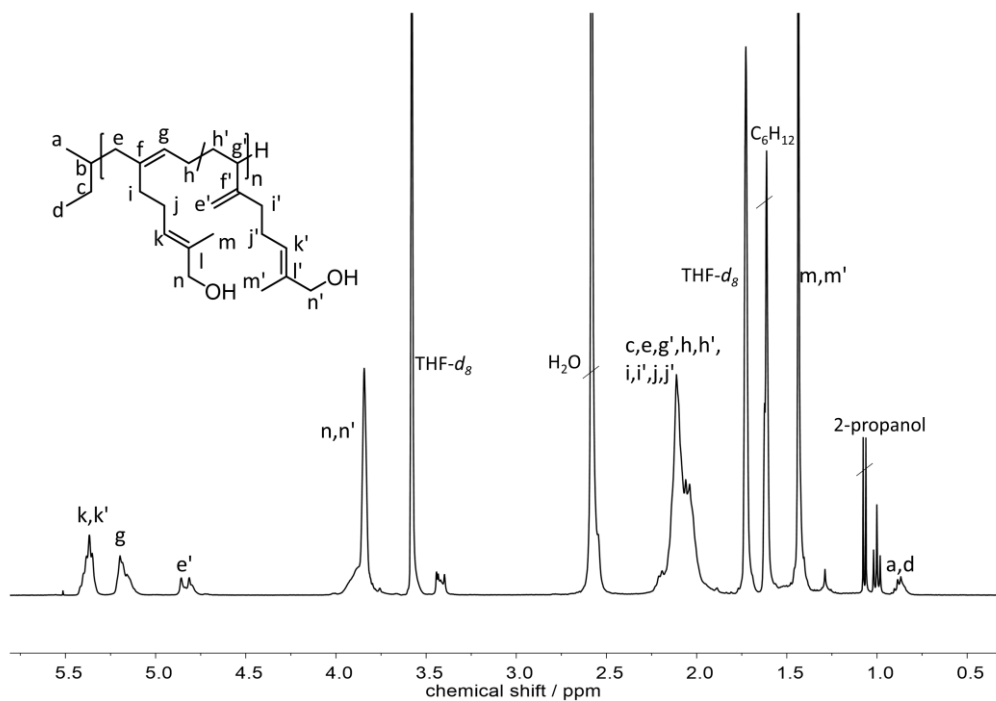


Figure S32. ¹H NMR spectrum (400 MHz) of PMyrOH (synthesized with TIPS protective group) in THF-*d*₈.

2.5 Determination of polydiene microstructure of homopolymers (content of 3,4-units)

The content of 3,4-units in the homopolymer backbone was calculated from the integrals (I) of the proton signals e' and g of the ^1H NMR spectrum (Figure S17, S18 and Figure S24) as follows:

$$3,4 \text{ content (\%)} = \frac{\frac{I(e', e''')}{2}}{I(g) + \frac{I(e', e''')}{2}} \quad (\text{S1})$$

2.6 SEC trace of $\text{PMyrOH}^{\text{TBDMS}}$

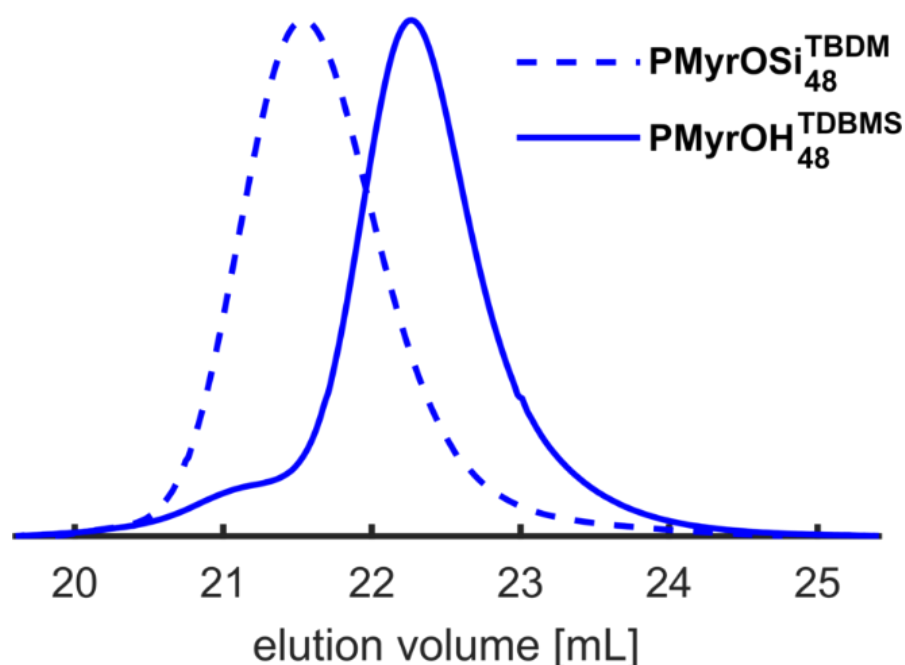


Figure S 33. SEC traces (THF, PI standard, RI signal) before ($\text{PMyrOSi}_{48}^{\text{TBDM}}$, dashed line) and after ($\text{PMyrOH}_{48}^{\text{TDBMS}}$, green line) removal of the protective groups.

2.7 DSC measurements

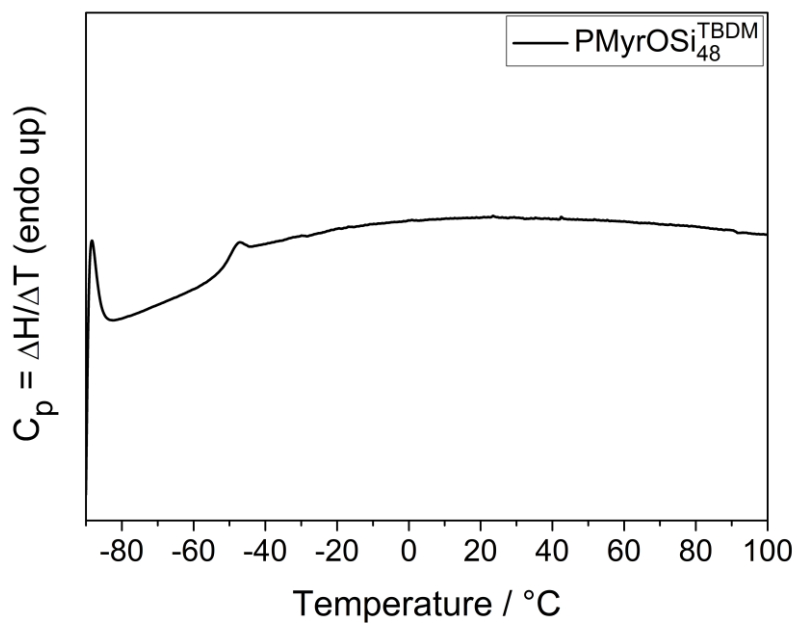


Figure S 34. DSC-Curves of PMyrOSi^{TBDM}₄₈ (heating rate of 10 °C min⁻¹).

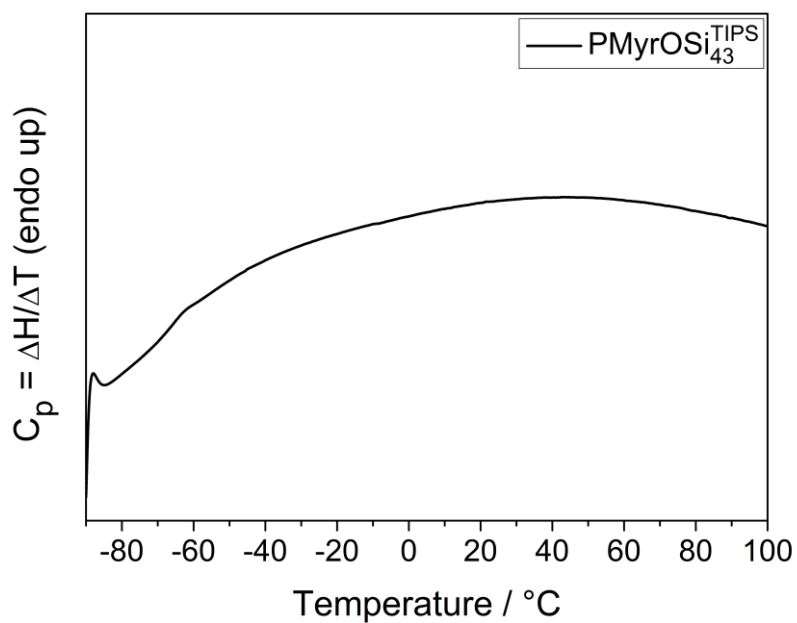


Figure S 35. DSC-Curves of PMyrOSi^{TIPS}₄₃ (heating rate of 10 °C min⁻¹).

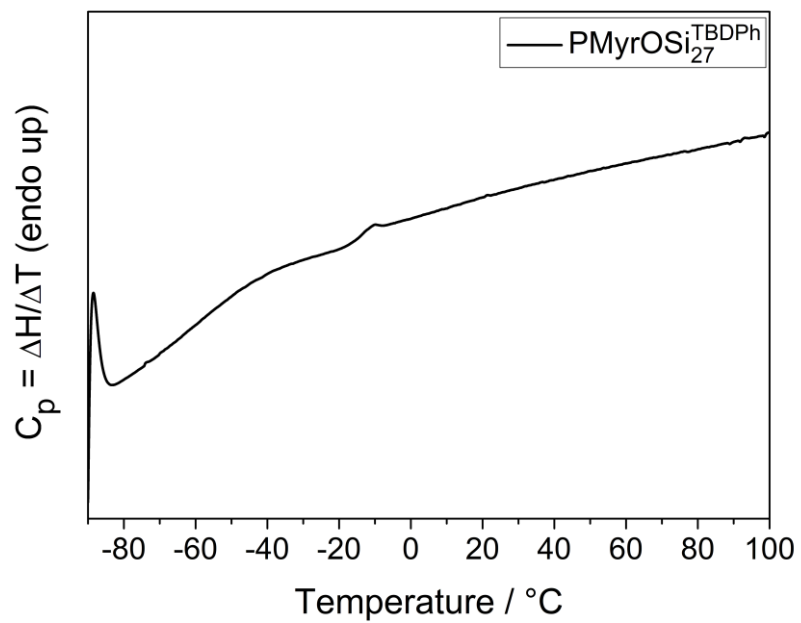


Figure S 36. DSC-Curves of PMyrOSi^{TBDPh}₂₇ (heating rate of 10 °C min⁻¹).

CHAPTER 4

Terpene-Based Thermoplastic Elastomers

CHAPTER 4

Tapered Multiblock Copolymers Based on Farnesene and Styrene: Impact of Bio-Based Polydiene Architectures on Material Properties

Christian Wahlen,^a Jan Blankenburg,^a Philipp von Tiedemann,^a Johannes Ewald,^a Pawel Sajkiewicz,^b Axel H. E. Müller^{*,a}, George Floudas^{*,c,d}, and Holger Frey^{*,a}

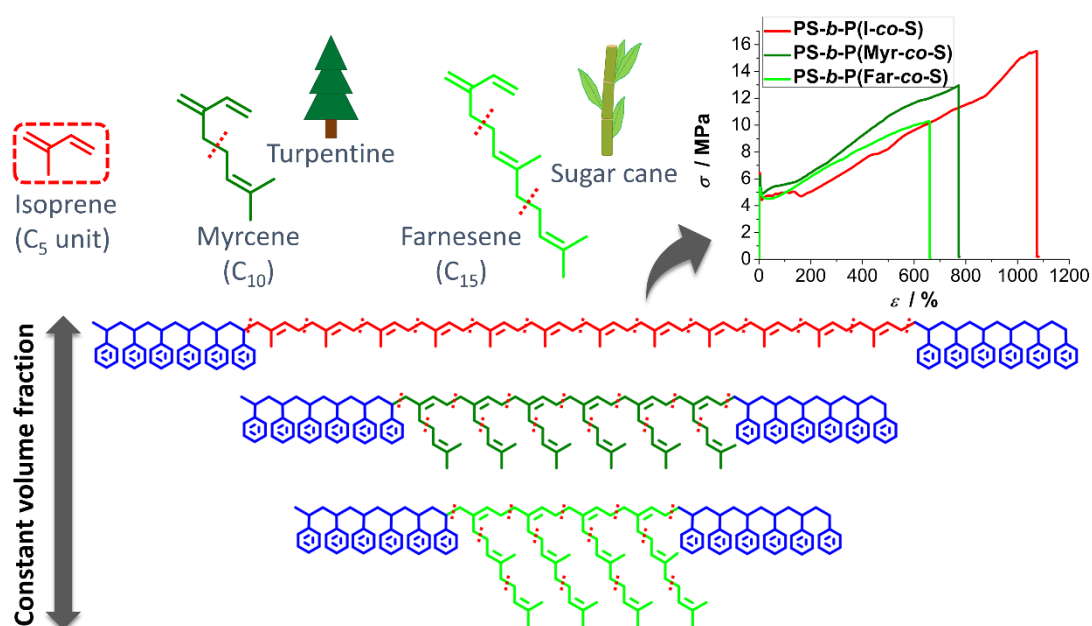
^a Department of Chemistry, Johannes Gutenberg University, Duesbergweg 10-14, 55128 Mainz, Germany

^b Institute of Fundamental Technological Research, Polish Academy of Sciences, Adolfa Pawińskiego 5b, 02-106 Warsaw, Poland

^c Max Planck Institute for Polymer Research, D-55125 Mainz, Germany

^d Department of Physics, University of Ioannina, P.O. Box 1186, 45110 Ioannina, Greece

Submitted to *Macromolecules*.



Abstract

The reactivity of the bio-based monomer β -farnesene in the statistical anionic copolymerization with styrene and the effect of the bottlebrush-like polyfarnesene structure on phase separation behavior were investigated. Furthermore, thermal and material properties of β -farnesene-based thermoplastic elastomers (TPEs), based on tri- and pentablock copolymers with styrene, and their processing behavior were investigated. As shown by ^1H NMR online kinetics, in analogy to both isoprene and β -myrcene, the direct (i.e. statistical) anionic copolymerization of β -farnesene and styrene in cyclohexane affords block-like, tapered copolymers due to the highly diverging reactivity ratios ($r_{\text{Far}} = 27$; $r_{\text{S}} = 0.037$). Algebraic expressions both for the molar and volume composition profiles were derived, which allow a mathematically accurate visualization of the tapered copolymer structure. The one-pot, tapered copolymer approach was used to synthesize series of tri- (ABA) and pentablock (ABABA) copolymers of styrene (A) and β -farnesene (B), varying the polydiene volume fraction between 0.50 and 0.68, respectively. Depending on the polydiene volume fraction, the tapered multiblock copolymers showed phase separation in lamellar or hexagonally packed cylindrical structures, as determined by small-angle X-ray scattering. Well-defined tapered tri- and pentablock copolymers with molecular weights of $120 \text{ kg}\cdot\text{mol}^{-1}$ and low dispersity ($\mathcal{D} = 1.05\text{--}1.16$) were obtained. The phase state of the poly(styrene-*co*-farnesene) copolymers bears many similarities (same morphology, practically the same domain spacing and a similar degree of segregation) to the corresponding polyisoprene copolymers with the same polydiene volume fraction. The similar domain spacing is suggestive of looped configurations mainly in the polyisoprene copolymers that are reduced in the polyterpene copolymers. The influence of the long alkenyl side chains of the polyfarnesene middle blocks on the mechanical properties of the multiblock copolymers was investigated by tensile testing. For this purpose, the respective tri- and pentablock copolymers of isoprene (C_5 unit) and β -myrcene (C_{10}) with styrene were synthesized as well, containing equal polydiene volume fractions as their β -farnesene-based (C_{15}) analogs. The mechanical toughness of the polymers increased with decreasing length of the alkenyl side chains (from β -farnesene to isoprene). Furthermore, tapered polyfarnesene tri- and pentablock copolymers with styrene exhibit reduced solution viscosity in comparison to e.g. polyisoprene-based tapered PS-*b*-P(I-*co*-S) triblock copolymers, resulting in improved processability by electrospinning. These

properties are discussed in terms of the different configurations of the polyterpene blocks and the pronounced differences in the entanglement molecular weights.

Introduction

Limited fossil feedstocks and the accumulating plastic waste in the environment have increased the prominence of research in the field of sustainable polymers within the last decade.¹⁻⁷ Terpenes like β -myrcene and β -farnesene are bio-based alternatives for the petroleum-based 1,3-diene monomers butadiene and isoprene, which are commercially used for the synthesis of thermoplastic elastomers (TPEs) on large scale.^{8,9} Due to the increasing interest in bio-based materials, monomers from renewable sources like β -myrcene are already used on limited scale as an alternative for isoprene.^{8,10,11} While β -myrcene is industrially produced by pyrolysis of β -pinene obtained from turpentine, β -farnesene is manufactured on large scale from sugar cane (by Amyris, Inc.), using fermentation technology.¹² In several approaches alternative routes to produce the – typically fossil source-based – monomers isoprene and styrene from biomass were also developed in recent works.¹³⁻¹⁶ However, these approaches are currently not scalable to an industrially relevant production volume. In analogy to isoprene and β -myrcene, the 1,3-diene moiety of β -farnesene enables its anionic polymerization. Obeying the isoprene rule for terpenes, β -myrcene (C_{10}) consists of two isoprene units (C_5), while β -farnesene (C_{15} , sesquiterpene) can be described as an isoprene trimer.¹⁷ Accordingly, the three diene monomers differ in the length of the alkenyl side chain linked to the polymerizable diene unit. The effect of the long alkenyl side chains on the polymer properties has been investigated for homopolymers of β -farnesene as well as for copolymers with butadiene in recent works.¹⁸⁻²² Due to the long C_{11} or C_{13} pendant groups, depending on the respective polydiene-microstructure (1,4- or 3,4-units), polyfarnesene can be described as a bottlebrush-like polymer. This structure of polyfarnesene (PFar) leads to reduced melt viscosity in comparison to polyisoprene (PI) and polymyrcene (PMyr), which is explained by the significantly higher entanglement molecular weight ($M_e(\text{PFar}) = 50 \text{ kg}\cdot\text{mol}^{-1} > M_e(\text{PMyr}) = 18 \text{ kg}\cdot\text{mol}^{-1} > M_e(\text{PI}) = 5.4 \text{ kg}\cdot\text{mol}^{-1}$).^{19,23} In addition, the unique bottlebrush-like structure of polyfarnesene results in a low glass temperature of 198 K. Furthermore, compared to polyisoprene, the polyfarnesene T_g exhibits a weak dependence on microstructure, because the compact branched structure dominates the effect of the backbone.¹⁸

At present there is little information available regarding copolymers of β -farnesene in general and in particular copolymers with styrene. The resulting materials are promising with respect to bio-based thermoplastic elastomers. Kuraray et al. developed the first ABA triblock copolymers based on styrene and β -farnesene, with hydrogenated polyfarnesene midblock.²⁴ However, to the best of our knowledge, the only work focusing on the copolymerization of this comonomer pair was published by Kirillov et al., who copolymerized styrene and β -farnesene, catalyzed by an *ansa*-lanthanidocene catalyst, resulting in random copolymers.²⁵ The statistical anionic copolymerization of analogous 1,3-diene monomers, like isoprene and β -myrcene with styrene (or its derivatives) in apolar solvents like cyclohexane affords block-like, tapered copolymers, mirroring the highly disparate reactivity ratios.²⁶⁻²⁸ Tapered copolymers of styrene and 1,3-diene monomers like isoprene or β -myrcene are known for their microphase separation behavior,^{26,27,29} which is mainly driven by the thermodynamic incompatibility. This is described by the Flory-Huggins interaction parameter (χ), the molecular weight and the molecular composition of the polymer, described in terms of the polymer volume fraction.³⁰⁻³³ Thermal and mechanical properties are mainly governed by the microphase separation and the resulting bulk morphologies of the copolymers.³⁴⁻³⁷

The vast potential of bio-based monomers for the synthesis of thermoplastic elastomers was pointed out in the work of Bolton et al., in which α -methyl-*p*-methyl-styrene based polymyrcene containing thermoplastic elastomers were synthesized by the sequential anionic copolymerization in THF at low temperatures, capitalizing on dichlorodimethylsilane coupling.³⁸ However, the respective polymerization of 1,3-diene monomers in THF is known to result in an increased content of side chain vinyl regioisomers (3,4- and 1,2-units) in the polymer backbone.³⁹ The side chain vinyl regioisomers increase the glass temperature of the rubbery polydiene phase, which is undesired for most applications.⁴⁰ As an alternative to the polymerization in THF, the one-step tapered copolymer approach can be used for the synthesis of styrene/diene-based tapered multiblock copolymers in cyclohexane, relying on sequential monomer addition of diene/styrene monomer-mixtures, resulting in a tapered diblock for each addition step. The multiblock copolymer synthesis in cyclohexane results in thermoplastic elastomer materials with high 1,4-unit content and consequently low T_g of the rubbery polydiene phase. These tapered multiblock copolymers show outstanding mechanical properties and microphase separation behavior.⁴¹⁻⁴³

In this work we aim at presenting a comprehensive picture of β -farnesene/styrene-based copolymers, starting from an investigation of the copolymerization kinetics to the synthesis of tapered multiblock copolymers. We also studied the resulting materials properties and processing behavior, keeping an eye on the comparison with the established isoprene and β -myrcene (multiblock) copolymers with styrene. A series of tri- and pentablock copolymers with constant molecular weights ($120 \text{ kg}\cdot\text{mol}^{-1}$), with two different polydiene volume fractions ($\phi_{\text{PDiene}} = 0.5$ and 0.68) were prepared. In the series of block copolymers, the brush length of the polydiene middle block increases from isoprene to β -farnesene. Consequently, for a valid comparison of the multiblock copolymers, the volume fraction of the polydiene middle blocks was kept constant for each diene monomer in order to study the effect of the bottle-brush architecture of polyfarnesene on the phase state and the mechanical properties.

Experimental Section

Reagents. Isoprene (99%), *sec*-butyllithium as a 1.3 M solution in cyclohexane/hexane (92/8) and calcium hydride were purchased from Acros Organics. β -Myrcene ($\geq 95\%$) was purchased from Sigma Aldrich. β -Farnesene with a purity of 95%, was received from BOC Sciences. Cyclohexane was acquired from Fisher Scientific. Cyclohexane- d_{12} was received from Deutero GmbH. Cyclohexane was dried using *sec*-butyllithium and 1,1-diphenylethylene (DPE) as an indicator (DPE-anion shows red color).

Instrumentation. SEC measurements were performed in THF as the mobile phase (flow rate $1 \text{ mL}/\text{min}$) on an SDV column set from PSS (SDV 10^3 , SDV 10^5 , SDV 10^6) and an RI detector. Calibration was carried out by using PS standards, provided by PSS Polymer Standard Service GmbH. NMR spectra were recorded on a Bruker Avance II 400 spectrometer with 400 MHz (^1H NMR). All spectra are referenced internally to the residual proton signals of the deuterated solvent. The thermal properties of the polymers were studied with a Q2000 (TA Instruments) differential scanning calorimeter (DSC). Two cooling and heating cycles were performed with a rate of $10 \text{ K}\cdot\text{min}^{-1}$ in a temperature range between 183 K and 403 K . The glass temperatures were extracted from the second cycle. Tensile tests were performed using a material testing machine Z005 (Zwick/Roell, Germany). The scanning electron microscopy (SEM) examinations of the fibers were conducted on a JEOL JSM-6010PLUS/LV scanning electron microscope with an acceleration voltage of 7 kV (secondary electron imaging mode, working distance: 10 mm ,

spot size: 50). For the sample preparation a SEM specimen stub was covered with adhesive carbon tape (NEM Tape, Nisshin EM. Co. Ltd.). A small piece of the nonwoven copolymer was glued onto the tape and coated twice for 2 minutes each with a thin layer of gold using a sputter coater (DII-29030SCTR Smart Coater, JEOL).

X-Ray scattering. Small-angle (SAXS) measurements were made using $\text{CuK}\alpha$ radiation (RigakuMicroMax 007 x-ray generator, Osmic Confocal Max-Flux curved multilayer optics). 2D diffraction patterns were recorded on an Mar345 image plate detector at a sample-detector distance of 2076 mm. Intensity distributions as a function of the modulus of the total scattering vector, $q = (4\pi/\lambda) \sin(2\theta/2)$, where 2θ is the scattering angle, were obtained by radial averaging of the 2D datasets. Samples in the form of thick films (~1 mm) were prepared by slow solvent casting (chloroform). Temperature-dependent measurements of 1 hour long were made by heating the films from 303 K to 453 K in 30 K steps and subsequent cooling to 303 K aiming at obtaining the phase state.

Synthesis of multiblock copolymers. A mixture of the diene monomer and styrene was dried over CaH_2 for 24 h, degassed by three freeze–thaw cycles, and distilled into a graduated ampule. In addition, the required amount of styrene was dried and degassed separately over CaH_2 for 24 h and was directly distilled into the reaction flask. Dried cyclohexane was distilled into the reaction flask, followed by flushing the flask with argon and the initiation of the polymerization of the first styrene block with a 1.3 M *sec*-BuLi solution. After 2 h a mixture of the diene monomer and styrene was added by an ampoule. For pentablock copolymers a second addition of the monomer mixture was carried out. The living polymerization was terminated by the addition of degassed 2-propanol. Afterwards the polymer was precipitated in 2-propanol and dried under vacuum. The equipment employed and the synthesis scheme are shown in Figure S12.

In situ ^1H NMR kinetics experiments. The monomers and the solvent were dried by the same procedure as for the multiblock copolymer synthesis. The monomer/solvent mixtures were prepared in an argon-filled glovebox (MBraun UNILAB, <0.1 ppm of O_2 and <0.1 ppm of H_2O). For the copolymerization at 23 °C a mixture of 0.1 mL β -farnesene (0.42 mmol, $[\text{Far}]_0 = 0.56 \text{ mol L}^{-1}$) and 0.05 mL styrene (0.42 mmol, $[\text{S}]_0 = 0.56 \text{ mol L}^{-1}$) in 0.6 mL of cyclohexane- d_{12}) was filled into NMR tubes and sealed with rubber septa. After initiation with 0.01 mL of *sec*-butyllithium ($[\text{Ini}]_0 = 0.017 \text{ mol L}^{-1}$) via syringe, the solution was vigorously homogenized by shaking several times. Subsequently, the NMR tube was

immediately inserted in the ^1H NMR spectrometer (Avance III HD 400 from Bruker; equipped with a 5 mm BBFO-SmartProbe (Z-gradient probe), ATM, and SampleXPress 60). A spectrum was recorded every 30 s with one scan until complete disappearance of the monomer signals. Additional to the kinetic experiment at 23 °C, ^1H NMR kinetic studies at increased sample temperatures (30 °C and 40 °C) were performed.

Electrospinning. The copolymer nanofiber preparation by electrospinning was adapted and modified from one of our previous works.⁴⁴ The copolymer was dissolved in a mixture of THF and DMF (80:20 v/v) to a concentration of 25-35 wt% (depending on the copolymer) by stirring at room temperature overnight. The spinning process was conducted using a rotating drum as collector (diameter: 2cm, length: 13 cm, rotation speed of 292 rpm), covered with aluminum foil. A distance between the needle tip (type Braun Sterican© 23G, with filed-down tip) and the collector drum of 10 cm was adjusted, and the spinning was conducted horizontally at a voltage of 17 kV and with a flow rate of 1.75 mL h⁻¹. The temperature inside the spinning chamber was 27-29 °C at a humidity of 45-50%. Scanning electron microscopy (SEM) was used for the characterization of the resulting fibers (as reported in Instrumentation). The diameters from 50 fibers were used in the calculation of the fiber diameter distribution using the software ImageJ. For the evaluation OriginPro 9.0 (OriginLab Corporation) was used.

Results and Discussion

***In situ* ^1H NMR copolymerization kinetics.** The kinetics of the statistical anionic copolymerization of styrene with isoprene and β -myrcene has been investigated in depth in the past and in recent years.^{26,27,45,46} In the current work we expand the understanding of the copolymerization kinetics of styrene with 1,3-diene derivatives to the copolymerization of styrene with β -farnesene. ^1H NMR kinetic experiments enable to determine the reactivity ratios, based on the non-terminal copolymerization model, which produces reliable results for modelling the anionic copolymerization in various systems.^{27,47,48} The *sec*-butyllithium ($[\text{Ini}]_0 = 0.017 \text{ mol L}^{-1}$) initiated copolymerization of β -farnesene ($[\text{Far}]_0 = 0.56 \text{ mol L}^{-1}$) and styrene ($[\text{S}]_0 = 0.56 \text{ mol L}^{-1}$) at 23 °C in deuterated cyclohexane was monitored by ^1H NMR spectroscopy, following the decrease of the methylene protons of styrene at 5.78-5.54 ppm (blue color) and β -farnesene at 6.41-6.28 ppm (green color) (stacked ^1H NMR spectra are shown in Figure 1, every 10th spectrum is shown, spectra were recorded every 30 s).

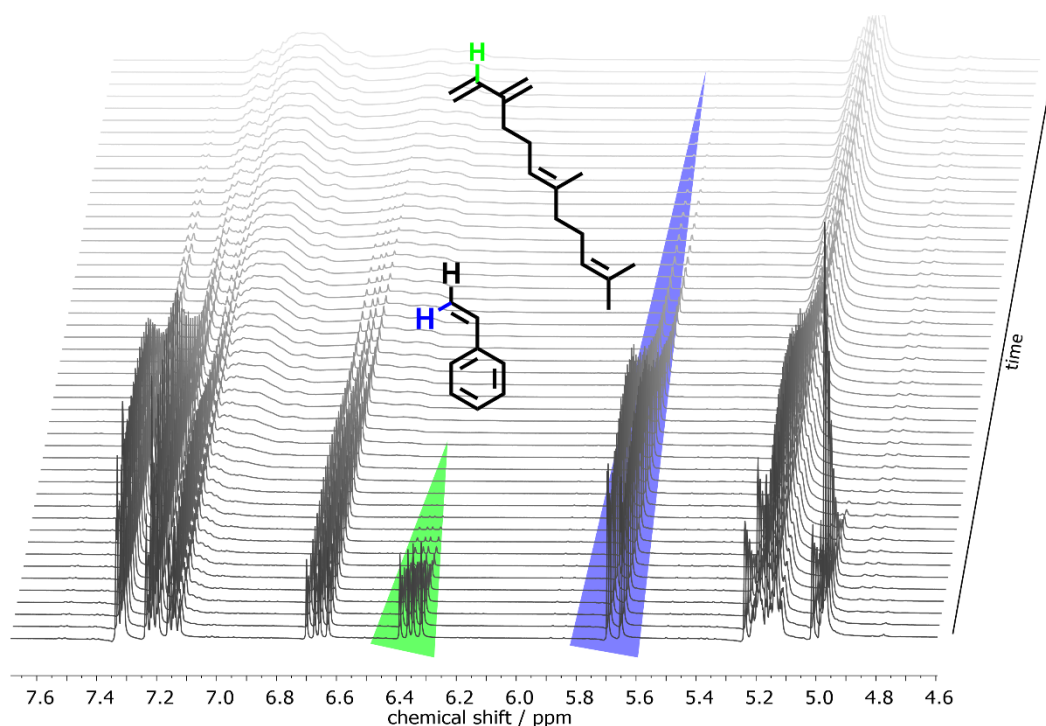


Figure 1. Stacked ¹H NMR spectra (400 MHz, C₆D₁₂) of the *in situ* NMR kinetics study of the copolymerization of styrene and β-farnesene at 23 °C (region from 7.7 to 4.6 ppm).

The normalized concentrations of both monomers, determined by integration of the monomer signals in the ¹H NMR spectra, were plotted as a function of time and function of total monomer conversion (Figures 2a and 2b). This shows the strongly preferred incorporation of β-farnesene at the early stage of the copolymerization, resulting in a polyfarnesene block with a small amount of incorporated styrene units, followed by a steep gradient. After complete conversion of β-farnesene, the remaining styrene forms a pure polystyrene block, resulting in a tapered copolymer. For the determination of the reactivity ratios the integrated equation⁴⁷ for the non-terminal (ideal) model according to Wall⁴⁸ was fitted to the experimental data, as shown in Figure S1. The value of the explanatory power (R^2) very close to unity verifies the accuracy of the fit and the adequate description of the copolymerization by the non-terminal model. Highly diverging reactivity ratios were determined for the copolymerization of β-farnesene and styrene ($r_{\text{Far}} = 27$, $r_{\text{S}} = 0.037$). In addition to the Integrated Ideal method, both the Jaacks⁴⁹ and the Meyer-Lowry⁵⁰ formalism were used to determine the reactivity ratios, as shown and discussed in the Supporting Information (Table S1 and Figures S1 and S2). The reactivity ratios were used for the calculation of the molar composition profile, shown in Figure 2b. Additional kinetic studies were performed at 30 °C and 40 °C, resulting in no significant

changes in the reactivity ratios (Figures S3 – S8). However, the fits for the terminal model by Mayo-Lewis⁵¹ (in the form of the Meyer-Lowry equation) resulted in a deviation of the reactivity ratios in comparison to the ideal/non-terminal model and in a clear temperature dependency of the reactivity ratios, without any tendency. For copolymerizations following the non-terminal model, the Meyer-Lowry treatment can be numerically unstable. These results illustrate the problem of overfitting, which results from using an overly complex model to describe experimental data, as is discussed in detail in the Supporting Information (Table S2 and Figure S9).^{52,53} Therefore the resulting values from the ideal model of Wall in the form of the Integrated Ideal equation were regarded to be more reliable and used for the depiction of the composition profiles.

In addition, the homopolymerization ¹H NMR kinetics of β -farnesene has been investigated, showing that the homopolymerization rate of β -farnesene ($k_{\text{FarFar}} = 3.2 \cdot 10^{-3} \text{ (L/mol)}^{1/4} \text{ s}^{-1}$, at 23 °C in cyclohexane) is significantly higher than the rate of isoprene ($k_{\text{II}} = 0.61 \cdot 10^{-3} \text{ (L/mol)}^{1/4} \text{ s}^{-1}$, at 23 °C)²⁸, resulting in a faster copolymerization with styrene, as shown and discussed in detail in the Supporting Information (Tables S3–S5 and Figure S10). The shorter reaction times of the copolymerization of β -farnesene and styrene are demonstrated on some exemplary Monte Carlo simulations in Table S6.

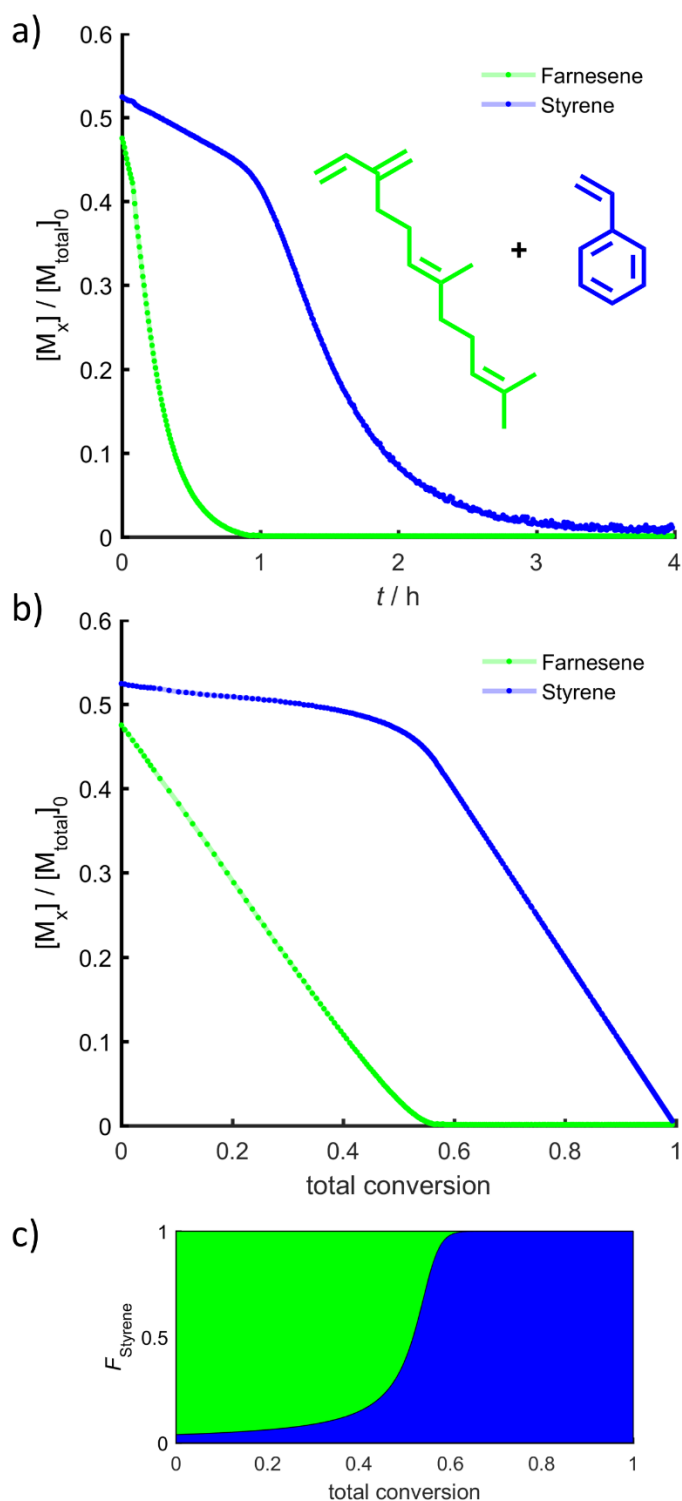


Figure 2. a) Time-conversion plots of the copolymerization of β -farnesene (green) and styrene (blue). Monomer concentrations were determined by *in situ* ^1H NMR spectroscopy in C_6D_{12} at $23\text{ }^\circ\text{C}$. b) Comonomer concentrations as a function of total conversion. c) Calculated molar composition profile of the corresponding tapered copolymer.

The resulting bulk morphologies of (block) copolymers, discussed in an ensuing section of this work, mainly depend on the volume fraction of the polymer blocks and their thermodynamic incompatibility.⁵⁴ Since the degree of phase separation can influence the related key material properties of (block) copolymers, understanding of the volume based monomer gradient profile is crucial.³⁰⁻³⁴ Thus, it is necessary to convert the molar composition profile into the volume composition profile. To the best of our knowledge, the molar and volume composition profiles have not been accessible by algebraic expressions to date. In the Supp. Inf. we show the analytical derivation of the explicit expressions both for the molar and volume composition profiles. These expressions can be directly implemented in simple spreadsheet software and in this way render the depiction of the copolymer composition profile easily accessible (as shown in Figure 3). Furthermore, this approach eliminates the risk of introducing numerical errors compared to previous approaches that use numerical integration to depict the composition profiles.^{29,55} The results of applying the related equations for the copolymerization of styrene with 1,3-dienes are shown in Figure 3. The difference in the molar and volume composition profile depends on the molecular weight and the corresponding volume of the 1,3-diene monomer. Obviously, the shift from the molar to volume composition profile strongly depends on the 1,3-diene monomer employed. While the shift for the isoprene-based copolymers is low, it increases with increasing volume of the diene monomer units from β -myrcene (C₁₀, isoprene dimer) to β -farnesene (C₁₅, isoprene trimer). The steepness of the gradient and the disparity of the reactivity ratios increases in the order I/S < Far/S < Myr/S.

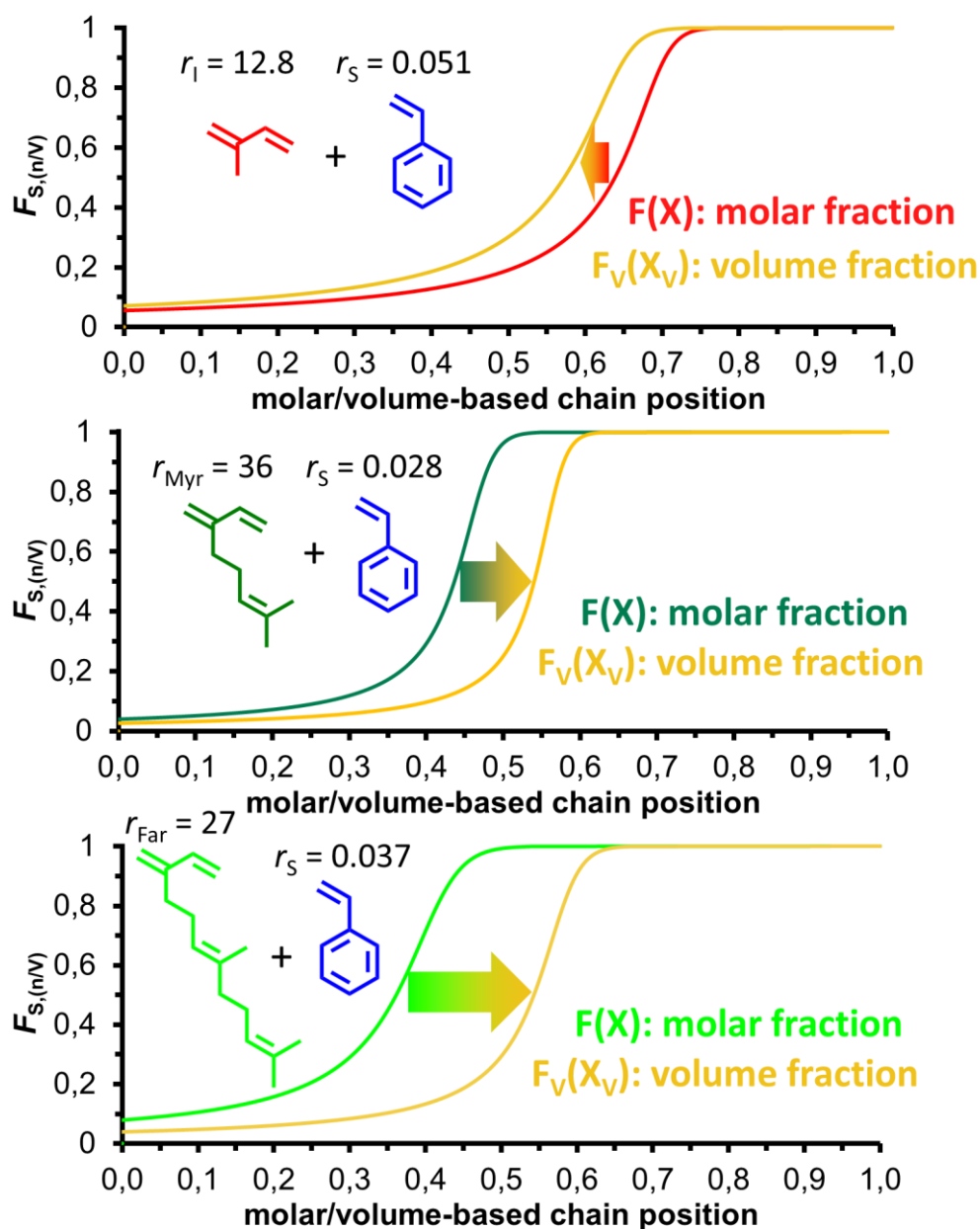


Figure 3. Shift from the molar composition profile of the tapered copolymers to the volume composition profile (orange) for equal total volume fractions (ϕ_{PDiene}) and the corresponding reactivity ratios.

Tapered multiblock copolymer synthesis and molecular characterization. The synthesis of tapered multiblock copolymers by the sequential addition of monomer mixtures was reported by our group for the monomer pairs isoprene/styrene and isoprene/4-methyl-styrene.^{41,42} In the concept of thermoplastic elastomers (TPEs), the polydiene blocks determine the elastic behavior of the material. To generate a TPE

material, an ABA triblock polymer structure is required, i.e. long polydiene B blocks have to be fixated by two terminal styrenic A-blocks that form the noncovalent crosslinking domains.⁵⁶ Thus, in contrast to our previous works on tapered multiblock copolymers, in the current work we prepared a pure polystyrene block before adding the diene/styrene mixture to generate the tapered blocks, as shown in Figure 4a. The concept of tapered triblock copolymers, based on styrene and isoprene (or butadiene), was developed by Geoffrey and Milkovich at Shell Co..⁵⁷ This concept for the polymer architecture was recently used for the synthesis of tapered multiblock star copolymers based on I/S to achieve optimized mechanical properties.⁵⁸ The procedure used in the current work results in two polystyrene end blocks, which in effect results in physical crosslinking of the polymer chains due to vitrification of the PS domains. A second addition of the respective diene/styrene monomer mixture enables the synthesis of tapered pentablock copolymers.

In this work, for each tapered tri- and pentablock copolymer composition, the analogous polyfarnesene, polymyrcene and polyisoprene-based copolymer was synthesized, keeping the total polydiene volume fraction (ϕ_{PDiene}) constant, as shown in depends on the different volume requirement of the 1,3-diene monomers, according to Figure 3. The three copolymer systems have the same polydiene volume fraction but very different chain length of the diene midblock. As we will see below in the SAXS measurements, this is a key feature of the copolymers that enables a direct comparison of the mechanical and processing behavior of the tapered block copolymers.

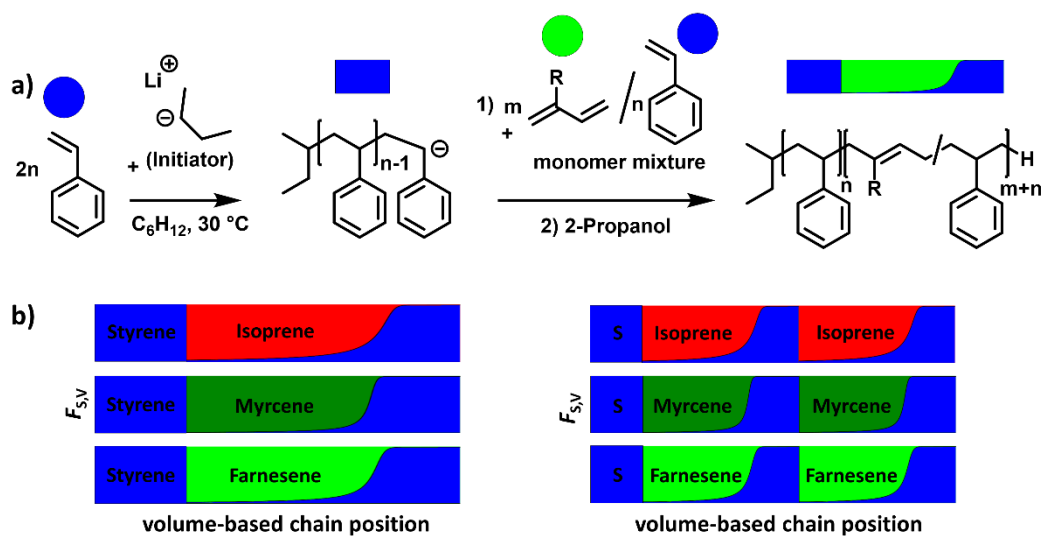


Figure 4. a) Synthetic strategy for tapered multiblock copolymers of styrene and 1,3-diene monomers (isoprene, myrcene or farnesene), b) volume composition profile (incorporation volume of styrene ($F_{\text{Styrene}}(V)$) vs. volume-based chain position) of tri- and pentablock copolymers with constant polydiene volume fraction ($\phi_{\text{PDiene}} = 0.5$) and constant molecular weight ($120 \text{ kg}\cdot\text{mol}^{-1}$).

The synthesis of the tri- and pentablock copolymers was performed with the three 1,3-diene monomers, resulting in molecular weights in a range of 107 to $140 \text{ kg}\cdot\text{mol}^{-1}$ and low dispersities between 1.05 and 1.16 (Figures S13-15; Table 1). The deviation of the SEC-data from the theoretical molecular weight can be explained by the overestimated molecular weight of polyisoprene when using a polystyrene standard. In addition, the increasing length of the side chain of the polydiene-units on going from isoprene to β -farnesene results in a bottlebrush-like structure of the polyfarnesene middle blocks, which alters the hydrodynamic volume and results in underestimated molecular weights of the tapered polyfarnesene copolymers in comparison to their polyisoprene analogs.⁵⁹ The polydiene microstructure of the tapered copolymers was determined by ^1H NMR spectroscopy (spectra are shown in Figures S16-18). For the polyisoprene based polymers a 3,4-regioisomer content around 5 % was found, which is in accordance with literature.⁶⁰ In the row of polyisoprene < polymyrcene < polyfarnesene-based tapered copolymers a slight increase of the 3,4-units up to 6.6 % is observable for the copolymerization in cyclohexane.

Table 1. Characterization data of synthesized series of tapered tri- and pentablock copolymers of styrene and different 1,3-diene monomers and with constant polydiene volume fractions ($\varphi_{\text{PDiene}} = 0.5$ or 0.68).

Sample	M_n^{th} (kg/mol)	M_n^a (kg/mol)	D^a	x_{Diene}^b	$\varphi_{\text{PDiene}}^b$	$T_{g,\text{PDiene}}^c$ (K)	$T_{g,\text{PS}}^c$ (K)	micro- structure ^b 1,4-units (%)	d_{norm}^d (nm)
PS _{0.25} - <i>b</i> -P(I _{0.5} - <i>co</i> -S _{0.25})	120	122.7	1.09	0.57	0.5	220	355	94.8	35.6
PS _{0.25} - <i>b</i> -P(My _{0.5} - <i>co</i> -S _{0.25})	120	106.8	1.12	0.40	0.5	214	366	93.9	36.0
PS _{0.25} - <i>b</i> -P(Far _{0.5} - <i>co</i> -S _{0.25})	120	107.6	1.14	0.31	0.5	205	366	93.6	36.0
PS _{0.17} - <i>b</i> -P(I _{0.25} - <i>co</i> -S _{0.17}) ₂	120	140.1	1.12	0.57	0.5	224	358	94.8	24.7
PS _{0.17} - <i>b</i> -P(My _{0.25} - <i>co</i> -S _{0.17}) ₂	120	136.5	1.15	0.40	0.5	214	356	93.5	25.2
PS _{0.17} - <i>b</i> -P(Far _{0.25} - <i>co</i> -S _{0.17}) ₂	120	123.3	1.16	0.31	0.5	209	361	93.4	25.5
PS _{0.16} - <i>b</i> -P(I _{0.68} - <i>co</i> -S _{0.16})	115	127.1	1.05	0.74	0.68	218	-	94.8	36.7
PS _{0.16} - <i>b</i> -P(My _{0.68} - <i>co</i> -S _{0.16})	115	119.3	1.08	0.59	0.68	212	-	94.1	37.7
PS _{0.16} - <i>b</i> -P(Far _{0.68} - <i>co</i> -S _{0.16})	115	108.7	1.09	0.49	0.68	203	-	93.6	36.5

^aDetermined by SEC measurements in THF at 25 °C using PS standards (Figs. S13-S15). ^bDetermined from ¹H NMR spectra (400 MHz, CDCl₃, Figs. S13-S15). ^cDetermined by DSC measurements (Fig. S19). ^dDetermined by SAXS measurements.

Thermal properties. The influence of the polydiene architecture on the thermal behavior was investigated by DSC measurements (DSC curves are shown in Figure S19). The occurrence of two glass temperatures for all tri- and pentablock copolymers (with $\varphi_{\text{PDiene}} = 0.5$) is an indication for phase separation of the polydiene- and the polystyrene domains, which is a precondition for thermoplastic elastomer behavior. More insight into the phase state requires a structural investigation (SAXS measurements below). The glass temperature of the flexible polydiene block ($T_{g,\text{PDiene}}$) decreases for all series of tri- and pentablock copolymers in the order polyisoprene > polymyrcene > polyfarnesene (Figure S20). The effect of the slightly increasing amount of 3,4-units in the series from polyisoprene to polyfarnesene, which is known to increase T_g ,^{40,61} is overcompensated by the bottlebrush-like structure of the polyfarnesene blocks.¹⁸ In the latter, the lower glass temperature results mainly from the longer side groups with the free ends that effectively plasticize the backbone. Since the glass temperature is mainly (but not solely)⁶² a property of the backbone (associated with the freezing of the backbone motions) a lower temperature is necessary for polyfarnesene to freeze.

For the triblock copolymers with a polydiene volume fraction of $\varphi_{\text{PDiene}} = 0.68$ merely the T_g of the polydiene phase was observable, which is even lower than for the corresponding triblocks with $\varphi_{\text{PDiene}} = 0.5$. The lack of a detectable T_g of the polystyrene domains is caused by the sensitivity limitation of the DSC measurement (the heat capacity step Δc_p

at T_g , is inversely proportional to temperature). In this case SAXS provides unambiguously the nanodomain morphology.

Morphology. The morphology of the tapered tri- and pentablock copolymers can be discussed with respect to the small-angle X-ray scattering (SAXS) curves depicted in Figures 5-7. The temperature-dependent SAXS patterns of all triblock copolymers share some features (Figure 5). All patterns exhibit a strong peak at low q followed by higher order reflections. The number and intensity of the higher order reflections depends on temperature. In general, all triblock copolymers show increased tendency for phase separation at temperatures above the polystyrene T_g . This might sound paradoxical as increasing temperature brings the copolymers closer to the disordered state. The increased nanophase separation here reflects the enhanced mobility of chains (e.g. annealing above the polystyrene T_g). Bragg reflections appear with relative q values of 1:2:3:4, corresponding to a lamellar structure (LAM) with periodicity (as $d_o=2\pi/q^*$, q^* is the modulus of the scattering vector corresponding to the first maximum) of 35.6 nm, 33.6 nm and 33.7 nm respectively for the polyisoprene, polymyrcene and polyfarnesene blocks. To account for the difference in the block molecular weights (Table 1, and further assuming Gaussian statistics for simplicity) we can obtain a normalized spacing as $d_{\text{norm}}=(d_o/M^{1/2})/(d_o/M^{1/2})_{\text{isoprene}}$ that amounts to 36 nm for the polymyrcene and polyfarnesene blocks.

The similarity in the domain spacing of the polyfarnesene triblock copolymers with the corresponding polyisoprene and polymyrcene copolymers has some important implications for the conformational properties of the diene blocks. In an SIS triblock copolymer the mid-block has a large fraction of looped configurations (in the range of 0.4-0.6 according to experiment, theory and simulation).⁶³ However, loops in polymyrcene - and even more so in polyfarnesene - blocks are increasingly more difficult because of the bottlebrush-like structure of the polydiene blocks that restrict such configurations. Hence the similar d -spacing is the result of the similar interaction parameters, $\chi_{S/\text{Myr}}$ and $\chi_{S/\text{Far}}$ with the respective $\chi_{S/I}$ and of the different configurations (loops vs bridges) of the polydiene blocks.

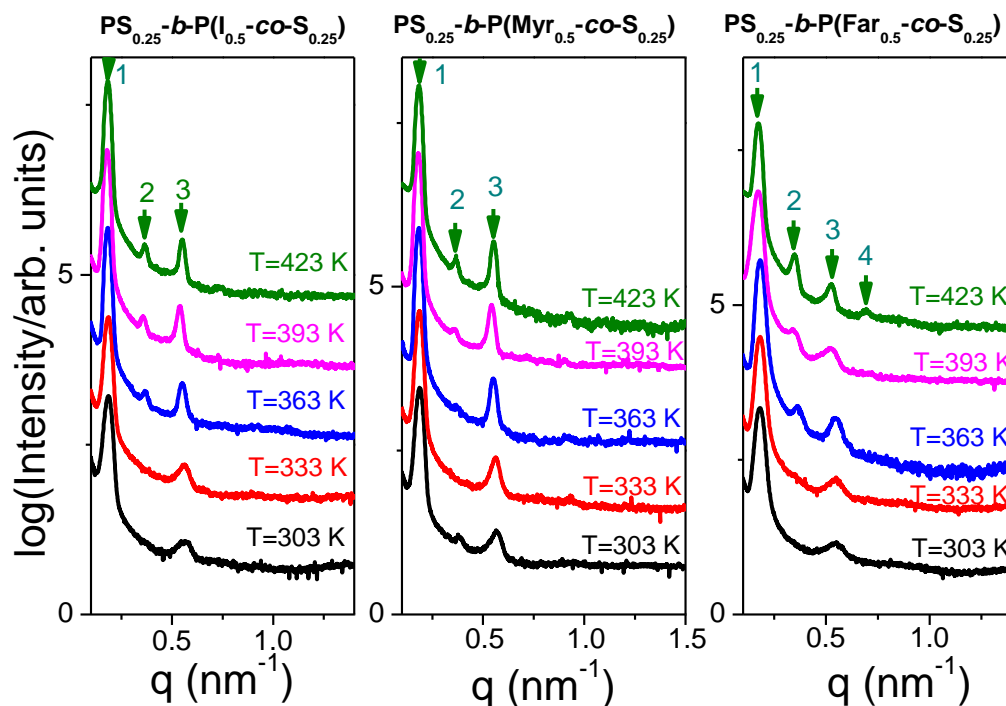


Figure 5. SAXS patterns of the triblock copolymers with polydiene volume fraction of $\varphi_{\text{PDiene}}=0.5$ shown at different temperatures obtained on heating. Arrows indicate the positions of the Bragg reflections corresponding to a lamellar morphology.

The reduced intensity for the even numbered reflections in the polyisoprene and polymyrcene copolymers reveal that the polydiene and PS domains have equal volumes (positions where the form factor has a minimum). Note that this is not case in the polyfarnesene copolymers (polyfarnesene and PS domains have slightly different volumes) where all reflections appear in similar intensity.

The corresponding SAXS results for the asymmetric triblock copolymers (polydiene volume fraction of $\varphi_{\text{PDiene}}=0.68$) are shown in Figure 6. SAXS patterns of the triblock copolymers with polydiene volume fraction of $\varphi_{\text{PDiene}}=0.68$ shown at different temperatures obtained on heating and cooling (cooling curves are indicated by c). Arrows indicate the positions of the Bragg reflections corresponding to a cylindrical morphology. All triblock copolymers exhibit Bragg reflections with relative q values of $1:3^{1/2}:4^{1/2}:7^{1/2}:9^{1/2}$ revealing a hexagonally packed cylindrical structure (HPC) composed of PS cylinders in a diene matrix. The periodicity ($d=d_0(4/3)^{1/2}$; $d_0=2\pi/q^*$), normalized for the difference in molecular weights, is now at 36.7 nm, 37.7 nm and 36.5 nm respectively for the polyisoprene, polymyrcene and polyfarnesene blocks. Again, this is suggestive of a similar degree of segregation but different diene configuration in the asymmetric triblock copolymers.

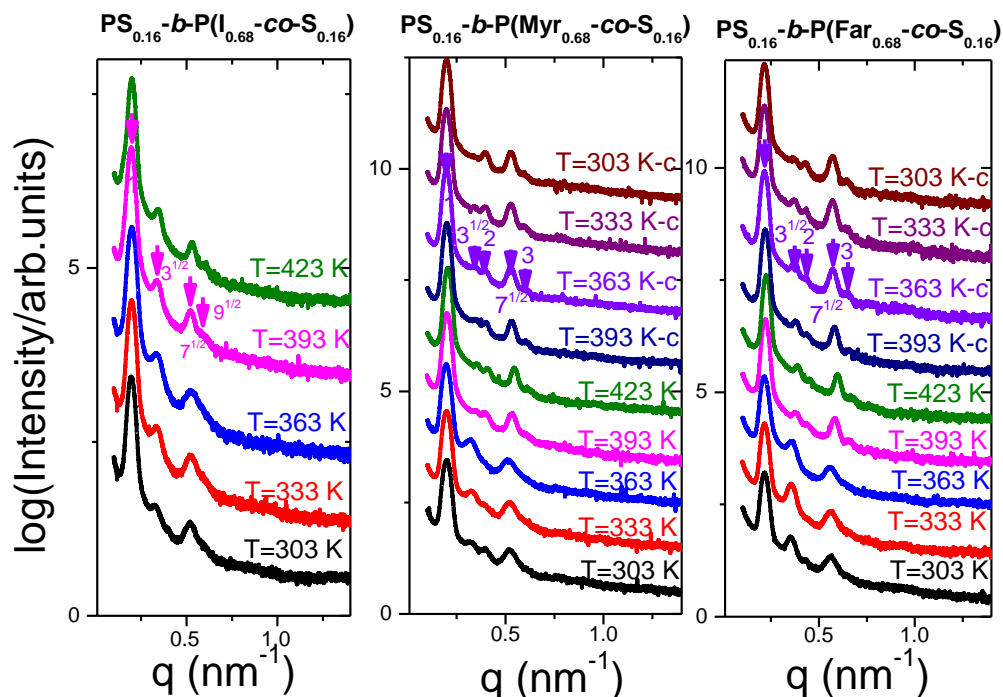


Figure 6. SAXS patterns of the triblock copolymers with polydiene volume fraction of $\varphi_{\text{PDiene}}=0.68$ shown at different temperatures obtained on heating and cooling (cooling curves are indicated by c). Arrows indicate the positions of the Bragg reflections corresponding to a cylindrical morphology.

All patterns of the pentablock copolymers translate to a LAM morphology of reduced periodicity as compared to the triblock copolymers. Domain-spacings normalized for the different molecular weights amount to 24.7 nm, 25.2 nm and 25.5 nm respectively for the polyisoprene, polymyrcene and polyfarnesene blocks (Fig. 7, Table 1). The reduced domain spacing relative to the triblock copolymers is a composite effect. In the case of the polyisoprene blocks it reflects the increased number of blocks at a fixed overall molecular weight and the configuration of the mid-blocks (e.g. further formation of loops), whereas in the case of polymyrcene and polyfarnesene blocks it mainly reflects the increase in block number.

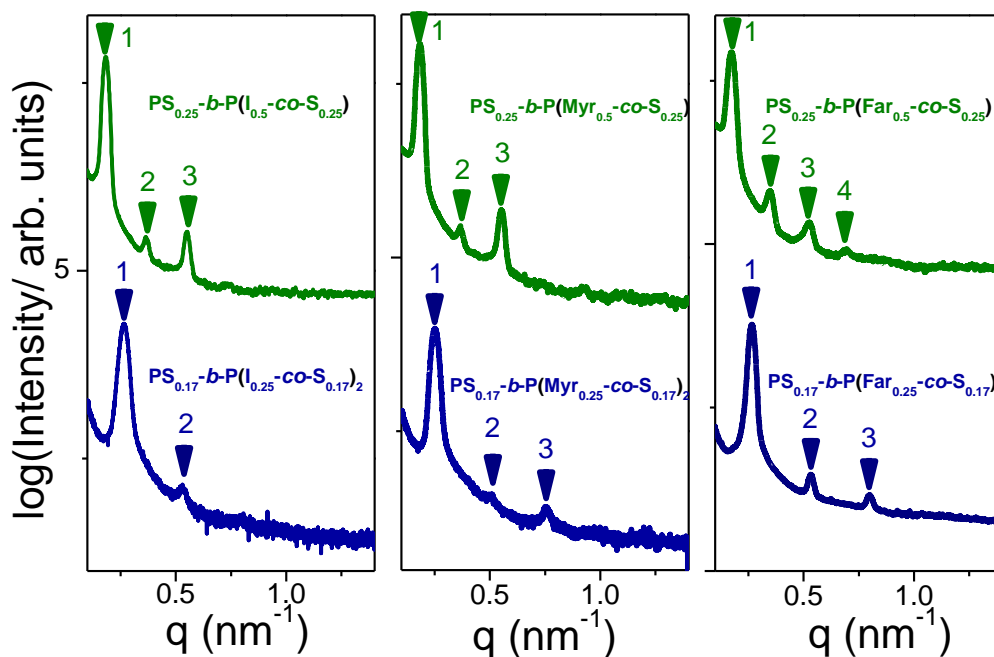


Figure 7. SAXS patterns of the triblock (top, blue) and pentablock copolymers (bottom, green) with polydiene volume fraction of $\phi_{\text{PDiene}}=0.5$, shown at 423 K. Arrows indicate the positions of the Bragg reflections corresponding to a lamellar morphology.

In summary, the phase state of the polymyrcene and polyfarnesene copolymers bears many similarities (same morphology, practically the same domain spacing and a similar degree of segregation) to the corresponding polyisoprene copolymers. The same domain spacing further suggests that specific chain configurations (loops) that are present in the polyisoprene copolymers are minimized in polymyrcene and polyfarnesene copolymers. The two effects (reduced entanglement molecular weight and increased bridging configurations in polymyrcene and polyfarnesene copolymers) are expected to influence the mechanical properties discussed below (in opposite ways), yet it is unknown which effect will prevail.

Mechanical properties. The mechanical properties of the tapered tri- and pentablock copolymers were investigated by uniaxial tensile measurements. The representative stress-strain plots for the tapered copolymers with a polydiene volume fraction of 0.5 and 0.68 are shown in Figure 8 and Figure 11. The investigation of the mechanical properties reveals striking differences between the different polydiene architectures of the tapered block copolymers, both regarding their yield point characteristics and the properties at the point of mechanical failure. Focusing on the point of mechanical failure, the stress at break (σ_b), strain at break (ϵ_b) and ultimate toughness decrease in the order polyisoprene

> polymyrcene > polyfarnesene (values are shown in Table S7). We recall here that all copolymers exhibit the same morphology (LAM), have similar degree of segregation but differ considerably in the configurations of the polydiene blocks. Based on the increasing bridging configurations of the polyterpene blocks one would expect increasing stress and strain at break, and ultimate toughness, whereas the opposite is observed. As discussed in the morphology section, polyterpenes have an increasing tendency to be less entangled (polymyrcene) or even to be unentangled (polyfarnesene). Comparing these two parameters, i.e. increasing bridging configurations and increasing propensity for unentangled chains it is the latter that prevails and eventually controls the mechanical response. This trend also occurs in the yield point characteristics. While the E_y modulus does not change significantly from the isoprene- to the β -myrcene-based triblocks, there is a slight decrease in the yield stress (σ_y). In contrast, all β -farnesene-based triblocks show clearly lower values for E_y and for the yield stress (see Table S7 and Figure 9 and S23).

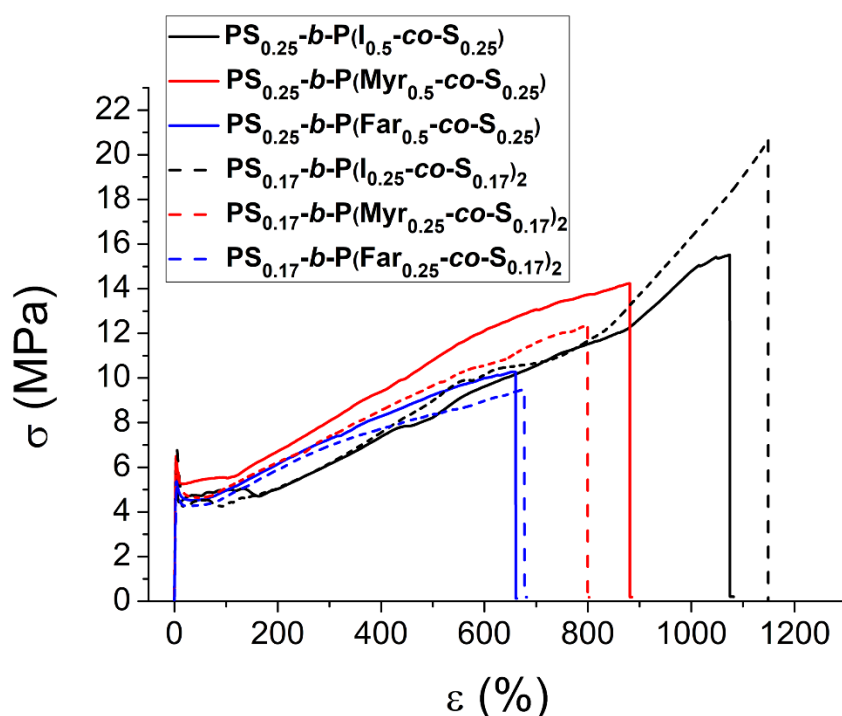


Figure 8. Representative stress–strain curves of the three series of tapered tri- (continuous lines) and pentablock (dashed lines) copolymers with different polydiene blocks: (a) polyisoprene (black), (b) polymyrcene (red) and (c) polyfarnesene (blue). The volume fraction of the polydiene phase is identical for all copolymers ($\varphi_{\text{PDiene}} = 0.5$).

With an increase of the block number from 3 to 5, keeping the overall molecular weight ($120 \text{ kg}\cdot\text{mol}^{-1}$) and the polydiene volume fraction ($\varphi_{\text{PDiene}} = 0.5$) constant, there are several factors that affect the mechanical properties: i) the increasing bridging fraction of the polydiene middle blocks,⁶⁴ ii) the decreasing molecular weights of the individual blocks, effectively reducing the number of entanglements, and iii) additional bridges in the glassy domains by the polystyrene midblock in the pentablock structures.^{65,66} In the pentablock series (dashed lines in Figure 8), the same trends regarding the ultimate mechanical properties and the yield point can be observed. Comparing the tapered tri- and pentablock copolymer series, for the isoprene-based samples, both the toughness, σ_b , and ε_b increase with increasing block number, as reported in literature.⁴² However, this trend is not followed by the terpene-based tapered block copolymer samples. The dependency of the ultimate toughness on the number of blocks of the tapered block copolymers with $\varphi_{\text{PDiene}} = 0.5$ and varying polydiene structures is presented in Figure 10. In contrast to the isoprene-based copolymers, the toughness in the β -myrcene-based samples slightly decreases with increasing number of blocks, while the toughness of the β -farnesene sample remains nearly constant ($U \approx 40 \text{ MJ}\cdot\text{m}^{-3}$). Given the similar phase state and degree of segregation, this trend can be correlated to the molecular weights of the single polydiene blocks in relation to the corresponding entanglement molecular weights (M_e) of the polydienes, listed in Table S9 and Table S10. An increasing block number under a constant overall molecular weight results in a decrease of the molecular weight of the single polymer blocks. For the polymyrcene-based series the molecular weights of the polymyrcene blocks approach the entanglement molecular weight of polymyrcene whereas for the polyfarnesene blocks the molecular weight is below than the M_e for the pentablock copolymer, resulting in no significant decrease in toughness. Accordingly, the decrease in toughness is attributed mainly to the absence of entanglements of the polydiene blocks between the terminal styrene blocks, which are known to contribute to the mechanical properties of thermoplastic elastomers.^{67,68} Furthermore, the values of E_y decrease with increasing number of blocks, as shown in Figure 9.

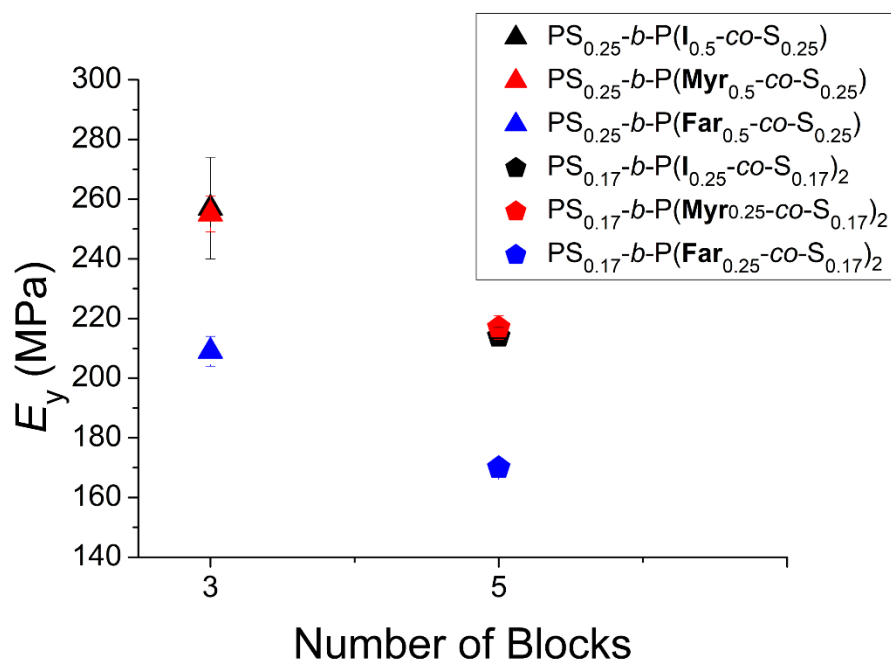


Figure 9. Young's modulus of the tapered tri- and pentablock copolymers ($\varphi_{PDiene} = 0.5$) in dependence of number of blocks and polydiene block (same color codes as used for the stress-strain curves). Values are determined as the average of 5 independent measurements. Errors are given in the 1σ interval.

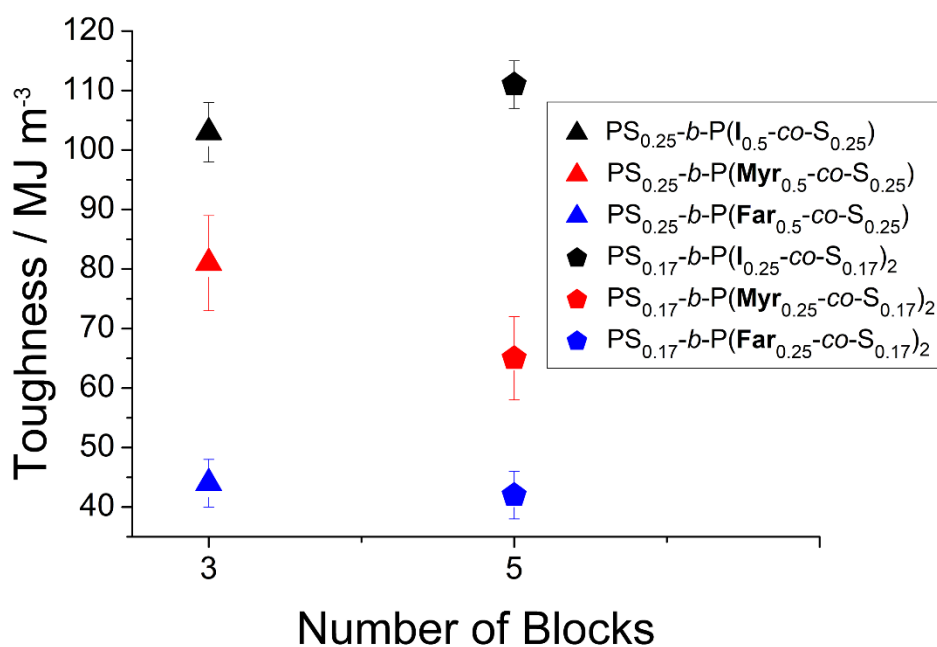


Figure 10. Toughness of the tapered tri- and pentablock copolymers ($\varphi_{PDiene} = 0.5$) in dependence of number of blocks and polydiene block (same color codes used as for the

stress-strain curves). Values are determined as the average of 5 independent measurements. Errors are given in the 1σ interval.

The series of tapered triblock copolymers with a higher polydiene volume fraction ($\varphi_{\text{PDiene}} = 0.68$), showing hexagonally packed cylindrical morphologies, was also investigated by tensile measurements. The stress-strain plots (Figure 11) show significantly different behavior in comparison to the samples with $\varphi_{\text{PDiene}} = 0.5$. The copolymers now exhibit the stress-strain behavior of conventional thermoplastic elastomers ($\varphi_{\text{PDiene}} \approx 0.65 - 0.8$), which do not show any yield point.^{34,35,69} In general, similar trends regarding toughness, stress at break (σ_b) and strain at break (ε_b) can be observed for the triblock series with $\varphi_{\text{PDiene}} = 0.68$, as given in Table S8 and Figure 11. The copolymer $\text{PS}_{0.16}\text{-}b\text{-P}(\text{I}_{0.68}\text{-}co\text{-S}_{0.16})$ shows different behavior in comparison to the corresponding β -myrcene and β -farnesene-based samples. The point of mechanical failure of $\text{PS}_{0.16}\text{-}b\text{-P}(\text{I}_{0.68}\text{-}co\text{-S}_{0.16})$ was not reached, due to the limitation of the testing machine. In contrast to $\text{PS}_{0.16}\text{-}b\text{-P}(\text{Myr}_{0.68}\text{-}co\text{-S}_{0.16})$ and $\text{PS}_{0.16}\text{-}b\text{-P}(\text{Far}_{0.68}\text{-}co\text{-S}_{0.16})$, that exhibit an elastomeric behavior, the copolymer $\text{PS}_{0.16}\text{-}b\text{-P}(\text{I}_{0.68}\text{-}co\text{-S}_{0.16})$ undergoes strain hardening, starting at $\varepsilon_b \approx 700\%$. In analogy to the stress-strain behavior of the samples with $\varphi_{\text{PDiene}} = 0.5$, the difference in the mechanical properties can be explained by the decreasing number of entanglements in the order $\text{PI} > \text{PMyr} > \text{PFar}$, as a consequence of the bottlebrush-like structure of polyfarnesene.

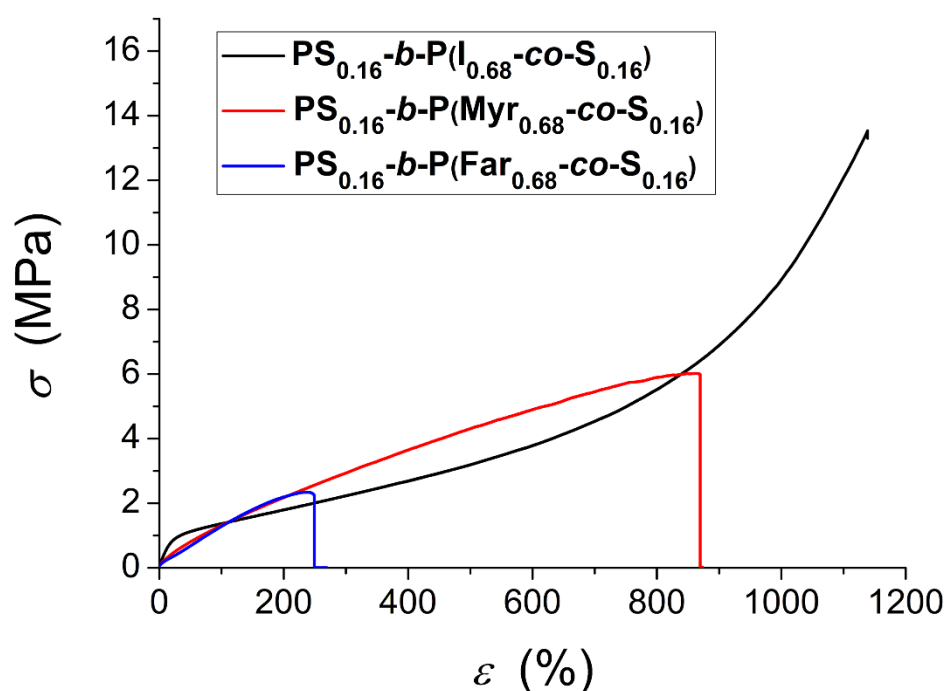


Figure 11. Representative stress–strain curves of the tapered triblock copolymers ($\varphi_{\text{PDiene}} = 0.68$) with varying polydiene blocks: (a) polyisoprene (black), (b) polymyrcene (red) and (c) polyfarnesene (blue).

Processing. Linear ABA type tri- or A(BA)_n multiblock copolymers show excellent mechanical properties, but there are limitations in the processing of the materials, due to their high melt and solution viscosity.⁷⁰ Branched structures are well-known for their reduced melt viscosities in comparison to their linear analogs. In comparison to the linear polyisoprene segments of the tapered copolymers, the polyfarnesene segments can be described as bottlebrush-like structures, due to their long C₁₁/C₁₃ side chains. As a consequence they possess very high entanglement molecular weight (50 kg·mol⁻¹) that results in a reduced melt viscosity.¹⁹ To demonstrate the impact of this unique architectural feature of polyfarnesene on the processing behavior of thermoplastic elastomeric materials, electrospinning was selected as exemplary processing technique to generate nanofibers of the tapered block copolymers. The experimental section of the electrospinning experiments can be found in the Supporting Information. Electrospinning is a versatile and viable processing method, which is attracting increased attention in academic research as well as in commercial applications.^{71–74} The solution viscosity is one of the most important parameters in electrospinning for the production of well-defined nanofibers.⁷⁵ There is a limited viscosity range, where electrospinning of a polymer

solution is possible. While too low viscosity results in the formation of droplets (so-called electrospraying) or “beads” on fibers (concentration dependency of morphology is shown in Figure S24), too high concentration of the polymer solution results in the formation of extremely thick fibers leading in a boundary case to prohibition of fiber formation (see Figure S25a).⁷⁶ The solution viscosities of the tapered tri- and pentablock copolymers dissolved in THF/DMF (80/20 v/v) were measured with a viscometer (Brookfield DV-III Ultra). The deviation of the diameter distribution is given by the standard deviation of the Gauss fit. The solution viscosity of the triblock copolymers dissolved in THF/DMF (80/20 v/v) decreased from polyisoprene to polyfarnesene-based samples, of the same molecular weight and total polydiene volume fraction, corresponding to the decreasing side chain length of the polydiene-units (viscosities and resulting fiber diameter are presented in Table 2) and the reduced number of entanglements.

Table 2. Solution viscosity of tapered triblock copolymers ($\phi_{\text{PDiene}} = 0.5$) dissolved in THF/DMF (80/20 v/v) with different concentrations (30 and 25 wt%) and the diameters of the resulting nanofibers.

Sample	η / mPa s	η / mPa s	d / μm
	(30 wt%)	(25 wt%)	
PS _{0.25} - <i>b</i> -P(I _{0.5} - <i>co</i> -S _{0.25})	5500	850	1.99 ± 0.39 ^a
PS _{0.25} - <i>b</i> -P(My _r 0.5- <i>co</i> -S _{0.25})	760	170	1.82 ± 0.50 ^b
PS _{0.25} - <i>b</i> -P(Far _{0.5} - <i>co</i> -S _{0.25})	420	140	1.88 ± 0.44 ^b

^a Spun from 25 wt% solution. ^b Spun from 30 wt% solution.

While the ABA triblocks containing polymyrcene and polyfarnesene segments were spinnable at high solution concentrations of 30 wt%, the polymer solution of the polyisoprene triblock had to be diluted to a concentration of 25 wt% to get in a processable viscosity range. In all cases well-defined fibers in a range of 1.82 – 1.99 μm diameter were obtained. As an example, the SEM image, as well as the fiber thickness distribution of the PS_{0.25}-*b*-P(Far_{0.5}-*co*-S_{0.25}) sample are shown in Figure 12.

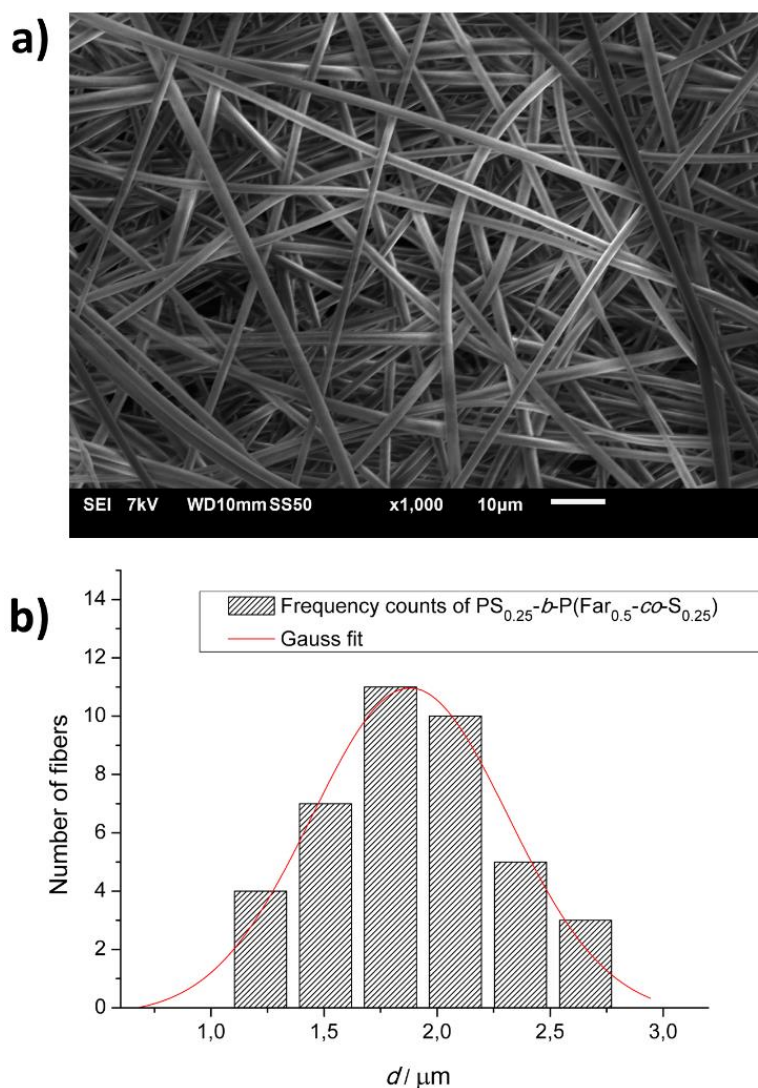


Figure 12. SEM image of electrospun $\text{PS}_{0.25}\text{-}b\text{-P}(\text{Far}_{0.5}\text{-}co\text{-S}_{0.25})$ tapered triblock copolymer nanofibers and distribution of the fiber diameters.

The same trend in solution viscosity could be observed for the pentablock copolymers. Due to the smaller polydiene domains of the pentablock copolymers, the solution viscosity decreases with increasing number of blocks (see Table S11). The complete results of the viscosity measurements of all sample and all SEM images as well as fiber distributions and diameters are available in the Supporting Information (Figures S25-S27). The results show the potential of β -farnesene (and even β -myrcene) based thermoplastic elastomers for simplified processing, exemplified by the processing method “electrospinning”. The reduced viscosity of polyfarnesene-based block copolymers enable to produce microfibers from concentrated polymer solutions, which offers an economical benefit over established isoprene/styrene-based TPEs. Furthermore, the reduced melt viscosity of the β -farnesene-based thermoplastic elastomers is of importance for

processing methods like melt extrusion.¹⁹ Electrospinning enables direct access to various microfiber assemblies, that are potentially suitable for membrane applications.⁷¹ Further work in this area is currently under way.

Conclusion

In this work we describe the direct, i.e. statistical anionic copolymerization of β -farnesene and styrene and the resulting monomer gradient in the polymer chains formed. Furthermore, we have investigated the consequences of the gradient composition on the morphology and mechanical properties of the resulting, partially bio-based thermoplastic elastomers. An online NMR kinetics study of the *sec*-butyllithium initiated statistical copolymerization in cyclohexane as well as the homopolymerization of β -farnesene was performed by *in situ* ^1H NMR kinetic experiments. The faster homopolymerization kinetics of β -farnesene ($k_{\text{FarFar}} = 3.2 \cdot 10^{-3} \text{ (L/mol)}^{1/4} \text{ s}^{-1}$, at 23 °C), in comparison to the established isoprene systems ($k_{\text{II}} = 0.61 \cdot 10^{-3} \text{ (L/mol)}^{1/4} \text{ s}^{-1}$, at 23 °C)²⁸, can be used to create tapered and block copolymers at reduced reaction times. Similar to the isoprene- and β -myrcene-based styrene copolymerization, the copolymerization kinetics of β -farnesene and styrene showed highly disparate reactivity ratios ($r_{\text{Far}} = 27$; $r_{\text{S}} = 0.037$, determined by the Integrated Ideal method), leading to block-like, tapered copolymers for the copolymerization in cyclohexane. For the design of tailor-made copolymers with adjustable material properties, the volume composition profile of the resulting tapered copolymers is essential. For this purpose, we introduced analytically derived algebraic expressions for the molar and volume composition profiles, which were directly implemented in a simple Microsoft Excel® spreadsheet, making the depiction of the copolymer composition profile directly accessible.

The tapered building blocks were used for the synthesis of both tri- (ABA) and pentablock (ABABA) copolymers of β -farnesene (B block) and styrene (A block) with total polydiene volume fractions of 0.50 and 0.68. In addition, the corresponding tri- and pentablock copolymers with isoprene (C_5) and β -myrcene (C_{10}) were synthesized, containing equal polydiene volume fractions as their β -farnesene-based (C_{15}) analogs. This approach resulted in well-defined tapered tri- and pentablock copolymers with molecular weights of $120 \text{ kg}\cdot\text{mol}^{-1}$ for all samples and low dispersities in the range of 1.05–1.16. This series of multiblock copolymers enabled a comprehensive study of the influence of the polydiene architecture on the thermal and mechanical properties of the thermoplastic

elastomers as well as their processability. The copolymers exhibit the same morphology. Depending on the polydiene volume fraction multiblock copolymers show phase separation in lamellar or hexagonally packed cylindrical morphologies, practically the same domain spacing and a similar degree of segregation. The similarity in domain spacing revealed that specific chain configurations (loops) that are present in the polyisoprene copolymers are minimized in polymyrcene and are practically absent in the polyfarnesene copolymers. The tensile properties of the tri- and pentablock copolymers depend strongly on the polydiene architecture. The toughness of the multiblock copolymers decrease from PI > PMyr > PFar-based block copolymers, which was ascribed to reduced number of entanglements of the polydiene midblocks ($(M_e(\text{PFar}) > M_e(\text{PMyr}) > M_e(\text{PI}))$).

Furthermore, the reduced solution viscosity of the tapered polyfarnesene tri- and pentablock copolymers in comparison with their linear polyisoprene analogs, leads to improved processability by electrospinning. The directly accessible microfiber meshes, with fiber diameters of 2 μm , are promising for use of the tapered multiblock copolymers for membrane applications. .

Acknowledgments

Andreas Hanewald and Dr. Kaloian Koynov are acknowledged for their valuable help with the mechanical characterization. The authors thank Monika Schmelzer for the valuable support with the SEC measurements and Ramona Barent for the support with the data evaluation.

References

- (1) Winnacker, M. Pinenes: Abundant and Renewable Building Blocks for a Variety of Sustainable Polymers. *Angew. Chem. Int. Ed.* **2018**, *57*, 14362–14371.
- (2) Winnacker, M.; Rieger, B. Recent progress in sustainable polymers obtained from cyclic terpenes: synthesis, properties, and application potential. *ChemSusChem* **2015**, *8*, 2455–2471.
- (3) Mühlaupt, R. Green Polymer Chemistry and Bio-based Plastics: Dreams and Reality. *Macromol. Chem. Phys.* **2013**, *214*, 159–174.
- (4) Gallezot, P. Conversion of biomass to selected chemical products. *Chem. Soc. Rev* **2012**, *41*, 1538–1558.
- (5) Gandini, A. Polymers from Renewable Resources: A Challenge for the Future of Macromolecular Materials. *Macromolecules* **2008**, *41*, 9491–9504.

- (6) Babu, R. P.; O'Connor, K.; Seeram, R. Current progress on bio-based polymers and their future trends. *Prog. Biomater.* **2013**, *2*, 8.
- (7) Zhao, J.; Schlaad, H. Synthesis of Terpene-Based Polymers; *Adv. Polym. Sci.* **2013**, *253*, 151-190.
- (8) Sarkar, P.; Bhowmick, A. K. Sustainable rubbers and rubber additives. *J Appl Polym Sci* **2018**, *135*, 45701.
- (9) Behr, A.; Johnen, L. Myrcene as a natural base chemical in sustainable chemistry: a critical review. *ChemSusChem* **2009**, *2*, 1072-1095.
- (10) Sahu, P.; Bhowmick, A. K.; Kali, G. Terpene Based Elastomers: Synthesis, Properties, and Applications. *Processes* **2020**, *8*, 553.
- (11) Marvel, C. S.; Hwa, C. C. L. Polymyrcene. *J. Polym. Sci.* **1960**, *45*, 25-34.
- (12) Benjamin, K. R.; Silva, I. R.; Cherubim, J. P.; McPhee, D.; Paddon, C. J. Developing Commercial Production of Semi-Synthetic Artemisinin, and of β -Farnesene, an Isoprenoid Produced by Fermentation of Brazilian Sugar. *J. Braz. Chem. Soc.* **2016**, *27*, 1339-1345.
- (13) Abdelrahman, O. A.; Park, D. S.; Vinter, K. P.; Spanjers, C. S.; Ren, L.; Cho, H. J.; Zhang, K.; Fan, W.; Tsapatsis, M.; Dauenhauer, P. J. Renewable Isoprene by Sequential Hydrogenation of Itaconic Acid and Dehydro-Decyclization of 3-Methyl-Tetrahydrofuran. *ACS Catal.* **2017**, *7*, 1428-1431.
- (14) Yang, J.; Zhao, G.; Sun, Y.; Zheng, Y.; Jiang, X.; Liu, W.; Xian, M. Bio-isoprene production using exogenous MVA pathway and isoprene synthase in *Escherichia coli*. *Bioresour. Technol.* **2012**, *104*, 642-647.
- (15) Azeem, M.; Borg-Karlson, A. K.; Rajarao, G. K. Sustainable bio-production of styrene from forest waste. *Bioresour. Technol.* **2013**, *144*, 684-688.
- (16) McKenna, R.; Nielsen, D. R. Styrene biosynthesis from glucose by engineered *E. coli*. *Metabolic engineering* **2011**, *13*, 544-554.
- (17) Breitmaier, E. *Terpene: Aromen, Düfte, Pharmaka, Pheromone*; Teubner Studienbücher Chemie; Vieweg+Teubner Verlag: Wiesbaden, 1999.
- (18) Yoo, T.; Henning, S. K. Synthesis and Characterization of Farnesene-based Polymers. *Rubber Chem. Technol.* **2017**, *90*, 308-324.
- (19) Iacob, C.; Yoo, T.; Runt, J. Molecular Dynamics of Polyfarnesene. *Macromolecules* **2018**, *51*, 4917-4922.
- (20) Lamparelli, D. H.; Paradiso, V.; Della Monica, F.; Proto, A.; Guerra, S.; Giannini, L.; Capacchione, C. Toward More Sustainable Elastomers: Stereoselective Copolymerization of Linear Terpenes with Butadiene. *Macromolecules* **2020**, *53*, 5, 1665-1673.
- (21) Newmark, R. A.; Majumdar, R. N. ^{13}C -NMR spectra of cis-polymyrcene and cis-polyfarnesene. *J. Polym. Sci. A Polym. Chem.* **1988**, *26*, 71-77.

- (22) Sahu, P.; Bhowmick, A. K. Redox Emulsion Polymerization of Terpenes: Mapping the Effect of the System, Structure, and Reactivity. *Ind. Eng. Chem. Res.* **2019**, *58*, 20946–20960.
- (23) Fetters, L. J.; Lohse, D. J.; Richter, D.; Witten, T. A.; Zirkel, A. Connection between Polymer Molecular Weight, Density, Chain Dimensions, and Melt Viscoelastic Properties. *Macromolecules* **1994**, *27*, 4639–4647.
- (24) Sasaki, H.; Uehara, Y; Kato, M; Thermoplastic elastomer composition and molded body. U.S. Patent 9752027B2, Sep 7, 2017.
- (25) Laur, E.; Welle, A.; Vantomme, A.; Brusson, J.-M.; Carpentier, J.-F.; Kirillov, E. Stereoselective Copolymerization of Styrene with Terpenes Catalyzed by an Ansa-Lanthanidocene Catalyst: Access to New Syndiotactic Polystyrene-Based Materials. *Catalysts* **2017**, *7*, 361.
- (26) Steube, M.; Johann, T.; Plank, M.; Tjaberings, S.; Gröschel, A. H.; Gallei, M.; Frey, H.; Müller, A. H. E. Kinetics of Anionic Living Copolymerization of Isoprene and Styrene Using in Situ NIR Spectroscopy: Temperature Effects on Monomer Sequence and Morphology. *Macromolecules* **2019**, *52*, 9299–9310.
- (27) Grune, E.; Bareuther, J.; Blankenburg, J.; Appold, M.; Shaw, L.; Müller, A. H. E.; Floudas, G.; Hutchings, L. R.; Gallei, M.; Frey, H. Towards bio-based tapered block copolymers: the behaviour of myrcene in the statistical anionic copolymerisation. *Polym. Chem.* **2019**, *10*, 1213–1220.
- (28) Tiedemann, P. von; Blankenburg, J.; Maciol, K.; Johann, T.; Müller, A. H. E.; Frey, H. Copolymerization of Isoprene with p -Alkylstyrene Monomers: Disparate Reactivity Ratios and the Shape of the Gradient. *Macromolecules* **2019**, *52*, 796–806.
- (29) Steube, M.; Johann, T.; Hübner, H.; Koch, M.; Dinh, T.; Gallei, M.; Floudas, G.; Frey, H.; Müller, A. H. E. Tetrahydrofuran: More than a “Randomizer” in the Living Anionic Copolymerization of Styrene and Isoprene: Kinetics, Microstructures, Morphologies, and Mechanical Properties. *Macromolecules* **2020**, *53*, 3042–3051.
- (30) Bates, F. S. Polymer-polymer phase behavior. *Science* **1991**, *251*, 898–905.
- (31) Bates, F. S.; Fredrickson, G. H. Block Copolymers—Designer Soft Materials. *Phys. Today* **1999**, *52*, 32–38.
- (32) Khandpur, A. K.; Foerster, S.; Bates, F. S.; Hamley, I. W.; Ryan, A. J.; Bras, W.; Almdal, K.; Mortensen, K. Polyisoprene-Polystyrene Diblock Copolymer Phase Diagram near the Order-Disorder Transition. *Macromolecules* **1995**, *28*, 8796–8806.
- (33) Matsen, M. W. Effect of Architecture on the Phase Behavior of AB-Type Block Copolymer Melts. *Macromolecules* **2012**, *45*, 2161–2165.
- (34) Adhikari, R.; Godehardt, R.; Lebek, W.; Weidisch, R.; Michler, G. H.; Knoll, K. Correlation between morphology and mechanical properties of different styrene/butadiene triblock copolymers: a scanning force microscopy study. *J. Macromol. Sci., Part B* **2001**, *40*, 833–847.
- (35) Dair, B. J.; Honeker, C. C.; Alward, D. B.; Avgeropoulos, A.; Hadjichristidis, N.; Fetters, L. J.; Capel, M.; Thomas, E. L. Mechanical Properties and Deformation Behavior

of the Double Gyroid Phase in Unoriented Thermoplastic Elastomers. *Macromolecules* **1999**, *32*, 8145–8152.

(36) Lach, R.; Weidisch, R.; Knoll, K. Morphology and mechanical properties of binary triblock copolymer blends. *J. Polym. Sci. B Polym. Phys.* **2005**, *43*, 429–438.

(37) Lach, R.; Weidisch, R.; Janke, A.; Knoll, K. Influence of Domain Size on Toughness of Poly(styrene-block-butadiene) Star Block Copolymer/Polystyrene Blends. *Macromol. Rapid Commun.* **2004**, *25*, 2019–2024.

(38) Bolton, J. M.; Hillmyer, M. A.; Hoyer, T. R. Sustainable Thermoplastic Elastomers from Terpene-Derived Monomers. *ACS Macro Lett.* **2014**, *3*, 717–720.

(39) Bywater, S.; Firat, Y.; Black, P. E. Microstructures of polybutadienes prepared by anionic polymerization in polar solvents. Ion-pair and solvent effects. *J. Polym. Sci. Polym. Chem. Ed.* **1984**, *22*, 669–672.

(40) Widmaier, J. M.; Meyer, G. C. Glass transition temperature of anionic polyisoprene. *Macromolecules* **1981**, *14*, 450–452.

(41) Galanos, E.; Grune, E.; Wahlen, C.; Müller, A. H. E.; Appold, M.; Gallei, M.; Frey, H.; Floudas, G. Tapered Multiblock Copolymers Based on Isoprene and 4-Methylstyrene: Influence of the Tapered Interface on the Self-Assembly and Thermomechanical Properties. *Macromolecules* **2019**, *52*, 1577–1588.

(42) Steube, M.; Johann, T.; Galanos, E.; Appold, M.; Rüttiger, C.; Mezger, M.; Gallei, M.; Müller, A. H. E.; Floudas, G.; Frey, H. Isoprene/Styrene Tapered Multiblock Copolymers with up to Ten Blocks: Synthesis, Phase Behavior, Order, and Mechanical Properties. *Macromolecules* **2018**, *51*, 10246–10258.

(43) Grune, E.; Appold, M.; Müller, A. H. E.; Gallei, M.; Frey, H. Anionic Copolymerization Enables the Scalable Synthesis of Alternating (AB)_n Multiblock Copolymers with High Molecular Weight in $n/2$ Steps. *ACS Macro Lett.* **2018**, *7*, 807–810.

(44) Tiedemann, P. von; Maciol, K.; Preis, J.; Sajkiewicz, P.; Frey, H. Rapid one-pot synthesis of tapered star copolymers via ultra-fast coupling of polystyryllithium chain ends. *Polym. Chem.* **2019**, *10*, 1762–1768.

(45) Grune, E.; Johann, T.; Appold, M.; Wahlen, C.; Blankenburg, J.; Leibig, D.; Müller, A. H. E.; Gallei, M.; Frey, H. One-Step Block Copolymer Synthesis versus Sequential Monomer Addition: A Fundamental Study Reveals That One Methyl Group Makes a Difference. *Macromolecules* **2018**, *51*, 3527–3537.

(46) Quinebèche, S.; Navarro, C.; Gnanou, Y.; Fontanille, M. In situ mid-IR and UV–visible spectroscopies applied to the determination of kinetic parameters in the anionic copolymerization of styrene and isoprene. *Polymer* **2009**, *50*, 1351–1357.

(47) Blankenburg, J.; Kersten, E.; Maciol, K.; Wagner, M.; Zarbakhsh, S.; Frey, H. The poly(propylene oxide-co-ethylene oxide) gradient is controlled by the polymerization method: determination of reactivity ratios by direct comparison of different copolymerization models. *Polym. Chem.* **2019**, *10*, 2863–2871.

- (48) Wall, F. T. The Structure of Vinyl Copolymers. *J. Am. Chem. Soc.* **1941**, *63*, 1862–1866.
- (49) Jaacks, V. *Makromol. Chem.* **1972**, *161*, 161–172.
- (50) Meyer, V. E.; Lowry, G. G. Integral and differential binary copolymerization equations. *J. Polym. Sci. A Gen. Pap.* **1965**, *3*, 2843–2851.
- (51) Mayo, F. R.; Lewis, F. M. Copolymerization. I. A Basis for Comparing the Behavior of Monomers in Copolymerization; The Copolymerization of Styrene and Methyl Methacrylate. *J. Am. Chem. Soc.* **1944**, *66*, 1594–1601.
- (52) R. Hoffmann, V. I. Minkin, B. K. Carpenter. Ockham's razor and chemistry. *Bull. Soc. Chim. Fr.*, *1996*, 117–130.
- (53) Hawkins, D. M. The problem of overfitting. *J. Chem. Inf. Comput. Sci.* **2004**, *44*, 1–12.
- (54) Ashraf, A. R.; Ryan, J. J.; Satkowski, M. M.; Lee, B.; Smith, S. D.; Spontak, R. J. Bicomponent Block Copolymers Derived from One or More Random Copolymers as an Alternative Route to Controllable Phase Behavior. *Macromol. Rapid Commun.* **2017**, *38*.
- (55) Skeist, I. Copolymerization; the composition distribution curve. *J. Am. Chem. Soc.* **1946**, *68*, 1781–1784.
- (56) Spontak, R. J.; Zielinski, J. M.; Lipscomb, G. G. Effect of looping on the microstructure of linear multiblock copolymers. *Macromolecules* **1992**, *25*, 6270–6276.
- (57) Geoffrey, H.; Milkovich, R. Blockpolymers of monovinyl aromatic hydrocarbons and conjugated dienes. U.S. Patent 3265765, Jan 29, 1962.
- (58) Tiedemann, P. von; Yan, J.; Barent, R. D.; Spontak, R. J.; Floudas, G.; Frey, H.; Register, R. A. Tapered Multiblock Star Copolymers: Synthesis, Selective Hydrogenation, and Properties. *Macromolecules* **2020**, *53*, 11, 4422–4434.
- (59) Gaborieau, M.; Castignolles, P. Size-exclusion chromatography (SEC) of branched polymers and polysaccharides. *Anal. Bioanal. Chem.* **2011**, *399*, 1413–1423.
- (60) Worsfold, D. J.; Bywater, S. Anionic Polymerization of Isoprene. *Can. J. Chem.* **1964**, *42*, 2884–2892.
- (61) Zhang, L.; Luo, Y.; Hou, Z. Unprecedented isospecific 3,4-polymerization of isoprene by cationic rare earth metal alkyl species resulting from a binuclear precursor. *J. Am. Chem. Soc.* **2005**, *127*, 14562–14563.
- (62) Pipertzis, A.; Hess, A.; Weis, P.; Papamokos, G.; Koynov, K.; Wu, S.; Floudas, G. Multiple Segmental Processes in Polymers with cis and trans Stereoregular Configurations. *ACS Macro Lett.* **2018**, *7*, 11–15.
- (63) Watanabe, H. Slow Dielectric Relaxation of a Styrene-Isoprene-Styrene Triblock Copolymer with Dipole Inversion in the Middle Block: A Challenge to a Loop/Bridge Problem. *Macromolecules* **1995**, *28*, 5006–5011.

- (64) Smith, S. D.; Spontak, R. J.; Satkowski, M. M.; Ashraf, A.; Heape, A. K.; Lin, J. S. Microphase-separated poly(styrene-*b*-isoprene)*n* multiblock copolymers with constant block lengths. *Polymer* **1994**, *35*, 4527–4536.
- (65) Mori, Y.; Lim, L. S.; Bates, F. S. Consequences of Molecular Bridging in Lamellae-Forming Triblock/Pentablock Copolymer Blends. *Macromolecules* **2003**, *36*, 9879–9888.
- (66) Hermel, T. J.; Hahn, S. F.; Chaffin, K. A.; Gerberich, W. W.; Bates, F. S. Role of Molecular Architecture in Mechanical Failure of Glassy/Semicrystalline Block Copolymers: CEC vs CECEC Lamellae. *Macromolecules* **2003**, *36*, 2190–2193.
- (67) Qiao, L.; Leibig, C.; Hahn, S. F.; Winey, K. I. Isolating the Effects of Morphology and Chain Architecture on the Mechanical Properties of Triblock Copolymers. *Ind. Eng. Chem. Res.* **2006**, *45*, 5598–5602.
- (68) Zhao, Y.; Su, B.; Zhong, L.; Chen, F.; Fu, Q. Largely Improved Mechanical Properties of a Poly(styrene-*b*-isoprene-*b*-styrene) Thermoplastic Elastomer Prepared under Dynamic-Packing Injection Molding. *Ind. Eng. Chem. Res.* **2014**, *53*, 15287–15295.
- (69) Knoll, K.; Nießner, N. Styrolux+ and styroflex+ - from transparent high impact polystyrene to new thermoplastic elastomers: Syntheses, applications and blends with other styrene based polymers. *Macromol. Symp.* **1998**, *132*, 231–243.
- (70) Zhang, J.; Li, T.; Mannion, A. M.; Schneiderman, D. K.; Hillmyer, M. A.; Bates, F. S. Tough and Sustainable Graft Block Copolymer Thermoplastics. *ACS Macro Lett.* **2016**, *5*, 407–412.
- (71) Xue, J.; Wu, T.; Dai, Y.; Xia, Y. Electrospinning and Electrospun Nanofibers: Methods, Materials, and Applications. *Chem. Rev.* **2019**, *119*, 5298–5415.
- (72) Greiner, A.; Wendorff, J. H. Electrospinning: a fascinating method for the preparation of ultrathin fibers. *Angew. Chem. Int. Ed.* **2007**, *46*, 5670–5703.
- (73) Li, D.; Xia, Y. Electrospinning of Nanofibers: Reinventing the Wheel? *Adv. Mater.* **2004**, *16*, 1151–1170.
- (74) Huang, Z.-M.; Zhang, Y.-Z.; Kotaki, M.; Ramakrishna, S. A review on polymer nanofibers by electrospinning and their applications in nanocomposites. *Compos. Sci. Technol.* **2003**, *63*, 2223–2253.
- (75) Chuangchote, S.; Sirivat, A.; Supaphol, P. Electrospinning of Styrene-Isoprene Copolymeric Thermoplastic Elastomers. *Polym. J.* **2006**, *38*, 961–969.
- (76) Lee, K. H.; Kim, H. Y.; Bang, H. J.; Jung, Y. H.; Lee, S. G. The change of bead morphology formed on electrospun polystyrene fibers. *Polymer* **2003**, *44*, 4029–4034.

Supporting Information

Tapered Multiblock Copolymers Based on Farnesene and Styrene: Impact of Bio-Based Polydiene Architectures on Material Properties

Christian Wahlen, Jan Blankenburg, Philipp von Tiedemann, Johannes Ewald, Pawel Sajkiewicz, Axel H. E. Müller*, George Floudas* and Holger Frey*

Table of Contents

1. <i>In situ</i> ¹ H NMR copolymerization kinetics	179
1.1. Evaluation of ¹ H NMR copolymerization kinetic experiment at 23 °C.....	180
1.2. Evaluation of ¹ H NMR copolymerization kinetic experiment at 30 °C.....	181
1.3. Evaluation of ¹ H NMR copolymerization kinetic experiment at 40 °C.....	183
1.4. Comparison of Integrated Ideal and Meyer-Lowry evaluation of the copolymerization kinetics for varying conversions.....	185
2. Homopolymerization kinetic experiments.....	187
3. Determination of reaction times of the copolymerization of β-farnesene with styrene.	190
4. Synthesis and characterization of tapered tri- and pentablock copolymers PS- <i>b</i> -P(Far- <i>co</i> -S) _n	191
5. SAXS measurements.....	196
6. Tensile tests	197
7. Electrospinning.....	200
8. Transformation of simulated molar composition profile to the corresponding volume composition profile.	204
8.2. Derivation of the copolymer molar composition profile expression for the terminal model (Mayo-Lewis).....	205
8.3. Derivation of the copolymer volume composition profile expression for the nonterminal/ideal model (Wall).....	206
8.4. Expression for the compositional drift of the volume fraction for the terminal model.....	208
8.5. Transformation of total conversion to chain position of the composition profile.....	209
References	209

1 *In situ* ¹H NMR copolymerization kinetics

The copolymerizations were both modelled by the ideal/non-terminal model (Wall, Jaacks) and the terminal model (Mayo-Lewis).^{1,2} The reactivity ratios of the Jaacks³ and Integrated Ideal⁴ fits show no significant dependence regarding the reaction temperature, as shown in Table S1, while the fits for the Mayo-Lewis model (in the form of the Meyer-Lowry equation)⁵ resulted in a deviation of the reactivity ratios from the ideal/non-terminal model and in a clear temperature dependency of the reactivity ratios, without any obvious tendency. The numerical instability of the Meyer-Lowry equation for copolymerizations that follow the non-terminal model, illustrates the problem of overfitting.^{6,7} It should be mentioned that it is necessary to compare models, which differ in their complexity, to reduce the problem of overfitting. In general a more complex model which results in no better predictions than a simpler model is an overfit.⁷ The linear correlation of the data points in the Jaacks plot indicate a nearly ideal copolymerization of β -farnesene and styrene, in comparison to the copolymerization of isoprene and styrene, which follows the terminal model.⁸

1.1 Evaluation of ^1H NMR copolymerization kinetic experiment at 23 °C

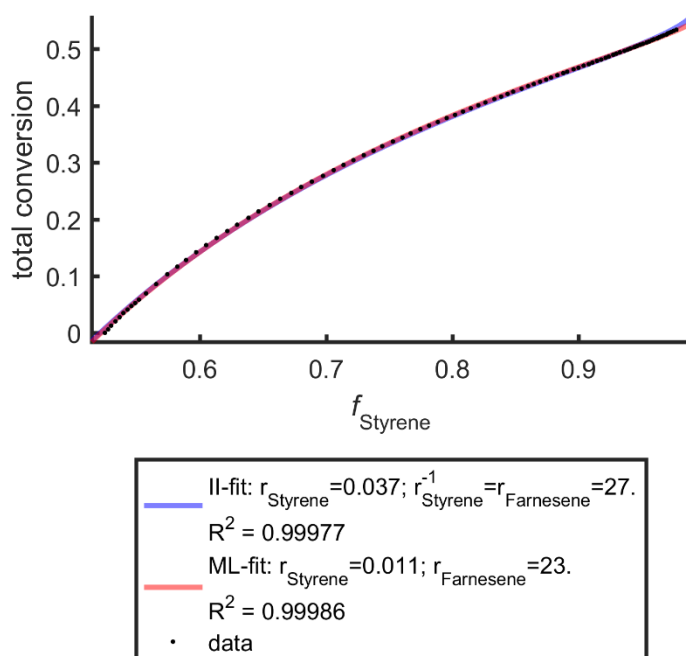


Figure S1. Integrated Ideal (II) and Meyer-Lowry (ML) fits of the copolymerization of styrene and β -farnesene at 23 °C with reactivity ratios determined by the fitting procedure (measured data points in black).

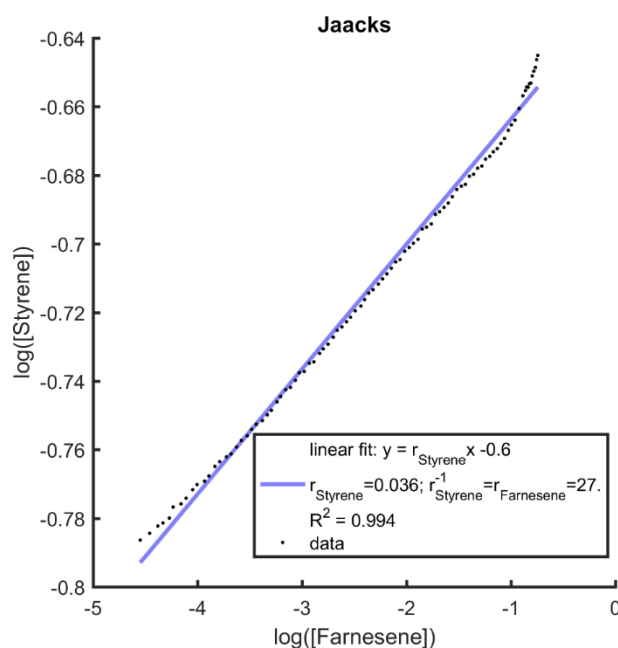


Figure S2. Jaacks fit of the copolymerization of styrene and β -farnesene at 23 °C with reactivity ratios determined by the fitting procedure (measured data points in black).

1.2 Evaluation of ^1H NMR copolymerization kinetic experiment at 30 °C

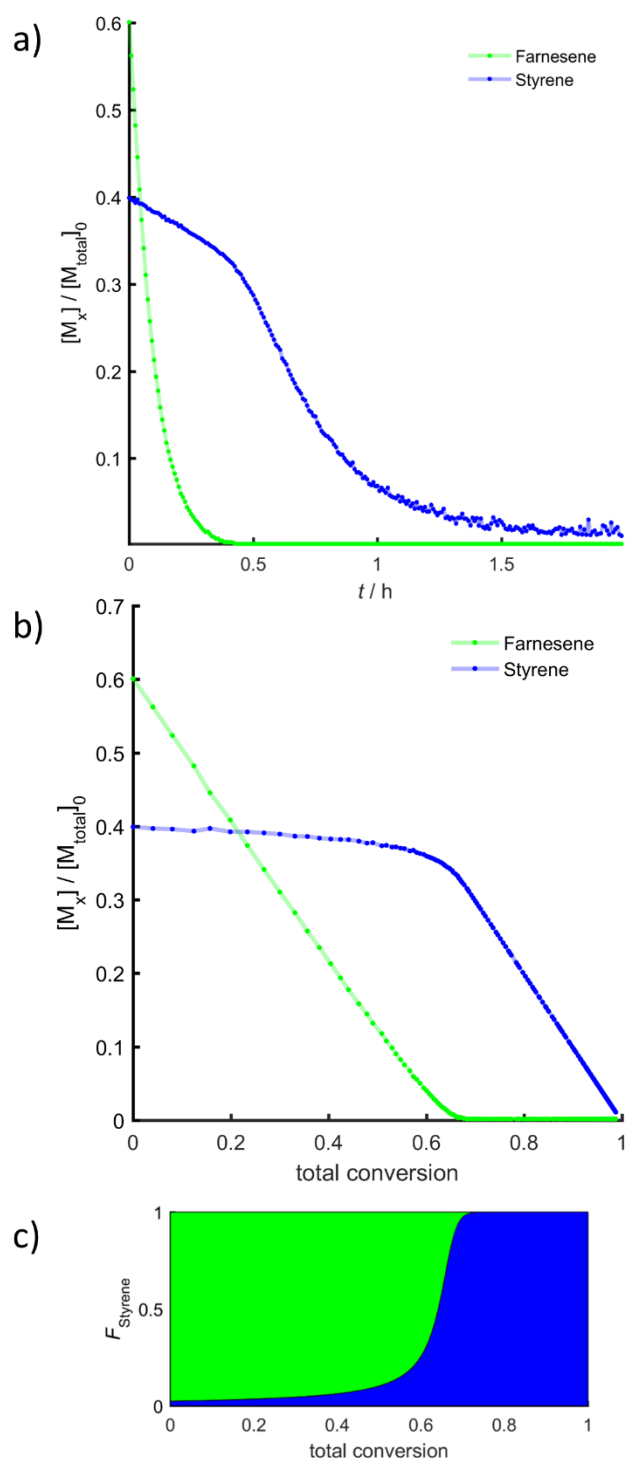


Figure S3. a) Time-conversion plots of the copolymerization of styrene and β -farnesene. Monomer concentrations were determined by *in situ* ^1H NMR spectroscopy in C_6D_{12} at 30 °C. b) Comonomer concentrations as a function of total conversion. c) Calculated molar composition profile of the corresponding tapered copolymer.

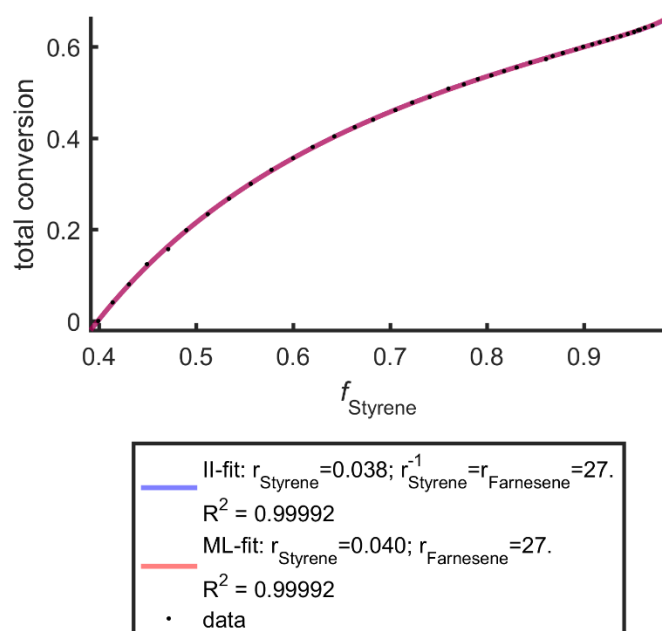


Figure S4. Integrated Ideal and Meyer-Lowry fit of the copolymerization of styrene and β -farnesene at 30 °C with reactivity ratios determined by the fitting procedure (measured data points in black).

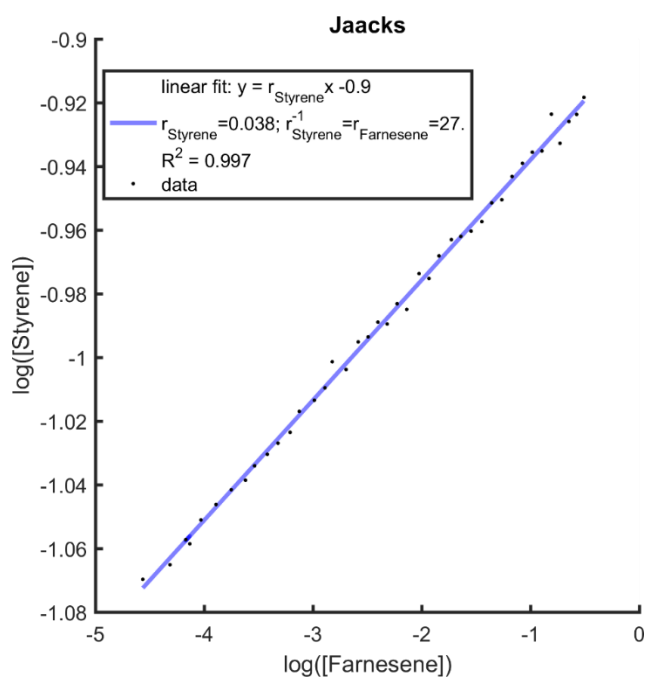


Figure S5. Jaacks fit of the copolymerization of styrene and β -farnesene at 30 °C with reactivity ratios determined by the fitting procedure (measured data points in black).

1.3 Evaluation of ^1H NMR copolymerization kinetic experiment at 40 °C

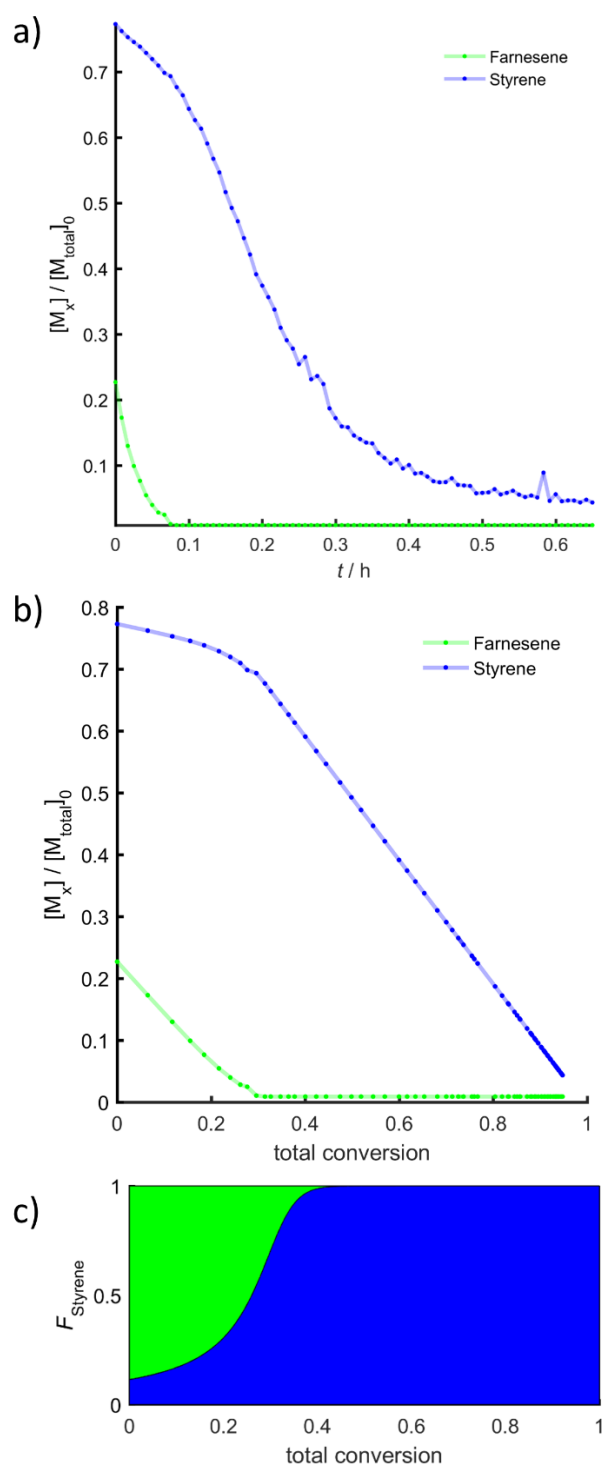


Figure S6. a) Time-conversion plots of the copolymerization of styrene and β -farnesene. Monomer concentrations were determined by *in situ* ^1H NMR spectroscopy in C_6D_{12} at 40 °C. b) Comonomer concentrations as a function of total conversion. c) Calculated molar composition profile of the corresponding tapered copolymer.

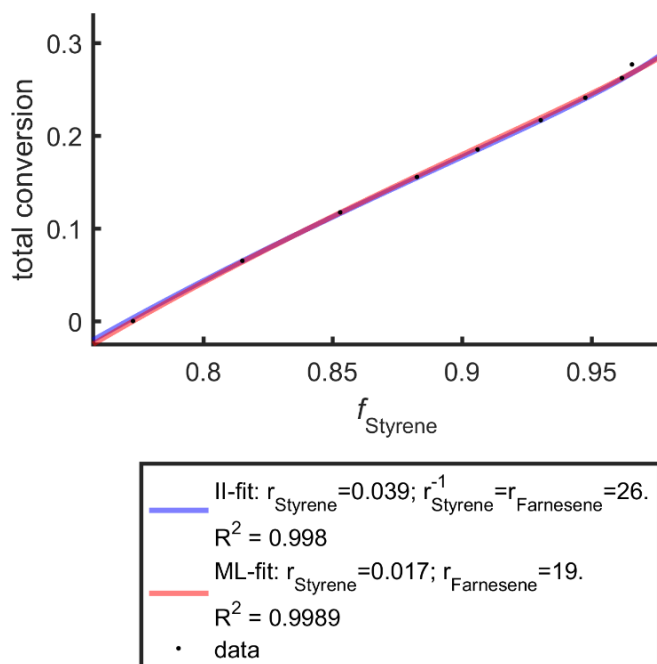


Figure S7. Integrated Ideal and Meyer-Lowry fit of the copolymerization of styrene and β -farnesene at 40 °C with reactivity ratios determined by the fitting procedure (measured data points in black).

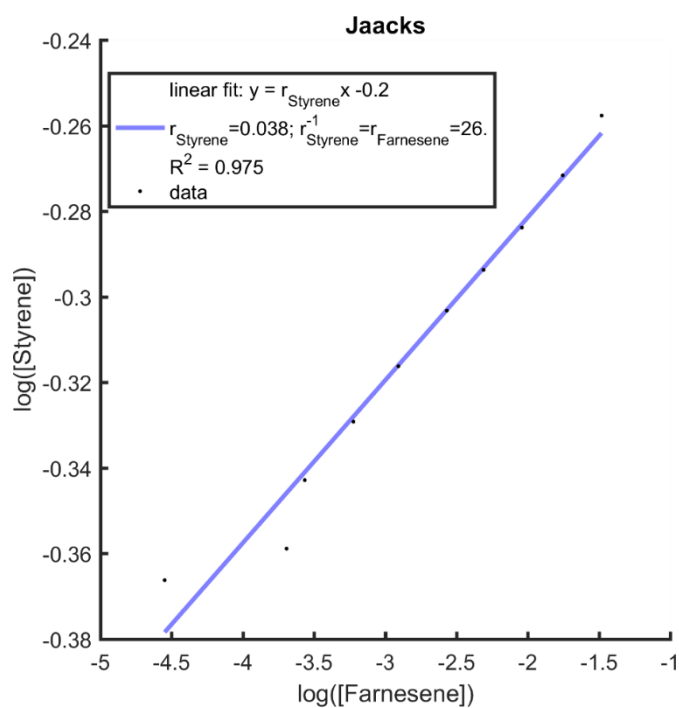


Figure S8. Jaacks fit of the copolymerization of styrene and β -farnesene at 40 °C with reactivity ratios determined by the fitting procedure (measured data points in black).

Table S1. Reactivity ratios for the copolymerization of β -farnesene with styrene at different temperatures, based on different methods.

Temperature / °C	Integrated Ideal		Jaacks		Meyer-Lowry		
	r_{Far}	r_{S}	r_{Far}	r_{S}	r_{Far}	r_{S}	$r_{\text{Far}} \cdot r_{\text{S}}$
23	27	0.037	27	0.036	23	0.011	0.24
30	27	0.038	27	0.038	27	0.040	1.06
40	26	0.039	26	0.038	19	0.017	0.33

1.4 Comparison of Integrated Ideal and Meyer-Lowry evaluation of the copolymerization kinetics for varying conversions

For an ideal polymerization the Meyer-Lowry fit is known to result in inaccurate reactivity ratios when dealing with systematic errors, as shown by several simulations.⁴ In ¹H NMR kinetic studies systematic errors, due to the baseline noise, especially in the range of low monomer concentrations, cannot be excluded. The well-known problem of overfitting can be identified by investigating the influence of varying the range, in which the data set is evaluated, on the model fitting.⁷ Accordingly, the numerical instability of the Meyer-Lowry equation regarding systematic errors is demonstrated by the evaluation of the β -farnesene/styrene copolymerization kinetic measurement at 23°C (shown in Figure S9). For this purpose the minimal trusted monomer concentration of β -farnesene $[M_{\text{Far}}]_{\text{min}}$ was varied. The minimal trusted monomer concentration defines the upper limit for the conversion interval that is evaluated in the fitting procedure. It is given as a fraction of the initial monomer concentration $[M_{\text{Far}}]_0$. While the reactivity ratios determined by the Meyer-Lowry equation show negative values for a minimal trusted concentration of $0.05 \cdot [M_{\text{Far}}]_0$ and $0.02 \cdot [M_{\text{Far}}]_0$, as well as a significant deviation along the series, the reactivity ratios determined by the Integrated Ideal fit evidence good stability against systematic errors (as shown in Table S2).

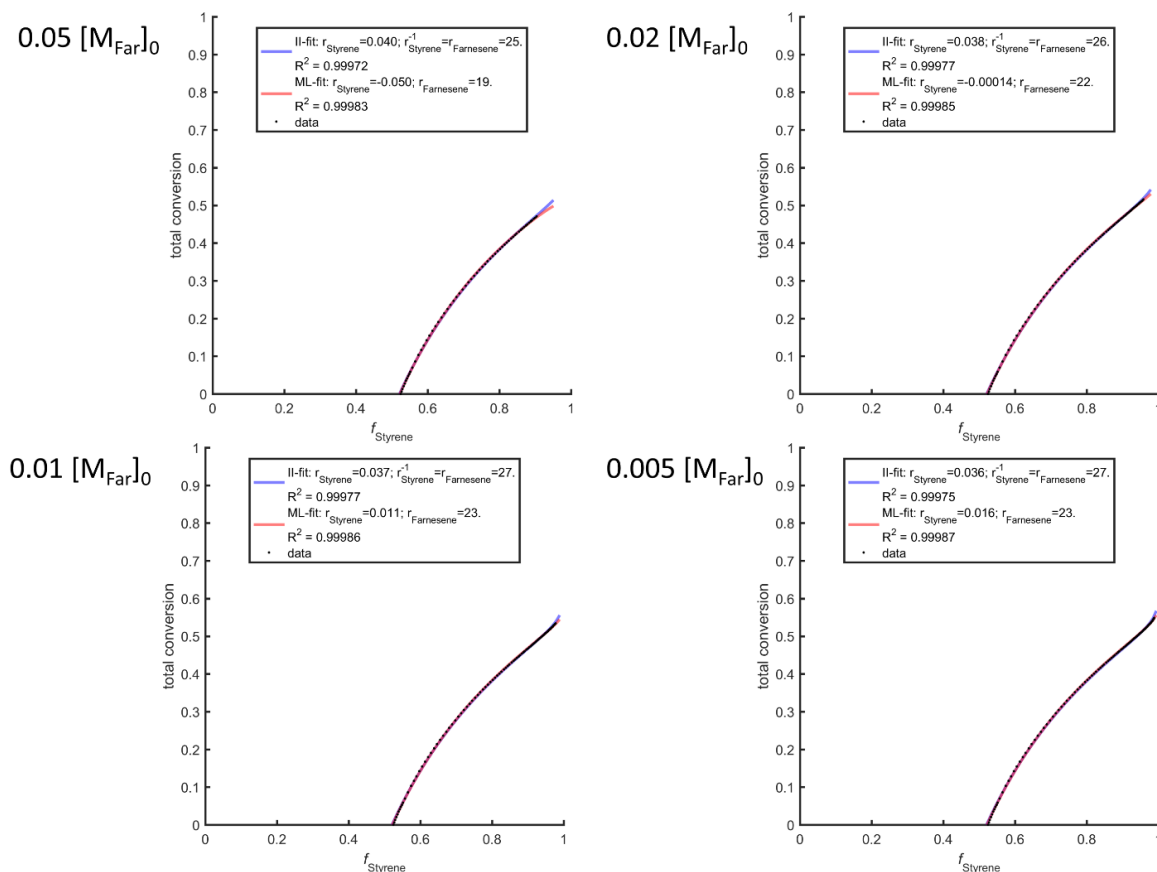


Figure S9. Comparison of Integrated Ideal and Meyer-Lowry fit of the copolymerization of styrene and β -farnesene at 23 °C, evaluated up to different minimal trusted monomer concentrations $[M_{Far}]_{min}$, which is given as fraction of $[M_{Far}]_0$. Reactivity ratios determined by the fitting procedure (measured data points in black).

Table S2. Overview of the reactivity ratios of the copolymerization of styrene and β -farnesene at 23 °C, determined by the Integrated Ideal and Meyer-Lowry fit and evaluated up to different minimal trusted monomer concentrations $[M_{\text{Far}}]_{\text{min}}$, which is given as fraction of $[M_{\text{Far}}]_0$.

Minimal trusted concentration $[M_{\text{Far}}]_{\text{min}}$	Integrated Ideal		Meyer Lowry		
	r_{Far}	r_{S}	r_{Far}	r_{S}	$r_{\text{Far}} \cdot r_{\text{S}}$
0.05 $[M_{\text{Far}}]_0$	25	0.040	19	(-0.050)	(-0.95)
0.02 $[M_{\text{Far}}]_0$	26	0.038	22	(-0.00014)	(-0.0031)
0.01 $[M_{\text{Far}}]_0$	27	0.038	23	0.011	0.25
0.005 $[M_{\text{Far}}]_0$	27	0.037	19	0.016	0.30

2 Homopolymerization kinetic experiments

The homopolymerization kinetic studies were performed analogous to the copolymerization kinetic studies. In Figure S10 the pseudo-first-order time-conversion plots for the homopolymerization of β -farnesene in C_6D_{12} at 23 °C (blue), 30 °C (black) and 40 °C (red) at different temperatures are shown. The linear dependence is an indication for the living character of the homopolymerization. By using eqs 1 and 2 (under the assumption of a tetrameric coordination of polyfarnesyllithium chains, in analogy to polyisoprenyllithium),^{9,10} the slope of the linear fits of the time-conversion plots (apparent rate constant, k_{app}) was used to calculate the homopolymerization rates k_{p} at different temperatures. The comparison with the corresponding homopolymerization rates of isoprene (Table S4) reveals a significantly higher homopolymerization rate for β -farnesene than isoprene. This also affects the total polymerization time of the copolymerization of β -farnesene and styrene, which is completed faster than the corresponding styrenic copolymerization with isoprene (according to eq. 2). From an industrial point of view, reduced reaction times may be a crucial advantage of homo- and copolymers of β -farnesene over isoprene, aiming at process optimization.

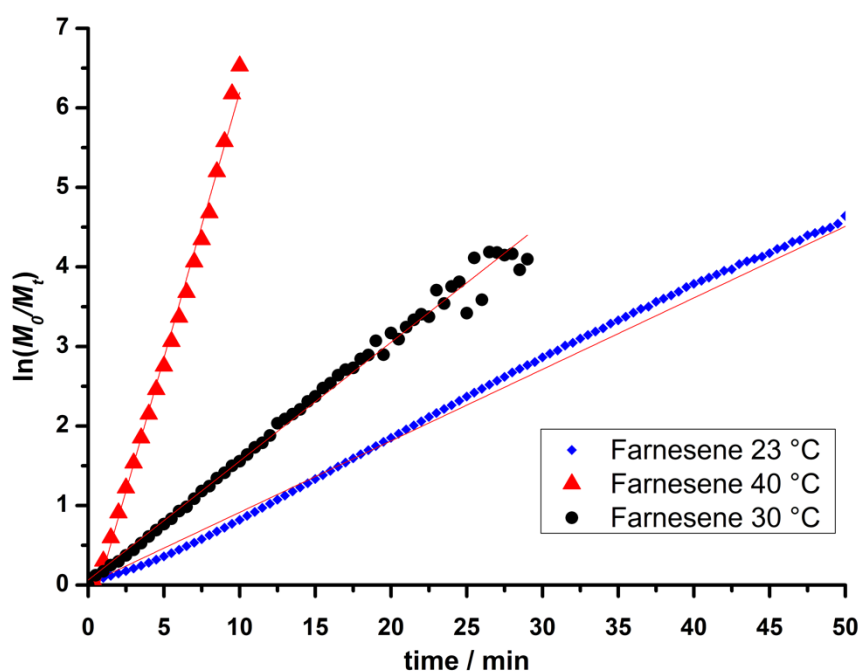


Figure S10. Pseudo-first-order time-conversion plots for the homopolymerization of β -farnesene in C_6D_{12} at different temperatures.

$$\ln \frac{[M_0]}{[M_t]} = k_{app}t \quad (S1)$$

$$k_p = k_{app}/[Ini]^{\frac{1}{4}} \quad (S2)$$

It should be noted that the so-called rate constant, k_p , still contains the unknown aggregation equilibrium constant, K_{agg} , of the polyfarnesene-Li chain ends:

$$k_p = k'_p(4K_{agg})^{-\frac{1}{4}} \quad (S3)$$

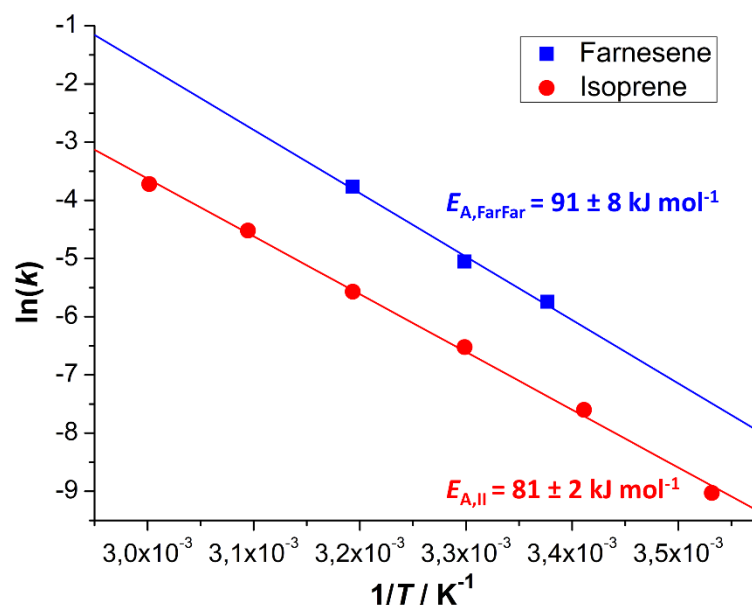
Table S3. Apparent rate constants from the homopolymerization kinetic measurements for different temperatures.

Temperature	$[Ini]_{0a} / \text{mol L}^{-1}$	$k_{app} \cdot 10^{-3} / \text{s}^{-1}$	$k_p \cdot 10^{-3} / (\text{L/mol})^{1/4} \text{s}^{-1}$
23 °C	0.038	1.49	3.23
30 °C	0.030	2.49	6.31
40 °C	0.045	11.1	23.1

^a $[Ini]_0 = [Far]_0 M_n / M_{\text{Monomer}}$, determination of the molecular weight of the polymer via end-group analysis via ^1H NMR spectroscopy ($[Far]_0 = 0.75 \text{ mol/L}$).

Table S4. Computed homopolymerization rate constants of β -farnesene and isoprene for different temperatures.

Diene-Monomer	$k_p \cdot 10^{-3} /$ $(\text{L/mol})^{1/4} \cdot \text{s}^{-1}$	$k_p \cdot 10^{-3} /$ $(\text{L/mol})^{1/4} \cdot \text{s}^{-1}$	$k_p \cdot 10^{-3} /$ $(\text{L/mol})^{1/4} \cdot \text{s}^{-1}$
	at 23 °C	at 30 °C	at 40 °C
Far	3.23	6.31	23.1
I ^{11,12}	0.61	1.47	3.81

**Figure S11.** Arrhenius plots of the homopolymerization rate constants of isoprene and β -farnesene in cyclohexane and the corresponding activation energies. Data for homopolymerization of isoprene are obtained from literature.¹¹

It might be surprising that the polymerization of the rather bulky β -farnesene is faster than that of isoprene. However, the k_p values still contain the aggregation constant of the chain ends, which – most probably due to steric reasons – for PFar-Li chain ends might be lower than that of the PI-Li chain ends. However, as expected, a linear correlation in the Arrhenius plot is observed for the homopolymerization of farnesene as well as for isoprene, as shown in Figure S11. The activation energy for the homopolymerization of β -farnesene ($E_{A, \text{FarFar}} = 91 \pm 8 \text{ kJ mol}^{-1}$), determined by the slope of the Arrhenius plot, shows a similar order of magnitude as the activation energy for the homopolymerization of isoprene ($E_{A, \text{II}} = 81 \pm 2 \text{ kJ mol}^{-1}$).

Table S5. Computed homo- and cross-propagation rate constants obtained for β -farnesene and styrene at different temperatures.

Temperature	$k_{\text{FarFar}} \cdot 10^{-3} / (\text{L/mol})^{1/4} \text{ s}^{-1}$	$k_{\text{SS}}^{11,13} \cdot 10^{-3} / (\text{L/mol})^{1/2} \text{ s}^{-1}$	$k_{\text{FarS}} \cdot 10^{-3} / (\text{L/mol})^{1/4} \text{ s}^{-1}$	$k_{\text{SFar}} \cdot 10^{-3} / (\text{L/mol})^{1/2} \text{ s}^{-1}$
23 °C	3.23	6.39	0.119	172
30 °C	6.31	10.9	0.233	287
40 °C	23.1	23.2	0.888	595

3 Determination of reaction times of the copolymerization of β -farnesene with styrene.

The reaction times of the copolymerizations of isoprene (I) or β -farnesene (Far) with styrene (S) in cyclohexane at different temperatures were simulated by kinetic Monte Carlo simulations, according to previous works of our group,¹⁴ for 5000 chains and monomer conversions of 99% with chain aggregation numbers of $N = 4$ for polydienyl and $N = 2$ for polystyryl lithium, respectively. For the β -farnesene/styrene copolymerization the rate constants listed in Table S5 were used. The rate constants of the isoprene/styrene copolymerization were obtained from literature.¹¹ As the presence of another monomer changes the environment slightly, and the homopropagation constants are derived from homopolymerization experiments, an additional time buffer of 10% is advisable.

Due to the higher homopolymerization rate of β -farnesene in comparison with isoprene, the copolymerization of β -farnesene and styrene is faster than the corresponding copolymerization of isoprene and styrene in the whole temperature range from 23 °C to 40 °C.

In Table S6 an overview of calculated reaction times for the copolymerization of isoprene or β -farnesene with styrene for copolymers with equal molar and volume composition is given. Striking differences between the copolymerization times of isoprene and β -farnesene are observable. To sum up, β -farnesene enables a faster synthesis of styrene-based thermoplastic elastomers in comparison to their isoprene analogs.

Table S6. Simulated reaction times of the copolymerizations of isoprene (I) or β -farnesene (Far) with styrene (S) in cyclohexane at different temperatures and with an initiator concentration of 1.1 mmol/L, with constant polydiene mole fraction or constant polydiene volume fraction. Homopolymerization rates of styrene were obtained from literature.^{3,5}

Copolymer	M_n / g·mol ⁻¹	[Ini] / mmol·L ⁻¹	ϕ_{PDiene}	x_{PDiene}	$t(23^\circ\text{C})$ /	$t(30^\circ\text{C})$ /	$t(40^\circ\text{C})$ /
					min	min	min
P(I _{0.43-co} -S _{0.57})	120	1.1	0.43	0.5	697	332	141
P(Far _{0.69-co} -S _{0.31})	120	1.1	0.69	0.5	388	223	93
P(I _{0.5-co} -S _{0.5})	120	1.1	0.5	0.57	727	342	144
P(Far _{0.5-co} -S _{0.5})	120	1.1	0.5	0.31	371	212	86

4 Synthesis and characterization of tapered tri- and pentablock copolymers PS-*b*-P(Far-co-S)_n

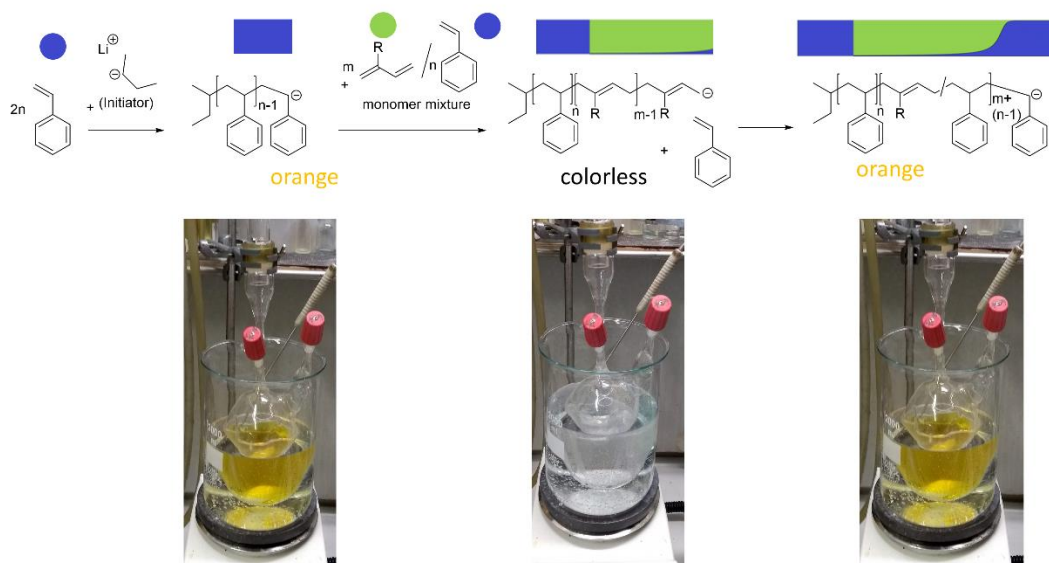


Figure S12. Synthesis scheme for tapered triblock copolymers.

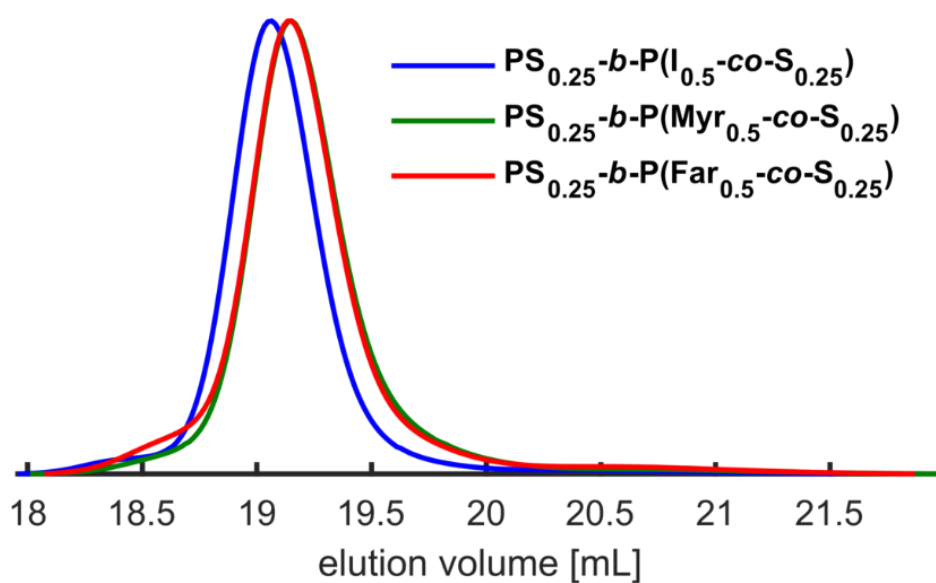


Figure S13. SEC traces (THF, PS standard) of triblock copolymers with $\varphi_{\text{PDiene}} = 0.5$.

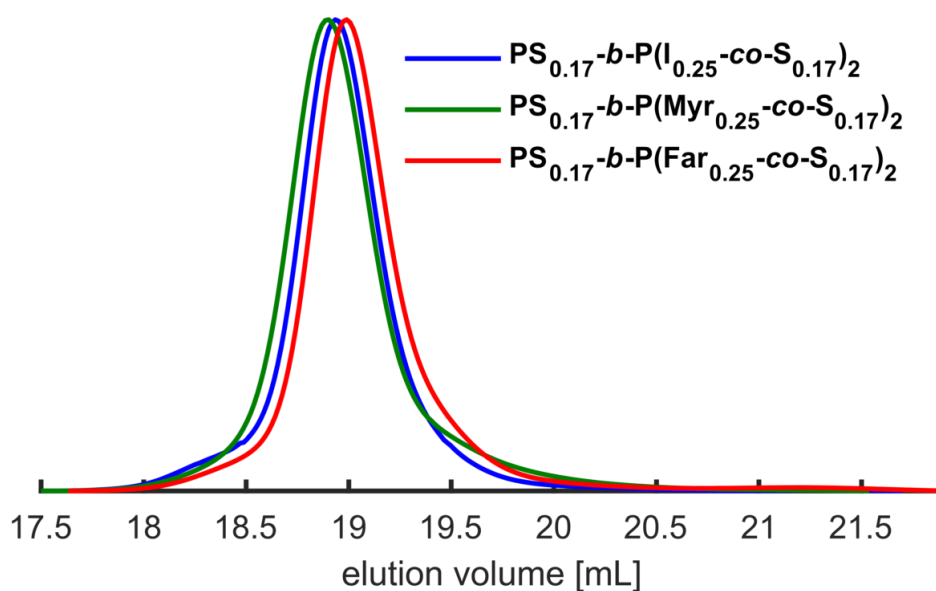


Figure S14. SEC traces (THF, PS standard) of pentablock copolymers with $\varphi_{\text{PDiene}} = 0.5$.

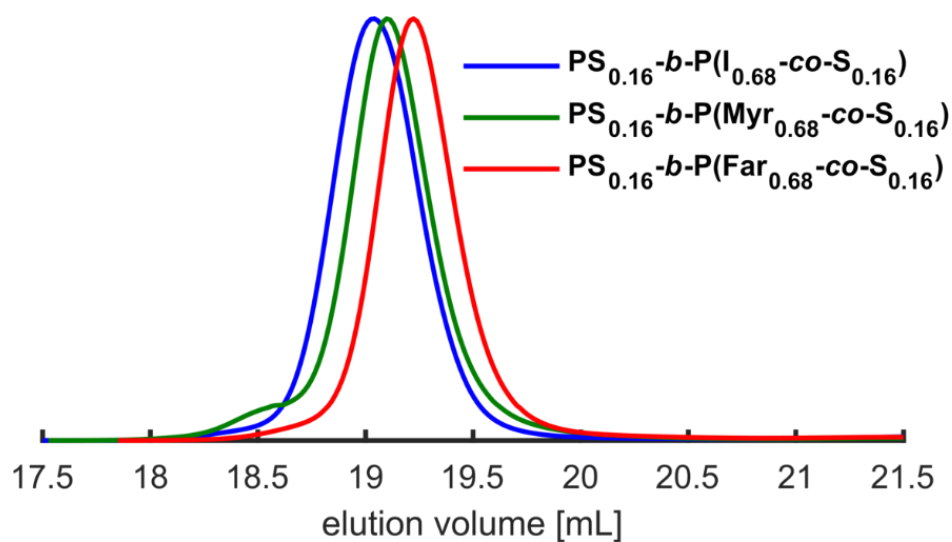


Figure S15. SEC traces (THF, PS standard) of triblock copolymers with $\varphi_{\text{PDiene}} = 0.68$.

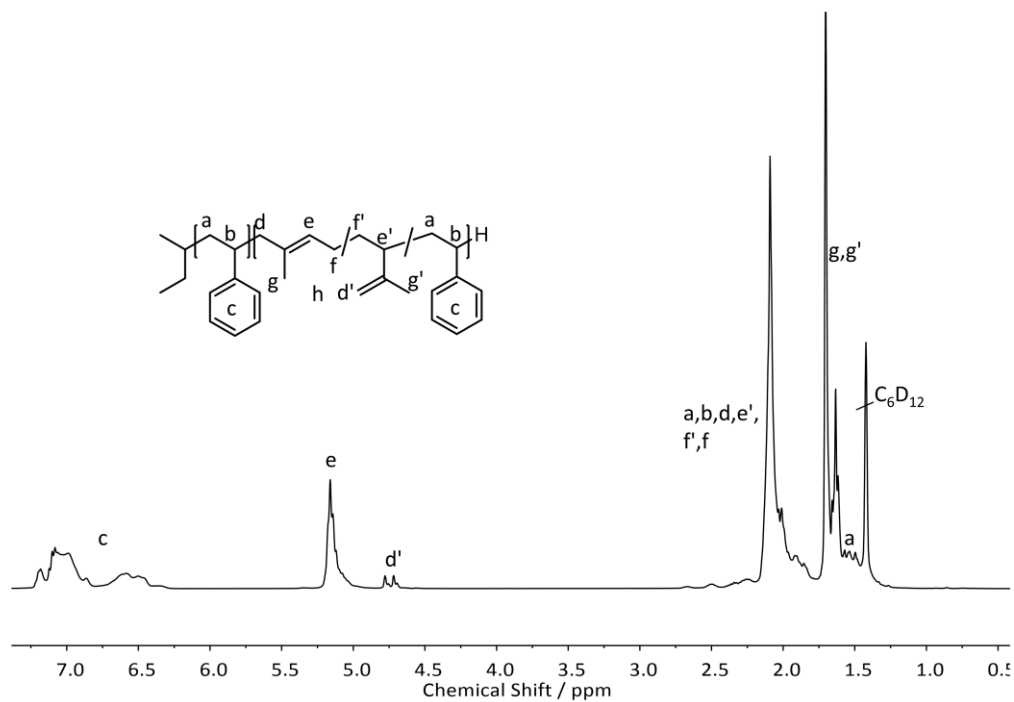


Figure S16. ^1H NMR spectrum (400 MHz) of $\text{PS}_{16}\text{-}b\text{-P}(\text{I}_{68}\text{-co-S}_{16})$ in C_6D_{12} .

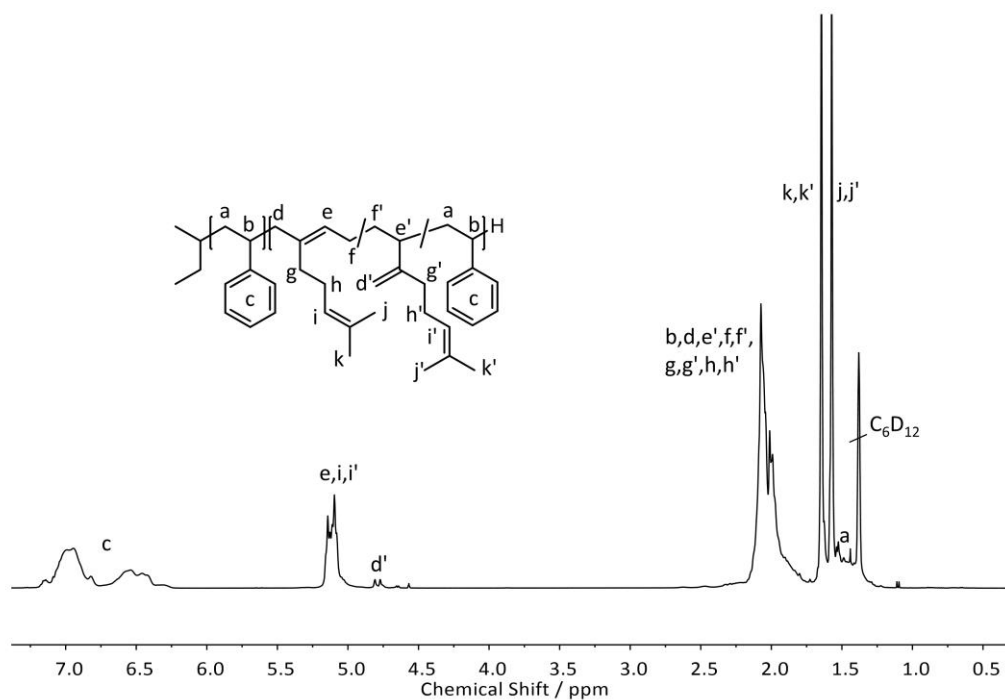


Figure S17. ¹H NMR spectrum (400 MHz) of PS₁₆-b-P(Myrc₆₈-co-S₁₆) in C₆D₁₂.

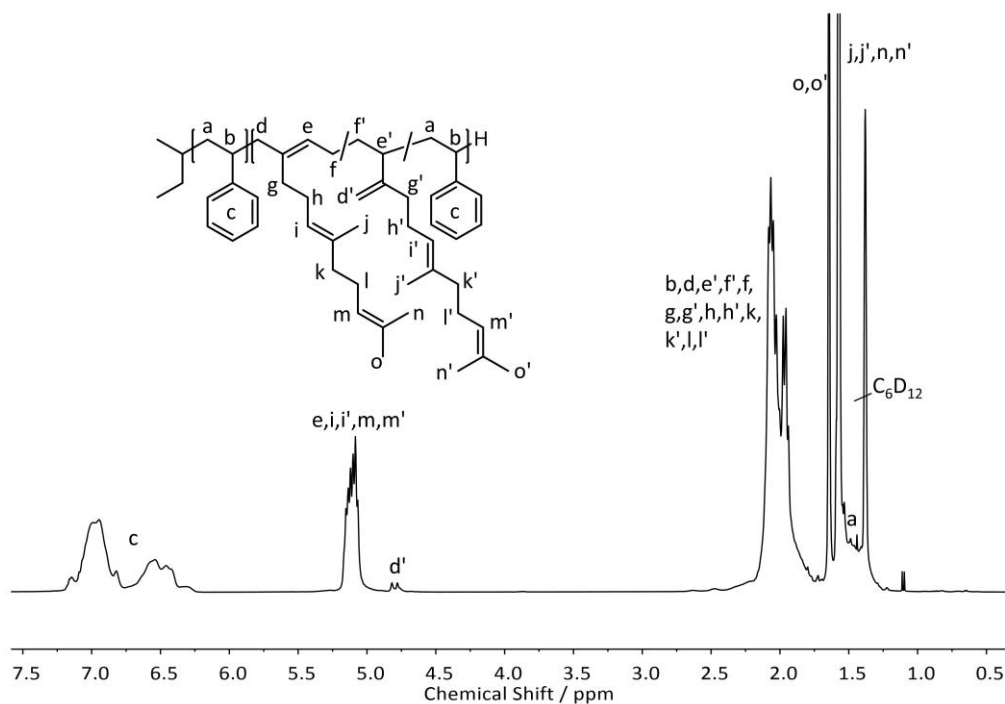


Figure S18. ¹H NMR spectrum (400 MHz) of PS₁₆-b-P(Far₆₈-co-S₁₆) in C₆D₁₂.

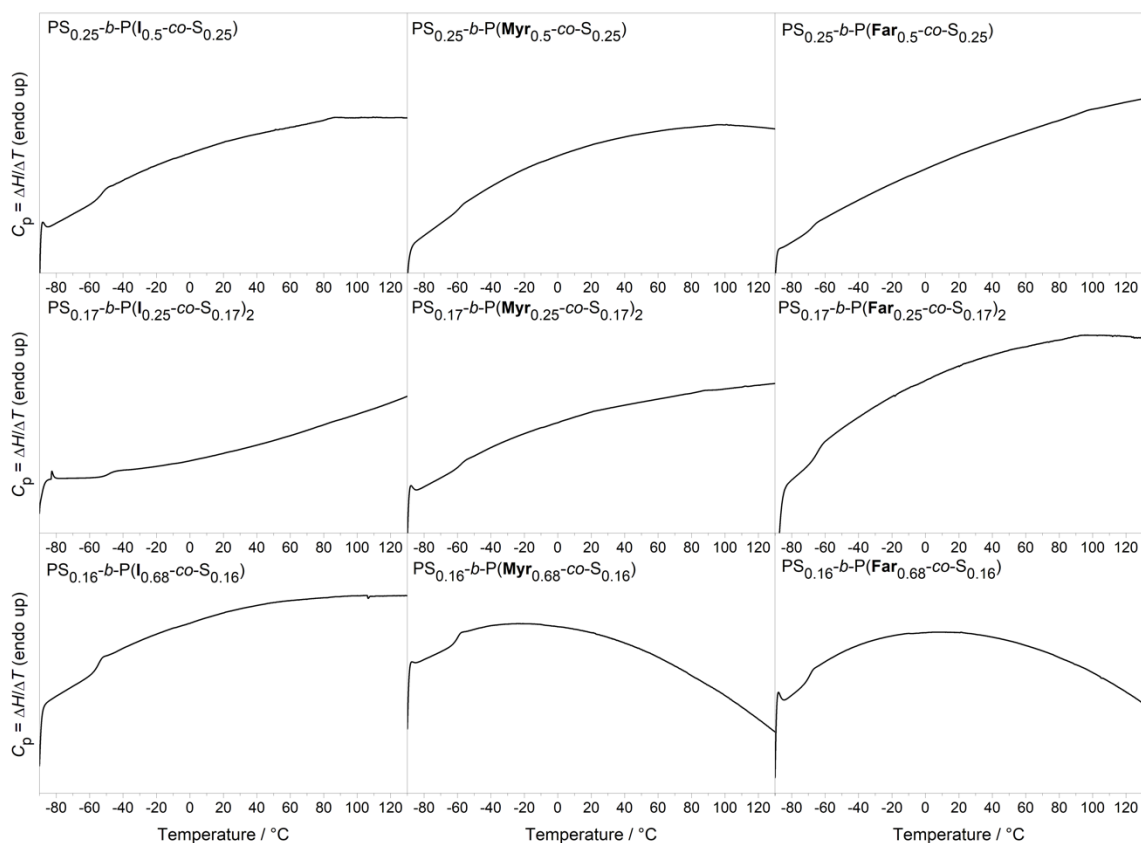


Figure S19. DSC-diagrams of the tri- and pentablock copolymers (2nd heating curve, from -90 °C to 130 °C, heating rate 10 °C/min).

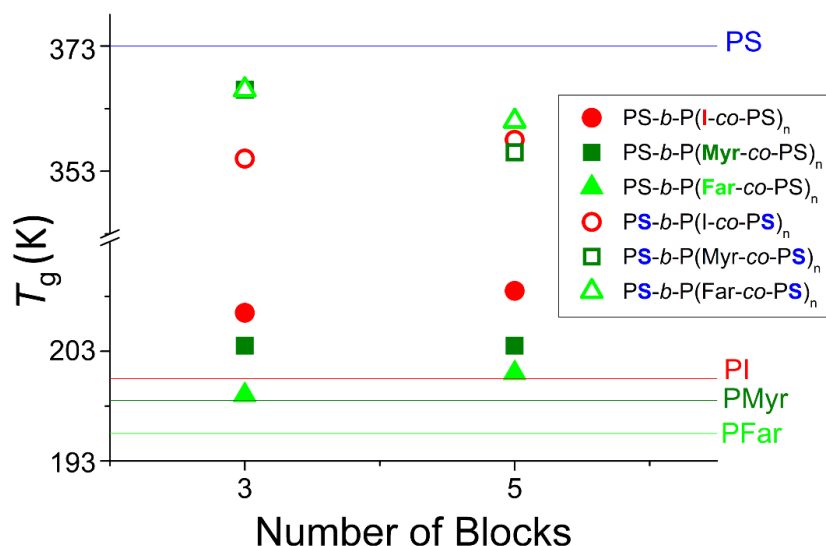


Figure S20. Glass temperatures of the tapered tri- and pentablock copolymers ($\varphi_{\text{PDiene}} = 0.5$) corresponding to PS (open symbols) and PDiene (filled symbols). Dashed lines give the glass temperature of PS and PDiene homopolymers.

5 SAXS measurements

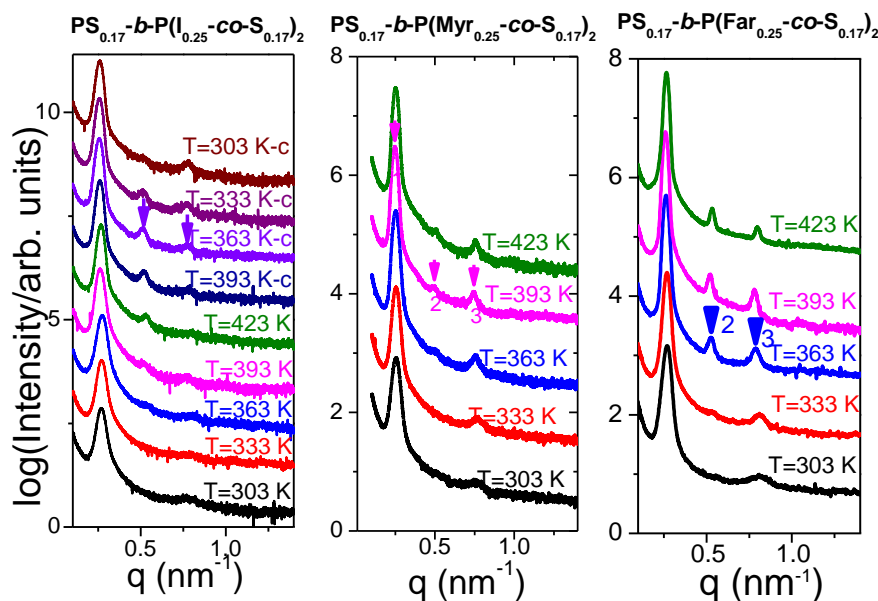


Figure S21. SAXS patterns of the pentablock copolymers with polydiene volume fraction of $\varphi_{\text{PDiene}}=0.5$ shown at different temperatures obtained on heating and cooling (cooling curves are indicated by c). Arrows indicate the positions of the Bragg reflections corresponding to a lamellar morphology.

6 Tensile Tests



Figure S22. Exemplary transparent film of $PS_{0.25}\text{-}co\text{-}P(\text{Far}_{0.5}\text{-}b\text{-}S_{0.25})$, cast by solvent evaporation of a chloroform solution ($c = 20 \text{ wt}\%$).

Table S7. Mechanical data of tri- and pentablock copolymers with $\varphi_{\text{PDiene}} = 0.5$. Values are determined as the average of 5 independent measurements. Errors are given in the 1σ interval.

sample	$E /$ MPa	$\epsilon_{\text{yield}} /$ %	$\sigma_{\text{yield}} /$ MPa	$\epsilon_{\text{break}} /$ %	$\sigma_{\text{break}} /$ MPa	$U /$ MJ m^{-3}
$PS_{0.25}\text{-}b\text{-}P(\text{I}_{0.5}\text{-}co\text{-}S_{0.25})$	257 ± 17	3.4 ± 0.42	6.2 ± 0.26	1119 ± 32	16.9 ± 1.04	103 ± 5
$PS_{0.25}\text{-}b\text{-}P(\text{Myr}_{0.5}\text{-}co\text{-}S_{0.25})$	255 ± 6	3.7 ± 0.26	6.3 ± 0.11	851 ± 56	13.7 ± 0.54	81 ± 8
$PS_{0.25}\text{-}b\text{-}P(\text{Far}_{0.5}\text{-}co\text{-}S_{0.25})$	209 ± 5	4.3 ± 0.15	5.3 ± 0.11	601 ± 42	10.1 ± 0.18	44 ± 4
$PS_{0.17}\text{-}b\text{-}P(\text{I}_{0.25}\text{-}co\text{-}S_{0.17})_2$	214 ± 3	4.6 ± 0.12	6.6 ± 0.18	1149 ± 33	19.6 ± 0.78	111 ± 4
$PS_{0.17}\text{-}b\text{-}P(\text{Myr}_{0.25}\text{-}co\text{-}S_{0.17})_2$	217 ± 4	4.2 ± 0.06	6.3 ± 0.09	806 ± 37	12.1 ± 0.18	65 ± 7
$PS_{0.17}\text{-}b\text{-}P(\text{Far}_{0.25}\text{-}co\text{-}S_{0.17})_2$	170 ± 1	4.9 ± 0.27	5.1 ± 0.02	577 ± 41	9.1 ± 0.26	42 ± 4

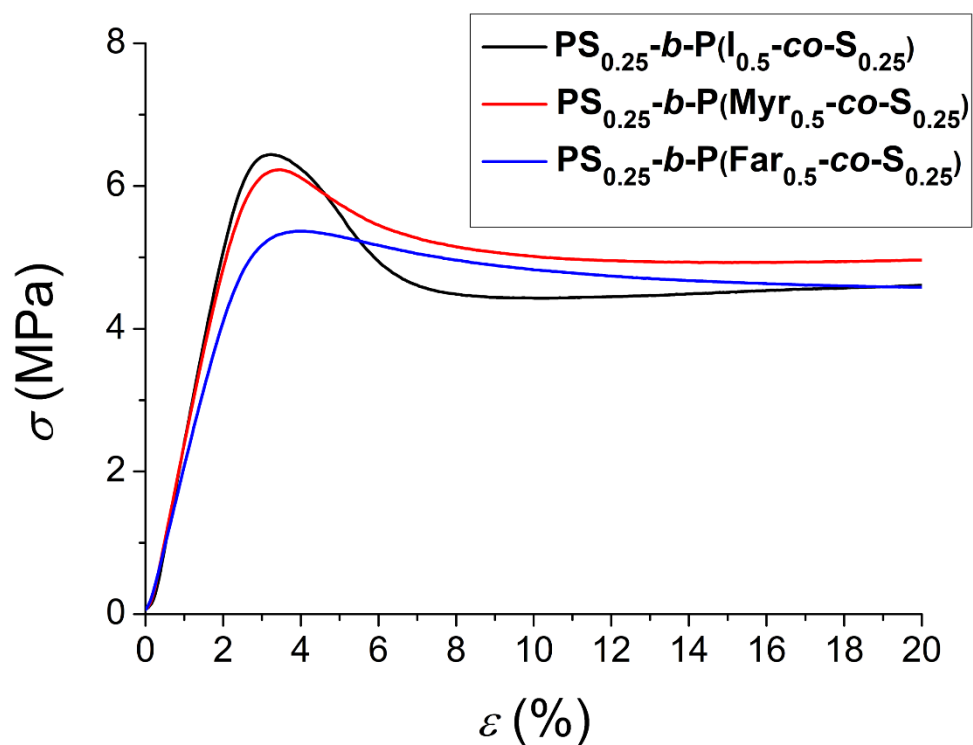


Figure S23. Representative stress–strain curves (zoomed into the range of the yield-point) of the three series of tapered triblock copolymers with varying polydiene blocks: (a) polyisoprene (black), (b) polymyrcene (red) and (c) polyfarnesene (blue) with $\varphi_{\text{PDiene}} = 0.5$.

Table S8. Mechanical data of triblock copolymers with $\varphi_{\text{PDiene}} = 0.68$. Values are determined as the average of 5 independent measurements. Errors are given in the 1σ interval.

sample	$\varepsilon_{\text{break}} / \%$	$\sigma_{\text{break}} / \text{MPa}$	$U / \text{MJ m}^{-3}$
$\text{PS}_{0.16}\text{-}b\text{-P}(\text{I}_{0.68}\text{-co-S}_{0.16})$	1279 ± 192	10.3 ± 2.2	3.7 ± 0.1
$\text{PS}_{0.16}\text{-}b\text{-P}(\text{Myr}_{0.68}\text{-co-S}_{0.16})$	934 ± 66	5.9 ± 0.2	36 ± 5
$\text{PS}_{0.16}\text{-}b\text{-P}(\text{Far}_{0.68}\text{-co-S}_{0.16})$	256 ± 5	2.1 ± 0.1	44 ± 4

Table S9. Overview of the molecular weights (M_n) of the single polystyrene (A) and polydiene (B) blocks of tri- and pentablock copolymers with different polymer volume fractions φ_{PDiene} , related to the synthesized isoprene-, myrcene- and farnesene-based tri- and pentablock copolymers of this work.

M_n / kg/mol	ABA ($\varphi_{\text{PDiene}} = 0.5$)	ABABA ($\varphi_{\text{PDiene}} = 0.5$)	ABA ($\varphi_{\text{PDiene}} = 0.68$)
first block (A)	32.1	21.4	20.1
second block (B)	55.8	27.9	74.8
third block (A)	32.1	21.4	20.1
fourth block (B)		27.9	
fifth block (A)		21.4	

Table S10. Overview of the entanglement molecular weights (M_e) of the building blocks of the tri- and pentablock copolymers.^{15,16}

	Polyisoprene	Polymyrcene	Polyfarnesene	Polystyrene
M_e / kg/mol	5.4	18	50	13.3

7 Electrospinning

Table S11. Solution viscosity of tapered tri- and pentablock copolymers ($\varphi_{\text{PDiene}} = 0.5$ or 0.68) dissolved in THF/DMF (80/20 v/v) with different concentrations (30 and 25 wt%) and the diameters of the resulting fibers.

Sample	$c /$ wt%	$\eta /$ mPa * s	$d / \mu\text{m}$
PS _{0.25} - <i>b</i> -P(I _{0.5} - <i>co</i> -S _{0.25})	25	850	1.99 ± 0.39
PS _{0.25} - <i>b</i> -P(My _{0.5} - <i>co</i> -S _{0.25})	30	760	1.82 ± 0.50
PS _{0.25} - <i>b</i> -P(Far _{0.5} - <i>co</i> -S _{0.25})	30	420	1.88 ± 0.44
PS _{0.17} - <i>b</i> -P(I _{0.25} - <i>co</i> -S _{0.17}) ₂	25	807	1.70 ± 0.35
PS _{0.17} - <i>b</i> -P(My _{0.25} - <i>co</i> -S _{0.17}) ₂	30	555	2.33 ± 0.57
PS _{0.17} - <i>b</i> -P(Far _{0.25} - <i>co</i> -S _{0.17}) ₂	30	337	2.68 ± 0.51
PS _{0.16} - <i>b</i> -P(Far _{0.68} - <i>co</i> -S _{0.16})	35	370	1.92 ± 0.75

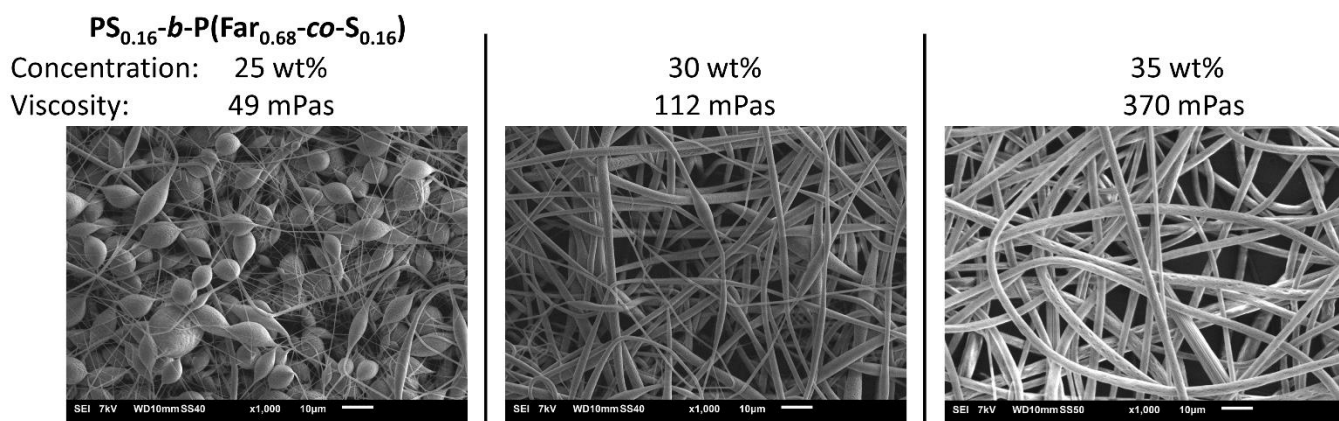


Figure S24. SEM images of electrospun PS_{0.16}-*b*-P(Far_{0.68}-*co*-S_{0.16}) tapered triblock copolymer, showing the influence of the concentration and viscosity of the polymer solution in THF/DMF (80/20 v/v) on the fiber formation: a) formation of beads mainly, b) formation of fibers with beads, c) formation of well-defined nanofibers without defects.

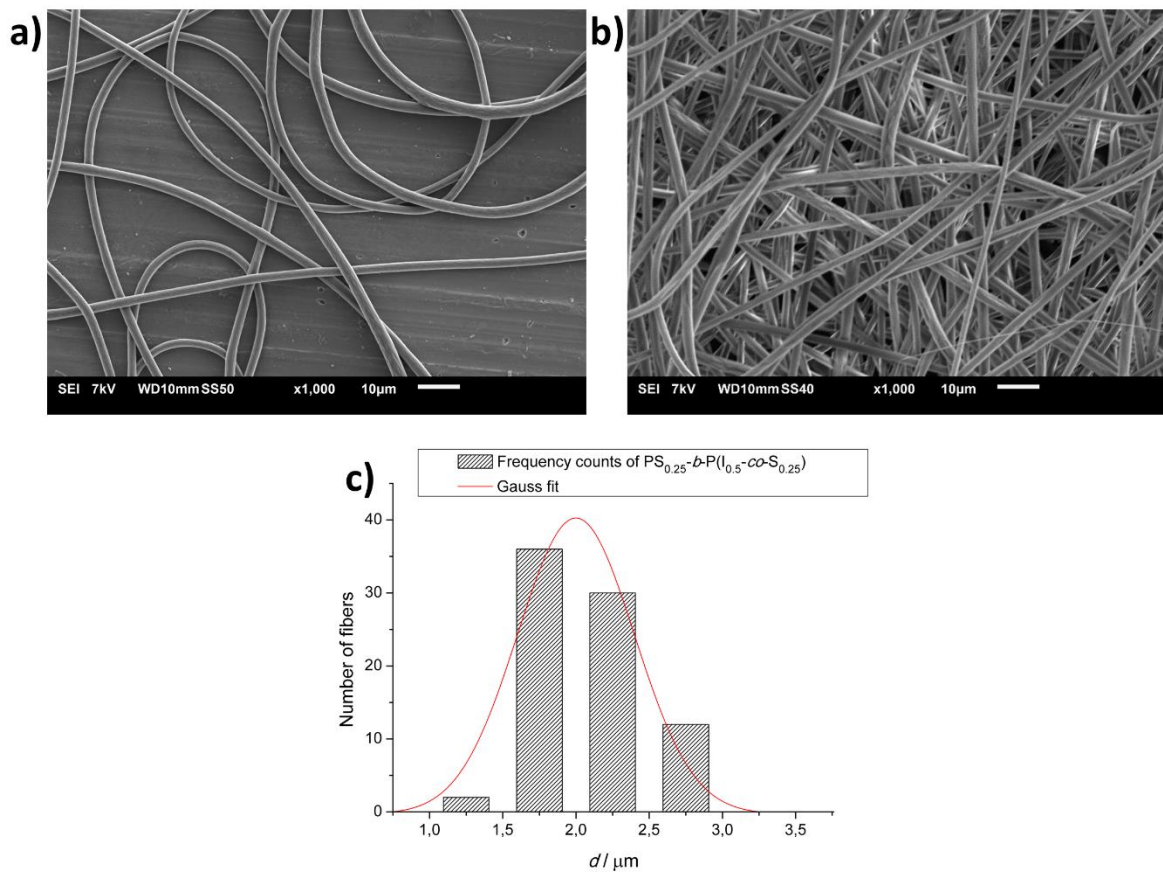


Figure S25. SEM image of electrospun $\text{PS}_{0.25}\text{-}b\text{-P}(\text{I}_{0.5}\text{-}co\text{-S}_{0.25})$ tapered triblock copolymer: a) with too high concentration/viscosity, resulting in very thick fibers (30 wt% polymer solution, $\eta = 5500 \text{ mPa s}$), b) with adequate concentration/viscosity (25 wt% polymer solution, $\eta = 850 \text{ mPa s}$), resulting in fibers with adequate diameters, c) distribution of the fiber diameters obtained by SEM imaging of b).

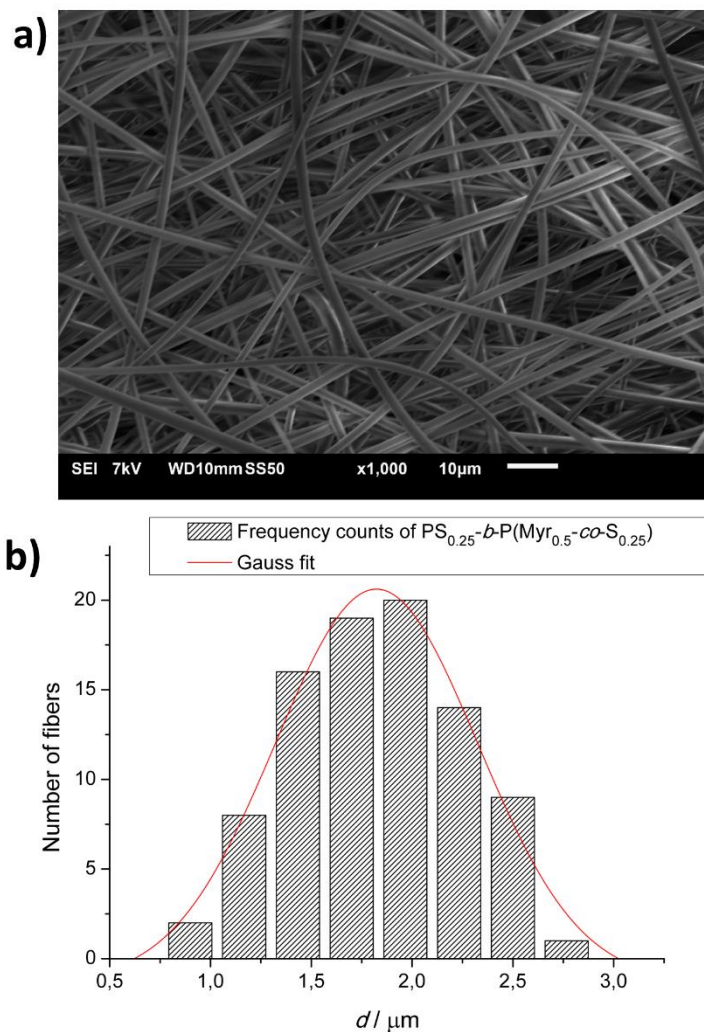


Figure S26. a) SEM image of electrospun $PS_{0.25}$ - b - $P(Myrg_{0.5}$ - co - $S_{0.25})$ tapered triblock copolymer (25 wt% polymer solution, $\eta = 760 \text{ mPa}^*\text{s}$), b) distribution of the fiber diameters.

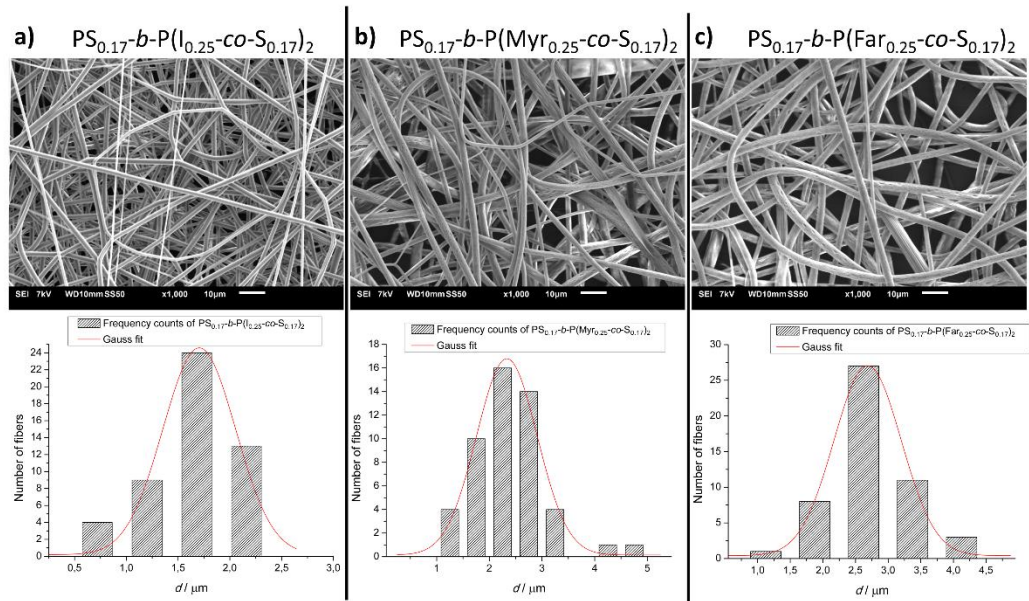


Figure S27. SEM images of electrospun pentablock copolymers (top, concentrations of Table S11 were used) and distribution of the corresponding fiber diameters (down).

8 Transformation of simulated molar composition profile to the corresponding volume composition profile

Basic definitions

In the following f always corresponds to f_1 and analogously f or F for F_1 .

$$F = \frac{d[M_1]}{d[M_2] + d[M_1]}; f = \frac{[M_1]}{[M_2] + [M_1]}; X = 1 - \frac{[M_2] + [M_1]}{[M_2]_0 + [M_1]_0} \quad (S4)$$

8.1 Derivation of the copolymer molar composition profile formula for the nonterminal/ideal model (Wall)

Wall's Ideal model in the fractional form can be transformed with the definitions of F and f in the following equation $F(f)$:¹

$$\begin{aligned} \frac{[M_1]}{[M_2]} &= r \frac{d[M_1]}{d[M_2]} \\ \Downarrow \\ F &= \frac{rf}{1-f+rf} \end{aligned} \quad (S5)$$

$F(f)$ can be solved for f to obtain an equation $f(F)$ (S6)

$$\begin{aligned} F(f) &= \frac{rf}{1-f+rf} \\ \Downarrow \\ f(F) &= \frac{F}{F+r-rF} \end{aligned} \quad (S7)$$

Substitution of $f(F)$ in the integrated ideal equation by $X(f)$ to yield an equation for the total conversion X in dependence of the instantaneous copolymer composition F .⁴

$$X(f) = 1 - \left(\frac{f}{f_0} \right)^{\frac{1}{r-1}} \left(\frac{1-f}{1-f_0} \right)^{\frac{r}{1-r}} \quad \text{substitute } f(F) = \frac{F}{F+r-rF} \quad (S8)$$

$$X(F) = 1 - \left(\frac{F}{F+r-rF} \right)^{\frac{1}{r-1}} \left(\frac{1 - \frac{F}{F+r-rF}}{1-f_0} \right)^{\frac{r}{1-r}} \quad (S9)$$

The equation $X(F)$ independent of the monomer feed f can be directly used to depict the copolymer composition profile for copolymerizations which can be described by the nonterminal model.

8.2 Derivation of the copolymer molar composition profile expression for the terminal model (Mayo-Lewis)

The derivation of the equation for the composition in case of the nonterminal model is analogous to the non-terminal model above. In the following only the intermediate results are given.

First the Mayo-Lewis equation in the fractional form is solved for f :

$$F = \frac{r_1 f^2 + f(1-f)}{r_1 f^2 + 2f(1-f) + r_2(1-f)^2} \quad (\text{S10})$$

↓ Solve for f

$$f(F) = \frac{1 + 2(r_2 - 1)F - \sqrt{(1 - 2F)^2 - 4r_1 r_2 (F - 1)F}}{2(1 - r_1 + [r_1 + r_2 - 2]F)} \quad (\text{S11})$$

This expression $f(F)$ can be substituted in the Meyer-Lowry equation.

$$X(F) = 1 - \left(\frac{f_F}{f_0} \right)^{\frac{r_2}{1-r_2}} \left(\frac{1-f_F}{1-f_0} \right)^{\frac{r_1}{1-r_1}} \left(\frac{f_F - \frac{1-r_2}{2-r_1-r_2}}{f_0 - \frac{1-r_2}{2-r_1-r_2}} \right)^{\frac{r_1 r_2 - 1}{(1-r_1)(1-r_2)}} \quad (\text{S12})$$

$$\text{where } f_F = \frac{1 + 2(r_2 - 1)F - \sqrt{(1 - 2F)^2 - 4r_1 r_2 (F - 1)F}}{2(1 - r_1 + [r_1 + r_2 - 2]F)}$$

The derived expressions enable the exact depiction of copolymer gradients with simple spreadsheet software with as little as 1000 data points. Previous methods either relied on numerical integration, which is prone to numerical errors especially in cases of extreme gradients. Another approach was to independently calculate values $X(f)$ and $F(f)$ and plotting these value pairs in a graph $X(F)$. Due to the uneven spacing of X and F , a large amount of data points was required to obtain a smooth depiction of the composition profile.

8.3 Derivation of the copolymer volume composition profile expression for the nonterminal/ideal model (Wall)

In recent work we already discussed the impact of the replacement of the mole fraction with any other fraction (e.g. volume fraction) for the nonterminal and terminal model.⁴ Based on these equation in the following we derive the expressions required to depict the volume-compositional profile.

The molar ratio is proportional to the volume ratio by the factor ν .

$$V_1 = \frac{M_1}{\rho_1}[M_1]; V_2 = \frac{M_2}{\rho_2}[M_2] \Rightarrow \frac{V_1}{V_2} = \frac{\rho_2 M_1 [M_1]}{\rho_1 M_2 [M_2]} = \frac{[M_1]}{\nu [M_2]} \quad (S13)$$

$$\frac{[M_1]}{[M_2]} = \nu \frac{V_1}{V_2} \text{ where } \nu = \frac{\rho_1 M_2}{\rho_2 M_1}$$

This equation is important to transform the molar to the fractional form of the models:

$$f = \frac{[x_1]}{[x_2] + [x_1]} \Rightarrow \frac{1}{f} = \frac{[x_2] + [x_1]}{[x_1]} = 1 + \frac{[x_2]}{[x_1]} \Rightarrow \frac{[x_2]}{[x_1]} = \frac{1}{f} - 1 = \frac{1-f}{f} \quad (S14)$$

$$\frac{[x_1]}{[x_2]} = \frac{f}{1-f}$$

In the fractional form the transformation from the molar to the volume-based equation is the following:

$$\frac{f}{1-f} = \frac{\nu f_V}{1-f_V} \Rightarrow \frac{1-f}{f} = \frac{1-f_V}{\nu f_V} = \frac{1}{f} - 1 \Rightarrow \frac{1}{f} = \frac{1-f_V + \nu f_V}{\nu f_V} \Rightarrow f = \frac{\nu f_V}{1-f_V + \nu f_V} \quad (S15)$$

In complete analogy the following equations can be obtained, which are required to transform the mole fraction to the volume fraction:

$$F = \frac{\nu F_V}{1-F_V + \nu F_V} \quad (S16)$$

$$F_V = \frac{F}{F + \nu - \nu F}; f_V = \frac{f}{f + \nu - \nu f};$$

In recent work we showed that the integrated ideal equation $X(f)$ is unchanged, when a constant factor (here ν) is introduced.⁵ $X(f)$ has the same form as $X_V(f_V)$. The same is true for $X(F)$. In $X_V(F_V)$ below, the uncommon initial volumetric feed fraction $f_{V,0}$ can be substituted by f_0 by the relation $f_V(f)$ derived above:

$$X_v(F_v) = 1 - \left(\frac{\frac{F_v}{F_v + r - rF_v}}{f_{v,0}} \right)^{\frac{1}{r-1}} \left(\frac{1 - \frac{F_v}{F_v + r - rF_v}}{1 - f_{v,0}} \right)^{\frac{r}{1-r}} ; f_{v,0} = \frac{f_0}{f_0 + \nu - \nu f_0} \quad (\text{S17})$$

$$X_v(F_v) = 1 - \left(\frac{\frac{F_v}{F_v + r - rF_v}}{\frac{f_0}{f_0 + \nu - \nu f_0}} \right)^{\frac{1}{r-1}} \left(\frac{1 - \frac{F_v}{F_v + r - rF_v}}{1 - \frac{f_0}{f_0 + \nu - \nu f_0}} \right)^{\frac{r}{1-r}} \quad \text{with } \nu = \frac{\rho_1 M_2}{\rho_2 M_1} \quad (\text{S18})$$

The equation $X_v(F_v)$ can be directly used for the depiction of the volume composition profile for copolymerizations that can be modeled with the nonterminal/ideal model.

8.4 Expression for the compositional drift of the volume fraction for the terminal model.

In contrast to the ideal model in the nonterminal model a constant factor has an influence on the form of the equations. A constant factor c results in the following equations:

$$\frac{x_1}{x_2} = c \frac{[M_1]}{[M_2]}; \quad (S19)$$

$$X_x(f_x) = 1 - \left(\frac{f_x}{f_{x,0}} \right)^{\frac{r_2}{1-r_2}} \cdot \left(\frac{1-f_x}{1-f_{x,0}} \right)^{\frac{r_1}{1-r_1}} \cdot \left(\frac{f_x - \frac{c(1-r_2)}{c(1-r_2)+1-r_1}}{f_{x,0} - \frac{c(1-r_2)}{c(1-r_2)+1-r_1}} \right)^{\frac{(1-r_1r_2)}{(1-r_1)(1-r_2)}} \quad (S20)$$

$$F_x = \frac{r_1 f_x^2 + c f_x (1-f_x)}{r_1 f_x^2 + (c+1) f_x (1-f_x) + r_2 c (1-f_x)^2} \quad (S21)$$

In the case of the volume fraction, $c = \frac{1}{\nu}$. Therefore $X_V(f_V)$ takes the following form:

$$X_V(f_V) = 1 - \left(\frac{f_V}{f_{V,0}} \right)^{\frac{r_2}{1-r_2}} \cdot \left(\frac{1-f_V}{1-f_{V,0}} \right)^{\frac{r_1}{1-r_1}} \cdot \left(\frac{f_V - \frac{1-r_2}{1-r_2+\nu(1-r_1)}}{f_{V,0} - \frac{1-r_2}{1-r_2+\nu(1-r_1)}} \right)^{\frac{r_1 r_2 - 1}{(1-r_1)(1-r_2)}} \quad (S22)$$

To eliminate f_V from this equation, $F_V(f_V)$ is solved for f_V :

$$F_V = \frac{r_1 f_V^2 + c f_V (1-f_V)}{r_1 f_V^2 + (c+1) f_V (1-f_V) + r_2 c (1-f_V)^2}$$

⇓ substitute $c = \frac{1}{\nu}$

$$F_V = \frac{\nu r_1 f_V^2 + f_V (1-f_V)}{\nu r_1 f_V^2 + (1+\nu) f_V (1-f_V) + r_2 (1-f_V)^2} \quad (S23)$$

⇓ Solve for f

$$f_V = \frac{1 + (2r_2 - \nu - 1)F_V - \sqrt{(1 - (1+\nu)F_V)^2 - 4\nu r_1 r_2 (F_V - 1)F_V}}{2(1 - \nu r + [\nu r_1 + r_2 - 1 - \nu_1]F_V)}$$

In this equation again $f_V, 0$ can be substituted by f_0 (equation above), and the variable $f_{V,F}$ is substituted by F_V

$$X_V(F_V) = 1 - \left(\frac{f_{V,F}}{f_0} \right)^{\frac{r_2}{1-r_2}} \cdot \left(\frac{1-f_{V,F}}{1-f_0} \right)^{\frac{r_1}{1-r_1}} \cdot \left(\frac{f_{V,F} - \frac{1-r_2}{1-r_2+\nu(1-r_1)}}{f_0 - \frac{1-r_2}{1-r_2+\nu(1-r_1)}} \right)^{\frac{r_1 r_2 - 1}{(1-r_1)(1-r_2)}} \quad (\text{S24})$$

$$\text{where } \nu = \frac{\rho_1 M_2}{\rho_2 M_1} \text{ and } f_{V,F} = \frac{1 + (2r_2 - \nu - 1)F_V - \sqrt{(1 - (1 + \nu)F_V)^2 - 4\nu r_1 r_2 (F_V - 1)F_V}}{2(1 - \nu r_1 + [\nu r_1 + r_2 - 1 - \nu]F_V)}$$

The equation $X_V(F_V)$ can be directly used for the depiction of the volume composition profile for copolymerization which are modeled with the terminal model.

8.5 Transformation of total conversion to chain position of the composition profile

Under the conditions of the living anionic polymerization, the total conversion X is a linear function of the degree of polymerization (P_n), with the constant factor of the initiator concentration $[I]_0$ and total initial monomer concentration $[M]_0$.^{17,18} In this case the total conversion X can be interchanged with the normalized chain length, as shown in eq S26. This allows to transform the conversion-based composition profile to the chain position-based composition profile.

$$P_n = \frac{[M]_0 - [M]}{[I]_0} \quad (\text{S25})$$

$$X = \frac{[M]_0 - [M]}{[M]_0} = \frac{[I]_0}{[M]_0} P_n$$

References

- (1) Wall, F. T. The Structure of Vinyl Copolymers. *J. Am. Chem. Soc.* **1941**, *63*, 1862–1866.
- (2) Mayo, F. R.; Lewis, F. M. Copolymerization. I. A Basis for Comparing the Behavior of Monomers in Copolymerization; The Copolymerization of Styrene and Methyl Methacrylate. *J. Am. Chem. Soc.* **1944**, *66*, 1594–1601.
- (3) Jaacks, V. *Makromol. Chem.* **1972**, *161*, 161–172.
- (4) Blankenburg, J.; Kersten, E.; Maciol, K.; Wagner, M.; Zorbakhsh, S.; Frey, H. The poly(propylene oxide- co -ethylene oxide) gradient is controlled by the polymerization method: determination of reactivity ratios by direct comparison of different copolymerization models. *Polym. Chem.* **2019**, *10*, 2863–2871.
- (5) Meyer, V. E.; Lowry, G. G. Integral and differential binary copolymerization equations. *J. Polym. Sci. A Gen. Pap.* **1965**, *3*, 2843–2851.

- (6) R. Hoffmann, V. I. Minkin, B. K. Carpenter. Ockham's razor and chemistry. *Bull. Soc. Chim. Fr.*, 1996, 117–130.
- (7) Hawkins, D. M. The problem of overfitting. *J. Chem. Inf. Comput. Sci.* **2004**, *44*, 1–12.
- (8) Steube, M.; Johann, T.; Hübner, H.; Koch, M.; Dinh, T.; Gallei, M.; Floudas, G.; Frey, H.; Müller, A. H. E. Tetrahydrofuran: More than a “Randomizer” in the Living Anionic Copolymerization of Styrene and Isoprene: Kinetics, Microstructures, Morphologies, and Mechanical Properties. *Macromolecules* **2019**, *52*, 9299–9310.
- (9) Worsfold, D. J.; Bywater, S. Anionic Polymerization of Isoprene. *Can. J. Chem.* **1964**, *42*, 2884–2892.
- (10) Worsfold, D. J.; Bywater, S. Degree of Association of Polystyryl-, Polyisoprenyl-, and Polybutadienyllithium in Hydrocarbon Solvents. *Macromolecules* **1972**, *5*, 393–397.
- (11) Steube, M.; Johann, T.; Plank, M.; Tjaberings, S.; Gröschel, A. H.; Gallei, M.; Frey, H.; Müller, A. H. E. Kinetics of Anionic Living Copolymerization of Isoprene and Styrene Using in Situ NIR Spectroscopy: Temperature Effects on Monomer Sequence and Morphology. *Macromolecules* **2019**, *52*, 9299–9310.
- (12) Tiedemann, P. von; Blankenburg, J.; Maciol, K.; Johann, T.; Müller, A. H. E.; Frey, H. Copolymerization of Isoprene with p -Alkylstyrene Monomers: Disparate Reactivity Ratios and the Shape of the Gradient. *Macromolecules* **2019**, *52*, 796–806.
- (13) Grune, E.; Johann, T.; Appold, M.; Wahlen, C.; Blankenburg, J.; Leibig, D.; Müller, A. H. E.; Gallei, M.; Frey, H. One-Step Block Copolymer Synthesis versus Sequential Monomer Addition: A Fundamental Study Reveals That One Methyl Group Makes a Difference. *Macromolecules* **2018**, *51*, 3527–3537.
- (14) Steube, M.; Johann, T.; Galanos, E.; Appold, M.; Rüttiger, C.; Mezger, M.; Gallei, M.; Müller, A. H. E.; Floudas, G.; Frey, H. Isoprene/Styrene Tapered Multiblock Copolymers with up to Ten Blocks: Synthesis, Phase Behavior, Order, and Mechanical Properties. *Macromolecules* **2018**, *51*, 10246–10258.
- (15) Iacob, C.; Yoo, T.; Runt, J. Molecular Dynamics of Polyfarnesene. *Macromolecules* **2018**, *51*, 4917–4922.
- (16) Fetters, L. J.; Lohse, D. J.; Richter, D.; Witten, T. A.; Zirkel, A. Connection between Polymer Molecular Weight, Density, Chain Dimensions, and Melt Viscoelastic Properties. *Macromolecules* **1994**, *27*, 4639–4647.
- (17) Waack, R.; Rembaum, A.; Coombes, J. D.; Szwarc, M. Molecular Weights of “Living” Polymers. *J. Am. Chem. Soc.* **1957**, *79*, 2026–2027.
- (18) Webster, O. W. Living polymerization methods. *Science* **1991**, *251*, 887–893.

CHAPTER 5

Tapered Multiblock Copolymers of Isoprene and 4 Methylstyrene

CHAPTER 5

Tapered Multiblock Copolymers Based on Isoprene and 4-Methylstyrene: Influence of the Tapered Interface on the Self-Assembly and Thermomechanical Properties

Eftyxis Galanos,^a Eduard Grune,^{b,c} Christian Wahlen,^b Axel H.E. Müller,^b Michael Appold,^d Markus Gallei,^d Holger Frey,^{*,b} George Floudas^{*,c}

^a Department of Physics, University of Ioannina, P.O. Box 1186, 45110 Ioannina, Greece

^b Department of Chemistry, Johannes Gutenberg University, Duesbergweg 10-14, 55128 Mainz, Germany

^c Graduate School Materials Science in Mainz, Staudinger Weg 9, 55128 Mainz, Germany

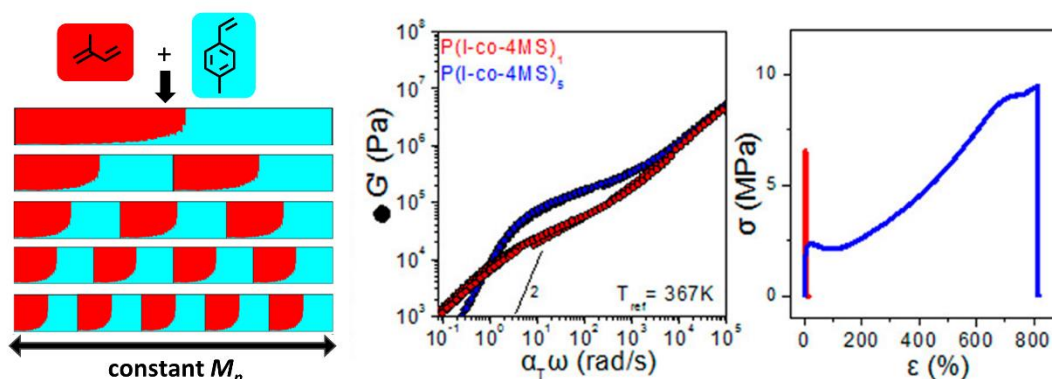
^d Macromolecular Chemistry Department, Technische Universität Darmstadt, Alarich-Weiss Str. 4, 64287 Darmstadt, Germany

^e Max Planck Institute for Polymer Research, D-55125 Mainz, Germany

E.Ga, E.Gr, C.W contributed equally.

Published in *Macromolecules* **2019**, 52 (4), 1577-1588.

DOI: 10.1021/acs.macromol.8b02669



Abstract

The synthesis of tapered multiblock copolymers by statistical living anionic copolymerization of a mixture of isoprene (I) and 4-methylstyrene (4MS) in cyclohexane is based on vastly different reactivity ratios of I and 4MS ($r_I = 25.4$ and $r_{4MS} = 0.007$). A library of tapered multiblock copolymers was prepared with different molecular weights (approximate molecular weights of 80 kg/mol, 240 kg/mol and 400 kg/mol) and number of blocks ($P(I-co-4MS)_n$ with $1 \leq n \leq 5$) and their thermomechanical properties were investigated by differential scanning calorimetry, rheology and tensile testing in relation to their nanodomain structure, the latter investigated by small-angle X-ray scattering. The interaction parameter between I and 4MS segments was obtained based on the order-to-disorder transition temperatures of a series of PI-*b*-P4MS diblock copolymers prepared by sequential addition of monomers. The obtained $\chi(T)$ dependencies ($\chi_{MFT} = 23.2/T - 0.024$ and $\chi_{FH} = 36.0/T - 0.041$) are weaker than in the corresponding PI-*b*-PS system, revealing that the different reactivity ratios of the monomers is not the sole factor that controls the miscibility of the tapered multiblock copolymers. The latter is controlled by the value of the interaction parameter, the width of the tapered interfaces as well as by the number of blocks and total molecular weight. Tapered multiblock copolymers undergo a fluctuation-induced first order transition from the ordered to the disordered state. The domain spacing scales as $d \sim n^{-0.83 \pm 0.02}$ when compared under a fixed total molecular weight reflecting the conformational properties of the middle blocks. In addition, domain spacing depends on molecular weight, as $d \sim N^{0.55}$, revealing stretching of chains and non-ideal configurations. These structural features of the tapered multiblock copolymer affected their mechanical properties. Tensile tests showed a dramatic enhancement of the strain at break with a concomitant increase in toughness. These mechanical properties can be fine-tuned by the judicious selection of molecular weight and number of blocks. The state of order (ordered, weakly ordered vs. disordered) and proximity to the glass temperature of the hard phase are additional parameters that affect the mechanical response. The improved mechanical properties reflect the enhanced interfacial strength the latter provided by the configurations of the middle blocks in the copolymers. The influence of methyl group substitution in the para position of styrene is discussed by comparing the self-assembly and thermomechanical properties of the current $P(I-co-4MS)_n$ with the $P(I-co-PS)_n$ system. We found that the shorter tapered interface in the former is

counterbalanced by its lower effective interaction parameter resulting to similar domain spacings.

Introduction

Applications of thermoplastic elastomers rely on anchoring of a rubbery center block between glassy end blocks.¹ Well-known examples are triblock copolymers based on poly(styrene-*b*-butadiene-*b*-styrene) (SBS) and poly(styrene-*b*-isoprene-*b*-styrene) (SIS) with respective trade names Kraton and Dexco.^{2,3} Other thermoplastic elastomers are based on more stiff resins and have a lower rubber content (the commercial product Styrolux is composed of SBS with a rubber content of 26 %) having a star polymer structure. Application of such copolymers (e.g. in molding, melt extrusion and film blowing) requires lowering the order-to-disorder transition temperature, T_{ODT} , while maintaining an ordered state at ambient temperature as to provide the desired mechanical properties. The multiblock copolymer strategy offers a versatile approach to obtaining useful and tunable physical properties.⁴⁻¹⁷ Increasing the number of blocks affects the chain configurations; a single chain in a multiblock copolymer can couple, (*i.e.*, “bridge”) over a number of glassy and rubbery domains, thus increasing the “bridging effect” that effectively controls the mechanical properties. The desired systems should be based on multiblock copolymers that are nanophase separated at ambient temperature and with an accessible T_{ODT} , located preferably in the vicinity of the glass temperature of the “hard” phase. Although controlling the T_{ODT} in multiblock copolymers by adjusting the number of blocks is still feasible, multiblock copolymers possessing a tapered interface provide additional degrees of freedom.¹⁸⁻²⁸ The latter exert control over the segregation strength (χN , where χ is the interaction parameter and N is the total degree of polymerization) by varying the mixing of unlike segments at the interface. Interfacial mixing gives rise to an effective interaction parameter, χ^{eff} , that is lower as compared to the bare χ .

Earlier important experimental studies have shown that controlled tapering allows access to higher molecular weight materials that reside in the weak-segregation limit.^{18-24,28} Block sequencing was also found to be an important factor controlling compatibility.^{19,20} Computer simulations²⁹ have also shown that T_{ODT} can be controlled by changing the composition gradient without any change in the nanodomain morphology. Most of the experimental studies were based on P(I-*co*-S) tapered tri- or multiblock copolymers with a taper generated by monomer addition protocols.^{18-23,28} There is a need to expand the published tapered multiblock copolymers with systems possessing varying interaction

parameters, interfacial widths, number of blocks and block lengths. Effectively, comparisons should be made (i) at a fixed total molecular weight and (ii) at a fixed block length, by varying the number of blocks.

Recently, the one-step synthesis of tapered block copolymers by statistical living anionic copolymerization of a mixture of isoprene (I) and 4-methylstyrene (4MS) in nonpolar media was reported.²⁵ The statistical copolymerization leads to tapered block copolymers because of the extremely slow crossover reaction from isoprene to the styrenic monomer. For the system I/4MS the reactivity ratios were highly disparate with values $r_I = 25.4$ and $r_{4MS} = 0.007$, resulting in a steep gradient of the comonomer composition. These synthetic efforts revealed the dual effect of a methyl group substitution in the *para* position of styrene: first, in controlling the reactivity ratios in nonpolar media and, secondly, in lowering the dispersity of the I/4MS copolymers in comparison to the I/S copolymers.²⁸ This strategy for block copolymer synthesis that avoids break-seal techniques, resulted in a series of tapered block copolymers from low to ultrahigh molecular weight (molecular weights exceeding 10^6 g/mol).^{25,26}

Herein, we are exploring the effect of the tapered interface in I/4MS multiblock copolymers of the $P(I-co-4MS)_n$ type (with $1 \leq n \leq 5$) on the thermomechanical properties by differential scanning calorimetry, rheology and tensile testing in relation to their nanodomain structure, the latter investigated by small-angle X-ray scattering. Three series of tapered multiblock copolymers with approximate molecular weights of 80 kg/mol, 240 kg/mol and 400 kg/mol were prepared. Addressing issues related to the phase state and the mechanical properties requires knowledge of the interaction parameter between I and 4MS segments. For this purpose, a series of diblock copolymers PI-*b*-P4MS was prepared by the sequential addition of monomers as well. The obtained $\chi(T)$ was extracted from the PI-*b*-P4MS copolymers and compared to the PI-*b*-PS case. It was shown that $\chi(T)$ has a weaker dependence than in the corresponding PI-*b*-PS copolymers revealing that miscibility of the tapered multiblock copolymers is controlled by the value of the interaction parameter, the difference in reactivities of the two monomers as well as by the number of blocks and total molecular weight. Tapered multiblock copolymers were shown to undergo a fluctuation-induced first-order transition from the ordered to the disordered state. Tensile tests showed a dramatic enhancement of the strain at break with a concomitant increase in toughness. The role of the configurations of the middle block on the improved mechanical properties is discussed.

Experimental Section

Synthesis. The synthesis of the P(I-co-4MS) copolymers was reported in a previous work.²⁵ However, in this work a systematic variation of chain architectures was achieved, keeping total molecular weights constant. Three series of copolymers with molecular weights of 80 kg/mol, 240 kg/mol and 400 kg/mol have been prepared, changing the number of segments in the range of 2-10. Herein we provide only a short description of the synthesis scheme (Figure 1). The I/4MS monomer mixture was dried over CaH₂ and trioctylaluminum. Cyclohexane was dried using a living polystyrene solution. All monomers and solvents were degassed by three freeze-thaw cycles prior to use. The monomer mixture was distilled into a graduated ampule equipped with a teflon stop cock. Cyclohexane was distilled directly into the all-glass reactor under reduced pressure. For the preparation of a tapered multiblock copolymer, a specific amount of the monomer mixture was added to the cyclohexane and initiated by *sec*-Butyllithium via syringe. All polymerizations were carried out at 30 °C and argon atmosphere. Depending on the block sizes, the next load of monomers was added after 12, 24 or 36 hours, the color change from the colorless polyisoprenyllithium to the dark orange poly(4-methylstyryl)lithium marked the successful crossover from the polyisoprene to the poly(4-methylstyrene) block segment. Due to the highly disparate reactivity ratios of isoprene and 4-methylstyrene ($r_I = 25.4$; $r_{4MS} = 0.007$) incorporation of isoprene is highly favored, yielding a block-like tapered copolymer subunit (AB) in one step. The monomer mixture addition was repeated until the desired number of blocks was achieved. The polymerization was terminated by degassed isopropyl alcohol and the polymer solution was precipitated into an eight-fold excess of isopropyl alcohol. Sample characterization via ¹H NMR and SEC are shown in Supporting Information section (Figure S1 and Figure S2, respectively).

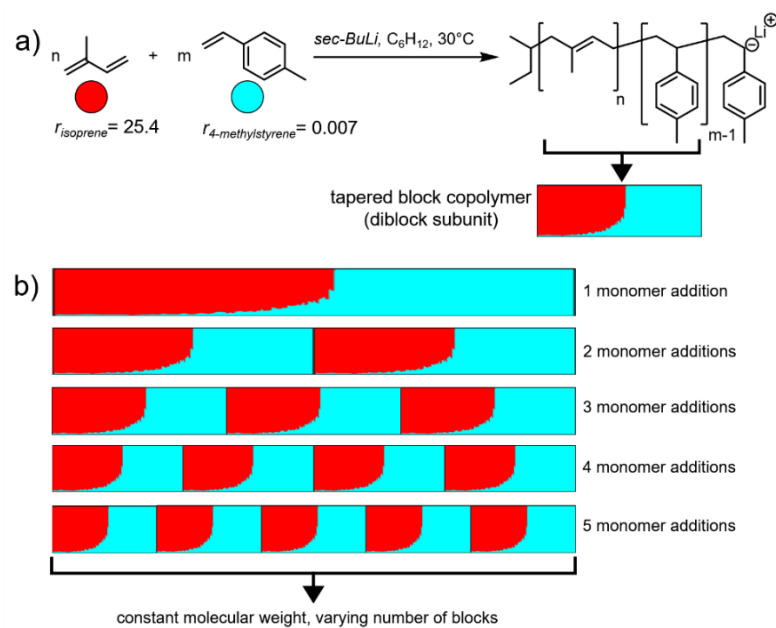


Figure 1. a) One-step tapered block copolymer formation; b) composition profile of multiblock copolymers with constant molecular weight and varied block number.

Table 1. Molecular characteristics of the tapered multiblock copolymers P(I-*co*-4MS) and of the sequential PI-*b*-P4MS (*i.e.* “normal”) and P4MS-*b*-PI (*i.e.* “inverse”) diblock copolymers.

Entry	Sample	number of blocks	M_n^{theo} (kg/mol)	M_n^a (kg/mol)	\bar{D}^a	Isoprene content ^{theo} (mol%)
1	80K 2B	2		94.7	1.06	50
2	80K 4B	4		82.4	1.12	50
3	80K 6B	6	80	81.1	1.10	50
4	80K 8B	8		78.7	1.15	50
5	80K 10B	10		77.5	1.18	50
6	240K 2B	2		237.8	1.11	50
7	240K 4B	4		227.2	1.11	50
8	240K 6B	6	240	308.1	1.26	50
9	240K 8B	8		253.1	1.24	50
10	240K 10B	10		232.2	1.17	50
11	400K 2B	2		481.2	1.09	50
12	400K 4B	4		313.4	1.05	50
13	400K 6B	6	400	356.3	1.11	50
14	400K 8B	8		431.7	1.22	50
15	400K 10B	10		423.9	1.23	50
16	30K P(I- <i>b</i> -4MS)	2	30	38.3	1.15	50
17	30K P(4MS- <i>b</i> -I)	2		37.7	1.17	50
18	35K P(I- <i>b</i> -4MS)	2	35	41.8	1.15	50
19	35K P(4MS- <i>b</i> -I)	2		40.3	1.16	50
20	40K P(I- <i>b</i> -4MS)	2	40	45.6	1.17	50
21	40K P(4MS- <i>b</i> -I)	2		46.4	1.18	50

^a Determined by SEC at 25°C in THF

Differential Scanning Calorimetry. The thermal properties of the tapered multiblock copolymers were studied with a Q2000 (TA Instruments) differential scanning calorimeter (DSC). The instrument was calibrated for best performance on the specific temperature range and heating/cooling rate. The calibration sequence included a baseline calibration for the determination of the time constants and capacitances of the sample and reference sensor using a sapphire standard, an enthalpy and temperature calibration for the correction of thermal resistance using indium as standard ($\Delta H = 28.71$ J/g, $T_m = 428.8$ K), and a heat capacity calibration with sapphire standard. Two cooling and

heating cycles were performed at a rate of 10 K/min in a temperature range between 173 K and 433 K and the glass temperatures corresponding to PI and P4MS were extracted from the second cycle.

Transmission Electron Microscopy (TEM). TEM experiments were carried out on a Zeiss EM 10 electron microscope operating at 60 kV. All shown images were recorded with a slow-scan CCD camera obtained from TRS (Tröndle) in bright field mode. The camera control was computer-aided using the ImageSP software from TRS.

X-Ray Scattering. Small-angle (SAXS) measurements were made using $\text{CuK}\alpha$ radiation (RigakuMicroMax 007 x-ray generator, Osmic Confocal Max-Flux curved multilayer optics). 2D diffraction patterns were recorded on an Mar345 image plate detector at a sample-detector distance of 2060 mm. Intensity distributions as a function of the modulus of the total scattering vector, $q = (4\pi/\lambda) \sin(2\theta/2)$, where 2θ is the scattering angle, were obtained by radial averaging of the 2D datasets. Samples in the form of thick films (~1 mm) were prepared by slow solvent casting (chloroform). Temperature-dependent measurements of 1 hour long were made by heating the films from 298 K to 473 K in 5 K steps aiming at obtaining the structure factor and further identifying the corresponding order-to-disorder transition temperatures.

Rheology. A TA Instruments, AR-G2, with a magnetic bearing that allows for nanotorque control was used for recording the viscoelastic properties of the polymer electrolytes. Measurements were made with the environmental test chamber (ETC) as a function of temperature. Samples were prepared on the lower rheometer plate (8 mm and 25 mm), the upper plate was brought into contact, and the gap thickness was adjusted. The linear and nonlinear viscoelastic regions were determined by the strain amplitude dependence of the complex shear modulus $|G^*|$ at $\omega = 10$ rad/s. Evidently, tapered multiblock copolymers orient easily by the application of strain. A low strain amplitude (typically below 1.5 %) was used to avoid non-linearities in the multiblock copolymers. Subsequent measurements involved (i) isothermal frequency scans within the range $10^{-1} < \omega < 10^2$ rad/s at several temperatures and (ii) isochronal temperature ramps with $\omega = 1$ rad/s between 298 K and 473 K.

Results and Discussion

Thermodynamics. It is known that DSC alone cannot account for thermodynamic miscibility/immiscibility in multicomponent polymer systems as even miscible blends/copolymers exhibit dual glass temperatures.^{30,31} Nevertheless, based on (i) the shift of the respective temperatures relative to the homopolymers and (ii) the broadening of the heat capacity curves at the respective T_g 's, some conclusions can be drawn on the purity of phases at the probed length scale. In accordance with the expectation, DSC curves of multiblock copolymers revealed two glass temperatures, independent of the phase state of the copolymers (ordered or disordered). This is depicted in Figure 2, where the first derivative of the heat flow obtained during the second heating runs are shown. The lower and higher peaks in this representation correspond to the PI and P4MS glass temperatures, respectively. Although the lower T_g – albeit broad – is always evident, the high T_g is less pronounced especially in the tapered multiblock (tetra-, hexa-, octa- and deca-block) copolymers. In the tapered copolymers with the lower molecular weight ($M_w \sim 80$ kg/mol) the two peaks approach each other especially in the octablock and decablock cases meaning that segmental mobilities are in proximity. In addition to the high and low glass temperatures another very broad peak around 303 K is evident for the 240 kg/mol and 400 kg/mol copolymers. This feature can be interpreted as an “interphase T_g ” of those segments that are intimately mixed within the I/4MS interface.

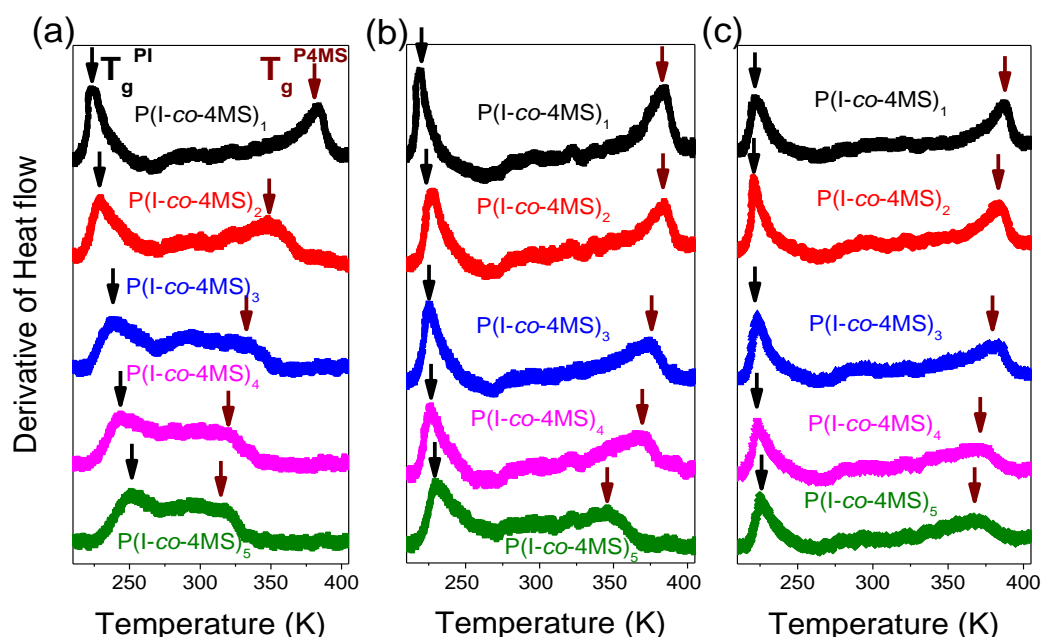


Figure 2. Derivative of heat flow obtained during the second heating runs of the P(I-co-4MS) tapered multiblock copolymers with overall molecular weights of 80 kg/mol (a), 240 kg/mol (b) and 400 kg/mol (c) with a rate of 10 K/min. Vertical arrows in black and orange colors indicate the PI and P4MS glass temperatures, respectively.

The results from the DSC investigation with respect to the PI and P4MS glass temperatures are summarized in Figure 3. The Figure shows dual glass temperatures in all copolymers with a temperature separation that decreases with the number of blocks and with decreasing total molecular weight. In addition, the PI T_g is higher than for a homopolymer PI ($T_g = -65$ °C) as a result of the incorporation of 4-methylstyrene segments within the PI chain. These findings for the dual T_g and for an intermediate T_g in the P(I-co-4MS) tapered multiblock copolymers bear certain similarities to the P(I-co-S) case.²⁸ The main difference between the P(I-co-4MS) and P(I-co-S) case is the location of the low (PI “phase”) glass temperature being approximately 15 K lower in the former system. This finding for the segmental mobility is in line with the vastly different reactivity ratios for isoprene, styrene and 4-methylstyrene resulting to a shorter tapered interface in the P(I-co-4MS) case.

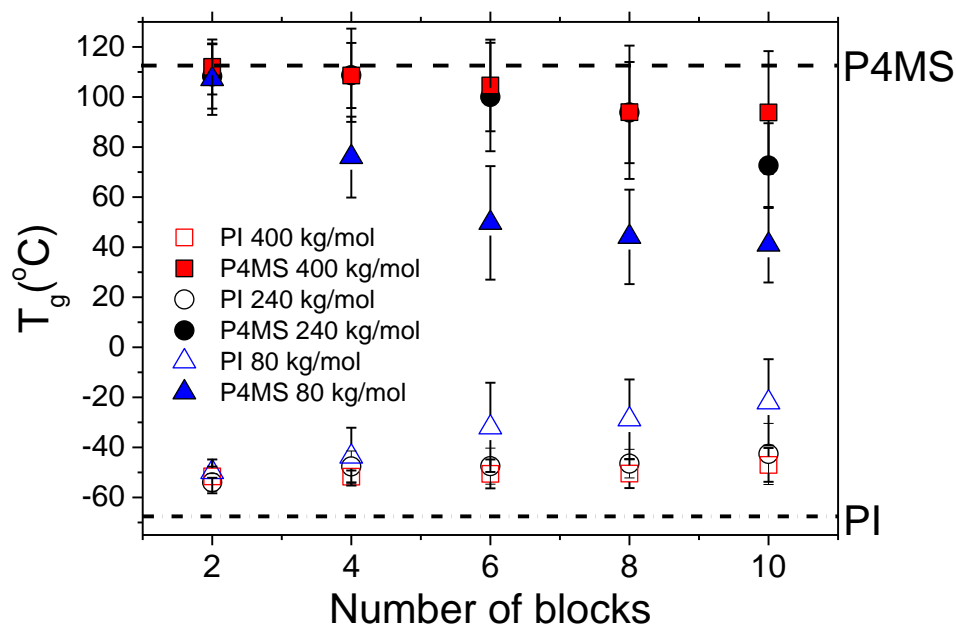


Figure 3. Glass temperatures in the tapered multiblock copolymers corresponding to P4MS (filled symbols) and PI (open symbols). Vertical bars indicate the temperature range of the respective glass temperatures (taken as the full width at half maximum). Dashed and dash-dotted lines give the glass temperature of P4MS and PI homopolymers, respectively.

Self-assembly. The phase state of the multiblock copolymers is controlled by (i) the interaction parameter between isoprene and 4-methyl styrene, (ii) the length of the tapered interface, (iii) the total molecular weight, and (iv) the number of blocks. The disparate reactivity ratios of I and 4MS ($r_1 = 25.4$, $r_{4MS} = 0.007$) is expected to lead to a short tapered midblock. To this end, the I/4MS system shows a better controlled monomer distribution composition and a shorter tapered structure in comparison to the known I/S copolymer ($r_1 = 11.0$, $r_{4MS} = 0.053$).^{25,28} The effect of methyl group substitution on the reactivity ratios in non-polar media is very strong. However, whether this effect will be the dominant factor controlling the phase state of the multiblock copolymers of P(I-co-4MS) and P(I-co-S) requires additional knowledge of the interaction parameter in the respective sequential copolymers (PI-*b*-P4MS and PI-*b*-PS).

Sequential and symmetric diblock copolymers, according to the mean-field theory (MFT),³² undergo a second order phase transition from the disordered to the lamellar phase by lowering temperature at the critical point ($\chi N = 10.495$, $f = 1/2$). The MFT structure factor in the disordered phase is predicted,³²

$$\frac{N}{S(q)} = F(x, f) - 2\chi N \quad (1)$$

where $F(x, f)$ is a combination of Debye functions and $x = q^2 R_g^2$; q , is the modulus of the scattering vector. However, the MFT predictions for the structure factor apply only at temperatures much above the order-to-disorder transition temperature, T_{ODT} . On approaching the T_{ODT} from higher temperatures, fluctuation corrections become important.^{30,31} This becomes evident as within MFT, $1/S(q)$, is proportional to $1/T$ in the disordered phase (in the simplest approximation χ is inversely proportional to T). However, at $T > T_{ODT}$ there exists a pronounced curvature which cannot be accounted by the MFT. Furthermore, the peak intensity at the transition remains finite and $S(q^*)$ is discontinuous at the transition. Subsequently, Fredrickson and Helfand³³ demonstrated that with the introduction of fluctuation corrections, the critical point is suppressed and is replaced by a weakly first order transition ($f = 0.6$) at

$$(\chi N)_{ODT} = 11.2 + \frac{46.1}{\bar{N}^{1/3}} \quad (2)$$

Fluctuation corrections apply to both the disordered and ordered phases in the vicinity of the transition. In the disordered phase the structure factor is³³

$$\frac{N}{S(q)} = F(x, f) - 2\chi N + \frac{c^3 d \lambda}{\bar{N}^{1/2}} \frac{\sqrt{S(q^*)}}{\sqrt{N}} \quad (3)$$

In eq. 3, $d = 3x^*/2\pi$ and c, λ are composition dependent coefficients, where $\bar{N} = N\alpha^6/u^2$, and α, u are the statistical segment length and volume, respectively (in the present case of $f = 0.6$; $c = 1.126$, $\lambda = 132$, and $d = 1.835$).³³ Thus, approaching the T_{ODT} from high temperatures the predicted intensities are lower than the ones expected from Leibler's theory and give rise to a non-linear dependence of $1/S(q)$ on $1/T$ which is in qualitative agreement with the non-linear dependence obtained experimentally (see below).

Herein we determine the interaction parameter, χ_{I-4MS} , based on the T_{ODT} values of three P(I-*b*-4MS) copolymers prepared by sequential addition. For this purpose, we employ rheology that is a sensitive probe of the order-to-disorder transition temperature.³⁴⁻⁴⁰ Figure 4 gives the storage moduli in three diblock copolymers under isochronal conditions ($\omega = 1$ rad/s). The fluctuation induced first order transition is evident by the drop in the shear storage modulus $G'(T)$ at the T_{ODT} . By forcing the MFT and FH predictions (Eqs. (1) and (2)) to the T_{ODT} we obtain (Figure 4) $\chi_{MFT} = 23.2/T - 0.024$ and $\chi_{FH} = 36.0/T - 0.041$; $\chi(300 \text{ K}) = 0.08$, respectively, for the interaction parameters in the

mean-field³² and fluctuation approach.³³ These dependencies are weaker than in the poly(isoprene-*b*-styrene) copolymers⁴¹ ($\chi_{\text{FH}} = 71.4/T - 0.0857$; $\chi(300 \text{ K}) = 0.15$) revealing that a methyl group in the former system is responsible for the change in polarizability and the alleviated immiscibility relative to PI-*b*-PS. In addition, block copolymers prepared by the reverse sequential addition of monomer, *i.e.*, reverse block copolymers (P4MS-*b*-PI), display small changes at the order-to-disorder transition temperatures relative to the respective normal copolymers (Figure S3, Supporting Information).

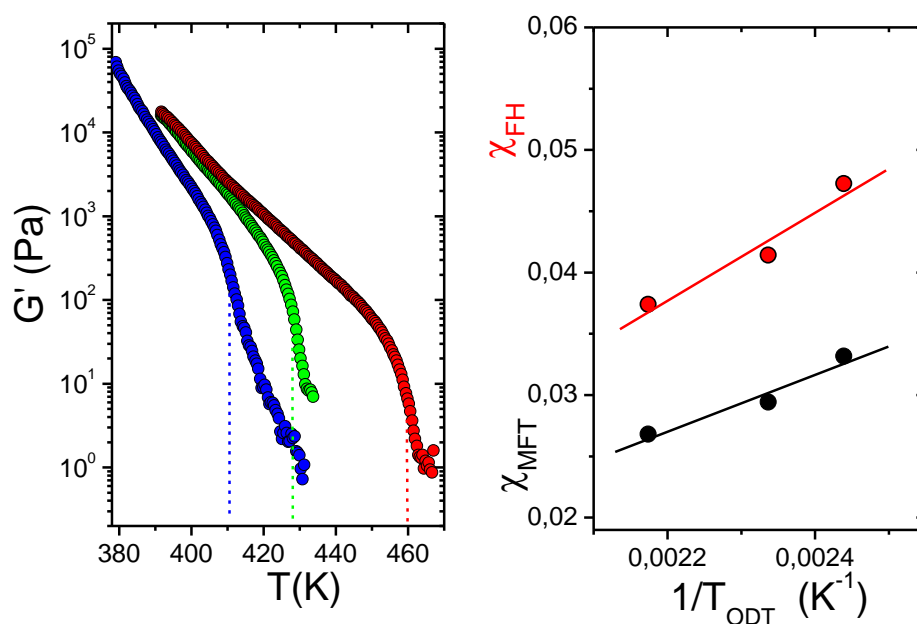


Figure 4. (Left) Temperature dependence of the storage modulus, G' , obtained at a frequency of $\omega = 1$ rad/s with a low strain amplitude on heating the sequential diblock copolymers PI-*b*-P4MS with $M_n = 30600$ g/mol (blue), 34800 g/mol (green) and 37950 g/mol (red). Vertical lines indicate the T_{ODT} 's. (Right) Temperature dependence of the interaction parameter within the MFT (black symbols) and the FH (red symbols) approach.

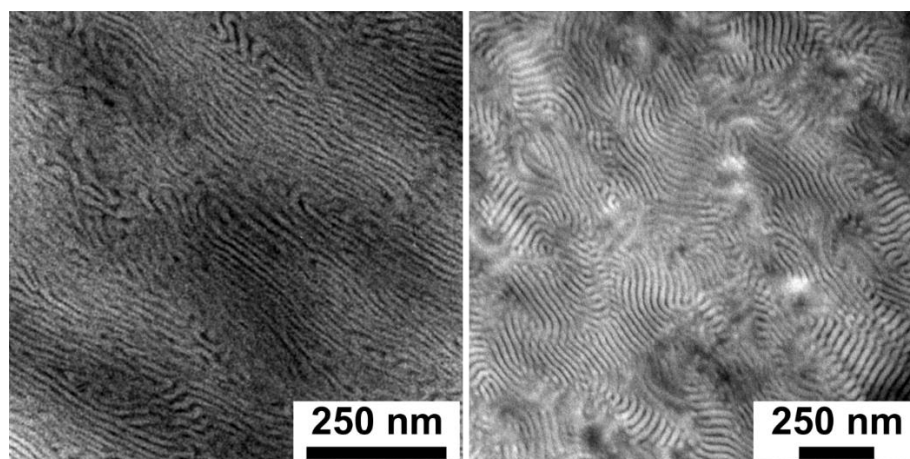


Figure 5. TEM images of 240K4B (left) and 400K4B (right).

The morphology of the tapered multiblock copolymers can be discussed based on the TEM results. The TEM images of Figure 5 depict well defined lamellar morphologies for the tetrablock copolymers with molecular weights of 240 kg/mol and 400 kg/mol and a much weaker phase segregation for the respective hexablock copolymers (Figures S5 and S6, Supporting Information Section).

The SAXS results for the tapered multiblock copolymers with approximate molecular weights of 80 kg/mol, 240 kg/mol and 400 kg/mol are shown in Figure 6 at ambient temperature. The curve for the tapered diblock copolymer with $M_w \sim 80$ kg/mol shows Bragg reflections with positions 1:2 relative to the first peak corresponding to a lamellar morphology. The curves for the tapered tetrablock, hexablock, octablock and decablock copolymers reveal a single and broad peak corresponding to scattering from the disordered state (correlation hole scattering⁴²). The SAXS results for the tapered multiblock copolymers with molecular weight of 240 kg/mol, reveal ordered phases with the expected nanodomain morphology (lamellar). This is evident by the Bragg reflections with positions 1:2:3:4:5 relative to the first peak in the tapered diblock copolymer. However, the curves of the octablock and decablock copolymers reflect only weakly ordered structures. Similarly, for the copolymers with molecular weight of 400 kg/mol, ordered phases are obtained (in the tapered diblock copolymer case with long-range order) with the exception of the decablock copolymer (disordered state). The final assignment of the exact phase state in the tapered multiblock copolymers (ordered vs disordered) as well as the location of the order-to-disorder transition temperature, T_{ODT} , requires temperature-dependent SAXS measurements and/or rheology (see below).

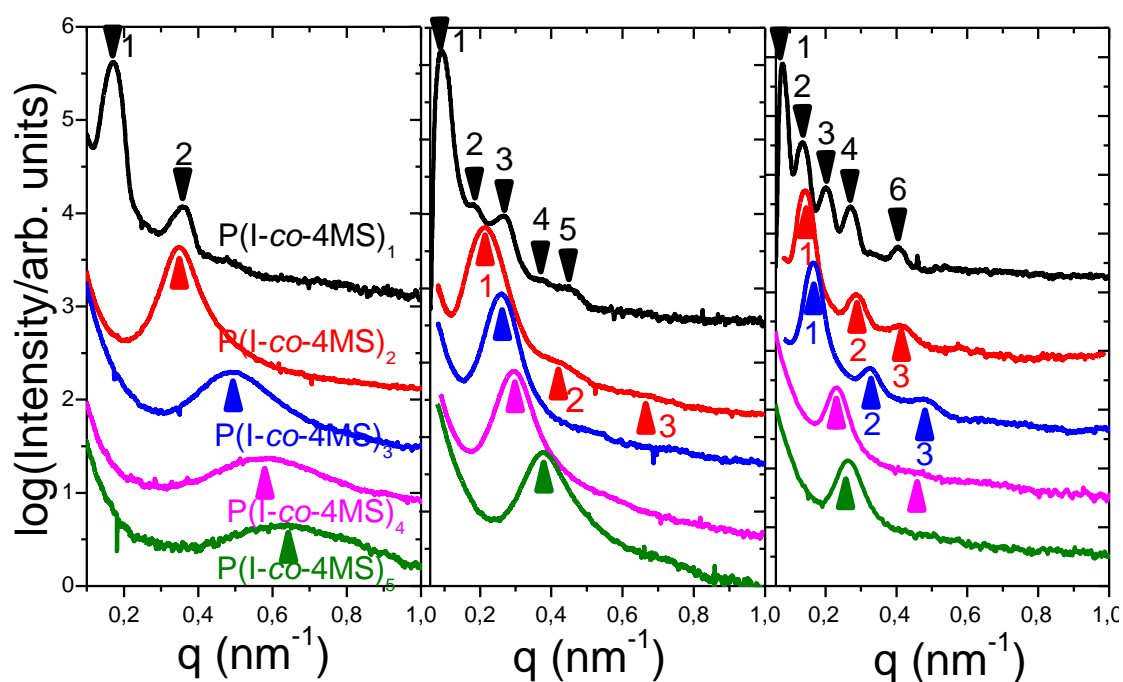


Figure 6. SAXS patterns for the tapered multiblock copolymers with approximate molecular weights of 80 kg/mol (left), 240 kg/mol (center) and 400 kg/mol (right) obtained at ambient temperature. Arrows give the positions of the Bragg reflections corresponding to a lamellar morphology. The same color code is used for the different samples.

The domain spacing, d , obtained from SAXS (as $d = 2\pi/q^*$, q^* is the modulus of the scattering vector corresponding to the first maximum) for the tapered multiblock copolymers can be compared to the corresponding spacing in PI-*b*-P4MS copolymers made by sequential addition (Figure 7). The figure depicts the domain spacing obtained at ambient temperature as a function of the number of blocks for the different molecular weights and as a function of the total molecular weight, the latter in a double logarithmic representation. For the sequential diblock copolymers the domain spacing varies as $\log(d/\text{nm}) = -1.61 + 0.65 \log(M_n/(\text{g/mol}))$ suggesting extended chains. Under conditions applicable to the strong segregation limit (SSL), the molecular weight dependence of the nanodomain spacing scales as $d \sim N^\delta$, with $\delta \sim 2/3$, as opposed to $\delta = 1/2$ for the unperturbed (Gaussian) chains. Helfand predicted⁴³ a nanodomain spacing scaling as: $d \sim \alpha N^{9/14} \chi^{1/7}$ whereas Semenov argued⁴⁴ that the copolymers are strongly segregated with $d \sim \alpha N^{2/3} \chi^{1/6}$. However, experiments on symmetric diblock copolymers spanning a broad range of molecular weights revealed that the picture is more complicated than theoretically predicted.⁴⁵ Interestingly, the molecular weight dependence in the tapered

multiblock copolymers is weaker, with $\delta \sim 0.55 \pm 0.02$ suggesting that chains are stretched - albeit to a lesser degree - with non-ideal (Gaussian) configurations.

Additional information on the chain configuration in the tapered multiblock copolymers can result by comparing their domain spacings with the corresponding diblock copolymers made sequentially. Strikingly, Figure 7b reveals that the tapered diblock copolymers have approximately the same domain spacing as the corresponding PI-*b*-P4MS copolymers made sequentially. The difference in domain spacing is even smaller considering that SEC overestimates the molecular weight of the copolymers. Evidently, the vastly different reactivity ratios of I and 4MS in cyclohexane lead to a tapered diblock with the same (narrow) interface as a block copolymer made by sequential addition. This feature permits an estimation of the width of the interface. In the limit of very long diblock copolymers (SSL), the interfacial width can be estimated according to Helfand and co-workers⁴³ as

$$\Delta_{\infty} = \frac{2a}{\sqrt{6\chi}} \quad (4)$$

where a is the statistical segment length (we further assumed $a_{\text{PI}} \approx a_{\text{P4MS}}$). For a diblock copolymer of finite molecular weight the interfacial width increases and now depends on block incompatibility as

$$\Delta \approx \Delta_{\infty} \left[1 + \frac{1.34}{(\chi N)^{1/3}} \right] \quad (5)$$

Based on the above equations, a typical interfacial thickness for a phase-separated PI-*b*-P4MS copolymer with $N = 1000$, $a \approx 0.635$ nm, and $\chi_{\text{FH}} = 0.076$ at 303 K, is $\Delta \sim 2.5$ nm, meaning that ~ 7 % of segments are at the interface. In the multiblock copolymers this interfacial width is expected to increase further by the length of the tapered interface.

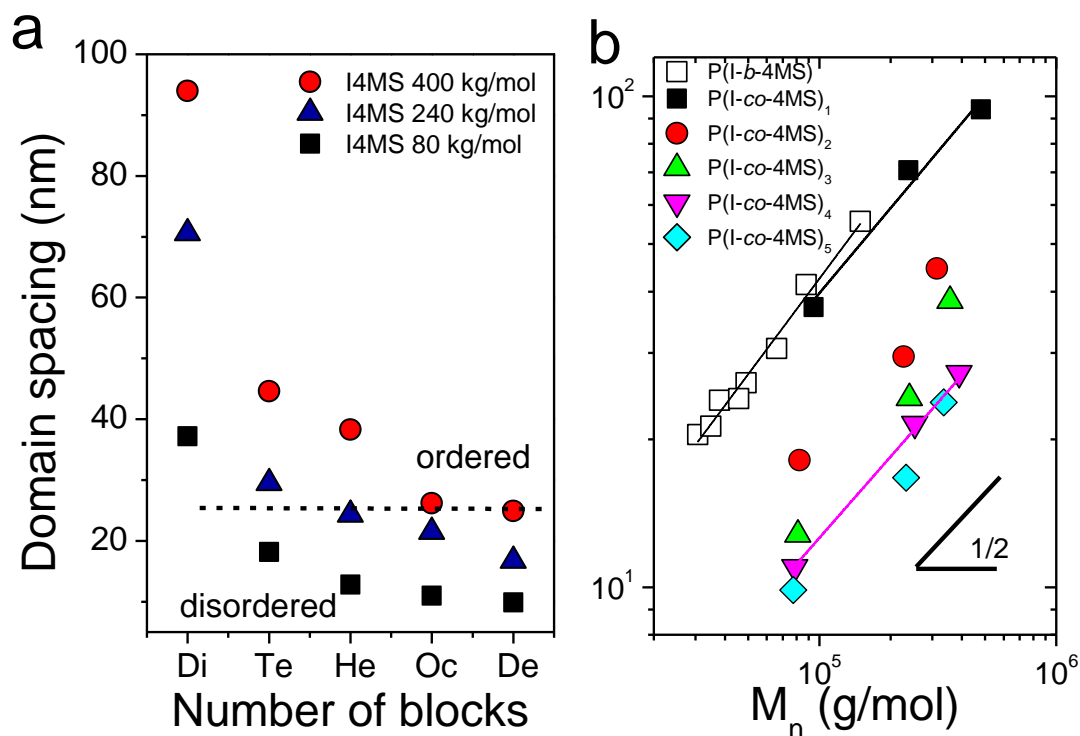


Figure 7. (a) Domain spacing obtained from SAXS plotted as a function of the number of blocks for the tapered multiblock copolymers with approximate molecular weights of 80 kg/mol (squares), 240 kg/mol (triangles) and 400 kg/mol (circles). The dashed line separates the ordered from the disordered states. (b) Domain spacing plotted as a function of molecular weight in a log-log representation for the tapered multiblock copolymers (filled symbols) and for sequential PI-*b*-P4MS copolymers (open squares). Lines are fits to the experimental data for the multiblock copolymers and have slopes of 0.57 and 0.55 for the diblock and octablock, respectively. A line with a slope of $\frac{1}{2}$ is also shown for comparison.

Multiblock copolymers prepared by the repeated addition of mixtures of 4-methyl styrene and isoprene show very different domain spacings when compared at a fixed overall molecular weight with increasing n . In the tetrablock copolymer the domain spacing is reduced by 52 %, relative to the diblock whereas in the octablock the reduction amounts to 74 %. The reduction in domain spacing by increasing the number of blocks at a fixed overall molecular weight is anticipated by the conformational properties of the middle blocks. The looping statistics of normal $(AB)_n$ multiblock copolymers under conditions of increasing n has been treated theoretically.⁶ $(AB)_n$ copolymers consist of two terminal blocks with only one junction site and of $2n-2$ middle blocks each having two junction sites. It was shown that increasing n increases the total number of loops as $2^{2(n-1)}$, with the average number of loops being equal to $n-1$. Two extreme cases were considered; fully

extended chains and fully looped chains and the predicted domain spacings scaled as $d \sim n^{-1.15}$ and $d \sim n^{-0.66}$, respectively. For an average number of loops, the scaling prediction follows $d \sim n^{-0.86}$.⁶ These predictions for normal (*i.e.*, not tapered) multiblock copolymers can be compared with the P(I-co-4MS)_n multiblock copolymers with the tapered interface. Figure 8a gives the domain spacing as a function on n for the three molecular weights in a log-log representation. First, we note that the scaling is obeyed despite some of the copolymers being in the ordered, weakly ordered or disordered states. Secondly, the scaling follows $d \sim n^{-0.83 \pm 0.02}$ in accord with the expectation for an average number of loops.

Informative is also the dependence of the domain spacing on n under fixed block length. From the series of molecular weights and number of blocks investigated there exist three copolymers that fulfill this requirement; P(I-co-4MS)₁ with $M_n = 94.7$ kg/mol; P(I-co-4MS)₃ with $M_n = 240.1$ kg/mol and P(I-co-4MS)₅ with $M_n = 335.3$ kg/mol with corresponding domain spacings of 37.2 nm, 24.4 nm and 9.9 nm. The domain spacings decrease strongly with increasing n , a property found also in multiblock copolymers when examined under a constant block length.⁷ In this case the domain spacing is corrected for the difference in the block molecular weights (assuming Gaussian statistics for simplicity) as $d_{\text{norm}} = (d/M^{1/2})_{n=1}/(d/M^{1/2})$ and the normalized domain spacing is depicted in Figure 8b. The domain spacing now follows $d \sim n^{-1.14}$. In any case, the reduction in domain spacing by increasing the number of blocks both at a fixed overall molecular weight and at a fixed block length reflect the conformational properties of the middle blocks and is expected to affect the mechanical properties of the multiblock copolymers (see below).

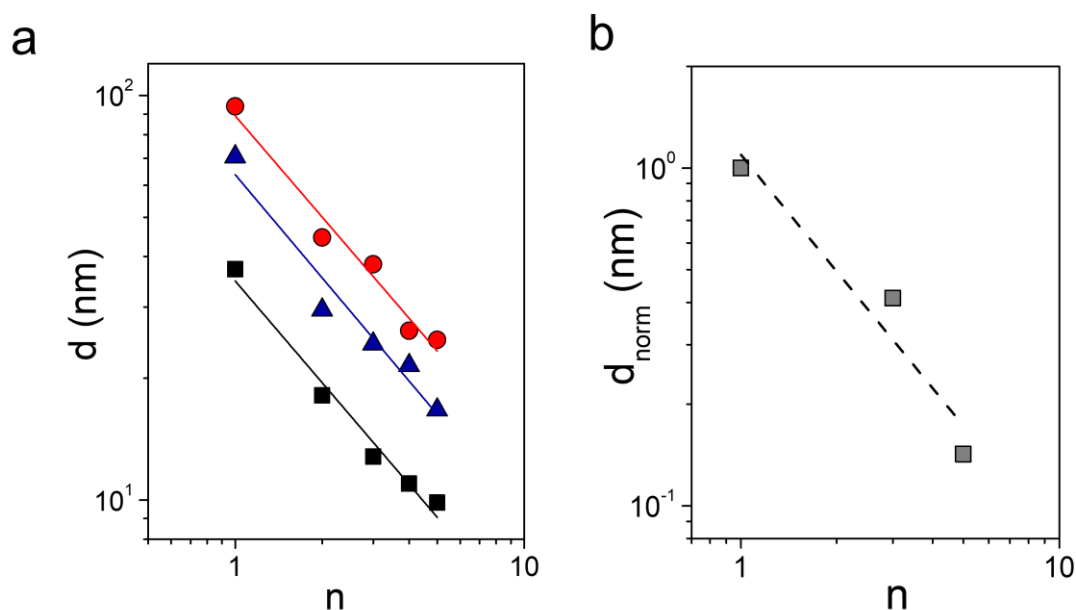


Figure 8. (a) Domain spacing obtained from SAXS plotted as a function of n for the tapered multiblock copolymers with approximate molecular weights of 80 kg/mol (squares), 240 kg/mol (triangles) and 400 kg/mol (circles) in a log-log representation. Lines represent linear fits to the data. (b) Normalized domain spacing plotted as a function of n under a fixed block length. The line gives the result of a linear fit.

More information on the phase state can be obtained by following the structure factor, $S(q)$, of the tapered multiblock copolymers as a function of temperature.³⁵ As an example, the static structure factor for the tapered tetrablock copolymer with a total molecular weight of 85.7 kg/mol is shown in Figure 9 as a function of temperature. A broad liquid-like peak is observed suggesting that all curves are located at $T > T_{\text{ODT}}$, *i.e.*, in the disordered phase. In accord with this expectation, there is no discontinuous change of the peak intensity as evidenced in the $1/S(q^*)$ vs $1/T$ representation. Furthermore, the $1/S(q^*)$ vs $1/T$ has a non-linear dependence as expected from the theory that includes fluctuation corrections (Eq. 3).³³ The latter representation shows, additionally, the role of the P4MS glass temperature in the $S(q)$. Crossing the T_g^{P4MS} influences the peak intensity through the change in macroscopic density and the concomitant change in the electron density for P4MS.

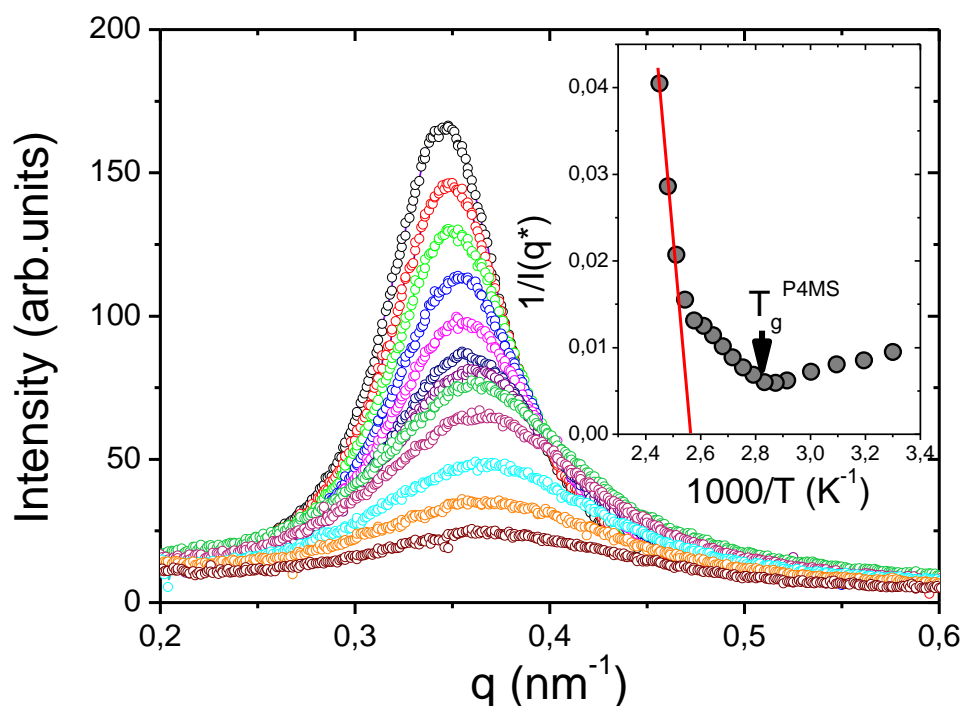


Figure 9. SAXS curves of the tapered tetrablock copolymer with a total molecular weight of 85.7 kg/mol plotted at different temperatures; $T = 353$ K (black); 358 K (red); 363 K (green); 368 K (blue); 373 K (magenta); 378 K (dark blue), 383 K (purple), 388 K (light green), 393 K (violet), 398 K (cyan), 403 K (orange) and 408 K (wine). The inverse peak intensity is plotted versus inverse temperature in the inset. The solid line indicates the MFT predictions. The vertical arrow indicates the T_g of the P4MS phase.

Rheology and mechanical properties. Rheology has been employed as a sensitive probe of the order-to-disorder transition and of the different ordered nanophases. This sensitivity originates from the large viscoelastic contrast of the disordered and the different ordered phases.³⁴⁻⁴⁰ Isochronal measurements of the storage modulus performed at low frequencies with low strain amplitudes by slowly heating the specimen provide a way of locating the T_{ODT} (Fig. 4). Figure 10a shows the result of the isochronal measurements of the storage (G') and loss (G'') moduli at $\omega = 1$ rad/s obtained on heating for the series of the tapered multiblock copolymers with molecular weight of ~ 80 kg/mol. The figure depicts one tapered copolymer that remains in the ordered phase over the whole temperature range (the diblock), and four multiblock copolymers (tetra-, hexa-, octa- and deca-block) that are in their disordered state. Overall, there is an excellent agreement with the SAXS results (Fig. 6) with respect to the phase state of the copolymers. In addition to the phase state the figure depicts the very different viscoelastic responses of the copolymers that are largely controlled by the glass temperature of the hard phase

(P4MS) being a strong function of the number of blocks (Figs 2 and 3) and the overall molecular weight.

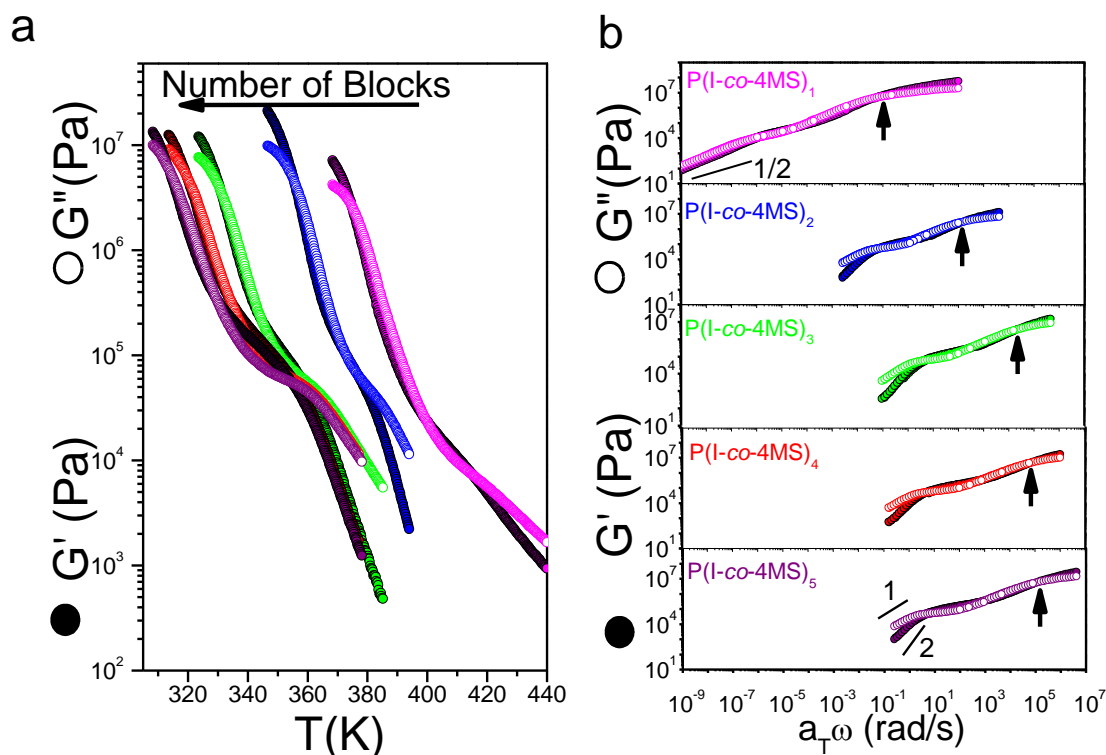


Figure 10. (a) Storage (filled symbols) and loss (open symbols) shear moduli during heating with a rate of 1 K/min at a frequency of 1 rad/s for the different tapered multiblock copolymers with a total molecular weight of 80 kg/mol. The strain amplitude was below 4% for the diblock and below 2% for the rest of the multiblock copolymers. (b) Master-curves of the storage (filled symbols) and loss (open symbols) shear moduli at a reference temperature of 367 K. Lines with slopes of 1 and 2 are shown for the $P(I-co-4MS)_5$ and a line with a slope of $1/2$ for the $P(I-co-4MS)_1$. Vertical arrows indicate the P4MS glass temperatures.

More informative of the viscoelastic response of block copolymers is the use of isothermal measurements as a function of frequency. The time-temperature superposition principle (tTs) allows the frequency ω dependence of the complex modulus G^* at any temperature T to be determined from a master curve at a reference temperature. At each temperature T , a single frequency-scale shift factor a_T allow superposition of all viscoelastic data at temperature T with the data at the reference temperature, T_{ref} , as:

$$G^*(\omega; T) = G^*(a_T \omega; T_{ref}) \quad (6)$$

As an example, master-curves of the storage and loss moduli for the same tapered multiblock copolymers are shown in Figure 10b at a reference temperature of 367 K. The

viscoelastic response of disordered block copolymers is usually similar to that observed for homopolymer melts. At high and intermediate frequencies two relaxation processes affect the viscoelastic response: the segmental and chain relaxation, respectively. At $T > T_{ODT}$, the time-temperature superposition (tTs) works well and the moduli exhibit typical terminal behavior ($G' \sim \omega^2$ and $G'' \sim \omega$). When examined over a broad temperature range, however, tTs is violated due to the order-to-disorder transition that drives the system from the disordered state to a nanophase separated state. At $T < T_{ODT}$ and at low frequencies, the moduli exhibit weak frequency dependencies of the order of $\omega^{1/2}$ (for symmetric block copolymers) to $\omega^{1/4}$. This results from the appearance of an ultra-slow relaxation process related to morphological rearrangements. As an example, the “master curve” for the P(I-co-4MS)₁ exhibits the segmental relaxation of P4MS, the chain relaxation and at lower frequencies the structural relaxation. The breakdown of tTs is observed at low frequencies where the Newtonian behavior of the disordered state is replaced by a rubbery state related to the un-relaxed morphology.

The linear viscoelastic properties of nanophase separated block copolymers have been the subject of theoretical studies. In the study by Rubinstein and Obukhov⁴⁶ both microscopic and mesoscopic mechanisms have been invoked which were attributed, respectively, to the dispersion in the number of entanglements of a chain with the opposite brush (high frequency response) and to the collective diffusion of copolymer chains along the interface. The latter mechanism is controlled by defects in lamellar orientation and contributes to the low-frequency side. For the disordered lamellar mesophase they predicted: $G'(\omega) \sim G''(\omega) \sim \omega^{1/2}$. On the other hand, Kawasaki and Onuki⁴⁷ proposed that overdamped second-sound modes in an orientationally disordered lamellar phase could result in a complex shear modulus proportional to $(i\omega)^{1/2}$. The experimental low-frequency data for P(I-co-4MS)₁ also show a parallel dependence of the moduli with $G'(\omega) \sim G''(\omega) \sim \omega^{1/2}$ as suggested from theory for a lamellar morphology.

The master-curves shown in Fig.10b contain additional information on the state of entanglements. A comparison for the different tapered multiblock copolymers for the 80 kg/mol series is made in Figure 11a that involves an additional horizontal shift factors, a_T' , that accounts for the difference in the glass temperatures of P4MS. The plateau modulus, G_e , of entangled polymers relates to the entanglement molecular weight, M_e , and the tube diameter, α , as⁴⁸

$$G_e \approx \frac{\rho RT}{M_e} \approx \frac{b^3 k_B T}{v_0 \alpha^2 b} \quad (7)$$

Here, ρ is the density, v_0 is the Kuhn monomer volume, and b is the monomer size. Despite the fact that the plateau is only marginally observed in the 80 kg/mol series, an increasing G_e (by approximately a factor of 3) is evident in going from $P(I-co-4MS)_1$ to the multiblock copolymers. There is also a smaller increase in going from $P(I-co-4MS)_2$ to $P(I-co-4MS)_5$. An increase of G_e reflects the bridged configuration of chains in the multiblock copolymers.¹³ The same comparison can also be made under conditions of a fixed block molecular weight. This is shown in Figure 11b where the master curves of $P(I-co-4MS)_1$ and $P(I-co-4MS)_3$, with respective total molecular weights of 80 kg/mol and 240 kg/mol, are compared. The figure depicts again an increasing plateau for $P(I-co-4MS)_3$ despite that it is only weakly segregated (Fig. 7).

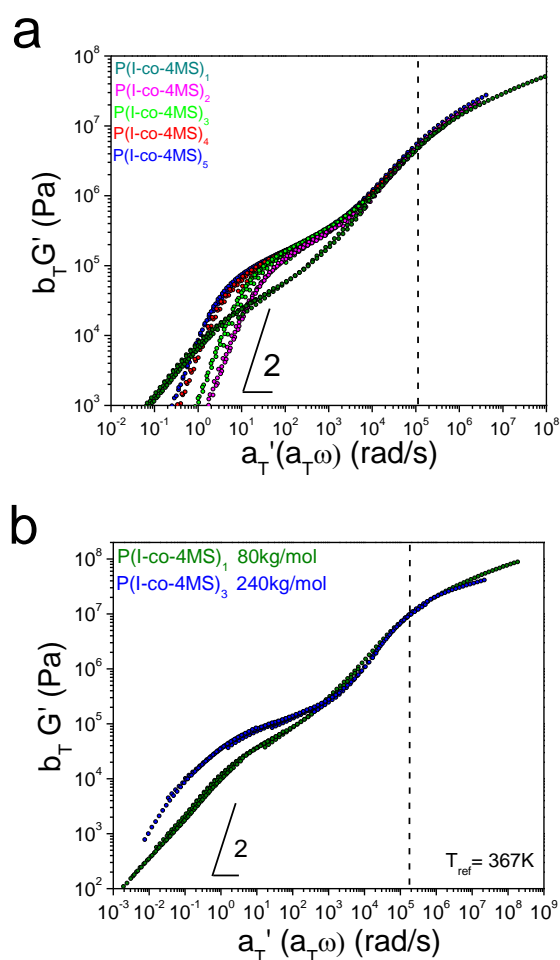


Figure 11. (a) Master-curves of the storage shear moduli for the different tapered multiblock copolymers with a total molecular weight of 80 kg/mol from Fig. 10b, shifted horizontally with additional shift factors (a_T') so as to coincide at the P4MS glass temperature. A small vertical shift (b_T) was also applied to the octablock and decablock cases. (b) Master-curves of the storage shear moduli for two tapered multiblock copolymers bearing the same block molecular weight. A line with a slope of 2 is shown in both cases.

Apart from the linear viscoelastic properties examined above with shear rheometry, of particular interest for applications are the tensile properties of the tapered multiblock copolymers. Some representative stress-strain curves for the different series of molecular weights all at ambient temperature are depicted in Figure 12. In general, all P(I-co-4MS)₁ copolymers are brittle with an elongation at break below 10 %, for the 80 kg/mol, and below 40 % for the 400 kg/mol series. Contrast this with the situation in the tetrablock copolymers with respective elongation at break of 300 % and about 600 % for the 80 kg/mol and 400 kg/mol copolymer series. Depending on the overall molecular weight, the number of blocks, the state of nanophase separation (ordered, weakly ordered vs disordered states) of the copolymers and the proximity to the P4MS glass temperature, a high elongation at break as high as 800% could be obtained. The tensile properties unambiguously show a transition from brittle to ductile behavior in going from the P(I-co-4MS)₁ to the tapered multiblock copolymers. In addition, all tapered copolymers show yielding followed by strain hardening (*i.e.* $d\sigma/d\varepsilon$ increases with increasing strain) prior to break. Strain hardening has also been observed in normal (AB)_n multiblock copolymers but only for large n values.¹² Here this effect is evident – especially for the higher molecular weights – even from the tetrablock ($n = 2$).

These results can also be discussed in terms of the increased toughness shown in Figure 13. As expected, P(I-co-4MS)₁ exhibits little toughness independent of the molecular weight. In the tapered multiblock copolymers there is a 35-fold (in the 400 kg/mol) to 200-fold (in the 80 kg/mol) increase in toughness. The figure reveals that, in addition to the number of blocks and total molecular weight, the state of order and proximity to the P4MS glass temperature also plays a role. The highest increase in toughness is obtained for nanophase separated copolymers where, in addition, P4MS is well into the glassy state. Similarly, the reduction in toughness obtained for the P(I-co-4MS)₅ with 80 kg/mol reflects the proximity of the temperature where the tensile test is performed (ambient temperature) to the P4MS glass temperature. These findings taken together suggest an enhanced interfacial strength as a result of the configurations of the middle blocks in the tapered multiblock copolymers.

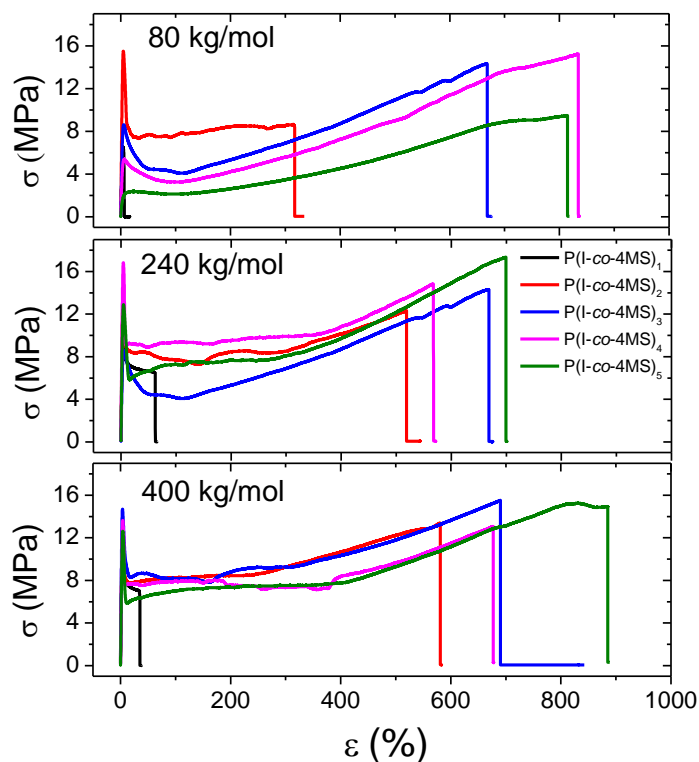


Figure 12. Representative stress-strain curves for the tapered multiblock copolymers with approximate molecular weights of 80 kg/mol (top), 240 kg/mol (center) and 400 kg/mol (bottom) obtained at ambient temperature. The same color code is used for the different samples.

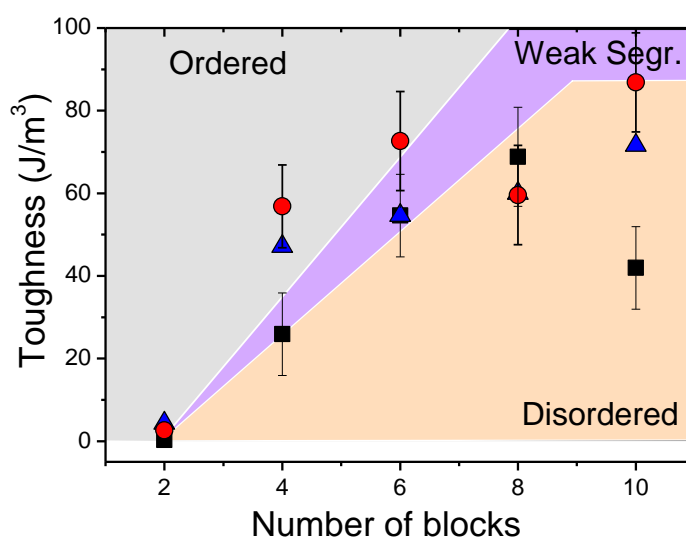


Figure 13. Toughness of the tapered multiblock copolymers with approximate molecular weights of 80 kg/mol (black squares), 240 kg/mol (blue triangles) and 400 kg/mol (red circles) obtained from the stress-strain curves at ambient temperature. Areas in grey, magenta and orange indicate, respectively, ordered, weakly ordered and disordered regimes.

Conclusions

The one-pot synthesis of tapered block copolymers by statistical living anionic copolymerization of a mixture of isoprene and 4-methylstyrene in cyclohexane provided a series of well-defined tapered multiblock copolymers with up to 10 blocks that exhibit much steeper gradients than the previously studied series of tapered multiblock copolymers based on isoprene and styrene.²⁸ The thermomechanical properties of these copolymers were found to be influenced by the phase state and the configurations of the middle blocks. More specifically:

Dual glass temperatures corresponding to P4MS-rich and PI-rich domains were obtained in all tapered multiblock copolymers. The two T_g s approach each other with the number of blocks and with decreasing total molecular weight. DSC provides evidence for an additional “interphase” T_g .

The interaction parameter between I and 4MS segments was obtained based on the order-to-disorder transition temperatures of PI-*b*-P4MS diblock copolymers prepared by sequential addition monomers. Forcing the T_{ODT} to the MFT and FH predictions resulted to the following $\chi(T)$ dependencies: $\chi_{MFT} = 23.2/T - 0.024$ and $\chi_{FH} = 36.0/T - 0.041$. Both dependencies are weaker than in the corresponding PI-*b*-PS system, revealing that the different reactivity ratios of the monomers and the associated steeper composition profile is not the only factor that controls the miscibility of the tapered multiblock copolymers. The latter is controlled by the value of the interaction parameter, the length of the tapered interface as well as by the number of blocks and total molecular weight. Temperature-dependent SAXS results show that tapered multiblock copolymers undergo a fluctuation-induced first-order transition from the ordered to the disordered state. The domain spacing in the P(I-co-4MS)_n series scales as $d \sim n^{-0.83 \pm 0.02}$ when compared under a fixed total molecular weight and as $d \sim n^{-1.14}$ when compared under a fixed block length both reflecting the conformational properties of the middle blocks. In addition, domain spacing depends on molecular weight, as $d \sim N^{0.55}$, and this dependence is weaker than in the corresponding diblock copolymers prepared by sequential addition ($d \sim N^{0.65}$). Nevertheless, it shows stretching of chains and non-ideal configurations.

The linear viscoelastic response of the tapered copolymers is controlled by the number of blocks *and* overall molecular weight. The plateau modulus in the tapered multiblock copolymers increases with the number of blocks as a result of the bridged configuration of chains. In the tapered multiblock copolymers a single chain can bridge over several

soft/rubbery domains. The non-linear mechanical properties obtained during the tensile tests revealed a dramatic enhancement of the strain at break; from about 10 % in the diblock copolymers to as high as 800 % in several tapered multiblock copolymers with a concomitant increase in toughness. These mechanical properties can be fine-tuned by the judicious selection of molecular weights and number of blocks. The state of order (ordered vs weakly ordered) and proximity to the glass temperature of the hard phase also plays a role. The improved mechanical properties reflect the enhanced interfacial strength as a result of the conformational properties of the middle blocks in the segmented polymer chains. In comparing the $P(I-co-4MS)_n$ and $P(I-co-PS)_n$ systems with respect to their phase state, we find that the shorter tapered interface in the former is counterbalanced by its lower effective interaction parameter, resulting in similar domain spacings.

In summary, we have demonstrated that the one-pot synthesis of tapered multiblock copolymers with controlled molecular weights, well-understood tapered interface, and defined number of blocks is feasible based on 4-methylstyrene and isoprene. We rely on a strategy that can be conveniently scaled up, permitting detailed mechanical characterization as well as processing studies. We believe that our results are highly relevant for thermoplastic elastomers (TPEs), in general, since the tapered multiblock copolymers are obtained in a one-pot procedure that relies on common vinyl monomers. We can demonstrate that tapered copolymers exhibit unique structural and thermomechanical properties enabled by the selection of the number of blocks and the total molecular weight and, in addition, by the mixing of unlike segments at the interface. This affords materials with an accessible (e.g., low) order-to-disorder transition temperature located in the vicinity of the glass temperature of the “hard” phase. This observation is important in view of processing of such materials. To sum up, these novel materials are highly promising for future applications as thermoplastic elastomers, especially when considering different block copolymer architectures or with blocks that in addition exhibit electrostatic interactions. A remaining challenge in the field is the quantification of the conformational properties of the middle blocks (bridges vs loops) that determine the mechanical properties.

Acknowledgments

The current work was supported by the Research unit on Dynamics and Thermodynamics of the UoI co-financed by the European Union and the Greek state under NSRF 2007-2013 (Region of Epirus, call 18). M.G. and M.A. acknowledge the German Research Foundation (DFG GA 2169/1-1) for partial financial support of this work. The authors also thank the RMU Mainz-Darmstadt for funding. Andreas Hanewald and Dr. Kaloian Koynov are acknowledged for their valuable help with the mechanical characterization.

References

- (1) Zelinski, R.; Childers, C. W. Linear Elastomeric Block Polymers. *Rubber Chem. Technol.* **1968**, *41*, 161–181.
- (2) Kraus, G.; Childers, C. W.; Gruver, J. T. Properties of Random and Block Copolymers of Butadiene and Styrene. I. Dynamic Properties and Glassy Transition Temperatures. *J. Appl. Polym. Sci.* **1967**, *11*, 1581–1591.
- (3) Knoll, K.; Nießner, N. Styrolux+ and Styroflex - From Transparent High Impact Polystyrene to New Thermoplastic Elastomers: Syntheses, Applications and Blends With Other Styrene Based Polymers. *Macromol. Symp.* **1998**, *132*, 231–243.
- (4) Benoit, H.; Hadziioannou, G. Scattering Theory and Properties of Block Copolymers with Various Architectures in the Homogeneous Bulk State. *Macromolecules* **1988**, *21*, 1449-1464.
- (5) Kavassalis, T. A.; Whitmore, M. D. On the Theory of Linear Multiblock Copolymers. *Macromolecules* **1991**, *24*, 5340-5345.
- (6) Spontak, R. J.; Zielinski, J. M.; Lipscomb, G. G. Effect of Looping on the Microstructure of Linear Multiblock Copolymers. *Macromolecules* **1992**, *25*, 6270-6276.
- (7) Smith, S. D.; Spontak, R. J.; Satkowski, M. M.; Ashraf, A.; Heape, A. K.; Lin, J. S. Microphase-Separated Poly(Styrene-*b*-Isoprene) Multiblock Copolymers with Constant Block Lengths. *Polymer* **1994**, *35*, 4527-4536.
- (8) Matsushita, Y.; Mogi, Y.; Mukai, H.; Watanabe, J.; Noda, I. Preparation and Morphology of Multiblock Copolymers of the (AB)*n* Type. *Polymer* **1994**, *35*, 246-249.
- (9) Spontak, R. J.; Smith, S. D. Perfectly-Alternating Linear (AB)*n* Multiblock Copolymers: Effect of Molecular Design on Morphology and properties. *J. Polym. Sci.: Polym. Phys.* **2001**, *39*, 947-955.
- (10) Wu, L.; Cochran, E. W.; Lodge, T. P.; Bates, F. S. Consequences of Block Number on the Order-Disorder Transition and Viscoelastic Properties of Linear (AB)*n* Multiblock Copolymers. *Macromolecules* **2004**, *37*, 3360-3368.
- (11) Wu, L.; Lodge, T. P.; Bates, F. S. Effects of Block Number on Multiblock Copolymer Lamellar Alignment Under Oscillatory Shear. *J. Rheol.* **2005**, *49*, 1231-1252.

- (12) Koo, C. M.; Hillmyer, M. A.; Bates, F. S. Structure and Properties of Semicrystalline-Rubbery Multiblock Copolymers. *Macromolecules* **2006**, *39*, 667-677.
- (13) Watanabe, H.; Matsumiya, Y.; Sawada, T.; Iwamoto, T. Rheological and Dielectric Behavior of Dipole-Inverted (SIS)_p-Type Multiblock Copolymers: Estimates of Bridge/Loop Fractions for Respective I Blocks and Effect of Loops on High Extensibility of Bridges. *Macromolecules* **2007**, *40*, 6885-6897.
- (14) Bates, F. S.; Hillmyer, M. S.; Lodge, T. P.; Bates, C. M.; Delaney, K. T.; Fredrickson, G. H. Multiblock Polymers: Panacea or Pandora's Box? *Science* **2012**, *336*, 434-440.
- (15) Lee, I.; Bates, F. S. Synthesis, Structure, and Properties of Alternating and Random Poly(Styrene-*b*-Butadiene) Multiblock Copolymers. *Macromolecules* **2013**, *46*, 4529-4539.
- (16) Xu, J.; Eagan, J. M.; Kim, S.-S.; Pan, S.; Lee, B.; Klimovica, K.; Jin, K.; Lin, T.-W.; Howard, M. J.; Ellison, C. J.; LaPointe, A. M.; Coates, G. W.; Bates, F. S. Compatibilization of Isotactic Polypropylene (iPP) and High-Density Polyethylene (HDPE) with iPP-PE Multiblock Copolymers. *Macromolecules* **2018**, *51*, 8585-8596.
- (17) Zhu, Y.; Radlauer, M. R.; Schneiderman, D. K.; Shaffer, M. S. P.; Hillmyer, M. A.; Williams, C. K. Multiblock Polyesters Demonstrating High Elasticity and Shape Memory Effects. *Macromolecules* **2018**, *51*, 2466-2475.
- (18) Zielinski, J. M.; Spontak, R. J. Thermodynamic Considerations of Triblock Copolymers with a Random Middle Block. *Macromolecules* **1992**, *25*, 5957-5964.
- (19) Hodorokoukes, P.; Floudas, G.; Pispas, S.; Hadjichristidis, N. Microphase Separation in Normal and Inverse Tapered Block Copolymers of Polystyrene and Polyisoprene. 1. Phase State. *Macromolecules* **2001**, *34*, 650-657.
- (20) Singh, N.; Tureau, M. S.; Epps, T. H. Manipulating Ordering Transitions in Interfacially Modified Block Copolymers. *Soft Matter* **2009**, *5*, 4757-4762.
- (21) Roy, R.; Park, J. K.; Young, W.-S.; Mastroianni, S. E.; Tureau, M. S.; Epps, T. H. Double-Gyroid Network Morphology in Tapered Diblock Copolymers. *Macromolecules* **2011**, *44*, 3990-3915.
- (22) Kuan, W.-F.; Roy, R.; Rong, L.; Hsiao, B. S.; Epps, T. H. Design and Synthesis of Network-Forming Triblock Copolymers Using Tapered Block Interfaces. *ACS Macro Lett.* **2012**, *1*, 519-523.
- (23) Luo, M.; Brown, J. R.; Remy, R. A.; Scott, D. M.; Mackay, M. E.; Hall, L. M.; Epps, T. H. Determination of Interfacial Mixing in Tapered Block Polymer Thin Films: Experimental and Theoretical Investigations. *Macromolecules* **2016**, *49*, 5213-5222.
- (24) Zhang, J.; Deubler, R.; Hartlieb, M.; Martin, L.; Tanaka, J.; Patyukova, E.; Topham, P. D.; Schacher, F. H.; Perrier, S. Evolution of Microphase Separation with Variation of Segments of Sequence-Controlled Multiblock Copolymers. *Macromolecules* **2017**, *50*, 7380-7387.
- (25) Grune, E.; Johann, T.; Appold, M.; Wahlen, C.; Blankenburg, J.; Leibig, D.; Müller, A. H. E.; Gallei, M.; Frey, H. One-Step Block Copolymer Synthesis versus Sequential Monomer Addition: A Fundamental Study Reveals That One Methyl Group Makes a Difference. *Macromolecules* **2018**, *51*, 3527-3537.

- (26) Appold, M.; Grune, E.; Frey, H.; Gallei, M., One-Step Anionic Copolymerization Enables Formation of Linear Ultra-High Molecular Weight Block Copolymer Films Featuring Vivid Structural Colors in the Bulk State. *ACS Appl. Mater. Interfaces* **2018**, *10*, 18202–18212.
- (27) Grune, E.; Appold, M.; Müller, A. H. E.; Gallei, M.; Frey, H. Anionic Copolymerization Enables the Scalable Synthesis of Alternating (AB)_n Multiblock Copolymers with High Molecular Weight in $n/2$ Steps. *ACS Macro Lett.* **2018**, 807–810.
- (28) Steube, M.; Johann, T.; Galanos, E.; Appold, M.; Rüttiger, C.; Mezger, M.; Gallei, M.; Müller, A. H. E.; Floudas, G.; Frey, H. Isoprene/Styrene Tapered Multiblock Copolymers with up to Ten Blocks: Synthesis, Phase Behavior, Order, and Mechanical Properties. *Macromolecules* **2018**, *51*, 10246–10258.
- (29) Pakula, T.; Matyjaszewski, K. Copolymers with controlled distribution of comonomers along the chain. 1. Structure, thermodynamics and dynamic properties of gradient copolymers. Computer simulation. *Macromol. Theory Simul.* **1996**, *5*, 987.
- (30) Lodge, T. P.; McLeish, T. C., Self-Concentrations and Effective Glass Transition Temperatures in Polymer Blends. *Macromolecules* **2000**, *33* (14), 5278-5284.
- (31) Harmandaris, V.; Floudas, G.; Kremer, K. Dynamic Heterogeneity in Fully Miscible Blends of Polystyrene with Oligostyrene. *Phys. Rev. Lett.* **2013**, *110*, 165701.
- (32) Leibler, L. Theory of Microphase Separation in Block Copolymers, *Macromolecules* **1980**, *13*, 1602.
- (33) Fredrickson, G. H.; Helfand, E. Fluctuation Effects in the Theory of Microphase Separation in Block Copolymers. *J. Chem. Phys.* **1987**, *87*, 697-705.
- (34) Matsen M. W.; Bates F. S. Block Copolymer Microstructures in the Intermediate-Segregation Regime. *J. Chem. Phys.* **1997**, *106*, 2436.
- (35) Hadjichristidis, N.; Pispas, S.; Floudas, G. *Block Copolymers. Synthetic Strategies, Physical Properties and Applications*. J. Wiley and Sons Inc.: 2002.
- (36) Bates, F.S.; Rosedale, J. H.; Fredrickson, G. H. Fluctuation Effects in a Symmetric Diblock Copolymer Near the Order-Disorder Transition. *J. Chem. Phys.* **1990**, *92*, 6255-6270.
- (37) Koppi, K. A.; Tirrell, M.; Bates, F. S.; Almdal, K.; Colby, R. H. Lamellae Orientation in Dynamically Sheared Diblock Copolymer Melts. *J. Phys. II* **1992**, *2*, 1941-1959.
- (38) Floudas, G.; Pakula, T.; Velis, G.; Sioula, S.; Hadjichristidis N. Equilibrium Order-to-Disorder Transition Temperature in Block Copolymers. *J. Chem. Phys.* **1998**, *108*, 6498-6501.
- (39) Han, C. D.; Baek, D. M.; Kim, J. K.; Ogawa, T.; Sakamoto, N.; Hashimoto, T. Effect of Volume Fraction on the Order-Disorder Transition in Low Molecular Weight Polystyrene-block-Polyisoprene Copolymers. 1. Order-Disorder Transition Temperature Determined by Rheological Measurements. *Macromolecules* **1995**, *28*, 5043–5062.

- (40) Floudas, G.; Vlassopoulos, D.; Pitsikalis, M.; Hadjichristidis, N.; Stamm, M. Order-Disorder Transition and Ordering Kinetics in Binary Diblock Copolymer Mixtures of Styrene and Isoprene. *J. Chem. Phys.* **1996**, *104*, 2083–2088.
- (41) Khandpur, A. K.; Förster, S.; Bates, F. S.; Hamley, I. W.; Ryan, A. J.; Almdal, K.; Mortensen, K. Polyisoprene-Polystyrene Diblock Copolymer Phase Diagram Near the Order-Disorder Transition. *Macromolecules* **1995**, *28*, 8796-8806.
- (42) de Gennes, P.-G. *Scaling Concepts in Polymer Physics*; Cornell University Press, Ithaca, NY, 1979.
- (43) Helfand, E. Block Copolymer Theory. III. Statistical Mechanics of the Microdomain Structure. *Macromolecules* **1975**, *8*, 552–556.
- (44) Semenov A. N. Contribution to the Theory of Microphase Layering in Block-Copolymer Melts. *Soviet Phys. JETP* **1985**, *61*, 733.
- (45) Papadakis, C. M.; Almdal, K.; Mortensen, K.; Posselt, D. Identification of an Intermediate-Segregated Regime in a Diblock Copolymer System. *Europh. Lett.* **1996**, *36*, 289-294.
- (46) Rubinstein, M.; Obukhov, S. P. Power-Law-Like Stress Relaxation of Block Copolymers: Disentanglement Regimes. *Macromolecules* **1993**, *26*, 1740-1750.
- (47) Kawasaki, K.; Onuki, A. Dynamics and Rheology of Diblock Copolymers Quenched into Microphase-Separated States. *Phys. Rev. A* **1990**, *42*, 3664-3666.
- (48) Rubinstein, M.; Colby, R. H. *Polymer Physics*, Oxford University Press: 2003.

Supporting Information

Tapered Multiblock Copolymers Based on Isoprene and 4-Methylstyrene: Influence of the Tapered Interface on the Self-Assembly and Thermochemical Properties

Eftyxis Galanos, Eduard Grund, Christian Wahlen, Axel H. E. Müller, Michael Appold, Markus Gallei, Holger Frey* and George Floudas*

Preparation of multiblock copolymers

In a previous short account we described a synthetic approach for $(AB)_n$ multiblock copolymers, based on the highly disparate reactivity ratios of isoprene (I) and 4-methylstyrene (4MS) ($r_I = 25.4$; $r_{4MS} = 0.007$).¹ Due to the highly favored incorporation of I, the statistical copolymerization of I/4MS yields tapered block copolymer in one step.² The living chain end permits further addition of I/4MS monomer mixtures, providing rapid access to linear tapered $(AB)_n$ multiblock copolymers (Figure S1 a). This general synthetic approach was used in our recent study to generate tapered multiblock copolymers based on isoprene and styrene.³ The resulting $(AB)_n$ multiblocks showed ordered structures for up to ten blocks ($n = 5$) and extraordinary toughness. To examine whether multiblock properties like state of order and mechanical response are affected by length and shape of the tapered interface, three series of $(AB)_n$ multiblock copolymers with varying block number, but constant molecular weights of 80 kg/mol; 240 kg/mol and 400 kg/mol were prepared based on isoprene and 4-methylstyrene (Figure S1 b).

For a better comparison of the samples, we aimed for a constant isoprene content of 50 mol% for all copolymers. The discrepancies between the targeted molecular weights and the molecular weights determined by SEC are, mainly caused by the calibration with polystyrene standards. However, the SEC results provide a sufficient estimation of the actual molecular weights (Table S1). The dispersities of the multiblock samples showed a broadening of the molecular weight distributions and the appearance of small shoulders at low molecular weights for increasing molecular weights and an increasing number of monomer additions (Supp. Inf. Figure S3). Both effects can be explained by a small percentage of termination during every monomer addition step. However, considering

the high molecular weights and the high number of blocks, the dispersities are still very narrow and demonstrate the potential and applicability of this synthetic approach for well-defined linear multiblock copolymers.

^1H NMR Analysis

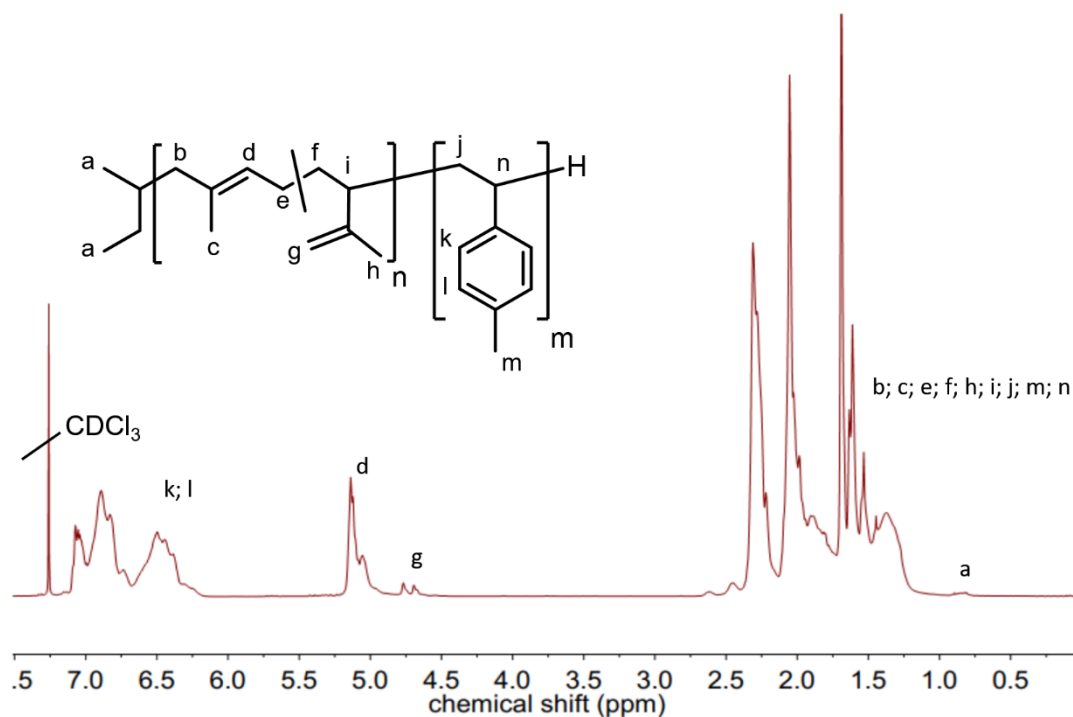
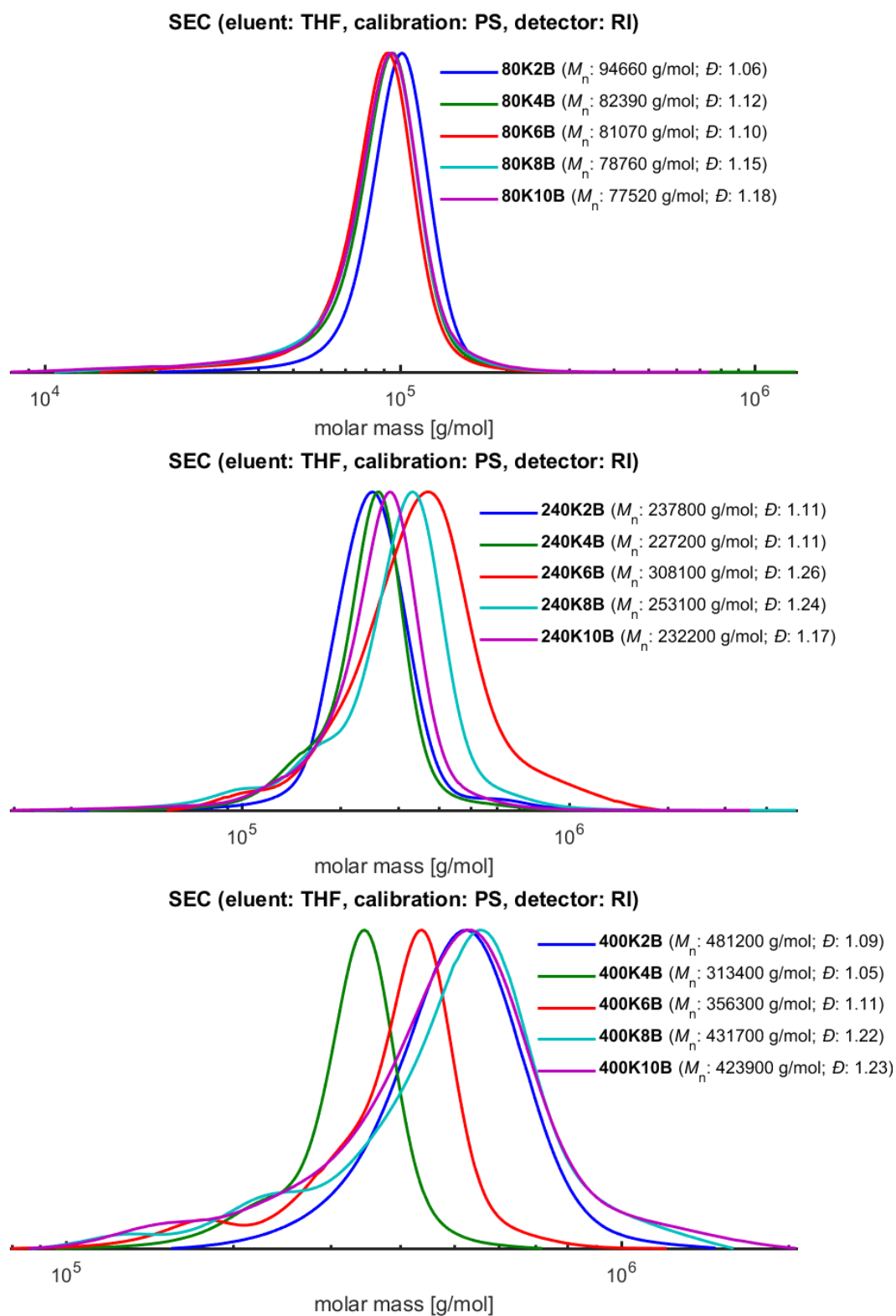


Figure S1. ^1H -NMR spectrum (400 MHz) of 400K 10B in CDCl_3 (Table S1 Entry 15).

SEC

**Figure S3.** SEC elugrams of I/4MS multiblock copolymers.

Rheology

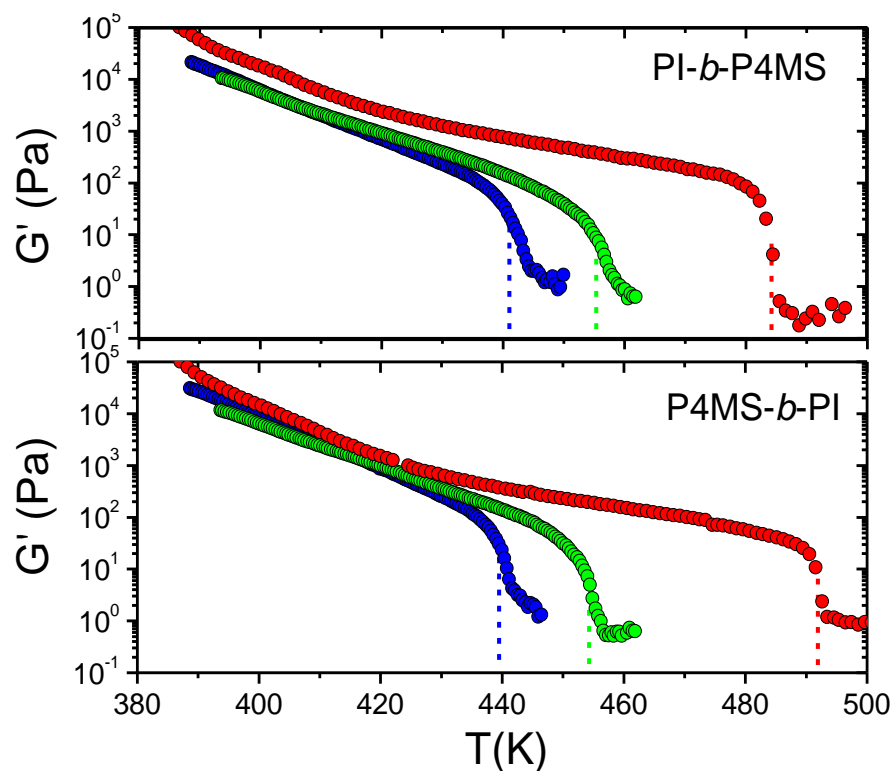


Figure S4: Temperature dependence of the storage modulus, G' , obtained at a frequency of $\omega = 1$ rad/s with a low strain amplitude on heating the sequential diblock copolymers 30KP(PI-*b*-P4MS) (Table S1 Entry 16) (blue), 35KP(PI-*b*-P4MS) (Table S1 Entry 18) (green) and 40KP(PI-*b*-P4MS) (Table S1 Entry 20) (red) (top) and the inverse diblock copolymers 30KP(P4MS-*b*-PI) (Table S1 Entry 17) (blue), 35KP(P4MS-*b*-PI) (Table S1 Entry 19) (green) and 40KP(P4MS-*b*-PI) (Table S1 Entry 21) (red) (bottom). Vertical dashed lines indicate the respective T_{ODT} 's.

Tensile Testing

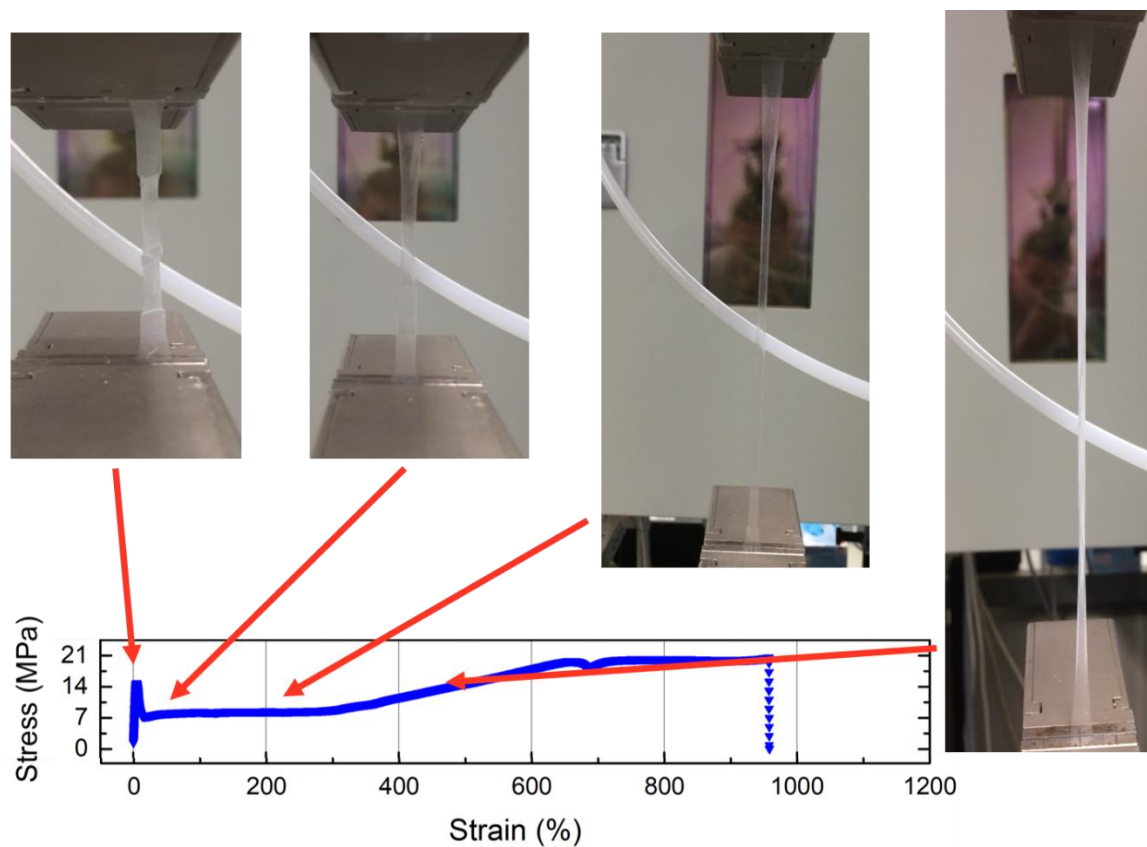


Figure S5. Tensile testing of a multiblock sample.

TEM

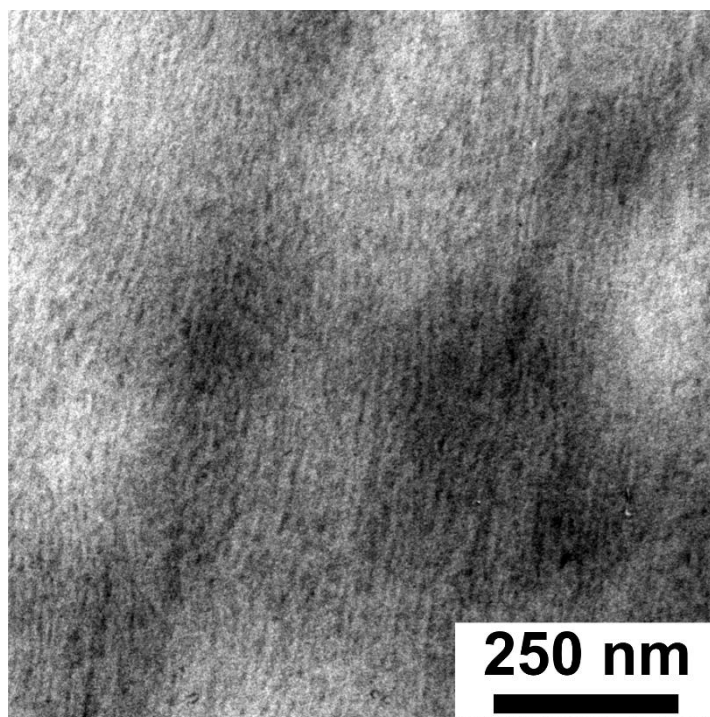


Figure S6: TEM image of a hexablock copolymer (240 kg/mol) (Table S1 Entry 8), showing very fine lamellar structures.

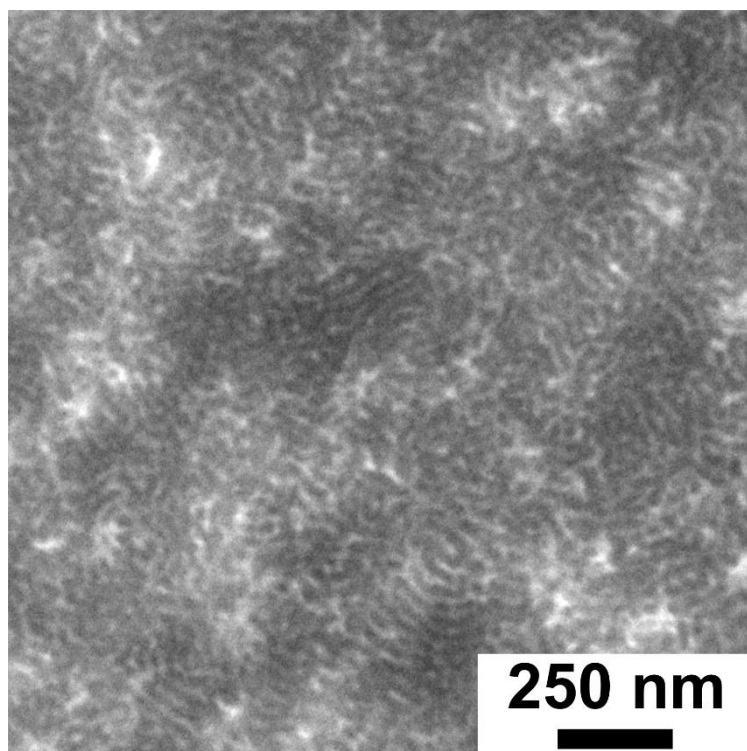


Figure S7: TEM image of a hexablock copolymer (400 kg/mol) (Table S1 Entry 13), showing a lamellar morphology.

References

- (1) Grune, E.; Appold, M.; Müller, A. H. E.; Gallei, M.; Frey, H. Anionic Copolymerization Enables the Scalable Synthesis of Alternating (AB)_n Multiblock Copolymers with High Molecular Weight in $n/2$ Steps. *ACS Macro Lett.* **2018**, 807–810.
- (2) Grune, E.; Johann, T.; Appold, M.; Wahlen, C.; Blankenburg, J.; Leibig, D.; Müller, A. H. E.; Gallei, M.; Frey, H. One-Step Block Copolymer Synthesis versus Sequential Monomer Addition: A Fundamental Study Reveals That One Methyl Group Makes a Difference. *Macromolecules* **2018**, 51, 3527–3537.
- (3) Steube, M.; Johann, T.; Galanos Eftyxis; Appold, M.; Rüttinger, C.; Metzger, M.; Gallei, M.; Müller, A. H.E.; Floudas, G.; Frey, H. Isoprene/Styrene Tapered Multiblock Copolymers with up to 10 Blocks: Synthesis, Phase Behavior, Order and Mechanical Properties. *Macromolecules* **2018**.

Appendix

CHAPTER A1

Tapered Multiblock Copolymers of Isoprene and 4 Methylstyrene

One-Step Block Copolymer Synthesis versus Sequential Monomer Addition: A Fundamental Study Reveals That One Methyl Group Makes a Difference

Eduard Grune,^{†,§} Tobias Johann,^{†,||} Michael Appold,[‡] Christian Wahlen,[†] Jan Blankenburg,^{†,§} Daniel Leibig,^{†,§} Axel H. E. Müller,^{*,†} Markus Gallei,^{*,‡,§} and Holger Frey^{*,†,§}

[†]Institute of Organic Chemistry, Johannes Gutenberg-University, Duesbergweg 10-14, 55128 Mainz, Germany

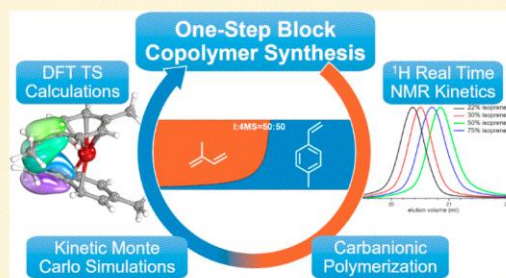
[‡]Macromolecular Chemistry Department, Technische Universität Darmstadt, Alarich-Weiss-Str. 4, 64287 Darmstadt, Germany

[§]Graduate School Materials Science in Mainz, Staudingerweg 9, 55128, Mainz, Germany

^{||}Max Planck Graduate Center, Staudingerweg 9, 55128, Mainz, Germany

Supporting Information

ABSTRACT: Block copolymers of polyisoprene and polystyrene are key materials for polymer nanostructures as well as for several commercially established thermoplastic elastomers. In a combined experimental and kinetic Monte Carlo simulation study, the direct (i.e., statistical) living anionic copolymerization of a mixture of isoprene (I) and 4-methylstyrene (4MS) in nonpolar media was investigated on a fundamental level. *In situ* ¹H NMR spectroscopy enabled to directly monitor gradient formation during the copolymerization and to determine the nature of the gradient. In addition, a precise comparison with the established copolymerization of isoprene and styrene (I/S) was possible. Statistical copolymerization in both systems leads to tapered block copolymers due to an extremely slow crossover from isoprene to the styrenic monomer. For the system I/4MS the determination of the reactivity ratios shows highly disparate values with $r_1 = 25.4$ and $r_{4MS} = 0.007$, resulting in a steep gradient of the comonomer composition. The rate constants determined from online NMR studies were used for a kinetic Monte Carlo simulation, revealing structural details, such as the distribution of the homopolymer sequences for both blocks, which are a consequence of the peculiar kinetics of the diene/styrene systems. DFT calculations were used to compare the established copolymerization of isoprene and styrene with the isoprene/4-methylstyrene system. A variety of gradient copolymers differing in molecular weight and monomer feed composition were synthesized, confirming strong microphase segregation as a consequence of the blocklike structure. The one-pot synthesis of such tapered block copolymers, avoiding high vacuum or break-seal techniques, is a key advantage for the preparation of ultrahigh molecular weight block copolymers ($M_n > 1.2 \times 10^6$ g/mol) in one synthetic step. These materials show microphase-segregated bulk structures like diblock copolymers prepared by sequential block copolymer synthesis. Because of the living nature of the tapered block copolymer structures, a vast variety of complex structures are accessible by the addition of further monomers or monomer mixtures in subsequent steps.



INTRODUCTION

Living anionic polymerization is still state of the art for the preparation of highly defined block co- and terpolymers with low molecular weight dispersity and high molecular weights, commonly by sequential addition of the monomers.^{1,2} Block copolymer architectures play a key role in current polymer research for a vast variety of commercial and prospective applications that capitalize on their nanophase-segregated structures, such as thermoplastic elastomers, compatibilization of polymer blends, block copolymer lithography, nanomedicine, nanoreactors, and highly ordered nanopatterns.^{3–9} Eminent examples for block copolymers established on large technical scale are Kraton, high impact polystyrene (HIPS), and more advanced, extremely elastic or tough thermoplastic materials

like Styroflex and Styrodur.^{10–12} The synthesis of block copolymers relies either on a living polymerization technique with consecutive addition of both monomers or highly efficient coupling reactions of prefabricated blocks.^{13,14} In both cases several reaction steps are required, increasing the risk of irreversible termination, leading to homopolymer impurities. Thus, one-step strategies for the preparation of block copolymers are desirable. Direct, i.e. statistical, copolymerization of a monomer pair using living anionic copolymerization can afford random or gradient monomer sequences,¹⁵ depend-

Received: February 23, 2018

Revised: April 13, 2018

Published: April 27, 2018

ing on the reactivity ratios of the respective monomers. Early works in the 1960s regarding the direct carbanionic copolymerization of isoprene (I) and styrene (S) in hydrocarbon solvents already suggested a block copolymer like structure that was (erroneously) attributed to strongly differing monomer reactivities.¹⁶ Several authors observed a correlation between homopolymerization and crossover reaction, concluding that a gradual incorporation of the less reactive monomer occurred instead of a sharp transition between the blocks.^{17,18} This type of block copolymer was designated “tapered block copolymer” and studied in several groundbreaking works, demonstrating the materials’ capability to undergo phase separation.^{19,20}

Nevertheless, tapered copolymers of isoprene and styrene differ in their mechanical properties from the corresponding block copolymers prepared by sequential monomer addition. Hadjichristidis et al. demonstrated that both shape and length of the taper define the properties of the copolymers and can be used to precisely adjust thermal and mechanical properties like the glass transition, T_g , and the order–disorder transition temperature, T_{ODT} .^{21,22} In elegant works of Epps and co-workers, deliberate manipulation of the tapered section was used to modify the nanosegregated morphologies both in bulk and in thin films.^{23–26} Alteration of the monomer gradient to manipulate the phase segregation and consequently macroscopic material properties requires the ability to adjust both length and shape of the gradient. Currently there are three approaches to manipulate the tapered section of I/S gradient copolymers: (i) the use of traces of THF as a randomizer, (ii) sequential addition of the pure monomers or monomer mixtures, and (iii) specific monomer addition protocols using automated syringes.^{20,21,25}

In this work we introduce a chemical approach to lower the reactivity of styrene, capitalizing on simple methyl substitution, aiming at deliberate manipulation of the gradient. For a detailed understanding of the impact on copolymerization kinetics and resulting copolymer structures, we have also reinvestigated the well-known copolymerization of I/S by *in situ* monitoring via ¹H NMR spectroscopy to compare it with the copolymerization of isoprene and 4-methylstyrene (4MS). *In situ* monitoring of a carbanionic copolymerization permits “mapping” the gradient structure of the growing copolymer chains. Especially near-infrared (NIR) and medium-infrared (MIR) in combination with UV–vis spectroscopy were employed for this purpose.^{27,28} In 2013, our group introduced real-time ¹H NMR kinetics studies as a key method to determine reactivity ratios in the living carbanionic polymerization of vinyl monomers.²⁹ Online monitoring of monomer consumption during the living polymerization in a sealed NMR tube enables the determination of the reactivity ratios by common evaluation methods like the Fineman–Ross, Kelen–Tüdös, and Meyer–Lowry approaches.^{30–32} The two reactivity ratios, r_1 and r_2 , for a monomer pair define the relative rates of homopolymerization vs crossover, i.e. copolymerization.³³ Since termination and transfer are absent in a living copolymerization, no compositional drift (nonhomogeneity of first order) is observed for the polymer chains formed. Instead, the comonomer composition along the chain reflects the reactivity ratios (nonhomogeneity of second order). Carbanionic copolymerization of isoprene and styrene (I/S) in a nonpolar medium, such as cyclohexane, represents this type of monomer system with markedly different reactivity ratios ($r_1 = 12.8$, $r_2 = 0.051$).^{18,27}

Here we present a fundamental study of the copolymerization of isoprene and 4-methylstyrene (4MS), with an in-depth characterization of the tapered block copolymers formed, capitalizing on *in situ* NMR kinetics, detailed kinetic calculations, kinetic Monte Carlo simulation, and DFT calculations. In this context, also the highly established monomer combination of isoprene and styrene is re-evaluated from a fundamental perspective. The combination of methods employed also sheds light on differences in comparison to block copolymers generated by sequential addition of the monomers isoprene and 4MS, demonstrating that the peculiar kinetics of the diene/styrene copolymerization has to be considered also for sequential block copolymer synthesis, particularly with respect to the succession of the synthesis of the respective blocks.

RESULTS AND DISCUSSION

Determination of Reactivity Ratios and Propagation Rate Constants Using Real-Time ¹H NMR. The determination of reactivity ratios for the statistical copolymerization commonly relies on terminating a series of polymerization reactions with different monomer feed at low conversion and characterization of the residual monomer concentration. Alternatively, samples can be withdrawn, while the polymerization proceeds.³⁴ Because of the high sensitivity of carbanions, this technique is not applicable to the living carbanionic copolymerization without irreversible termination of living chain ends.

Aiming at tapered block copolymers with a short gradient, we have studied the copolymerization of isoprene (I) with 4-methylstyrene (4MS), a readily available styrene derivative. For comparison, the reactivity ratios of copolymers of styrene (S) and isoprene were also determined in cyclohexane-*d*₁₂, using real-time ¹H NMR spectroscopy with *sec*-butyllithium as an initiator at 23 °C. The reactivity ratios determined from *in situ* NMR for styrene and isoprene ($r_1 = 11.0$, $r_2 = 0.049$, see Supporting Information Figures S1 and S2, Table S1) are in good agreement with literature values determined by other methods.^{16,18} In the case of copolymerization of 4MS, a styrene derivative with slightly enhanced electron density due to the methyl group, with isoprene highly divergent reactivity parameters ($r_1 = 25.4$, $r_{4MS} = 0.007$) were observed (Figures S3 and S4). For this monomer pair Figure 1 demonstrates the rapid incorporation of isoprene in the copolymers and formation of a second homopolymer block P4MS in the subsequent stage after full isoprene consumption.

Besides the reactivity ratios r_1 and r_2 , the homopolymerization rate constants play a crucial role in understanding the resulting gradient microstructure of the copolymers formed (*vide infra*). The homopolymerization rate constant of 4MS in cyclohexane-*d*₁₂ was also determined by real-time ¹H NMR spectroscopy in a sealed NMR tube at 23 °C. Taking into account that the P4MS chain ends are present as dimers, the propagation of 4MS can be described by the following kinetic equation in analogy to work of Fontanille et al.²⁷

$$\frac{d[4MS]}{dt} = k_{4MS}[4MS][P4MSLi]^{1/2} \quad (1.1)$$

After fast initiation the polymerization follows pseudo-first-order kinetics. Therefore, the apparent propagation rate constant, k , can be determined using a logarithmic representation of the measured values and linear regression (Figure S5, eqs 1.1 and 1.2).

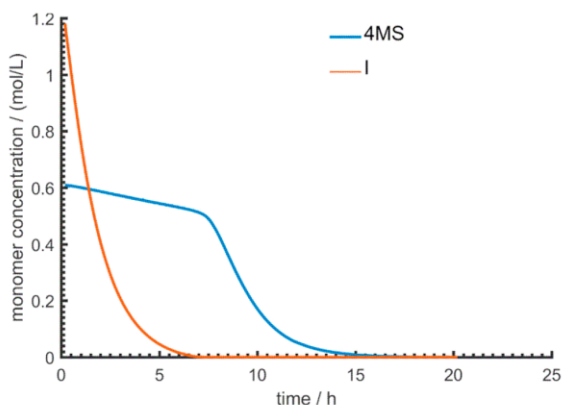


Figure 1. Plot of the single monomer concentrations versus time for the copolymerization of 4-methylstyrene (4MS, blue, $c_0 = 0.61$ mol/L) and isoprene (red, $c_0 = 1.18$ mol/L) in cyclohexane- d_{12} determined from *in situ* NMR monitoring.

$$\ln\left(\frac{[4MS]_0}{[4MS]_t}\right) = k_{4MS}[BuLi]_0^{1/2}t \quad (1.2)$$

The apparent propagation rate constant of 4MS ($k_{4MS} = 1.26 \times 10^{-3}$ (L/mol) $^{1/2}$ s $^{-1}$) was determined as well. The homopolymerization rate constant of styrene in cyclohexane at 40 °C ($k_{S,40^\circ C} = 2.4 \times 10^{-2}$ (L/mol) $^{1/2}$ s $^{-1}$) was reported by Fontanille et al.²⁷ Direct comparison of styrene and 4MS can be achieved by applying the Arrhenius equation using the reported activation energy and adjusting the rate constant of styrene k_S to 23 °C ($k_{S,23^\circ C} = 6.4 \times 10^{-3}$ (L/mol) $^{1/2}$ s $^{-1}$). Thus, the styrene homopolymerization rate is 5.1 times higher than the homopolymerization rate of 4MS. These different reactivities can be attributed to the small positive inductive effect of the methyl group in the *para* position, which both decreases monomer reactivity and increases the reactivity of the living chain end. This will be discussed in detail below.

DFT Calculations. To obtain theoretical insight into the effect of the *para*-methyl group on the reactivity of the styrene derivative 4MS, we performed DFT calculations of the polymerization pathway of styrene and 4MS. Since transition states are inaccessible for direct observation, e.g., by NMR spectroscopy, theoretical considerations by means of quantum chemical calculations can give valuable insight regarding the polymerization on a molecular level. In recent work, Morita and Van Beylen³⁴ reported an approach to model the total reaction pathway starting from poly(styryl)lithium dimers to form a monomer–poly(styryl)lithium precursor complex, the propagation transition state, and finally the extended polymer product. Following this approach, we performed DFT calculations (B3LYP-D3-gCP/def2-TZVP//B3LYP-D3-gCP/def2-TZVP) to investigate the reaction pathway of the homopolymerization both for styrene and 4MS. Furthermore, the reactions of both monomers with H–Li were calculated to compare the resulting partial charges as a rough estimate of monomer reactivities.

In line with expectation, styrene exhibits a lower partial charge ($-0.3686e$) at the vinyl β -carbon compared to 4MS ($-0.3751e$). This position is attacked in the propagation step and can therefore be used for an assessment of monomer reactivity (Figure 2). After addition of H–Li as a model

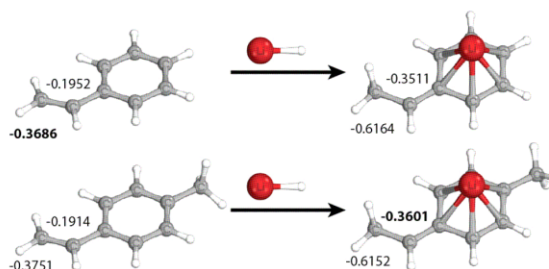


Figure 2. 3D representation of the reaction of styrene (top) and 4MS (bottom) with H–Li to form H–S–Li or H–4MS–Li, respectively. The annotated values show the corresponding partial charge calculated by the NBO method.^{35,36}

compound for carbanionic propagation, H–4MS–Li shows higher partial charge ($-0.3601e$) at the vinyl α -carbon compared to H–S–Li ($-0.3511e$). From these calculations styrene can be expected to be more easily attacked by nucleophiles, resulting in higher reactivity as compared to 4MS. In contrast, poly(4-methylstyryl)lithium (P4MS–Li) chain ends can be expected to be more reactive than poly(styryl)lithium chain (PS–Li) ends. These estimates can be further verified by investigating the reaction pathway for propagation of styrene and 4MS (Figure S6 and Table S2). As expected, unimeric H–4MS–Li shows higher dissociation energy than the corresponding H–S–Li unimer. Even though propagation transition states show similar activation energies, the homopolymerization of 4MS (51.1 kJ/mol) requires slightly higher activation energy for propagation as compared to styrene (50.1 kJ/mol). One has to take into account that these calculated energies are electronic energies only and do not include entropic or solvent effects. In case of the free energy a difference of 5.8 kJ/mol was calculated, which translates to a rate constant ratio of styrene to 4MS of approximately 10. We note that these calculations are in good agreement with our experimentally determined differences of the reactivity of styrene and 4MS.

Comparison of the Tapered Microstructure of 4MS/I and S/I Copolymers. The microstructure of 4MS/I and S/I copolymers, i.e., the shape and steepness of the taper plays a crucial role for the mechanical properties of the respective copolymers.^{21–23} Real-time 1H NMR kinetics gives access to the mean microstructure by determination of the resulting rate constants and mean incorporation rates.

Direct comparison of the copolymerization rate constants (Table 1) reveals that the probability for crossover from polyisoprenyllithium (PI–Li) chain ends toward styrene in the I/S system is approximately double compared to PI–Li and 4MS. On the other hand, the crossover from PS–Li to isoprene is 40% less probable than from P4MS–Li chain ends. This explains that in the case of the I/4MS monomer system the formation of long homosegments consisting of isoprene and 4MS is more likely, and therefore formation of a block copolymer with a steep monomer gradient (i.e., a short taper) can be expected.

The different gradient structures of I/S and I/4MS can be directly derived from the real-time 1H NMR kinetic measurements (Figure 3, Figures S1–S4). The overall mean monomer composition, F , versus total conversion reveals that in the initial stages primarily isoprene is consumed, and following a steep gradient, a pure block of P4MS is formed. Compared to the I/S

Table 1. Reaction Rate Constants for the S/I and 4MS/I Systems Determined from *in Situ* NMR

system	$10^{-4}k_{II}$ [(L/mol) ^{1/4} s ⁻¹]	$10^{-5}k_{I(4MS)S}$ [(L/mol) ^{1/4} s ⁻¹]	$10^{-3}k_{(4MS)S(4MS)S}$ [(L/mol) ^{1/2} s ⁻¹]	$k_{(4MS)SI}$ [(L/mol) ^{1/2} s ⁻¹]	r_1^b	$r_{(4MS)S}^b$
I/S ^a	6.12	5.57	6.39	0.121	11.0	0.053
I/4MS ^b	6.12	2.41	1.26	0.180	25.4	0.007

^aValues for styrene (k_{SS}) and isoprene (k_{II}) taken from Fontanille et al.²⁷ and corrected to 23 °C. ^bThis work.

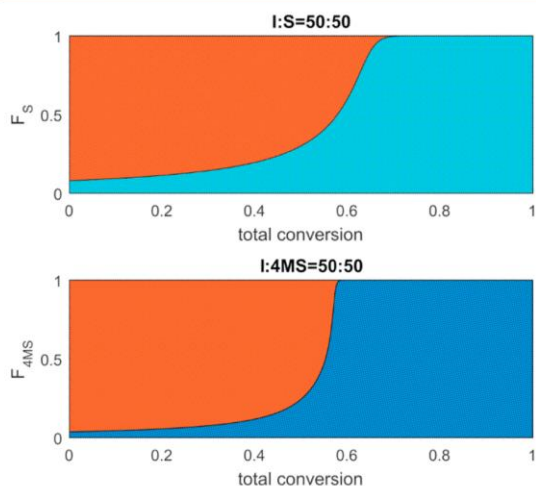


Figure 3. Reactivity ratios obtained from real-time ¹H NMR measurements enable to simulate plots of the monomer incorporation profiles of isoprene (red) and styrene (light blue) or 4MS (blue) versus total conversion, reflecting the mean composition (F) of the polymer chains formed.

system, the gradient of I/4MS copolymerization is considerably steeper (Figure 3, bottom).

The determined reactivity ratios permit to simulate monomer incorporation profiles for any monomer feed composition (cf. Figures S7 and S8 for different initial monomer feeds).

Kinetic Monte Carlo Simulation of the Formation of Tapered Block Copolymer Chains. Real-time ¹H NMR monitoring of copolymerization kinetics provides excellent access to the overall mean monomer composition in the polymer chains formed at any conversion throughout the living copolymerization. The Mayo–Lewis equation is a function of only two reactivity parameters and monomer concentrations.³³ From this globally derived equation no detailed insights regarding the monomer composition distribution can be extracted. In addition, the explicit sequence length distribution within the copolymers is not accessible with the currently available experimental methods. Broadbelt and co-workers developed a comprehensive kinetic Monte Carlo (KMC) model to describe the chemical composition distribution (CCD) and segment length distribution of copolymers by tracking the monomer-by-monomer sequence of each chain.³⁷ In particular, the segment length distribution can provide an excellent description of the gradient structure of copolymers. The KMC of the model of Broadbelt et al. was primarily developed for radical polymerization, taking into account termination reactions, but no aggregation phenomena. In contrast, in an ideal anionic copolymerization no termination is present, but the copolymerization kinetics of isoprene with styrene derivatives is strongly dependent on the aggregation behavior of the living chain ends. Worsfold and Bywater

proposed tetrameric aggregated PI–Li as the dominant species in nonpolar solvents at not extremely low chain-end concentration. For PS–Li chain ends the presence of a dimeric species is widely accepted.¹⁸ However, only unimeric chain ends, which form a dynamic equilibrium with their aggregated counterpart, are assumed to propagate. The following kinetic equations for copolymerization of 4MS and isoprene can be formulated in analogy to the equations for styrene and isoprene used by Fontanille et al. (Supporting Information Equation Set S2).²⁷ To reveal the exact structure of the gradient and define the length of the tapered section both in the S/I and 4MS/I copolymers, we developed a KMC model based on the kinetic equations (Equation Sets S1 and S2). This permits to illustrate the monomer-by-monomer sequence of each chain, thus enabling evaluation of mean segment length and segment length distribution. Because of the influence of initiator concentration, degree of polymerization and monomer ratio, copolymers consisting of 200 units each of isoprene and styrene (or 4MS, respectively) were selected as a typical sample to elucidate the structure of the gradient.

The segment length weight distribution is shown in Figure 4. The segment length is defined as the number of consecutive monomer units of one type without interruption by the other monomer unit. For both tapered block copolymers the noninterrupted isoprene homopolymer segments are rather small, i.e., below 50 (for I/S) or 100 (for I/4MS) units (Figure

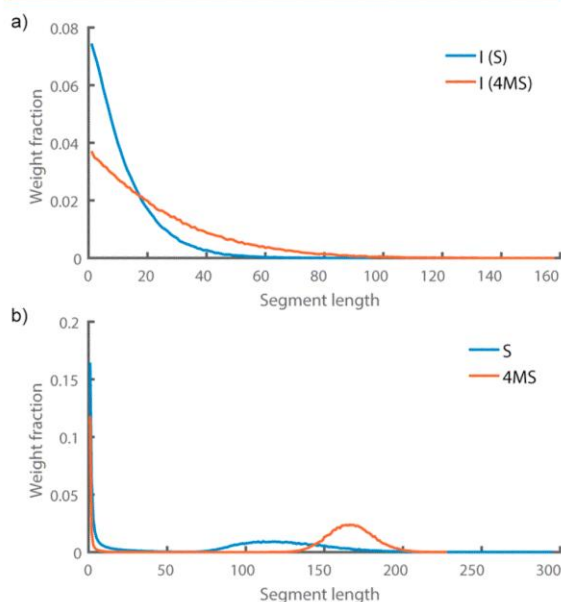


Figure 4. Plot of segment length weight distribution obtained from the KMC simulation for tapered copolymers of I/S (blue line) and I/4MS (red line): (a) distribution for isoprene; (b) distribution for styrene/4MS. Simulation conditions: $DP_n(I) = DP_n(S) = 200$.

5a) with a number-average at 4.6 (I/S) and 7.8 (I/4MS) (Table 2). The mean weight-average length of the isoprene segments is

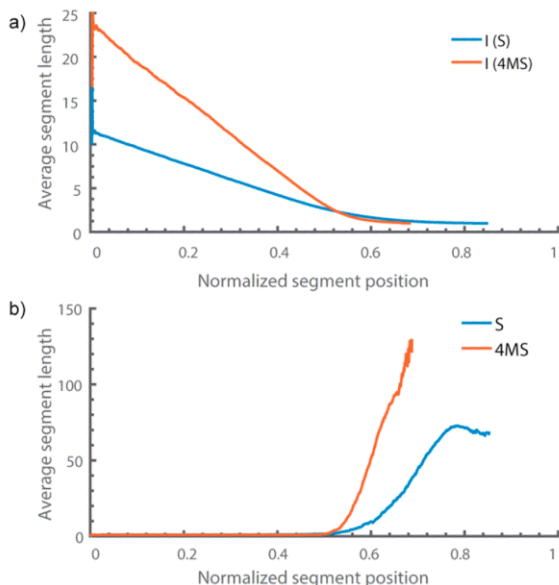


Figure 5. Plot of average segment length versus normalized segment position (relative position of the start of the segment) for I/S (blue lines) and I/4MS (red lines). (a) Plot for isoprene; (b) plot for styrene (blue) and 4MS (red).

11.9 for I/S and 23.9 for I/4MS. These segments are nearly exclusively interrupted by exactly one unit of S or 4MS (see bimodal distribution in Figure 5b with one maximum at $\langle N_{4MS} \rangle_w = 1$). The reason for this high discrepancy between number- and weight-average is initially in the copolymerization nearly all chains start with the largest isoprene segment (Figure 6). This is attributed to the ratio of the rates of isoprene homopolymerization, R_{II} , versus crossover reaction rate, R_{I4MS} (eqs 2.1 and 2.2, the same equations apply for styrene).

$$R_{II} = k_{II}[I][PILi]^{1/4} \quad (2.1)$$

$$R_{I4MS} = k_{I4MS}[4MS][PILi]^{1/4} \quad (2.2)$$

At the start of the reaction the monomer concentrations can be assumed to equal the initial monomer feed. Therefore, in the case of equivalent feed of comonomers, the initial segment length equals the reactivity ratio r_1 (eq 2.3).

$$\frac{R_{II}}{R_{I4MS}} = \frac{k_{II}}{k_{I4MS}} = r_1 \quad (2.3)$$

With increasing incorporation of isoprene, the average PI segment length decreases, leading to a gradient. Following the gradient part of the chain, a nearly pure block of P4MS (or PS,

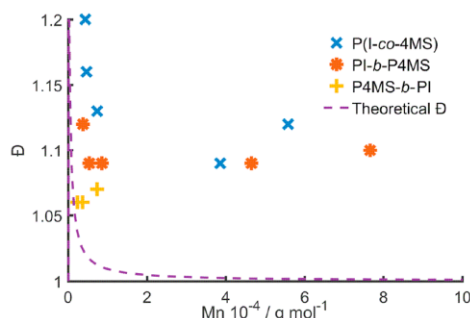


Figure 6. Dispersity D of prepared low to mid molecular weight ($M_n < 10^5$ g/mol) (block) copolymers with 50 mol % isoprene content versus molecular weight of the polymer.

respectively) is formed, which is only rarely interrupted by isoprene residues. In the case of styrene a mean weight-average of 80.4 and 141.3 units, respectively, for 4MS is calculated (Table 2). As shown in Figure 4b, the segment length distribution of S and 4MS is split into two separated parts consisting of either one unit or a distribution with a maximum of 166 units for 4MS and 115 for S. This leads to the conclusion that 4MS or S is mainly distributed as one large block at the end of the chains or as single units that disrupt the isoprene block. The segment length distribution of the 4MS block is less broadened compared to styrene in the I/S system. Considering these results, a shorter gradient and thus a highly blocklike copolymer are confirmed for the I/4MS system. Both the isoprene and 4MS homosegments are larger and less frequently interrupted.

Synthesis of Tapered and Sequential Block Copolymers of Isoprene and 4-Methylstyrene. Based on the kinetics and simulation results, several series of copolymers were prepared both in statistical copolymerization reactions and by conventional sequential monomer addition. Our observations regarding the monomer sequence motivate the fundamental question, whether the tapered I/4MS copolymers with the steep gradient determined by *in situ* NMR kinetics may actually be viewed as block copolymers rather than gradient structures. Commonly an enhancement of phase mixing of two incompatible blocks is observed with increasing gradient length. Shortening the tapered intermediate segment results in a reduced compatibilization effect, diminishing the differences between block copolymers and tapered copolymers prepared by statistical copolymerization.^{21,22,38} To elucidate the consequences of the blocklike nature of copolymers based on I/4MS, a comparison with the corresponding block copolymers synthesized by sequential monomer addition in two steps is important. Several gradient and block copolymers varying in composition and molecular weight were prepared by anionic copolymerization and examined by SEC, ¹H NMR, and DSC (Table 3 and Figures S9–S16 and Table S3). We emphasize that all polymers were prepared in a glovebox or in Schlenk

Table 2. Calculated Number-Average ($\langle N \rangle_n$) and Weight-Average ($\langle N \rangle_w$) Segment Lengths for Isoprene, Styrene, and 4MS Monomer Units Obtained from Monte Carlo Simulation

system	$\langle N_I \rangle_n$	$\langle N_I \rangle_w$	$\langle N_I \rangle_w / \langle N_I \rangle_n$	$\langle N_{4MS} \rangle_n$	$\langle N_{4MS} \rangle_w$	$\langle N_{4MS} \rangle_w / \langle N_{4MS} \rangle_n$
I/S	4.6	11.9	2.55	4.5	80.4	18.06
I/4MS	7.8	23.9	3.06	7.4	141.3	19.22

Table 3. One-Step Tapered Block Copolymers (-*co*-) and Sequential Block Copolymers (-*b*-) Based on Isoprene (I) and 4-Methylstyrene (4MS)

entry	polymer composition ^a	isoprene content [mol %]	target M_n [kg/mol]	$M_n(\text{SEC})^b$ [kg/mol]	$D = M_w / M_n$	v_1^c [%]	T_g^d (I/4MS) [°C]
1	P(I- <i>co</i> -4MS)	50	40	38.6	1.09	39	-50/86
2	PI- <i>b</i> -P4MS	50	40	46.5	1.09	41	-65/89
3	P(I- <i>co</i> -4MS)	30	60	76.3	1.12	24	-46/93
4	PI- <i>b</i> -P4MS	30	60	71.1	1.14	23	-70/97
5	P(I- <i>co</i> -4MS)	50	60	55.8	1.12	40	-51/102
6	PI- <i>b</i> -P4MS	50	60	76.6	1.10	39	-65/98
7	P(I- <i>co</i> -4MS)	50	400	360	1.07	40	-55/99
8	P(I- <i>co</i> -4MS)	60	130	133	1.09	50	-52/115
9	P(I- <i>co</i> -4MS)	90	1300	1250	1.32	86	-54/116
10	P(I- <i>co</i> -4MS)	50	2.5	4.4	1.20	29	26
11	PI- <i>b</i> -P4MS	50	2.5	3.8	1.12	30	-/-
12	P4MS- <i>b</i> -PI	50	2.5	2.4	1.06	40	20
13	P(I- <i>co</i> -4MS)	50	5	4.7	1.16	30	-15/21
14	PI- <i>b</i> -P4MS	50	5	5.4	1.09	36	-41/11
15	P4MS- <i>b</i> -PI	50	5	3.7	1.06	40	-47/6
16	P(I- <i>co</i> -4MS)	50	10	7.4	1.13	38	-31/16
17	PI- <i>b</i> -P4MS	50	10	8.6	1.09	39	-43/21
18	P4MS- <i>b</i> -PI	50	10	7.4	1.07	39	-43/23

^aPolymer composition and preparation route with targeted isoprene/4MS content; ^b sequential addition; ^c *co* direct copolymerization. ^d Size exclusion chromatography (SEC) in THF at 25 °C. ^e Calculated volume fractions based on densities from ref 39. ^f Via differential scanning calorimetry (DSC).

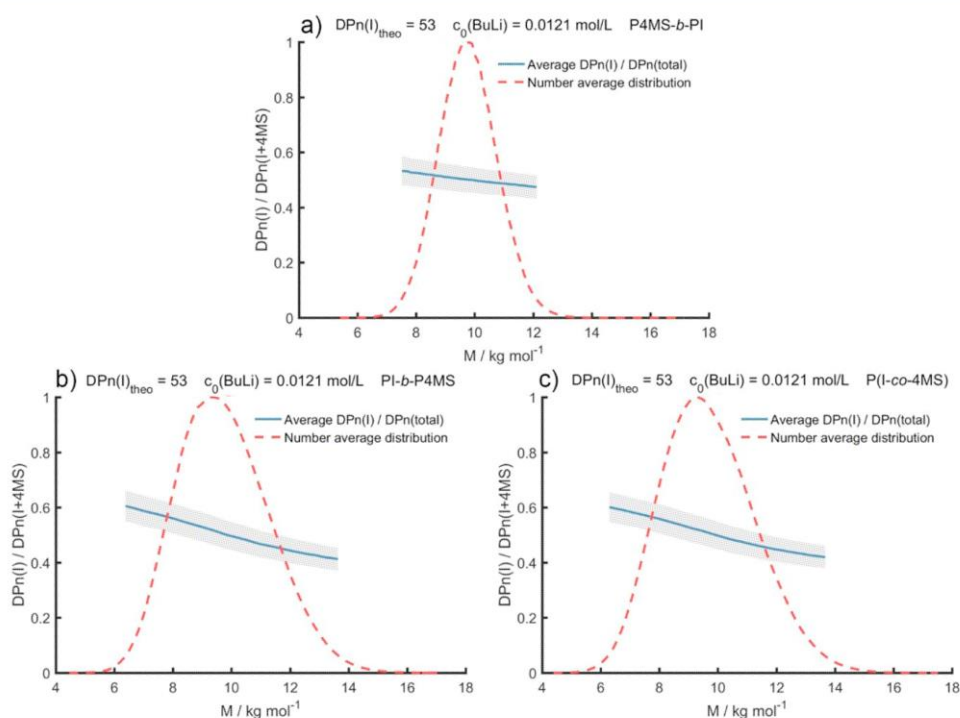


Figure 7. Average ratio of the degree of polymerization of isoprene ($DP_n(I)$) to the total DP_n (blue) versus total molecular weight, simulated for the synthesized samples with molecular weights of 10 kg/mol (Table 3). The shaded area shows the standard deviation of the average $DP_n(I)/DP_n(\text{total})$ ratio. The red curve shows the normalized number-average distribution of the simulated copolymers. (a) Sequential addition of (i) 4MS followed by (ii) isoprene; (b) sequential addition of (i) isoprene followed by (ii) 4MS. (c) Statistical copolymerization of 4MS and isoprene to form a tapered block copolymer.

flasks, avoiding high-vacuum or break-seal techniques. Except for the low molecular weight samples 10–12 all examined copolymers exhibit two glass transitions, indicating phase

separation, regardless of their synthesis in a statistical one-pot or sequential (i.e., conventional) two-step copolymerization, as summarized in Table 3.

Comparison of Synthetic Approaches for the Preparation of I/4MS Copolymers. As shown in Figure 6, the different synthetic approaches for the block copolymer synthesis lead to a significant effect on the resulting molecular weight distribution, leading to a distinct deviation from an ideal Poisson distribution (dashed line). Only when the P4MS block is prepared first, followed by consecutive addition of isoprene to generate P4MS-*b*-PI, low dispersities approaching the theoretical limit are obtained. Both for the direct copolymerization of isoprene with 4MS and for the sequential addition of 4MS to a living poly(isoprenyl)lithium block broadening of the molecular weight distribution is observed. To shed light on these observations, we considered the initiation step of the second P4MS or PI block and the crossover reaction from an isoprene chain-end toward 4MS based on the kinetic equations, employing kinetic Monte Carlo simulation (*vide infra*).

One key requirement for a narrow molecular weight distribution is that the initiation rate is considerably faster than the rate of chain propagation, as it was shown mathematically by Gold long ago.⁴⁰ Slow initiation leads to broadening of the molecular weight distribution, depending on the ratio k_i/k_p and the desired DP_n . Considering the crossover rate constants versus the homopolymerization rate constants of isoprene and 4MS (Table 1), fast initiation of the second block only occurs for the crossover starting from a living P4MS-Li block to the isoprene monomer. In this case the rate of initiation is approximately 300 times faster than the propagation rate ($k_{11}/k_{4MS1} = 294$), ensuring conditions of a controlled polymerization for both blocks.

One has to consider that every direct copolymerization of two monomers with strongly differing reactivity ratios exhibits low crossover rates to the less favored monomer. Assuming reasonable propagation rates of both monomers on same order of magnitude, this inevitably leads to slow initiation rate compared to the propagation rate (k_{12}/k_{22}) (eqs 3.1 and 3.2), thus hampering the controlled nature of an anionic polymerization.

$$r_1 = \frac{k_{11}}{k_{12}} \gg 1 \quad \text{and} \quad k_{11} \approx k_{22} \quad (3.1)$$

$$\frac{1}{r_1} = \frac{k_{12}}{k_{11}} \approx \frac{k_{12}}{k_{22}} \ll 1 \quad (3.2)$$

Monomer Composition Distribution. To further elaborate via theoretical approaches whether tapered block copolymers of isoprene and 4MS obtained by statistical copolymerization can be compared to block copolymers prepared by common sequential monomer addition, we utilized our developed KMC model to predict the monomer composition distribution. In addition, we aim at elucidating to which extent the polymerization of the second block is controlled.

The simulated monomer compositions of the three different synthesis approaches are shown in Figure 7 and clearly demonstrate that the order of the monomer additions—diene or styrene derivative first—plays a crucial role. As expected, the 4MS-first approach produces a narrow molecular weight distribution of 4MS and isoprene with nearly invariant monomer composition ($DP_n(I)/DP_n(\text{total}) \sim 0.5$) (Figure 7a). The dispersity of the P4MS block calculated from the simulation displayed in Figure 7 is 1.02 for a sequential copolymerization, when the P4MS block is prepared first (rapid

crossover). However, if the PI block is generated first, the sequential approach leads to a simulated dispersity of 1.056 for the P4MS block. Remarkably, this is exactly the same result as obtained for the direct (statistical) copolymerization of the equimolar I/4MS mixture.

The mean isoprene content of the P4MS-*b*-PI block copolymer exhibits only a subtle change as a function of molecular weight. The ideal living anionic copolymerization should lead to an invariant mean monomer composition of the copolymer without any dependence on the molecular weight. Only in this ideal case the distribution of monomer units changes within the chain in dependence on the reactivity ratios. However, in both Figures 7b and 7c broadened molecular weight distributions are observed, in agreement with the experimental results. A distinct drift of the chemical monomer composition over the molecular weight can be seen. It is remarkable that virtually no difference of the molecular weight distribution and the respective drift of the monomer composition between the statistical copolymerization of 4MS and isoprene and the sequential addition of 4MS to a PILi macroinitiator is detectable. Thus, the direct copolymerization of 4MS and isoprene may be considered to be initiated by a PILi macroinitiator that is interrupted by 4MS in several places but essentially follows the same kinetics as the conventional two-step approach. In both cases the crossover rate is rather slow (see Table 1). Therefore, not all chains start their growth at the same time to form the second P4MS block. This leads to inhomogeneous growth of the P4MS block, resulting in increased 4MS content at higher molecular weights. Because of statistics and mass conservation, some chains lack 4MS and therefore show increased isoprene content and lower molecular weights.

The compositional drift resulting from the slow crossover from PI-Li to 4MS can also be evaluated by comparing the distribution of isoprene and 4MS units to an ideal Poisson distribution (Figure 9). The distributions have been simulated for three synthesized polymers with a molecular weight of 2.5, 5, and 10 kg/mol according to the experimental conditions. In all cases isoprene polymerization affords a Poisson distribution. The distributions of 4MS are broader than the ideal Poisson distribution except for the case of P(4MS-*b*-1), leading to a broadened overall molecular weight distribution. This is also observed experimentally by slightly increased dispersity values (Figure 6 and Table 3, see above) of these polymers. Comparing experimental values with simulation results, one has to consider that at higher molecular weights increased polydispersity indices are also influenced by impurities in addition to kinetic effects.

Effect of the Degree of Polymerization on the Molecular Weight Distribution. According to the Poisson distribution the dispersity of polymers made by a living polymerization decreases with increasing degree of polymerization. In our polymer syntheses we observed that especially at low molecular weights (samples 10, 13, and 16; Table 3) the obtained molecular weight distributions are broader than expected, which we ascribe to the kinetic effects described above. To investigate the influence of the degree of polymerization on the dispersity, we simulated the monomer composition of the statistical copolymerization of I/S and I/4MS, using the KMC model for different degrees of polymerization at an initial initiator concentration of 10^{-3} mol/L (see Figures S17 and S18 for number-average molecular

weight distribution and average monomer composition in dependency of the molecular weight).

As expected, the simulated dispersity decreases with increasing molecular weight of the copolymers (Figure 9). This is in good agreement with the experimental findings in Table 3 and Figure 8. In all considered cases the dispersity of

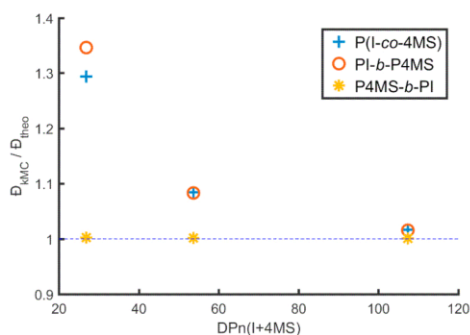


Figure 8. Comparison of the dispersity of the simulated monomer distribution (D_{MMC}) with ideal Poisson distribution (D_{theo}) versus degree of polymerization DP_n according to the synthesized polymers with molecular weights of 2.5, 5, and 10 kg/mol (Table 3). A ratio of 1 equals the dispersity in an ideal living anionic polymerization.

copolymers of 4MS is superior to the dispersity obtained for those of styrene. In contrast to styrene in the I/S system, 4MS nearly approaches an ideal Poisson distribution at degrees of polymerization exceeding 200 (Figure 9). This can be

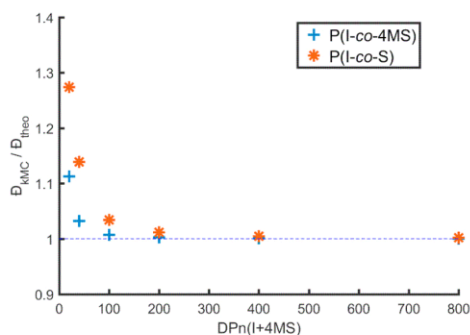


Figure 9. Comparison of simulated dispersities, D_{MMC} , with those of ideal Poisson distribution, D_{theo} , versus final degree of polymerization at an initial initiator concentration of 10^{-3} mol/L. A ratio of unity represents an ideal living anionic polymerization.

rationalized by the lower homopolymerization rate constant of 4MS in comparison to styrene, thus increasing the controlled nature of the polymerization by the higher ratio of initiation rate versus propagation rate.

Influence of Initiator and Monomer Concentration.

During our kinetic simulations, we unexpectedly observed an influence of the initial initiator concentration on the resulting monomer composition distribution at a constant degree of polymerization. As shown in Figure 10, with increasing initial initiator concentration the deviation from an ideal Poisson distribution increases (Figure S19). Even though the overall deviation is rather small as compared to the influence of the targeted DP_n and the respective synthetic approach, as

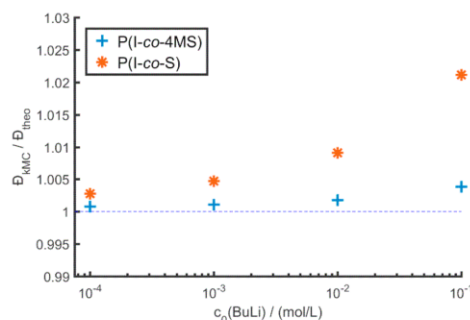


Figure 10. Comparison of simulated dispersity, D_{MMC} , to the ideal Poisson distribution versus initial initiator concentration (simulation conditions: $DP_n(I) = DP_n(4MS) = DP_n(S) = 200$). A ratio of unity equals ideal living anionic polymerization. The concentration of 10^{-1} mol/L is only shown as a reference and cannot be obtained experimentally due to maximum bulk concentration.

discussed before, the 4MS/I system shows a lower dependence on the concentration compared to the copolymerization of styrene with isoprene.

We performed a mathematical derivation for the simplified case of sequential addition. The ratio of initiation from a PILi chain end as a macroinitiator and propagation rate of 4MS can be defined as $\alpha_{\text{PILi} \rightarrow 4\text{MS}} = R_{\text{I}4\text{MS}}/R_{4\text{MS}4\text{MS}}$. By simplifying the equations (see Supporting Information Equation Set S3 for the complete derivation), it can be shown that this ratio of initiation to propagation rate is independent of any monomer concentration:

$$\frac{\alpha_{\text{PILi} \rightarrow 4\text{MS}}([\text{PILi}]_1)}{\alpha_{\text{PILi} \rightarrow 4\text{MS}}([\text{PILi}]_2)} = \left(\frac{[\text{PILi}]_1}{[\text{PILi}]_2} \right)^{-1/4} \quad (4.1)$$

Consequently, with a 10-fold dilution the rate of initiation to propagation increases by approximately 1.7 times (Figure S20a). As a direct result the control over the polymerization of the second block is improved, leading to narrowing of the monomer distribution. The inverse approach of isoprene addition to a P4MSLi macroinitiator can be derived analogously (Figure S20b). In this case a 10-fold dilution decreases the ratio of initiation to propagation rate by a factor of approximately 0.6.

$$\frac{\alpha_{\text{P4MSLi} \rightarrow 1}([\text{P4MSLi}]_1)}{\alpha_{\text{P4MSLi} \rightarrow 1}([\text{P4MSLi}]_2)} = \left(\frac{[\text{P4MSLi}]_1}{[\text{P4MSLi}]_2} \right)^{1/4} \quad (4.2)$$

We emphasize that this scaling behavior is independent of reactivity ratios and monomer concentrations and is valid for every system where one chain end forms dimeric and the other forms tetrameric chain ends.

Consequences for the Design of Tapered Block Copolymers. The formation of tapered block copolymers is affected by various experimental parameters. As shown in this work, the small inductive effect of one methyl group on going from styrene to 4MS changes the system significantly. The ratio of initiation and propagation rates plays an important role to obtain chemically homogeneous, tapered block copolymers with narrow size distribution. However, this ratio is inherently low for monomers with divergent reactivity ratios. In the previous paragraphs we have demonstrated that high molecular weights and high dilution of the polymerization solutions are

favorable to increase control of the copolymerization and to obtain well-defined tapered block copolymers. However, at very high dilution the presence of impurities may not be negligible, particularly when relying on carbanionic techniques. As a good starting point, an initiator concentration of 10^{-4} mol/L and a targeted degree of polymerization of at least 200 monomers per block are recommended, based on our simulation results. We believe that these fundamental results derived at the example of the I/4MS system are generally valid for the copolymerization of styrene derivatives with diene monomers like isoprene or butadiene.

Thermal Properties and Segregated Morphologies of the Tapered Copolymers. A comparison of the glass transitions for block and gradient copolymers shows negligible differences for the higher glass transition temperature, $T_{g,4MS}$, as expected due to the homopolymer nature of this block in the tapered block copolymers. Larger differences are found for $T_{g,I}$. An increase of the $T_{g,I}$ for the PI block in gradient copolymers (-50 °C vs -65 °C to -70 °C for PI homopolymer in sequential block copolymers) is attributed to the incorporation of the 4MS monomer in the PI segment, as already detailed in the simulations above.

We emphasize that in this work we do not present a comprehensive study of the morphology of all polymer samples prepared, but rather show some typical results obtained for selected samples to illustrate the potential of the I/4MS copolymerization. Microphase-segregated morphologies, well-known for I/S block copolymers, were obtained by varying the molecular weight and isoprene content (Figure 11 and Figure

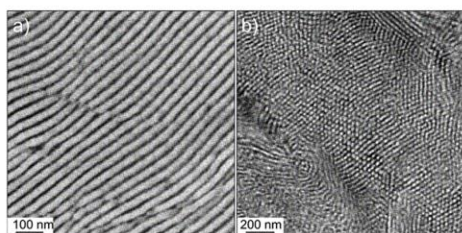


Figure 11. Typical TEM micrographs of I/4MS tapered block copolymers: (a) P(I-co-4MS) (entry 13 in Table S3), lamellae, lamellar distance 14.8 nm; (b) P(I-co-4MS) (entry 3 in Table 3), hexagonal cylinder morphology, cylinder diameter 11.8 nm. PI was stained with OsO_4 .

S21). Both parameters determine phase separation in the same manner as known for PI-block-PS diblock copolymers.⁴¹ PI/P4MS can be reasonably assumed to exhibit a similar Flory–Huggins interaction parameter as PI/PS and thus a similar phase diagram. This behavior supports the concept of a “one-pot block copolymer synthesis” put forward in this work for the I/4MS system. Detailed morphological characterization will be reported elsewhere.

This also leads to the question whether there are advantages for a one-pot synthesis of block copolymers as opposed to the highly established sequential procedures. Obviously, the preparation of ultrahigh molecular weight block copolymers by sequential addition of monomers represents a difficult task, since the extremely low concentration of sensitive carbanionic chain ends does not permit to introduce a second monomer in the reaction vessel without significant chain termination, necessitating a one-pot strategy. In this case direct statistical

copolymerization like in the case of the I/4MS systems is highly favored.

Tapered block copolymers featuring overall molecular weights as high as 1.25×10^6 g/mol were accessible as determined by SEC vs PS standards (see Table 3 and Figure 12a). First studies of the morphology of the tapered block

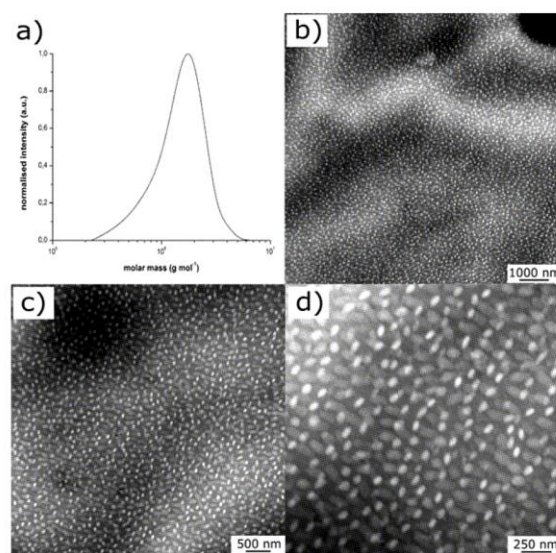


Figure 12. (a) Molecular weight distribution of gradient block copolymer P(I-co-4MS) with 16 wt % 4MS (entry 9 in Table 3) obtained by SEC vs. PS standards. (b–d) TEM micrographs showing spherical domains; PI was stained with OsO_4 .

copolymer with an overall number-average molecular weight of 1.25×10^6 g/mol, featuring a volume fraction of 86% I and 14% 4MS, are given in Figure 12b–d. The spherical domains correspond to the P4MS blocks, while the dark matrix represents PI (staining with osmium tetroxide). It has to be mentioned that the observable P4MS spherical domains exhibit an average diameter of ca. 90 nm, which is larger than the thin slices prepared by ultramicrotomy (ca. 50 nm). For this reason, deformation of the spherical domains occurs during the cutting procedure, as seen in image Figure 12d. However, all images evidence phase segregation into large spherical domains for the ultrahigh molecular weight block copolymers (UHMW BC). A detailed study of the properties of such systems is reported separately.⁴²

CONCLUSIONS

This combined experimental and simulation work introduces the one-step synthesis of tapered block copolymers from isoprene and 4-methylstyrene (4MS) in cyclohexane by statistical living anionic copolymerization. Detailed understanding of the monomer gradient was achieved via real-time NMR kinetics, determined from the monomer consumption during copolymerization, DFT calculations, and kinetic Monte Carlo simulation. To the best of our knowledge, no example of a kinetic Monte Carlo model has been applied to the living carbanionic copolymerization to date, considering both the tetrameric polyisoprenyllithium and dimeric poly(styryl)lithium chain ends. We demonstrate that for the I/4MS system in a

statistical copolymerization a very short tapered midblock is formed as a consequence of the markedly different reactivity ratios ($r_1 = 25.4$, $r_{4MS} = 0.007$). In all cases considered, the I/4MS system shows better controlled monomer distribution compositions and a shorter gradient structure in comparison to the established isoprene/styrene (I/S) copolymerization. The polyisoprene segments are less frequently interrupted by 4MS units compared to the I/S copolymerization. The results emphasize the striking effect of a methyl group in the para-position of styrene on the reactivity ratios in nonpolar media as well as its effect of significantly lowering the dispersity of the I/4MS copolymers in comparison to the I/S copolymers.

The potential of this one-pot strategy for block copolymer synthesis has been demonstrated at the example of a series of tapered block copolymers from low to ultrahigh molecular weight materials with molecular weights exceeding 10^6 g/mol. We emphasize that high-vacuum or break-seal techniques were avoided in all cases; thus, the syntheses can be conveniently scaled up. For comparison, copolymers were also synthesized by the two possible sequential (i.e., conventional two-step) approaches starting both from 4MS and isoprene.

Finally, we emphasize the general nature of the results: we believe that the influence of both initiator concentration and targeted degree of polymerization are generally valid for every system combining a diene monomer like isoprene or butadiene and a styrene derivative. These monomer combinations play a key role for well-known and industrially established thermoplastic elastomers (TPEs). We emphasize that the direct copolymerization essentially follows the same kinetics as the two-step approach; i.e., no significant difference can be detected in monomer composition distribution, thermal properties, and phase segregation behavior, if the flexible PI block is prepared first, since the slow crossover to the styrene monomer leads to broadening of the molecular weight distribution. It is obvious that the direct copolymerization of isoprene and 4-methylstyrene holds great promise for a large variety of complex polymer architectures, since the block structures formed remain living and permit further addition of monomers or monomer mixtures, greatly simplifying for instance the synthesis of well-defined high molecular weight multiblock copolymers. The impact of the one-step method for a variety of complex block copolymer architectures and in particular for high molecular weight multiblock copolymers will be presented in a forthcoming work.

■ ASSOCIATED CONTENT

Supporting Information

The Supporting Information is available free of charge on the ACS Publications website at DOI: 10.1021/acs.macromol.8b00404.

Polymerization methods, synthetic details, equations used for the kinetic Monte Carlo (KMC) calculations, parameters of DFT calculations, *in situ* NMR characterization and further characterization of the resulting copolymers (PDF)

■ AUTHOR INFORMATION

Corresponding Authors

*E-mail: hfrey@uni-mainz.de (H.F.).

*E-mail: muellax@uni-mainz.de (A. H. E. M.).

*E-mail: M.Gallei@MC.tu-darmstadt.de (M. G.).

ORCID

Markus Gallei: 0000-0002-3740-5197

Holger Frey: 0000-0002-9916-3103

Author Contributions

E.G. and T.J. contributed equally.

Notes

The authors declare no competing financial interest.

■ REFERENCES

- (1) Hadjichristidis, N.; Iatrou, H.; Pitsikalis, M.; Mays, J. Macromolecular architectures by living and controlled/living polymerizations. *Prog. Polym. Sci.* **2006**, *31*, 1068–1132.
- (2) Tanaka, S.; Goseki, R.; Ishizone, T.; Hirao, A. Synthesis of Well-Defined Novel Reactive Block Polymers Containing a Poly(1,4-divinylbenzene) Segment by Living Anionic Polymerization. *Macromolecules* **2014**, *47*, 2333–2339.
- (3) Kim, H.-C.; Park, S.-M.; Hinsberg, W. D. Block Copolymer Based Nanostructures: Materials, Processes, and Applications to Electronics. *Chem. Rev.* **2010**, *110*, 146–177.
- (4) Park, C.; Yoon, J.; Thomas, E. L. Enabling nanotechnology with self assembled block copolymer patterns. *Polymer* **2003**, *44*, 6725–6760.
- (5) Bates, C. M.; Bates, F. S. 50th Anniversary Perspective: Block Polymers - Pure Potential. *Macromolecules* **2017**, *50*, 3–22.
- (6) Stefik, M.; Mahajan, S.; Sai, H.; Epps, T. H.; Bates, F. S.; Gruner, S. M.; Disalvo, F. J.; Wiesner, U. Ordered three- and five-ply nanocomposites from ABC block terpolymer microphase separation with niobia and aluminosilicate sols. *Chem. Mater.* **2009**, *21*, 5466–5473.
- (7) Schacher, F. H.; Rupa, P. A.; Manners, I. Functional Block Copolymers: Nanostructured Materials with Emerging Applications. *Angew. Chem., Int. Ed.* **2012**, *51*, 7898–7921.
- (8) Ma, H.; Wang, Q.; Sang, W.; Han, L.; Liu, P.; Chen, J.; Li, Y.; Wang, Y. Synthesis of Bottlebrush Polystyrenes with Uniform, Alternating, and Gradient Distributions of Brushes Via Living Anionic Polymerization and Hydrosilylation. *Macromol. Rapid Commun.* **2015**, *36*, 726–732.
- (9) Lee, J. H.; Kim, Y.; Cho, J.-Y.; Yang, S. R.; Kim, J. M.; Yim, S.; Lee, H.; Jung, Y. S. In Situ Nanolithography with Sub-10 nm Resolution Realized by Thermally Assisted Spin-Casting of a Self-Assembling Polymer. *Adv. Mater.* **2015**, *27*, 4814–4822.
- (10) Kraus, G.; Childers, C. W.; Gruver, J. T. Properties of random and block copolymers of butadiene and styrene. I. Dynamic properties and glassy transition temperatures. *J. Appl. Polym. Sci.* **1967**, *11*, 1581–1591.
- (11) Knoll, K.; Nießner, N. Styrolux and styroflex from transparent high impact polystyrene to new thermoplastic elastomers. *Macromol. Symp.* **1998**, *132*, 231–243.
- (12) Angelo, R. J.; Ikeda, R. M.; Wallach, M. L. Multiple glass transitions of block polymers. *Polymer* **1965**, *6*, 141–156.
- (13) Ito, S.; Goseki, R.; Ishizone, T.; Hirao, A. Successive synthesis of well-defined multiarmed miktoarm star polymers by iterative methodology using living anionic polymerization. *Eur. Polym. J.* **2013**, *49*, 2545–2566.
- (14) Ntaras, C.; Polymeropoulos, G.; Zapsas, G.; Ntetsikas, K.; Lontos, G.; Karanastasis, A.; Moschovas, D.; Rangou, S.; Stewart-Sloan, C.; Hadjichristidis, N.; Thomas, A.; Avgeropoulos, A. Synthesis, characterization and self-assembly of well-defined linear heptablock quaterpolymers. *J. Polym. Sci., Part B: Polym. Phys.* **2016**, *54*, 1443–1449.
- (15) Zaremski, M. Y.; Kalugin, D. I.; Golubev, V. B. Gradient copolymers: Synthesis, structure, and properties. *Polym. Sci., Ser. A* **2009**, *51*, 103–122.
- (16) Zelinski, R.; Childers, C. W. Linear Elastomeric Block Polymers. *Rubber Chem. Technol.* **1968**, *41*, 161–181.
- (17) van Beylen, M.; Bywater, S.; Smets, G.; Szwarc, M.; Worsfold, D. J. Developments in anionic polymerization - A critical review. In

Polysiloxane Copolymers/Anionic Polymerization; Springer: Berlin, 1988; pp 87–143.

(18) Worsfold, D. J. Anionic copolymerization of styrene and isoprene in cyclohexane. *J. Polym. Sci., Part A-1: Polym. Chem.* **1967**, *5*, 2783–2789.

(19) Hashimoto, T.; Tsukahara, Y.; Tachi, K.; Kawai, H. Structure and properties of tapered block polymers. 4. “Domain-boundary mixing” and “mixing-in-domain” effects on microdomain morphology and linear dynamic mechanical response. *Macromolecules* **1983**, *16*, 648–657.

(20) Hashimoto, T.; Shibayama, M.; Kawai, H. Domain-boundary structure of styrene-isoprene block copolymer films cast from solution. 4. Molecular-weight dependence of lamellar microdomains. *Macromolecules* **1980**, *13*, 1237–1247.

(21) Hodrokoukes, P.; Floudas, G.; Pispas, S.; Hadjichristidis, N. Microphase Separation in Normal and Inverse Tapered Block Copolymers of Polystyrene and Polyisoprene. 1. Phase State. *Macromolecules* **2001**, *34*, 650–657.

(22) Hodrokoukes, P.; Pispas, S.; Hadjichristidis, N. Controlling Micellar Properties of Styrene/Isoprene Copolymers by Altering the Monomer Arrangement along the Chain. *Macromolecules* **2002**, *35*, 834–840.

(23) Luo, M.; Brown, J. R.; Remy, R. A.; Scott, D. M.; Mackay, M. E.; Hall, L. M.; Epps, T. H., III Determination of Interfacial Mixing in Tapered Block Polymer Thin Films: Experimental and Theoretical Investigations. *Macromolecules* **2016**, *49*, 5213–5222.

(24) Morris, M. A.; Gartner, T. E.; Epps, T. H., III Tuning Block Polymer Structure, Properties, and Processability for the Design of Efficient Nanostructured Materials Systems. *Macromol. Chem. Phys.* **2017**, *218*, 1600513.

(25) Roy, R.; Park, J. K.; Young, W.-S.; Mastroianni, S. E.; Tureau, M. S.; Epps, T. H. Double-Gyroid Network Morphology in Tapered Diblock Copolymers. *Macromolecules* **2011**, *44*, 3910–3915.

(26) Luo, M.; Epps, T. H., III Directed Block Copolymer Thin Film Self-Assembly: Emerging Trends in Nanopattern Fabrication. *Macromolecules* **2013**, *46*, 7567–7579.

(27) Quinebèche, S.; Navarro, C.; Gnanou, Y.; Fontanille, M. In situ mid-IR and UV-visible spectroscopies applied to the determination of kinetic parameters in the anionic copolymerization of styrene and isoprene. *Polymer* **2009**, *50*, 1351–1357.

(28) Long, T. E.; Liu, H. Y.; Schell, B. A.; Teegarden, D. M.; Uerz, D. S. Determination of solution polymerization kinetics by near-infrared spectroscopy. 1. Living anionic polymerization processes. *Macromolecules* **1993**, *26*, 6237–6242.

(29) Natalello, A.; Werre, M.; Alkan, A.; Frey, H. Monomer Sequence Distribution Monitoring in Living Carbanionic Copolymerization by Real-Time ¹H NMR Spectroscopy. *Macromolecules* **2013**, *46*, 8467–8471.

(30) Meyer, V. E.; Lowry, G. G. Integral and differential binary copolymerization equations. *J. Polym. Sci., Part A: Gen. Pap.* **1965**, *3*, 2843–2851.

(31) Fineman, M.; Ross, S. D. Linear method for determining monomer reactivity ratios in copolymerization. *J. Polym. Sci.* **1950**, *5*, 259–262.

(32) Kelen, T.; Tüdös, F. A new improved linear graphical method for determining copolymerization reactivity ratios. *React. Kinet. Catal. Lett.* **1974**, *1*, 487–492.

(33) Mayo, F. R.; Lewis, F. M. Copolymerization. I. A Basis for Comparing the Behavior of Monomers in Copolymerization; The Copolymerization of Styrene and Methyl Methacrylate. *J. Am. Chem. Soc.* **1944**, *66*, 1594–1601.

(34) Morita, H.; van Beylen, M. New Vistas on the Anionic Polymerization of Styrene in Non-Polar Solvents by Means of Density Functional Theory. *Polymers* **2016**, *8*, 371.

(35) Reed, A. E.; Weinstock, R. B.; Weinholt, F. Natural population analysis. *J. Chem. Phys.* **1985**, *83*, 735–746.

(36) Nikolaienko, T. Y.; Bulavin, L. A.; Hovorun, D. M. JANPA: An open source cross-platform implementation of the Natural Population

Analysis on the Java platform. *Comput. Theor. Chem.* **2014**, *1050*, 15–22.

(37) Cho, A. S.; Broadbelt, L. J. Stochastic modelling of gradient copolymer chemical composition distribution and sequence length distribution. *Mol. Simul.* **2010**, *36*, 1219–1236.

(38) Tsukahara, Y.; Nakamura, N.; Hashimoto, T.; Kawai, H.; Nagaya, T.; Sugimura, Y.; Tsuge, S. Structure and Properties of Tapered Block Polymers of Styrene and Isoprene. *Polym. J.* **1980**, *12*, 455–466.

(39) Wu, L.; Lodge, T. P.; Bates, F. S. Bridge to Loop Transition in a Shear Aligned Lamellae Forming Heptablock Copolymer. *Macromolecules* **2004**, *37*, 8184–8187.

(40) Gold, L. Statistics of Polymer Molecular Size Distribution for an Invariant Number of Propagating Chains. *J. Chem. Phys.* **1958**, *28*, 91–99.

(41) Khandpur, A. K.; Foerster, S.; Bates, F. S.; Hamley, I. W.; Ryan, A. J.; Bras, W.; Almdal, K.; Mortensen, K. Polyisoprene-Polystyrene Diblock Copolymer Phase Diagram near the Order-Disorder Transition. *Macromolecules* **1995**, *28*, 8796–8806.

(42) Appold, M.; Grune, E.; Frey, H.; Gallei, M. One-Step Anionic Copolymerization Enables Formation of Linear Ultra-High Molecular Weight Block Copolymer Films Featuring Vivid Structural Colors in the Bulk State. *ACS Appl. Mater. Interfaces*, in revision.

Supporting Information

One-Step Block Copolymer Synthesis versus Sequential Monomer Addition: A Fundamental Study Reveals that one Methyl Group Makes a Difference

Eduard Grune,^{a,c} Tobias Johann,^{a,d} Michael Appold,^b Christian Wahlen,^a Jan Blankenburg,^{a,c}
Daniel Leibig,^{a,c} Axel H. E. Müller,^{*a} Markus Gallei,^{*b} Holger Frey^{*a}

^a Institute of Organic Chemistry, Johannes Gutenberg-University, Duesbergweg 10-14, 55128 Mainz (Germany); E-mail: hfrey@uni-mainz.de

^b Macromolecular Chemistry Department, Technische Universität Darmstadt, Alarich-Weiss Str. 4, 64287 Darmstadt (Germany)

^c Graduate School Material Science in Mainz, Staudinger Weg 9, 55128, Mainz (Germany)

^d Max Planck Graduate Center, Staudinger Weg 9, 55128, Mainz (Germany)

The first two authors contributed equally

1. Experimental Procedures

Materials: All chemicals and solvents were purchased from Acros Organics Co. and Sigma-Aldrich Co. Isopropyl alcohol and methanol were used as received without further purification. Cyclohexane was purified via distillation over sodium and degassed by three freeze-thaw cycles prior to use. Isoprene, styrene and 4-methylstyrene were purified by distillation over CaH₂ and degassed by three freeze-thaw cycles prior to use.

General polymerization procedure for one-step and sequential block copolymers: All copolymerizations were carried out in cyclohexane under argon atmosphere and room temperature in a glove box in 30 ml glass flasks equipped with septa. The degassed monomer/solvent (20 wt%) was initiated by *sec*-butyllithium (1.3 M in cyclohexane/hexane 92/8) via syringe. The solution was stirred over night to ensure full monomer conversion. The polymerization was terminated by adding 0.5 ml of degassed methanol via syringe. The polymers were precipitated in methanol, dried at reduced pressure and stored at -18 °C. For the preparation of block copolymers a mixture of isoprene/cyclohexane (10 wt%) was initiated by *sec*-butyllithium (1.3 M in cyclohexane/hexane 92/8). When full monomer conversion was achieved, 4-methylstyrene was added via syringe.

General polymerization procedure for ultrahigh molecular weight block copolymers:

P(I-*co*-4MS) (entry 17 in Table S3) (PI_{20,310}-*co*-P4MS_{t_{2,240}})

In an ampule equipped with a stir bar 320 mg (2.7 mmol) neat 4-methylstyrene and 1654 mg (24.29 mmol) isoprene were dissolved in 100 mL of dry cyclohexane inside a glove box. The polymerization was initiated by quick addition of 92 µL *sec*-butyllithium (0.0012 mmol, 0.013 M solution in hexane) with a syringe. The solution was stirred at room temperature for 1 week to ensure complete conversion. After adding a small amount of degassed methanol, the polymer was poured into a 10-fold excess of methanol. The polymer was collected by filtration, washed with methanol, dried in vacuum and stored under argon or nitrogen at -18 °C (yield: 1170 mg, 97.5 %).

P(I-*co*-4MS) (entry 16 in Table S3) (PI₆₉₀-*co*-P4MS_{t₄₅₀})

In an ampule equipped with a stir bar, 826 mg (7 mmol) neat 4-methylstyrene and 714 mg (10.48 mmol) isoprene were dissolved in 50 mL dry cyclohexane inside a glove box. The polymerization was initiated by quick addition of 11 µL *sec*-butyllithium (0.0149 mmol, 1.4 M solution in hexane) with a syringe. The solution was stirred at room temperature for 1 day to ensure complete conversion. After adding a small amount of degassed methanol, the polymer was poured into a 10-fold excess of methanol. The polymer was collected by filtration, washed with methanol, dried in vacuum and stored under argon or nitrogen at -18 °C (yield: 1480 mg, 99.3 %).

¹H-NMR kinetics studies: The monomer/solvent mixtures (20 wt% in cyclohexane-*d*₁₂) were prepared in a glove box. All compounds were purified via distillation over CaH₂ prior to use. The mixtures were filled in conventional NMR tubes and sealed with rubber septa. A NMR spectrum of the mixture was measured prior to the initiation step. After the initiation with one drop of *sec*-butyllithium (1.3 M in cyclohexane/hexane 92/8) the NMR experiments were started without locking and shimming of the polymerization mixture. All spectra were measured with 4 scans at 400 MHz, and the time intervals between the spectra varied from 20 seconds to 1 minute due to the gradual decrease of the polymerization rate. The reaction temperature was kept constant at 23 °C. Typically, 150-250 ¹H NMR spectra were recorded and evaluated.

TEM Measurements: TEM experiments were carried out on a Zeiss EM 10 electron microscope operating at 60 kV. All images presented were recorded with a slow-scan CCD camera obtained from TRS (Tröndle) in bright field mode. Camera control was computer-aided using the ImageSP software from TRS.

Instrumentation: Additional NMR spectra were recorded on a Bruker Avance II 400 spectrometer working 400 MHz (¹H NMR). NMR chemical shifts are referenced relative to tetramethylsilane. Standard SEC was performed with THF as the mobile phase (flow rate 1 mL min⁻¹) on a SDV column set from PSS (SDV 10³, SDV 10⁵, SDV 10⁶) at 30 °C. Calibration was carried out using PS standards

(from Polymer Standard Service, Mainz). For determining the thermal properties of the polymers differential scanning calorimetry (DSC) was performed with a Mettler Toledo DSC-1 in a temperature range of -100 °C to 150 °C with a heating rate of 10 K min⁻¹.

Determination of reactivity ratios: To determine the reactivity ratios by the Fineman-Ross¹, Kelen-Tüdös² and Meyer-Lowry³ formalism, respectively, the proton signals at 5.54-5.64 ppm (4-methylstyrene), 5.6-5.7 ppm (styrene) and 6.34-6.44 (isoprene) were used. In case of 4MS/I copolymerization the Meyer-Lowry formalism was used. Evaluation methods based on the differential form of the Mayo-Lewis equation did not perform well in case of 4MS/I copolymerization due to strongly curved compositional shift. This means that incorporation determination by segmental linear fits is not sufficient. The integrated Meyer-Lowry equation can directly fit the composition shift during the copolymerization experiment and is superior to the differential version of the Mayo-Lewis equation. Relative errors of the reactivity ratios are not trivially determined for a non-linear fit with errors in both independent variables. The used Least Squares fit does not provide a concise prediction of the possible errors.⁴ Therefore, no errors for the reactivity ratios are indicated, since this would be speculative.

DFT: All DFT calculations have been performed using the ORCA 3.0.2 software suite.⁵ Each geometry was optimized with the B3LYP DFT hybrid function with geometrical counterpoise correction (gCP) and dispersion correction (D3)^{6,7} with def2-TZVP basis set.^{8,9} To reduce the calculation effort the RIJCOSX approximation method was used.¹⁰ For all ground states no imaginary frequency was detectable. For the transition state exactly one imaginary frequency corresponding to the desired reaction pathway was detected. For further verification the transition state was connected to the precursor and product by intrinsic reaction pathway calculations.

Kinetic Monte Carlo calculations (KMC) (Equation Set SI): The model was developed based on the stochastic simulation algorithm by Gillespie.^{11,12} Continuum-based reaction rates were converted to number-based probabilities using the following equations:

$$kMC_{II} = \frac{k_{II}}{(NV)^{1/4}} \quad (1.1)$$

$$kMC_{4MS4MS} = \frac{k_{4MS4MS}}{(NV)^{1/2}} \quad (1.2)$$

$$kMC_{I4MS} = \frac{k_{I4MS}}{(NV)^{1/4}} \quad (1.3)$$

$$kMC_{4MSI} = \frac{k_{4MSI}}{(NV)^{1/2}} \quad (1.4)$$

Concentrations have been converted by multiplying with Avogadro's number N and simulation volume V. The typical simulation volume was in the range of 8E-16 L to 8E-19 L. For each simulation 500000 chains were used. All simulations were performed up to 99 % conversion. Each reaction probability was calculated based on the fraction of the total reaction rate:

$$P_v = \frac{R_v}{\sum_{M=1}^v R_M} \quad (1.5)$$

The corresponding reaction was chosen using a uniform distributed random number $r_1 = [0..1]$ based on the reaction probabilities:

$$\sum_{v=1}^{\mu-1} P_v < r_1 < \sum_{v=1}^{\mu} P_v \quad (1.6)$$

The time interval corresponding to the chosen reaction step was calculated using another uniformly distributed random number $r_2 = [0..1]$:

$$\tau = \frac{1}{\sum_{M=1}^{\mu} R_M} \ln\left(\frac{1}{r_2}\right) \quad (1.7)$$

After a reaction was stochastically selected, one randomly corresponding chain was chosen and used to proceed the reaction step. The monomer composition of all chains was tracked. The number and weight average sequence length was calculated using the following equations:

$$\langle N \rangle_n = \frac{\sum_i i N_i}{\sum_i N_i} \quad (1.8)$$

$$\langle N \rangle_w = \frac{\sum_i i^2 N_i}{\sum_i i N_i} \quad (1.9)$$

N_i represents the number of segments with the size i .

For performance improvement the main stochastic model was implemented in C code, compiled using MinGW GCC compiler 5.1.0, while evaluation of the computed data was performed using custom written MATLAB scripts.

2. Real time NMR kinetics results and evaluation

Real time (*in situ*) ^1H -NMR kinetics studies of the copolymerization of isoprene and styrene (I/S)

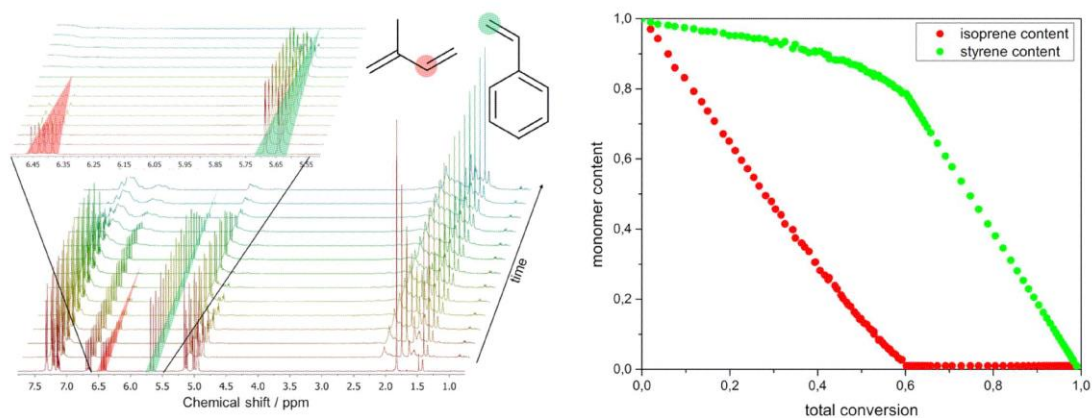


Figure S1: Left: real-time ^1H -NMR measurements of the copolymerization of isoprene and styrene (selected spectra), right: monomer concentration of isoprene (red) and styrene (green) vs. total conversion.

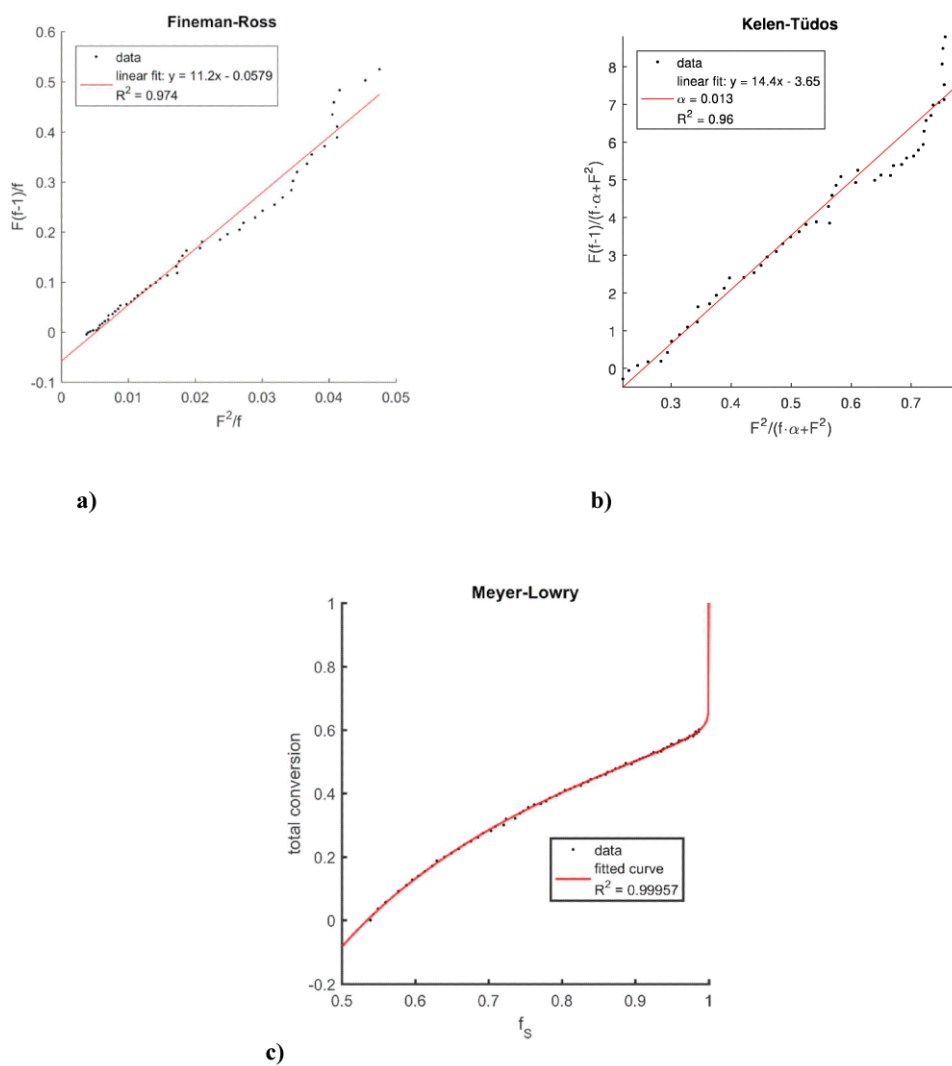


Figure S2 a,b,c: Determination of reactivity ratios by a) Fineman-Ross, b) Kelen-Tüdös and c) Meyer-Lowry formalism for the copolymerization of isoprene and styrene in cyclohexane.

Table S1: Summarized reactivity ratios for styrene/isoprene system in cyclohexane from all used methods and literature.

Method	r_{isoprene}	r_{styrene}
Fineman Ross	11.21	0.058
Kelen Tüdös	10.71	0.049
Meyer-Lowry	11.07	0.040
Average Value	11.0	0.049
Literature Value ¹³	14.4	0.045
Literature Value ¹⁴	12.8	0.051

Real time NMR-kinetics studies of the copolymerization of isoprene and 4-methylstyrene (I/4MS)

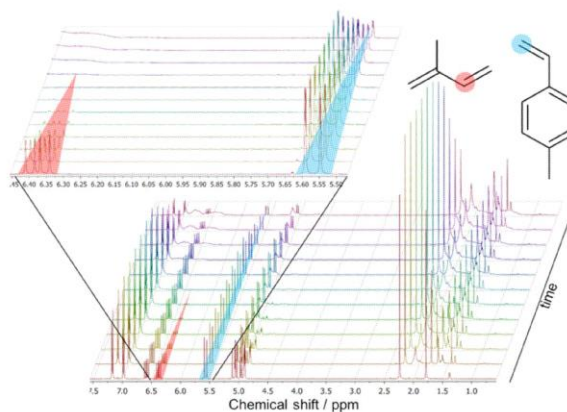


Figure S3: Real time ^1H -NMR measurement of the copolymerization of isoprene and 4-methylstyrene

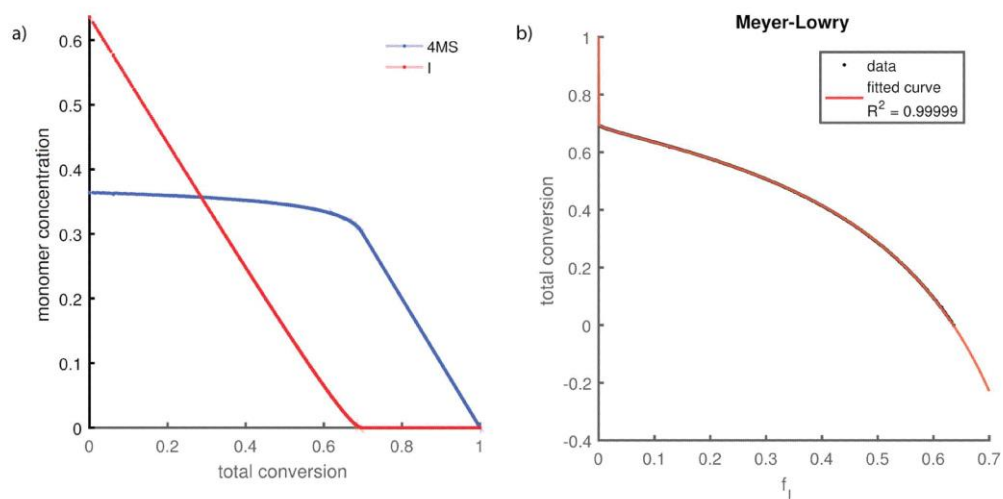


Figure S4 a,b: a) Normalized monomer concentration (total = 1) versus total conversion of 4MS (blue) and isoprene (red). b) Total conversion versus instantaneous monomer incorporation, f_1 , of isoprene, and Meyer-Lowry fitted curve.

Real time $^1\text{H-NMR}$ kinetics studies of 4MS homopolymerization

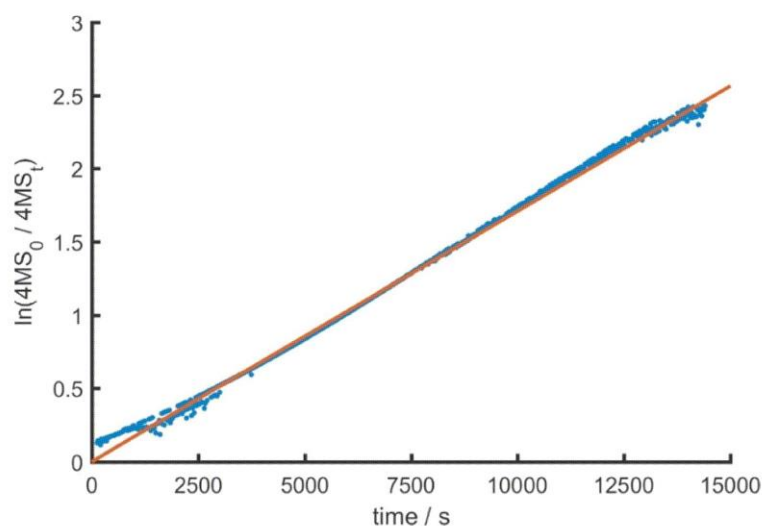


Figure S5: First-order time-conversion plot of the homopolymerization of 4MS determined from NMR measurements. The slope of the linear regression is the apparent rate constant, $k_{\text{app}} = 1.71 \times 10^{-4} \text{ s}^{-1}$.

3. DFT studies and simulated monomer distributions for tapered copolymers

DFT Studies of 4MS and styrene homopolymerization

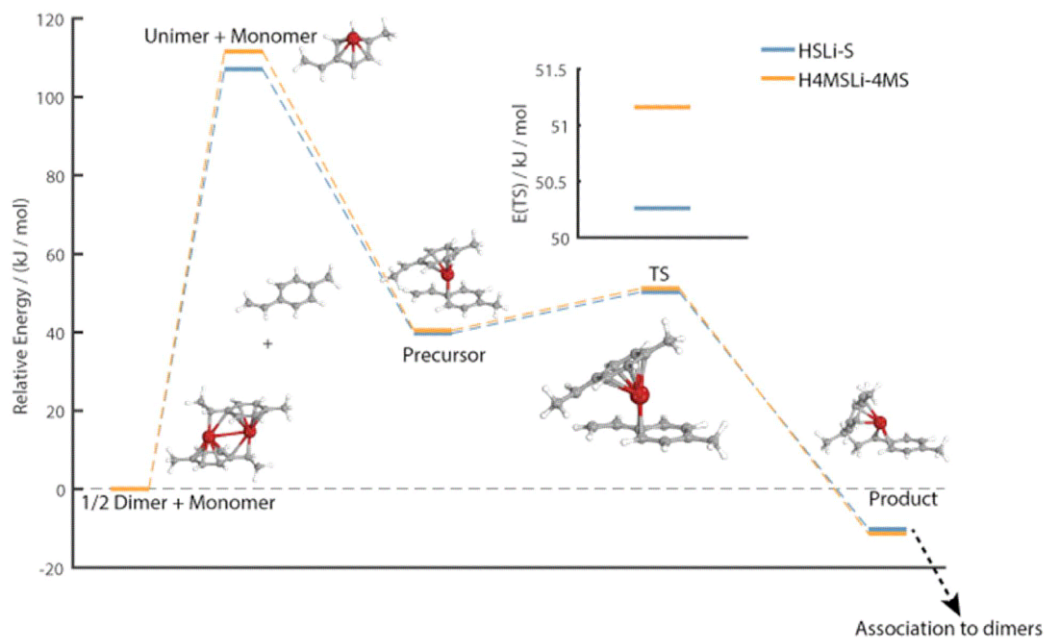


Figure S6: Energy diagrams of homopolymerization of 4MS (orange) and S (blue), respectively. 3D representation show the corresponding structures for 4MS.

Table S2, left: calculated energies (B3LYP-D3-gCP/def2-TZVP//B3LYP-D3-gCP/def2-TZVP) of styrene and 4MS homopolymerization normalized to the energy level of the sum $\frac{1}{2}$ dimer and one monomer (right side).

	Electronic energy / Hartree		Normalized electronic energy / kJ / mol		
	Styrene	4MS	Styrene	4MS	
H-Li	-8.0727743	-8.0727743	1/2 Dimer + Monomer	0	0
Monomer	-309.5797979	-348.8853499	Unimer + Monomer	107.089747	111.639804
Dimer	-635.4888281	-714.0959984	Precursor	39.7871027	40.5174511
Unimer	-317.7036257	-357.0054778	Transition state	50.2616137	51.1589702
Precursor	-627.3090579	-705.9179168	Product	-10.1596742	-11.3480936
Transition state	-627.3050683	-705.9138637			
Product	-627.3280816	-705.9376713			

Equation Set S2: Copolymerization kinetics equations for 4MS / I


$$\frac{d[I]}{dt} = k_{11}[I][PILi]^{1/4} - k_{4MSI}[I][P4MSLi]^{1/2} \quad (2.7)$$

$$\frac{d[4MS]}{dt} = k_{4MS4MS}[4MS][P4MSLi]^{1/2} - k_{14MS}[4MS][PILi]^{1/4} \quad (2.8)$$

$$\frac{d[P4MSLi]}{dt} = k_{4MSI}[I][P4MSLi]^{1/2} + k_{14MS}[4MS][PILi]^{1/4} \quad (2.9)$$

$$\frac{d[PILi]}{dt} = -\frac{d[P4MSLi]}{dt} \quad (2.10)$$

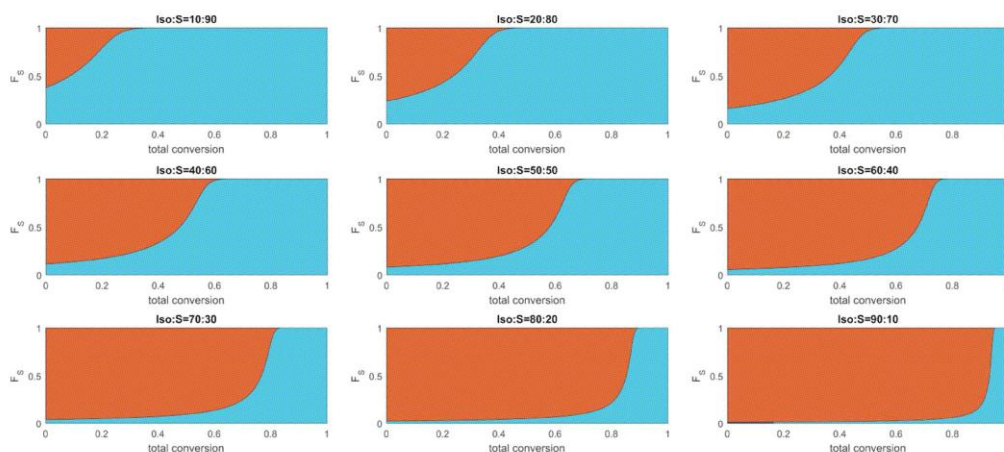


Figure S7, isoprene/styrene system: simulated plots of incorporated fraction of styrene (F_S , light blue) and isoprene (red) versus total conversion for different initial monomer feed ratios. The reactivity ratios were directly derived from 1H real-time NMR measurements.

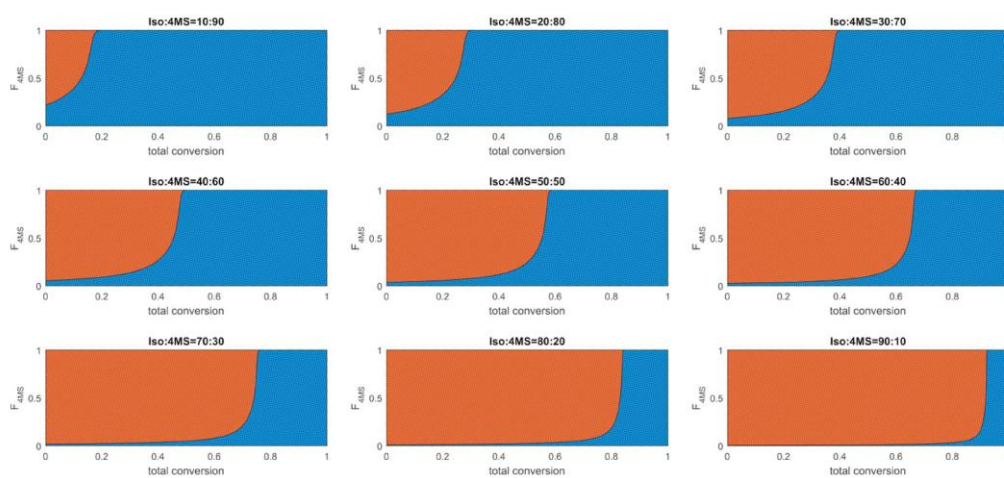


Figure S8, isoprene/4-methylstyrene system: Simulated plots of the incorporated fraction of 4MS (F_{4MS} , blue) and isoprene (blue) versus total conversion for different initial monomer feed ratios I/4MS. The data employed for the simulation are directly derived from ^1H real-time NMR kinetics measurements.

4. Characterization of the copolymers prepared by statistical copolymerization

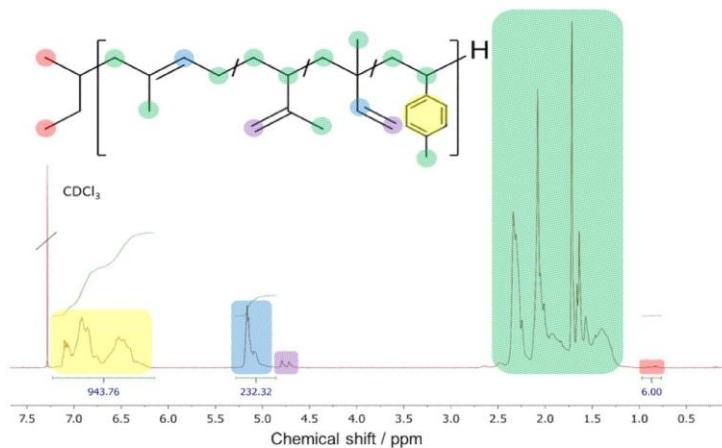


Figure S9: $^1\text{H-NMR}$ spectrum (400 MHz) of a statistical copolymer of I/4MS in CDCl_3 (entry 3 in Table S3).

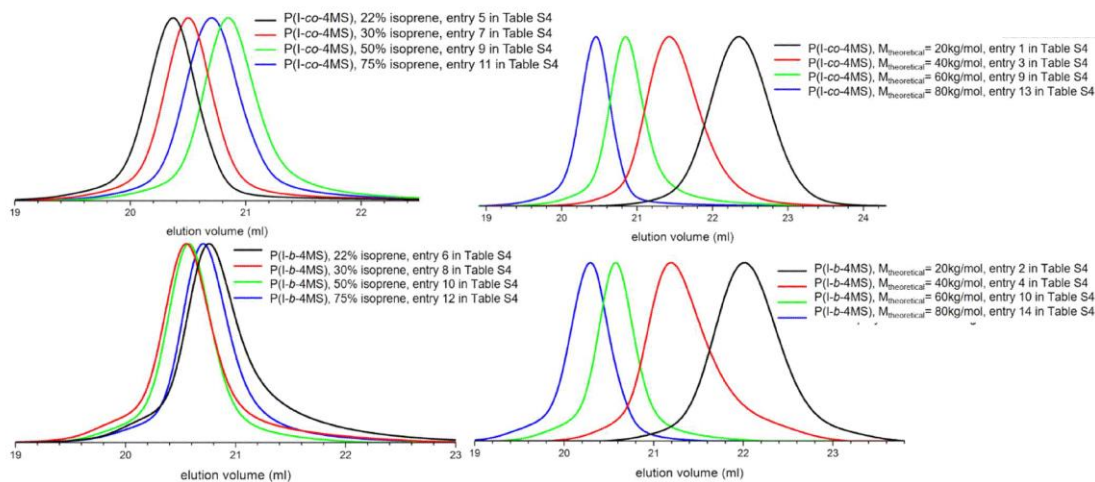


Figure S10: SEC traces of gradient and block copolymers of I/4MS prepared under argon atmosphere in a glove box. Dispersity range of the polymers: 1.08 – 1.16.

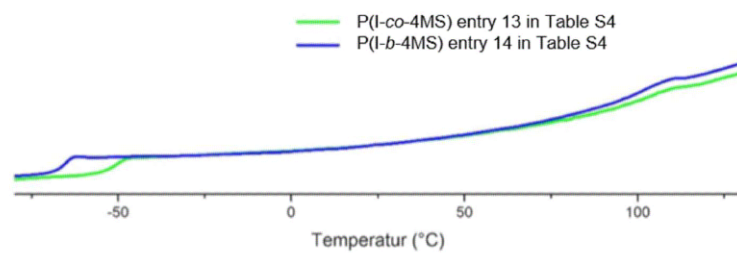


Figure S11: DSC thermogram of entry 13 (green) and 14 (blue) (Table S3). Heating rate: 10 K min⁻¹.

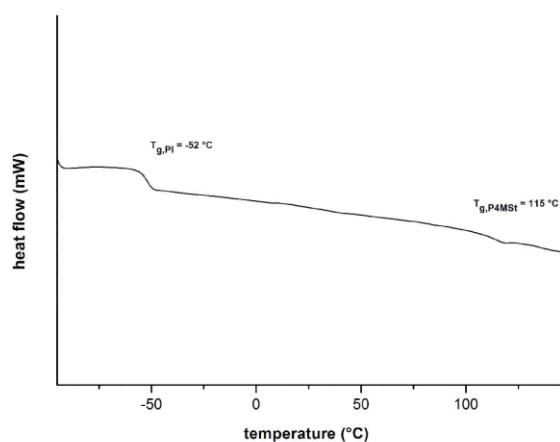


Figure S12. DSC thermogram of sample entry 16 (Table S3). Heating rate: 10 K min⁻¹.

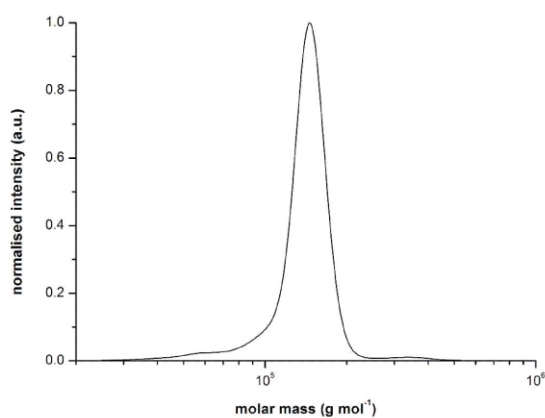


Figure S13. Typical molar mass distributions obtained by SEC measurements vs. PS standards in THF obtained for sample entry 16 (Table S3).

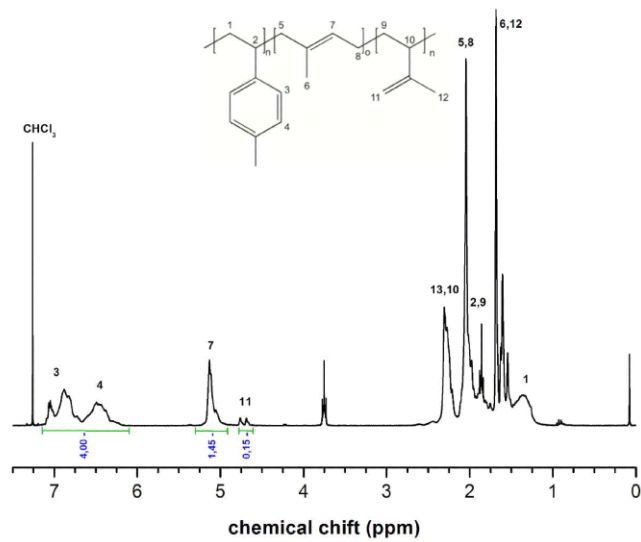


Figure S14. ^1H NMR spectrum of entry 16 (Table S3) in CDCl_3 .

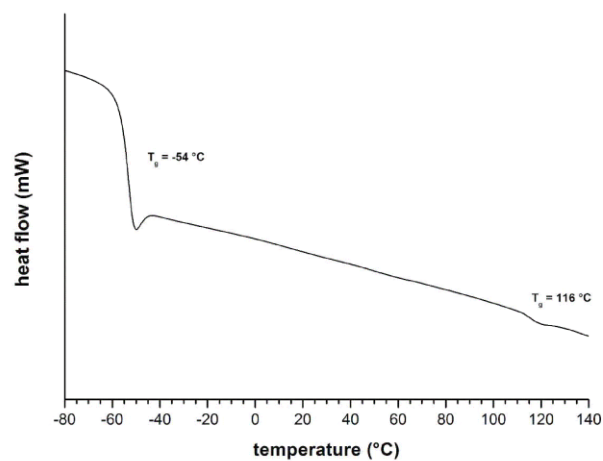


Figure S15. DSC thermogram of entry 17 (Table S3) (heating rate 10 K min^{-1}).

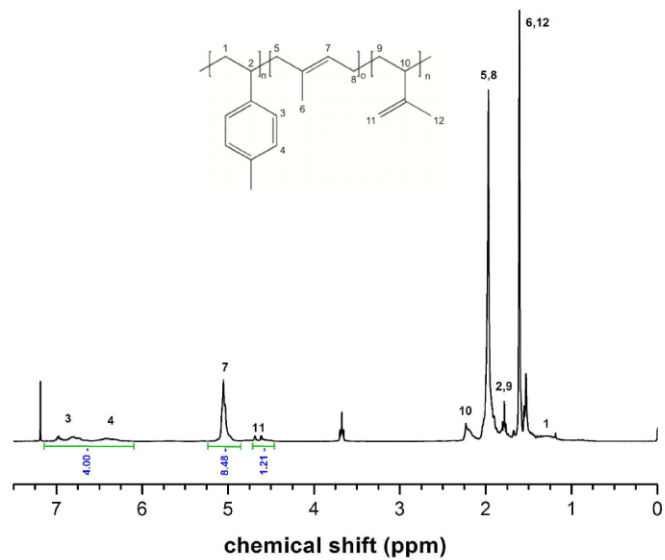


Figure S16. ¹H NMR spectrum of entry 17 (Table S3) in CDCl₃.

Table S3: Summarized results of copolymer characterization by NMR, SEC and DSC.

Entry	Polymer composition ^[a]	Isoprene content / %	Target M_n [kg/mol]	M_n (SEC) ^[b] [kg/mol]	$\bar{D} = M_w/M_n$	v_1 ^[c] [%]	T_g ^[d] (I/4MS) [°C]
1	P(I-co-4MS)	50	20	38.6	1.08	40	-45/45
2	PI- <i>b</i> -P4MS	50	20	46.5	1.08	41	-63/70
3	P(I-co-4MS)	50	40	38.6	1.09	39	-50/86
4	PI- <i>b</i> -P4MS	50	40	46.5	1.09	41	-65/89
5	P(I-co-4MS)	22	60	77.3	1.10	18	-/87
6	PI- <i>b</i> -P4MS	22	60	57.6	1.11	17	-/87
7	P(I-co-4MS)	30	60	76.3	1.12	24	-46/93
8	PI- <i>b</i> -P4MS	30	60	71.1	1.14	23	-70/97
9	P(I-co-4MS)	50	60	55.8	1.12	40	-51/102
10	PI- <i>b</i> -P4MS	50	60	76.6	1.10	39	-65/98
11	P(I-co-4MS)	75	60	65.4	1.11	60	-56/-
12	PI- <i>b</i> -P4MS	75	60	62.4	1.12	61	-57/-
13	P(I-co-4MS)	50	80	77.4	1.08	41	-52/100
14	PI- <i>b</i> -P4MS	50	80	101.9	1.08	40	-65/105
15	P(I-co-4MS)	50	400	360	1.07	40	-55/99
16	P(I-co-4MS)	60	130	133	1.09	50	-52/115
17	P(I-co-4MS)	90	1300	1250	1.32	86	-54/116
18	P(I-co-4MS)	50	2.5	4.4	1.20	29	26
19	PI- <i>b</i> -P4MS	50	2.5	3.8	1.12	30	-/-
20	P4MS- <i>b</i> -PI	50	2.5	2.4	1.06	40	20
21	P(I-co-4MS)	50	5	4.7	1.16	30	-15/21
22	PI- <i>b</i> -P4MS	50	5	5.4	1.09	36	-41/11
23	P4MS- <i>b</i> -PI	50	5	3.7	1.06	40	-47/6
24	P(I-co-4MS)	50	10	7.4	1.13	38	-31/16
25	PI- <i>b</i> -P4MS	50	10	8.6	1.09	39	-43/21
26	P4MS- <i>b</i> -PI	50	10	7.4	1.07	39	-43/23

[a] Polymer composition and preparation route with targeted isoprene and 4MS content: “*b*” sequential addition of both monomers, “*co*” translates to direct (i.e., statistical) copolymerization; [b] Size exclusion chromatography (SEC) in THF at 25 °C. [c] calculated volume fractions based on densities from reference¹⁵ [d] via differential scanning calorimetry (DSC).

Samples 16 and 17 (entry 16 and 17 in Table S3) show higher glass transition temperatures for the 4MS block due to their higher molecular weight and the use of a different experimental setup than the other samples.

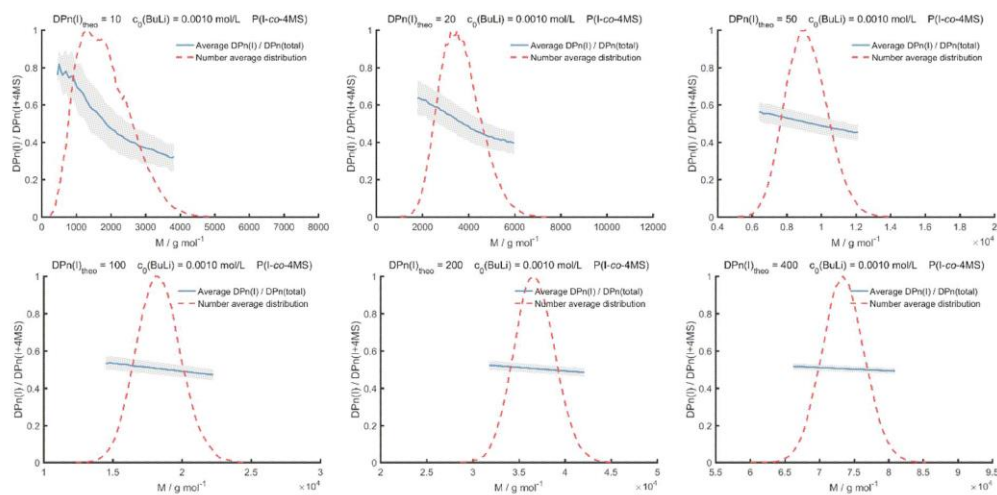


Figure S17: Average ratio of the degree polymerization of isoprene ($DP_n(I)$) and the total DP_n (blue) of P(I-co-4MS) copolymers versus total molecular weight at an initial initiator concentration of 10^{-3} mol/L. The shaded area shows the standard deviation of the average $DP_n(I) / DP_n(\text{total})$ ratio. The red curve shows the normalized number average distribution of the simulated copolymers.

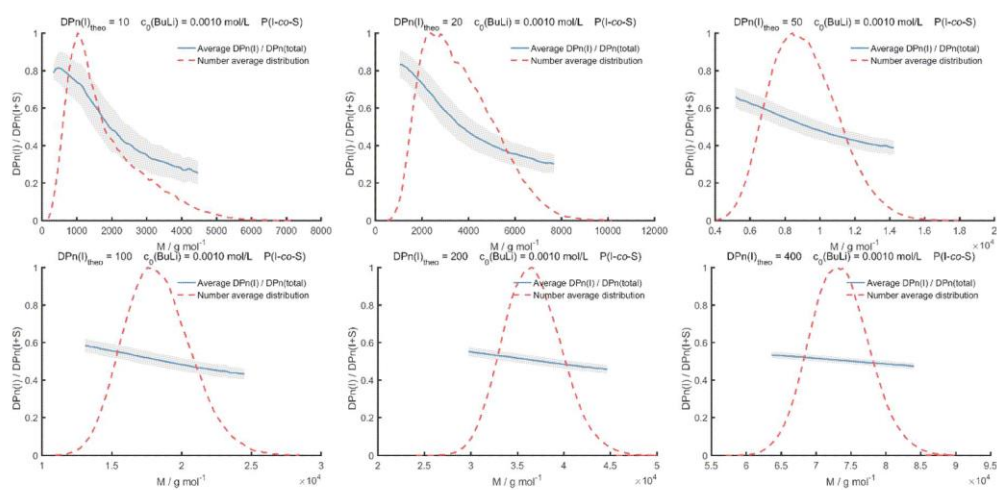


Figure S18: Average ratio of the degree polymerization of isoprene ($DP_n(I)$) and the total DP_n (blue) of P(I-co-S) copolymers versus total molecular weight at an initial initiator concentration of 10^{-3} mol/L. The shaded area shows the standard deviation of the average $DP_n(I) / DP_n(\text{total})$ ratio. The red curve shows the normalized number average distribution of the simulated copolymers.

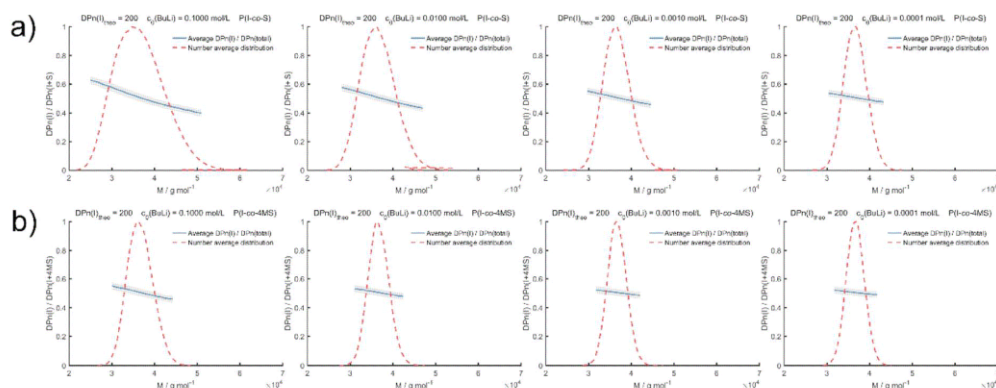


Figure S19: Average ratio of the degree polymerization of isoprene ($DP_n(I)$) and the total DP_n (blue) of (a) P(I-co-S) and (b) P(I-co-4MS) copolymers versus total molecular weight at different initial initiator concentrations. The shaded area shows the standard deviation of the average $DP_n(I) / DP_n(\text{total})$ ratio. The red curve shows the normalized number average distribution of the simulated copolymers.

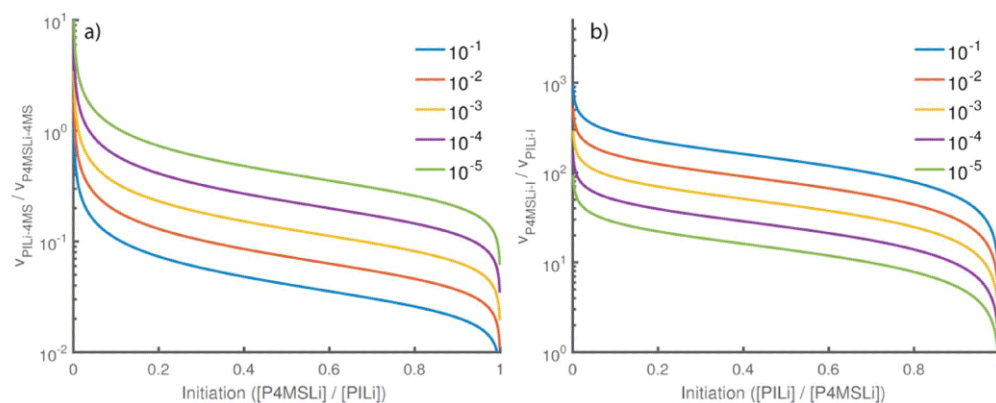


Figure S20: Ratio of initiation rate to propagation rate versus initiation amount at various initiator concentrations. At an initiation amount of 1 all chains have been successful initiated. a) Initiation of a 4MS block by a PILi macroinitiator. b) Initiation of an isoprene block by a P4MSLi macroinitiator.

Equation Set S3: Mathematical derivation of initiation rate versus propagation rate dependence from initiator concentration in case of dimeric polystyryllithium and tetrameric polyisoprenyllithium chain ends starting from a PILi macroinitiator.

$$R_{I4MS} = k_{I4MS}[4MS][PILi]^{1/4} \quad (3.1)$$

$$R_{4MS4MS} = k_{4MS4MS}[4MS][P4MSLi]^{1/2} \quad (3.2)$$

$$[PILi] + [P4MSLi] = [PILi]_0 \quad (3.3)$$

$$\frac{R_{I4MS}}{R_{4MS4MS}} = \frac{k_{I4MS}}{k_{4MS4MS}} \frac{[PILi]^{1/4}}{[P4MSLi]^{1/2}} = \frac{k_{I4MS}}{k_{4MS4MS}} \frac{([PILi]_0 - [P4MSLi])^{1/4}}{[P4MSLi]^{1/2}} = \alpha_{ini} \quad (3.4)$$

$$\beta = \frac{[PILi]_1}{[PILi]_2} \quad \gamma = \frac{[PILi]_n}{[P4MSLi]_n} \quad (3.5)$$

$$\frac{\alpha_{ini,1}}{\alpha_{ini,2}} = \frac{([PILi]_1 - [P4MSLi]_1)^{1/4} [P4MSLi]_2^{1/2}}{([PILi]_2 - [P4MSLi]_2)^{1/4} [P4MSLi]_1^{1/2}} = \frac{([PILi]_1 - \gamma [PILi]_1)^{1/4} (\gamma [PILi]_2)^{1/2}}{([PILi]_2 - \gamma [PILi]_2)^{1/4} (\gamma [PILi]_1)^{1/2}} \quad (3.6)$$

$$\frac{\alpha_{ini,1}}{\alpha_{ini,2}} = \left(\frac{[PILi]_1(1-\gamma)}{[PILi]_2(1-\gamma)} \right)^{1/4} \left(\frac{[PILi]_2}{[PILi]_1} \right)^{1/2} = \beta^{1/4} \beta^{-1/2} = \beta^{-1/4} \quad (3.7)$$

TEM measurements (transmission electron microscopy)

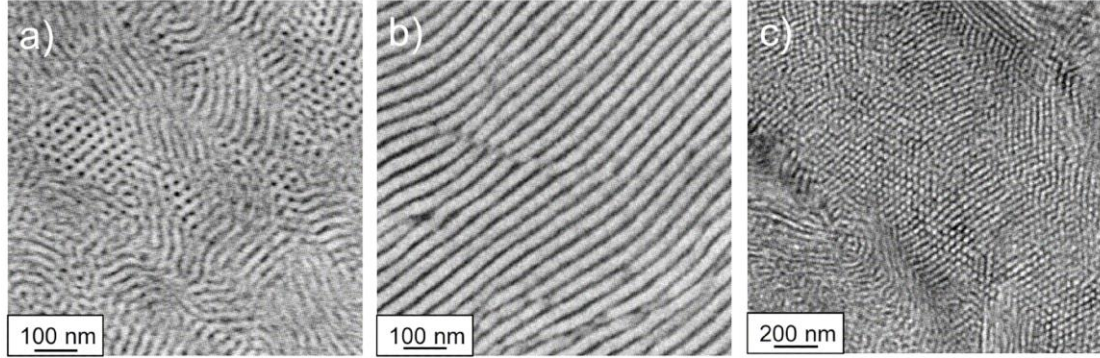


Figure S21: TEM images of gradient copolymers of isoprene and 4-methylstyrene after staining with osmium tetroxide, a) P(I-co-4MS) (entry 7 in Table S3), isoprene cylinders in poly(4-methylstyrene) matrix; b) P(I-co-4MS) (entry 9 in Table S3), lamella; c) P(I-co-4MS) (entry 11 in Table S3), *p*-methylstyrene cylinders in polyisoprene matrix.

References

- (1) Fineman, M.; Ross, S. D. Linear method for determining monomer reactivity ratios in copolymerization. *J. Polym. Sci.* **1950**, *5*, 259–262, DOI: 10.1002/pol.1950.120050210.
- (2) Kelen, T.; Tüdös, F. A new improved linear graphical method for determining copolymerization reactivity ratios. *React Kinet Catal Lett* **1974**, *1*, 487–492, DOI: 10.1007/BF02074484.
- (3) Meyer, V. E.; Lowry, G. G. Integral and differential binary copolymerization equations. *J. Polym. Sci. A Gen. Pap.* **1965**, *3*, 2843–2851, DOI: 10.1002/pol.1965.100030811.
- (4) van den Brink, M.; van Herk, A. M.; German, A. L. Nonlinear regression by visualization of the sum of residual space applied to the integrated copolymerization equation with errors in all variables. I. Introduction of the model, simulations and design of experiments. *J. Polym. Sci. A Polym. Chem.* **1999**, *37*, 3793–3803, DOI: 10.1002/(SICI)1099-0518(19991015)37:20<3793:AID-POLA8>3.0.CO;2-Q.
- (5) Neese, F. The ORCA program system. *WIREs Comput Mol Sci* **2012**, *2*, 73–78, DOI: 10.1002/wcms.81.
- (6) Grimme, S.; Antony, J.; Ehrlich, S.; Krieg, H. A consistent and accurate ab initio parametrization of density functional dispersion correction (DFT-D) for the 94 elements H–Pu. *The Journal of chemical physics* **2010**, *132*, 154104, DOI: 10.1063/1.3382344.
- (7) Grimme, S.; Ehrlich, S.; Goerigk, L. Effect of the damping function in dispersion corrected density functional theory. *Journal of computational chemistry* **2011**, *32*, 1456–1465, DOI: 10.1002/jcc.21759.
- (8) Schäfer, A.; Horn, H.; Ahlrichs, R. Fully optimized contracted Gaussian basis sets for atoms Li to Kr. *The Journal of chemical physics* **1992**, *97*, 2571–2577, DOI: 10.1063/1.463096.
- (9) Weigend, F.; Ahlrichs, R. Balanced basis sets of split valence, triple zeta valence and quadruple zeta valence quality for H to Rn: Design and assessment of accuracy. *Physical chemistry chemical physics : PCCP* **2005**, *7*, 3297–3305, DOI: 10.1039/b508541a.
- (10) Neese, F.; Wennmohs, F.; Hansen, A.; Becker, U. Efficient, approximate and parallel Hartree–Fock and hybrid DFT calculations. A ‘chain-of-spheres’ algorithm for the Hartree–Fock exchange. *Chemical Physics* **2009**, *356*, 98–109, DOI: 10.1016/j.chemphys.2008.10.036.
- (11) Gillespie, D. T. A general method for numerically simulating the stochastic time evolution of coupled chemical reactions. *Journal of Computational Physics* **1976**, *22*, 403–434, DOI: 10.1016/0021-9991(76)90041-3.
- (12) Gillespie, D. T. Exact stochastic simulation of coupled chemical reactions. *J. Phys. Chem.* **1977**, *81*, 2340–2361, DOI: 10.1021/j100540a008.
- (13) Worsfold, D. J. Anionic copolymerization of styrene and isoprene in cyclohexane. *J. Polym. Sci. A-1 Polym. Chem.* **1967**, *5*, 2783–2789, DOI: 10.1002/pol.1967.150051106.
- (14) Quinebèche, S.; Navarro, C.; Gnanou, Y.; Fontanille, M. In situ mid-IR and UV–visible spectroscopies applied to the determination of kinetic parameters in the anionic copolymerization of styrene and isoprene. *Polymer* **2009**, *50*, 1351–1357, DOI: 10.1016/j.polymer.2009.01.041.
- (15) Wu, L.; Lodge, T. P.; Bates, F. S. Bridge to Loop Transition in a Shear Aligned Lamellae Forming Heptablock Copolymer. *Macromolecules* **2004**, *37*, 8184–8187, DOI: 10.1021/ma048635w.

Christian Wahlen

CURRICULUM VITAE

Address

[REDACTED]

[REDACTED]

Phone

[REDACTED]

E-Mail

[REDACTED]

Date and place of birth

20/12/1991 / Mainz

Nationality

German



Education

04/2017 – now

PhD candidate

Johannes Gutenberg University Mainz

Research group of Prof. Dr. Holger Frey

Topic: “Anionic polymerization of terpenes and bio-based thermoplastic elastomers”

- Analytical methods: NMR, DSC, SEC, SAXS, TEM, tensile test
- Protective group chemistry
- Copolymerization kinetics
- Supervision of 2 Bachelor students and 1 Master student
- Interdisciplinary collaborations with Prof. Dr. George Floudas (SAXS, rheology), Prof. Dr. Paweł Ł. Sajkiewicz (Electrospinning) and Prof. Dr. Markus Gallei (TEM)

10/2014 – 03/2017

Master of Science (1.4) Chemistry

Johannes Gutenberg University Mainz

Master thesis (1.0)

Supervisor: Prof. Dr. Holger Frey

Topic: “End-functionalization of block-like gradient copolymers“

- End-group analysis (NMR spectroscopy, MALDI-ToF-MS)
- Carbanionic und oxyanionic polymerization

09/2016 – 12/2016

Erasmus traineeship Durham University (UK)

Research group of Prof. Dr. Lian R. Hutchings

Topic: “Synthesis, characterization and purification of cyclic polymers via the macromonomer approach”

- End-group analysis via temperature gradient interaction chromatography

- 04/2011 – 08/2014** **Bachelor of Science** (2.1) Chemistry
Johannes Gutenberg University Mainz
Bachelor thesis (1.0):
Supervisor: Prof. Dr. Frederik Wurm
Topic: “Application of the Horner-Wadsworth-Emmons reaction on polyphosphonates synthesized via ADMET”
- 08/2008 – 03/2011** **High-school diploma (Abitur)** (3.1)
Gutenberg-Gymnasium, Mainz

Languages, Skills and Interests

- Languages** German (first language), English (fluent)
- IT** MS-Office, Origin, Mestrenova, Chemdraw, Web of Science, Citavi, Reaxys, Scifinder
- Hobbies** [REDACTED]

Further Education

- 02/2019** GDCh course “Business Administration for Chemists”
- 06/2017** MAINZ Summer School “From Polymers to Functional Systems”
- 08/2017 – 03/2019** Courses of the General Postgraduate Program (GPP) of Johannes Gutenberg University Mainz
- Project Management
 - Intercultural Communication
 - Presenting in English
 - Academic Writing in English
 - Good Scientific Practice

Conferences

- 05/2019** Sixth International Symposium Frontiers in Polymer Science, Budapest (Hungary)
Poster presentation: “A novel myrcenol-based monomer for carbanionic polymerization: Adjustable polarity by copolymerization with myrcene”
- 09/2017** 12th International Symposium on Ionic Polymerization, Durham (UK)
Poster presentation: “One-pot synthesis of amphiphilic block terpolymers using potassium *tert*-butoxide and crown ether additives”

List of Publications

Contribution as first author or equally

2020

- (1) Wahlen, C.; Rauschenbach, M.; Blankenburg, J.; Kersten, E.; Ender, C. P.; Frey, H. Myrcenol-Based Monomer for Carbanionic Polymerization: Functional Copolymers with Myrcene and Bio-Based Graft Copolymers. *Macromolecules*, **2020**, DOI: 10.1021/acs.macromol.0c01734.
- (2) Wahlen, C.; Blankenburg, J.; von Tiedemann, P.; Ewald, J.; Sajkiewicz, P.; Müller, A. H. E.; Floudas, G.; Frey, H. Tapered Multiblock Copolymers based on Farnesene and Styrene: Impact of Bio-based Polydiene Architectures on Material Properties, *submitted to Macromolecules*.

[REDACTED] to be submitted.

[REDACTED] to be submitted.

2019

- (5) Galanos, E.; Grune, E.; Wahlen, C.; Müller, A. H. E.; Appold, M.; Gallei, M.; Frey, H.; Floudas, G. Tapered Multiblock Copolymers Based on Isoprene and 4-Methylstyrene: Influence of the Tapered Interface on the Self-Assembly and Thermomechanical Properties. *Macromolecules* **2019**, *52*, 1577–1588, DOI: 10.1021/acs.macromol.8b02669.

Contribution as coauthor

2018

- (6) Grune, E.; Johann, T.; Appold, M.; Wahlen, C.; Blankenburg, J.; Leibig, D.; Müller, A. H. E.; Gallei, M.; Frey, H. One-Step Block Copolymer Synthesis versus Sequential Monomer Addition: A Fundamental Study Reveals That One Methyl Group Makes a Difference. *Macromolecules* **2018**, *51*, 3527–3537, DOI: 10.1021/acs.macromol.8b00404.

2015

- (7) Steinbach, T.; Wahlen, C.; Wurm, F. R. Poly(phosphonate)-mediated Horner–Wadsworth–Emmons reactions. *Polym. Chem.* **2015**, *6* (7), 1192–1202, DOI: 10.1039/C4PY01365D.

2014

- (8) Steinbach, T.; Alexandrino, E. M.; Wahlen, C.; Landfester, K.; Wurm, F. R. Poly(phosphonate)s via Olefin Metathesis: Adjusting Hydrophobicity and Morphology *Macromolecules* **2014**, *47*, 4884–4893, DOI: 10.1021/ma5013286.